Universiteit Antwerpen

Faculty of Science

Department of Biology

Morphology of the Tapir Forelimb

anatomy, function and implications for perissodactyl locomotor evolution

– Anatomie van de voorpoot van de tapir –

– implicaties op de evolutionaire geschiedenisvan de voortbeweging bij onevenhoevigen –

Thesis submitted for the degree of doctor in Biology at the University of Antwerp to be defended by

Jamie A. MACLAREN

Promotors: Dr. Sandra Nauwelaerts

Prof. Dr. Peter Aerts

Antwerp 2019

– CONTENTS –

– SUMMARY –

The shape of the mammalian forelimb is inexorably tied to the functional demands of the species in question. The versatility of this morphological unit has enabled mammals to meet the locomotor needs involved in swimming, flying, climbing, digging and running. Mammals which utilise their forelimbs for walking and running on the ground possess a multitude of forelimb shapes and postures adapted to achieve the basic functions of gravitational support, directional change, shock absorption, and propulsion. The shape of the forelimb has undergone no greater changes in terrestrial mammals than that of the perissodactyl family Equidae (horses, zebras and asses). Widely regarded as the posterchild for terrestrial locomotor macroevolution, the so-called 'equid transition' charts the changes in limb morphology – most importantly the adaptation and reduction of digits – through the numerous lineages of equids. The earliest equids were small-bodied, four-toed (tetradactyl) forest-dwellers living approximately 56 million years ago. Through time, equids have adapted their limbs though digit reduction, distal element elongation, and tendonisation of distal muscles, ultimately leading to the evolution of the modern, single-toed (monodactyl) genus *Equus*. This transition has been studied for over 150 years, and is broadly believed to be a result of an increasingly cursorial lifestyle necessitating an increase in stride length and reduction in rotational inertia. Despite a diverse range of studies investigating the locomotor transition in equids, the timing, mechanisms and driving forces behind the changes are not yet fully resolved.

To provide insights into this presumably adaptive locomotor transition from four to one digit, this thesis takes an alternative taxonomic approach by investigating the forelimb functional morphology of a modern family of tetradactyl perissodactyls – the Tapiridae (tapirs). By quantifying the anatomy of tapir forelimb bones and muscles, I am able to gain an understanding of the functional anatomy of a living tetradactyl perissodactyl, which in turn enables informed comparisons between extinct tetradactyl perissodactyls and their modern counterparts. Furthermore, identification of important shifts in osteology and muscular arrangements (with known functional outcomes) can be highlighted during the transition between four and three functional forelimb digits in equids and their kin.

Quantifying the functional morphology of the tapir forelimb forms the integral backbone of this thesis. Historically, tapirs have been considered uniform in their bauplan, with some morphological changes in the cranium due to the development of their characteristic proboscis, and in the post-cranium only as an artefact of increases in body size. To offer insights into the evolution of the equid forelimb, it was therefore

important to ascertain the morphological variation in the tapir forelimb before any comparisons could be drawn. The thesis was therefore divided roughly into two sections: 1) quantifying the variation in tapir forelimb functional morphology, both in extant and extinct species; and 2) using information gained in the first section, to draw inferences on the functional morphology of the Equidae and their closest relatives (the Palaeotheriidae). To quantify morphology in both sections, I used a three-dimensional geometric morphometric approach based on laser surface scans of the bones of the forelimb. In addition, I also implemented limb long-bone ratios (speed proxies), lever-arm measurements (proxy for mechanical advantage), area ratios of muscle attachments / joint articular surfaces, body mass estimates, phylogenetic comparative methods, and quantified muscular architecture in order to achieve a holistic understanding of tapir forelimb functional anatomy.

Initial results of the thesis revealed the interspecific variation present in the forelimb of the tapir genus *Tapirus*, across both extant and extinct species. I also revealed hitherto unrecognised interspecific variation in the forelimbs of tapirs which suggests: a) differential load application across the four toes during movement, b) a spectrum of muscular application at the shoulder and beneath the foot-pad, c) potential shifts in resting posture between modern tapir species based on their upper forelimb bone shape, and d) the postcranial skeleton of tapirs has undergone morphological changes independent of both body size and phylogenetic relatedness. Investigating the muscular attachments and their resultant action on the skeleton revealed that tapirs share a series of features in common with tetradactyl Eocene equids and palaeotheres (centrally placed scapular spine; unspecialised humerus; extended volar process of the magnum; reduced flexion / increased adduction and abduction of the phalanges), which are rapidly lost in the equid locomotor transition. The shift in shape of these features indicate that early three-toed (tridactyl) equids and palaeotheres interacted with their underfoot substrate in a different manner, with equids exhibiting reduced upper limb stability and reduced potential for digit adduction/abduction early in their shift from four to three functional digits. This is not observed in palaeotheres or tapirs, leading to the conclusion that both these groups were better adapted for locomotion on compliant surfaces (e.g. rainforest floor) than the tridactyl equids.

The inclusion of both osteological and muscular quantification of the tetradactyl forelimb of tapirs in this thesis has made it possible, and justifiable, to draw inferences on the evolution of locomotion in equids. Aspects which warrant further study beyond the work presented here include the quantification of shape change in bones defining origination and insertion of muscle groups which have 1) undergone radical reorganisation through the equid transition, and 2) pertain to established outcomes

relevant for locomotion. This thesis represents the first quantification of such data in a tetradactyl perissodactyl, and can act as a springboard for further study of locomotor functional morphology across the Perissodactyla.

– SAMENVATTING –

De voorpoot van een zoogdier is morfologisch divers, wat hen in staat stelt verschillende habitats in te nemen. De vorm van het skelet is functioneel verwant met de manier van voortbewegen waardoor ze kunnen zwemmen, vliegen, klimmen, graven en rennen. Specifiek voor stappen en rennen is de vorm van de voorpoot aangepast aan de mechanische vereisten voor ondersteuning, richtingsverandering, schokabsorptie en kracht. Binnen de landzoogdieren zijn de vormveranderingen van de voorpoot bij familie van de Equidae (paarden, zebra's en ezels) waar de voorpoot een sterke reductie van het aantal vingers onderging. De schijnbare graduele veranderingen met al hun tussenvormen van een voorouder met vier vingers die tot het moderne paard met een vinger werd lang beschouwd als het schoolvoorbeeld van macro-evolutie. Buiten de reductie in aantal vingers, onderging de voorpoot in verschillend evolutieve lijnen een reeks drastische veranderingen: verlenging van de distale pootelement en het verpezen van de distale pootspieren. Momenteel wordt algemeen aangenomen dat deze drastische veranderingen in morfologie veroorzaakt zijn door een toenemende selectie op snelheid, waarvoor een grotere paslengte en een reductie van de rotationele inertia van de poten noodzakelijk zijn. Ondanks het grote aantal studies naar de locomotorische transitie bij paardachtigen zijn het tijdsverloop en de evolutieve mechanismen en selectieve drukken resulterend in de vormveranderingen, nog steeds niet volledig gekend.

Om verder inzicht te verschaffen in deze locomotorische transitie van een vier- naar ééntenige vorm bij paardachtigen, wordt in dit proefschrift gefocust op een nauw verwante groep aan de paardachtigen, de tapirs, die aan de voorpoot vier vingers hebben. Door de anatomie van de botten en spieren van de voorpoot van de tapir te kwantificeren, verkreeg ik inzicht in de functionele anatomie van hedendaagse tetradactyle onevenhoevigen. Dit liet op zijn beurt gefundeerde vergelijkingen toe tussen de uitgestorven tetradactyle Perissodactyla en hun moderne tegenhangers. Bovendien kon zo ook de belangrijke veranderingen in skelet en spierstelsel tijdens de overgang tussen vier- en functionele drietenige paardachtigen worden geïdentificeerd.

Kwantificering van de functionele morfologie van de tapirvoorpoot vormt de ruggengraat van dit proefschrift. Historisch gezien werd het tapir-bauplan als vrij uniform beschouwd, met enkel beperkte morfologische veranderingen in de schedel wegens de ontwikkeling van de karakteristieke proboscis. In de post-cranium, echter,

werden verschillen eerder gezien als lauter een effect van verschillen in lichaamsgrootte. Om inzicht te verkrijgen in de evolutie van de voorpoot bij paardachtigen, was het noodzakelijk om eerst de morfologische variatie in de tapirvoorpoot te kennen. Het proefschrift bestaat daarom uit twee grote delen.

In het eerste deel concentreer ik me op het kwantificeren van de variatie in de functionele morfologie van de tapirvoorpoot, zowel bij hedendaagse als uitgestorven soorten. In het tweede deel maak ik gebruik van de opgedane kennis om hypotheses te testen betreffende de functionele morfologie van de Equidae en hun naaste verwanten (de Palaeotheriidae).

Tijdens mijn doctoraat paste ik driedimensionale geometrische morfometrie toe op laseroppervlakscans van de voorpootbotten. Daarnaast gebruikte ik ratio's van de lange pootbeenderen als benadering voor voortbewegingssnelheid. Hefboomlengtes werden geïnterpreteerd als een maat voor mechanisch voordeel. Vervolgens gebruikte ik verhoudingen van spierinserties en gewrichtsoppervlakken, spierarchitectuur maten, schattingen van lichaamsgewicht, en fylogenetische vergelijkende methoden om een holistisch beeld van de functionele anatomie van de voorpoot van de tapir te verkrijgen.

De eerste resultaten van het proefschrift tonen de verschillen in voorpoot morfologie de van hedendaagse en uitgestorven soorten binnen het geslacht Tapirus. Onderzoek naar de spierinserties en het effect ervan op de werking van het musculo-skeletale systeem onthulde dat tapirs een aantal kenmerken gemeen hebben met tetradactyle Eocene paardachtigen en met palaeotheres. Deze kenmerken verdwenen echter tijdens de verdere 'equid transition'. De vormveranderingen van deze kenmerken lijken er op te wijzen de vroege drietenige (tridactyle) paardachtigen en de palaeotheres op een ander substraat liepen dan de latere sooorten. De vroege paardachtigen vertoonden in hun evolutie van een vier- naar drietenige vorm een verminderde proximale stabiliteit en tegelijkertijd lijken de vingers minder tot adductie-abductie in staat. Dit is niet waargenomen bij palaeotheres of tapirs, wat doet concluderen dat deze beide groepen beter aangepast waren om zich voort te beweging op zachtere bodems dan de tridactyle vormen.

Het samenvoegen van kwantitatieve osteologische en musculaire gegevens van de tetradactyle voorpoot van de tapirs laat conclusies betreffende de evolutie van de voortbeweging van paardachtigen toe. Dit proefschrift levert de eerste kwantificering van botkenmerken gelinkt aan oorsprong en insertie van spiergroepen in een tetradactyle onevenhoevige en kan fungeren als springplank voor de verdere studie van de functionele morfologie van het locomotor in de Perissodactyla.

“you’ll learn things you

never knew you never knew”

- Pocahontas

– INTRODUCTION –

From the unicorn, Pegasus and Karkadann of hallowed antiquity, to Rhyhorn, Drowzee and My Little Pony of modern popular culture, perissodactyls have long been a source of fascination and intrigue for mankind. In reality, the story of the Perissodactyla (horses, rhinoceroses, tapirs, and their extinct relatives) rivals the imaginations of any wise scholar or creative video-gamer. It is a story over 56 million years in the making, from humble, diminutive beginnings in Eurasia through a vicariance and diversity renaissance in the Oligocene and Miocene, and finally a steady decline in the bitter chill of the Pleistocene. Throughout their evolution, families within this group have undergone a host of morphological changes, evolving horns, tusks, proboscises, a range of craniodental adaptations, very large and small body sizes, and numerous changes to the locomotor apparatus (e.g. limbs). It is the variation in morphology and function in the limbs of this clade which will be the focus of this project, with the intention of understanding morphofunctional variation in the past by investigating shape and functional change in the present.

Here, I present an overview of the Perissodactyla, an in-depth summary of the specific study group I will investigate (tapirs), the methodologies I will implement, and a guide to the composition of the thesis.

– Perissodactyla: the 'odd-toed' ungulates –

The Perissodactyla (Owen, 1848) represent an order of terrestrial, quadrupedal mammals with a deeply rooted evolutionary history. Perissodactyls (from Ancient Greek: "uneven toes") can be defined by several features of their anatomy, most notably in the limbs (odd number of toes on the hind limb; saddle-shaped facet between astragalus and navicular bones in the ankle; lack of clavicle). Three perissodactyl families remain extant: the Equidae (Gray, 1821) (horses, zebras and asses; six-nine species); the Rhinocerotidae (Gray, 1820) (rhinoceroses; five species); and the Tapiridae (Gray, 1821) (tapirs; four-five species) (Cozzuol et al., 2013; Groves, Fernando, & Robovský, 2010; Rubenstein, 2011). This low modern species diversity is in stark contrast to that of extinct forms, representing a minute numerical diversity (between 15 and 19 species) for an order of mammals which dominated terrestrial mammalian communities in the Eocene (56-34 million years ago; Mya) and Miocene (23–5.3 Mya) epochs (Franzen, 2010a). At least 13 extinct perissodactyl families have been described, dependent upon nomenclature used, each with multiple species assigned to each. Several families of extinct perissodactyls sported bauplans ('body forms') which are no longer present in modern ecosystems. Examples include the

Hyracodontidae (Cope, 1879) – the "running rhinoceroses" – which exhibited elongated, three-toed (tridactyl) limbs, and include the largest perissodactyls of all (paraceratheres) (Prothero, 2005; W. B. Scott, 1941); the Chalicotheriidae (Gill, 1872), which evolved long, claw-hooved forelimbs and reduced hind limbs, giving them a "gorilla-like" appearance (Franzen, 2010a; Holbrook, 2001); and the Brontotheriidae (Marsh, 1873), a group of rhinoceros-like behemoths with four massively built digits on the forelimbs aiding in supporting the weight of colossal bony protuberances on the head and nose (Gregory, 1929; Mihlbachler, 2008) (**Box 1).** A recurring theme of these extinct clades is the importance and variation in shape of the forelimb elements. However, the variation in this locomotor unit is not restricted to the extinct perissodactyls, as crown perissodactyls vary greatly in their forelimb disparity (morphological diversity). Understanding the differences in shape between modern perissodactyl forelimbs, and discerning what may have driven those morphological changes through time, is therefore a key aspect to understanding the evolution of the group as a whole.

– Forelimbs of crown Perissodactyla –

The three extant families of Perissodactyla (Equidae, Tapiridae and Rhinocerotidae) are currently believed to have diverged from one another between 55 and 60 Mya (Bai, Wang, & Meng, 2018b; Steiner & Ryder, 2011), with the Equoidea (equids, palaeotheres + relatives) splitting off first, and then the Tapiroidea (tapirs + relatives) and Rhinocerotoidea (rhinoceroses + relatives) diverging from one another shortly after. Consequently, extant crown groups have had a great deal of time to diversify in morphology, ecology and behaviour within their own respective phylogenetic clades. It is important to note that, despite exhibiting morphological diversification, the limbs themselves have retained their basic functions for terrestrial locomotion: propulsion, gravitational support, directional change, shock absorption etc. (e.g. Prothero 2005; Watson and Wilson 2007; Lanovaz et al. 2010; Warner et al. 2013; Biewener and Patek 2018*a*). No known perissodactyl has modified its limbs for an arboreal (e.g. felids, primates) or aquatic lifestyle (e.g. pinnipeds, sirenians). Keeping this overall uniformity in function of the locomotor apparatus in mind, the forelimb skeleton of extant perissodactyl families exhibits three quite different morphologies, all the while sharing the key perissodactyl feature of 'mesaxonic symmetry' (Klaits 1972). All perissodactyls demonstrate anatomical mesaxonic symmetry in their hand (manus) (Klaits 1972); that is to say, the longest digit is the central third digit, with the second and fourth digits of approximately equal length, and the fifth digit shorter still or absent (Klaits 1972; Holbrook 2001) (**Box 2**). The first digit (pollux) is always absent in perissodactyls

Box 1. Major lineages of Perissodactyla through time

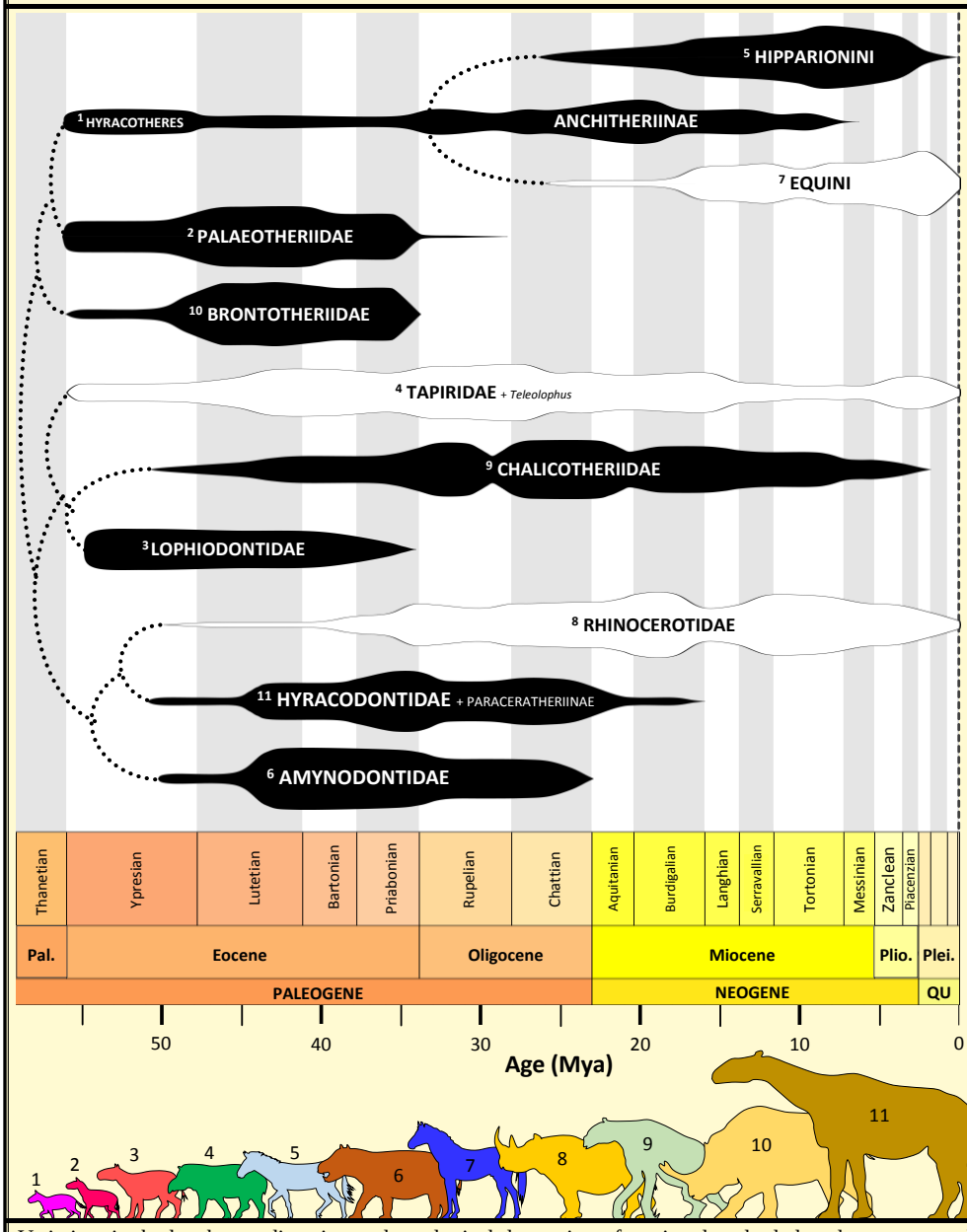

Variation in body shape, diversity and geological longevity of perissodactyl clades demonstrates the adaptability of this group to a variety of habitats through time. Here, black (extinct) and white (extant) 'balloons' chart approximate species diversity of 11 perissodactyls clades, duration of which in some cases tracks extinction events, e.g. Eocene-Oligocene turnover (33.9 Mya) and Pleistocene megafaunal extinctions (c.1 Mya) (species counts taken from occurrences in the Paleobiology Database). A notable aspect of perissodactyl evolution and variation is their great range of body sizes, summarised in a simplified form by silhouettes of exemplar taxa (bottom). Species silhouettes from left: *Sifrhippus* [1], *Plagiolophus* [2], *Lophiodon* [3], *Tapirus* [4], *Nannippus* [5], *Metamynodon* [6], *Equus* [7], *Diceros* [8], *Moropus* [9], *Megacerops* [10], *Paraceratherium* [11].

(Franzen, 2010b). Within the mesaxonic manus of crown perissodactyls, the number of remaining digits varies between families.

Tapiridae - the tapirs

Modern tapirs (Tapiridae) retain the ancestral (plesiomorphic) condition of four forelimb digits – they are tetradactyl (Hulbert, 2005) (**Box 2**). This trait has been assumed to be beneficial in the muddy and compliant substrates in which tapirs currently live (de Thoisy et al., 2014), and are believed to have inhabited in the past (DeSantis & MacFadden, 2007). Within the broader superfamily Tapiroidea (under its current definition; McKenna and Bell 1997), of which extant tapirs are one family, multiple tetradactyl taxa also exist. Known examples include members of the Helaletidae (e.g. *Heptodon, Colodon*) and Lophiodontidae (e.g. *Paralophiodon*; Holbrook 2009), with tentative evidence of tetradactyly in Deperetellidae (Bai, Wang, & Meng, 2018a). The Lophiodontidae, while often considered tapiroids, share phylogenetic affinity with the Chalicotheroidea (e.g. *Moropus*; **Box 1**), and may be more closely related to that superfamily (Holbrook, Lucas, & Emry, 2004; Hooker & Dashzeveg, 2004). In the Eocene and Oligocene, members of both Helaletidae and Tapiridae exhibited a tetradactyl manus with elongate metacarpals and phalanges (Wortman & Earle, 1892); this feature is commonly found among the early members of perissodactyl clades (Franzen, 2006; Radinsky, 1965b; W. B. Scott, 1941; Wood, Bebej, Manz, Begun, & Gingerich, 2011; Wortman & Earle, 1892). The extant genus *Tapirus* (Brisson 1762) first appears in the fossil record c.14 Mya, following the so-called 'tapir vacuum' in Europe and North America (van der Made & Stefanovic, 2006), and maintains the tetradactyl forelimb condition to the present day. Differences in the tetradactyl manus of extant tapirs were qualitatively investigated in the late 1800s (Earle, 1893, 1896; Wortman & Earle, 1892), with more quantitative work being carried out in the 20th Century (Radinsky, 1965b; Simpson, 1945). Tapirs are known from multiple fossil localities in North America and Eurasia, and were one of the more successful megafauna to migrate into South America during the Great American Biotic Interchange (Cione, Gasparini, Soibelzon, Leopoldo, & Eduardo, 2015). Currently, there are four widely accepted extant species: the Malayan tapir (*Tapirus indicus* Desmarest), the Central American or Baird's tapir (*T. bairdii* Gill), the Brazilian or lowland tapir (*T. terrestris* Linnaeus) and the mountain or wooly tapir (*T. pinchaque* Roulin). Modern tapirs are distributed in the neotropics of Central and South America (Baird's, lowland and mountain tapirs), with an additional fragmented distribution in South-East Asia (Malayan tapir) (de Thoisy et al., 2014). Modern Malayan tapirs are believed to have diverged from New World tapirs approximately 15-20 Mya (Steiner and Ryder 2011; Ruiz-Garcia et al. 2016), with the divergence and biogeographical interrelationships

Box 2. Digit reduction in the mesaxonic manus

PERISSODACTYLA

S. AMERICAN NATIVE FAUNA

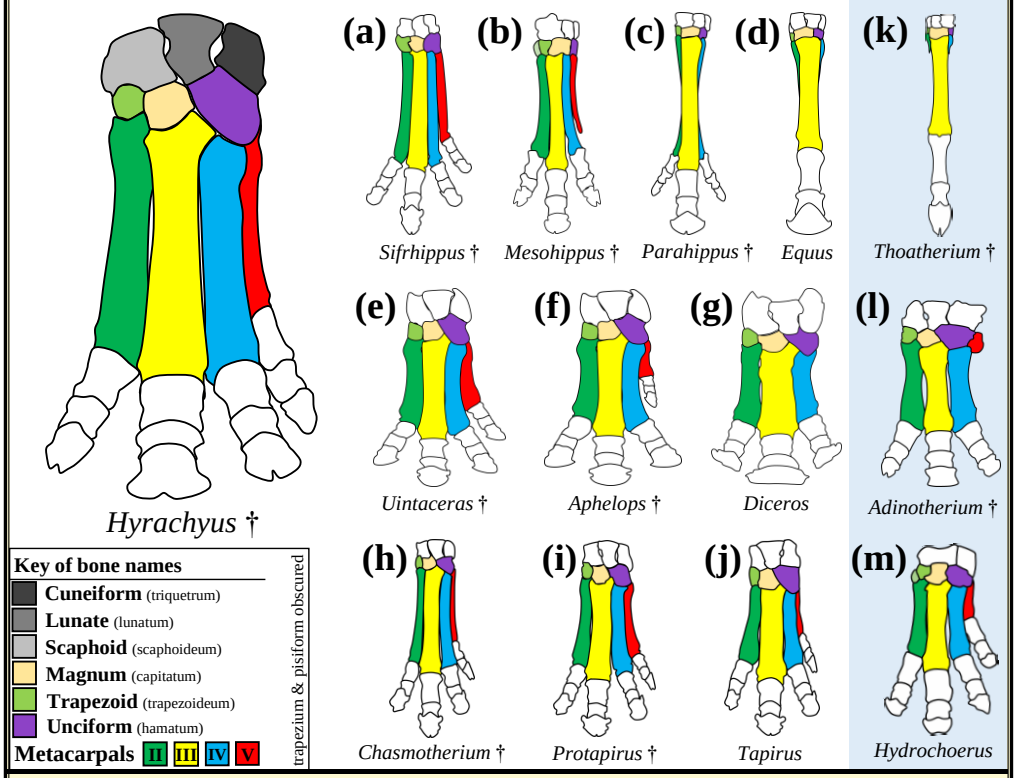

Different groups of crown perissodactyls have reduced their forelimb toe number from the plesiomorphic tetradactyl condition throughout their evolution. Equids reduced their functional digit number from four **(a)** to three **(b)** in the middle Eocene (c.40 Mya); subsequent lineages exhibited further lateral and medial toe reduction **(c)**, maintaining anatomical mesaxonic symmetry. Following the taxonomic split between Equini and Hipparionini, the equinine lineage fully reduced their functional digit count to one, ultimately leading to the evolution of the modern monodactyl genus *Equus* **(d)**. Rhinocerotids retained four functional digits throughout the Eocene (e.g. **(e)** *Uintaceras*), with the reduction of the lateral fifth digit occurring in the early to mid-Oligocene (c.30–25Mya). Some species of rhinoceros in the 'acerathere' clade retained a small, fully formed fifth digit, seemingly functionless for locomotion **(f)**. Modern rhinoceroses have only three toes, although in most individuals a vestigial fifth metacarpal is retained, acting as a tendon attachment site **(g)**. Tapirs have undergone little to no digit reduction, with the earliest 'tapirs' (e.g. **(h)** *Chasmotherium*) possessing four functional digits, and both the Oligocene-Miocene *Protapirus* **(i)** and modern *Tapirus* **(j)** also demonstrating four well developed toes on the manus.

Interestingly, parallels can be drawn between perissodactyl digit condition and reduction and that of endemic South American mammal faunas **(k-m)**. *Thoatherium* (Litopterna) demonstrated a high level of digit reduction, preceding the evolution of monodactyly in equids by up to 15 Ma. The large, stocky *Adinotherium* (Toxodontidae), may have appeared very much like hornless rhinoceroses, and similarly reduced their functional toe number to three. Lastly, within modern endemic South American faunas, we observe a tetradactyl, mesaxonic contemporary of extant tapirs: the capybara (Rodentia: *Hydrochoerus*).

between New World tapirs still hotly debated (e.g. Cozzuol et al. 2013; Holanda and Ferrero 2013; Ruiz-Garica et al. 2015; 2016). All tapir species are considered large ungulates within their respective ecosystems, although the Malayan tapir is not the largest in its entire range, which overlaps with that of the one-horned Indian rhinoceros (*Rhinoceros unicornis*). Following the extinction of proboscideans and equids in South America (Prado & Alberdi, 2014), tapirs became the defacto largest ungulates in Central and South America. Both Malayan and lowland tapirs are predominantly inhabitants of low-lying forest and wetlands (de Thoisy et al., 2014), with occasional ranging into drier shrublands which undergo seasonal inundation (Bodmer & Brooks, 1997; Wallace, Ayala, & Viscarra, 2012). The Baird's tapir is currently found in forested areas (including palm swamps, mangroves and cloud forest), across a greater altitudinal range than observed in either lowland or Malayan species (0 – 3620m; García et al. 2012). The aptly named mountain tapir exists at elevations from 1400m to the snowline, which can vary from 4000 to 5000m (Downer, 1997; Fox & Bloom, 1994); this species frequents boggy, high altitude grassland (paramó) and cloud forest. All modern tapirs are solitary (aside from mothers and calves), although occasional aggregations of lowland tapirs have been observed at salt licks (Harald Beck, pers. comm.). Home ranges for males are approximately 1–2 hectares, with limited or no exclusive territoriality; females tend to roam to a greater extent (de Thoisy et al., 2014), although specific data on how far and fast this occurs is currently deficient. Tapirs are naturally predated by large cats, e.g. tiger (Malayan tapir), puma (mountain tapir) and jaguar (all New World tapirs), with evidence of predation by other large carnivorous species e.g. *Tremarctos* (Stirling & Derocher, 1990) and crocodilians (Platt et al., 2007). To combat the threat of such ambush predators, tapirs are capable of explosive bursts of speed (Hames, 1979; Kaplan & Kopischke, 1992; Koster, 2006), young tapirs are patterned to break up their outline (camouflaging themselves against the forest floor), and all tapirs are strong swimmers, which may have additional predator escape benefits.

Of the modern groups of perissodactyls, tapirs are known to spend the most time in water; this has led some researchers to suggest that their limbs may have become adapted to a semi-aquatic lifestyle (Endo et al., 2019). Although there is some evidence suggesting behavioural adjustments in hind limb use during locomotion in water, adaptations in bone shape were not observed. At present, tapirs remain enigmatic in terms of their morphological variation, albeit with recent attempts to quantify shape changes in the cranium (Cozzuol et al., 2013; Dumbá, Dutra, & Cozzuol, 2018). Indeed, a great deal more is known about extinct tapir limb osteology than modern taxa (e.g. Wortman and Earle 1892; Simpson 1945; Radinsky 1965; Hulbert 1995, 2005, 2010); this is a void in the understanding of the Perissodactyla which will be addressed in this thesis.

Rhinocerotidae – the true rhinoceroses

Although many tetradactyl taxa are known within the Rhinocerotidae, all extant rhinoceroses have three functioning digits on the fore- and hind limbs (tridactyly) (**Box 2**). Rhinocerotids from the Eocene through to the Miocene of both North America and Europe demonstrate a continuum of decreasing functionality of the lateral fifth digit the forelimb (*Uintaceras*; Holbrook and Lucas, 1997; *Trigonias* and *Aphelops*; Prothero, 2005; *Hoploaceratherium*; Heissig, 2012; among others). This suggests that the transition from four to three digits in rhinocerotids was not fully complete for some clades until more recently than 13.6 Mya (Prothero, 2005). The extant rhinceroses (genera *Ceratotherium*, *Diceros*, *Dicerorhinus* and *Rhinoceros*) exhibit only three functional forelimb digits, supported by a large fatty foot-pad (Panagiotopoulou, Pataky, & Hutchinson, 2018). Many groups of rhinoceroses evolved mediolaterally broad metacarpals, especially when compared to the same bones in tapirs and equids. The broadening of the metacarpals offered greater surface area for the attachment of a large fatty foot-pad beneath them, and the passage of large, broad flexor tendons (Gregory, 1929); both these features can be considered adaptations for efficient locomotion while bearing greater weight than can be supported by the skeletal digits alone. The proximal limb also has a suite of adaptations for conferring gravitational support, such as large tubercles of the humerus and a strongly recurved olecranon process of the ulna; these adaptations confer greater mechanical advantage to the lateral shoulder muscles and the *triceps brachii* respectively (Gregory, 1929; Hermanson & MacFadden, 1992). Within the forelimb of rhinoceroses, there is a division in limb morphology between modern African (*Ceratotherium* and *Diceros*; Dicerotina) and tropical Asian (*Rhinoceros* spp., and *Dicerorhinus*) species (Maclaren, Mallet, pers. comms.; see also Guérin 1980; Hermanson and MacFadden 1992). This likely corresponds with phylogenetic relatedness (Mallet, In prep.): African taxa exhibit mediolaterally broad and dorsoventrally compressed metacarpals when compared to their modern Asian counterparts, indicative of increased mass in the shoulder region and resultant increases in loading over the manus (Prothero, 2005). African rhinoceroses also exhibit an incipient intermediate tubercle of the humerus, associated with the presence of a rudimentary stay apparatus for locking the shoulder and minimising energetic output while standing (Hermanson & MacFadden, 1992), a feature not present in the forest-dwelling rhinoceroses of Asia. By comparison to extinct rhinocerotids, modern rhinoceroses are more uniform in their postcranial morphology; for example, although capable of comparatively rapid movement, no modern rhinoceroses have adapted their limbs for running in the manner that their predecessors have done (e.g. *Subhyracodon*, Scott 1941; *Protaceratherium*, Roman 1914). These Eocene and Oligocene rhinoceroses were contemporaries of the 'running rhinoceroses' (Hyracodontidae), and

exhibited similarly elongated metapodials and zeugopodia (radius, ulna, tibia, fibula) with an associated shortening of the humerus and femur characteristic of cursorial species (Bai, Meng, Wang, Wang, & Holbrook, 2017; Gregory, 1929). The perissodactyl group which took these cursorial adaptations to the greatest extreme are the equids.

Equidae - the true horses

The Equidae demonstrate the most extreme digit reduction in the Perissodactyla, having reduced their forelimb (and hind limb) digit number to one (monodactyly) (MacFadden, 1992a) (**Box 2**). Within Mammalia, such radical digit reduction is only known to have occurred three times in large-bodied species: Sthenurine kangaroos (Marsupialia; Macropodidae) (Janis, Buttrill, & Figueirido, 2014); Proterotheriid meridiungulates (Meridiungulata; Proterotheriidae) (MacFadden 1992*b*; Franzen 2010*a*; see also **Box 2**); and Equinine equids (Perissodactyla; Equidae) (MacFadden, 2005). Tetradactyl and tridactyl equids are known from the Palaeogene and Neogene fossil record, and are often termed as 'transitional' equids. From the discovery of the first horses by Othniel Charles Marsh (Marsh, 1874), transitional equids have long been a focal point of perissodactyl research. Thomas Huxley's so-called "horse sequence", an adaptation of Marsh's discoveries, represented a poster-child for terrestrial macroevolution for decades (MacFadden, 2005), with the gradual progression from tetradactyl Eohippus, through three-toed species (e.g. *Palaeotherium*, *Hipparion*) to one-toed species (*Equus*). The sequence has since been proven to be flawed due to the inclusion of (a) non-equids (e.g. *Palaeotherium*) and (b) equids within the hipparionine lineage (*Hipparion* spp), a group of tridactyl equids which never adopted anatomical monodactyly (Sondaar 1968; Maguire and Stigall 2008; Prado and Alberdi 2017*a*). However, the currently understood evolution of the equid locomotor apparatus is not far removed from that original horse sequence, albeit with many more transitional species. Equids are generally accepted to have evolved from tetradactyl ancestors in the genus *Sifrhippus* and *Eohippus* (Froehlich, 2002; Mihlbachler, Rivals, Solounias, & Semprebon, 2011; Wood et al., 2011), and proliferated in North America. Recent evidence of early equids in east Asia suggests a complex biogeographical dispersal of Equidae as a family early in their evolution, potentially explaining the presence of contemporaneous early equid faunas in North America and Eurasia (Bai et al., 2018b). Through this transition, there is inferred to have been a postural change from a semi-crouched, digitigrade state in tetradactyl equids to an erect, subunguligrade posture (i.e. ungual phalange interacts with substrate with assistance of a foot-pad) in early tridactyl equids (Sondaar 1968; Thomason 1985, 1986; Reilly et al. 2007; Kubo et al. 2019) (**Box 3**). These postural changes are associated with a number of adaptations, including modifications to the

Box 3. Posture and Mechanical Advantage

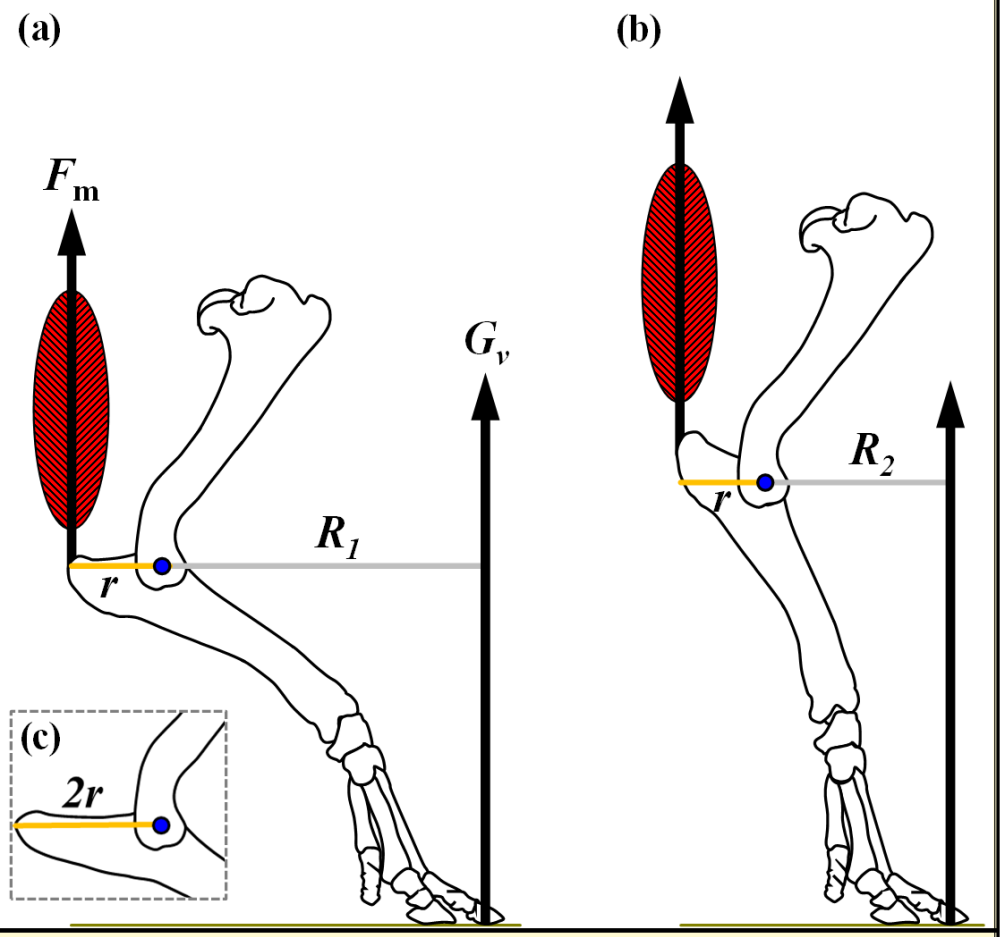

When quadrupeds move across a substrate, they will experience ground reaction forces when their forelimb is in contact with the surface. The ground reaction force (or GRF) relative to forelimb posture during the support phase largely determines the moments (rotational equivalent of a linear force) around a joint. A moment acting at a joint must be balanced by a muscle force (F_m). When the foot is in contact with the ground, the magnitude of required muscle force is mostly determined by the muscle moment arm (r) relative to the moment arm of the GRF (R). By defining the moment arm as the perpendicular distance from the direction of force application to the centre of joint rotation, the relationship between the ratio of moment arms (mechanical advantage) and forces can be described: $r / R = \text{GRF} / F_m$

A simplified example is shown in the diagram above, describing forces and moment arms around the elbow. Neither limb is moving; muscle moment arms and GRF are uniform (r = 2 cm, G_v = 10 N). In crouched posture **(a)**, animals possess a relatively long moment arm (R_1 = 8 cm) to the point of vertical GRF (G_v), whereas in an upright posture **(b)** animals exhibit a shorter GRF moment arm (R_2 = 4 cm) while standing (or in mid-stance of running). When input into the equation ($r / R = \text{GRF} / F_m$), the crouched animal must exert 40 N of muscle force to maintain equilibrium, compared to 20 N in the more upright posture. To reduce muscle force, crouched animals must either reduce GRF (i.e. weigh less / move more slowly), or modify bone shape to increase the muscle moment arm **(c)**. Morphology of muscle attachment sites is therefore very important for comparative anatomists interested in ascribing functional outcomes to shape differences.

olecranon, curvature of the forearm, and arrangement of the carpal complex (Day & Jayne, 2007; Gregory, 1929; Milne, 2016) (**Box 3**). Following the evolution of the functionally three-toed *Mesohippus*, tridactyly in equids became widespread. No forelimb remains are known from the genera immediately preceding *Mesohippus* (*Epihippus* and *Haplohippus*), and therefore the current concensus is that *Mesohippus* was the first tridactyl equid (MacFadden, 2005). *Mesohippus* was the first of a series of tridactyl equids with gradually more reduced lateral and medial digits (the 'anchitheres'), evolving through the Oligocene and early Miocene of North America, and culminating in *Parahippus*. The 'anchitheres' colonised Eurasia in the Miocene, specialising as browsing equids with low-crowned molars and retaining three functional digits (Alberdi & Rodriguez, 2012; MacFadden, 1992b, 2005). Two lineages of equids (Equinines and Hipparionines) diverged from a common ancestor with *Parahippus* around the Burdigalian stage in the early Miocene (c. 16–20 Mya), with both lineages including multiple tridactyl taxa. Hipparionines diversified greatly in the late Miocene and Pliocene (c.15–3 Mya) of North America, Eurasia and Africa (Maguire & Stigall, 2008; Prado & Alberdi, 2017b), and retained their lateral second and fourth digits with fully developed (though functionally restricted) phalanges until their extinction in the Pleistocene (Prado & Alberdi, 2017b). Equinines flourished in the latest Miocene, further reducing their lateral and medial digits resulting in the exclusion of functional phalanges. Several equinine species from the mid– to late Miocene are known from specimens which include both monodactyl and tridactyl individuals, e.g. *Pliohippus pernix* (MacFadden, 1984) and *Dinohippus* sp. (Voorhies, 1981). The terminal genera of the equinine lineage are represented by the Pleistocene *Hippidion* from South America and the modern genus *Equus*, both of which evolved true monodactyly (MacFadden, 2005). The evolution of digital reduction in the forelimbs of equids, rhinoceroses and tapirs was preceded by another characteristic feature of perissodactyl locomotor evolution: distal limb elongation.

Distal Limb Elongation

The elongation of the distal fore– and hind limb occurred in several clades of perissodactyls (e.g. hyracodontids, helaletids), but most notably in equids. The metapodials of the fore– and hindlimbs (metacarpals and metatarsals) of equids narrowed during the division between equids and their widely accepted sister taxa (Palaeotheriidae; see Bai et al. 2014 for discussion on this). The earliest equids (e.g. *Sifrhippus*; Wood et al. 2011) already exhibited narrow, elongate metacarpals; these lengthened through the transition from tetradactyl 'hyracotheres' to the transitional, browsing 'anchitheres' (MacFadden, 1992b). Other perissodactyls (e.g. plagiolophines, hyracodontids and helaletids), artiodactyls (e.g. antilopes, camels, giraffes) and

meridioungulates (e.g. litopterns) underwent similar distal limb telescoping compared to their more stoutly built ancestors (Gregory, 1929; MacFadden, 1992b; K. M. Scott, 1990). The conventional thinking behind the acquisition of telescoped distal limb elements is that stride length was increased for greater speed; when combined with digital reduction, this elongated stride would also benefit from reduced (or at least no increase in) rotational inertia (MacFadden, 1992b; Thomason, 1985). This decreased the energetic cost of moving at speed over large distances (Biewener & Patek, 2018a), greatly beneficial for animals beginning to exploit more open environments than the rainforest homes of their ancestors (Blondel, 2001; Boardman & Secord, 2013; Radinsky, 1965b; W. B. Scott, 1941). Added to the reductions in energetic input for gravitational support (i.e. postural changes reducing muscle exertion), the suite of adaptations equids underwent to promote efficient locomotion in open environments is impressive. However, as equids increased in size through time (MacFadden, 1992b), limb bone telescoping alone presented the biomechanical issue of resistance to bending forces on the limb during locomotion. Larger equids overcame this by reinforcing the central third digit at the expense of the side digits, losing their digital foot-pad in the process (Thomason, 1985, 1986). The reduction of the medial and lateral toes in favour of a single reinforced central digit (more suitable to resist bending forces than multiple thin digits of equivalent mass) would therefore have benefited derived equids during migration, predator escape and for other high speed locomotor needs (Janis & Wilhelm, 1993; MacFadden, 1992b; McHorse, Biewener, & Pierce, 2017). Greatly telescoped equid metacarpals are unsurprisingly only found in taxa with low estimated body masses such as the transitional anchitheres *Archaeohippus* and *Parahippus*, and also in several derived hipparionines such as *Pseudhipparion* and *Nannippus* (MacFadden & Hulbert, 1990; K. M. Scott, 1990). The increased length of the metapodials relative to the other long bones in the limbs (humerus, radius, ulna; femur, tibia, fibula) in equids and other modern species exhibiting rapid locomotion has led to this feature being considered indicative of cursoriality (i.e. running locomotor mode) (Bai et al., 2017; Gregory, 1929; MacFadden, 1992b; Wood et al., 2011).

– Perissodactyl Locomotor Modes –

Within living perissodactyls, it is widely accepted that three different locomotor ‘modes’ are represented: cursoriality (rapid running; e.g. equids), graviportality (slow, ponderous movement; e.g. many rhinoceroses), and mediportality (neither cursorial nor graviportal; e.g. tapirs) (Gregory, 1929). These locomotor ‘modes’ are associated with a suite of morphological characteristics which, when assessed critically, are less three separate modes and more of a spectrum of features which some taxa exhibit and others lack (e.g. “elongated tuberosity of the humerus in graviportal species” (Gregory, 1929),

a feature present in rhinoceroses regardless of the elongation or abbreviation of other bones in the forelimb). Perhaps this qualitative and often subjective terminology is best summarised in a recent quote from an eminent palaeontologist:

"*Cursoriality is like pornography – it is difficult to quantify, but we all know it when we see it*"

– Dr. Thomas R. Holtz Jr

This inherent lack of a quantitative definition for locomotor 'modes' will not be directly addressed in this thesis; rather, it is an example of the early precedent set for defining the locomotor potential of perissodactyls (especially the crown groups) with respect to their anatomy. Relative length measurements for the long bones of the limbs have been taken for perissodactyls with *a priori* locomotor mode assignment (e.g. Gregory 1929; Bai et al. 2017), and 'speed ratios' assigned for those taxa. The quantification of perissodactyl 'speed ratios' and 'locomotor modes' may be somewhat subjective; however, the fact that quantitative efforts were made (rather than qualitatively stating that one bone is larger than another) was a positive step forward. When such analyses have been applied to perissodactyls, the relative changes in forelimb proportions through the equid lineage show a striking trajectory towards rapid distal limb elongation (Gregory, 1929). On the other hand, tapirs and rhinoceroses (both extant and extinct) exhibit a more limited range of speed ratio values (Bai et al., 2017; Gregory, 1929), broadly categorised as 'mediportal' locomotor modes (i.e. designed for intermediate speeds). Extinct perissodactyl groups with no living descendants have been afforded little attention with regards to locomotor modes, with clades such as the Chalicotheriidae and Palaeotheriidae not being represented in the literature despite exhibiting highly specialised locomotor apparatus (Holbrook, 2001; Rudwick, 2008). Recent research on Miocene rhinoceros locomotor ratios highlights the problems with assigning such labels to groups of taxa. Hind limb long-bone ratios suggest that 'sub-cursorial' rhinoceroses (species likely capable of sustained running, but lacking certain adaptations such as telescoped distal limb elements) plot within a 'mediportal' category, whereas species widely considered as 'graviportal' in their limb structure (e.g. the extinct rhinoceros *Teleoceras* and the modern *Hippopotamus*) also plot within 'mediportal' locomotor modes (Schellhorn, 2018). Rhinoceroses pose an additional problem for the quantification of locomotor style. Despite possessing many skeletal indicators of graviportality (Gregory, 1929), modern rhinoceroses are capable of galloping locomotion (up to 27 kph; Alexander and Pond 1992), and exhibit strongly angled limbs and low duty factors (fraction of a stride during which the foot is in contact with the ground) when running (Alexander & Pond, 1992). The label of graviportal may

therefore be unwarranted for rhinoceroses in general, and due to the rather ambiguous description of locomotor styles like 'mediportal', it is important that researchers do not over-rely on terms like 'graviportal' or 'cursorial' locomotor modes without explicitly defining it within the context of their study, as such terms can often be reliant on many other factors than just ratios of bone lengths.

Semantics aside, ratios of limb element lengths give a viable, if rather simplistic, proxy for the style of locomotion an animal is (or was) capable of. The shape of the bones, rather than simply length or ratio of lengths, offers a much greater pool of information. Combinations of lengths, widths, depths and areas are now widely used for quantification of multiple morphological features and the comparative function of bones within the skeleton. The use of these techniques falls within the bracket of morphometrics (i.e. shape measurement).

– Morphometrics and the Quantification of Locomotor Morphology –

The study of perissodactyl locomotion and limb bones through linear morphometric methods has a long history, with a strong bias toward equid evolution. There exist a number of studies utilising simple but effective linear morphometric measurements to define shape of perissodactyl limb bones for species identification or functional inference in equids (Eisenmann 1979, 1995, 2006; Eisenmann and Karchoud 1982; Eisenmann and Beckouche 1986; Dive and Eisenmann 1991; Alberdi et al. 2003; Scott et al. 2003; Bernor et al. 2005, 2011, 2013; Orlando et al. 2006; Bernor and Kaiser 2006; Alrtib et al. 2013; Machado et al. 2018; etc.), tapirs (Scott 1941; Simpson 1945; Eisenmann and Guérin 1992; Guérin and Eisenmann 1994; Hulbert 1995, 2005, 2010; etc.) and rhinoceroses (Guérin 1980; Prothero and Sereno 1982; Prothero 2005; de Soler et al. 2012; Heissig 2012; Guérin and Tsoukala 2013; etc.). In general, these measurements offer an accurate overview of the dimensions of the bones, while not necessarily providing information as to how those measurements relate to one another spatially (Zelditch, Swiderski, & Sheets, 2012). This method of morphometric data collection is cost and time efficient, and can be performed in the field as easily as in the lab or museum collections. However, linear morphometric measurements are often highly dependent on size (e.g. for a metacarpal this would manifest as 'maximum length'; see **Box 4a**). Any measurements taken parallel to, or in similar orientation to, the 'size' measurements are likely to correlate strongly with that size variable. For example, the distance from the proximal joint surface of a metacarpal to the medial-most point of the metacarpophalangeal joint (**Box 4a**, L1) is likely to be highly correlated with the maximum proximodistal length of the bone (**Box 4a**, L2). Any variation in the shape of that section of the metacarpophalangeal joint may therefore be

masked by its correlation with the size variable. In fact, all measurements incorporate aspects of both shape and size, as do combinations of these measurements (e.g. principal component scores). Separation of size from shape is intuitively erroneous for biological analyses – the size of a bone has as many implications for the function of that bone in the skeleton as its shape does (Zelditch et al., 2012). Therefore, when using a methodology which removes aspects of size from the data, it is important to keep in mind that size and shape share an intimate link in biology. Lines of questioning should therefore investigate how the relationship between the two affects the function of the object in question. Linear morphometrics can answer some of these queries; however, to examine how homologous features vary in position between objects without losing shape information due to the confounding factor of size, an alternative approach to shape quantification is required: geometric morphometrics (**Box 4**).

Geometric Morphometrics

Geometric morphometrics is a field of shape quantification which has been in use for many decades now, and relies on the following definition of shape: "all geometric information that remains when location, scale and rotational effects are filtered out from an object." (Kendall, 1977). In practice, this involves the analysis of coordinate data, and the removal of information between configurations of coordinates pertaining to location, scale and orientation. A generalised superimposition is performed using a least-squares fit, aligning all configurations to minimise the sum of the squared distances between corresponding shape coordinates (Zelditch et al., 2012) – this is known as a Generalised Procrustes Analysis (GPA), and from this point I will refer to the sums of squared distances as 'Procrustes distances'. A simplified example of this alignment of configurations is presented in **Box 4**. In geometric morphometrics, coordinate data are collected as 'landmarks'. For the purposes of this thesis, landmarks are defined as biologically or operationally homologous points on a series of limb bones. Biologically homologous points are the same corresponding point between different species or specimens, likely due to phylogenetic relatedness; these are the best types of landmarks – examples include the vertices of a metacarpal joint facet, or the exact centre of the orbit in the skull. Operationally homologous points are here defined as performing the same operational function; these are often maxima and minima – examples include the anterior tip of the dinosaurian mandible (not the same bone in all species, therefore not biologically homologous; MacLaren et al. 2017), or the most proximal point of the greater tubercle of the mammalian humerus (different place along the tubercle for different species). Both biologically and operationally homologous landmarks can be defined according to the classification of landmarks by Bookstein (1991):

Box 4. Morphometrics and Procrustes Alignment

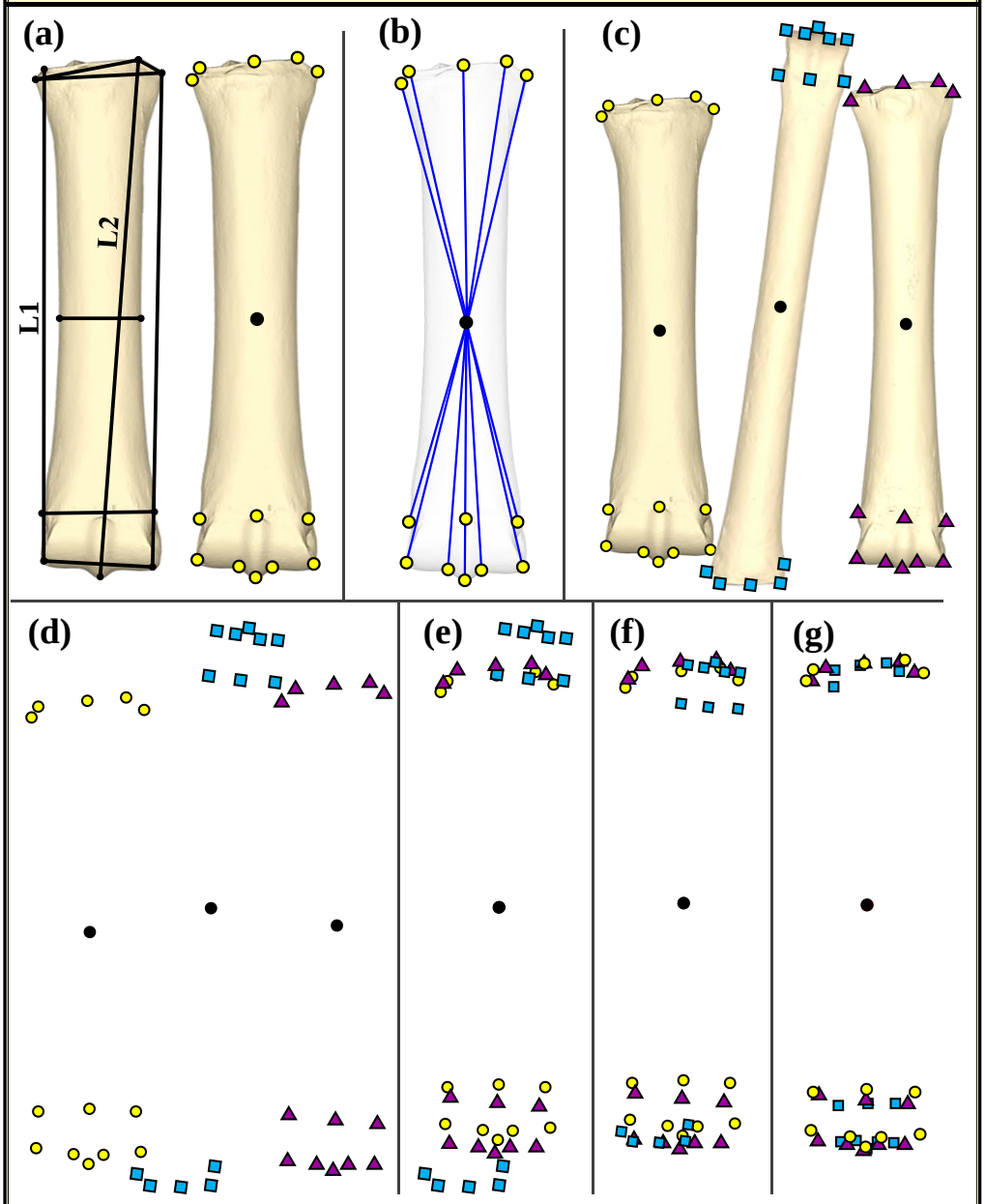

(a) Traditional morphometric measurements on an equid metacarpal describing eight linear distances (from Eisenmann 1986) compared to 13 landmark points. **(b)** Instead of taking a maximum linear distance as a size variable, geometric morphometric analyses can produce an intrinsic size measure based on the square-root sum of square distances (blue lines) from the geometric centre (centroid; black circle). **(c)** Three examples of equid metacarpals with landmarks applied. **(d)** The three configurations of equid metacarpal landmarks are then **(e)** aligned based on common centroid, **(f)** scaled to a common long axis, and **(g)** rotated to minimise sum of square distances between corresponding landmark points across all configurations in the analysis.

Type of landmark	Definition	Examples
Type I	Point at the discrete juxtaposition of tissues	Three-point suture in cranium
Type II	Local definition of a construct; localised maxima or minima	Anterior-most tip of mandible
Type III	Defined by proximity or distance from other landmarks or features	Mid-point of the dorsal surface of the metacarpal
Semi-landmark	Non-discrete points across an edge or surface; position defined relative to fixed landmarks or other semi-landmarks	10x10 patch across metacarpal head; 10 point curve along supracondylar ridge of the humerus

For analyses of the locomotor apparatus, Type I landmarks are rare, as the confluence of three tissues on long-bones is uncommon; examples of Type I landmarks that could be implemented in locomotor analysis would be foveae or neural canals. A caveat to this is that the definition of Type I landmarks and the juxtaposition of tissues does seem to be subject to interpretation in some cases (e.g. Arias-Martorell et al. 2012; Rosas et al. 2015). Ultimately, Type II and Type III landmarks are most prevalent in shape analyses of long bones, with many studies utilising this technique to quantify both two- and three-dimensional shape variation (e.g. Milne et al. 2009; Curran 2012; Walmsley et al. 2012; Fabre et al. 2013*a*, 2014; Martín-Serra et al. 2014; Acuña et al. 2017; de Oliveira and Santos 2018). With the advent of more advanced computational techniques to analyse data, studies using semi-landmarks have become much more widespread in biological sciences, using curves and patches to define morphological changes in regions absent of homologous features; e.g. ventral surface of the mandible (e.g. Anderson et al. 2011, 2013; Stubbs et al. 2013; Maclaren et al. 2017) and articular surfaces of limb bones (e.g. Milne et al. 2009; Fabre et al. 2013*b*, 2015*a*, *b*; Botton-Divet et al. 2017; Fabre et al. 2017; Muñoz et al. 2017). Semi-landmarks can be very useful for describing functional surfaces of bones (e.g. Fabre et al. 2015*a*); however, they contain less information (fewer degrees of freedom) than true 'fixed' landmarks, and few or no homologous features. Semi-landmarks also require the removal of tangential variation (i.e. equalising the distance between semi-landmark points along a curve or area), known as 'sliding'. The process of sliding semi-landmarks can be based on minimising the bending energy or minimising the Procrustes distances with respect to the mean average form. As these two methods can yield different results (Perez, Bernal, & Gonzalez, 2006; Slice, 2007), extra caution must be exercised when drawing

conclusions from quantitative shape analysis based on semi-landmark data alone. Irrespective of the type of landmark used to describe the shape, configurations of landmarks are aligned to a common centroid, and once differences which are not shape-related have been removed, intuitively only shape information remains (Zelditch et al., 2012).

As previously mentioned, size must be considered intricately linked to shape. Therefore, the geometric scale of objects (an intrinsic size metric extracted from geometric morphometric analyses) can be highly informative. Moreover, the geometric scale calculated from landmark coordinates, known as 'centroid size' (**Box 4b**), is mathematically independent of shape (Zelditch et al., 2012), although potentially correlated with aspects of shape in biological analyses (size-dependent, or 'allometric shape') (Klingenberg, 2016). The complete removal of size from shape (i.e. removing the effects of allometry on shape data) can be statistically performed by regressing shape variables against a size variable, and performing analyses on the regression residuals. In the case of geometric morphometrics, this could be the centroid size (or log-transformed centroid size for groups where size range is large or not normally distributed), or independently measured body mass, snout-vent length etc. (Klingenberg, 2016; Monteiro, 1999). For biological investigations, accounting for allometric influence may be necessary to ascertain what morphological features of a bone involved in gravitational support change independent of body mass, or what features of a bone exhibit disproportionately different shapes between large and small taxa. At this point it is important to highlight the influence of taphonomy on the fossil record, especially as pertains to geometric morphometric analyses (**Box 5**). Studies exploring patterns of shape variation and including both extant and extinct species must always be aware, and where possible account for, taphonomic degradation of morphological features and sampling biases throughout the fossil record.

Over the years, the application of geometric morphometric techniques to the understanding of perissodactyl biology has included examinations of dental morphology (e.g. Seetah et al. 2014; Cucchi et al. 2017; Heck et al. 2018), cranial anatomy and systematics (e.g. Bales 1996; Piras et al. 2010; Moyano and Giannini 2017; Parés-Casanova et al. 2017; Dumbá et al. 2018; Heck et al. 2018), and some work on the locomotor apparatus (Bignon, Baylac, Vigne, & Eisenmann, 2005; Hanegraef, 2015; Hanot, Guintard, Lepetz, & Cornette, 2017; Hanot, Herrel, Guintard, & Cornette, 2017; K. E. Jones, 2016). However, considering the large quantity of well-preserved limb fossil material and attention on the locomotor evolution of perissodactyls (especially equids), the dearth of geometric morphometric analyses is somewhat surprising. Recent work has looked to build upon the extensive linear morphometric databases available

for equids, rhinoceroses and tapirs, and to investigate shape variation and covariation in the limb skeleton of these taxa using geometric morphometrics (e.g. Hanegraef 2015; Hanot et al. 2017*b*, *a*; Mallet et al. 2018). Contributing to this new wave of quantifying perissodactyl locomotor morphology will form a key aspect of this thesis.

To capture the shape of the bone prior to quantification with geometric morphometrics, I will use a laser surface scanner to digitise the surface of each bone. There are several benefits to laser scanning bones for geometric morphometric assessments rather than using a hand-held landmark digitizer (e.g. microscribe) to collect coordinate data: 1) landmark placement – within a digital framework, landmarks can be placed, checked and rearranged where necessary, whereas this is not always possible for landmarks attained using a microscribe; 2) repeatable use – scanning objects for one project does not limit those scans to be used only for that project. Researchers can therefore utilise the scans they have taken for multiple analyses rather than relying on the data taken by using a microscribe in (e.g.) a museum collection, in addition to sharing their scan data with other researchers; 3) versatility – three-dimensional models attained by laser scanning are not limited to being used for geometric morphometrics, but can also be used for measuring absolute distances, 3D printing for education purposes, and virtual reconstructions (e.g. musculoskeletal modelling; interactive museum exhibits). The FARO ScanArm Platinum V2 system with integrated FARO laser line probe owned by the Functional Morphology Labo of the Universiteit Antwerpen is an ideal tool for scanning bones, and will be the primary means by which I digitise osteological material for landmarking throughout this project. This apparatus offers the opportunity to quantify tapir anatomy in a manner previously unavailable to researchers investigating this group of enigmatic perissodactyls.

– Comparative Functional Morphology of the Tapir Forelimb – – Aims and Objectives –

The main aim of this project is to investigate differences in forelimb morphology of perissodactyls, and to use the acquired knowledge to comment on the evolutionary transition in the morphology of the forelimb in equids. To ground the thesis within this broad evolutionary background, this study will set out to investigate the locomotor morphology of perissodactyls with the most plesiomorphic forelimb condition (i.e. tetradactyly). The ancestors of all modern and extinct perissodactyls possessed four functional toes on the forelimb (MacFadden, 1992b; W. B. Scott, 1941), exhibited anatomical mesaxonic symmetry (Klaits, 1972), and – from the evidence of dental and palaeohabitat analyses – were forest dwelling (Boardman & Secord, 2013; Hellmund, 2016; Kaiser et al., 2013). Within modern perissodactyl clades, one family is known to

Box 5. Taphonomy and the Fossil Record

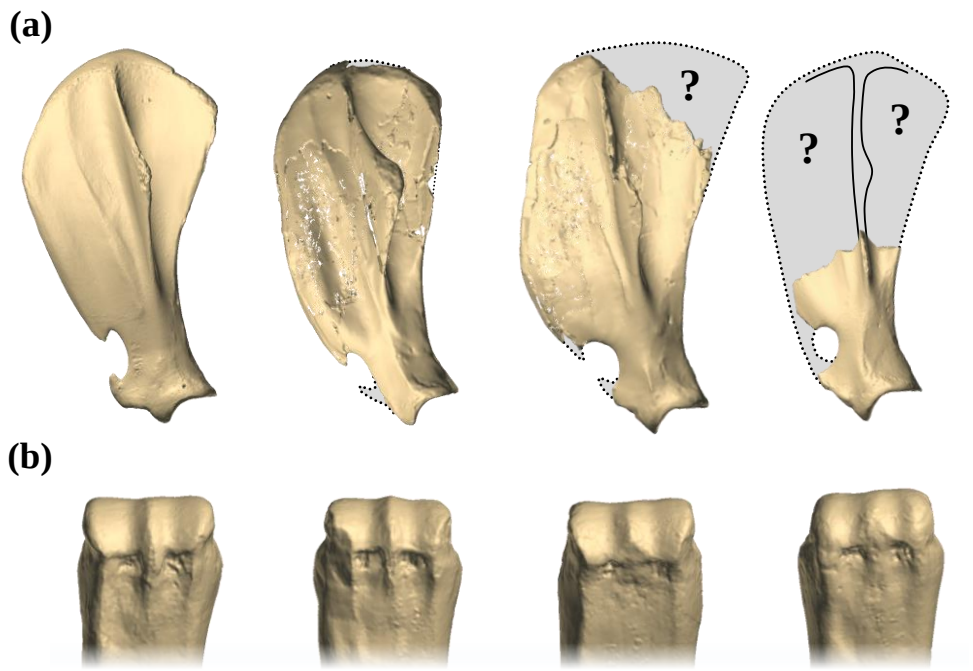

The fossil record is inherently incomplete. Palaeontologists have long been aware of the factors influencing the completeness of the fossil record; here the factors are summarised, adapted from David Raup's classic series of filters which affect fossil preservation (Raup 1972):

(1) Anatomy – hard, skeletal elements will fossilise more easily than soft tissues; **(2)** Population Dynamics – organisms with low population densities will have a reduced probability of fossilisation; **(3)** Ecological – where an organism lives affects fossilisation potential, e.g. species living near water-bodies will have a higher likelihood of fossilisation; **(4)** Sedimentary – some environments are typically sites of sedimentary deposition, and organisms are more likely to be buried there; e.g. shallow lagoons and lakes offer ideal sedimentary conditions; **(5)** Preservation – if sediment is constantly being deposited and then reworked (e.g. a river), biological remains may be disarticulated, worn or damaged by physical movement and buffeting; **(6)** Exposure – to be collected, fossil material must be in rocks which have been raised to the surface via tectonic activity, or eroded down over time following previous tectonic uplift; **(7)** Human – ultimately, to be incorporated into a palaeontological study, the fossil must be seen, excavated, catalogued and then studied. An extra factor to keep in mind is the effect of human error in excavating and cataloguing the fossil, either by accidental damage or incorrect classification.

Examples of taphonomy can be seen in a sample of tapir scapulae (lateral view) and tapir distal third metacarpals (palmar view). **(a)** The scapula is a thin, plate-like bone, and as such is highly susceptible to crushing during fossilisation. From left: complete scapula of modern *Tapirus bairdii*; near complete scapula of *T. polkensis* (crushed and reconstructed); incomplete scapula of *T. webbi* – large portions of the caudal angle have been lost, and as such this bone could not be used in a comprehensive geometric morphometric analysis of scapulae; partial scapula of *T. haysii* – very little of the scapula blade remains; the comparatively robust glenoid fossa (articulation with humerus) is invariably the only part of the scapula preserved. **(b)** The distal third metacarpal is a robust section of bone resistant to crushing. However, edges of the joint facets are highly susceptible to abrasion and chipping of key morphological features. Third metacarpals of *T. webbi* from Love Bone Bed, from left: undamaged; chipped; sagittal ridge worn and chipped; heavily abraded.

possess all these characteristics of the ancestral perissodactyls: the tapirs (Tapiridae). Therefore, this project will be built around the comparative anatomy and functional morphology of the tapir forelimb, predominantly using a three-dimensional geometric morphometric approach based on laser surface scan data.

Despite their initial formal classification by Carl Linnaeus in the mid-1700s, the functional anatomy of tapirs has been afforded little attention through the centuries, certainly by comparison with their modern relatives the equids and rhinoceroses. This may have been due to the superficially uniform bauplan and habitat of modern tapirs. However, as a result of this lack of morphological scrutiny, there are no comprehensive reports on the functional morphology of tapir prior to the work of George Gaylord Simpson and Leonard Radinsky in the 1900s (Radinsky, 1963, 1965b, 1965a, 1967; Simpson, 1945), and these works do not specifically deal with adaptive differences in the locomotor apparatus. Consequently, there is a lack of knowledge regarding the comparative limb morphology of modern tapirs, with any qualitative comparisons that have been performed focussing on the differences between the lowland tapir (*Tapirus terrestris*) and Malayan tapir (*T. indicus*) (Earle, 1893, 1896), two species hypothesised to have diverged approximately 25 million years ago (Mya) (Steiner and Ryder 2011). With the current lack of quantitative data on tapir limb osteology, the first objective within this project is to establish whether there are discernible shape differences in the forelimb bones of modern tapir species; these aspects of the thesis are addressed in the first two research chapters. These initial comparative studies stand alone as research projects, despite also representing companion pieces which together quantify modern tapir forelimb shape. They allow me to question whether modern tapirs have diverged from one another in their forelimb functional morphology during their long evolutionary history. If so, can we quantitatively discriminate between tapir species based on forelimb bones? And does any shape variation exhibited by modern tapirs hint at differences in load application during locomotion? The third research chapter is intricately linked to the previous two; however, rather than focussing on the osteology of multiple tapir species, it will examine muscular arrangements and quantify muscle architecture of a single tapir species (*Tapirus indicus*), and compare it to the modern monodactyl horse *Equus* in order to establish how the muscles of the forelimb interact with the bones in tetradactyl perissodactyls compared to monodactyls. This will provide an extant phylogenetic bracket (Witmer, 1995), with which to draw evolutionary conclusions. Using this comparison, I am able to question which muscles of the tapir forelimb are the most massive relative to those of equids? How do muscle attachment areas and intrinsic properties (such as pennation angle) differ between muscles of a tetradactyl and monodactyl perissodactyl forelimb? And can functional outcomes be

predicted from the differences observed between tetradactyl and monodactyl forelimb muscle architecture and arrangements?

Using the knowledge gained from the three initial, descriptive sections of the thesis, I then test two as yet unquantified statements concerning tetradactyl perissodactyls. Firstly, a statement on scaling in tapirs: Radinsky (1965*a*) mentions in his comparative work on the osteology of helaletids and tapirs that "The postcranial skeleton of *Tapirus* has remained basically similar to that of *Heptodon*, and most of the differences observed are correlated with larger size of *Tapirus*…including relatively broader and more robust limbs". This statement was in support of previous claims that the tapir postcranial skeleton has not changed through time other than under the influence of changes in body size (Hershkovitz, 1954), and later quoted in more recent literature (Padilla, Dowler, & Downer, 2010). The specific aim of the fourth research chapter is therefore to test whether forelimb bone shape scales allometrically in tapirs – i.e. are shape differences in tapir postcrania correlated with changes in size? If not, how much effect does phylogenetic relatedness have on bone shape? And finally, is there any evidence of non-allometric shape change in keeping with variation in habitat?

Secondly, a statement on tapirs as analogues for extinct perissodactyls: as early as the 1800s, qualitative comparisons have been drawn between modern tapirs and the extinct sister taxa to equids – the palaeotheres. These comparisons hark back to the days of Georges Cuvier, who in his descriptions of the Eocene fauna of the Gypsum Beds surrounding Paris stated "there is nothing easier than to represent [*Palaeotherium magnum*] in its living state, for it is only necessary to imagine a tapir as large as a horse…[*Palaeotherium crassum*] resembled the tapir still more than [*Pa. magnum*], for it did not differ even in its size and proportions…I am persuaded that most travellers would have confused [*Tapirus* and *P. crassum*] if they had existed at the same epoch" (Cuvier 1812; translated in Rudwick 2008). Given this deep-seeded, though as yet unquantified, analogisitc relationship between tapirs and palaeotheres – which are themselves tragically understudied – I focus on using the rich fossil record of palaeothere postcrania to quantitatively assess the validity of such claims. Using the comparative dataset from previous research chapters, I am able to question claims of morphological analogy between tapirs and palaeotheres, including: does the forelimb of *Pa. magnum* or *Pa. crassum* closely resemble that of modern tapirs? Do the forelimb bones of tetradactyl palaeotheres exhibit morphological similarities to those of modern tapirs? If so, what aspects of the overall biology of palaeotheres (e.g. body size, reliance on lateral digit etc.) may negate analogies being drawn between tapirs and palaeotheres?

My comparative study of palaeotheres and tapirs in the previous research chapter leads smoothly to a comparison between tapirs and equoids (palaeotheres + equids) through time. This final research chapter builds upon all the previous works, incorporating knowledge gained from all research chapters to look into the morphological variation across equoids and tapirs in a specific morphological feature – the distal third metacarpal. The joint facet and ligamentous attachments of the distal metacarpal are integral to the fetlock joint, which in modern equids forms an intricate part of the highly specialised elastic recoil mechanism in the distal limb. This mechanism, and other modifications to the distal limb of equoids (e.g. digit reduction, autopodial elongation), has been associated with a shift in equoid ecology to favour efficient running at high speed (i.e. reducing inertia; increasing stride length, etc.). For the purposes of this study, reducing the number of bones studied to a single, functionally informative element enables me to incorporate a large number of taxa from multiple time periods, and degrees of digital specialisation, in order to investigate links between shape change and ecological shifts in deep time. I will therefore be able to question whether the equoid fetlock ever resembled that of a tapir? If so, when did equoid fetlock morphology shift away from that of tapirs? Did the morphological diversity of the fetlock joint in tapirs remain conservative through time? What impact did palaeotheres have on morphological variation in equoids? At what point did the fetlock of transitional equids resemble that of modern horses, asses or zebra? And did body mass, feeding regime, or global ecological turnover events correlate with changes in the shape of the equoid fetlock?

Research Chapter Breakdown

From this point, the thesis will consist of six Research Chapters and a general synthesis and discussion. **Research Chapter 1** focusses on the comparative anatomy of the upper forelimb (the region of most muscular attachment) of tapirs, revealing hitherto unrecognised interspecific variation within the genus *Tapirus* in the attachment sites of muscles involved in gravitational support and shoulder stability. Following on from and building upon the results of Research Chapter 1, **Research Chapter 2** concentrates on the tapir carpus and metacarpus, which are more closely involved with the interaction between limb and substrate. Both carpal and metacarpal shape analyses indicate that the possession of four toes in the manus does not necessarily dictate that all four are loaded to the same degree during locomotion, and that within tapirs there is a spectrum of functionality in the digits of the manus. Using knowledge gained from differences in bone shape to form specific investigative questions, **Research Chapter 3** adds flesh to the bones by assessing the muscular architecture of a Malayan tapir forelimb. Comparisons with published muscle architecture from equids suggest different levels of

functionality for the shoulder musculature between tetradactyl and monodactyl perissodactyls, with implications for the evolution of the pectoral girdle in equoids. In **Research Chapter 4**, I broaden the taxonomic, temporal and geographical scope of my sample from Research Chapters 1 and 2 to incorporate extinct *Tapirus* species from Europe, North America and Asia, including both dwarf (*T. polkensis*) and giant (*T.* (*Megatapirus*) *augustus*) species. In an effort to ascertain the influences of body size, phylogeny and habitat use on the forelimb morphology of *Tapirus* species, this chapter demonstrates that body size is not the exclusive driver behind shape variation that was previously assumed. Continuing to test current assumptions of tapir locomotor biology, **Research Chapter 5** involves utilising the forelimb anatomy of modern *Tapirus* species (using data from Research Chapters 1, 2 and 3) in a comparison with numerous palaeothere taxa (both tetradactyl and tridactyl), with which George Cuvier originally drew his qualitative comparisons. High degrees of intra-generic variation are observed in palaeotheres, with quantitative results supporting the conclusions of George Cuvier with regards to *Pa. magnum* and its morphological affinity to modern tapirs. However, tetradactyl palaeotheres exhibit notable differences to tapirs in their forelimb morphology and their body size, suggesting that tapirs would make poor modern analogues for locomotion in tetradactyl palaeotheres. Finally, in **Research Chapter 6** I investigate shape variation of the distal region of the third metacarpal (the fetlock) of tapirs, palaeotheres and equids through time, using the comparative results of all previous Research Chapters to inform hypotheses and conclusions on the driving forces behind observed variation. I demonstrate effects of diet, size, dispersal, origination/extinction, climate and provincialism on the morphological variation observed in the tapir and equoid fetlock, driving differences across 56 million years of evolution.

“time it is for you to look

past a pile of old books”

- Yoda

– RESEARCH CHAPTER ONE –

A three-dimensional morphometric analysis of upper forelimb morphology in the enigmatic tapir (Perissodactyla: *Tapirus*) hints at subtle variations in locomotor ecology

Jamie A. MacLaren - Sandra Nauwelaerts

adapted from *Journal of Morphology*
(2016) **277**:1469-1485

Forelimb morphology is an indicator for terrestrial locomotor ecology. The limb morphology of the enigmatic tapir (Perissodactyla: *Tapirus*) has often been compared to that of basal perissodactyls, despite no quantitative studies comparing forelimb variation in modern tapirs. Here, we present a quantitative assessment of tapir upper forelimb osteology using three-dimensional geometric morphometrics to test whether the four modern tapir species are monomorphic in their forelimb skeleton. The shape of the upper forelimb bones across four species (*T. indicus*; *T. bairdii*; *T. terrestris*; *T. pinchaque*) was investigated. Bones were laser scanned to capture surface shape and 3D landmark analysis was used to quantify shape. Discriminant function analyses were performed to reveal features which could be used for interspecific discrimination. Overall our results show that the upper forelimb skeleton of tapirs contains notable interspecific differences. We demonstrate that upper forelimb bones can be used to discriminate between species (>91% accuracy), with the scapula proving the most diagnostic bone (100% accuracy). Features that most successfully discriminate between the four species include the placement of the cranial angle of the scapula, depth of the humeral condyle, and the caudal deflection of the olecranon. Previous studies comparing the limbs of *T. indicus* and *T. terrestris* are corroborated by our quantitative findings. Moreover, the mountain tapir *T. pinchaque* consistently exhibited the greatest divergence in morphology from the other three species. Despite previous studies describing tapirs as functionally mediportal in their locomotor style, we find osteological evidence suggesting a locomotor variability in the tapirs. We conclude that modern tapir forelimbs are neither monomorphic, nor are tapirs as conserved in their locomotor habits as previously described.

Introduction

The Tapiridae (tapirs) represent a deep-rooted clade of large-bodied hoofed mammals within the order Perissodactyla (odd-toed ungulates). Modern tapirs are widely accepted to belong to a single genus (*Tapirus*), containing four extant species (Hulbert, 2005; Ruiz-García et al., 2016): the Baird's tapir (*T. bairdii*), lowland tapir (*T. terrestris*), mountain tapir (*T. pinchaque)*, and the Malayan tapir (*T. indicus*). Extant tapirs primarily inhabit lowland tropical rainforest (*T. indicus* and *T. terrestris*), with some populations of neotropical tapirs (e.g. *T. pinchaque*) also occupying chaparral, cloud forest and high altitude grassland (páramo) biomes (Padilla & Dowler, 1994; Padilla et al., 2010). Tapirs historically had a very extensive Holarctic distribution (Dumbá et al. 2018), but are now geographically split between the neotropics (*T. bairdii*, *T. pinchaque* and *T. terrestris*) and South-East Asia (*T. indicus*). Most populations are patchily distributed, with the exception of *T. terrestris*, which exhibits a broad range across much of northern South America, with several populations being granted subspecies status (e.g. *T. t. colombianus*, *T. t. spegazzinii*) (Padilla & Dowler, 1994; D. E. Wilson & Reeder, 2005).

The genus *Tapirus* has frequently been compared morphologically to extinct perissodactyls (M. W. Colbert, 2005; Hershkovitz, 1954; Holbrook, 2001, 2009, Radinsky, 1965b, 1966; Rose, 1996), sometimes earning tapirs the colloquially used title of 'living fossil' (Janis 1984; Rustioni and Mazza 2001). The title of 'living fossil' implies limited changes in tapir skeletal shape throughout evolutionary history (Radinsky 1965*a*). Within the Radinsky (1965) study, the upper forelimb description was based on two specimens of *Tapirus pinchaque* (MCZ 6037 and AMNH 149424). He noted several key features common to all tapir forelimbs, including the scapular spine lacking an acromion, an expanded supraglenoid tubercle forming the distal arm of a deep coracoscapular notch, a medially directed anterior hook of greater tubercle of the humerus and the absence of intermediate tubercle or bursa. Assuming the tapir forelimb skeleton has been morphologically conserved through time except in overall size, as suggested by Radinsky (1965*a*) and subsequent authors, interspecific differences in limb bone shape would not be expected if analysed using size-independent shape analyses, such as geometric morphometrics.

Morphometric studies investigating variation in limb morphology have been presented on a range of mammalian species, particularly on carnivorans (Fabre, Cornette, et al., 2015; Fabre et al., 2014; Fabre, Cornette, Slater, et al., 2013; Fabre, Salesa, et al., 2015; Martín-Serra et al., 2014; Meloro, 2011; Samuels, Meachen, & Sakai, 2013; Van Valkenburgh, 1987) but also rodents (Elissamburu & DeSantis, 2011; Kuncova &

Frynta, 2009; Samuels & Van Valkenburgh, 2008) and marsupials (Astúa, 2009; Bassarova, Janis, & Archer, 2008; Weisbecker & Warton, 2006). Ungulate limb bone variation has also been assessed successfully using geometric morphometrics (e.g. Bernor et al. 2005; Bignon et al. 2005; Curran 2012, 2015). Geometric morphometrics is a technique for quantifying shape independent of size, often by using homologous single points (landmarks) on the surface of a series of objects (Zelditch et al., 2012). This allows quantitative morphometric data to be used for a wide variety of shape analyses. These methods have been used to discriminate populations or species, and detect variation across multiple limb bones of ungulate mammals (Alrtib et al., 2013; Bernor et al., 2005; Bignon et al., 2005; Curran, 2012; Kaushik, 2009; Martínez-Navarro & Rabinovich, 2011).

In this study, we used a three-dimensional geometric morphometric approach to perform a quantitative, comparative study on the upper forelimb skeleton of tapirs. Forelimb morphology has been suggested as a good indicator for terrestrial locomotor ecology (Andersson, 2004; Andersson & Werdelin, 2003; Fabre, Cornette, et al., 2015; Fabre, Cornette, Slater, et al., 2013; Flores & Díaz, 2009; Halenar, 2011; Hawkins, 2011), in both extant and extinct taxa. The forelimbs not only provide gravitational support and stability in quadrupedal mammals (Evans & de Lahunta, 2013; Jenkins Jr., 1973), but are also used to an extent in forward propulsion (Clayton, Chateau, & Back, 2013; J. C. Watson & Wilson, 2007a) and shock absorption on ground impact (Astúa, 2009; Payne, Veenman, & Wilson, 2004). Here, we test whether the bones of the tapir upper forelimb exhibit interspecific variation. Other authors have hypothesised that interspecific differences in the postcranial skeleton of modern tapirs will be minimal (Hershkovitz 1954; Radinsky 1965; Padilla and Dowler 1994). However, the deep phylogenetic divisions between most modern tapir species (Steiner and Ryder 2011; Ruiz-García et al. 2012; Cozzuol et al. 2013) have offered a broad timescale for adaptive variation to take place, based on habitat use and other aspects of tapir ecology. Consequently, we hypothesise that tapir upper forelimbs will exhibit osteological variation that may pertain to differing locomotor ecologies.

Materials and Methods

Specimens

A total of 24 fully disarticulated tapir forelimbs (dry bones) were collected from museums in Europe and the United States of America (USA) (Table 1.1). Multiple

specimens of four species of extant tapir (*Tapirus terrestris*, *T. pinchaque*, *T. bairdii* and *T. indicus*) were collected for analysis to account for intraspecific variation. As the tapir cranium is highly recognisable and species specific for modern taxa, species assignment was checked using visual inspection of the cranium where possible. Morphologically mature limb specimens (adult; Table 1.1) were used where possible. As the scapula cartilage is the final region of the forelimb to fully ossify in tapirs, forelimb maturity was defined based on the full ossification of the dorsal border of the scapula (Liebich, Konig, & Maierl, 2007). Specimens with non-ossified dorsal borders (sub-adult; Table 1.1) were also scanned to maintain good sample sizes; these specimens are noted in Table 1.1, and were excluded for comparisons of bone size. Sexual size dimorphism is known to be present in tapirs (de Thoisy et al., 2014; Padilla & Dowler, 1994), although it has been described as non-significant for morphological comparisons (Simpson 1945). Due to the fact that intraspecific variation in size within male and female tapirs is reported in the literature (e.g. Simpson 1945), and that all tapirs use their forelimbs for locomotion and are not under any sexual selection, sex bias was not taken into account. To compliment information from published articles on tapir osteology and myology (Bressou, 1961; Campbell, 1936; Murie, 1871; Pereira, 2013; Windle & Parsons, 1902) a dissection was performed on the limbs of a juvenile *Tapirus indicus* that was made available by the Royal Zoological Society of Antwerp (KMDA). Muscular attachments available from the dissection, in addition to published literature, assisted in the description of osteological features and potential functional outcomes. Where necessary, interpretations were supplemented with veterinary accounts of equid osteology and myology (Budras, Sack, & Rock, 2003; Clayton et al., 2013; Constantinescu et al., 2012; Liebich et al., 2007).

Scanning

The scapula, humerus, radius and ulna from one forelimb of each specimen were scanned using a FARO ScanArm Platinum V2 system with integrated FARO Laser Line Probe capable of scanning to a resolution of 50 μm. Bones were suspended using clamps and supports, which were positioned on regions of the specimen surface that landmarks would not be placed on (e.g. shaft of long bone). A three-dimensional virtual point cloud was produced for each limb element, which was visualised in GeoMagic (GeoMagic Qualify v.10, Morrisville, NY, USA). Outlying surfaces in the point clouds were pruned to remove excess surface information (e.g. incidental scanning of clamps or support structures). Point clouds were subsequently converted into detailed polygon-based surface models. Models ranged in detail from 200k to 1000k polygons, dependent on the size of the bone and the detail required around joint surfaces.

Table 1.1. List of specimens scanned for geometric morphometric analysis. Limb elements used: S = scapula, H = humerus, U = ulna, R = radius, UR = fused ulna and radius (radioulna). M = male, F = female, dashes represent specimens of unknown sex; (w) = wild.

Taxon	Specimen No.	Bone	Sex	Age	Provenence
Tapirus indicus	NMHW 1938	S, H, UR	-	adult	unknown
	NMHW 42298	S, H, UR	F	adult	unknown
	RMNH 17923	S, H, UR	-	adult	unknown
	RMNH 43543	S, H, R, U	-	adult	unknown
	RMNH 21056	S, H, U	-	adult	unknown
	RMNH 1014	S, H, R, U	-	adult	unknown
	ZMB MAM 47503	S, H, UR	F	adult	unknown
	ZMB MAM 4950	S, H, UR	-	adult	Malaysia (w)
Tapirus bairdii	RMNH 43495	S, H, R, U	-	adult	unknown
	AMNH 90128	S, H, R, U	-	sub-adult	zoo
	AMNH 130104	S, H, R, U	-	adult	zoo
	MVZ 141173	S, H, UR	F	adult	Guatamala (w)
	MVZ 141296	S, H, UR	M	sub-adult	Belize (w)
Tapirus pinchaque	MNHN 1982-34	S, H, R, U	-	adult	unknown
	MEO 2203a	S, H, UR	M	adult	zoo (Berlin)
	ZMB MAM 62085	S, H, R, U	F	adult	unknown
	AMNH 149424	S, H, R, U	F	sub-adult	zoo
Tapirus terrestris	NMHW 58178	S, H, UR	F	adult	unknown
	MEO 2204e	S, H, R, U	M	adult	zoo
	MEO 2204b	S, H, R, U	M	adult	zoo (Olmen)
	RMNH 12827	S, H, UR	M	adult	Paramaribo (w)
	RMNH 12913	S, H, UR	-	adult	unknown
	RMNH 1163.2b	S, H, UR	M	adult	unknown
	ZMB MAM 12999	S, H, UR	F	adult	unknown

Institutional Abbreviations – AMNH, American Museum of Natural History, New York; **MEO,** MuseOs Natuurhistorisch Museum, Koksijde; **MNHN**, Muséum National d'Histoire Naturelle, Paris; **MVZ**, Museum of Vertebrate Zoology, Berkeley; **NHMW**, Naturhistorisch Museum Wien, Vienna; **RMNH**, Naturalis Biodiversity Centre, Leiden; **ZMB**, Museum für Naturkunde, Berlin.

Geometric Morphometrics

Landmark-based geometric morphometrics is a widely used and appropriate method for quantifying morphological differences between three-dimensional objects (Gould, 2014; Zelditch et al., 2012). The technique is based on landmarks: discrete, biologically (or operationally) homologous points placed onto a series of objects (Zelditch et al., 2012). Type II (maxima and minima) and Type III (calculated from Type II positioning) landmark points were used to define the morphology of the four bones of the shoulder and forearm (stylopodium + zeugopodium). For ease of description, landmarks are labelled with subscript letters pertaining to the bones they describe: e.g. scapula (18 $_{S}$Lms), humerus (42 $_{H}$Lms), radius (25 $_{R}$Lms) and ulna (27 $_{U}$Lms) (Figure 1.1). Finalised surface models were imported into Landmark Editor v.3.0 software (Wiley et al., 2006) for three-dimensional landmark application. Raw landmark coordinates were exported to MorphoJ v1.06d (Klingenberg, 2011) and aligned using Generalised Procrustes Analysis (GPA). GPA eliminated the effects of size, location and orientation by aligning raw coordinate configurations based on geometric centre (centroid) and minimised distances between corresponding landmarks. The resulting Procrustes coordinates and centroid sizes were then exported from MorphoJ into SPSS v.23 (IBM Corp. 2013) for further analysis. Centroid sizes represent a composite size measure that can be used to scale a configuration of landmarks. The centroid sizes for full adult specimens were retained for intra- and inter-specific size comparisons. A multivariate analysis of variance (MANOVA) was performed on the Procrustes coordinates of the four bones to demonstrate the power of our analysis, given unequal and potentially small sample sizes. The MANOVAs were performed in SPSS v.23.

Discriminant Function Analysis

Procrustes coordinates (x, y, z) for all landmarks for each specimen were used in discriminant function analysis (DFA), which was used to ascertain what combination of continuous variables could best discriminate between the four species. DFA relies on accurate *a priori* assignment of specimens to groups (in this case, species), in addition to sample sizes within the groups exceeding the total number of groups under study (Zelditch et al., 2012). Highly disparate groups can be reliably discriminated with

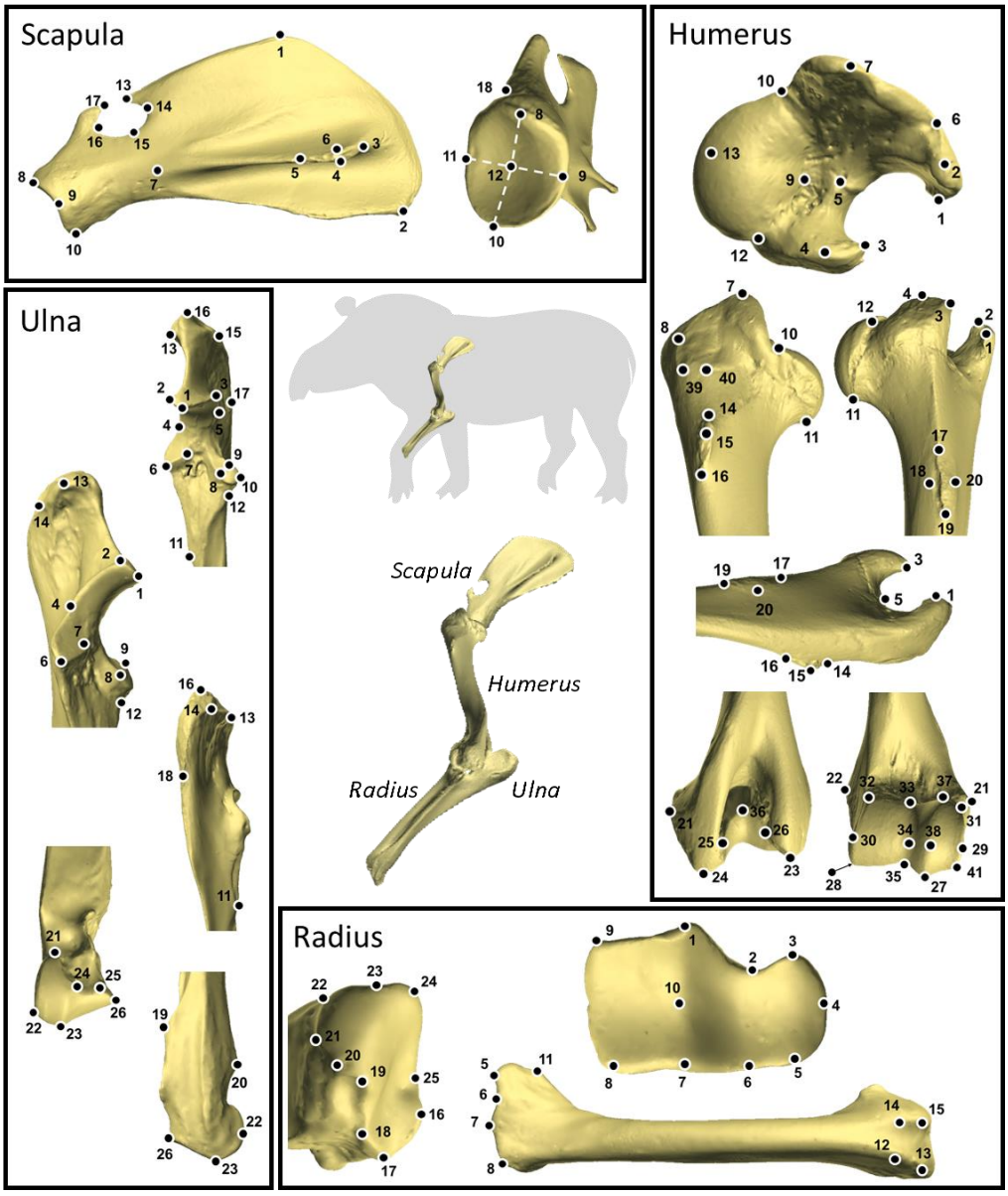

Figure 1.1. Three-dimensional landmark placements on four largest forelimb bones of *Tapirus*. Placement of bones within forelimb tapir (centre). Landmark placement exemplified on bones of *Tapirus pinchaque* (MEO 2203a). Descriptions of landmark placements can be found in the Appendix One.

modest to low sample sizes (Lachenbruch, 1968). DFAs were performed in SPSS v.23 (IBM Corp. 2013), entering Procrustes coordinates using a forward step-wise method to remove independent variables that were not significant to the discrimination process. Predicted species membership, expressed as a % accuracy, was produced and cross-validated by jack-knifing the dataset, producing a classification table. Tests for sensitivity and specificity were also performed and reported in the classification table.

The Wilk's lambda test was used to assess whether species means were equal (0 – 1; 0 = highest likelihood of inequality, 1 = high likelihood of species means being equal). Territorial maps were produced to visualise how species would be classified dependent upon the particular discriminant functions. Territorial maps were calculated based upon the mean values for each species used in the DFA. These were visualised on linear discriminant function plots, based on the first two discriminant functions (DF1 and DF2). The first two functions account for the highest percentage of variance in the datasets, and were used for graphical representations and discriminant function coefficient interpretation. The third function accounted for between 0.3% and 11.5% of total variance. Cut-off values between species were determined as the weighted mean of the discriminant scores of the group centroids. Classification tables and territorial maps were created in SPSS v.23 (IBM Corp. 2013), with resultant discriminant function plots formatted in R Studio (R Core Development Team 2008).

Scapular Fossa Ratio

Initial observations of the tapir scapula suggested interspecific variation in the attachment sites for the large, lateral shoulder muscles: the scapular fossae. The lateral scapular fossae (supraspinous and infraspinous) represent principle origination sites for the *supraspinatus* and *infraspinatus* muscles, which together act to support the shoulder, and secondarily extend (*supraspinatus*) and flex (*infraspinatus*) the upper limb. To compliment the interpretation of discriminant function results of the scapula, scapular fossa ratios were calculated from adult specimens of all taxa (Table 1.1). Areas of the two lateral scapular fossae were calculated by pruning the 3D laser scans in GeoMagic (GeoMagic Qualify v.10, Morrisville, NY, USA). These were imported into MeshLab (Cignoni et al., 2008) to calculate surface area (*A*). Scapular fossa ratios were calculated using the equation:

$$\frac{A_{supraspinous}}{A_{supraspinous} + A_{infraspinous}}$$

For comparison with other perissodactyl scapulae, 11 specimens of equids from seven species (*Equus ferus caballus*; *E. f. przewalksi*; *E. hemionus*; *E. kiang*; *E. africanus*; *E. quagga*; *E. zebra*) and four specimens of rhinoceros from three species (*Ceratotherium simum*; *Diceros bicornis*; *Dicerorhinus sumatrensis*) were added to the analysis of scapular fossa ratio. SFR specimen information are listed in Appendix I. Differences between perissodactyl clades were assessed using one-way analysis of variance (ANOVA) and Tukey HSD (honest significant difference) post-hoc test for significant differences, both performed in RStudio.

Results

Overall, discriminant function analyses successfully discriminated between the four species of extant tapirs when calculated from the scapula, humerus, ulna and radius. A classification table with jack-knifed classifications (reporting sensitivity and specificity results) was used to quantify the success of discrimination between species for each bone (Table 1.2). Accuracy of jack-knifed species classification exceeds 90% for all upper forelimb bones, with the scapula representing the most diagnostic bone with 100% accurate discrimination between the four species. The radius is the second most diagnostic bone with a classification accuracy of 95.7%. *Tapirus indicus* and *T. pinchaque* are consistently discriminated across all bones with 100% accuracy. However, at least one specimen of *T. terrestris* was misclassified for three bones (humerus, radius and ulna). Wilks' lambda testing revealed that for all bones the group centroids were significantly different ($\lambda \leq 0.001$). Function scores at group centroids (canonical group means; mean group position in canonical variate-space) are reported in Table 1.3, with cut-off scores based on weighted mean discriminant scores between two group centroids reported in Table 1.4. Discriminant plots for each bone are presented in Figure 1.2, with discriminant function coefficients (loadings) for landmarks that contributed toward accurate discrimination highlighted in Table 1.5. Results of the MANOVA and power analyses revealed statistical power for the scapula, humerus and ulna in excess of 0.8 (high power); the radius recorded a power of 0.57 (medium power) (Supplementary Table S1.5).

Scapula

Discriminant function plots of the scapula reveal isolated occupation of variate-space by each tapir species. The first two discriminant functions (DF1 and 2) based on the scapula landmarks account for 88.5% of variance (Figure 1.2a). Scapulae from each species were classified 100% correctly, both prior to and after jack-knifing (Table 2). The analysis was revealed as both highly sensitive (1.000) and specific (1.000),

Table 1.2. Jack-knifed classification table of specimen assignments for scapula, humerus, radius and ulna using linear discriminant analysis. *T. = Tapirus*; *bai = T. bairdii*; *ind = T. indicus*; *pin = T. pinchaque*; *ter = T. terrestris*.

	Species	Predicted Species Membership				Total	Sensitivity	Specificity
Scapula		*bai*	*ind*	*pin*	*ter*			
Specimen	*T. bairdii*	5	0	0	0	5	1.000	1.000
Count	*T. indicus*	0	8	0	0	8	1.000	1.000
	T. pinchaque	0	0	4	0	4	1.000	1.000
	T. terrestris	0	0	0	7	7	1.000	1.000
Overall % Correctly Classified:						**100**		
Humerus		*bai*	*ind*	*pin*	*ter*			
Specimen	*T. bairdii*	5	0	0	0	5	1.000	1.000
Count	*T. indicus*	0	8	0	0	8	1.000	1.000
	T. pinchaque	0	0	4	0	4	1.000	1.000
	T. terrestris	2	0	0	5	7	1.000	0.714
Overall % Correctly Classified:						**91.7**		
Radius		*bai*	*ind*	*pin*	*ter*			
Specimen	*T. bairdii*	5	0	0	0	5	1.000	1.000
Count	*T. indicus*	0	7	0	0	7	1.000	1.000
	T. pinchaque	0	0	4	0	4	1.000	1.000
	T. terrestris	1	0	0	6	7	1.000	0.857
Overall % Correctly Classified:						**95.7**		
Ulna		*bai*	*ind*	*pin*	*ter*			
Specimen	*T. bairdii*	5	0	0	0	5	1.000	1.000
Count	*T. indicus*	0	8	0	0	8	1.000	1.000
	T. pinchaque	0	0	4	0	4	1.000	1.000
	T. terrestris	2	0	0	5	7	1.000	0.714
Overall % Correctly Classified:						**91.7**		

suggesting no false positive or false negative results. Discriminant functions at the group centroids show that taxa overlapping along one DF show separation along the other DF (Figure 1.2; Tables 1.3 and 1.4); both DFs are necessary for successful discrimination between species. The proximodistal positioning of the cranial angle ($_{S}$Lm 1) and the mediolateral placement of the *biceps brachii* origin ($_{S}$Lm 18) influence both DF1 and DF2; the lateral expansion of the glenoid cavity ($_{S}$Lm 9) also influences discrimination along DF1. Landmarks that show greatest discrimination along DF2 include the craniocaudal enlargement of the scapular spine tuberosity ($_{S}$Lm 3), the proximodistal expansion of the cranial margin of the glenoid cavity ($_{S}$Lm 8) and the proximal-most point of the supraglenoid tubercle ($_{S}$Lm 17) (Figure 1.2; Table 1.5). Centroid size varies both inter- and intra-specifically, with *T. terrestris* and *T. bairdii* exhibiting the greatest

Table 1.3. Discriminant functions at group centroids

Scapula	**Discriminant Function**	
Species	1	2
T. bairdii	-5.154	3.163
T. indicus	0.013	1.881
T. pinchaque	-6.837	-5.466
T. terrestris	7.573	-1.286

Humerus	**Discriminant Function**	
Species	1	2
T. bairdii	-17.145	-3.477
T. indicus	4.434	10.13
T. pinchaque	39.467	-7.458
T. terrestris	-15.374	-4.832

Radius	**Discriminant Function**	
Species	1	2
T. bairdii	3.869	2.73
T. indicus	4.063	-4.872
T. pinchaque	-23.318	0.396
T. terrestris	6.498	2.696

Ulna	**Discriminant Function**	
Species	1	2
T. bairdii	3.06	-1.005
T. indicus	-6.696	-0.829
T. pinchaque	1.716	7.345
T. terrestris	4.486	-2.531

range of centroid sizes. *T. indicus* show the largest mean average centroid size (409.79 ± 16). *T. terrestris* displays the largest individual centroid size (431.45). *T. bairdii* displays a smaller mean centroid size (379.76 ± 30) to that of *T. terrestris* (399.17 ± 25), with *T. pinchaque* displaying the smallest (352.69 ± 13). Scapular fossa ratios (SFRs) for the four tapir species and two perissodactyl outgroups are presented in Figure 1.3.

Results from Tukey HSD post-hoc testing from ANOVA of scapula fossa ratios (SFRs) revealed that *T. indicus* was significantly separate from all neotropical taxa ($p < 0.01$) (Table 1.6). *T. bairdii* does not differ significantly from other neotropical species, whereas *T. pinchaque* is statistically separated from *T. terrestris* ($p = 0.037$). The exclusion of a single outlying *T. terrestris* (MEO 2204e) polarises this result with a very strong significant difference ($p = 0.002$). The highest SFR is calculated for *T. pinchaque*, with a mean SFR of 0.610 ± 0.026. Mean SFRs in the larger neotropical species were similar to one another: *T. terrestris* (0.557 ± 0.03) and *T. bairdii* (0.572 ± 0.01). *T. indicus* displayed a mean SFR closer to extant rhinoceroses than to other extant tapirs (Figure 1.3). *Equus* displayed the lowest SFR of the species studied (mean SFR: 0.369 ± 0.013).

Humerus

Discriminant function plots of the humerus show a substantial separation between three groups: *T. indicus*, *T. pinchaque* and a combined *T.bairdii* + *T.terrestris* grouping (Figure 1.2b). Combined, DF1 and DF2 account for 98.3% of humeral variance, with DF 1 alone accounting for 86.7% of humeral variance (Figure 1.2b). Humeri from all species are classified 100% correctly; in addition *T. indicus*, *T. bairdii* and *T. pinchaque* are correctly classified 100% when classifications are jack-knifed. 28.6% of *T. terrestris* (two specimens: RMNH 12913 and ZMB MAM 12999) are incorrectly classified as *T. bairdii*. Overall, tapir humeri are correctly classified 91.7% after jack-knifing (Table 1.2). This humeral discriminant analysis was shown to be highly sensitive (1.000); two false positives were reported, and thus specificity fell to 0.714 (Table 1.2). Functions at the group centroids support the presence of three morphotypes, with *T. terrestris* and *T. bairdii* group centroids falling very close to one another, but far separated from *T. indicus* and *T. pinchaque* along both DF1 and DF2 (Figure 1.2; Tables 1.3 and 1.4). DF1 successfully discriminates between the three morphotypes present. Morphological features that contribute most toward accurate interspecific classifications along DF1 include the proximodistal positioning of the distal margin of the teres major tuberosity ($_{H}$Lm 18) and the craniocaudal expansion of the medial humeral condyle ($_{H}$Lm 22, 26, 27 and 30). Classification along DF2 (accounting for 11.6% of variance) is influenced by the medial deflection of the greater tubercle ($_{H}$Lm 2) and the proximal expansion of the lesser tubercle ($_{H}$Lm 4 and 9); in addition DF2 is also influenced by the mediolateral and craniocaudal expansion of the humeral condyle ($_{H}$Lm 22, 26, 27 and 30) (Figures 1.1 and 1.2; Table 1.5). Humeral centroid size is greatest in the largest species, *T. indicus* (individual: 724.55; mean average: 689.92 ± 21). The smallest species by body mass (*T. pinchaque*) displays the second largest average humeral centroid size (681.67 ± 12), with *T. terrestris* exhibiting the smallest (642.09 ± 34).

Radius

Discriminant function plots of the radius show a large separation of *T. pinchaque* from the other taxa, with *T. terrestris* and *T. bairdii* again showing some spatial overlap (Figure 1.2c). The first discriminant function (DF1) accounts for 89.3% of radial variance, with DF 2 accounting for only 8.6%. Radii from all species are classified 100% correctly prior to jack-knifing. One specimen of *T. terrestris* (MEO 2204e) was incorrectly classified as *T. bairdii* after jack-knifing, resulting in an overall classification accuracy of 95.7%. Radius discriminant analysis was highly sensitive (1.000); a single false positive was reported, reducing specificity 0.857. Functions at the group centroids show that *T. pinchaque* is far removed from the other taxa along DF1, with the other

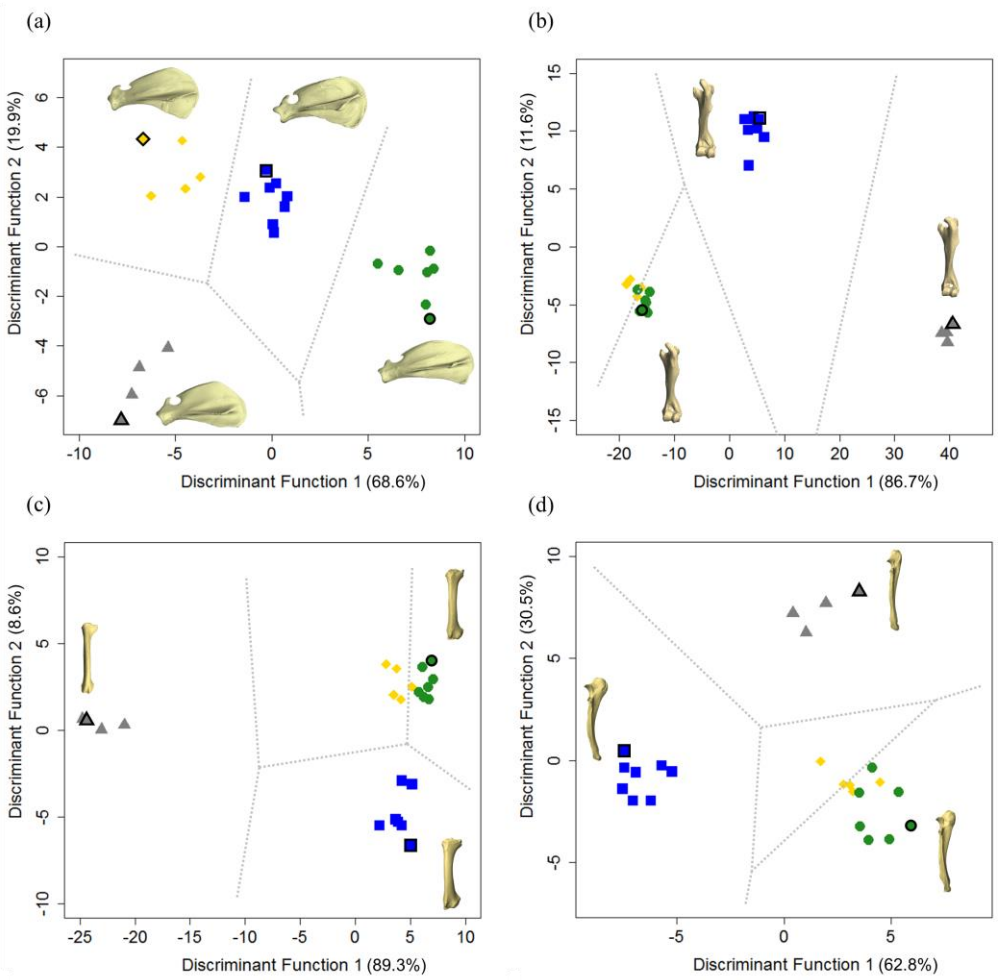

Figure 1.2. Linear discriminant function plots for the upper forelimb bones of four extant species of *Tapirus*. Discriminant function plots of **(a)** scapula, **(b)** humerus, **(c)** radius, and **(d)** ulna of extant *Tapirus* species. Percentage of variance accounted for by each discriminant function is presented in brackets. Species key: *T. bairdii* (gold diamonds); *T. indicus* (blue squares); *T. pinchaque* (grey triangles); *T. terrestris* (green circles); dotted line = territorial map lines separating each group based on mean average values. Outlined points and representative bone morphologies denote specimens furthest from other species clusters.

three species possessing similar mean discriminant functions along DF1 (Figure 1.2; Tables 1.3 and 1.4). *T. bairdii* and *T. terrestris* group centroids are very similarly placed on DF2 (*T. bairdii* = 2.730; *T. terrestris* = 2.696). This similar placement for three species may account for medium statistical power for the radius compared to high power

Table 1.4. Discrimination between species based on cut-off scores on either Discriminant Function 1 or Discriminant Function 2. Cut-off scores (means) weighted by number of specimens per group.

Scapula	**Description of Discrimination**
Discriminant Function 1	*T. bairdii*+*T. pinchaque* < -0.989 < *T. indicus* < 2.023 < *T. terrestris* (discriminates between 3 of 4 groups; *T. bairdii* and *T. pinchaque* not separated)
Discriminant Function 2	*T. pinchaque* < -0.815 < *T. bairdii* (discriminates between *T. bairdii* and *T. pinchaque*)
Humerus	**Description of Discrimination**
Discriminant Function 1	*T. bairdii*+*T. terrestris* < -2.444 < *T. indicus* < 13.895< *T. pinchaque* (discriminates between 3 of 4 groups; *T. bairdii* and *T. terrestris* not separated)
Discriminant Function 2	1.075 < *T. indicus* (discriminates *T. indicus*)
Radius	**Description of Discrimination**
Discriminant Function 1	*T. pinchaque* < -5.403 (discriminates *T. pinchaque*)
Discriminant Function 2	*T. indicus* < -0.759 (discriminates *T. indicus; T. bairdii* and *T. terrsetris* not separated)
Ulna	**Description of Discrimination**
Discriminant Function 1	*T. indicus* < -0.699 (discriminates *T. indicus*; *T. bairdii* and *T. terrestris* not separated)
Discriminant Function 2	*T. pinchaque* < 2.310 (discriminates *T. pinchaque*)

for all other bones. Both *T. indicus* and *T. pinchaque* group centroids are positioned separate to the *T. bairdii* + *T. terrestris* group along DF2 (Figure 1.2; Tables 1.3 and 1.4). Positioning along DF1 is influenced by the lateral deflection ($_{R}$Lm 4 and 11) and craniocaudal expansion ($_{R}$Lm 9) of the fovea of the radial head, in addition to the proximodistal positioning of $_{R}$Lm 14 (apex of lateral border of the *extensor carpi radialis* groove). $_{R}$Lm 14 also contributes to discrimination along DF2, in addition to both the lateral expansion ($_{R}$Lm 4) and the positioning of the deepest point on the medial sagittal crest of the fovea capitis radii ($_{R}$Lm 10). Average centroid size of the radius is notably larger in *T. indicus* (575.91 ± 15). The radii of both *T. bairdii* and *T. pinchaque*

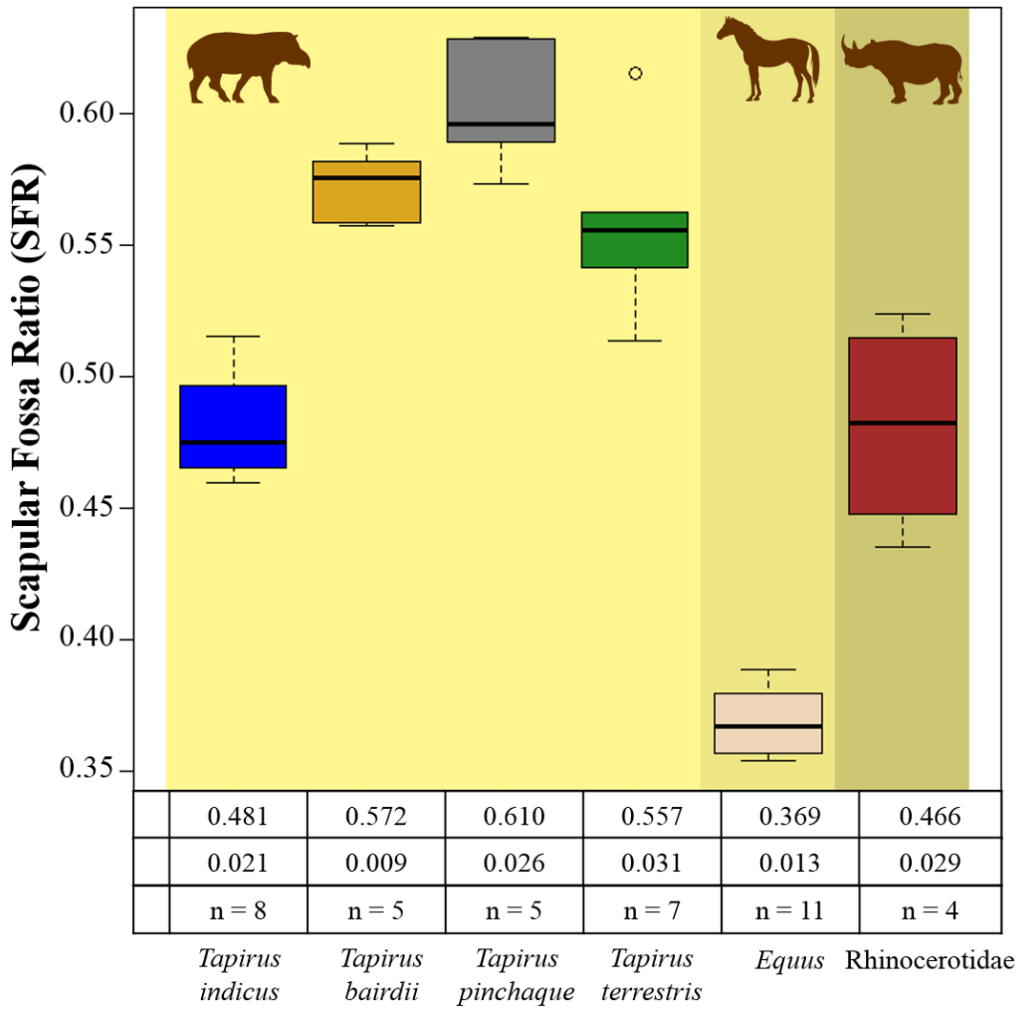

Figure 1.3. Scapular fossa ratios (SFRs) for four extant tapir species and representatives of other modern perissodactyls (equids and rhinocerotids). Table beneath boxplot provides mean SFR value (top), standard deviation (middle) and number of specimens (n). Coloured boxes define upper and lower quartile; vertical whiskers = highest and lowest value within the group (excluding outliers); bold black line = median value; black circles = statistical outlier. Silhouettes represent relevant families of perissodactyl (from left: Tapiridae, Equidae, Rhinocerotidae).

show similar average centroid sizes (527.53 ± 27 and 521.01 ± 19 respectively). As in the humerus, *T. terrestris* exhibits the smallest average radial centroid size (506.63 ± 26).

Ulna

Linear discriminant function plots of the ulna show a large separation of *T. pinchaque* from the other American taxa, with *T. terrestris* and *T. bairdii* again showing some spatial overlap. As in all other plots, *T. indicus* positions away from the neotropical species (Figure 1.2d). The first two discriminant functions account for 93.3% of ulna variance (DF1 = 62.8%; DF2 = 30.5). Ulnae from all species are classified 100% correctly. Jack-knifed ulna classification falls to 91.7% accuracy, with two *T. terrestris* specimens (RMNH 12827 and RMNH 1163.2b) incorrectly classified as *T. bairdii* (Table 1.2). Ulnar discriminant analysis was shown to be highly sensitive (1.000). Two false positives were reported, reducing specificity to 0.714 (Table 1.2). Ulnar functions at group centroids show that *T. indicus* is far removed from the other taxa along DF1, with centroid and cut-off points all present in negative DF1 variate-space (Figure 1.2; Tables 1.3 and 1.4). *T. bairdii* and *T. terrestris* group centroids are positioned close to each other for both DF1 and DF2, representing a *T. bairdii* + *T. terrestris* ulnar morphotype. Both the group centroid and cut-off points for *T. pinchaque* are found in positive DF2 variate-space (Figure 1.2; Tables 1.3 and 1.4), whereas group centroids for all other species are placed in negative DF2 variate-space. Discrimination along DF1 is influenced by the proximodistal positioning of the lateral coronoid process ($_{U}$Lm 11), the craniocaudal depth of the distal ulna ($_{U}$Lm 20), and the mediolateral narrowing of the pisiform facet ($_{U}$Lm 24) (Figure 1.1; Table 1.5). Discrimination on DF2 is influenced by the morphology of the medial anconeal process ($_{U}$Lm 2), the proximodistal positioning of the *triceps brachii* insertion (on the olecranon tuber) ($_{U}$Lm 15), and the lower margin of the *flexor carpi ulnaris* ulnar origination site ($_{U}$Lm 19) (Figure 1.1; Table 1.5). Average ulnar centroid size is largest in *T. indicus* (572.75 ± 14). Similarly to the radius and humerus, *T. bairdii* and *T. pinchaque* display comparable average centroid sizes (527.70 ± 25 and 525.44 ± 21 respectively) for the ulna. *T. terrestris* exhibits the smallest average ulnar centroid size (501.77 ± 24).

Discussion

Our results support our hypothesis of interspecific variation in modern tapir upper forelimbs. Discriminant function analyses revealed interspecific patterns across all upper limb bones. The scapula is the only bone to be 100% successfully discriminated across all species. Our MANOVAs and power analysis results (Supplementary Table

Table 1.5. Standardized linear discriminant function coefficients for upper arm bones of *Tapirus*. Bold numbers highlight coordinates of greatest influence for each discriminant function.

Scapula	Discriminant Functions	
$_{bone}$Lm n_{axis}	1	2
$_{s}$Lm 1_{x}	**1.855**	**-1.346**
$_{s}$Lm 3_{y}	-0.255	**1.597**
$_{s}$Lm 5_{x}	-0.017	-0.782
$_{s}$Lm 6_{y}	0.814	0.715
$_{s}$Lm 8_{z}	-0.716	**-1.454**
$_{s}$Lm 9_{x}	**2.004**	-0.159
$_{s}$Lm 17_{y}	-0.484	**1.284**
$_{s}$Lm 18_{z}	**-1.31**	**1.017**

threshold for interpretation of Function: 1 = **>1**; 2 = **>1**

Humerus	Discriminant Functions	
$_{bone}$Lm n_{axis}	1	2
$_{H}$Lm 2_{y}	1.255	-0.768
$_{H}$Lm 2_{z}	-0.471	**-1.173**
$_{H}$Lm 4_{x}	2.052	**-1.024**
$_{H}$Lm 7_{x}	1.439	**1.687**
$_{H}$Lm 11_{y}	-2.509	0.231
$_{H}$Lm 18_{x}	**5.11**	-0.507
$_{H}$Lm 22_{z}	**5.69**	**1.00**
$_{H}$Lm 26_{x}	**-6.333**	0.319
$_{H}$Lm 27_{x}	**-5.77**	**-1.297**
$_{H}$Lm 29_{y}	1.953	0.622
$_{H}$Lm 30_{z}	**8.881**	**1.269**
$_{H}$Lm 41_{y}	2.802	0.375

threshold for interpretation of Function: 1 = **>5**; 2 = **>1**

Radius	Discriminant Functions	
$_{bone}$Lm n_{axis}	1	2
$_{R}$Lm 1_{x}	2.764	-0.436
$_{R}$Lm 4_{x}	4.247	**1.594**
$_{R}$Lm 4_{y}	**5.036**	0.851
$_{R}$Lm 9_{z}	**-5.347**	-0.706
$_{R}$Lm 10_{x}	2.003	0.91
$_{R}$Lm 10_{z}	-2.478	**-1.753**
$_{R}$Lm 11_{y}	**-5.4**	-0.29
$_{R}$Lm 14_{x}	**8.086**	**1.276**
$_{R}$Lm 20_{x}	2.954	0.714

threshold for interpretation of Function: 1 = **>5**; 2 = **>1**

Ulna	Discriminant Functions	
$_{bone}$Lm n_{axis}	1	2
$_{U}$Lm 2_{x}	-0.985	**1.163**
$_{U}$Lm 11_{x}	**1.321**	0.709
$_{U}$Lm 15_{x}	0.558	**1.791**
$_{U}$Lm 16_{y}	0.43	0.214
$_{U}$Lm 18_{z}	0.813	-0.171
$_{U}$Lm 19_{x}	0.446	**1.643**
$_{U}$Lm 20_{z}	**-1.336**	0.912
$_{U}$Lm 24_{z}	**-1.23**	0.293

threshold for interpretation of Function: 1 = **>1**; 2 = **>1**

S1.5) suggest that sample sizes in this study are more than sufficient to test interspecific differences (statistical power between 0.51 and 0.87), despite superficially low specimen counts. Results may suffer from assumptions associated with discriminant analyses (Zelditch et al., 2012). For example, the number of specimens of *T. pinchaque* does not exceed the number of predetermined groups (n=4). There may be an over-reliance on accurate species identification *a priori*, especially as we did not conduct a corresponding genetic analysis on the specimens under study, although qualitative examination of the highly distinctive tapir crania was used where possible to identify specimens to the species level. Finally, although our effect sizes (partial eta^2) and

statistical power are high (Table S1.5), it is known that lower samples sizes can result in overly high effect size; unfortunately, we were unable to include high or equal sample sizes for the species in this investigation. Knowing the true extent of the bias on the effect size would warrant the inclusion of more specimens; however, despite low sample sizes, our results suggest high shape variation between species. As such, we are confident in the effect size and power of our analysis, and here present the major morphological differences within our sample of extant tapirs, with functional interpretations. The divergent upper forelimb morphology of the mountain tapir (*Tapirus pinchaque*) is of particular note, with numerous morphological features in this species indicative of increased stride frequency and potentially higher locomotor speeds. Our study corroborates previous qualitative research on Malayan tapir (*T. indicus*) morphology, confirming a number of adaptations for increased weight-bearing in this species compared to others. We also identify similarities in the stylopodium and zeugopodium of the lowland (*T. terrestris*) and Baird's tapirs (*T. bairdii*), which may be correlated more closely with loading patterns (due to similar range of body mass) and habitat preferences rather than common ancestry.

Morphological separation of the mountain tapir

Our results show that the upper forelimb bones of the mountain tapir (*Tapirus pinchaque*) are consistently distinct from those of other extant tapirs. When inspecting landmark placement in the scapula of *T. pinchaque*, the cranial angle ($_{S}$Lm 1) midway along the cranial margin and the posteroventral placement of the scapular spine tuberosity ($_{S}$Lm 3) increase the area of the supraspinous fossa (Figure 1.4). The scapular

Table 1.6. One-way ANOVA and Tukey HSD (honest significance difference) test results for scapular fossa ratios in *Tapirus*. Significant differences set at $p \leq 0.05$, with significant values in bold. DF = degrees of freedom.

ANOVA	**DF**	**Sum of Squares**	**F-value**	**p-value**
Clade groupings	5	0.286	99.39	<0.01
Residuals	33	0.019		
Tukey HSD	*T. bairdii*	*T. indicus*	*T. pinchaque*	*T. terrestris*
T. bairdii		**0.000**	0.353	0.901
T. indicus	**0.000**		**0.000**	**0.000**
T. pinchaque	0.353	**0.000**		**0.037**
T. terrestris	0.901	**0.000**	**0.037**	

spine of *T. pinchaque* is more posteroventral than in any other modern tapir, and the supraspinous fossa subsequently becomes much greater in relative area compared to the infraspinous (Figure 1.4). Functionally, the supraspinous fossa is the attachment site for the *supraspinatus* and *subclavius*, which stabilise the scapula (Budras et al., 2003; J. C. Watson & Wilson, 2007a). The infraspinous fossa is the principal attachment site for the *infraspinatus*, which primarily acts as a shoulder stabiliser (acting as a lateral collateral ligament with the *subscapularis*), while secondarily flexing the shoulder joint (Budras et al., 2003; Liebich et al., 2007). In other quadrupedal species, an enlarged *supraspinatus* has been suggested to allow for greater energy absorption on ground impact during locomotion (equids, Watson and Wilson 2007; didelphid marsupials, Astúa 2009). Despite recent research highlighting that the relationship between muscle attachment site and muscle volume is not necessarily a direct one (Bello-Hellegouarch, Potau, Arias-Martorell, Pastor, & Pérez-Pérez, 2013; Larson & Stern, 2013), the *supraspinatus* in published studies of both *T. indicus* and *T. terrestris* is described as filling or exceeding the supraspinous fossa (MacLaren pers. obs.; Murie 1871; Windle and Parsons 1901; Campbell 1936; Bressou 1961). Using this information, we interpret that a large *supraspinatus* is present in *T. pinchaque* relative to other tapir species, facilitating greater stabilisation and shock absorption for the proximal limb (Astúa, 2009; J. C. Watson & Wilson, 2007a). This has been shown to be useful for taxa that employ half-bounds during running locomotion (e.g. cursorial rodents and lagomorphs, Seckel and Janis 2008; terrestrial New World possums, Astúa 2009), a form of movement which is advantageous for rapid acceleration or deceleration (Walter & Carrier, 2007). All tapirs exhibit half-bound locomotion in captivity (pers. obs. MacLaren), though this is restricted to predominantly level surfaces. A relatively enlarged *supraspinatus* may therefore enable *T. pinchaque* to employ rapid bursts of speed and abrupt deceleration when travelling through dense undergrowth on both level and inclined surfaces, without the innovation of more complex shock absorbers such as those present in equid fetlock (W. Back et al., 1995).

The ratio of the scapular fossae areas (here described as the scapular fossa ratio; SFR) quantifies differences in supraspinous and infraspinous fossa size, confirming that *T. pinchaque* exhibits a larger supraspinous compared to infraspinous fossa than any other tapir in this study (Figure 1.3). Although *T. pinchaque* displays the highest SFR of extant tapirs, all the neotropical tapirs exhibit higher SFRs than *T. indicus* and other extant perissodactyls (equids and rhinocerotids) (Figure 1.3). The supraspinous fossa morphology of *T. pinchaque* does not greatly resemble that of any modern ungulates (Maynard Smith & Savage, 1956), bearing more resemblance to the scapulae of felids (Martín-Serra et al., 2014; Zhang et al., 2012) and some basal perissodactyls (Hellmund, 2005; Kitts, 1956; Wood et al., 2011).

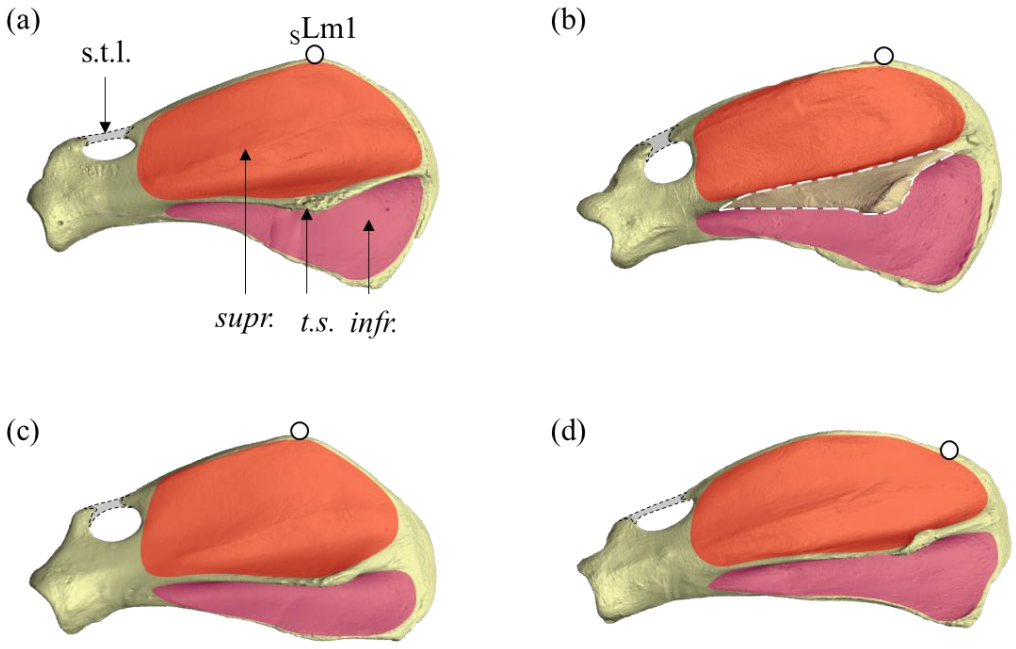

Figure 1.4. Comparison of scapular blade morphology in tapirs. (a) *Tapirus bairdii*; (b) *T. indicus*; (c) *T. pinchaque*; (d) *T. terrestris*. Lateral view. Scapular features: $_{S}$Lm 1; *supr.* = supraspinous fossa (red); *infr.* = infraspinous fossa (purple); *t.s.* = tuber of the scapular spine; s.t.l.; superior transverse ligament.

In addition to possessing a SFR higher than other tapir species, *T. pinchaque* exhibits the shallowest glenoid cavity of all the tapirs in this study (defined by $_{S}$Lm 9). A shallow glenoid cavity has been suggested to facilitate a high degree of mobility (Argot, 2013; Spoor & Badoux, 1986), rather than restricting the shoulder to a purely rotational movement. The higher degree of mobility in the shoulder joint may also help generate greater stride lengths in *T. pinchaque* by allowing more parasagittal movement of the humeral head within the shoulder joint. The combination of large supraspinous fossae and shallow glenoid cavities may act as a shock absorber in the proximal forelimb of *T. pinchaque*, in addition to a distal footpad. When compared to the impact resistance adaptations of other modern perissodactyls such as horses (A. M. Wilson, McGuigan, Su, & van Den Bogert, 2001), the modifications to the forelimb skeleton of *T. pinchaque* are less complex. In equids, the long tendons of the digital flexor muscles of the

zeugopodium have evolved to act as impact dampeners (A. M. Wilson et al., 2001), associated with the loss of a foot-pad (MacFadden, 1992a; Thomason, 1985). This represents a derived, distal impact dampening adaptation to the distal limb. The osteological adaptations in *T. pinchaque* may have evolved to facilitate stable locomotion on the spongey páramo grassland, while also resisting impact forces when moving down inclined, alpine habitats (Downer, 1995, 2001; Hawkins, 2011; Padilla et al., 2010; J. C. Watson & Wilson, 2007a), rather than providing impact resistance for sustained running in open habitats (equids) (MacFadden, 1992a). Morphological adaptations in the scapular blade in *T. pinchaque*, in addition to overall scapular variability between extant tapir species (Figures 1.3–1.4), offer evidence supporting the integral role the scapula plays in the kinematics of locomotion in quadrupeds, affecting stride length (Gasc, 2001; Schmidt & Fischer, 2009; Spoor & Badoux, 1986), stability (Argot, 2013; Spoor & Badoux, 1986; Wood et al., 2011) and impact cushioning (Watson and Wilson 2007; Astúa 2009; this study). However, it also highlights the capacity for large mammals within a single genus to display notable variation in their locomotor capabilities.

In addition to an unusual scapula shape, the humerus of *T. pinchaque* is more mediolaterally and craniocaudally narrow than those of other tapir species, giving the upper forelimb a more gracile appearance. The gracile nature of the upper forelimb elements in this study compliments similar observations of lower hind limb elements in *T. pinchaque* (Hawkins, 2011). The mediolateral narrowing of the limb bones reduces bone mass, creating less inertia for muscular action to overcome (Carrano, 1999; Fedak, Heglund, & Taylor, 1982); this has been described as a 'cursorial' adaptation, enabling an increased stride frequency (Anton, Galobart, & Turner, 2005; Carrano, 1999; Gambaryan, 1974; Hildebrand, 1985; MacFadden, 1992a; Samuels et al., 2013; Van Valkenburgh, 1987).

The insertion sites of humeral flexors (e.g. teres tuberosity of the humerus) are more proximal to the joint centre of the shoulder than in any other tapir ($_{H}$Lm 18) (Figure 1.5). In addition, the posteroventral positioning of the scapular spine alters the origination site for another shoulder flexor, the scapular head of the *deltoideus*. The proximal placement of muscle insertions (coupled with the posteroventral scapular spine) shortens the flexion lever arm around the shoulder joint for both the *teres major* and *deltoideus*, allowing less torque around the joint while enabling rapid flexion of the shoulder and adduction of the humerus (de Muizon & Argot, 2003; Gambaryan, 1974; Hildebrand, 1985; Pereira, 2013). This is another adaptation indicative of increased cursoriality (Gambaryan, 1974; Gregory, 1929; Hildebrand, 1985), and suggests that *T. pinchaque* may be capable of increased stride frequency compared to other extant tapirs.

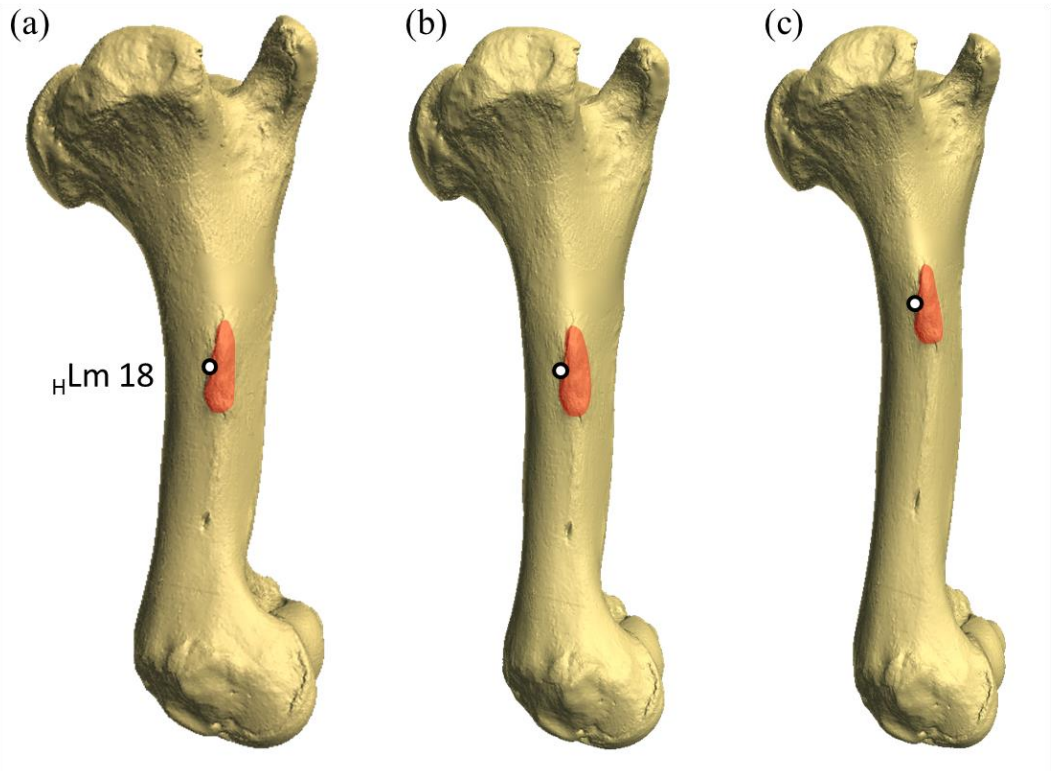

Figure 1.5. Comparison between teres tuberosity positioning in *Tapirus*. From left: (a) *T. indicus*, (b) *T. terrestris*, and (c) *T. pinchaque*. All bones scaled to same size to make differences relative. Bone shapes based on mean average shape of species mapped onto surface scans of ZMB MAM 12999).

In the zeugopodium (radius and ulnar), *T. pinchaque* displays the least prominent lateral tuberosity of the radius (RLms 4 and 11), the site of attachment of the lateral collateral ligament. This tuberosity is described as prominent in most tapirs (Holbrook 2001), cervids and sheep (Blagojević & Aleksić, 2012). The tuberosity is even more prominent in equids, rhinoceroses and large bovids, projecting further than the lateral margin of the radial head (pers. obs.; Gregory 1929; Liebich et al. 2007). The lateral collateral ligament attachment of *T. pinchaque* is consistently found beneath the lateral extent of the radial head, a morphology more reminiscent of basal perissodactyls (Gregory, 1929;

Holbrook, 2001; Radinsky, 1965b; Wood et al., 2011), canids and felids (Argot, 2013; Liebich et al., 2007). The functional interpretation of the lateral tuberosity placement beneath the radial head in *T. pinchaque* remains uncertain.

Finally, *T. pinchaque* exhibits the least amount of posterior rotation in the olecranon process of the ulna (Figure 1.6). Caudal deflection of the olecranon (i.e. the angle of the olecranon to the long axis of the ulna) has been shown to increase with overall body mass (de Muizon & Argot, 2003; Van Valkenburgh, 1987), and is described as an adaptation to weight-bearing in large ungulates (Gregory, 1929). When the two-dimensional angle between the long axis of the ulna and the olecranon is compared across modern *Tapirus* species (Figure 1.6), *T. pinchaque* exhibits the lowest angle of the olecranon ($_{U}$Lm 15) to the long axis of the ulna (48.2°), compared to *T. terrestris* (62.8°) and *T. indicus* (66.5°) (Figure 1.6). The angle at which the olecranon is offset from the long axis of the ulna determines the forelimb position in which the *triceps brachii* (zeugopodium extensor) has the greatest leverage. In the case of *T. pinchaque*, the lower angle of deflection may imply a marginally more flexed forelimb position for maximum triceps leverage compared to other tapir species. Similar variations in olecranon morphology and caudal deflection have been observed in large felids (Christiansen & Adolfssen, 2007). These species possess similar overall body masses and implement their forelimbs in prey capture; thus, care should be taken when comparing variation in osteological features in carnivores to similar variation observed in herbivores. However, tapirs in this study show a far greater range of body masses than those exhibited by large felids (Christiansen & Adolfssen, 2007), and we therefore interpret the more acute degree of olecranon rotation in *T. pinchaque* as indicative of lower loading on the forelimb in this species. In combination with the mediolaterally narrow humerus, radius and ulna, muscular and ligamentous attachment sites in the upper forelimb of *T. pinchaque* imply this species may be capable of higher stride frequency and potentially higher locomotor speeds than other modern tapirs.

The upper forelimb bones of *T. pinchaque* show a marked morphological contrast with its closest phylogenetic relative: *T. terrestris* (Figure 1.2–1.6). Phylogenetic divergence estimates from molecular studies suggest these species began divergence recently in geological time (2–4 Mya; Steiner and Ryder 2011; Cozzuol et al. 2013; Ruiz-García et al. 2012; Ruiz-García et al. 2016), with genetic differentiation between these species in some genes as low as 1% (Ruiz-García et al., 2016). There are significant differences between *T. pinchaque* and *T. terrestris* forelimb bone shapes, despite few differences in bone centroid size or overall bone length (Appendix I; Tables S1.1–S1.2). As such, we conclude that the suite of morphological differences between *T. pinchaque* and other extant tapirs result from functional adaptations to a different locomotor style, most

likely triggered by differences in habitat exploitation (Lizcano, Pizarro, Cavelier, & Carmona, 2002; Padilla et al., 2010; Ruiz-García et al., 2012).

Adaptations to weight-bearing in the Malayan tapir

Tapirus indicus is the only remaining Old World tapir (de Thoisy et al., 2014; Holanda & Ferrero, 2013), and has been shown to be morphologically and molecularly separate from the neotropical taxa (Cozzuol et al., 2013; Ferrero & Noriega, 2007; Ferrero et al., 2013; Holanda & Ferrero, 2013; Ruiz-García et al., 2012). Our results corroborate findings from previous qualitative comparisons of forelimb osteology between *T. indicus* and *T. terrestris* (Earle, 1893; Gregory, 1929). Features of the upper forelimb which discriminate *T. indicus* correspond with results from previous studies claiming *T. indicus* is the most 'graviportal' extant tapir (capable of powerful but slow locomotion) (Gregory, 1929). The scapular spine ($_{S}$Lm 3) of *T. indicus* is more central on the blade than in other tapirs. Scapular spine placement reduces the supraspinous fossa area compared to the infraspinous, so reducing the SFR. The SFR of *T. indicus* is similar to that of modern rhinocerotids (Figure 1.3), all of which exhibit numerous adaptations to weight-bearing (Gregory, 1929). A caudal deflection of the scapular spine, present in all our *T. indicus* specimens (visible in Figure 1.4b), is described as indicative of species with high body masses (Gregory, 1929; Maynard Smith & Savage, 1956), and is interpreted as a further adaptation to greater body mass in *T. indicus* compared to other tapirs. This caudal deflection of the scapular spine was also present in the juvenile specimen of *T. indicus* (MacLaren pers. obs.; see Research Chapter 3), suggesting that this is a species-specific morphology and not correlated with increased body mass through ontogeny. This morphology is also present in ungulates such as suids (including pygmy hogs *Porcula salvania* and wild boar/domestic pigs *Sus*; Oliver 1993; Liebich et al. 2007; Deka et al. 2013), and rhinoceroses (e.g. *Dicerorhinus*, *Subhyracodon*; Prothero 2005), suggesting an additional functional role potentially uncorrelated with overall body size or phylogeny.

The lesser and greater tubercles of the humerus (defined by $_{H}$Lms 2, 4 and 7) are expanded both proximal and lateral to the shoulder articulation. Tubercle morphology discriminates *T. indicus* humeri from those of other modern tapirs. The tubercles provide large insertion sites and confer greater mechanical advantage to the muscles that stabilise the shoulder joint (Hermanson & MacFadden, 1992). In a similar fashion, the craniocaudally thickened olecranon offers a greater insertion site for the heads of the *triceps brachii*, suggesting a larger elbow extensor. Greater leverage is accomplished during elbow extension by the angle of caudal deflection of the olecranon in *T. indicus* (Van Valkenburgh, 1987), which is greater than in other species (Figure

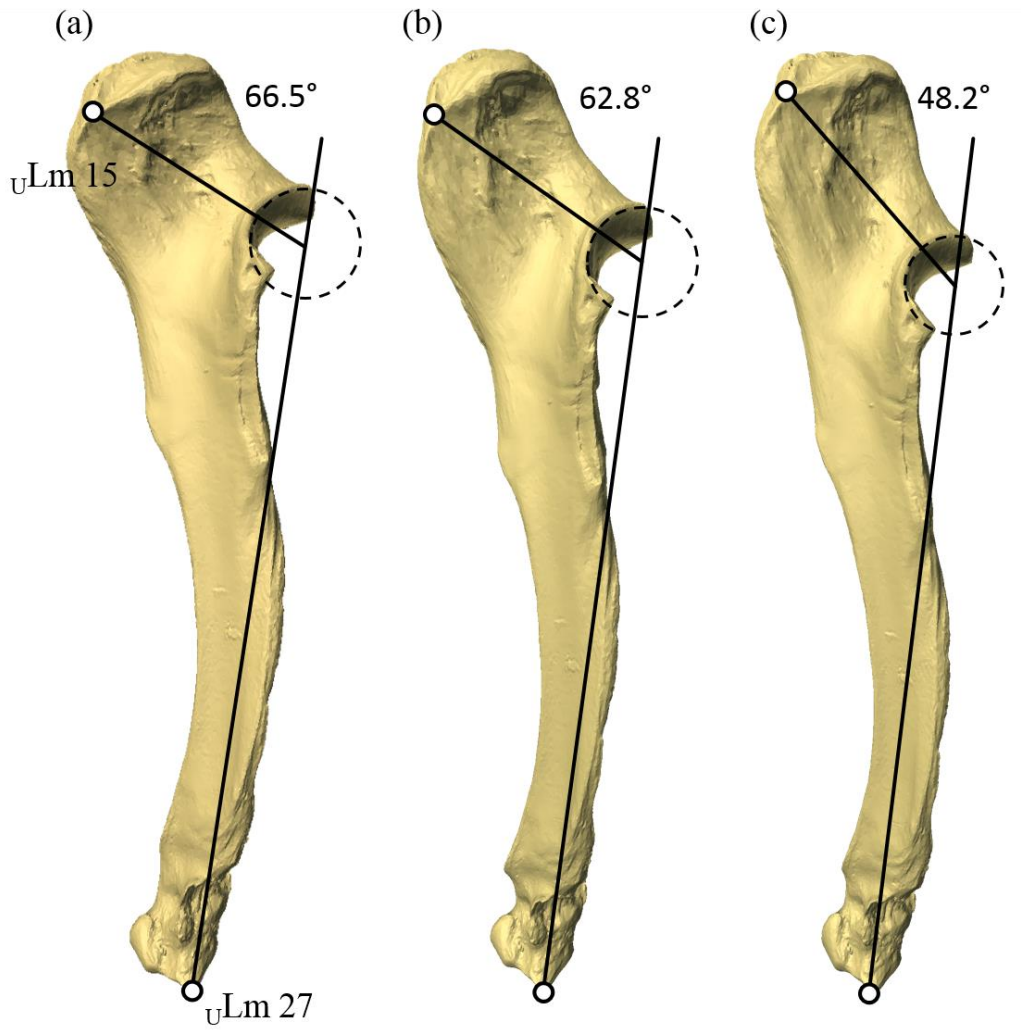

Figure 1.6. Comparison between olecranon deflections in *Tapirus*. From left: **(a)** *T. indicus*, **(b)** *T. terrestris*, and **(c)** *T. pinchaque*. Angle between the long axis of the ulna and olecranon defined by a line from the mediodistal extreme of the ulna ($_{U}$LM 27) to the centre of rotation, and a corresponding line from the centre of rotation to the posteromedial apex of *triceps brachii* attachment site ($_{U}$Lm 15). All measurements were based on 2D images of bones digitally aligned in identical orientation. All bones scaled to same size to make differences relative. Bone shapes based on mean average shape of species mapped onto surface scans of RMNH 43495.

1.6). From this morphology, we infer that the forelimb of *T. indicus* confers greater gravitational supportand experiences higher loads than other extant tapirs during both locomotion and stationary stance. Features of the shoulder and elbow joints observed in *T. indicus*, such as the relatively large infraspinous fossa, expanded humeral tubercles, and relatively large caudal deflection of the olecranon are typical of 'graviportal' ungulates (Gregory, 1929; Hermanson & MacFadden, 1992; Maynard Smith & Savage, 1956). Thus, the osteological features of the upper forelimb which contributed toward successful discrimination between *T. indicus* and other tapirs highlight adaptations for maintaining gravitational support and successful locomotion with higher body mass in *T. indicus*.

Morphological affinity between lowland and Baird's tapirs

Our landmark-based shape differences did not always result in successful discrimination, especially between species with similar overall body mass ranges (de Thoisy et al., 2014). The neotropical lowland tapir (*T. terrestris*) and Baird's tapir (*T. bairdii*) overlap in their range of body masses (*T. terrestris*: 160–295 kg; *T. bairdii*: 180–340 kg; de Thoisy et al. 2014), and in several of their forelimb bone shapes (this study; Figure 1.2 and 1.3). The scapular shape of *T. bairdii* is significantly dissimilar to that of *T. terrestris*. Despite the scapula of *T. terrestris* having a characteristic shape, with several features discriminating between these two species, the ratio of lateral scapular fossae (SFR) was not shown to be significantly different (Figure 1.3; Table 1.6). This may in part be due to the greater variation in *T. terrestris*, which in turn may be accounted for by the broad geographic range and subspecific diversity. Multiple populations of *T. terrestris* from different regions of their home range are known to exhibit different external appearance (colouration, hair length etc.) (Heshkovitz 1954; Padilla and Dowler 1994). It is possible that the variability in features such as the SFR of *T. terrestris* may be highlighting interspecific variability driven by morphologically variable populations, although specific information on subspecies classification was not available for the individuals in this study.

By contrast to the highly divergent scapula morphologies between the species, the long bone shape of *T. bairdii* and *T. terrestris* are shown to be the most similar of any extant tapir species. On several occasions *T. terrestris* and *T. bairdii* bones were so similar that the discriminant analysis could not separate these species. Similarities may be due to comparable loading on the limb during locomotion, influenced by a similar range of body masses in these species (de Thoisy et al., 2014). In addition, similarities in morphology may have arisen through common ancestry or similar habitat preferences. The lineages leading to these two species diverged from one another 9–11 Mya (M. W.

Colbert, 2005; Ruiz-García et al., 2012), and thus represent two separate lineages of neotropical tapirs (García et al., 2012; Hulbert, 2010; Ruiz-García et al., 2012). The lineage of *T. bairdii* has been suggested to have originated in North America, migrated south during the Great American Biotic Interchange (GABI), and secondarily migrated north again into Central America following the colonisation of South America by the ancestors of *T. terrestris* and *T. pinchaque* during the late Pleistocene (Cione et al., 2015; García et al., 2012). *T. bairdii* shows greater phylogenetic affinity to the now extinct North American tapir subgenus *Helicotapirus* (Ferrero & Noriega, 2007; Holanda & Ferrero, 2013; Hulbert, 2010), which may have originated from a South American ancestor rapidly after the GABI (Holanda & Ferrero, 2013; Hulbert, 2010). Phylogenetically, *T. terrestris* is most closely related to *T. pinchaque*, having diverged approximately 2–4 Mya (Ruiz-García et al., 2016, 2012; Steiner & Ryder, 2011). These two sister taxa exhibit extensive morphological differences, despite sharing a more recent common ancestor than *T. bairdii* and *T. terrestris* (Cozzuol et al., 2013; Ruiz-García et al., 2016, 2012; Steiner & Ryder, 2011). The similarity between the long bones of *T. terrestris* and *T. bairdii* may be explained by other biotic and abiotic factors (e.g. body mass, habitat), although common ancestry cannot be entirely ruled out as an influencing factor. Populations of *T. bairdii* and *T. terrestris* are known to occur in similar habitats in their respective geographical ranges, with some sympatric populations in upland forest regions of Colombia (González-Maya et al., 2012; Padilla et al., 2010; Ruiz-García et al., 2012). We therefore conclude that these two species exhibit similarities in their stylopodium and zeugopodium due to influences of phylogenetic relatedness (common ancestry), behaviour (comparable habitat use) and comparable body size. However, factors affecting the dissimilarity in scapular shape between *T. terrestris* and *T. bairdii* are less easy to determine, and may be influenced by phylogenetic separation. Investigations into the forelimb osteology of extinct South American tapirs most closely related to *T. terrestris* (e.g. *T. cristatellus*, *T. rondoniensis*) may reveal whether phylogenetic relatedness is a factor influencing the divergence in scapular morphology between *T. terrestris* and *T. bairdii*. An increased sample size may reveal more subtle variations between these two misclassified species. Small sample sizes in highly disparate *a priori* groups is not as problematic as it is for morphologically similar groups. Increasing the sample size for groups that are more frequently misclassified may increase the power of the analyses, and increase accurate classification (Brennan, Buchanan, Schick, & Herman, 1991; Davis & McHorse, 2013; Lachenbruch, 1968). This represents an intrinsic limitation for our study.

Conclusions

Modern tapirs exhibit interspecific differences in the bone morphologies in their upper forelimb skeleton. The scapula exhibits the greatest degree of interspecific variation, and is revealed as the most diagnostic bone in the upper forelimb (using a stepwise discriminant function analysis of three-dimensional landmark data). Our study corroborates all previous analyses comparing the Malayan (*T. indicus*) and lowland (*T. terrestris*) tapirs: *T. indicus* not only possesses the largest bones of the extant tapirs, but also exhibits a suite of osteological features associated with higher limb loading. Key morphological differences between tapirs revealed in this study centre around the mountain tapir (*T. pinchaque*). The morphological features of the scapula that discriminate *T. pinchaque* (large supraspinous fossa, posteroventrally positioned scapular spine) are unique within modern ungulates. This species also possesses long humeri, radii and ulnae compared to its more massive neotropical relatives (e.g. *T. terrestris* and *T. bairdii*). All these adaptations hint at subtly different locomotion styles in extant tapirs. Acquisition of comparative data on autopodial bones (carpals, metacarpals and phalanges) will be the next step in further understanding differences in locomotor morphology between modern tapirs.

“Change is hard - you can either
run from it, or learn from it”

- Rafiki -

– RESEARCH CHAPTER TWO –

Interspecific variation in the tetradactyl manus of modern tapirs (Perissodactyla: *Tapirus*) exposed using geometric morphometrics

Jamie A. MacLaren - Sandra Nauwelaerts

adapted from *Journal of Morphology*
(2017) 278**(11)**:11517-1535

The distal forelimb (autopodium) of quadrupedal mammals is a key morphological unit involved in locomotion, body support and interaction with the substrate. The manus of the tapir (Perissodactyla: *Tapirus*) is unique within modern perissodactyls, as it retains the plesiomorphic tetradactyl (four-toed) condition also exhibited by ancestral tapirs, equids and rhinoceroses. Tapirs are known to exhibit anatomical mesaxonic symmetry in the manus, although interspecific differences and biomechanical mesaxony has yet to be rigorously tested. Here, we investigate variation in the manus morphology of four modern tapir species (*Tapirus indicus*, *T. bairdii*, *T. pinchaque* and *T. terrestris*) using a geometric morphometric approach. Autopodial bones were laser scanned to capture surface shape and morphology was quantified using 3D landmark analysis. Landmarks were aligned using Generalised Procrustes Analysis, with discriminant function and partial least square analyses performed on aligned coordinate data to identify features that significantly separate tapir species. Overall, our results support the previously held hypothesis that *T. indicus* is morphologically separate from neotropical tapirs; however, previous conclusions regarding function from morphological differences are shown to require reassessment. We find evidence indicating that *T. bairdii* exhibits reduced reliance on the lateral fifth digit compared to other tapirs. Morphometric assessment of the metacarpophalangeal joint and the morphology of the distal facets of the lunate lends evidence towards high loading on the lateral digits of both the large *T. indicus* (large body mass) and the small, long limbed *T. pinchaque* (ground impact). Our results support other recent studies on *T. pinchaque*, suggesting subtle but important adaptations to a compliant but inclined habitat. In conclusion, we demonstrate further evidence that the modern tapir forelimb is a variable locomotor unit with a range of interspecific features tailored to habitual and biomechanical needs of each species.

Introduction

Modern tapirs (Tapiridae; *Tapirus* Brünnich) are enigmatic, forest-dwelling representatives of the order Perissodactyla (odd-toed ungulates) (Cozzuol et al., 2013; Ruiz-García et al., 2012; Steiner & Ryder, 2011). In addition to equids (horses, asses and zebras) and rhinoceroses, tapirs represent the last members of a formerly highly speciose order of small to very large herbivores (Janis, 1989; Norman & Ashley, 2000). The tetradactyl (four-toed) manus of the modern tapir is a unique feature in extant perissodactyls, with equids and rhinoceroses having reduced their functional digit number to one and three respectively (MacFadden, 1992a); the earliest ancestors of rhinoceroses, tapirs and equids also displayed a tetradacyl manus (Holbrook, 2001). The small, basal members of the Perissodactyla (e.g. *Propalaeotherium*, *Hyracotherium*, *Heptodon*) are interpreted as forest-dwelling browsers with a 'primitive' digital condition, bearing three toes on the hind foot (tridactyly) and four on the forefoot (Hellmund, 2005; Holbrook, 2001; Radinsky, 1965b; Wood et al., 2011). This plesiomorphic characteristic of the tapir manus, among other features of tapir anatomy, has contributed to the traditional interpretation of tapirs as 'living fossils' (Hershkovitz, 1954; Janis, 1984; Padilla et al., 2010; Schoch, 1989). Consequently, extant tapirs have been the object of numerous morphological and ecological comparisons to extinct tetradactyl perissodactyls (including Radinsky 1965; Janis 1984; Holbrook 2001, 2009). However, these studies often treat *Tapirus* either as a single morphological unit (e.g. Holbrook 1999, 2001), or compare only one or two species of *Tapirus* with extinct tetradactyl perissodactyls (e.g. Simpson 1945; Radinsky 1965). Recent studies on the extinct tapirs of North America increased species counts for comparative analyses, albeit with predominantly qualitative techniques (Holanda, Ribeiro, & Ferigolo, 2012; Hulbert, 1995, 2005, 2010; Hulbert, Wallace, Klippel, & Parmalee, 2009). Using *Tapirus* as a solitary morphological unit is greatly beneficial for phylogenetic comparisons with more basal tapiromorph perissodactyls, e.g. *Lophiodon* (Holbrook, 2009) and *Colodon* (M. W. Colbert, 2005), as it does not require exhaustive character comparisons across all species of tapir through time. However, to test evolutionary questions on the functional morphology of the postcranial skeleton in basal, tetradactyl perissodactyls, a comprehensive understanding of limb variation in their modern relatives is essential. One such question concerns the true axis of symmetry in the mesaxonic autopodium.

Perissodactyls, including tetradactyl, tridactyl and monodactyl taxa, possess mesaxonic symmetry in their manus (Klaits 1972); the axis of symmetry passes through the third digit. The term 'mesaxonic' has been used to describe autopodia in a variety of tetrapod groups. Anatomical and morphometric studies determine a mesaxonic autopodium to

exhibit a third digit that is longer than all the others, flanked by digits two and four, which are shorter than digit three but of comparable length to one another (J. C. Brown & Yalden, 1973a; Lockley, 2009; Rajkumar & Klein, 2014; Reghem, Byron, Bels, & Pouydebat, 2012; Tougard, Delefosse, Hänni, & Montgelard, 2001). Other studies approach the subject of mesaxony from a more functional and biomechanical standpoint, suggesting that mesaxonic symmetry is not exclusively defined by longer third digits, but that the central third digit is loaded most greatly during locomotion. Lateral digits are then loaded approximately equally (J. C. Brown & Yalden, 1973b; Holbrook, 2001; Klaits, 1972), with the third digit acting as the centre of rotation during lift-off of the foot (Klaits 1972). The first, anatomical definition of mesaxonic symmetry has been known to be true for perissodactyls for many years (Earle, 1893, 1896; Gregory, 1929; Simpson, 1945); the second, biomechanical interpretation has yet to be explored in all living perissodactyl groups. Understanding the comparative morphology of the manus in modern tapirs, which are known to exhibit anatomical mesaxonic symmetry, may reveal osteological evidence for variation in load application across the four manual digits that also support the biomechanical interpretation of mesaxonic symmetry. Unfortunately the majority of tapir postcranial research has centred on qualitative descriptions, with little by way of quantitative morphological investigation required for proper functional interpretations.

Previous qualitative studies of modern tapir postcranial morphology have revealed interspecific differences, almost exclusively between the lowland tapir (*T. terrestris* Linnaeus) and the Malayan tapir (*T. indicus* Desmarest) (Earle, 1893; Gregory, 1929). Results often align, with *T. indicus* shown to possess longer, heavier and more graviportally adapted limb elements compared to *T. terrestris* in all analyses (Earle, 1893; Hulbert, 1995; Osborn, 1929). In addition, *T. terrestris* has been stated to have a smaller lateral toe (fifth metacarpal) relative to tapirs of greater body size, e.g. *T. indicus*, *T. haysii* Leidy (Earle, 1893; Hulbert, 1995; Osborn, 1929). When interpreted functionally, the graviportal adaptations of the upper arm, carpus and the metacarpals in *T. indicus* have been suggested to imply greater loading on the forelimb, and in turn greater reliance on the lateral digits than the smaller *T. terrestris* (Earle, 1893). Many of these qualitative observations may have functional consequences and also associated changes in surrounding bones which have not yet been quantified.

Quantitative comparisons of tapir postcrania have recently been undertaken, with results suggesting that differences in both forelimb (MacLaren and Nauwelaerts 2016; Nauwelaerts et al. 2016) and hindlimb (Hawkins, 2011) morphology pertain to subtle variations in locomotor ecology across extant tapir species. These quantitative studies corroborate qualitative observations on the large Malayan tapir (*T. indicus*),

demonstrating that this species exhibits subtle adaptations to the upper forelimb bones consistent with increased necessity for gravitational support (MacLaren and Nauwelaerts 2016). The mountain tapir (*T. pinchaque* Roulin) has been shown to possess more gracile upper forelimb and lower hindlimb bones (MacLaren and Nauwelaerts 2016; Hawkins 2011), and morphological features pertaining to proximal shock absorption and increased stride frequency (MacLaren and Nauwelaerts 2016). The upper forelimb morphologies of the Baird's (*T. bairdii* Gill) and lowland (*T. terrestris*) tapirs have been shown to differ significantly from both *T. pinchaque* and *T. indicus*, despite presenting only subtle osteological differences from one another (corroborating qualitative observations of these species by Simpson 1945; MacLaren and Nauwelaerts 2016). From the results of the few quantitative studies on tapir limbs that have been performed, ecological conclusions have been drawn (Hawkins 2011; MacLaren and Nauwelaerts 2016; Nauwelaerts et al. 2016). Here, we present a quantitative assessment of the autopodium of extant tapirs to further our understanding of interspecific differences in the locomotor apparatus of modern tapirs.

Using results and interpretations from qualitative studies on the perissodactyl carpus and metacarpus, combined with recent quantitative results on tapir postcranial anatomy (Hawkins 2011; MacLaren and Nauwelaerts 2016), we will investigate several hypotheses concerning tapir autopodial variation. Firstly, we will quantitatively test the hypotheses presented by Earle (1893), Osborn (1929) and Simpson (1945), detailing differences in the morphology of the carpals and metacarpals between *T. indicus* and *T. terrestris*. Furthermore, due to its larger average body dimensions and mass (de Thoisy et al., 2014), we hypothesise that *T. indicus* will display shape differences in keeping with greater loading on the autopodium compared to all other extant species across all autopodial bones. Recent work on the limb morphology of modern tapirs has shown distinct morphological differences between the mountain tapir (*T. pinchaque*) and other neotropical tapirs (Hawkins, 2011; MacLaren & Nauwelaerts, 2016); in keeping with these results, we predict significant differences in the autopodial anatomy of *T. pinchaque* relative to other neotropical tapirs. Finally, we hypothesise that mean average carpal and metacarpal shapes for *T. terrestris* and *T. bairdii* will not show significant differences, based on results from both qualitative (Simpson 1945) and quantitative (MacLaren and Nauwelaerts 2016) studies. By testing these hypotheses, we aim to shed light on potential differences in the mesaxonic manus of modern tapirs (Klaits 1972), and infer biomechanical outcomes based on any variation revealed. We will use discriminant function analyses to identify features of the autopodium that contribute to accurate discrimination between species, and aim to formulate functional interpretations from these discriminant features.

Material and Methods

Specimens

As study material, 22 disarticulated forelimbs (dry bones) of tapirs were collected from museums in Europe and the USA (Appendix II, Section 1 and 2). Four species of modern tapir (*Tapirus terrestris*, *T. pinchaque*, *T. bairdii* and *T. indicus*) were collected for analysis, with multiple specimens accounting for intraspecific variation. Whenever possible, morphologically mature specimens were scanned (adult; Appendix II, Section 1), as defined by the complete ossification of the epiphyses, including the scapular cartilage (Liebich et al., 2007; Simpson, 1945). Specimens without fully ossified dorsal borders (sub-adult; Appendix II, Section 1) were also included to maintain viable specimen counts for statistical analyses. Sexual dimorphism has been described as non-significant for morphological comparisons in tapirs, and therefore was not considered as a limiting factor for specimens (Simpson 1945). Seven carpals and all four metacarpals were included in the study (Figure 2.1). Trapezium, sesamoids and phalanges were not included in this study due to poor sample sizes for these elements. The bones were split into three groupings: the proximal carpal row, distal carpal row, and metacarpals. The proximal row included the pisiform (*accesorium*), cuneiform (*ulnare*), lunate (*intermedium*) and scaphoid (*radiale*). The distal row included the trapezoid (*carpale II*), magnum (*carpale III*) and unciform (*carpale IV*). The trapezium (*carpale I*) was observed in the juvenile *T. indicus* after dissection and is known to be exhibited in living perissodactyls, although with little consistency (Constantinescu et al., 2012); the trapezium was omitted from this analysis as few scanned specimens had the bone readily preserved and available for study. All available metacarpals (MCII, MCIII, MCIV, MCV) were included in the analysis (Figure 2.1).

A dissection was performed on the limbs of a juvenile *Tapirus indicus* to supplement functional interpretations from published tapir osteology and myology (Campbell, 1936; Murie, 1871; Pereira, 2013). The juvenile tapir was provided by the Royal Zoological Society of Antwerp (KMDA). Muscular and ligamentous attachment sites available from the dissection and published literature assisted in the identification of osteological features and interpreting functional outcomes. Veterinary accounts of equid and rhinocerotid osteology and myology (Yalden 1971; Barone 2000; Budras et al. 2003; Liebich et al. 2007; Constantinescu et al. 2012; Clayton et al. 2013) were used where necessary to assist identification and interpretations.

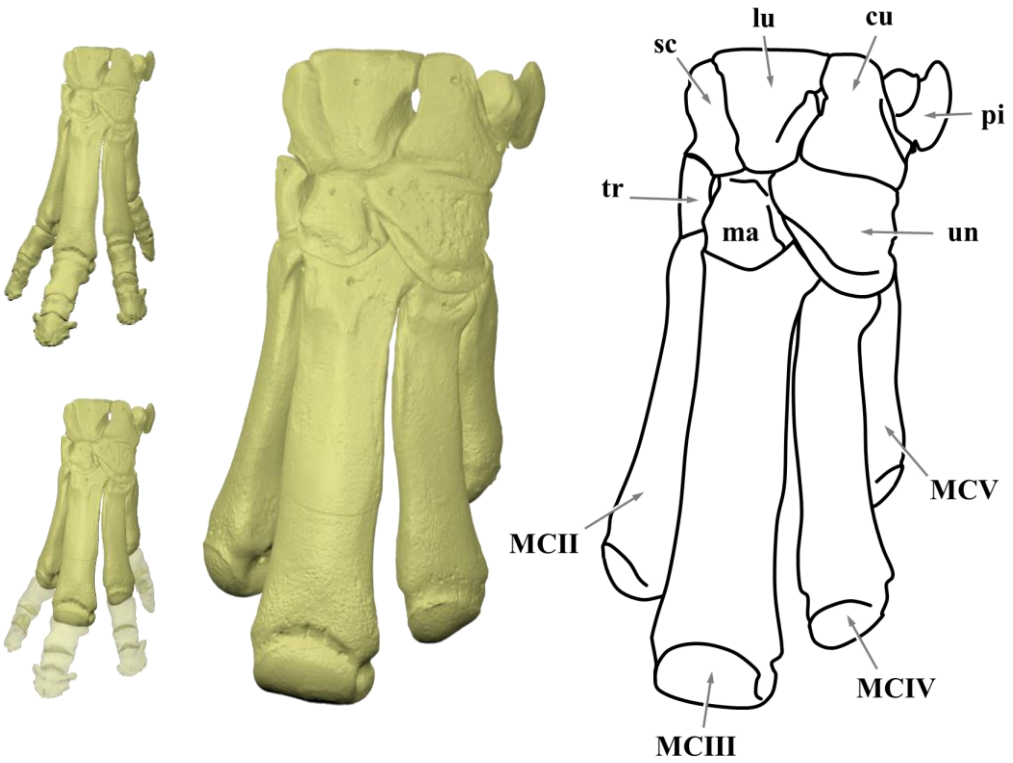

Figure 2.1. Bones of the tapir autopodium. Fully articulated left forefoot (based on scans of RMNH 43495), with enlarged autopodium representing bones used in this study: **sc** = scaphoid; **lu =** lunate; **cu** = cuneiform; **pi** = pisiform; **tr** = trapezoid; **ma** = magnum; **un** = unciform; **MCII** = second metacarpal; **MCIII** = third metacarpal; **MCIV** = fourth metacarpal; **MCV** = fifth metacarpal.

Scanning

The disarticulated carpus and metacarpals from one forelimb of each specimen were laser scanned using a FARO ScanArm Platinum V2 system with integrated FARO Laser Line Probe (up to 50 μm resolution). Bones were balanced on supports positioned on regions of the specimen surface on which landmarks could not be placed (e.g. shaft of metacarpal). A three-dimensional virtual point cloud was produced for each autopodial bone, visualised in GeoMagic (GeoMagic Qualify v.10, Morrisville, NY, USA). Any

outlying surfaces in the point clouds (e.g. incidental scanning of support structures) were digitally removed to focus only on surface information from the bones. Point clouds were then converted into polygon-based surface models, ranging in detail from 200k to 500k polygons, dependent upon bone and the detail necessary around articular surfaces.

Geometric Morphometrics

Landmark-based geometric morphometrics has been extensively used and is an appropriate technique for quantifying differences in shape between three-dimensional objects (Gould, 2014; Rohlf & Slice, 1990). The technique is based on selection of a series of discrete, biologically or operationally homologous points (landmarks) placed onto a succession of objects (Zelditch et al., 2012). Type II landmark points (representing maxima and minima) were used in this study to define the shape of the carpals and metacarpals. Landmark placement on representative bones in this analysis are visualised in Figure 2.2 (carpals) and Figure 2.3 (metacarpals). To aid in the description of discriminant features, landmarks were annotated with subscript denominations pertaining to the bone the landmark describes (as in MacLaren and Nauwelaerts 2016) (Appendix II, Section 3: Table S2.1). Surface models were imported into Landmark Editor v.3.0 software (Wiley et al., 2006) for three-dimensional landmark application. Raw landmark coordinates were then exported into MorphoJ v1.06d (Klingenberg, 2011) and aligned using Generalised Procrustes Analysis (GPA). This technique removed the effect of size, location and orientation and aligned raw coordinate configurations based on geometric centre (centroid), minimising inter-landmark distance (D. C. Adams, Rohlf, & Slice, 2004; Rohlf & Slice, 1990; Zelditch et al., 2012). Resultant Procrustes coordinates and centroid sizes were then exported into SPSS v.23 (IBM Corp. 2013) for discriminant analyses and post-hoc testing. Centroid size represents an intrinsic size measure that can be used to scale a configuration of landmarks, for example to assess metric distances between landmarks. Centroid sizes for adult specimens were retained for size comparisons. A multivariate analysis of variance (MANOVA) was performed on the Procrustes coordinates calculated for each bone. MANOVA was used to test differences in the means of the groups (species), and the observed power of our MANOVA using small sample sizes was retrieved from the analysis. The MANOVA and power analysis was performed in SPSS v.23.

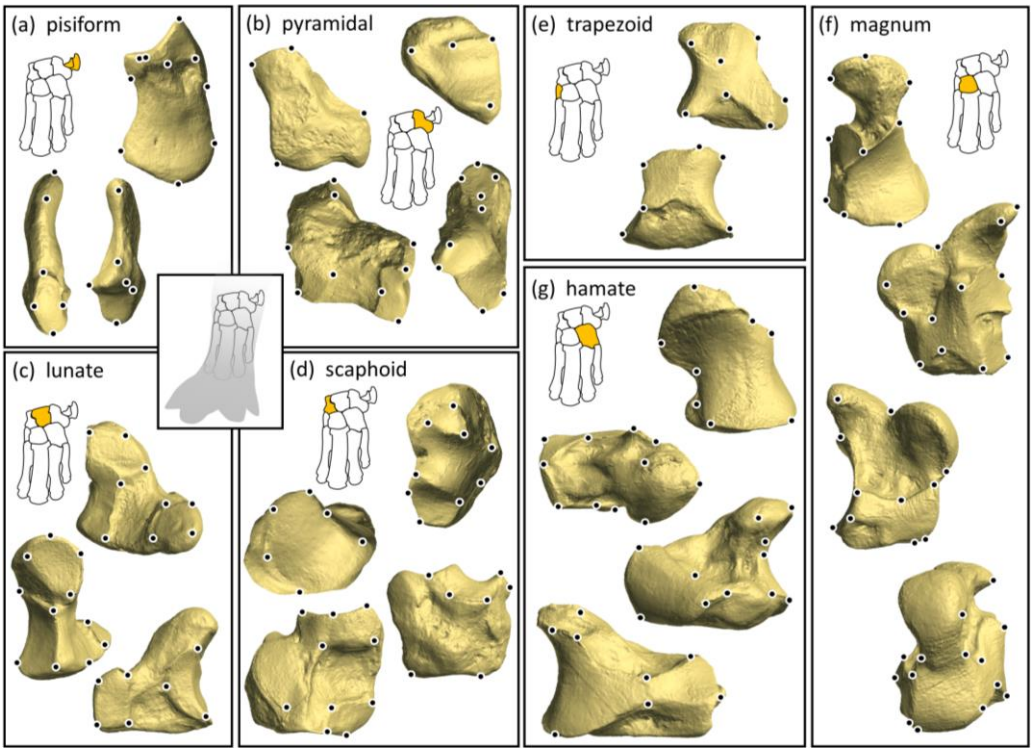

Figure 2.2. Landmark placement on the seven bones of the tapir carpus. Proximal row **(a)** – **(d)** and distal row **(e)** – **(g)**. Carpus position in the foot depicted within the grey outline (left). Position of the bone in the carpus relative to other elements demonstrated on each autopodium diagram (orange bone). Specific landmark denomination for each bone can be found in Supplementary Information 3. Representative bones from scans of MEO 2203a.

Discriminant Function Analysis

A discriminant function analysis (DFA) was performed on the Procrustes coordinates (x, y, z) for all bones. DFA was used to determine what combination of continuous variables for each bone best discriminated between the four species. DFAs were performed in SPSS v.23 (IBM Corp. 2013) using a forward step-wise method for Procrustes coordinate input; this removed independent variables that were not significant for discrimination. A classification table was produced by predicting group membership and cross-validating by jack-knifing the dataset. Sensitivity and specificity

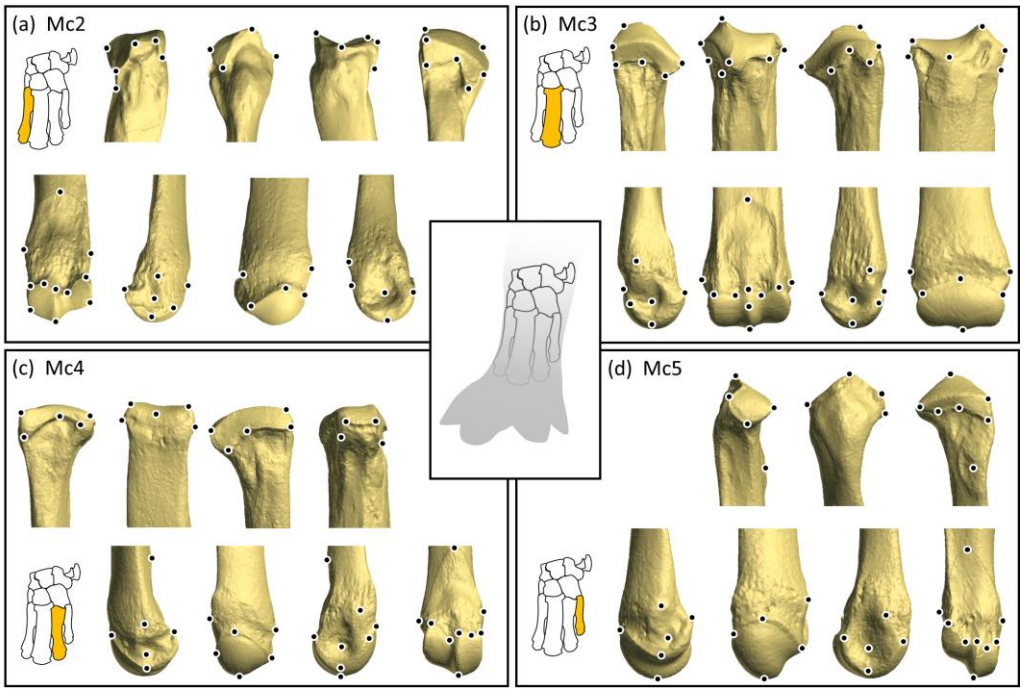

Figure 2.3. Landmark placement on the four tapir metacarpals. **(a)** metacarpal II, **(b)** metacarpal III, **(c)** metacarpal IV and **(d)** metacarpal V. Metacarpal position in the foot depicted within the grey outline. Position of each metacarpal relative to other bones portrayed in each autopodium diagram (orange bone). Specific landmark denomination for each bone can be found in Supplementary Information 3. Representative bones from scans of MEO 2204b.

tests were also performed. To assess differences in group means, we employed a multivariate analysis of variance with Wilk's lambda test statistic (0 – 1; 0 = highest likelihood of inequality, 1 = high likelihood of group means being equal). For visualisation of results, discriminant function plots were produced based on the first two discriminant functions (DF1 and DF2), which accounted for the highest percentage of variance. Territorial maps were added to demonstrate how groups were divided and where cut-off values were placed dependent on DF1 and DF2 scores. The third discriminant function accounted for between 0.3% and 11.6% of total variance; DF3 is reported in the results, but is not plotted in discriminant function plots. Cut-off values between groups were based on the weighted mean of the discriminant score for each group centroid. Classification tables and territorial maps were produced in SPSS v.23

(IBM Corp. 2013), and resultant discriminant function plots were configured in R Studio (R Core Development Team 2008).

Partial Least Squares (PLS) analysis

Within the carpal complex there are a variety of bones with multiple facets interacting with one another. Changes in morphology in one joint facet which may signal a shift in mechanical capabilities should correspond to similar changes in adjoining bones. In order to assess whether bones and joint facets covary in morphology with neighbouring carpals, we utilised a two-block partial least square analysis (2B-PLS) accompanied by a permutation test (10000 repetitions) to test for significance of covariance (Fadda & Corti, 2001; Rohlf & Corti, 2000). The RV coefficient of integration (multivariate generalisation of squared Pearson correlation coefficient; Klingenberg 2009) produced by PLS analyses is used to predict the degree of covariation between two blocks of data (in this case, landmark coordinates and facet areas). RV coefficient is measured between 0 (no covariation) and 1 (complete covariation)(Klingenberg, 2009). This analysis was used for adjoining carpals which demonstrated key features which both discriminated between species and pertained to possible biomechanical differences during locomotion. When area measurements were tested for covariance (as opposed to landmark coordinates) the raw area data were log-transformed prior to 2B-PLS analysis. The PLS analyses were performed in MorphoJ v1.06d (Klingenberg, 2011), with graphical representations compiled in R Studio (R Core Development Team 2008).

Joint Facet Comparisons

To compliment carpal shape differences detected using 3D landmark analysis, the relative areas of joint surfaces were also calculated. Variation in joint surfaces (facets) have been reported in tapirs through qualitative comparisons (Earle, 1893; Osborn, 1929; Simpson, 1945); here we used landmark analyses to detect differences in the shape of facets using only the landmarks that define the joint facet in question. In addition, we calculated relative areas of a series of joint surfaces of the scaphoid, lunate and unciform to quantify previous qualitative claims about interactions between carpals within the autopodium (Earle 1893; Osborn 1929; Simpson 1945; Klaits 1972). We identified and tested two inter-carpal facet relationships: the distal lunate facet ratio (highlighted by Earle 1893) and the unciform-magnum facet ratio (again pertaining to the lunate, Osborn 1929; Simpson 1945). The distal lunate possesses two large facets: anteriorly the unciform facet and posteriorly the volar magnum facet. The anterior magnum facet is found alongside the unciform facet. In the densely packed carpus, a relatively larger facet intuitively implies greater loading rather than greater mobility,

with a larger surface area available for force transmission. The three-dimensional scans of the carpal bones provided smooth articular surfaces for quantitative comparison between carpals. Facet areas were calculated by pruning the full 3D laser scans of bones until only the joint facet under study remained; this was performed in GeoMagic Qualify v.10 (Morrisville, NY, USA). These reduced surface scans were then imported into MeshLab (Cignoni et al., 2008) to calculate surface areas. Ratios were formulated by dividing the posterior or anterior magnum facet area (whichever was appropriate) by the combined total of the unciform joint facet and the respective magnum facets. To test for covariation between the joint facets of the distal lunate (both between anterior unciform-magnum and posterior unciform-magnum), a two-block partial least square analysis (2B-PLS) was performed on the log-transformed area data. 2B-PLS analyses and 10000 permutations were performed in MorphoJ v1.06d (Klingenberg, 2011).

Distal Metacarpophalangeal Facet Variation

The distal metacarpal shape was further investigated using a subset of landmarks to test for interspecific differences exclusively in the distal joint surface. Eight landmarks, homologous for all four metacarpals across tapir species, were selected, describing the palmar distal joint facet (metacarpophalangeal joint). In order to test for differences concurrently between both metacarpals and species, a Procrustes ANOVA was performed in MorphoJ. This analysis was used to complement and inform functional interpretations of morphological changes in the distal metacarpals pertaining to interactions with the proximal phalanges (pastern) and the proximal sesamoids.

Results

Overall, discriminant functions successfully discriminated between the four extant species of tapir for all autopodial bones. Jack-knifed classification tables for all bones in the autopodium are presented in Table 2.1, reporting sensitivity and specificity of the analyses. Accuracy of jack-knifed species classification for autopodials exceeded 75% accuracy for all cases. *T. indicus* is classified 100% accurately for all carpal bones, whereas *T. terrestris* is the most frequently misclassified species (six different bones). *T. bairdii* is the most accurately classified neotropical tapir, with only the cuneiform demonstrating inaccuracy in classification (Table 2.1). Power analyses revealed high statistical power for all MANOVAs (mean power = 0.88 ± 0.08); full tabulated results can be found in Appendix II, Section 4: Table S2.2. We are therefore confident in the power of this analysis and the morphological differences between the taxa. Here, we describe results of discriminant function analysis for all autopodials (proximal carpal

row, distal carpal row, and metacarpals). Descriptions of landmarks affecting discrimination can be found in Appendix II.

Proximal Carpal Row

The proximal carpal row (scaphoid, lunate, cuneiform and pisiform; Figure 2.1) contains the bones that interface with the radius and ulna; the scaphoid, lunate and cuneiform also articulate with the distal carpal row. Interspecific classification in the proximal carpal row ranges from 100% accuracy (scaphoid) to 75% accuracy (cuneiform) (Figure 2.4), with bones that articulate with the radius (scaphoid and lunate) showing more accurate classification than those articulating with the ulna

---

Table 2.1. Jack-knifed classification accuracy for autopodial specimen assignments from linear discriminant analysis. Specificity of classification for each bone are presented alongside % accuracy following jack-knifing the dataset.

Bone	**Specificity**				**% accuracy**
	T. bairdii	*T. indicus*	*T. pinchaque*	*T. terrestris*	
Pisiform	1.00	1.00	1.00	0.80	**94.7**
Cuneiform	0.60	1.00	0.75	0.60	**75.0**
Lunate	1.00	1.00	1.00	0.80	**95.0**
Scaphoid	1.00	1.00	1.00	1.00	**100**
Trapezoid	1.00	1.00	1.00	1.00	**100**
Magnum	1.00	1.00	0.67	1.00	**95.2**
Unciform	1.00	1.00	1.00	1.00	**100**
MCII	1.00	1.00	1.00	1.00	**100**
MCIII	1.00	1.00	1.00	1.00	**100**
MCIV	1.00	1.00	0.75	0.83	**90.9**
MCV	1.00	1.00	1.00	0.83	**95.5**

(cuneiform and pisiform) (Table 2.1). Here we present results for discriminant function analysis on the bones of the proximal carpal row:

Scaphoid – The scaphoid is the largest carpal of the tapir proximal carpal row, and articulates proximally with the radius, medially with the lunate, and distally with the magnum, trapezoid and in some cases the trapezium. The first two discriminant functions (DF1 and DF2) based on scaphoid landmarks account for 97.9% of variance (Appendix II, Figure S2.1a). The features that most greatly influence accurate species

classification include the anteroposterior morphology of the palmar lunate facet ($_{sc}$Lm 20), and the upper margin of the trapezoid-magnum facet, defined by $_{sc}$Lm 11. *T. bairdii* shows the greatest distinction in scaphoid morphology from other tapirs. In *T. bairdii*, $_{sc}$Lm 11 is placed more distally and $_{sc}$Lm 20 is more posterior than in other species. Average species centroid sizes for the scaphoid show that *T. indicus* possess the largest scaphoid, with *T. pinchaque* displaying the smallest (Table 2.2).

Lunate – The lunate, or semi-lunar, represents the central carpal in the proximal carpal row. The proximal surface articulates with the radius, medially and laterally it articulates with the scaphoid and cuneiform respectively. Distally the lunate has three articular facets: one to the unciform and two to the magnum (one dorsal, one palmar). Discriminant function 1 accounts for 93.1% of variation (Figure S1b); interspecific discrimination along DF1 is most greatly influenced by placement of $_{lu}$Lm6, the edge of the palmar magnum facet closest to the dorsal facet. Dorsal deflection and elongation of this facet in *T. indicus* brings the distal lunate facets into closer proximity to each other. Proximodistal expansion of the entire dorsal surface of the lunate is observed along DF2 between neotropical taxa (Figure S1b), driven by placement of $_{lu}$Lms 3 and 18. Average centroid sizes differ to those of the scaphoid, revealing *T. indicus* to possess the largest lunates and *T. terrestris* the smallest (Table 2.2).

Cuneiform – The cuneiform, pyramidal or ulnar carpal, is the most lateral bone in the proximal carpal row; it articulates proximally with the pisiform and ulna, medially with the lunate, and distally with the unciform (Figure 2.1). The cuneiform is the most poorly discriminated bone in the autopodium, with one in four bones being misclassified (Figure 2.4). The first two discriminant functions describe 92.4% of total variance (Appendix II, Figure S2.1c). One or more specimens of all neotropical species are misclassified as *T. indicus*, with additional misclassification between *T. bairdii* and *T. terrestris*; the first discriminant function successfully separates only *T. pinchaque* from the other species (Appendix II, Figure S2.1c; also Section 5, Table S2.3). The most discriminatory feature is the shape of the mediodistal facet articulating with the lunate ($_{cu}$Lm 3); the orientation of the cuneiform (defined by $_{cu}$Lm 3 and 4) also contributes to successful discrimination of *T. pinchaque*. Average centroid sizes for the cuneiform show a similar pattern to that of the scaphoid, with *T. indicus* displaying the largest and *T. pinchaque* the smallest cuneiform carpals (Table 2.2).

Pisiform – The pisiform, or accessory carpal, is the most palmar bone in the carpus and facilitates the passage of flexor tendons through the carpal tunnel. The pisiform articulates distally with the cuneiform and proximally via two facets with the ulna. The first two discriminant functions describe 89.1% of variance, with each species

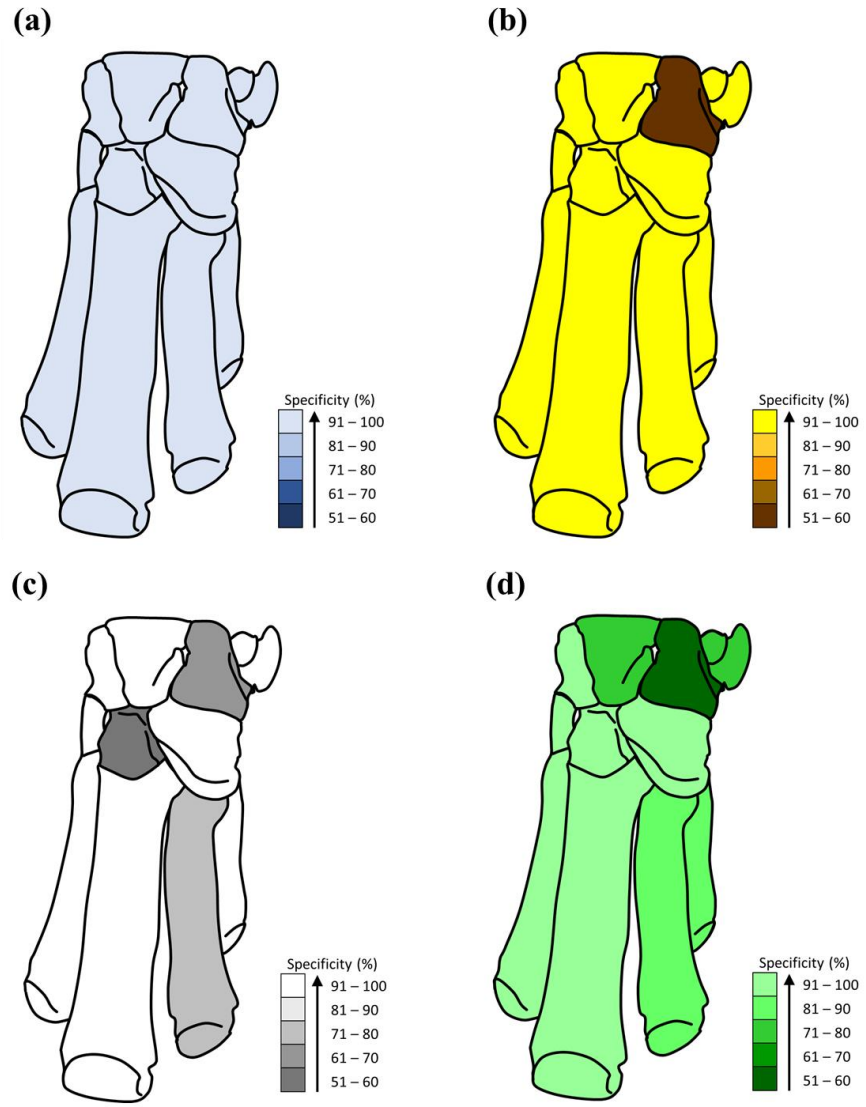

Figure 2.4. Specificity of autopodial discrimination across four tapir species. From top left: **(a)** *Tapirus indicus*; **(b)** *T. bairdii*; **(c)** *T. pinchaque*; **(d)** *T. terrestris*. Bones of the autopodium shaded to represent the accuracy of classification from Linear Discriminant Analysis. Darker colours represent lower % specificity, with light colours representing high % accuracy of interspecific discrimination. *T. indicus* demonstrates 100% classification accuracy; the cuneiform represents the bone most frequently misclassified across neotropical taxa.

occupying a discrete region of canonical variate-space (Appendix II, Figure S2.1d). Placement of $_{pi}$Lm 4 (distal extremity of ulnar facet) shows variation along DF1, with *T. indicus* displaying a distinct morphology from *T. bairdii*. DF2 discriminates between *T. terrestris* and *T. pinchaque* with the placement of $_{pi}$Lm12 (accessory ulnar facet) discriminating between these two taxa. As with the scaphoid and cuneiform, *T. indicus* demonstrates the largest centroid sizes for the pisiform, and *T. pinchaque* the smallest centroid size (Table 2.2).

Distal Carpal Row

The distal carpal row (trapezoid, magnum, unciform) is the most successfully classified group of autopodials (mean classification accuracy = 98.4%). Within this grouping, both the trapezoid and unciform achieved 100% interspecific classification, whereas the magnum was classified with 95.2% accuracy. Graphical results are presented in Appendix II, Figure S2.2.

Trapezoid – The trapezoid, or second carpal, is the second smallest carpal in the tapir carpus (after the trapezium, which was not investigated here). It has a proximal articulation with the scaphoid, a lateral facet for the magnum, a distal facet for the second metacarpal (MCII) and a small medial facet for articulation with the trapezium (first carpal; not available in all specimens and therefore not included in the analysis). The first discriminant function accounts for 93.6% of interspecific variation, and successfully discriminates the four taxa (Appendix II, Figure S2.2a). Separation along this function is influenced by the landmarks describing the palmar region ($_{tr}$Lm 7) and the laterodistal margin ($_{tr}$Lm 10) of the of the magnum facet. The difference in the magnum facet morphology is greatest between *T. bairdii* and *T. indicus*. The centroid size for the trapezoid mirrors that of the scaphoid, cuneiform and pisiform (Table 2.2).

Magnum – The magnum, capitate or third carpal, is the central carpal of the tapir autopodium. The magnum articulates proximally with the scaphoid and lunate (via two facets), proximolaterally with the unciform, medially with the trapezoid and distally with a small facet for the second metacarpal (MCII) and a large facet for the third metacarpal (MCIII). The first discriminant function accounts for 95.8% of magnum variation (Appendix II, Figure S2.2b). *T. indicus* and *T. bairdii* are the most easily discriminated taxa along DF1; however, specimens of *T. pinchaque* and *T. terrestris* are misclassified along DF1. Landmarks that most heavily influence interspecific discrimination along DF1 include $_{ma}$Lm 7 (expansion-contraction of the unciform facet) and $_{ma}$Lm 15 (defining the concavity of the dorsal trapezoid facet). *T. bairdii* exhibits a highly concave trapezoid joint plane. The volar process (palmar projection of the

magnum for attachment of the superficial interossei) demonstrates a large degree of variation between *T. indicus* and *T. bairdii* ($_{lu}$Lms 16 and 17). As with the majority of the carpals (excluding the lunate), *T. indicus* displays the largest average magnum centroid size and *T. pinchaque* exhibits the smallest (Table 2.2).

Unciform – The unciform, hamate or fourth carpal, is the largest carpal in the distal carpal row; it articulates proximally with the lunate and cuneiform, medially with the magnum, and distally with the third, fourth and fifth metacarpals (MCIII, MCIV and MCV). The first two discriminant functions describe 88.4% of total variance (Appendix II, Figure S2.2c). The placement of taxa along DF1 is greatly affected by $_{un}$Lm 3 (lateral morphology of the MCV joint facet) and $_{un}$Lm 10 (anteroposterior expansion or constriction of the lunate facet). *T. indicus* displays an expanded lunate-cuneiform facet relative to neotropical taxa. DF2 (32.9%) is most greatly influenced by $_{un}$Lm 8, which tracks a relative expansion of the medial edge of the cuneiform facet. DF2 is also influenced by $_{un}$Lm 5, which describes the antero-posterior constriction (*T. bairdii*) and expansion (*T. indicus* and *T. pinchaque*) of the MCIV facet, and by extension the entire distal unciform. The average centroid size is once again greatest in *T. indicus* and smallest in *T. pinchaque* (Table 2.2).

Metacarpals

Overall results for the metacarpals (MCs) suggest that the lateral bones exhibit marginally less interspecific variation than the medial metacarpals. MCs II and III were classified 100% accurately after jack-knifing, whereas MCIV and MCV exhibited occasional misclassification. Centroid sizes for the metacarpals do not follow the same pattern as in the carpals.

Metacarpal II – Metacarpal II (MCII), or the second metacarpal, is the most medial hand bone in the tapir autopodium. It has a proximal articulation with the trapezoid and trapezium (absent in this analysis), a lateral articulation with MCIII, and a distal articular facet for the proximal phalange II and proximal sesamoids. DF1 accounts for 99.8% or variation, with *T. indicus* greatly separated from the neotropical taxa (Appendix II, Figure S2.3a). Separation along DF1 is heavily influenced by the placement of $_{2}$Lm 26 (palmar margin of trapezoid facet), and also $_{2}$Lms 4 and 5, which describe the morphology of the proximolateral sesamoid joint facet, in addition to affecting the dorsopalmar depth of the metacarpal head. The largest average centroid size for the MCII is found in *T. indicus*, with the smallest exhibited by *T. terrestris. T. pinchaque* exhibits the second largest MCII centroid size (Table 2.2).

Table 2.2. Average centroid sizes per species for each bone in the autopodium. Mean average and standard deviation are reported for each species. Centroids based on full adult specimens (excluding sub-adults), with number of adult specimens for each bone also listed (*n*).

Bone		***T. bairdii***	***T. indicus***	***T. pinchaque***	***T. terrestris***
Pisiform	mean	54.73 ± 5.6	64.46 ± 3.3	51.42 ± 5.6	53.55 ± 3.3
	n	*3*	*5*	*3*	*5*
Cuneiform	mean	59.48 ± 1.5	64.81 ± 1.2	54.65 ± 2.4	55.59 ± 5.1
	n	*3*	*6*	*3*	*5*
Lunate	mean	74.09 ± 2.1	83.86 ± 3.0	69.67 ± 1.0	68.40 ± 7.1
	n	*3*	*6*	*3*	*5*
Scaphoid	mean	71.43 ± 2.7	86.83 ± 3.5	68.13 ± 3.5	69.24 ± 6.8
	n	*3*	*7*	*3*	*5*
Trapezoid	mean	37.52 ± 1.6	43.08 ± 2.1	32.28 ± 0.4	34.41 ± 2.4
	n	*3*	*4*	*3*	*5*
Magnum	mean	76.50 ± 0.7	87.01 ± 3.0	70.90 ± 1.3	74.15 ± 4.7
	n	*3*	*7*	*3*	*6*
Unciform	mean	71.61 ± 2.0	79.44 ± 2.8	66.00 ± 0.5	69.52 ± 5.5
	n	*3*	*6*	*3*	*5*
MCII	mean	214.74 ± 9.5	228.14 ± 3.7	218.25 ± 9.5	214.27 ± 9.2
	n	*3*	*7*	*3*	*6*
MCIII	mean	256.57 ± 15	272.32 ± 7.4	263.21 ± 7.9	256.65 ± 11
	n	*3*	*7*	*3*	*6*
MCIV	mean	202.86 ± 11	218.12 ± 7.0	202.33 ± 7.3	202.03 ± 11
	n	*5*	*7*	*3*	*6*
MCV	mean	124.66 ± 5.3	153.21 ± 4.4	130.82 ± 4.3	131.20 ± 9.8
	n	*3*	*7*	*3*	*6*

Metacarpal III – Metacarpal III (MCIII), or the third metacarpal (cannon bone) is the largest metacarpal in the tapir autopodium. Proximally it articulates with the magnum and unciform, proximomedially with MCII and proximolaterally with MCIV; MCIII articulates distally with the proximal sesamoids and proximal phalange III. The first two discriminant functions account for 92.0% of variation (Appendix II, Figure S2.3b). Landmarks that contribute most greatly to interspecific classification along DF1 include $_3$Lm 19 (proximodistal depth of the magnum facet) and $_3$Lm 23 (palmar edge of the MCII joint facet). Classification along DF2 is dominated by $_3$Lm 17 (describing the breadth of the unciform joint facet). Average centroid size for MCIII suggests that *T. indicus* have the largest metacarpal; both *T. terrestris* and *T. bairdii* display very similar average centroid sizes, smaller than the other two species (Table 2.2).

Metacarpal IV – Metacarpal IV (MCIV), or the fourth metacarpal, is the intermediate metacarpal between the central third and lateral fifth. MCIV articulates with the unciform proximally, MCIII proximomedially and MCV proximolaterally; as with other metacarpals, MCIV distally articulates with the corresponding proximal phalange IV and paired proximal sesamoids. MCIV is accurately classified for 90.9% of specimens (Table 2.1), with the first discriminant function accounting for 94.8% of variation (Appendix II, Figure S2.3c). The landmarks which contribute most greatly toward interspecific discrimination describe the concave shape of the unciform facet ($_4$Lm 15) and the expansion-contraction of the medial margin of the metacarpophalangeal joint facet ($_4$Lm 8). The MCIVs of the neotropical tapirs show very similar average centroid sizes, with *T. terrestris* marginally displaying the smallest (Table 2.2); *T. indicus* exhibits the largest MCIVs.

Metacarpal V – The fifth metacarpal (MCV) is the most lateral hand bone, and the smallest metacarpal in the tapir autopodium. Proximally, MCV articulates with the unciform, proximomedially with MCIV, and distally with the proximal phalange V and paired proximal sesamoids. The first two discriminant functions account for 94.5% of interspecific variation. Along DF1, three morphotypes are separated (Appendix II, Figure S2.3d). Landmarks that display high loading on DF1 include those describing the morphology of the lateral sesamoid facet ($_5$Lms 3 and 5), which divides modern tapirs into three morphotypes (Appendix II, Figure S2.3d). *T. bairdii* displays a notably smaller average centroid size than other neotropical taxa, with *T. indicus* exhibiting the largest average centroid size for MCV (Table 2.2).

Metacarpophalangeal Facets

The palmar metacarpophalangeal joint of the tapir metacarpal comprises of three principal regions: the medial sesamoid facet, lateral sesamoid facet and metacarpal sagittal ridge. The subset of eight landmarks describe the proximopalmar margin of the metacarpophalangeal joint, incorporating the sesamoid facets and sagittal ridge. Results for the subset of eight landmarks for all four metacarpals demonstrated notable interspecific differences. Procrustes ANOVA results detected significant differences ($p < 0.01$) between individual species and between the four metacarpals in the morphology of the distopalmar metacarpal facet (Table 2.3).

Partial Least Squares analyses (*2B-PLS*)

Results from discriminant function analyses suggest bones along the medial autopodium (scaphoid, trapezoid and MCII) are most accurately discriminated across all tapir

Table 2.3. Procrustes ANOVA significance test results for subset of landmarks describing metacarpophalangeal facet of MCII, MCIII, MCIV and MCV across four tapir species. Bold values denote significant differences.

Variable	Sum of Squares	Mean Squares	df	F	Parametric p-value
Species	0.0839	0.001645	51	3.38	**<0.01**
Metacarpal	0.9891	0.019394	51	39.81	**<0.01**

species (Figure 2.4). To investigate specific articulations in the medial autopodium, 2B-PLS was performed between the trapezoid and magnum (examining the joint facet between the two bones) and the respective facet morphologies of the trapezoid and scaphoid. Overall 2B-PLS analyses between the trapezoid and magnum revealed a strong covariation in joint facet morphology (RV = 0.778), with high statistical significance from permutation test ($p < 0.001$). The first PLS axes account for over 80% of covariance between the bones (Figure 2.5c; Table 2.4), which is also highly significant following permutation testing ($p < 0.001$). Coordinates which most greatly influence covariation for PLS1 include $_{tr}$Lm8 (anterior concave edge of magnum facet), $_{ma}$Lm14 and $_{ma}$Lm15 (anterior and posterior concave margins of trapezoid facet).

The overall 2B-PLS analyses between the trapezoid and scaphoid shows modest covariation in joint facet shape (RV = 0.415), albeit with no statistical significance after permutation test ($p = 0.089$). The fist PLS axes account for over 60% of covariance between the bones (Figure 2.5d; Table 2.4), which does exhibit high statistical significance with permutation testing ($p = 0.005$). Procrustes coordinates which most greatly influence covariation for PLS1 include $_{tr}$Lm3, 4 and 6 (proximal extremities of both anterior and posterior margins), and $_{sc}$Lm11 and $_{sc}$Lm13 (anterior margin of trapezoid facet and deepest point on the concave facet for the trapezoid).

Joint Facet Ratios

Unciform–Magnum Facet Ratio (*HMF Ratio*) – The unciform-magnum facet ratios show a different pattern to that of the distal lunate facets. *T. pinchaque* displays the largest average anterior magnum facet, and shows a significant difference to *T. indicus* in the ratio of unciform to anterior magnum facets ($p = 0.014$; Table 2.5). *T. indicus* displays the greatest range of ratios, with one outlying specimen exhibiting a ratio

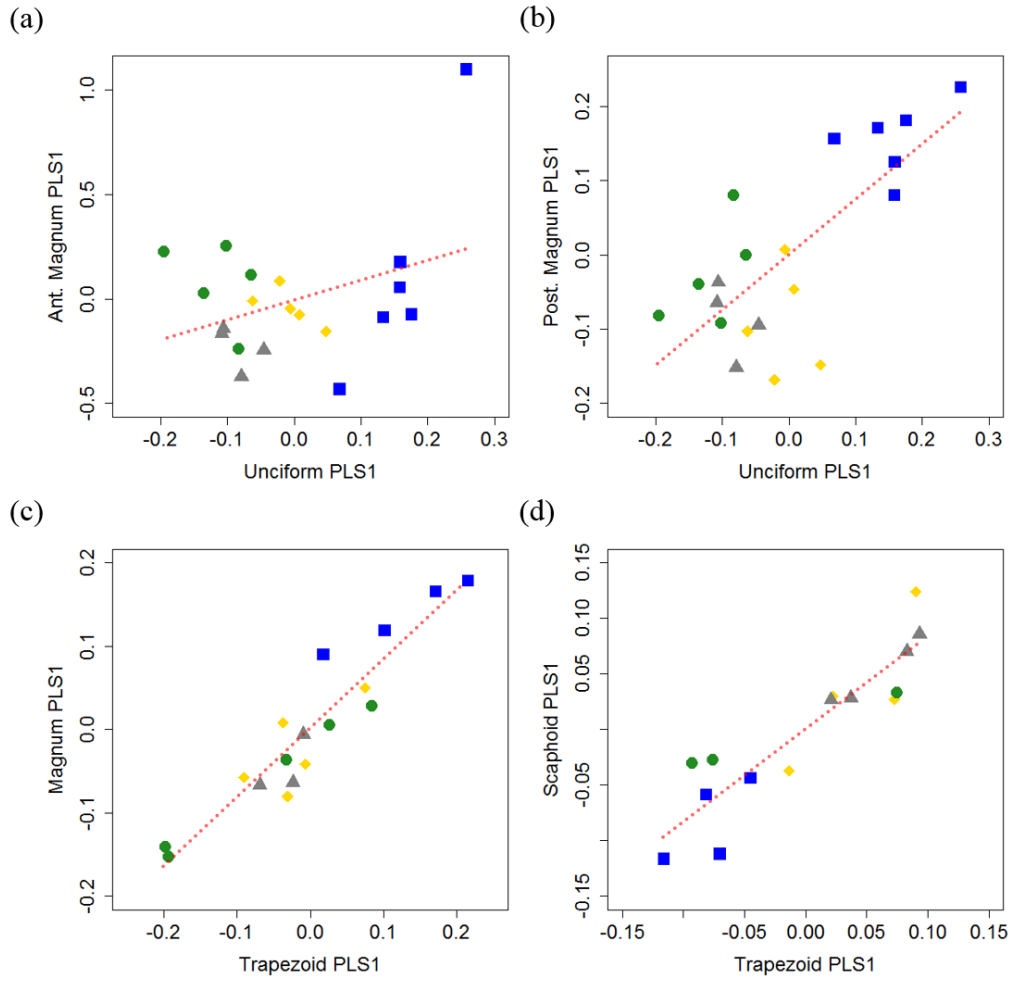

Figure 2.5. Results of 2B-PLS regression analyses comparing **(a)** unciform and anterior magnum facet area, **(b)** distal lunate facet areas, **(c)** trapezoid and magnum articulation facets, and **(d)** trapezoid and scaphoid articulation facets. Symbols: *Tapirus indicus* (squares), *T. bairdii* (diamonds), *T. pinchaque* (triangles) and *T. terrestris* (circles); dotted line denotes line of best fit for all data-points. Statistical data for these plots can be found in Table 2.4.

comparable to *T. pinchaque* (Figure 2.6). *T. indicus* displays no significant difference to *T. terrestris*, and *T. bairdii* and *T. terrestris* display similar HMF ratios. Covariation based on 2B-PLS analyses of the unciform and anterior magnum facet areas do not support covariation between these facets. PLS1 axes account for 100% of covariation;

however, PLS axes do not correlate highly (RV = 0.363) (Figure 2.5a; Table 2.4). Overall correlation is weak and not statistically significant after permutation (RV = 0.132; p = 0.117).

Distal Lunate Facet Ratio (*DLF Ratio*) – The comparison between the distal lunate facets (DLFs) show that there is a spectrum of variation across neotropical species (Figure 2.7). *T. bairdii* demonstrates the greatest difference between anterior and posterior distal facets (Figure 2.7), showing a significant difference to *T. terrestris* (Table 2.6) which exhibits the smallest difference between facet areas. *T. indicus* and *T. pinchaque* demonstrate near identical mean values for distal facet area ratios (*T. indicus*: 0.663 ± 0.036; *T. pinchaque*: 0.663 ± 0.031). Covariation analyses based on 2B-PLS analysis of the unciform and posterior magnum facet areas support a covariation relationship between these facets. Again, PLS1 axes account for 100% of covariation, with a strong positive co-relationship between PLS axes (RV = 0.738) (Figure 2.5b; Table 2.4). Overall correlation is fairly strong (RV = 0.545) and statistical significance from the permutation test is very high (p < 0.001).

Discussion

Variation in the carpal and metacarpal arrangement within Perissodactyla has been studied with various qualitative techniques, with both morphological and functional conclusions being drawn at the genus level (*Tapirus*) (Earle, 1893; Holbrook, 2001; Klaits, 1972; Osborn, 1929; Simpson, 1945). However, the comparative morphology and interspecific variation within the manus of the genus *Tapirus* has only briefly been touched upon in previous studies (Earle, 1893; Osborn, 1929; Simpson, 1945), and has not taken all extant taxa into account. Observed interspecific variation in tapir autopodials may reflect subtle variation in locomotor style, and possibly variation in application of loading forces on the anatomically mesaxonic manus of tapirs. Here, we discuss the major osteological differences in the autopodium of extant *Tapirus* species, and their implications for locomotor variability in this group.

Facets of the lunate

Throughout previous comparisons between tapir postcrania, several key differences in the autopodium have been postulated. In particular, clear differences between *T. indicus* and other modern tapirs have been suggested (Earle, 1893; Osborn, 1929). We find strong support for this distinction between *T. indicus* and other modern tapirs. However, our findings do not correlate with the specific conclusions from previous qualitative studies (Earle 1893; Osborn 1929). For example, Earle noted little to no contact between

Table 2.4. Two-Block Partial Least Squares analysis results for pairwise comparisons between key joint articulations. Number of covariance occurrences per combination tested (n), PLS axes accounting for the greatest covariance are included with % accounted for, and correlation coefficient (*r*) and significance (*p*) for those axes are presented. Bold RV coefficient of integration and *p*-values represent overall results for the covariation analysis. Species specific comparisons are presented for trapezoid-magnum facet.

Facet combination (*n*)	**PLS axis**	**% covar.**	***r***	***p***	**RV**	***p*-value**
Unciform-Magnum (*20*)	PLS1	100.0	0.363	0.117	**0.132**	**0.117**
Distal Lunate facets (*20*)	PLS1	100.0	0.738	<0.001	**0.545**	**<0.001**
Trapezoid-Magnum (*17*)	PLS1	80.7	0.937	<0.001	**0.778**	**<0.001**
	PLS2	12.7	0.892	0.006		
Tapirus indicus (*4*)	PLS1	78.5	0.959	0.259	**0.915**	**0.086**
Tapirus baridii (*5*)	PLS1	71.6	0.978	0.205	**0.667**	**0.446**
Tapirus pinchaque (*3*)	PLS1	86.3	0.999	0.170	**0.992**	**0.170**
Tapirus terrestris (*5*)	PLS1	93.3	0.992	0.009	**0.931**	**0.009**
Trapezoid-Scaphoid (*15*)	PLS1	60.6	0.903	0.005	**0.415**	**0.089**
	PLS2	19.5	0.727	0.205		

the lunate and magnum (Figure 2.1) in *T. terrestris* when compared to *T. indicus*, and that the approximately equal facets for unciform and magnum in *T. indicus* allows equal transmission of force to the medial and lateral digits (Earle 1893). Our investigation reveals that the lunate contact with the magnum in *T. indicus* possesses the smallest facet (on average) relative to the unciform joint (Figure 2.6), which is in direct contrast to the findings of Earle (1893). A relatively larger unciform facet on the lunate would

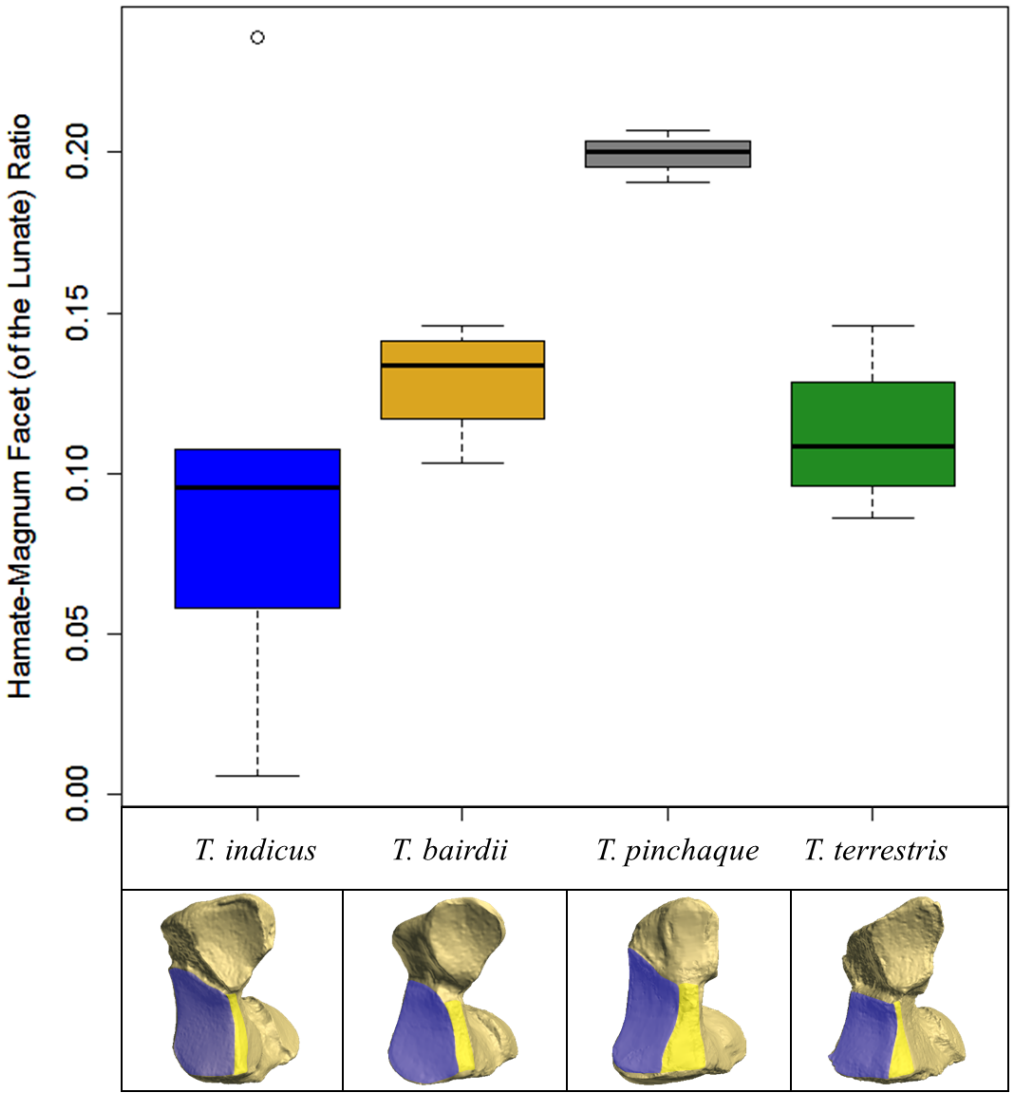

Figure 2.6. Ratio of areas for unciform (blue) and anterior magnum (yellow) facets of the lunate (intermediate carpal). Box plots represent intraspecific variation, with black bar highlighting the mean value; open circles represent outlying specimens. Representative bones (nearest to mean facet value) and ratios: *T. indicus* (RMNH 17923; 0.09), *T. bairdii* (MVZ 141173; 0.13), *T. pinchaque* (MNHN 1982-34; 0.21), *T. terrestris* (RMNH 12827; 0.15).

Table 2.5. Tukey-HSD significance test results from one-way ANOVA of unciform-magnum facet area ratios. Bold values denote significant differences.

	Species			
	T. indicus	*T. bairdii*	*T. pinchaque*	*T. terrestris*
T. indicus		0.731	**0.014**	0.668
T. bairdii	0.731		0.110	1.000
T. pinchaque	**0.014**	0.110		0.131
T. terrestris	0.668	1.000	0.131	

conceivably enable greater force transmission to the unciform and the digits beneath it (the lateral digits IV and V) in *T. indicus*. As such, our results for the lunate facets suggest that *T. indicus* may not exhibit biomechanical mesaxonic symmetry, but rather allows for increased loading on lateral digits. Additionally, results for *T. terrestris* suggest no significant difference to *T. indicus* in the distal lunate facets (Figure 2.6; Table 2.3), which also contrasts with previous observations (Earle 1893). Finally, we found no statistically significant support for covariation between the areas of these facets across the four tapir species. Individual variation in facet size may be a key factor here, as demonstrated by the large error bars for this ratio in *T. indicus* (Figure 2.6). These findings lead us to conclude that, contrary to the deductions of Earle (1893), tapirs with an enlarged unciform facet will not necessarily display reduction in their anterior magnum facet.

Our study suggests that *T. pinchaque* exhibits the largest anterior magnum facet of the lunate (Figure 2.6), which combined with a large unciform facet enables a more even spread of loading forces to the anterior carpal row and both MCIII and MCIV. Although we find no statistical evidence that there is a strong correlation between these facets in our sample, a morphological similarity to extinct tetradactyl perissodactyls is nevertheless present. The carpal arrangement is reminiscent of early, functionally tetradactyl perissodactyls (e.g. *Lophiodon* and *Hyrachyus*) (Osborn, 1929), and supports quantitative results from scapulo-humeral morphology suggesting *T. pinchaque* displays a number of osteological features in common with Eocene perissodactyls (MacLaren & Nauwelaerts, 2016). It should also be emphasised that our results for the distal lunate facets and anterior magnum-unciform ratios suggest only very small

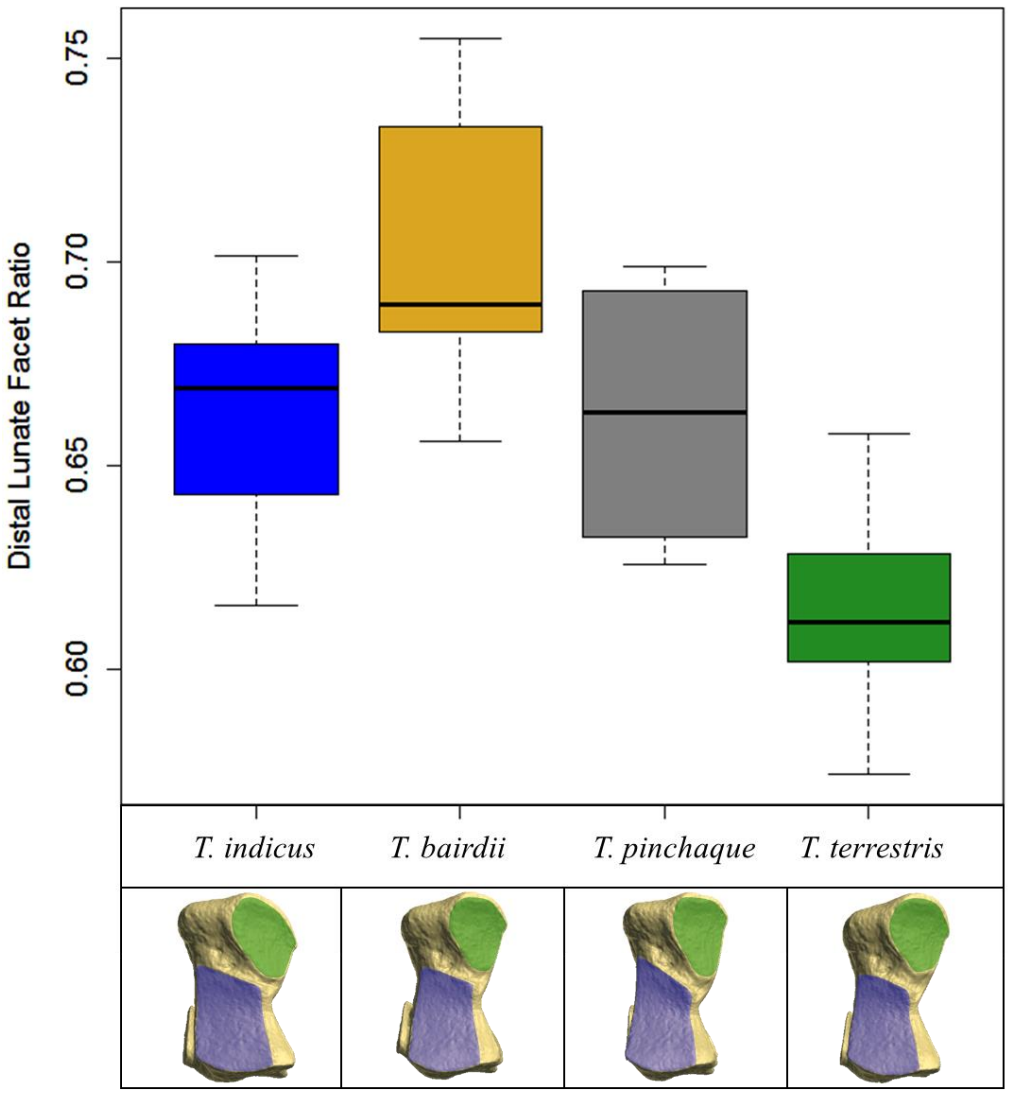

Figure 2.7. Ratio of areas for distal facets of the lunate. Box plots represent intraspecific variation, with black bar highlighting the mean value. Representative bones warped mean landmark configurations applied to RMNH 43495. Facets highlighted on representative bones: anterior distal facet (to proximal unciform) (blue); posterior distal facet (to volar process of magnum) (green).

Table 6. Tukey-HSD significance test results from one-way ANOVA of distal lunate facet area ratios. Bold values denote significant differences.

	Species			
	T. indicus	*T. bairdii*	*T. pinchaque*	*T. terrestris*
T. indicus		0.249	1.000	0.134
T. bairdii	0.249		0.324	**0.004**
T. pinchaque	1.000	0.324		0.199
T. terrestris	0.134	**0.004**	0.199	

differences in overall area (~10% between largest and smallest). However, we did find significant covariation in the distal lunate facets, suggesting that the lunate articulation with the posterior magnum is linked to changes in area of unciform facet and *vice versa*. We believe that extrapolating differences in loading regime and further functional outcomes from these small differences would involve over-interpretation of the data. We also stress that the morphological conclusions from Earle (1893) and Osborn (1929) remain on the whole accurate, although their functional interpretations require rigorous re-examination (as recommended by Klaits 1972) with modern quantitative kinematic methods before any solid conclusions on locomotor function can be made.

Mobility of the pisiform

The accessory carpal (pisiform) of tapirs is flattened dorsopalmarly and curves inwards toward the medial border of the autopodium. The curvature of the pisiform enables the passage of the flexor tendons of the *flexor digitorum superficialis + profundus* through the carpal tunnel (Bressou, 1961; Campbell, 1936; Murie, 1871), and the spatulate tip of the bone is the site for attachment of the *flexor carpi ulnaris* (proximal) and *abductor digiti minimi* (distal). A recent quantitative analysis revealed two different morphologies for the pisiform facet of the ulna in *Tapirus* (MacLaren & Nauwelaerts, 2016); *T. terrestris* and *T. indicus* demonstrated mediolaterally broad pisiform facets on the posterior ulna, whereas *T. bairdii* and *T. pinchaque* exhibited more proximodistally elongate facets. Results from the present analysis of the pisiform (accessory carpal) suggest a similar pattern of morphological disparity, especially between *T. terrestris* and *T. pinchaque* (Figure 2.8), further corroborating previous analyses revealing differences in forearm osteology between these closely related taxa (MacLaren & Nauwelaerts, 2016). In *T. terrestris*, the pisiform facet is sub-rhomboidal with

approximately parallel edges, and the articulating facet of the ulna is semi-circular in lateral view (Figure 2.8a; also MacLaren and Nauwelaerts 2016). This offers the pisiform of *T. terrestris* a relatively smaller surface with which to articulate compared to the other neotropical tapirs, while concurrently allowing a greater range of mobility for the pisiform during carpus flexion. The flatter, more elongate pisiform facet for the ulna may limit the functional capabilities of the lateral autopodium in *T. pinchaque* and *T. bairdii*, whereas *T. terrestris* does not appear to be under such mechanical constraints. In addition, the insertion area for the *flexor carpi ulnaris* on the proximoposterior edge of the pisiform (Figure 2.8i) is accentuated in neotropical taxa (most greatly so in *T. bairdii*), whereas *T. indicus* shows no great proximal expansion. The prominent insertion point in neotropical taxa offers a greater surface area for tendon attachment, suggesting increased resistance to carpal over-extension (by the antagonistic *flexor carpi ulnaris*). By contrast, the broader distal edge of the pisiform in *T. indicus* offers greater attachment surface for the *abductor digiti minimi* (abductor of the fifth digit) (Campbell, 1936; Murie, 1871); this is mirrored in the expanded volar process of the magnum (offering larger attachment for fifth digit interossei) in *T. indicus*. Enlarged attachment sites for the *abductor* and *adductor digiti minimi* on the pisiform and volar process of the magnum respectively implies that *T. indicus* has potentially greater muscular control over the fifth digit, allowing it to splay the toes and resist hyperextension, enabling support of greater mass on soft substrates. This result supports previous claims that *T. indicus* utilises the fifth digit to a greater extent than its living neotropical relatives (Earle, 1893; Gregory, 1929). To assess whether this morphology is common to all large tapir species, similar analyses on extinct taxa of high estimated body mass (e.g. *T. haysii*, *T. augustus*) will be necessary.

Medial digit loading

Within a biomechanically mesaxonic autopodium, the digits immediately lateral (fourth) and medial (second) of the central third digit will typically be loaded approximately equally (Klaits 1972; Holbrook 2001). The lateral digits and corresponding unciform (fourth carpal) have been shown to display morphological differences in modern tapirs; therefore, corresponding morphologies in the trapezoid (second carpal) may be expected. One of the most discriminatory features of the trapezoid was the morphology of the joint facet with the magnum (third carpal). The corresponding facet on the magnum was also highly discriminatory (visualised in Appendix II, Figure S2.2b). For simplicity, we discuss the articulation from here as the trapezoid-magnum facet. The anterior border of the facet is highly concave in *T. bairdii*, affording relatively less surface for articulation between the bones in this species

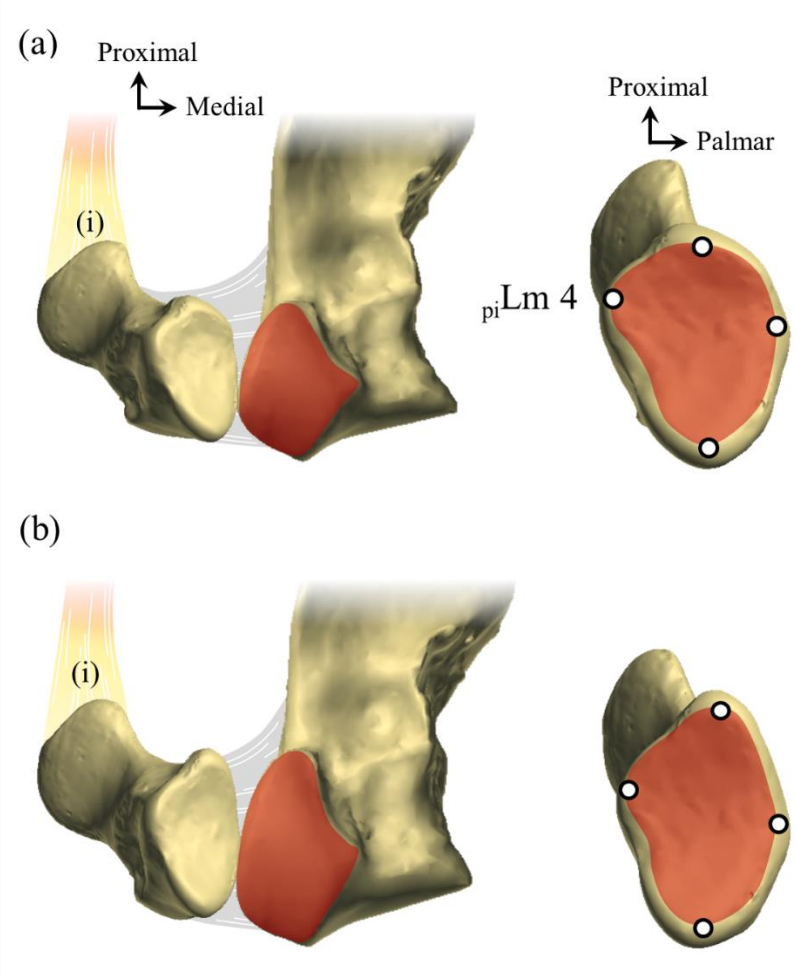

Figure 2.8. Comparison of pisiform-ulna articular morphology in *Tapirus terrestris* **(a)** and *T. pinchaque* **(b)**. Ulnae scaled to same size. Red shaded areas on both ulnae and pisiforms represent articular surface. Ulnae and pisiform depicted in posterior view (pisiform reflected from joint facet; pisiform with landmarks depicted from dorsolateral view. Approximate placement of *flexor carpi ulnaris* insertion **(i)** and carpal retinaculum (grey; connecting pisiform and ulna) is shown. $_{pi}$Lm 4 represents landmark most heavily affecting classification along DF 1 for pisiform. Bones represented depict average morphology for *T. terrestris* and *T. pinchaque* applied to scans of MNHN 1982-34 (*T. pinchaque*).

(Figure 2.9a). By contrast, *T. indicus* displays a much less concave anterior or posterior border to the facet, enlarging the relative area of the facet (Figure 2.9b). This morphology is mirrored in the trapezoid, and the relationship is strongly supported with results from PLS analyses for covariance (Table 2.4). Landmarks defining the concave margins of the facet on both trapezoid and magnum contribute most greatly toward the high covariation coefficient. The high covariance between these bones implies a tightly associated morphological relationship between trapezoid and magnum. In the larger *T. indicus*, the less concave margins and relatively greater articular surface suggest greater immobility across this joint. In addition, we find that the scaphoid facet for the trapezoid is more concave, thus allowing less mobility for the trapezoid within the *T. indicus* carpus; this finding should be treated with some caution, as this feature was not revealed to be statistically significant after covariation analysis ($p = 0.08$). Despite the poor co-variation between the trapezoid and scaphoid, evidence from the trapezoid-magnum facet implies the morphology of *T. indicus* is adapted for greater loading on the medial digit than other modern tapirs, allowing greater force transmission through the medial carpus. This conclusion is further supported by results for metacarpal morphology in this study (see below) and conclusions from previous qualitative assessments (Earle, 1893; Gregory, 1929). When combined with other subtle differences in the carpal complex of *T. indicus*, the adaptation of the trapezoid-magnum joint suggests the medial manus of *T. indicus* may be loaded more heavily relative to other tapirs, despite maintaining anatomical mesaxonic symmetry. By contrast, *T. bairdii* displays the least concave trapezoid facet on the scaphoid, with both *T. terrestris* and *T. pinchaque* displaying very similar trapezoid-magnum (Figure 2.9c–d) and trapezoid-scaphoid facet morphologies, intermediate between *T. indicus* and *T. bairdii*. This similarity may signify a phylogenetic aspect to this morphological difference (Ruiz-García et al., 2016, 2012). Further investigation into the carpal morphology of closely related South American taxa (e.g. the extinct *T. cristatellus* and *T. rondoniensis*) may shed more light on the evolutionary history of this morphology.

Metacarpophalangeal facet variation

The tapir metacarpals display anatomical mesaxonic symmetry (axis of symmetry passing through the third digit), both in absolute length and in average centroid size (Table 2.2). Whereas the central third metacarpal exhibits discriminant variation in the proximal joint surfaces, the second, fourth and fifth metacarpals are most successfully discriminated interspecifically using landmarks describing the palmar metacarpopalangeal joint (Figure 2.10). The metacarpophalangeal joint includes three main regions (the medial sesamoid facet, lateral sesamoid facet and metacarpal sagittal ridge), all of which are described in part by the landmark analysis. The palmar section

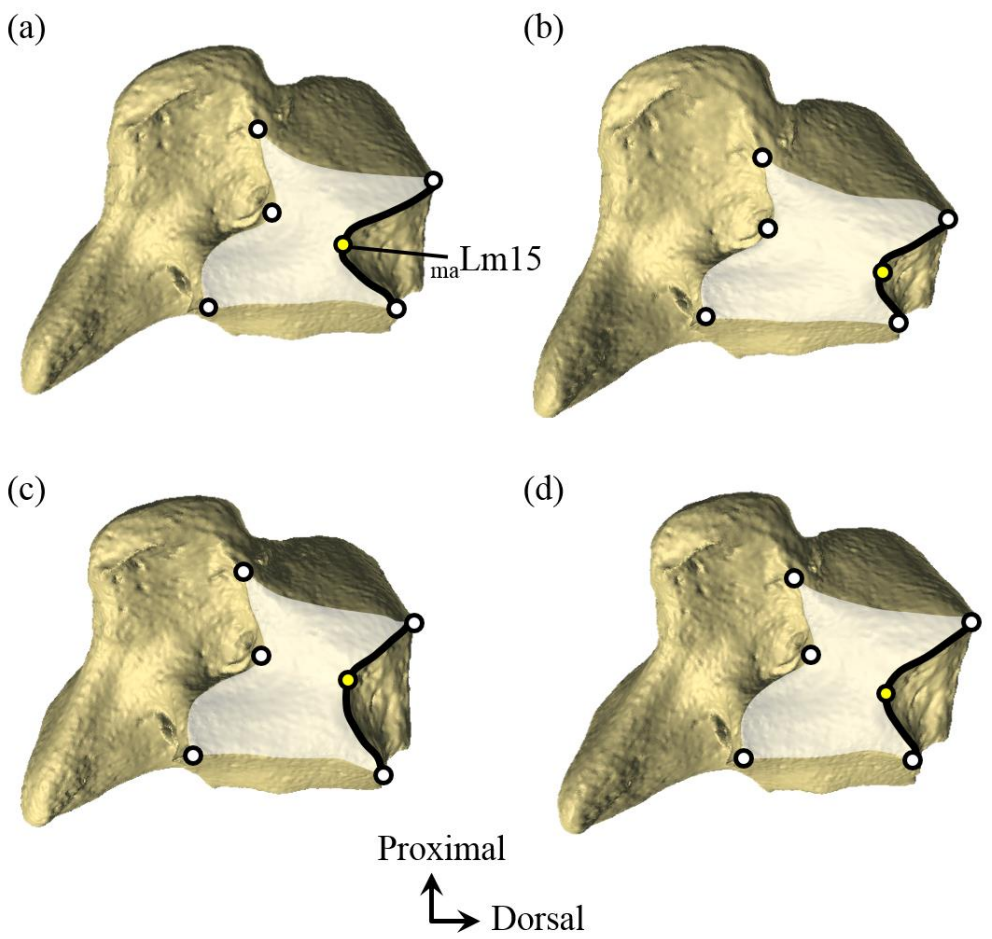

Figure 2.9. Comparison of trapezoid (second carpal) facet morphology of the magnum (third carpal) in extant *Tapirus*. Medial view. From top left: **(a)** *T. bairdii*; **(b)** *T. indicus*; **(c)** *T. pinchaque*; **(d)** *T. terrestris*. Representative facet areas shaded and outlined with landmarks (white circles) used in morphometric analysis; maLm 15 (yellow circle) highly discriminatory along DF 1 for magnum. Concave dorsal margin of trapezoid facet marked in bold black.

of the metacarpophalangeal joint facet articulates with the proximal phalange in addition to the paired sesamoid bones, which slot either side of the sagittal ridge (Constantinescu et al., 2012; Liebich et al., 2007). Quantitative comparisons of this facet across the four metacarpals demonstrated that the facet morphology of each type of metacarpal is

significantly different, as are the differences between species ($p < 0.001$) (Table 2.3). Two taxa stand out as notably different in their palmar metacarpophalangeal joint morphology: *T. indicus* and *T. pinchaque*.

T. indicus demonstrates a suite of morphological features associated with increased forelimb loading, as has been shown in previous literature and in this study (Earle, 1893; Gregory, 1929; Hulbert, 1995; MacLaren & Nauwelaerts, 2016). The palmar facet of the metacarpals also shows shape differences consistent with increased bone-bone contact, with *T. indicus* demonstrating a relatively broad facet on all metacarpals (Figure 2.10), in addition to discriminatory features in the medial and lateral carpus enabling dissipation of compressive forces (Figure 2.9). Furthermore, the sagittal ridge of the metacarpals in *T. indicus* is elongated proximally, with mediolaterally broad sesamoid facets, offering large sesamoids a greater surface area with which to articulate. We interpret this as a morphological feature contributing to load distribution across each metacarpal, and by extension the entire foot (Easton & Kawcak, 2007). Interestingly, this morphology of the palmar sagittal ridge is mirrored in *T. pinchaque*, which is on average the smallest and least massive of the neotropical taxa. As it is unlikely that *T. pinchaque* would require increased sesamoid-metacarpal contact to overcome high loading due to increased mass (i.e. graviportalism), we hypothesise that this shift in morphology in *T. pinchaque* is consistent with conferring greater stability to each toe (Hildebrand, 1985) and spreading the forces more evenly during limb loading (Easton & Kawcak, 2007). We also infer that, as this feature is seen in all the metacarpals of *T. pinchaque*, that the distal forelimb of this species has developed increased stability in all its digits. Impact of the fifth digit on the substrate would greatly benefit the animal, especially under potentially high loading conditions such as running up a steep, forested incline. Increased loading and necessity for stability in this comparatively small tapir may be due to a number of factors. Reduced reliance on the digital pad in favour of the toes, as is seen through equid evolution (MacFadden, 1992a; Thomason, 1985), would cause a shift in loading forces to the toes and may account for increased sesamoid facets and necessity for toe stability in *T. pinchaque*. No quantitative comparisons of toepad size has been reported in *T. pinchaque*, and so this interpretation remains speculative until further investigation has been undertaken. In addition, moving up or down sub-alpine habitats and over uneven, high altitude wet-grassland (Downer, 1996; Padilla et al., 2010) would necessitate increased digital stability; this supports previous quantitative results on forelimb morphology and biomechanics in this species (MacLaren and Nauwelaerts 2016). We find further support for previous quantitative works (Hawkins, 2011; MacLaren & Nauwelaerts, 2016) in the overall shape of *T. pinchaque* metacarpals, which demonstrate a more gracile morphology than those of other extant taxa. Overall, the morphologies observed in *T. pinchaque* in this and other

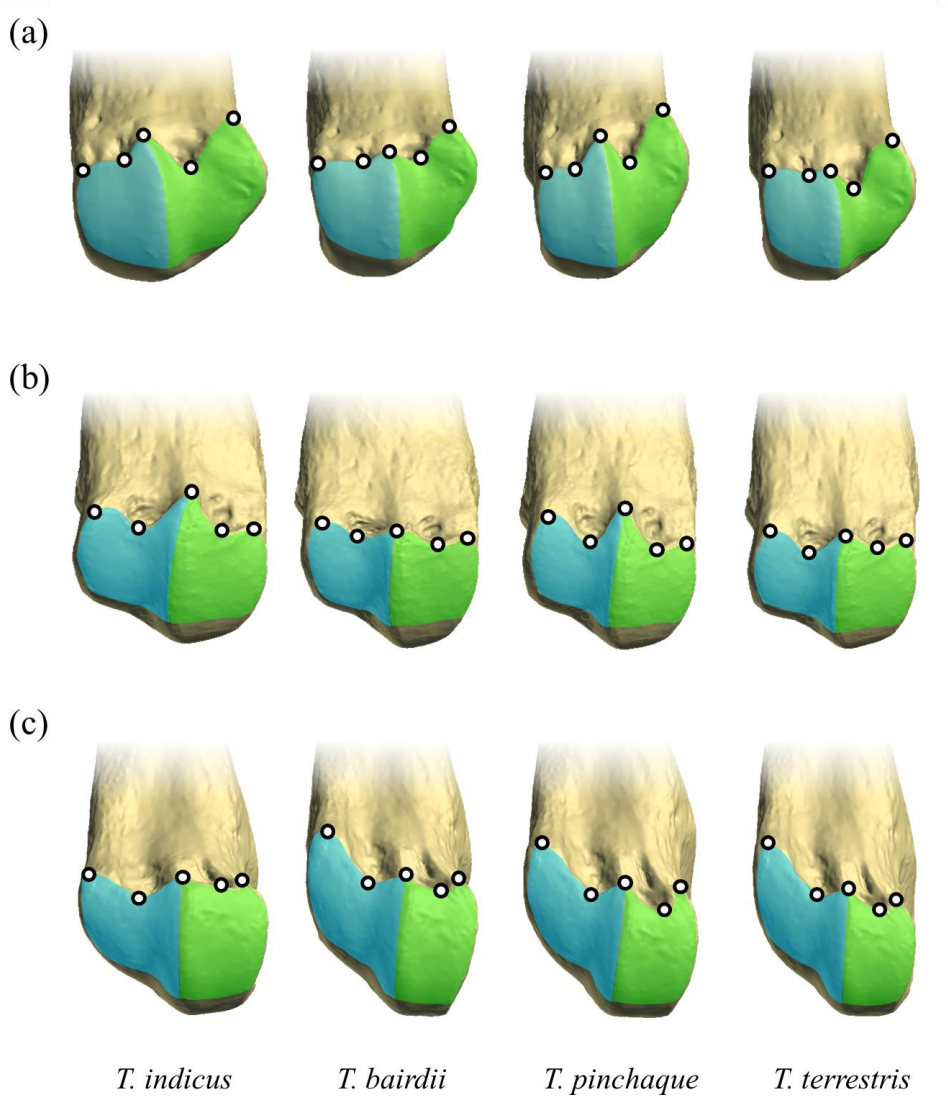

Figure 2.10. Comparison of the morphology of the palmar metacarpophalangeal joint facet in extant *Tapirus*. Medial and lateral metacarpals represented: **(a)** MCII; **(b)** MCIV; **(c)** MCV. Shaded regions represent approximate facet surface for articulation with the proximal sesamoids either side of the palmar sagittal ridge: green = medial sesamoid; blue = lateral sesamoid. White circles = landmark placement on palmar metacarpophalangeal joint. Average landmark configurations warped onto metacarpals of MEO 2204e (*Tapirus pinchaque*).

osteological studies hint at the retention or re-exploration of putatively 'primitive' perissodactyl forelimb traits (e.g. equal force distribution from lunate to unciform and magnum; functional fifth digit; gracile long bones), while concurrently developing novel anatomical features to both the upper and lower forelimb (e.g. large supraspinous fossa as potential proximal shock absorber; braced resting stance; strongly keeled metacarpophalangeal joints increasing stability for the phalanges during locomotion) (this study; MacLaren and Nauwelaerts 2016).

Finally, when compared to the metacarpals of other extant taxa, *T. bairdii* demonstrates the least proximal enlargement of the palmar sagittal ridges, more notably on MCII and MCIV (Figure 2.10). *T. bairdii* also demonstrates a compressed proximal carpal row, indicative of resistance to compressive forces in large quadrupeds (Prothero, 2005), which may represent an adaptation towards graviportalism not seen in the upper forelimb of this species (MacLaren and Nauwelaerts 2016). The manus of *T. bairdii* demonstrates greater potential for mobility of the medial digit (MCII; Figure 2.9), and small centroid size of MCV compared to that of other neotropical species (Table 2.2). From these observations, we posit that *T. bairdii*, despite its large size, has reduced functionality of the most lateral digit in favour of the second, third and fourth digits, strongly supporting both anatomical and biomechanical mesaxonic symmetry in this taxon. In contrast, the autopodium of *T. indicus* demonstrates anatomical features enabling broader force dissipation across the four digits of the manus; as such, *T. indicus* is the only extant tapir that may not adhere to both anatomical and biomechanical interpretations of mesaxonic symmetry. Kinematic and kinetic research will be necessary to shed greater light upon actual limb loading regimes in this enigmatic, and potentially variable, group of mammals.

Conclusions

From both qualitative and quantitative comparisons of the tapir fore-foot, we formulated several hypotheses regarding the morphology of modern tapir carpals and metacarpals, investigating whether the anatomy of the tapir autopodium supports both anatomical and biomechanical interpretations of mesaxonic symmetry (Klaits 1972). Discriminant function results support our hypothesis that *T. indicus* is most easily discriminated from neotropical tapirs, although conclusions from previous studies regarding carpal morphology and function are shown to require rigorous reassessment. Interspecific differences among neotropical taxa do not align with previous quantitative comparisons of the forelimb (MacLaren and Nauwelaerts 2016), with *T. bairdii* rather than *T. pinchaque* displaying the most divergent neotropical morphologies. Interspecific comparisons and covariance analyses of the autopodials offer evidence that *T. indicus*

has adapted its metapodials and distal carpals to cope with higher loading forces than other tapirs, which supports all previous assessments on tapir limb morphology. Morphometric analysis suggests that *T. bairdii* places greater reliance on digits II, III and IV than other species, with a decreased load predicted for digit V due to size and distal joint morphology. Testing this will require further analysis of the kinematics of locomotion in living tapirs. Conversely, *T. indicus* and *T. pinchaque* demonstrate osteological evidence for functional use of the fifth digit, widely considered as redundant in neotropical tapirs (Earle, 1893; Osborn, 1929). These and other features of the autopodium lead us to believe that both *T. indicus* and *T. pinchaque* have retained a fully functional tetradactyl manus, and *Tapirus* as a genus may not necessarily display both anatomical and biomechanical mesaxonic symmetry as has previously been assumed. We conclude that the tetradactyl tapir manus should be considered as a variable locomotor unit with a spectrum of functional adaptations, rather than simply a lingering plesiomorphy.

"it's not who you are on the inside –

it's what you do that defines you "

- Rachel Dawes -

– RESEARCH CHAPTER THREE –

Forelimb myology and muscular architecture of a juvenile Malayan tapir *Tapirus indicus* (Perissodactyla: Tapiridae)

Jamie A. MacLaren - Brianna K. McHorse

adapted from submission to *Journal of Anatomy*
(accepted pending revisions)

The absence of preserved soft tissues in the fossil record is frequently a hindrance for palaeontologists wishing to understand musculoskeletal movements, such as locomotion. Understanding the soft tissue composition of the limbs of modern species can aid in interpreting macroevolutionary changes in related groups. The Perissodactyla (horses, rhinoceroses, tapirs and their relatives) are known to have originated with a plesiomorphic, four-toed (tetradactyl) forelimb condition. Horses proceeded to lose all but their central digit, and rhinoceroses lost the lateral digit, whereas tapirs retained the basal tetradactyl state. The modern Malayan tapir (*Tapirus indicus*) represents the largest tetradactyl perissodactyl alive today. The skeletal anatomy of *T. indicus* has been known for over two centuries; however, muscle architectural quantification has never been attempted for this (or any other) species of tapir. Here, we report comprehensive muscle architecture of the forelimb of a juvenile Malayan tapir and compare patterns of mass and physiological cross-sectional area with a monodactyl (single-toed) relative of tapirs: the modern caballine horse (*Equus ferus caballus*). Each muscle of the tapir forelimb was dissected out from a cadaver and measured for architectural properties: muscle-tendon unit (MTU) length, MTU mass, muscle mass, pennation angle, and resting fibre length. Comparative parameters were then calculated from the raw measurements: physiological cross-sectional area (PCSA), muscle volume, and % muscle mass. At the shoulder, the *infraspinatus* of *T. indicus* is here shown to exhibit dual origination sites: the principal head is enclosed in the infraspinous fossa, with an accessory head originating from the deflected cranial surface of the scapular spine; the same condition is observed in pigs and their relatives (suids). Quantitative results suggest that the *triceps brachii caput longum* (656.2 ± 22g) and *supraspinatus* (464.3 ± 15g) are the heaviest muscles in the *T. indicus* forelimb. The PCSA of the juvenile *T. indicus* was smaller than those of the adult *Equus*; however, PCSAs for the *supraspinatus*, *subscapularis*, *coracobrachialis*, *triceps brachii* (all heads), and *extensor digitorum lateralis* of the tapir were comparable with those of adult reindeer

(*Rangifer*). The *supraspinatus* constituted 27.2% of muscle mass in the tapir upper forelimb compared to 14.1% in a comparative sample of *Equus*; the *extensor carpi lateralis* constituted more than double the % mass of lower forelimb musculature in *T. indicus* (5.4%) compared to *Equus* (1.9%). Differences between the tapir and horse in % muscle mass (especially for *supraspinatus*, *flexor carpi ulnaris* and lateral digital flexors) reflect adaptations that equids have undergone to their muscular architecture during their evolution from tetradactyl forest-dwellers to monodactyl, open-habitat specialists. This quantitative dataset of muscle architecture in a juvenile, functionally tetradactyl tapir is a pivotal first step towards reconstructing the locomotor capabilities of similarly small, extinct ancestors of modern perissodactyls.

Introduction

The Malayan tapir (*Tapirus indicus* Desmaret) represents the largest of the four widely accepted extant tapir species (de Thoisy et al. 2014). Malayan tapirs are considered to have diverged from the lineage which lead to the modern neotropical tapirs approximately 25Mya (MacLaren, Hulbert, Wallace, & Nauwelaerts, 2018; Steiner & Ryder, 2011). The cranial and postcranial elements have been known to differ from those of neotropical taxa for many years (Earle, 1893), with recent quantitative analyses demonstrating clear divergences between Malayan and neotropical tapir osteology (Dumbá et al., 2018; MacLaren & Nauwelaerts, 2016, 2017). Morphological comparisons of the forelimb anatomy strongly suggest that the Malayan tapir possesses obligate function of its lateral fifth digit (Earle, 1893; MacLaren et al., 2018; MacLaren & Nauwelaerts, 2017), akin to some of the earliest extinct tetradactyl (four-toed) perissodactyls, such as *Propalaeotherium* (Palaeotheriidae), *Lophiodon* (Lophiodontidae) and *Palaeosyops* (Brontotheriidae) (Franzen, 2010b; Gregory, 1929; Holbrook, 2009), and the ancestors of modern equids (e.g. *Sifrhippus*; Froehlich, 2002; Wood et al., 2011; Secord et al., 2012).

Unfortunately for the study of extinct vertebrates, muscular and ligamentous remains are almost invariably lost during the fossilisation process. As a result, the muscular arrangements and physiological cross-sectional area (PCSA), both critical inputs for modelling skeletal processes such as feeding and locomotion, can only be estimated based on available phylogenetic bracketing (Witmer, 1995). To further understand the transition from tetradactyl (four-toed) forelimbs to the modern monodactyl (one-toed) condition in equids, myological and skeletal information from their closest relatives will be of great value. Such functional myological data is readily available for derived equids

(e.g. domestic horse *Equus ferus caballus*) (Liebich et al., 2007; Payne et al., 2004; J. C. Watson & Wilson, 2007b). However, for understanding extinct tetradactyl perissodactyl locomotion, modern tetradactyl perissodactyls (i.e. tapirs) may be considered as more appropriate musculoskeletal analogues than modern, monodactyl horses. Within the four modern tapir species, the Malayan tapir represents most functionally tetradactyl taxon (Bressou, 1961; Earle, 1893; MacLaren & Nauwelaerts, 2016, 2017; Steiner & Ryder, 2011). This study will draw on the existing tapir literature describing muscular arrangements (Bressou, 1961; Campbell, 1936; Murie, 1871; Pereira, 2013) to inform a systematic dissection and muscular analysis of a juvenile Malayan tapir. In the absence of functional muscular data for tapirs, we will quantify muscular masses and PCSAs for all the major limb muscles, and comment upon the potential utility of these data in future biomechanical modelling of ancestral hippomorphs (equids and relatives) and tapiromorphs (tapirs, rhinos and relatives).

The specific action of a muscle during locomotion and gravitational support can be influenced by several characteristics, including activity pattern, fibre type and muscular architecture (Biewener & Roberts, 2000). The arrangement of fibres within the muscles relative to the axis of force generation (muscle architecture) can be described using several parameters (including pennation angle and PCSA). To our knowledge, these parameters are here investigated for the first time in the forelimb of the genus *Tapirus*. The upper forelimb muscles of tapirs are known to correspond to those of modern equids (Campbell 1936; Bressou 1961; Barone 2000; Pereira 2013). However, the highly specialised nature of the equid distal limb causes direct comparisons to distal tapir myology to be more problematic, although tendon and ligamentous attachments sites on the one functional and two ancillary digits of equids remain constant (Campbell, 1936). It may be expected that muscles which flex and extend the lateral and medial digits of tapirs (and are lost in Equus) will exhibit architectural differences between these two clades. We therefore formulate the working hypothesis that muscles in the upper forelimb of *Tapirus* with demonstrate similar patterns of muscular architecture (e.g. % mass, PCSA etc.) to the upper forelimb of *Equus* (using values from Watson and Wilson 2007). Conversely, we predict large inter-genus differences in muscle architectural in lower forelimb muscles, most notably for muscles which shift in function between tetradactyl (i.e. *Tapirus*) and monodactyl (i.e. *Equus*) species (e.g. lateral digit flexors and extensors).

Methodology

Specimens

The two forelimbs of a juvenile Malayan tapir from the Koninklijke Maatschappij Dierkunde Antwerpen (KMDA) became available for study in 2016. The juvenile, a female approximately five months old, died from rapid onset viral encephalomyocarditis (Vercammen, Bosseler, Tignon, & Cay, 2017). The myocardial infection which caused the death of the juvenile tapir did not cause prolonged sickness or associated muscular atrophy. Medical conditions associated with captive perissodactyls which may affect skeletal musle architecture and mass (e.g. obesity, capture myopathy, stress atrophy) have not been reported in tapirs (Duncan, 2018). Additional comparative material became available from an elderly male Malayan tapir, also from the KMDA; the left forelimb was examined (but not dissected) following its death due to natural causes. Dissection was not possible as this animal cadaver was being used for another, invasive experiment. A dislocated manus of an adult lowland tapir (*Tapirus terrestris*) was also made available for visual inspection and comparison to the manus of *T. indicus*. We were unable to record muscular architecture information for either the adult male (different experiment) or the *T. terrestris* manus (degradation), although visual examination of key muscle arrangements enabled qualitative interpretations. The dissection of the forelimbs took place over four weeks in the spring and autumn of 2016, performed at the laboratory of Applied Veterinary Morphology of the Universiteit Antwerpen (Gebouw U, Campus Drie Eiken, Wilrijk, Antwerp).

Muscle Architecture

The anatomy, attachment sites and functional action of the forelimb muscles under investigation can be found in Figures 3.1 and 3.2, and Table 3.1. Each forelimb muscle was isolated from the surrounding tissues and removed from the cadaver, following confirmation of origination and insertion sites. Where there were multiple heads to the muscle (e.g. *triceps brachii*), the locations of each head of the muscle were determined prior to removal, whereupon each head of the muscle was weighed and measured. Measurements were made for the following parameters: muscle belly length; tendon length; fascicle length; fascicle pennation angle. Total muscle tendon unit (MTU), tendon and muscle belly lengths were measured using a flexible ribbon tape, with incisions made into the muscular flesh to identify the extent of the tendons into the muscle. Muscle mass was measured using an OHAUS Scout-Pro (SPU 602) measuring balance with 0.01g precision; muscles weighing in excess of 200g were weighed in several pieces and the combined total used. Tendinous tissue was carefully removed

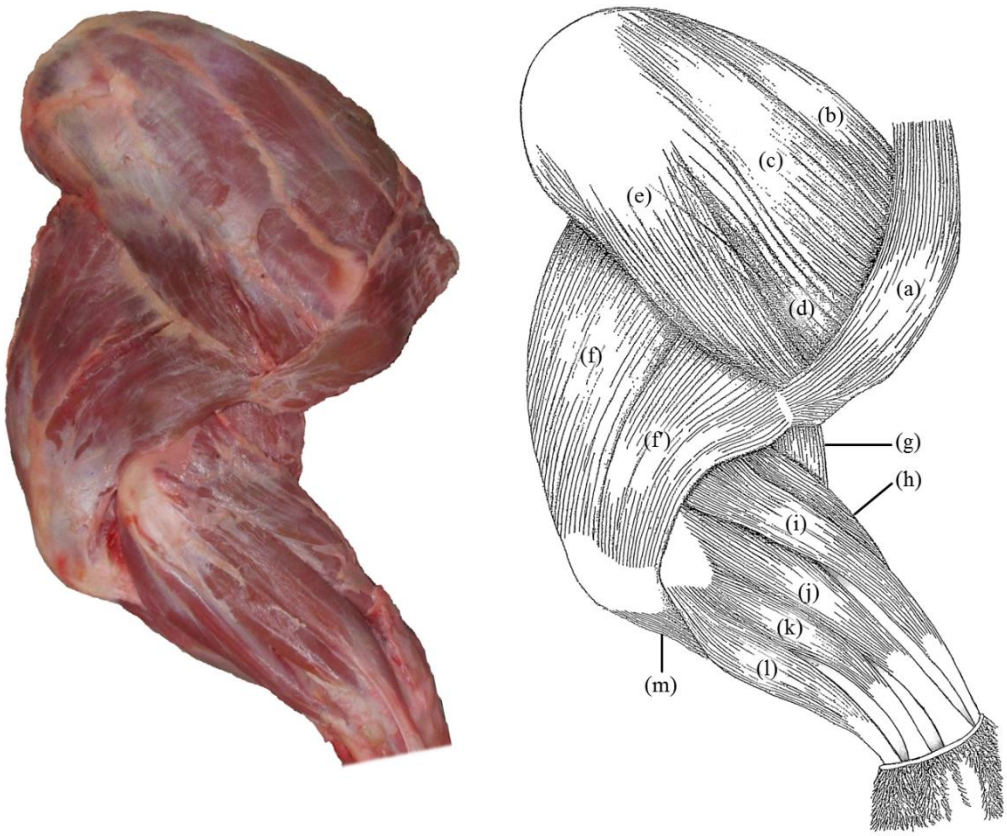

Figure 3.1. Muscles of *Tapirus indicus* right forelimb in lateral aspect. Photograph of muscles (left) with annotated diagram (right). Muscles: (a) *m. cleidobrachialis*; (b) *m. subclavius*; (c) *m. supraspinatus*; (d) *m. infraspinatus*; (e) *m. deltoiudeus pars scapularis*; (f) *m. triceps brachii caput longum*, (f') *caput laterale*; (g) *m. brachialis*; (h) *m. brachioradialis*; (i) *m. extensor carpi radialis* (ECR); (j) *m. extensor digitorum communis* (EDC); (k) *m. extensor digitorum lateralis* (EDL); (l) *m. extensor carpi ulnaris* (*ulnaris lateralis* in equids) (UL); (m) *m. flexor carpi ulnaris caput ulnare* (ulnar head of FCU).

from the muscle following pure muscle mass measurement, with the mass of the tendinous tissue subtracted from the total muscle mass. Muscle fascicle lengths were recorded along the line of muscle action by measuring the distance from the fibre origin at the tendon to the end of the muscle fibre. Muscle and fascicle lengths were recorded using a ribbon tape, with repeated measurements (four to eight) being performed at regular intervals along the length of the muscle belly to generate a representative

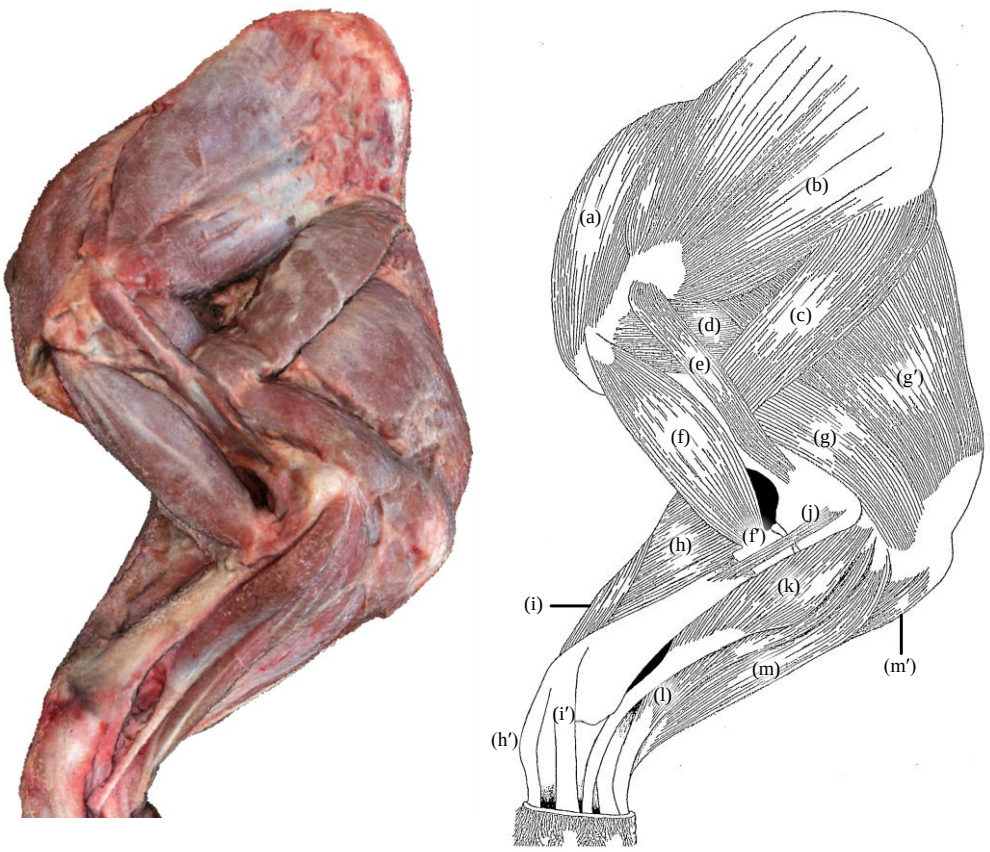

Figure 3.2 Muscles of *Tapirus indicus* right forelimb in medial aspect. Photograph of muscles (left) with labelled diagram (right). Muscles: (a) *m. subclavius*; (b) *m. subscapularis*; (c) *m. teres major*; (d) *m. brachialis*; (e) *m. coracobrachialis*; (f) m. *biceps brachii*, (f′) *lacerta fibrosus*; (g) *m. triceps brachii caput mediale*, (g′) *caput longum*; (h) *m. extensor carpi radialis* (ECR), (h′) insertion tendon of ECR; (i) *m. adductor pollicis longus* (APL), (i′) insertion tendon of APL; (j) *m. pronator teres*; (k) *m. flexor carpi radialis* (FCR); (l) *m. flexor digitorum profundus caput humerale* (FDP); (m) *m. flexor digitorum superficialis caput humerale* (FDS), (m′) *caput ulnare*. FDS (l) and FDP (m, m′) closely combined after separate origination sites (see Table 3.1).

average length per muscle. Pennation angle to the tendon was calculated using a transparent protractor, again with repeated measures to provide an overall average pennation angle. Resting pennation angles of less than 5° were given a zero value (after

the methods of Brown et al. 2003). Pennation angles were therefore not recorded for *subclavius*, *teres major*, medial *triceps brachii*, *anconeal*, *pronator teres*, *brachioradialis*, EDC and EDL. All measurements were recorded on both right and left forelimbs, with overall averages representative of the individual. Inferred muscular volume was calculated by dividing the mass of the muscle by a constant muscle density ($1.06 cm^{-3}$; Mendez and Keys, 1960). The estimated muscle volume was then divided by the average fascicle length for the muscle to generate the physiological cross-sectional area (PCSA):

$$\text{PCSA} = \text{muscle volume } (cm^3) \div \text{muscle fascicle length (cm)}$$

PCSAs were compared among the upper and lower limb muscles. Upper limb muscles were determined as those muscles intrinsic to the forelimb and which act upon the shoulder and elbow joint (Table 3.1). Lower forelimb muscles are designated as muscles which act upon the carpus and digits; several lower forelimb muscles cross the elbow joint, although their primary function is not the flexion or extension of the joint (e.g. *brachialis*, *extensor digitorum communis*). Data on *Equus* muscle architecture were taken from published sources (Brown et al. 2003; Payne et al. 2005; Watson and Wilson 2007), and comparisons were therefore limited to the muscles which have architecture reported for equids. Muscle mass and PCSA data from those available muscles were compared with corresponding muscles of the dissected *Tapirus*. These muscles included the *subclavius*, *supraspinatus*, *biceps brachii*, *triceps brachii* (three heads), APL, FDS+P, EDC, EDL, FCU, FCR, ECR and ECU (homologous to UL in equids; Barone, 2000) (Table 3.1). Published literature sources for *Equus* included Brown et al. (2003) (APL, FDS+P, EDC, EDL, FCU, FCR, ECR and ECU), Payne et al. (2005) (*subclavius*), and Watson and Wilson (2007) (*supraspinatus*, *biceps brachii*, *triceps brachii*). PCSA from other ungulates were also used for comparisons across the entire forelimb (*Rangifer*, Wareing et al. 2011; *Sus*, Matthewson et al. 2011; *Capra*, Gewaily et al. 2017).

Statistical Comparisons

As equids are much larger than juvenile tapirs, direct comparison of muscle mass was considered unsuitable. Ontogenetic studies of mammalian and avian muscle and tendon anatomy suggest that limb muscles can scale both allometrically and isometrically through ontogeny, dependent upon the muscle and the taxon (M. L. Martin, Warburton, Travouillon, & Fleming, 2019; Miller, Basu, Fritsch, Hildebrandt, & Hutchinson, 2008; Olson, Glenn, Cliffe, & Butcher, 2018). Unfortunately, no data is presently available for ontogenetic variation or scaling in muscle architecture for perissodactyls, and

Table 3.1. Origin, insertion and functional action of forelimb muscles of juvenile *Tapirus indicus*. Abbreviations: *E.*= extensor; *F.* = flexor; *Ab.*= Abductor; *d.* = digitorum; apo. = aponeurosis; MC = metacarpal

Muscle	Abbr.	Origin	Insertion	Function
Subclavius	**SBC**	Cranial angle of scapula (dorsal), extending to rib cartilage	Fascia of *Pectoralis profundus*	Supports and fixes the scapula; shoulder extension
Supraspinatus	**SUP**	Supraspinous fossa.	Greater and lesser tubercules of humerus.	Shoulder extension.
Infraspinatus	**INF**	1. Infraspinous fossa 2. partial on the supraspinous fossa (see text)	Greater tubercle of humerus.	Supports shoulder as lateral collateral 'ligament'; shoulder flexion (after initial flexing)
Subscapularis	**SUB**	Dorsal border of scapula (medial).	Lesser tubercle of humerus.	Supports shoulder; medial collateral 'ligament'.
Deltoideus	**DEL**	Tuber spinae.	Deltoid tuberosity.	Shoulder flexion.
Teres major	**TMJ**	Caudal border of scapula (medial).	Teres tuberosity (deep to *Latissumus dorsi*).	Shoulder flexion.
Teres minor	**TMN**	Caudal border and neck of scapula.	Humeral shaft between greater tubercle and deltoid tuberosity.	Shoulder flexion.
Brachialis	**BR**	Distal to lesser tubercle of humerus.	Cranial surface of radius.	Elbow flexion.
Coracobrachialis	**CBR**	Coracoid process (medial).	Distal humeral shaft (medial).	Upper arm adduction.
Biceps brachii	**BB**	Supraglenoid and coracoid processes.	Lacerta fibrosus (and coronoid process of ulna).	Elbow flexion; shoulder extension and stabilisation (during stance phase)
Triceps brachii *caput longum* *caput laterale* *caput mediale*	**TBlo** **TBla** **TBme**	Long: caudal angle and scapular border. Lateral: ridge proximal to deltoid tuberosity. Medial: medial shaft of humerus.	Long: caudodistal part of olecranon. Lateral: lateral olecranon. Medial: medial epicondyle and anconeal process.	Shoulder extension (*caput longum*) Elbow extension and stabilisation
Anconeus	**ANC**	Distal humeral shaft and olecranon fossa.	Anconeal process and cranial olecranon.	Elbow extension

Table 3.1. continued Origin, insertion and functional action of forelimb muscles of juvenile *Tapirus indicus*. Abbreviations: *E.*= extensor; *F.* = flexor; *Ab.*= Abductor; *d.* = digitorum; apo. = aponeurosis; MC = metacarpal

Muscle	Abbr.	Origin	Insertion	Function
Pronator Teres	**PT**	Proximal margin of medial epicondyle of humerus.	Centre of radial shaft (medial).	Lower forelimb pronation
Brachioradialis	**BRA**	Supracondylar ridge (lateral) of the humerus.	Styloid process of radius (medial).	Lower forelimb supination
E. d. communis	**EDC**	Supracondylar ridge and lateral epicondyle of humerus.	Dorsal surface of all four ungual phalanges.	Carpus and digital extension (all digits).
E. d. lateralis	**EDL**	Lateral epicondyle of humerus (distal to EDC).	Lateral digit IV and dorsal digit V.	Digital extension (digit IV and V).
E. carpi ulnaris (*Ulnaris lateralis*)	**UL**	Lateral condyl of humerus (distal to EDL).	MC V (dorsolateral).	Metacarpal extension (MC V).
E. carpi radialis	**ECR**	Trochlear ridge, radial fossa and lateral epicondyle of humerus.	Proximal MC III (dorsal).	Carpus extension and fixation
Ab. pollicis longus	**APL**	Interosseous space between radius and ulna.	Lateral MC II and trapezium (second carpal).	Digit II abduction (modified from digit I abductor)
F. carpi ulnaris	**FCU**	Humeral head: medial epicondyle of humerus. Ulnar head: medial olecranon	Posterior pisiform (accessory carpal).	Carpus flexion
F. carpi radialis	**FCR**	Medial epicondyle of humerus	Palmar surface of MC III	Carpus flexion
F. d. superficialis + *F. d. profundus*	**FDS+P**	Combined heads (Campbell, 1936). Ulna head: medial olecranon. Humeral head: distal medial epicondyle. Radial head: interosseous space between radius and ulna.	FDS: intermediate phalanges II, III and IV. FDP: ungual phalanges of digit II, II and IV; ulnar head shares fibres with UL insertion on digit V.	FDS: forefoot and digital flexion; metacarpo-phalangeal joint support. FDP: Digital joint flexion

therefore scaling of juvenile *Tapirus* data to an adult size was not performed. We therefore compare patterns of mean % muscle mass and mean PCSA between *Tapirus* and *Equus*, rather than statistically comparing absolute or log-transformed values. Muscle mass and calculated PCSA for five upper forelimb muscles of *Equus* was taken from Watson and Wilson (2007), and for nine lower forelimb muscles from Brown et al. (2003). In the absence of total body mass data for all subjects in the analysis, individual muscle masses were calculated as a percentage of the sum of available limb muscle mass. The comparative dataset for *Equus* muscles included *supraspinatus*, *biceps brachii*, *triceps brachii* (three heads), *flexor digitorum superficialis*, *flexor digitorum profundus*, *flexor carpi ulnaris*, *flexor carpi radialis*, *extensor digitorum communis*, *extensor digitorum lateralis*, *extensor carpi radialis*, and *extensor carpi ulnaris* (*ulnaris lateralis* in equids, where it has lost its extensor function; Brown et al. 2003). % mass for each tapir muscle was compared to that of *Equus* to inspect whether *Tapirus* % muscle mass fell within the standard deviations exhibited by the forelimb muscles of *Equus*.

Within the tapir limb itself, one-way analyses of variance (ANOVAs) and Tukey-B post-hoc tests were performed to test for significant differences between pennation angles (following successful normality testing using Shapiro-Wilk test) (Arruda et al., 2018; Hady, Fosgate, & Weh, 2015; Lang, Motta, Habegger, & Hueter, 2012). Significant differences in pennation angle were tested for between the lower forelimb flexors (FDS+P, FCU, FCR) and extensors (UL, ECR). Pennation angles of less than 5° (e.g. TBme) were excluded from ANOVAs.

Results

Tapir Muscle Mass and Volume

The *triceps brachii* (long head; 619.5g), *supraspinatus* (444.9g), and *infraspinatus* (315.5g) represent the heaviest muscles in the upper forelimb of the tapir in this analysis. The combined deep and superficial digital flexors (*flexor digitorum superficialis* + *profundus* (FDS+P): 151g), radial carpus extensor (*extensor carpi radialis* (ECR); 96g) and common digital extensor (*extensor digitorum communis* (EDC); 53g) were the heaviest muscles of the tapir lower forelimb (Table 3.2). Combined muscle volume of carpal flexors was substantially lower (47.2cm^3) than carpal extensors (128.9cm^3), whereas combined digital flexor volume (143.1cm^3) was double that of digital extensors (71.8cm^3).

Table 3.2. Muscular architecture of forelimb muscles of juvenile *Tapirus indicus*

Muscle	MTU Mass (g)	Muscle Mass (g)	Muscle L (mm)	Tendon L (mm)	Fascicle L (mm)	Pennation Angle (°)
SBC	208.6	207.7	34.5 ± 1	9.2	30.1 ± 1	< 10
SUP	464.3 ± 15	444.9 ± 1	27.4 ± 1	18.3 ± 1.8	9.3 ± 3	30 ± 1
INF	358.9 ± 1	315.5 ± 6	26.8 ± 2	33.3 ± 1	5.7 ± 1	37 ± 8
SUB	200.2 ± 24	183.8 ± 15	17.2 ± 1	14.4 ± 3	4.2 ± 1	38 ± 16
DEL	78.8 ± 1	77.6 ± 3	17.4 ± 3	16.3 ± 1	7.3 ± 3	16 ± 6
TMJ	143.5 ± 22	141.2 ± 19	22.7 ± 2	8.7	18.1 ± 1	< 10
TMN	19.8 ± 4	17.8 ± 2	10.3 ± 1	12.5 ± 1	5.3 ± 1	31 ± 5
BR	160.1 ± 9	157.5 ± 6	21.5 ± 1	12.5	13.7 ± 1	47 ± 7
CBR	14.4 ± 5	11.6 ± 3	14.9 ± 2	17.3 ± 1	2.2 ± 1	22 ± 7
BB	123.8	107.7	15.3 ± 1	26.2 ± 1	4.2 ± 1	35 ± 13
TBlo	656.2 ± 22	619.5 ± 15	24.1 ± 2	18.1 ± 1	9.9 ± 2	26 ± 9
TBla	203.8 ± 12	197.8 ± 6	21.7 ± 1	14.0	11.6 ± 2	29 ± 10
TBme	63.9	58.9	16.5	12.2	10.9 ± 2	< 10
ANC	53.4	48.4	13.8	7.2	9.1 ± 2	< 10
PT	7.7	0.6	4.4	17.8	-	< 10
BRA	25.0	22.9	22.0 ± 4.2	24.1 ± 3.7	20.9 ± 3.7	< 10
EDC	66.9 ± 11	53.7 ± 0.3	15.2 ± 1.6	35.5 ± 4.9	8.9 ± 2.2	< 10
EDL	33.7	22.4	17.4	38.8	4.6 ± 0.5	< 10
UL	53.9 ± 12	40.5 ± 3.1	17.7 ± 0.4	27.5 ± 0.7	1.6 ± 0.5	41 ± 5
ECR	110.3	96.2	20.0	33.5	9.5 ± 4.4	44 ± 3
APL	25.6	21.1	11.0	22.5	2.7 ± 0.3	26 ± 8
FCU	22.2 ± 7	17.7 ± 4.8	18.6	23.0 ± 1.4	1.6 ± 0.6	37 ± 8
FCR	37.2	32.3	16.3	28.2	3.2 ± 2.0	9 ± 5
FDS + FDP	247.3	151.7 / 15.1	20.9 / 35.1	40.1	3.2 ± 2.8	11 ± 8
AdDV	5.42	3.87	9.1	10.4	2.1 ± 0.8	28.75 ± 3
AbDV	7.14	3.89	6.9	11.1	1.7 ± 1.0	55 ± 7

Tapir Muscle-Tendon Unit (MTU) Length

The longest muscle-tendon units in the tapir upper forelimb were the *infraspinatus* (33.3mm) and *subclavius* (34.5mm), with the tendons of the *biceps brachii*, *coracobrachialis*, *teres minor* and *infraspinatus* exceeding muscle belly length (Table 3.2). The longest muscles in the lower forelimb include the *brachioradialis*, ECR and the FDS+P; the longest tendons belong to the digital extensors and flexors (Table 3.2).

Tapir Pennation Angle

The highest average pennation angles in the upper limb were recorded for the *brachialis* (47°), *subscapularis* (38°) and *infraspinatus* (37°), whereas the ECR (44°), *extensor carpi ulnaris* (= *ulnaris lateralis*; UL) (41°) and *flexor carpi ulnaris* (FCU; 37°) exhibited the steepest pennation angles for the lower forelimb muscles. The highest pennation angles in the entire forelimb were recorded for the fifth digit abductor (AbDV; 55°) in the manus. ANOVA between carpo-digital flexor (FCU, FDS+P, FCR) and extensor (UL, ECR) pennation suggests that the extensor muscles of *Tapirus* are significantly more pennate than flexors ($p < 0.01$).

Comparative Muscular Parameters

Percentage Muscle Mass – Percentages of upper and lower forelimb muscle mass are compared between *Tapirus* and *Equus* in Figure 3.3. For the muscles available for direct comparison, the greatest percentage mass differences between *Tapirus* and *Equus* were observed in the *supraspinatus*, EDL and FCU (Figure 3.3; Table 3.3). The long head of the *triceps brachii* accounted for the greatest percentage of muscle mass in the upper forelimb of both *Tapirus* and *Equus*, with the FDS+P and ECR constituting the largest percentages of muscle mass for the lower limb in both genera (Figure 3.3; Table 3.3).

PCSA – Comparisons between physiological cross-sectional area (PCSA) in *Tapirus* and *Equus* forelimb muscles are presented in Figure 3.4, with additional comparisons with selected artiodactyls in Table 3.4. PCSA in *Tapirus* is greatest for the long head of the *triceps brachii* (58.8cm^2), with the *infraspinatus*, *supraspinatus*, *subscapularis* and FDS+P all exhibiting relatively high PCSAs between 40 and 55cm^2 (Table 3.4). The *brachioradialis* (*supinator longus*) exhibits the smallest PCSA for *Tapirus* in this study. When compared to other ungulate taxa, the juvenile tapir exhibits comparable PCSAs to adult *Sus* and *Rangifer* in rotator cuff muscles (*infraspinatus*, *supraspinatus*, *subscapularis*), although not in the *teres minor*, for which *Tapirus* exhibits a relatively low PCSA (3.2cm^2). The *triceps brachii* complex of *Tapirus* is very similar in PCSA to

Table 3.3. Comparison of available forelimb muscle masses between *Equus* and *Tapirus.* Percentage mass based on upper and lower forelimb segments.

Muscle	*Tapirus*		*Equus**	
	Muscle Mass (g)	**% Mass**	**Muscle Mass (g)**	**% Mass**
SCL	207.67	12.7	1303.00	15.8
SUP	444.95	27.2	1161.56	14.1
BB	107.74	6.6	663.66	8.1
TBlo	619.49	37.9	4059.17	49.3
TBla	197.795	12.0	887.53	10.8
TBme	58.88	3.6	159.94	1.9
FDS+P	151.65	36.6	946.98	32.2
EDC	53.71	13.0	315.97	10.7
EDL	22.44	5.4	57.14	1.9
FCU	17.69	4.3	262.26	8.9
FCR	32.29	7.7	179.71	6.1
UL	40.51	9.8	364.07	12.5
ECR	96.18	23.2	814.75	27.7

* measurements from published literature (N. A. T. Brown et al., 2003; Payne et al., 2004; J. C. Watson & Wilson, 2007b)

that of *Rangifer* (Table 3.4). When compared to *Equus*, the patterns of PCSA (rather than absolute values) for available muscles were in general similar (Figure 3.4), with the greatest differences present in the *biceps brachii* and FCU (notably larger in *Equus*).

Discussion

The muscular arrangement, muscle mass and architecture of a Malayan tapir (*Tapirus indicus*) was here investigated and compared to similar architectural data available for the modern horse *Equus ferus caballus*. The arrangement of muscles in the forelimb of *Tapirus* is very similar to that of *Equus*, although the relative size (percentage mass) of certain muscles in the lower and upper forelimb differ between these genera. It would be remiss of the authors to not address the limitations of sample size, specimen age, and comparative data availability. This study was conducted on juvenile material made available due to tragic and unfortunate circumstances, based on a non-domesticated animal registered as endangered by the IUCN Red List (Momin Khan, 1997). Multiple specimens were therefore unavailable for dissection. Comparative material based on numerous equid individuals is well documented (Brown et al. 2003; Watson and Wilson

Table 3.4. Comparison of physiological cross-sectional area (PCSA) calculations for *Tapirus* and other ungulate taxa.

Muscle	PCSA (cm^2)				
	Tapirus	***Equus***[a]	***Rangifer***[b]	***Capra***[c]	***Sus***[d]
SBC	6.5	23.0	14.3	-	-
SUP	45.3	150.3	46.5	4.9	31.2
INF	52.1	-	83.6	2.6	47.5
SUB	41.3	-	40.6	2.6	33.8
DEL	9.99	-	17.2	1.2	-
TMJ	7.4	-	5.9	7.0	-
TMN	3.2	-	11.1	8.4	8.7
BR	10.8	-	6.3	0.9	-
CBR	4.9	-	3.8	4.1	-
BB	24.1	244.8	46.1	1.0	-
TBlo	58.8	168.3	54.3	4.2	
TBla	16.1	38.4	11.5	2.4	
TBme	5.1	12.3	3.6	0.8	
ANC	5.0	-	2.8	0.5	-
BRA	1.0	-	-	-	-
EDC	5.7	36.3	3.7	0.7	-
EDL	4.6	12.1	5.5	0.3	-
UL	24.7	193.8	73.9	0.8	-
ECR	9.6	99.3	27.7	1.1	-
APL	7.3	19.1	-		-
FCU	10.6	133.9	33.0	0.4	-
FCR	9.5	18.5	3.8	0.3	-
FDS + FDP	44.4	363.3	62.4	1.9	-

[a] Brown et al., 2003, Payne et al. 2004, Watson and Wilson, 2007; [b] Wareing et al. 2011; [c] Gewaily et al. 2017; [d] Mathewson et al., 2011.

2007*a*), although a complete assessment of the muscular architecture of the *Equus* forelimb was unavailable. Despite the low sample sizes and specimen counts, observations made on the single tapir specimen offer a comprehensive account of forelimb muscular architecture in this genus, which to the authors' knowledge has not been attempted until now. Within the tapir forelimb itself, several features were

observed that were not previously noted in dissection reports and comparative studies (Bressou, 1961; Campbell, 1936; Murie, 1871; Pereira, 2013). These are discussed below, along with comparative interpretations of both equid and tapir forelimb muscular architecture.

Forelimb Musculature of Tapirus indicus

Within the forelimb of the tapir in this study, the largest muscles by mass and by PCSA include the *triceps brachii*, *supraspinatus*, *infraspinatus* and FDS+P (Tables 3.2 and 3.3). These muscles are heavily involved in propulsion and gravitational support, extending and supporting the shoulder (*infraspinatus*, *supraspinatus*), elbow (*triceps brachii*) and manus (FDS+P) (Liebich et al., 2007). When compared to other ungulate taxa (*Equus*, *Sus*, *Capra* and *Rangifer*; Table 3.4), the physiological cross-sectional area (PCSA) of the tapir deep lateral shoulder muscles (*supraspinatus* and *infraspinatus*) shows similarities to *Rangifer* and *Sus*, albeit with different absolute values; the ratio of the PCSAs of these muscles is more similar to *Sus* than *Rangifer*, potentially explained by the relatively smaller attachment site (supraspinous fossa) in cervids and bovids compared to suids and tapirs. The *supraspinatus* and *infraspinatus* have been shown to be of particular interest for tapir locomotion (MacLaren & Nauwelaerts, 2016), with the mountain tapir *T. pinchaque* exhibiting a very large supraspinous fossa, interpreted as an adaptation for shock absorption at the shoulder (MacLaren & Nauwelaerts, 2016). In this study, the *infraspinatus* of *T. indicus* was observed to occupy not only the infraspinous fossa, but also to pass over the scapular spine with an accessory head originating from the supraspinous fossa as well. This muscular arrangement is also observed in suids (Barone, 2000), with the attachment of the accessory head of the *infraspinatus* on the dorsal region of the scapular spine, in part explaining the peculiar morphology of the spine in *T. indicus* (as observed in MacLaren and Nauwelaerts 2016). This muscular arrangement is observed in both juvenile and adult specimens of *T. indicus*, whereby the *infraspinatus* lies in the infraspinous fossa and a secondary head of the muscle originates from the dorsal scapular spine, distal to the ridge running along the scapular spine on the supraspinous side (MacLaren & Nauwelaerts, 2016). Previous studies did not report this morphology in *T. indicus* (Bressou, 1961; Murie, 1871); published muscular assessments of other tapirs are uncommon (Campbell, 1936; Pereira, 2013), and do not suggest this muscle arrangement is present in neotropical tapirs. None of the modern neotropical tapirs possess the clear ridge on the dorsal aspect of the scapular spine (MacLaren & Nauwelaerts, 2016). Assuming this scapular blade morphology is directly linked with the *infraspinatus* extending above the scapular spine in *T. indicus* (present in adult and juvenile specimens; MacLaren and Nauwelaerts, 2016), it seems likely that the *infraspinatus* of modern neotropical species is restricted

to the infraspinous fossa. This is an avenue of investigation beyond the scope of this study, but represents a clear and testable hypothesis for future comparative dissections and descriptions of muscle architecture in tapirs.

When compared to dissections of other tapir species, we are limited to comparing *T. indicus* to the lowland tapir *T. terrestris*. Unfortunately, no muscular architecture is available for this species, despite rigorous comparative dissections having been performed (Campbell, 1936; Pereira, 2013). When comparing muscular arrangements to those described for *T. terrestris*, we find differences to several origination and insertion sites reported in Pereira (2013); however, the majority of the muscle locations observed corroborate other myological investigations into both *T. indicus* and *T. terrestris* (Bressou, 1961; Campbell, 1936; Murie, 1871). Variation between these two taxa in the muscles of the manus may be expected due to the significant differences in carpal and metacarpal morphology (Earle, 1893; MacLaren & Nauwelaerts, 2017), possibly pertaining to different functional outcomes. From a brief comparison with a *T. terrestris* manus, the size of the digital interossei (*flexores breves profundi manus*; Campbell, 1936) in *T. indicus* (despite the young age of this specimen) were comparable with those of the adult *T. terrestris*. The most notable difference is that of the interossei of the fifth digit (IDV), the only interosseus of the manus that originates solely from the unciform, which in *T. indicus* is broad and (in our specimen) presented an additional belly to the muscle on the lateral side. Within the interossei of the *T. indicus* specimen, muscle pennation angles in the IDV were much lower than the other interossei (average IDII = 43°, IDIII = 30°, IDIV = 30°, IDV < 5°). This suggests that the amount of force transmitted to the tendon of the IDV will be less affected by pennation angle than in the other interossei. By contrast, the fifth digit abductor (AbDV) was the most pennate muscle in the forelimb (in this study), suggesting that the muscle force transmitted to the AbDV tendon to abduct the fifth digit (i.e. spread the digits) may be comparatively reduced. Further investigations into the comparative manus musculature between in the functionally tetradactyl *T. indicus* and other modern tapirs with less obligate use of the fifth digit (e.g. *T. bairdii*; Maclaren and Nauwelaerts 2017) will doubtless provide further information on how, and potentially why, modern tapirs differ in their interaction with their underfoot substrate.

Forelimb Muscle Similarities between Tapirus *and* Equus

In this study, we put forward the hypothesis that muscular arrangement in *Tapirus* and *Equus* would differ more greatly in the lower forelimb than the upper forelimb, due to the highly specialised distal limb of *Equus*. We found this hypothesis to be only partially supported. Percentage masses of lower forelimb muscles in *Equus* differed notably to

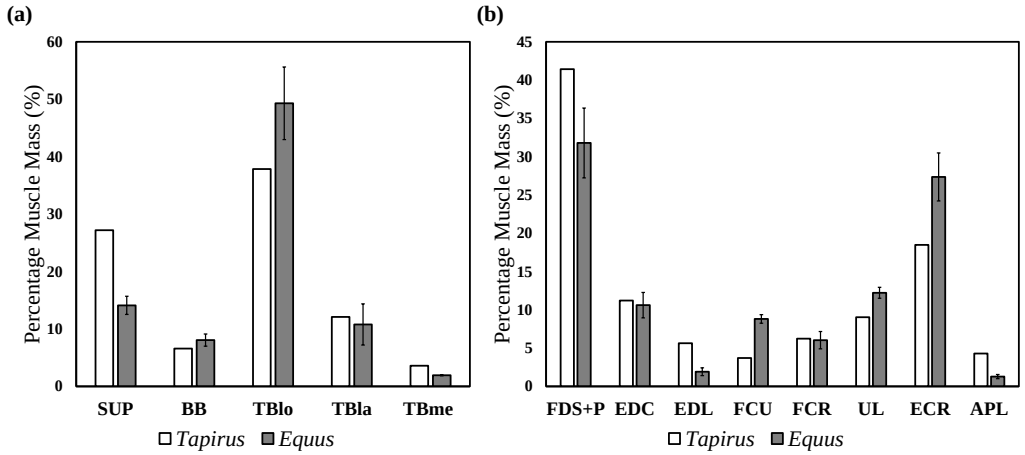

Figure 3.3. Comparison of percentage muscle mass in a comparative sample of **(a)** upper and **(b)** lower forelimb muscle in *Tapirus* (white) and *Equus* (grey). Muscle abbreviations: SUP, *supraspinatus*; BB, *biceps brachii*; TBlo, *triceps brachii* (*caput longum*); TBla, *triceps brachii* (*caput laterale*); TBme, *triceps brachii* (*caput mediale*); FDS+P, merged *flexor digitorum sublimis + profundus*; EDC, *extensor digitorum communis*; EDL, *extensor digitorum lateralis*; FCU, *flexor carpi ulnaris*; FCR, *flexor carpi radialis*; UL, *extensor carpi radialis* (in tapirs), *ulnaris lateralis* (in equids); ECR, *extensor carpi radialis;* APL, *abductor pollicis longus*. (a) Average % masses for upper limb muscles of *Tapirus* (this study) and Equus (from Watson and Wilson 2007; n = 2). (b) Average % masses for lower limb muscles of *Tapirus* (this study) and *Equus* (from Brown et al. 2003; n = 7).

those of *Tapirus* (Table 3.3; Figure 3.3) in this study. Across both upper and lower forelimbs, the greatest differences in % mass were represented by the abductor pollicis longus (APL; 235% higher in *Tapirus*), *extensor digitorum lateralis* (EDL; 194% higher in *Tapirus*), the *flexor carpi ulnaris* (FCU; 137% larger in *Equus*) and the *supraspinatus* (SUP; 92% larger in *Tapirus*). Unfortunately only five muscles were available for comparison between *Tapirus* and *Equus* in the upper forelimb, and these did not include the *infraspinatus* or *subscapularis*, which are intimately associated with the *supraspinatus* in function of the shoulder (Barone, 2000; Mathewson, Kwan, Eng, Lieber, & Ward, 2014). Nevertheless, with the muscles that were available for comparison we show that 60% of upper forelimb muscle masses exhibited by *Tapirus* fell outside the standard deviations of the *Equus* sample (Figure 3.3a; error bars). By contrast, 75% of lower forelimb muscle masses displayed by *Tapirus* fell outside the

range of standard deviations from the % muscle mass calculations for the *Equus* sample (Figure 3.3b; error bars). This strongly supports our hypothesis of greater differences in patterns of muscle mass between *Tapirus* and *Equus* in the lower forelimb.

PCSA results were not tested for significant differences, due to the large mass differences between these two taxa, and the fact that a juvenile (*Tapirus*) was compared to adults (*Equus*). Behavioural surveys of Malayan tapirs suggest that juveniles mature rapidly between four and eight months, weaning as early as six months of age (Gilmore, 2001). However, as there is no current data on how ontogeny may affect perissodactyl muscular architecture, the potential issues that scaling up juvenile muscle mass or architectural properties may cause (e.g. isometric vs. allometric scaling in different muscles; Miller et al., 2007) precluded us from pursuing this as an option. Encouragingly, the limited number of previous studies investigating ontogenetic variation in architecture of mammalian limb muscles have shown that, although absolute values do differ, the patterns of PCSA across forelimb muscles do not vary greatly between adults and juveniles (Olson et al., 2018). Therefore, for the comparisons presented in this study, we believe that the juvenile tapir offers a viable approximation of the pattern of muscular architecture that may be observed in an adult of the same species. Trends in PCSA across the forelimb suggest that both the upper and lower forelimb muscles follow a similar pattern in *Equus* and *Tapirus*, which does not directly support our hypothesis. Two muscles show a clear deviation from the trend in PCSA between *Equus* and *Tapirus*: the *biceps brachii* and the *flexor carpi ulnaris* (FCU; Figure 3.4). The more representative % mass results for the EDL and FCU (based on mass calculations for the entire lower forelimb) and the muscle architecture of the *biceps brachii* and FCU will be further discussed from a comparative functional standpoint.

The *biceps brachii* is proximomedially positioned in the upper forelimb, antagonistic to the *triceps brachii*, and one of the principal flexors of the elbow. The origination tendon of the *biceps brachii* passes from the coracoid process of the scapula through the intertubercular groove, passing along the long axis of the humerus to insert on the proximal radius (Liebich et al., 2007; J. C. Watson & Wilson, 2007b). The biceps stores elastic energy within its internal tendon during the stance phase to initiate limb protraction during swing phase (A. M. Wilson, Watson, & Lichtwark, 2003), which is of great value for a large animal running at consistent high speeds (e.g. equids). The relatively large PCSA of the *biceps brachii* in *Equus* compared to *Tapirus* may be explained by this reliance by equids on retaining energy in flexor tendons for swift, efficient movement over long distances. By comparison, the *supraspinatus* of *Equus* has a much lower PCSA (150.3 cm^2) than the *biceps brachii* (244.8 cm^2), whereas *Tapirus* demonstrates the opposite condition (*supraspinatus* = 45.3 cm^2; *biceps brachii*

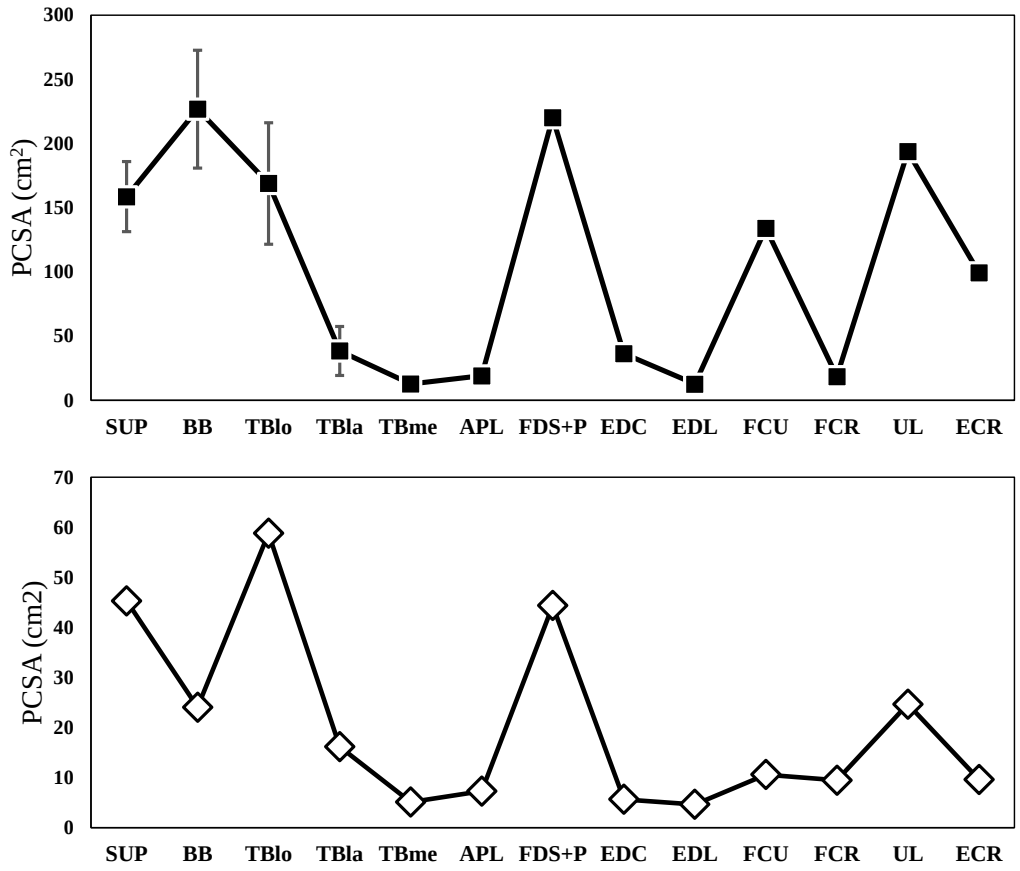

Figure 3.4. Comparison of physiological cross-sectional area (PCSA) in the forelimb muscles of *Equus* (squares; top) and *Tapirus* (diamonds; bottom). PCSAs for *Equus* taken from values in previous studies (Brown et al. 2003; Watson and Wilson 2007); error bars denote standard deviation, with number of individuals presented above bar. Muscle abbreviations: SCL, *subclavius*; SUP, *supraspinatus*; BB, *biceps brachii*; TBlo, *triceps brachii* (*caput longum*); TBla, *triceps brachii* (*caput laterale*); TBme, *triceps brachii* (*caput mediale*); APL, *abductor pollicis longus*; FDS+P, merged *flexor digitorum sublimis + profundus*; EDC, *extensor digitorum communis*; EDL, *extensor digitorum lateralis*; FCU, *flexor carpi ulnaris*; FCR, *flexor carpi radialis*; UL, *extensor carpi ulnaris* (in tapirs), *ulnaris lateralis* (in equids); ECR, *extensor carpi radialis*. PCSAs for upper limb muscles of *Equus* from Watson and Wilson (2007; n = 2) and average PCSAs from lower limb of *Equus* from Brown et al. (2003; n = 7).

= 24.1 cm^2). We may conclude from this that, in relative terms, the *biceps brachii* is more important than the *supraspinatus* as a shoulder extensor in *Equus* (as shown by Watson and Wilson 2007), whereas the *supraspinatus* is of greater importance in this role for *Tapirus*. It is possible that this difference between shoulder extensor PCSAs has an ecological signal; open-habitat sprinting cheetahs (*Acinonyx*) exhibit a large biceps brachii PCSA compared to the predominantly rainforest-based jaguar (*Panthera onca*) (Cuff et al., 2016). However, although both comparisons demonstrate similar patterns of PCSA variation between species, establishing a true ecological signal would require more rigorous testing across a greater sample of taxa.

In accordance with our hypothesis, we observe notable differences in the lower forelimb of *Tapirus* when compared to that of *Equus*. As previously noted by several authors (Campbell, 1936; Murie, 1871), the *flexor digitorum superficialis* and *flexor digitorum profundus* in our specimen share sufficient muscle fibres to be considered combined (FDS+P) rather than separate as in equids, although the separate origination heads are homologous to those in *Equus*. We note that the *extensor carpi ulnaris* (*ulnaris lateralis* in *Equus* and many other ungulates) does perform an extensor function rather than a modified flexor, corroborating previous observations on both *T. indicus* and *T. terrestris* (Campbell, 1936; Murie, 1871; Pereira, 2013). Due in part to this extensor function of the *ulnaris lateralis* (UL), the mean muscle volumes of carpal and digital flexor and extensors differs between tapirs and equids (N. A. T. Brown et al., 2003). The flexor : extensor volume ratio for muscles acting on the carpus in *Tapirus* (0.37:1.00) is lower than that exhibited by *Equus* (0.95:1.00), and overall flexor:extensor muscle volume ratio (0.95:1.00) suggests that the lower forelimb flexors are relatively greater in importance for *Equus* (1.43:1.00) (N. A. T. Brown et al., 2003). This volume difference is partially explained by the relatively greater mass (and PCSA) of the FCU in *Equus* compared to *Tapirus* (Table 3.3; Figures 3.3–3.4). In turn, the greater % mass and PCSA of the FCU in *Equus* is in keeping with the necessity for energy retention in the stance phase and explosive release as the hoof leaves the ground during locomotion in equids. The rapid flexion of the carpus (and indeed the entire forelimb facilitated by the *biceps brachii*) expedites the initiation of the swing phase, a vital adaptation for running at high speed over large distances.

The muscle with the lowest % mass and smallest PCSA in the equid lower limb is the *extensor digitorum lateralis* (EDL). While also having the smallest PCSA in *Tapirus*, this muscle has more than double the % mass for *Tapirus* than is observed in *Equus*. The function of this muscle goes some way to explaining the differences in % mass for the EDL, as it is an extensor of the two lateral digits in *Tapirus* (digit IV and V) (Bressou, 1961; Campbell, 1936; Murie, 1871; Pereira, 2013). Equids, having lost full

function of their fifth digit over 40 million years ago (MacFadden, 2005), are therefore likely to have reduced this muscle relative to those which still act upon the functional third digit (e.g. EDC). The insertion tendon which passed to the functional fourth digit in basal equids is retained in modern equids, and now inserts on the lateral surface of the medial phalanx of digit III (Liebich et al., 2007). As a result, we may conclude that tapirs with reduced functionality of the fifth digit compared to *T. indicus* (e.g. *T. bairdii*; MacLaren and Nauwelaerts 2016) may exhibit a reduction in % mass in the EDL. Furthermore, this result has implications for modelling changes in equid locomotion through time. Greater understanding and quantification of muscular architecture in modern tapir species will be of great importance for estimating changes of muscular morphology and action during digit reduction through equid evolution.

Conclusion

In this study, we present the first published muscular architecture of the forelimb of the Malayan tapir (*Tapirus indicus*). We successfully quantify the muscles of the forelimb in this functionally tetradactyl perissodactyl using architectural measures including muscle mass, volume, pennation angle and physiological cross-sectional area (PCSA). To our knowledge, this is the first attempt to quantify these data in the genus *Tapirus*, which remains enigmatic and somewhat understudied in its functional anatomy. By comparing the muscular architecture of *Tapirus* with that of previously published studies on forelimb muscles, we identify multiple similarities between tapirs and their monodactyl relative *Equus*. Significant differences in % muscle mass accounted for by the *supraspinatus*, *flexor carpi ulnaris* and lateral digital flexor muscles were observed, in addition to relative divergence in PCSA of the *biceps brachii* and *flexor carpi ulnaris*. These differences graphically demonstrate several adaptations that equids have undergone to their muscular architecture during the progression from tetradactyl forest-dwellers to monodactyl, open-habitat specialists. When investigating locomotion in the small, closed-habitat ancestors and relatives of modern equids (e.g. *Sifrhippus*, *Hallensia*, *Propalaeotherium*), it will be essential to understand how different muscle groups in the limbs have adopted greater or more reduced importance through evolutionary transitions such as that of equids. Results from this study are an ideal first step towards developing viable locomotor models of early equid ancestors. Further studies, hopefully adding more comparative material of neotropical tapirs and comprehensive assessments from modern *Equus* muscular architecture, may also focus on correlating differences observed in muscular architecture patterns with changes in bone morphology across locomotor transitions in Perissodactyls.

“all you have to decide is what to do
with the time that is given to you”

- Gandalf -

– RESEARCH CHAPTER FOUR –

A morphometric analysis of the forelimb in the genus *Tapirus* (Perissodactyla: Tapiridae) reveals influences of habitat, phylogeny and size through time and across geographical space

Jamie A. MacLaren - Richard C. Hulbert - Steven C. Wallace - Sandra Nauwelaerts

adapted from *Zoological Journal of the Linnean Society* (2018) **184**:499–515

The limb skeleton of tapirs (Perissodactyla: *Tapirus* spp.) was traditionally thought to exhibit morphological variation correlated with changes in body size. Here, we test whether forelimb variation exhibited by *Tapirus* is a byproduct of size fluctuations through the tapir fossil record, or whether it is influenced by habitat differences. We investigated the forelimb osteology of 12 species of *Tapirus* using 3D geometric morphometrics on laser surface scans. Aligned shape coordinates were regressed against intrinsic bone size to account for allometry. Stable carbon isotope values were averaged per species as a proxy for habitat density. Multivariate regressions of the humerus, pisiform, cuneiform, unciform, third and fourth metacarpals revealed no significant influence of size on shape. Taxa of equivalent predicted body mass (e.g. *T. pinchaque*, *T. lundeliusi*) were shown to exhibit significant differences in bone shape both before and after correction for allometric influence. The lateral carpals (pisiform, cuneiform, unciform) demonstrated variation across the habitat density gradient. Observed variation is likely driven by species in the extinct subgenus *Helicotapirus* which inhabited drier, more open woodland areas than modern taxa. We conclude that tapir forelimb variation is not exclusively an artefact of body size, with lateral wrist bones displaying notable differences across a habitat density gradient, beyond that resulting from size and phylogenetic effects.

Introduction

For many years the skeleton of the modern tapir *Tapirus* Brisson (Perissodactyla: Tapiridae) has been considered pleisiomorphic (Earle, 1893; Gregory, 1929; Radinsky, 1965b; Simpson, 1945). The combination of a tetradactyl (four-toed) forelimb, unspecialised lophodont dentition and closed-habitat environments in which tapirs are

currently found are analogous to the earliest ancestors of other modern perissodactyl groups including rhinoceroses (Rhinocerotidae), equids (Equidae) and tapirs themselves (Bai et al., 2017; DeSantis & MacFadden, 2007; Holbrook, 2001; Secord, Wing, & Chew, 2008). Tapir postcranial anatomy has undergone little quantitative attention due to historical claims that tapir limb bones vary in shape only as an influence of changes in body size (Hershkovitz, 1954; Radinsky, 1965b). Extant tapirs share several morphological features in common with Paleogene tapiroids (M. W. Colbert, 2005; Holbrook, 1999; Radinsky, 1965b), with differences reported in the forelimb limited to the robusticity of the limb bones (associated with greater mass), and several features associated with greater cursoriality (e.g. loss of acromion of the scapula; Radinsky 1965). This reported lack of variation in the tapir skeleton through time has in the past lead authors to describe it as a 'living fossil' (Janis, 1984; Rustioni & Mazza, 2001), and utilise tapir fossils as a robust indicator of forested habitats through time (DeSantis & MacFadden, 2007). However, recent quantitative examinations of forelimb osteology in modern *Tapirus* have revealed unexpected interspecific variation within this locomotor unit.

Quantitative investigations into extant tapir forelimb skeleton have recently revealed interspecific differences in keeping with different locomotor outcomes (MacLaren & Nauwelaerts, 2016, 2017). Most notably, variation was observed between tapirs sharing close phylogenetic affinity (*Tapirus pinchaque* and *T. terrestris*) but inhabiting different ecological biomes (Padilla & Dowler, 1994; Padilla et al., 2010). Forelimb bone shape in *T. pinchaque*, a species inhabiting tropical yet high-altitude shrubland and cloud forest species, was most divergent of all the modern taxa (MacLaren & Nauwelaerts, 2016, 2017; Ruiz-García et al., 2016). Within these quantitative studies, differences were also found between taxa of greatly different body masses (e.g., *T. indicus* and *T. terrestris*), supporting the historical viewpoint on postcranial shape variation being correlated with size in tapirs (Earle, 1893; Hershkovitz, 1954; Radinsky, 1965b). However, the range of body sizes within extant tapirs is not representative of the genus *Tapirus* as a whole, which includes at least 21 valid extinct species, with several proposed subgenera (e.g., *Acrocodia*, *Helicotapirus*, *Megatapirus*). To truly test whether the morphology of the tapir postcranial skeleton is correlated with body size, a greater range of taxa than the four extant species should be incorporated in a morphological analysis, free of both isometric and allometric (size-dependent) shape variation.

In addition to studies revealing locomotor disparity within this apparently ecologically conserved clade (Hulbert, 2005; MacLaren & Nauwelaerts, 2016, 2017), ranges in habitat exploitation and dietary preferences have also been demonstrated in tapirs

(DeSantis, 2011; DeSantis & MacFadden, 2007; Padilla et al., 2010; Ruiz-García et al., 2012) using stable carbon isotope ratios ($\delta^{13}C$) from tooth enamel (including DeSantis and MacFadden 2007; Secord et al. 2008; Boardman and Secord 2013). Disparity in stable isotope ranges has not been specifically linked to any morphological differences in either the cranial or post-cranial skeleton of tapirs, despite evidence that tapirs in different time periods inhabited more open biomes compared to their current range of dense rainforest and *páramo* shrubland (Bocherens et al., 2017; DeSantis, 2011; DeSantis, Feranec, MacFadden, Robinson, & Roeder, 2009; DeSantis & Wallace, 2008; Feranec & MacFadden, 2006; Hoppe & Koch, 2006; Koch, Hoppe, & Webb, 1998; Kohn, McKay, & Knight, 2005; MacFadden & Cerling, 1996; Nelson, 2014; Padilla et al., 2010; Perez-Crespo, Arroyo-Cabrales, Alva-Valdivia, Morales-Puente, & Cienfuegos-Alvarado, 2012). The functional and locomotor challenges of occupying a dense, closed forest environment will differ to those of a more open habitat (Curran, 2015), and morphological differences may be expected between closed-canopy rainforest taxa and those existing in drier and more open woodland realms. Alternatively, the influence of phylogenetic relatedness may cause morphological conservancy within limb bones of closely related taxa, irrespective of their habitat preference (e.g. giraffid humeri; Owen 1838; Basu et al. 2016).

Here, we investigate whether forelimb variation exhibited by a broad sample of *Tapirus* is correlated only with changes in size through the tapir fossil record (as suggested by previous authors; Simpson 1945; Radinsky 1965; cited in Padilla and Dowler 1994; Rustioni and Mazza 2001), or whether differences in limb osteology are also influenced by phylogenetic relatedness or habitat variation. Based upon recent quantitative findings (Hulbert, 2005; MacLaren & Nauwelaerts, 2016, 2017), we use a three-dimensional geometric morphometric approach to test the hypothesis that habitat influences forelimb shape variation in tapirs after accounting for allometry (size-dependent shape). This approach is conducted on a series of extant and extinct *Tapirus* species across a spectrum of body sizes within a phylogenetic context.

Institutional Abbreviations:– AMNH, American Museum of Natural History, New York; **ETMNH**, East Tennessee State University and General Shale Brick Museum of Natural History, Gray; **UF**, Florida Museum of Natural History, Gainesville; **UF/FGS**, collection of the Florida Geological Survey, housed at the Florida Museum of Natural History; **FSL**, Université Claude Bernard Lyon, Lyon; **MEO,** MuseOs Natuurhistorisch Museum, Koksijde; **MNHN**, Muséum National d'Histoire Naturelle, Paris; **MVZ**, Museum of Vertebrate Zoology, Berkeley; **NHMW**, Naturhistorisches Museum Wien, Vienna; **RMNH**, Naturalis Biodiversity Centre, Leiden; **ZMB MAM**, Museum für Naturkunde (Mammal Collections), Berlin.

Methodology

Specimens

Forelimb material from extinct tapir species was laser scanned at the Florida Museum of Natural History (Gainesville, FL) and the Gray Fossil Site and General Shale Natural History Museum (Gray, TN). Species included *T. webbi* Hulbert, *T. polkensis* Olsen, and the *Helicotapirus* species *T. lundeliusi* Hulbert, *T. haysii* Leidy and *T. veroensis* Sellards (Hulbert, 2010) (Table 4.1). These North American specimens were supplemented with scans from available postcranial elements of the giant Asian tapir *Tapirus* (*Megatapirus*) *augustus* (American Museum of Natural History, NY) and the European tapirs *T. priscus* (Museum für Naturkunde, Berlin) and *T. arvernensis* (Université Claude Bernard Lyon). Individual limb elements were scanned with a FARO ScanArm Platinum V2 system with integrated FARO Laser Line Probe (≥50 μm resolution), and visualised using GeoMagic (GeoMagic Qualify v.10, Morrisville, NY, USA). Scans of fossil specimens were combined with previously analysed material representing the four extant tapir species (*T. terrestris*, *T. pinchaque*, *T. bairdii* and *T. indicus*) (MacLaren & Nauwelaerts, 2016, 2017). Bones included the humerus, radius, pisiform, cuneiform, lunate, scaphoid, magnum, unciform and the second, third, fourth and fifth metacarpals. Extant specimens were collected from museums in Europe and the USA (see Table 1.1 in MacLaren and Nauwelaerts 2016).

Geometric Morphometrics

Landmark-based geometric morphometrics has been widely used for quantifying variation in shape between objects (e.g. Zelditch et al. 2012; Klingenberg 2016). A series of discrete points (landmarks), detailing biologically and operationally homologous features, were digitally placed onto each bone using Landmark Editor v.3.0 software (Wiley et al., 2006). For full details on the 3D landmark points selected, see MacLaren and Nauwelaerts 2016 (upper arm; Table 1.1) and 2017 (autopodium; Table S2.1) (see also Appendix I, Section 1; Appendix II, Section 3). Raw landmark coordinates were exported to MorphoJ v1.06d (Klingenberg, 2011) and aligned using Generalised Procrustes Analysis (GPA) (Rohlf & Slice, 1990). GPA removes the effect of scale, location and orientation, aligning coordinate configurations based on a geometric centre (centroid). GPA produces an intrinsic size measure (centroid size; the sum of the squared distances from each landmark to the geometric centre), which was log-transformed and used for correcting shape data for allometric influence (Monteiro 1999; Klingenberg 2016). For full details regarding the choice of analysis to correct for allometric effects, see Appendix III; Table S3.1.

Body Mass Estimation

To establish whether forelimb bone size could be used as a viable proxy for overall size, we estimated tapir body masses using linear regression equations based on humeral measurements for all ungulates described in Scott (1990); these were successfully applied to tapirs previously in Hulbert et al. (2009). Linear measurements for estimating body mass were chosen based on the highest squared correlation coefficients ($R^2 \geq 0.95$) from ungulate regression equations (H3, H4 and H5; Scott 1990; also see Damuth and MacFadden (1990): Appendix). Linear measurements were performed on scanned humeri using the measuring tool in Geomagic Studio 10. Mass estimates for extant species were compared against published body mass brackets from live specimens (de Thoisy et al. 2014). Body mass estimates from individual linear measurements were averaged, log-transformed and regressed against log-transformed centroid sizes ($_{log}$CS, from geometric morphometric analysis) to assess validity of using $_{log}$CS as a representative size measure. Full details on body mass estimations can be found in the Appendix III; Section 1.

Regression, PCA and perMANOVA

Procrustes coordinates produced from GPA were regressed against log-transformed centroid size ($_{log}$CS) using multivariate regression (Klingenberg, 2016; Monteiro, 1999; Zelditch et al., 2012) producing shape variables (regression residuals) entirely independent of allometric size effects (Klingenberg, 2016). Regression residuals were subsequently subjected to principal components analyses (PCAs). PCAs produced principal component scores of regression residuals (rPCs), with species variation visualised in morphospace constructed in RStudio (RStudio Team 2016). A permutational multivariate analysis of variance (perMANOVA) of regression residuals was used to test for interspecific differences (M. J. Anderson, 2001) in aligned coordinates. PerMANOVA was chosen because dependent variables exceeded sample (specimens) number, and group sizes did not vary greatly. PerMANOVA testing was performed in PAST v.3 (Hammer, Harper, & Ryan, 2001), with pairwise perMANOVA testing (10000 permutations) performed in RStudio using the 'RVAideMemoire' package (Hervé, 2014); *p*-values were corrected using false discovery rate protocol (Benjamini & Hochberg, 1995).

Ecological Traits

Carbon isotope values ($\delta^{13}C$) extracted from tooth enamel samples of tapir species were collated from published literature and averaged per species (Table 4.1; raw values in Appendix III, Section 7). More depleted $\delta^{13}C$ values are indicative of a high level of C3 plants in the diet, with values below -14‰ suggesting the animal resided in a closed canopy, heavily forested area. Less depleated values (e.g. -12 to -10‰ are more indicative of open woodland, and values above -9‰ indicate a mixed C3/C4 plant diet. Therefore, in a clade known to occupy wooded or forest biomes, variations in stable carbon isotope values may be used as a proxy for habitat density. No isotope recordings were available for European tapir taxa. Average $\delta^{13}C$ recordings were assigned to one of four ranges, with each species falling within one range: > -13‰ (*T. haysii, T. lundeliusi, T. veroensis*); -13‰ to -14‰ (*T. webbi, T. polkensis*); -14‰ to -15‰ (*T. bairdii, T. pinchaque*); < -15‰ (*T. indicus, T. terrestris*). Interspecific differences in raw $\delta^{13}C$ values were tested for using one-way analysis of variance (ANOVA) in Past v.3 (Hammer et al., 2001) with Tukey's pairwise comparisons between *a priori* groups. Estimated body mass was regressed against average $\delta^{13}C$ values (habitat proxy) using a Generalised Least Square regression (incorporating the influence of phylogeny) to test for a correlation between size and habitat; this was performed in RStudio using the 'phytools' package (Revell 2012), fitted with .

Informal Tapir Phylogeny

Tapirus has a deep rooted evolutionary history (Holbrook, 1999; Norman & Ashley, 2000; Steiner & Ryder, 2011). To account for influence of phylogenetic relatedness on forelimb morphology, a composite phylogeny was assembled from published literary sources (M. W. Colbert, 2005; Eisenmann & Guérin, 1992; Holanda & Ferrero, 2013; Hulbert, 1995, 2005, 2010; Ruiz-García et al., 2016; Steiner & Ryder, 2011; Tong, 2005). No forelimb postcranial characters were used to construct the published trees. A phylogenetic tree was constructed in Mesquite v. 3.04, with branch lengths generated in RStudio v.1.0.143 (RStudio Team 2016) using the 'paleotree' package (Bapst, 2012). Branch lengths were calculated based on first/last occurrence dates compiled from the literature (E. H. Colbert & Hooijer, 1953; Czaplewski, Puckette, & Russell, 2002; Eisenmann & Guérin, 1992; Guérin & Eisenmann, 1982; Hulbert, 1995, 2005, 2010; Hulbert et al., 2009; Ruiz-García et al., 2016; Steiner & Ryder, 2011; Tong, 2005; Tong, Liu, & Han, 2002; van der Made, 2010). The resultant time-calibrated phylogeny was used to visually inspect variation in body mass across *Tapirus*, and statistically to account for the effect of phylogeny on shape data. The first two rPCs for bones demonstrating size-independence (after multivariate regression) were tested for

phylogenetic signal using the 'phytools' and 'geiger' packages (Revell, 2012) in RStudio. Pagel's λ was chosen as a test statistic, with a *p*-value testing for a significant departure from λ = 0 (no correlation between species). Maximum likelihood ancestral states were estimated using the 'phytools' package in RStudio (Revell, 2012, 2013) for all nodes and branches to illustrate variation in body mass across the tree topology (Labonte et al., 2016; Revell, 2013); however, no quantitative or statistical conclusions were drawn from these node estimates. Finally, forelimb shape data across ecological ranges were analysed using phylogenetic multivariate analysis of variance (phyMANOVA), based on species-averaged rPCs accounting for over 70% of shape variation; phyMANOVAs were performed in the RStudio package 'geiger' (Garland, Dickerman, Janis, & Jones, 1993). Wilks' lambda (Λ) was calculated for the phyMANOVAs, with associated *F* and *p*-values (significant ≤ 0.05), and used to test for differences between isotopic group means while simultaneously accounting for phylogenetic relatedness.

Results

Body Mass and Phylogeny

Body mass calculations for *Tapirus* species in this study are presented in Table 4.1, with log-transformed body mass (logBM) plotted onto the informal phylogenetic tree (Figure 4.1). Mass estimates range from the dwarf tapir *T. polkensis* (117 ± 18 kg) to the giant tapir *T.* (*M.*) *augustus* (631.4 kg). Phylogenetic signal is high for body mass (Pagel's λ > 0.999), although this influence is not statistically significant ($p = 0.155$). Similar results are observed when centroid size and log-transformed centroid size are tested for phylogenetic signal, with no bones significantly deviating from λ = 0 (Table 4.3; Appendix III, Table S3.15). Log-transformed centroid size was strongly correlated with estimated body mass across the forelimb (average $r^2 = 0.70$); $_{log}$CS was therefore accepted as a viable proxy for size in the remainder of the study to test against individual shape variables (rather than average values). Branch length generation from first and last occurrence dates for tapir species in this study suggest that the genus *Tapirus* divided into two geographically separated lineages in the early-middle Aquitanian (~22 Mya), prior to the 'tapir vacuum' (van der Made, 2010). The extinct subgenus *Helicotapirus* (including *T. lundeliusi*, *T. haysii* and *T. veroensis*) is estimated to have split from modern *T. bairdii* around 7 Mya; modern neotropical taxa are predicted to have diverged 9–10 Mya, with subsequent divergence of *T. terrestris* and *T. pinchaque* lineages around 5 Mya (Figure 4.1).

Table 4.1. Body mass estimates for *Tapirus* species based on humeral linear measurements; number of specimens (*n*), geographical origin (location), mean estimated BM ($\bar{x}$) in kg, standard deviation (*s*), log-transformed body mass used in comparative analyses ($_{log}$BM), and average stable carbon isotope recording from literature (δ^{13}C).

Species	*n*	location	$\bar{x}$	*s*	$_{log}$BM	δ^{13}C
T. (*M.*) *augustus*	1	SE Asia	631.4	-	6.45	-
T. priscus	1	Europe	349.8[a]	-	5.86	-
T. indicus	8	SE Asia	326.4	14.53	5.79	15.4
T. webbi	6	N America	293.3	31.59	5.68	13.0
T. sanyuanensis	1	SE Asia	284.0[b]	-	5.64	-
T. haysii	1	N America	279.2	-	5.63	12.2
T. veroensis	5	N America	232.1	18.46	5.45	12.7
T. bairdii	5	CS America	228.7	15.25	5.43	14.8
T. terrestris	5	S America	216.6	25.57	5.38	15.6
T. arvernensis	1	Europe	215.0[a]	-	5.37	-
T. lundeliusi	8	N America	202.8	23.62	5.31	12.8
T. pinchaque	4	S America	202.4	19.28	5.31	14.3
T. polkensis	6	N America	116.9	18.26	4.76	13.1

[a] mass predicted from radius-humerus regression (see Appendix III)
[b] measurements taken with permission from scaled images of humerus in Tong and Qiu (2008)

Shape Variable Regression

Results from multivariate regression of shape variables (Procrustes coordinates) against $_{log}$CS for each bone in this study are presented in Table 4.2. Half of the bones (six of 12) demonstrated a significant correlation between size and morphological variables (bold *p*-values; Table 4.2), most notably in the radius and MCII. The humerus, pisiform, cuneiform, unciform, MCIII and MCIV demonstrate non-significant influence by both $_{log}$CS and $_{log}$BM on the shape variables (Table 4.2). These bones were further analysed and are described as 'size-independent' bones forthwith. All correlations from multivariate regressions are displayed in Appendix III, Figure S3.2.

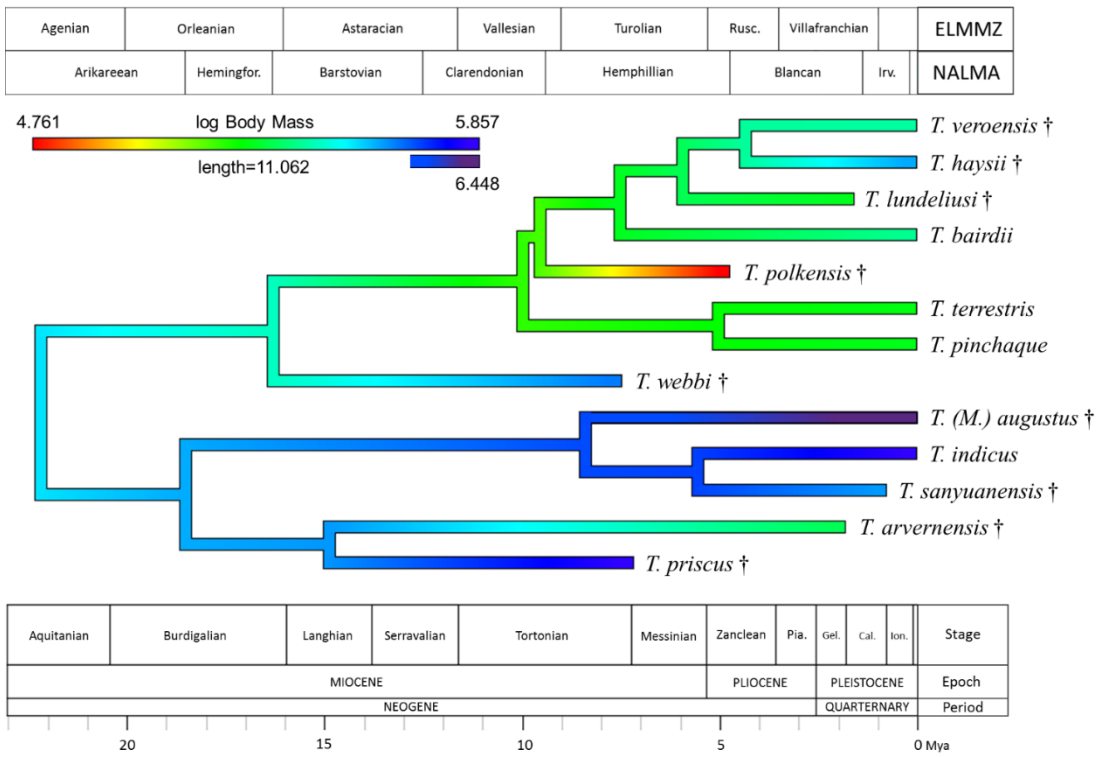

Figure 4.1. Tapir body mass ($_{log}$BM) plotted onto informal phylogenetic tree. Maximum and minimum trait values shown. Time calibration based upon first-last occurrences. Extinct taxa denoted with †. Outsized *T.* (*M.*) *augustus* plotted with separate scale. Abbreviations of **ELMMZ** (European Land Mammal Mega-Zones): Rusc. = Ruscinian; **NALMA** (North American Land Mammal Ages): Irv. = Irvingtonian, Rancholabrean follows Irvingtonian; **ICS**: Pia. = Piacenzian, Gel. = Gelasian, Cal. = Calabrian, Ion. = "Ionian".

Size-Independent Shape Variation

Size-independent shape variation in the six bones shown to display non-significant allometric influence (humerus, pisiform, cuneiform, unciform, MCIII and MCIV) was examined using principal components analysis of the multivariate regression residuals (Figure 4.2). Overall, the extinct North American taxa (*T. webbi*, *T. polkensis*, *T. lundeliusi*, *T. haysii* and *T. veroensis*) cluster in separate regions of morphospace to those of modern neotropical and Asian species (Figure 4.2), although overlaps in morphospace occupation do occur for most bones. Results of phylogenetic signal testing

for the first two rPCs of all bones are presented in Table 4.3, with the pisiform and unciform demonstrating significant influence from species relatedness. PerMANOVA testing suggests overall significant differences in the species means for all bones (Table 4.4; see also Appendix III, Table S4.2). Pairwise comparisons between species for all bones can be found in the Appendix III, Tables S4.3–S4.14).

Table 4.2. Multivariate regressions (shape variables vs. size variables) for tapir forelimb bones. Permutation test (x10000) against a null hypothesis of size-independence (***p***), correlation cooefficient (R^2), % sum of squares predicted by size variable (*% pred.*) reported with significant *p*-values in bold.

Bone	**log Centroid Size**		
	n	**% predicted**	***p***
Humerus	37	5.5	*0.06*
Radius	44	11.9	***<0.01***
Pisiform	46	1.8	*0.54*
Cuneiform	39	2.5	*0.50*
Lunate	47	3.7	***0.03***
Scaphoid	42	5.5	***<0.01***
Magnum	48	5.1	***<0.01***
Unciform	48	3.1	*0.10*
Metacarpal II	51	7.9	***<0.01***
Metacarpal III	50	2.2	*0.15*
Metacarpal IV	45	3.6	*0.10*
Metacarpal V	51	5.3	***<0.01***

In humeral morphospace, the extant mountain tapir *T. pinchaque* is revealed as an outlier to other species (Figure 4.2a); the largest taxon in the humeral analysis (*T.* (*M.*) *augustus*) does not cluster with the other large taxa (*T. indicus* and *T. webbi*). The humerus of *T. indicus* is found to be significantly different in size-independent morphology to all taxa in the analysis represented by >1 specimen. Results from phylogenetic signal for the humerus suggest very little influence of interspecific relatedness (rPC1 $\lambda < 0.01$, $p = 1.00$; rPC2 $\lambda < 0.01$, $p = 0.47$).

Table 4.3. Phylogenetic signal testing on first two principal components of regression residuals and on centroid size (rPC1; rPC2; $_{log}$CS) for species-averaged tapir forelimb bones. Variance % accounted for by each rPC reported, with Pagel's Lambda (λ) and significance of departure from 0 for λ statistic (*p*; significant <0.05). Significant *p*-values for λ statistic in bold.

Bone	rPC1			rPC2			$_{log}$Centroid Size	
	Var. %	**λ**	***p***	**Var. %**	**λ**	***p***	**λ**	***p***
Humerus	54.8	<0.01	*1.00*	18.6	0.85	*0.47*	<0.01	*1.00*
Radius	25.7	0.99	*0.09*	22.7	0.99	*0.13*	0.99	*0.28*
Pisiform	57.6	0.99	***0.04***	18.1	<0.01	*1.00*	0.99	*0.29*
Cuneiform	38.8	<0.01	*1.00*	22.1	<0.01	*1.00*	<0.01	*1.00*
Lunate	37.9	<0.01	*1.00*	19.3	<0.01	*1.00*	0.98	*0.77*
Scaphoid	38.3	<0.01	*1.00*	18.4	<0.01	*1.00*	0.96	*0.560*
Magnum	39.2	<0.01	*1.00*	21.2	<0.01	*1.00*	0.99	*0.52*
Unciform	36.4	0.99	***0.03***	22.4	<0.01	*1.00*	<0.01	*1.00*
MCII	34.2	0.91	*0.46*	18.8	<0.01	*1.00*	<0.01	*1.00*
MCIII	49.7	<0.01	*1.00*	16.7	0.59	*0.53*	<0.01	*1.00*
MCIV	48.6	0.99	*0.23*	18.3	<0.01	*1.00*	<0.01	*1.00*
MCV	44.8	0.99	*0.23*	19.8	<0.01	*1.00*	0.99	*0.51*

For pisiform morphospace, the two largest species (*T. indicus* and *T. webbi*) represent the two extremes of morphology along rPC1 (Figure 4.2b); *T. webbi* demonstrates a pronounced proximal protrusion of the spatulate process for the insertion of the *flexor carpi ulnaris*, causing the process to appear triangular in this species. Pairwise comparisons suggest that the pisiform of *T. webbi* is the most distinct, exhibiting significant differences to all species except *T. haysii*. Of the modern taxa, *T. bairdii* and *T. indicus* demonstrate significant differences (p = 0.033), and both *T. indicus* and *T. terrestris* are significantly separated from all extinct species. Phylogenetic signal for the pisiform along rPC1 is high and significantly differs from 0 (rPC1 λ = 0.99; p = 0.040) (Table 4.4).

Cuneiform morphospace suggests the larger North American species (*T. webbi* and *T. haysii*) exhibit similar morphologies to one another, but divergent from the large

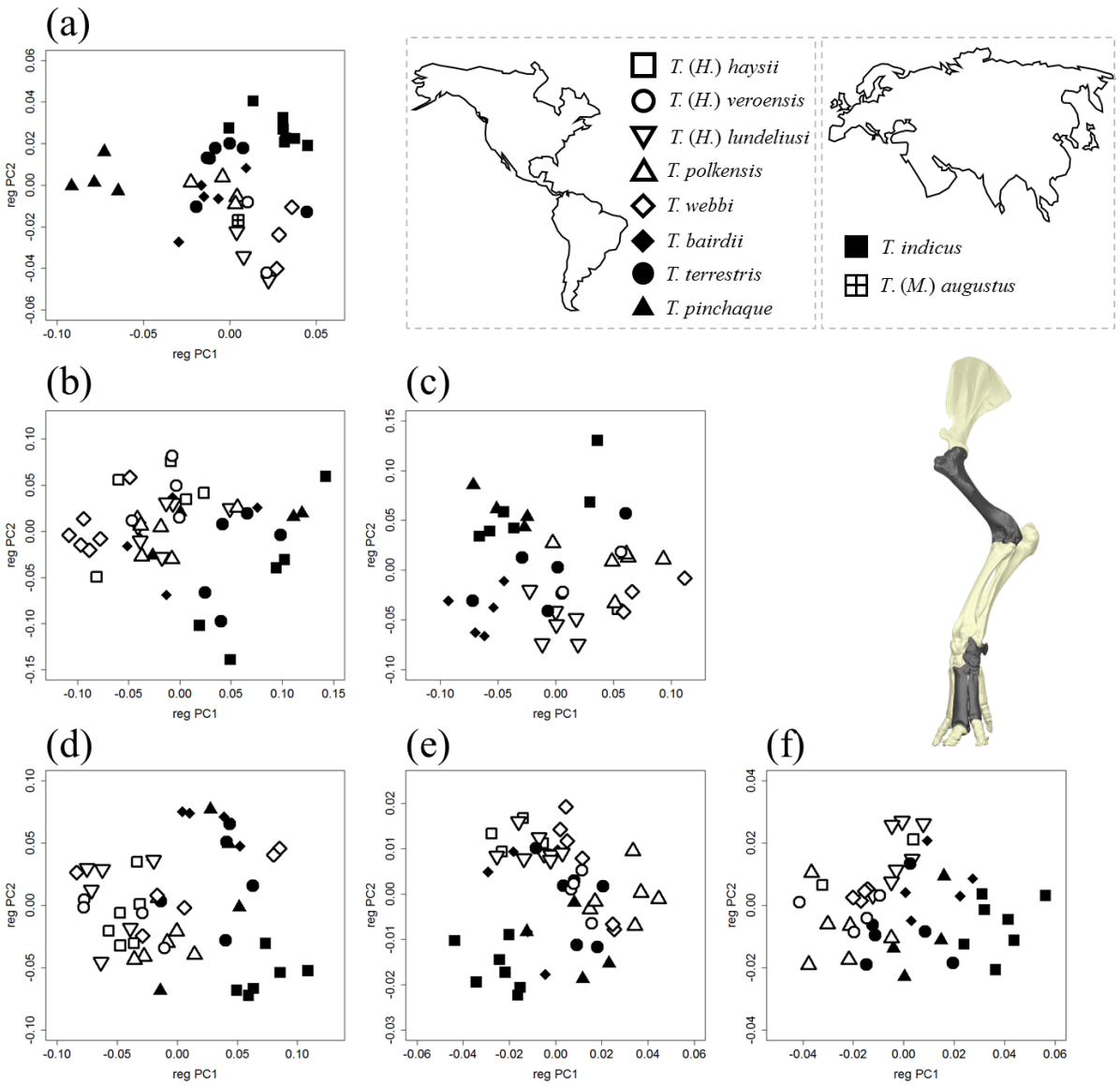

Figure 4.2. Morphospace occupation based on multivariate regression residuals (shape vs. log-transformed centroid size) for six *Tapirus* forelimb bones: **(a)** humerus; **(b)** pisiform; **(c)** cuneiform; **(d)** unciform; **(e)** metacarpal III; **(f)** metacarpal IV. Representative bones are shown in situ on left forelimb of *T. bairdii* (RMNH 43495).

Malayan tapir (*T. indicus*) (Figure 4.2c). *T. bairdii* displays the greatest difference in cuneiform morphology to other taxa, with significant differences found between it and

all taxa represented by >1 specimen. Phylogenetic signal for the cuneiform is very low (rPC1 $\lambda < 0.01$; rPC2 $\lambda < 0.01$) (Table 4.3); along with the humerus, the cuneiform displays the least influence from both body mass and species relatedness.

The spread of species in unciform morphospace suggests a splitting of taxa into three groups with minimal overlap: a *T. indicus* group, an extant neotropical grouping and a North American group (Figure 4.2d); two *T. webbi* are removed from the main North American group. The unciform displays significant phylogenetic signal for rPC1 ($\lambda > 0.99$; $p = 0.03$), but not for rPC2 ($\lambda < 0.01$).

Metacarpal III (MCIII) morphospace patterns show the greatest degree of overlap between extant and extinct species (Figure 4.2e). The only Eurasian taxon (*T. indicus*) plots separately to all New World tapirs. *T. webbi* possesses the largest MCIIIs, and is the only taxon to exhibit non-significant differences in MCIII morphology (to *T. pinchaque*, *T. terrestris* and *T. veroensis*). Phylogenetic signal for the MCIII is overall low (rPC1 $\lambda < 0.01$; rPC2 $\lambda = 0.59$).

Metacarpal IV (MCIV) morphospace occupation suggests a gradual size-independent shape difference spectrum from North American taxa, through South American taxa to Eurasian taxa along rPC1 (Figure 4.2f). *T. webbi* and *T. haysii* occupy different regions of morphospace to the equally large *T. indicus*. Both *T. indicus* and *T. bairdii* differ significantly from all other tapirs in the analysis, with *T. webbi* and *T. lundeliusi* exhibiting significant differences to all other taxa except *T. haysii*. Phylogenetic signal for the MCIV is high (rPC1 $\lambda = 0.99$; rPC2 $\lambda < 0.01$), suggesting patterns of morphospace occupation along rPC1 for this bone are heavily influenced by phylogenetic relationships.

Shape and Habitat Variation

One-way ANOVA results comparing habitat mean and species mean $\delta^{13}C$ values demonstrated overall significant differences between group means ($p < 0.01$; Table 4.5; species means in Appendix III, Table S3.16); post-hoc Tukey's pairwise differences are also listed in Table 4.5. PhyMANOVA results comparing shape data across isotopic ranges (habitat proxy) are reported in Table 4.6. Two out of the six bones examined (MCIII and MCIV) demonstrated no significant differences in morphology across the habitat gradient. Three of the remaining bones (all carpals: pisiform, cuneiform and unciform) demonstrated significant differences in morphology across the habitat gradient prior to phylogenetic correction (Table 4.6). Following correction for phylogeny, these bones continued to exhibit morphological

Table 4.4. PerMANOVAs of *Tapirus* species based on regression residuals for six forelimb bones corrected for false discovery rate (10000 permutations). Sum of squares and within-group sum of squares reported alongside F-statistic (***F***) and associated *p*-values (***p***). Significant differences in bold.

Bone	Sum of squares	Within group sum.	*F*	*p*
Humerus	0.116	0.051	4.400	***<0.001***
Pisiform	0.578	0.364	2.714	***<0.001***
Cuneiform	0.513	0.295	2.772	***<0.001***
Unciform	0.581	0.349	3.249	***<0.001***
Metacarpal III	0.059	0.031	4.661	***<0.001***
Metacarpal IV	0.077	0.042	3.722	***<0.001***

differences across the habitat density gradient, although corrected p-values were outside the 95% threshold (corrected p = 0.051–0.072; Table 4.6). Additional testing of two subsets of data (all bones subset and New World species subset) did not greatly differ from results in the initial analysis, although the morphology of the size-dependent second metacarpal was shown to be significantly different across the habitat gradient (Appendix III, Table S4.17–S4.18). The lunate, scaphoid (proximomedial carpus) and the fifth metacarpal (lateral autopodium) also demonstrate significant differences in the New World subset (Appendix III, Table S4.18). Average body mass exhibited a strong negative correlation with $\delta^{13}C$ values, albeit with a non-significant test statistic (R^2 = -0.988; p-value = 0.897).

Discussion

In this study, we used estimates of body mass, phylogenetic relationships, and quantitative three-dimensional shape analysis to test whether forelimb shape variation observed in tapirs is correlated body size (as hinted at by Radinsky 1965, and cited by subsequent authors), or whether differences in habitat density play a role in influencing morphology in the postcranial skeleton of *Tapirus*. We demonstrate that habitat does influence forelimb shape variation in tapirs after allometry (size-dependent shape) is accounted for, contradicting size-dependence in tapir limb morphology. Due to the fact that we incorporated extinct taxa in this experiment, it is important that abiotic influences on fossilised bone shape be addressed. Specimen descriptions and excavation accounts from fossiliferous sites in Florida and Tennessee (including Gray Fossil Site,

Table 4.6. phyMANOVAs of size-independent shape variables against average stable carbon isotope ($\delta^{13}C$) ranges, based on rPC scores accounting for >70% variance of species averaged shape data (10000 simulations). Significant values for Wilks' Lambda statistic (Λ) and associated p-value (*p*) and phylogenetically corrected *p*-values (corr. *p*) are in bold.

Bone	DF	Λ	*F*	*p*	corr. *p*
Humerus	3	0.060	3.078	*0.099*	*0.054*
Pisiform	3	0.050	4.605	***0.026***	*0.066*
Cuneiform	3	0.009	4.842	***0.022***	*0.051*
Unciform	3	0.012	4.225	***0.031***	*0.072*
Metacarpal III	3	0.099	1.315	*0.362*	*0.587*
Metacarpal IV	3	0.079	1.519	*0.291*	*0.494*

Love Bone Bed, Leisey Shell Pit and Haile 7 sites, among others; Hulbert et al. 2006; Hulbert et al. 2009; Hulbert 2010) report exceptional preservation of three-dimensional structure of vertebrate remains, including that of numerous tapirs species used in this study. Accordingly, we reject the notion that differences in morphospace occupation observed in extant and extinct tapirs are caused by post-mortem deformation. The limited postcranial remains available for this study from Eurasian and extinct South American *Tapirus* species should also be noted as an unfortunate drawback of the analysis. The results of morphological comparisons of the radius suggest that European taxa resemble one another more greatly than they do other Asian or American taxa; this result is not highlighted in the main discussion as it is based on only one bone from two species (*T. priscus* and *T. arvernensis*). Nevertheless, expanding the sample of scanned tapir limbs to include more European, Asian and American specimens has the potential to greatly improve resolution and biogeographical scope of the results presented here. Despite these methodological limitations, tapir body sizes observed in this study provide a perfect range for testing the hypotheses laid out by the authors. Hereafter we discuss the results of biotic influences on tapir forelimb morphology in relation to fluctuations in body size and variation in habitat.

Size-Independence in Forelimb Shape

The historical viewpoint on tapir postcranial variation suggests that the limb shape has remained basically unchanged, with any modifications correlated with changes in size

Table 4.5. One-way analysis of variance (ANOVA) comparing raw stable isotopic values within ranges, with Tukey's pairwise comparisons. Average values on the border of two ranges (e.g. *T. webbi* $\delta^{13}C$ = -13‰) are placed in the more depleted range (e.g. *T. webbi* within 'closed canopy' range). Tukey's Q below pairwise diagonal and *p*-values above the diagonal; significant *p*-values in bold.

Test	**Sum of squares**	**DF**	***F***	***p***
Equal Means	135.328	3.00	39.78	***<0.001***
Welch *F* test	-	44.5	34.11	***<0.001***
Group	dry open canopy	wet open canopy	closed canopy	dense canopy
dry open canopy		*0.277*	***<0.001***	***<0.001***
wet open canopy	2.56		***<0.001***	***<0.001***
closed canopy	9.99	7.44		***0.044***
dense closed canopy	13.76	11.21	3.77	

(Radinsky 1965; Padilla et al. 2010). We demonstrate that 50% of bones from the forelimb of tapirs exhibit no significant influence of size on morphological variation (six of 12 bones; scapula, trapezoid, trapezium and phalanges excluded) (Table 4.2; Figure 4.2). Our morphospace results, based on bones demonstrating no significant influence of size on shape (Figure 4.2), demonstrate a number of interspecific groupings implying differences between *Tapirus* taxa independent of size effects.

In the humerus we observe *T. pinchaque* as an outlier in morphospace (Figure 4.2a). This is likely as a result of adaptations for increased speed of shoulder flexion (detailed in MacLaren and Nauwelaerts 2016). We also observe that the giant Asian tapir *T.* (*Megatapirus*) *augustus* does not plot near to its closest relative (*T. indicus*) in morphospace, but rather is found proximate to *Helicotapirus* taxa and *T. webbi*. These North American tapirs demonstrate large but less robust humeri than *T. indicus*. Rather than exhibiting similar limb morphology to other large bodied tapirs, *T. indicus* in fact represents a highly robust morph of *Tapirus*, demonstrating significant differences in shape to other large tapirs with limbs of similar or greater absolute size (e.g. *T. haysii*, *T. webbi*) (Appendix III, Tables S3.3–S3.14).

Previous observations on the size of the limbs in *T. webbi* (Hulbert, 2005) are supported by centroid size results in this study. In our morphospace results, *T. webbi* is frequently observed occupying regions proximal to *T. polkensis* (Figure 4.2; hollow triangles and hollow diamonds). These tapirs are both Miocene in age (Figure 4.1), and although they

are phylogenetically separated they share several morphological features of the forelimb. Shared features include a prominent process on the pisiform for insertion of carpal flexor tendons, long and relatively slender metacarpals, and an emarginated scapho-lunate joint facet (primitive feature for Perissodactyla, although derived for *Tapirus*; Holbrook, 1999); it is worthy of noting that the emargination of the distal scapho-lunate joint facet may not be homologous to the cladistic feature described in Holbrook (1999). The large and long-limbed *T. webbi* is in many cases more comparable in form to other North American tapirs rather than to similarly large tapirs from Eurasia (e.g. *T. indicus, T. priscus*) (Supplementary Tables S3.3–3.14). This result would not be expected were tapir limb morphology correlated only with size. Body mass estimates for *T. webbi* (293 ± 31 kg) do suggest it is, on average, smaller than large Eurasian species such as *T. indicus* (326 ± 14 kg), thus morphological differences are to be expected; however, we also find evidence for a decoupling between mass and morphology in the forelimb of two small tapir taxa of equal estimated body mass: *Tapirus lundeliusi* and *T. pinchaque*.

Decoupling Mass and Morphology in Tapirus

During the process of body mass estimation, two taxa presented comparable average body masses: the Early Pleistocene *Tapirus lundeliusi* from Florida (202 ± 24 kg) and the extant mountain tapir *T. pinchaque* (202 ± 19 kg; Figure 4.3a). Despite similar mass estimates, *T. lundeliusi* and *T. pinchaque* are statistically separated from one another in forelimb bone shape (Table S3.3–S3.13). These two species represent an ideal example of divergent morphologies irrespective of size in the forelimb of *Tapirus*. We find that several features previously shown to be of adaptive advantage for *T. pinchaque* (MacLaren & Nauwelaerts, 2016) contribute greatly to the distinction from *T. lundeliusi* (Appendix III, Tables S3.3–S3.8). Shoulder flexor muscle insertions proximal to the humeral head suggests more rapid shoulder flexion in *T. pinchaque*, at the expense of power (Gambaryan, 1974; Hildebrand, 1985; MacLaren & Nauwelaerts, 2016). When combined with the gracile morphology of the proximal limb bones, this feature implies that *T. pinchaque* is capable of more rapid upper forelimb flexion than the extinct *T. lundeliusi*. The humerus of *T. pinchaque* displays greater torsion than *T. lundeliusi*, reducing supination of the entire forelimb at the shoulder (Figure 4.3b) and bringing the entire forelimb into the parasagittal plane (associated with increased cursoriality; Gregory 1929; Wood et al. 2010). We hereby highlight a further adaptation toward a divergent locomotor style in the forelimb of *T. pinchaque* that have been previously discussed (MacLaren and Nauwelaerts 2016; 2017).

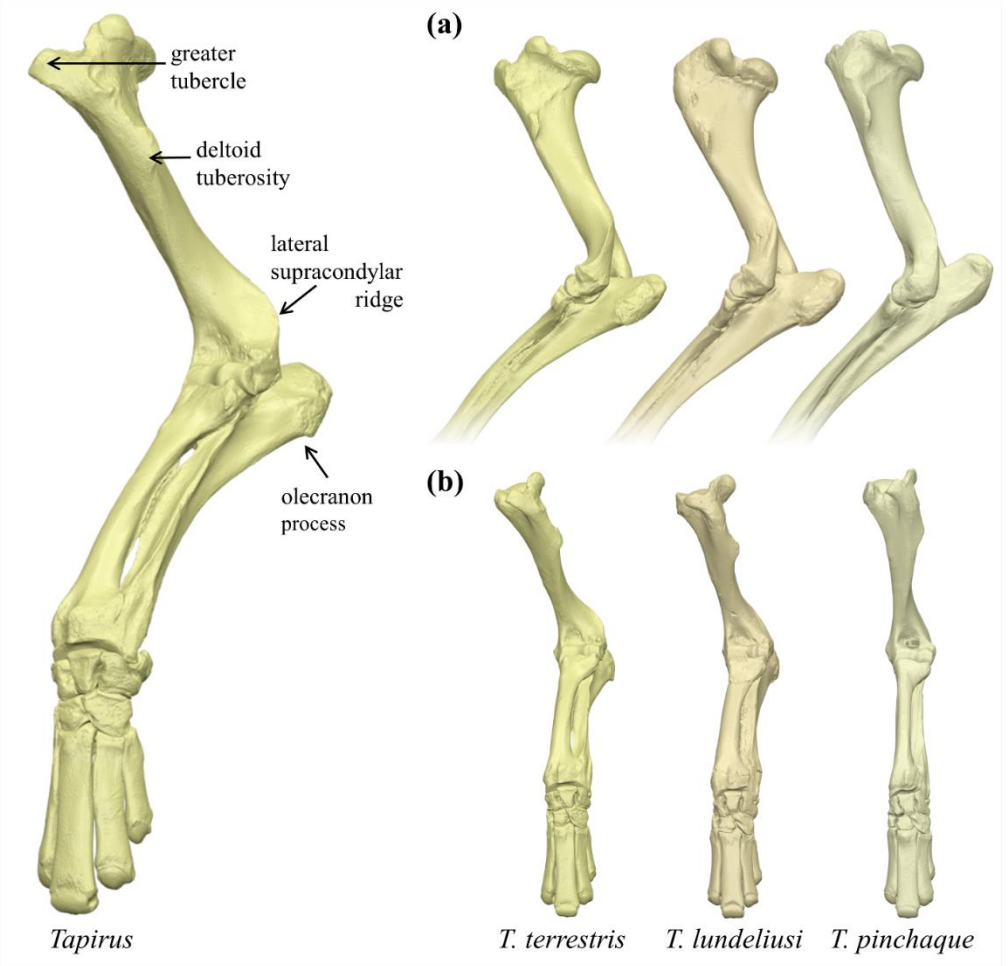

Figure 4.3. Forelimb morphology in three tapir species of comparable body masses. Full forelimb of *Tapirus* alongside **(a)** elbow morphology in lateral view and **(b)** stylopodial profile in frontal view (manus fixed in identical orientation). Specimens: *T. terrestris* ZMB MAM 12999 (216.5kg); *T. lundeliusi* UF 121736 (202.8kg); *T. pinchaque* ZMB MAM 62085 (202.4kg).

Overall, forelimb morphology in *T. lundeliusi* is more in keeping with New World tapirs exhibiting much greater body mass than predicted for this taxon in the present study. *T. lundeliusi* exhibits more distally placed shoulder flexors and a posteriorly deflected olecranon process than *T. pinchaque* (MacLaren & Nauwelaerts, 2016), features enabling *T. lundeliusi* to bear greater loads at the shoulder and elbow joints. A thickened proximal humerus (Figure 4.3a), distally positioned deltoid tuberosity (Figure 4.3a and

4.3b) and posteriorly deflected olecranon process (Figure 4.3a) all imply that the forelimb of the Florida endemic *T. lundeliusi* was adapted for slow and powerful shoulder flexion, and potentially greater gravitational support than tapirs of similar (and sometimes greater) predicted body mass (e.g. *T. terrestris*, *T. bairdii*, *T. veroensis* and *T. pinchaque*) (Gregory, 1929; Hermanson & MacFadden, 1992; MacLaren & Nauwelaerts, 2016, 2017). In addition to features of the forelimb highlighted in this study (e.g. thickened humeral shaft, deflected olecranon, locked cuneiform-pisiform joint), *T. lundeliusi* demonstrates a series of primitive cladistic characteristics of the skull (including long nasals and a short maxilliary flange) (Hulbert, 1995, 2010). We suggest that the upper arm morphology and cuneiform-pisiform interaction are plesiomorphic for the *Helicotapirus* clade, and are lost in the youngest taxon (*T. veroensis*).

When compared to medium sized tapirs (e.g. *T. bairdii*, *T. terrestris*, *T. veroensis*), *T. lundeliusi* displays upper limb and lateral carpal adaptations in keeping with a taxon of much higher mass (MacLaren and Nauwelaerts 2016; 2017), with thicker bones and more tightly locked carpal joints than is evident in the largest modern tapir (*T. indicus*). Contrastingly, *T. pinchaque* demonstrates a suite of features associated with rapid limb flexion and shock absorption (MacLaren & Nauwelaerts, 2016, 2017). These two small taxa perfectly demonstrate that tapirs of comparable size display species-specific adaptations to the forelimb to suite their individual biological requirements, challenging the historical perspective of size-dependent postcranial disparity.

Manus variation across habitat gradient

This study compliments previous findings by demonstrating that limb disparity in tapirs is affected by intrinsic (e.g. phylogeny) and extrinsic (e.g. environmental) factors in combination with fluctuations in body size (MacLaren & Nauwelaerts, 2016, 2017). One extrinsic factor – habitat density – was here shown to affect tapir forelimb morphology to a more significant extent than was expected, given the restricted niche occupied by modern tapirs. The general ecological role of tapirs in modern ecosystems is well documented (Bocherens et al., 2017; de Thoisy et al., 2014; DeSantis & MacFadden, 2007; Downer, 2001; Gregory, 1929; MacFadden & Hulbert, 1990; Perez-Crespo et al., 2012; Stacklyn et al., 2017). Extant tapirs represent medium-to-large crepuscular and nocturnal browsers, existing in low densities within wet, tropical biomes (de Thoisy et al., 2014; Padilla & Dowler, 1994; Padilla et al., 2010; Ruiz-García et al., 2012). It is evident from this study and others (Czaplewski et al., 2002; DeSantis & Wallace, 2008; Graham, 2003; MacFadden & Hulbert, 1990) that tapirs have not

always been restricted to dense rainforest habitats, as demonstrated by stable carbon ($\delta^{13}C$) isotopic values.

Levels of $\delta^{13}C$ in tooth enamel are indicative of the proportion of C3 and C4 plant material in the diet (Cerling, Harris, Ambrose, Leakey, & Solounias, 1997; Cerling, Harris, & Leakey, 1999; Cerling, Hart, & Hart, 2004; DeSantis & MacFadden, 2007). Values above -9‰ suggest mixed C3/C4 diet, with higher values suggestive of a drier and more open habitat (MacFadden and Cerling 1996). Stable carbon isotopic values of -13‰ to -10‰ have been shown to represent open canopy forest, with less depleted values demonstrating decreasing moisture available for vegetation (Codron et al., 2005; Ehleringer, Lin, Field, Sun, & Kuo, 1987; Mooney, Bullock, & Ehleringer, 1989; Secord et al., 2008). Values of $\delta^{13}C$ more depleted than -14‰ strongly suggest a closed canopy tropical biome (Cerling et al., 2004; Codron et al., 2005; Secord et al., 2008).

When stable carbon isotope recordings for modern and extinct tapirs are compared, both the average and range of $\delta^{13}C$ show dense forest environments for modern tapir taxa (Figure 4.4; Appendix III, Table S3.16). The most depleted $\delta^{13}C$ values in this study are found in the modern *T. terrestris* (average = -15.6‰) and *T. indicus* (average = -15.4‰); these values are equivalent to those of other extant rainforest browsers, such as duikers (Cephalophinae) and chevrotains (Tragulidae) in Central Africa (Cerling et al., 2004) and banteng in South China (Bocherens et al., 2017; Qu et al., 2014). By contrast, the least depleted average $\delta^{13}C$ value is that of *T. haysii* (average = -12.2‰), including a population from Mexico exhibiting $\delta^{13}C$ values averaging -10.7‰ (Perez-Crespo et al. 2016). Similar $\delta^{13}C$ values are reported for white tailed deer *Odocoileus* (-12.1‰; MacFadden and Cerling 1996), red deer *Cervus elaphus* (-11.4‰; Garcia et al. 2009) and the European forest horse *Equus germanicus* (-11.7‰; Scherler et al. 2014), all of which are regarded as open woodland taxa existing in temperate forest biomes. The average isotopic values for *T. haysii* also approximate that of the gracile Oligocene tapiroid *Colodon* (-12.2‰) from the White River fauna in Nebraska (Boardman & Secord, 2013), suggested as the first representation of tapiromorphs exploiting riparian refugia within an otherwise dry, open habitat (Boardman & Secord, 2013; Zanazzi & Kohn, 2008). This may also be the case for the Pleistocene tapirs *T. haysii* and *T. veroensis* (-12.7‰), whose ranges included areas proximate to the continental glacial front during the Pleistocene ice age (Czaplewski et al., 2002; Graham, 2003). Therefore, both *T. haysii* and *T. veroensis* were able to exist in a drier habitat than that typical of modern tapirs. The forest environments inhabited by these Pleistocene tapirs would have been composed of different flora, likely with a reduced canopy coverage (as indicated by the more enriched $\delta^{13}C$ values; Figure 4.4). Variation in forest density (i.e. canopy cover) is a vital factor for a large-bodied ungulate negotiating its way through

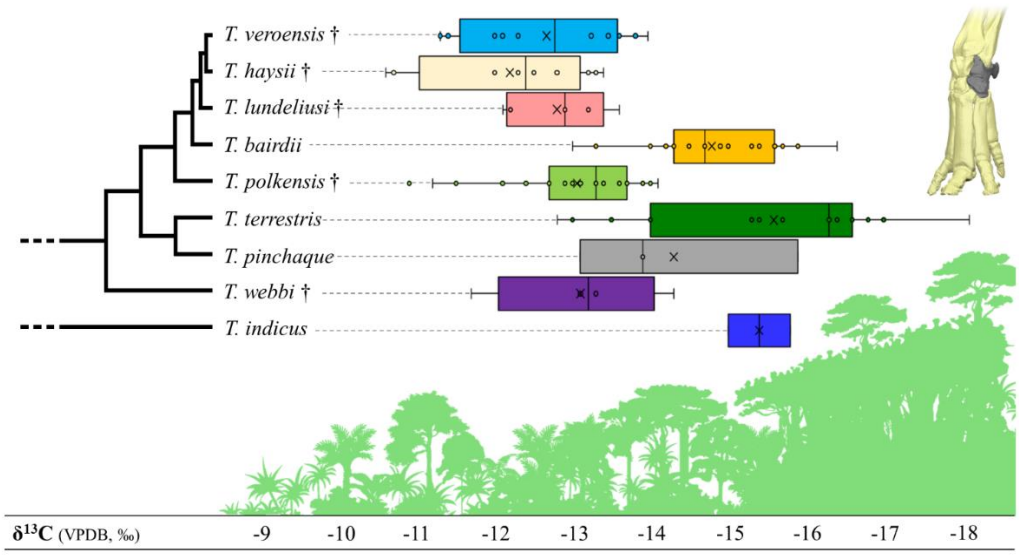

Figure 4.4. Stable carbon isotope ranges across *Tapirus*. Composite phylogeny of taxa (left) in this study alongside diagrammatic canopy cover (bottom) with corresponding stable carbon isotopic levels, and manus bones exhibiting significant differences between isotopic ranges (top right). X = mean value; central bar = median; filled boxes denotes 50% between first and third quartiles. Isotope values from MacFadden and Cerling 1996; Koch et al. 1998; Kohn et al. 2005; Hoppe and Koch 2006; DeSantis and Wallace 2008; DeSantis et al. 2009; DeSantis 2011; Perez-Crespo et al. 2012. Treeline design after Arini lighting (www.hess.eu).

its environment, potentially limiting size and locomotor style (Curran, 2015). In this study we found not only that extinct tapir species inhabit less dense forest environments (Figure 4.4), but also that the morphology of the lateral manus is significantly different across the forest density gradient (Table 4.6; see also Appendix III, Tables S3.17–S3.18).

In this study we reveal that the lateral carpus (consisting of the pisiform, cuneiform and unciform carpals) exhibits significant morphological variation in tapirs across a habitat density gradient (Table 4.6). Despite phylogenetic correction on shape variables within isotopic ranges becoming elevated above the threshold of 0.05 for the pisiform ($p = 0.066$), cuneiform (0.051) and unciform (0.072) (Table 4.6), we believe that the morphological signal between ecological groups that these bones demonstrate is worthy

of recognition and discussion. Both the pisiform and unciform rPC scores were shown to exhibit significant departure from a strong phylogenetic signal (Table 4.3), suggesting the morphology of these bones is less restricted by species relatedness than that of other bones in the analysis. These carpals are all located on the lateral autopodium, a region previously highlighted as being of morphological interest in modern tapir species (Earle, 1893; MacLaren & Nauwelaerts, 2016, 2017; Simpson, 1945). For example, both *T. indicus* and *T. pinchaque* possess a more expanded unciform joint facet for the lateral metacarpals than either *T. terrestris* or *T. bairdii*; this adaptation implies greater reliance on the fifth metacarpal in *T. pinchaque* and *T. indicus* than in other extant taxa (MacLaren & Nauwelaerts, 2017). When we consider the position in morphospace of the extinct *Helicotapirus* species (the three taxa with highest carbon isotopic values), both the pisiform and unciform of these taxa are greatly separated from the isotopically depleted *T. indicus* and *T. terrestris* (Figure 4.2b and 4.2d). There has been little research into the effect of habitat differences on carpal morphology within ungulate clades. One previous investigation into the carpus of cervids in relation to habitat use found no direct evidence for morphological differences in the carpal complex between closed and open habitat (Schellhorn and Pfretzschner 2014). In the present study, however, we do identify differences in morphology of the lateral carpus across a habitat density gradient. The unciform demonstrates a trend towards a relatively increased cuneiform facet in more open-woodland taxa; accordingly, the cuneiform facet for the unciform is more elongate anteroposteriorly in tapirs inhabiting less dense woodland. In addition, the pisiform facet becomes relatively smaller, more posteriorly deflected and more laterally positioned as tapirs inhabit denser forest habitats. Finally, the ulnar joint facet on the pisiform becomes gradually more asymmetrical as taxa are found in denser habitats, with a strong medial process present in dense-habitat tapirs compared to an elliptical facet found in open woodland taxa. As these three bones are closely associated, it may not be surprising that they all demonstrate significant differences across the habitat gradient prior to phylogenetic corrections. The change in significance values between phylogenetically corrected and non-corrected *p*-values across the habitat groups may be explained by monophyly of the *Helicotapirus* clade (*T. haysii*, *T. lundeliusi* and *T. veroensis*). The *Helicotapirus* tapirs demonstrate morphological divergence in the lateral carpus (in particular the cuneiform), in addition to being the only tapir taxa in this analysis with average $\delta^{13}C$ values greater than -13‰ (DeSantis et al., 2009; Hoppe & Koch, 2006; Koch et al., 1998; Kohn et al., 2005).

From the data currently available, formulating direct functional outcomes from the morphological variation observed across the habitat density gradient would require an over-interpretation of the findings. Unfortunately, a lack of stable carbon isotopic and extensive morphological data for the postcrania of European tapirs, including *T. priscus*,

T. arvernensis and others, prevented these taxa playing a greater role in this analysis. Increased taxon and specimen counts, additional palaeoenvironmental data (e.g. stable oxygen isotopes, widespread palaeobotanical assessments etc.), and digital simulations or *in-vivo* experiments on the functional morphology of the carpal complex in tapirs will be necessary before more conclusive interpretations can be made on the influence of habitat density on the tapir forelimb. The isotopic signal in this study is intriguing, and promotes future studies to compare morphological and habitual data in this fashion.

Conclusion

Using a size-independent, three-dimensional approach to quantify forelimb shape, we have shown that the forelimb of *Tapirus* demonstrates notable variation not significantly influenced by size. As part of this study, we present the first published body mass estimates for several *Tapirus* species (including *T.* (*Megatapirus*) *augustus*, *T. priscus*, *T. lundeliusi*, *T. veroensis* and *T. arvernensis*), the results of which suggest that Eurasian tapirs attained greater masses on average than those in the Americas. Addition of extinct tapir specimens from southern Europe, China and South America may offer more resolution to this apparent geographical signal. Our findings highlight occurences of decoupling between tapir size and limb morphology, typified by the comparison of two small taxa of near-equal estimated mass (*T. pinchaque* and *T. lundeliusi*). We observe previously undescribed adaptations in the forelimb skeleton of the modern mountain tapir *T. pinchaque*, shedding further light on the divergent locomotor capabilities of this elusive and endangered taxon. Variation across an ecological gradient is observed in the lateral autopodium of *Tapirus*, although phylogenetic analyses suggest that morphological variation observed in the lateral autopodium may be at least in part driven by tapirs in the subgenus *Helicotapirus*, which in general occupied drier and more open woodland habitats than their extant, rainforest relatives.

The sample of taxa used in this study all fall within the genus *Tapirus* which, while being a deep-rooted clade, does not account for all morphologies within the Tapiridae or Tapiromorpha. To gain a holistic viewpoint on postcranial scaling in tapirs throughout their evolutionary history, further investigation into body size, limb proportions, habitat ecology and locomotor capabilities must be carried out on multiple extinct tapiromorphs outside crown Tapiridae (e.g. *Heptodon*, *Colodon* and *Protapirus*). Understanding the locomotor capabilities of these early taxa, prior to the origination of crown Tapiridae, will expose further insights into this bizarre clade of browsing ungulates and their plesiomorphic, yet variable, locomotor apparatus.

“it is not our abilities who make us
who we truly are– it is our choices”

- Prof. Dumbledore -

– RESEARCH CHAPTER FIVE –

Modern tapirs as morphofunctional analogues for locomotion in endemic Eocene European perissodactyls

Jamie A. MacLaren - Sandra Nauwelaerts

adapted from *Journal of Mammalian Evolution*
(2019) xx:xxx-xxx

Tapirs have historically been considered as ecologically analogous to several groups of extinct perissodactyls, based on dental and locomotor morphology. Here, we investigate comparative functional morphology between living tapirs and endemic Eocene European perissodactyls to ascertain whether tapirs represent viable analogues for locomotion in palaeotheres and lophiodontids. Forelimb bones from 20 species of Eocene European perissodactyls were laser scanned and compared to a forelimb dataset of extant *Tapirus*. Bone shape was quantified using 3D geometric morphometrics; coordinates were Procrustes aligned and compared using Principal Component Analysis and neighbour-joining trees. Functional traits included lever-arm ratios (LARs; proxy for joint angular velocity), long-bone proportions (speed proxy), and estimated body mass. Results suggest that *Paralophiodon* and *Palaeotherium magnum* resemble Neotropical tapirs in humeral morphology and LARs. Palaeotheres demonstrate extensive forelimb shape disparity. Despite previous assessments, metacarpal shape analyses do not support a strong morphological similarity between palaeotheres and tapirs, with *Tapirus pinchaque* representing the closest analogue for Eocene European equoid manus morphology. Our analyses suggest lophiodontids were not capable of moving as swiftly as tapirs due to greater loading over the manus. We conclude that the variation within modern tapir forelimb morphology confounds the assignment of one living analogue within *Tapirus* for extinct European equoids, whereas tapirs adapted for greater loading over the manus (e.g., *T. bairdii, T. indicus*) represent viable locomotor analogues for lophiodontids. This study represents a valuable first step toward locomotor simulation and behavioural inference for both hippomorph and tapiromorph perissodactyls in Eocene faunal communities.

Introduction

The modern tapirs (Tapiridae: *Tapirus*) represent the crown group of a deeply rooted lineage of perissodactyls (odd-toed ungulates) that diverged from their closest living relatives (rhinoceroses and equids) during the earliest Eocene (approximately 56 Mya; Ryder 2009; Steiner and Ryder 2011; Rose et al. 2014). The skeleton of many members of the Tapiridae (both extinct and extant) demonstrates superficial similarities to the earliest ancestors of extant equoids (e.g., horses) (Holbrook, 2001; Holbrook & Lucas, 1997; Prothero, 2016; Rudwick, 2008; Wood et al., 2011). Similarities between tapirs and Eocene European equoids (e.g., *Eurohippus*, *Palaeotherium*) include inhabiting moist, forest habitats (DeSantis, 2011; DeSantis & Wallace, 2008; Hooker, 2010b; Secord et al., 2008; Zanazzi & Kohn, 2008), comparable dental morphology (lophodont dentition; (Froehlich, 2002; Holanda & Ferrero, 2013; Hulbert et al., 2009; Mihlbachler et al., 2011; Simpson, 1945), and in many cases a tetradactyl (four-toed) forelimb (Holbrook & Lucas, 1997; MacLaren & Nauwelaerts, 2017; Prothero, 2005, 2016; Rose et al., 2014; Wood et al., 2011). The similarities in forelimb morphology of the European equoid family Palaeotheriidae (palaeotheres) have in the past led to tapirs being described as analogues for species within this clade (e.g., *Palaeotherium magnum* and *Pa. crassum;* Cuvier 1812; Adams and Meunier 1872; Gregory 1929*)*, with the exclusion of the derived, cursorial plagiolophines. The diminutive palaeotheres *Eurohippus* and *Propalaeotherium*, both of which exhibited functionally tetradactyl forelimbs (as tapirs do), have also been compared with tapirs based on appearance and ecology (MacFadden, 1992b; Prothero, 2016). However, explicit quantitative data on comparisons between tapir and palaeothere functional forelimb morphology (bone shape, locomotor mechanics, etc.) have not been previously published.

When establishing modern analogues for extinct taxa, understanding morphological similarities is a key first step toward reconstructing locomotion of ancestral species (Carrano, 1998, 1999; Hutchinson & Gatesy, 2006; Thewissen & Fish, 1997). The close phylogenetic relationships between palaeotheres and the earliest horse ancestors (e.g., *Sifrhippus*; Hooker 2010a) demonstrate that the identification of a viable extant analogue for palaeothere locomotion will greatly benefit investigations into modelling the transition from early tetradactyl to extant monodactyl equids (Bronnert, Gheerbrant, Godinot, & Métais, 2017; Danilo et al., 2013; Froehlich, 1999, 2002). Forelimb shape variation, and consequent functional differences, have been described in tapirs both qualitatively and quantitatively in recent years (Hulbert, 2005; MacLaren et al., 2018; MacLaren & Nauwelaerts, 2016, 2017). Here, we will use a previously established three-dimensional forelimb dataset from extant tapirs (MacLaren et al., 2018; MacLaren & Nauwelaerts, 2016, 2017) and compare these to the forelimb bones of Eocene

European perissodactyls (including palaeotheres and contemporaneous lophiodontids). Due to the tetradactyl nature of their forelimbs, we hypothesise that a three-dimensional geometric morphometric analysis of bone shape will group tetradactyl Eocene equoid (e.g., *Eurohippus*, *Propalaeotherium*) limb bones with those of extant tapirs, with significant differences between tapirs and more derived, cursorial tridactyl palaeotheres (e.g., *Plagiolophus, Pa. medium*).

Historically, ratios of forelimb and hind limb bone lengths have been used to estimate the locomotion style (long-bone or 'speed' ratios) of extinct taxa, based on comparable ratios in living species (Gregory, 1929; Samuels & Van Valkenburgh, 2008; Van Valkenburgh, 1987). The ratios of the humerus to radius (radiohumeral ratio; HR) and humerus to third metacarpal (metacarpohumeral ratio; HMC) have been used to predict or demonstrate cursoriality (i.e., running locomotion) and graviportalism (i.e., slow, ponderous locomotion) in quadrupedal taxa (Bai et al., 2017; Gregory, 1929; Van Valkenburgh, 1987). Radiohumeral ratios increase with the elongation of the radius (and ulna), a feature observed throughout the evolution of numerous fast-moving taxa (e.g., equids, giraffes, canids; Gregory 1929; Van Valkenburgh 1987; Bai et al. 2017). The metacarpohumeral ratio increases as the third metacarpal lengthens relative to the humerus; such distal limb element lengthening is observed in cursorial groups (e.g., equids). HMC decreases with the shortening of the third metacarpal relative to the humerus, indicative of slower locomotion and higher mass over the center of the manus (Gregory, 1929). Here, we calculate and compare HR and HMC ratios for tapirs and Eocene European perissodactyls. When these ratios are high, we expect the animal to exhibit cursorial locomotor style (e.g., equids); as extant tapirs are not considered as cursorial, we predict that tapirs will be poor analogues for Eocene European perissodactyls with high HR and HMC ratios. Ultimately, we reason that extant tapirs will represent a viable extant analogue for forelimb locomotion in Eocene European perissodactyls that exhibit fewest significant differences in both form (limb morphology; long-bone ratios) and function (lever-arm ratios; posture).

Institutional Abbreviations:– **ETMNH**, East Tennessee State University and General Shale Brick Museum of Natural History, Gray; **FSL**, Geology Department of the Universite Claude Bernard Lyon, Lyon; **GMH**, Geiseltalmuseum Halle, Halle; **MEO**, Museos Natuurhistorische Museum, Koksijde; **MNHN**, Museum National d'Histoire Naturelle, Paris; **NHMUK**, British Museum of Natural History, London; **NMW**, Naturhistorich Museum Wien, Vienna; **RBINS**, Royal Belgian Institute of Natural Sciences, Brussels; **SMNK**, Staatliches Museum fur Naturkunde Karlsruhe, Karlsruhe; **ZMB MAM** (**MfN**), Mammal Collections, Museum für Naturkunde, Berlin.

Methodology

Specimens

To examine claims of morphological analogy between tapir and palaeothere locomotor anatomy, forelimb bones from a range of extinct equoids and contemporaneous tapiromorphs were collected. The specimens under study include several of the most well-preserved holotype postcranial remains from early Eocene perissodactyls known worldwide. These were combined with many three-dimensionally preserved perissodactyl forelimb bones from fossil lagerstätte such as Geiseltal (Saxony-Anhalt, Germany), the Quercy Phosphorites (France), and La Debruge (Vaucluse, France). Selected limb elements were scanned with a FARO ScanArm Platinum V2 system combined with an integrated FARO Laser Line Probe (≥50 μm resolution). Resultant models were visualised using GeoMagic (GeoMagic Qualify v.10, Morrisville, NY, USA). Species studied are listed in Table 5.1. Tapirs represented in this analysis included the four widely recognised extant *Tapirus* species (*Tapirus terrestris*, *T. pinchaque*, *T. bairdii* and *T. indicus*; Cozzuol et al. 2013; Dumbá et al. 2018) and the dwarf *T. polkensis* from the Miocene of USA. *Tapirus polkensis* was included as an approximate size analogue for several extinct European perissodactyls. Eocene European perissodactyl species were scanned in museum collections in France (Lyon and Paris), Germany (Karlsruhe, Berlin, and Halle), and the United Kingdom (London). Fossil locality information can be found in Appendix IV, Figure S4.5. Additional specimens used for comparative limb ratios represented perissodactyl taxa widely considered as graviportal (e.g., teleoceratine and metamynodont rhinoceroses; *Teleoceras* spp. and *Metamynodon*) and cursorial (e.g., tri- and tetradactyl equids; *Sifrhippus* and *Mesohippus* spp.) (Prothero, 2005; W. B. Scott, 1941; Wood et al., 2011).

Geometric Morphometrics

Geometric morphometrics was used to quantify variation in shape between the forelimb bones (Klingenberg, 2016; Zelditch et al., 2012). A series of discrete landmark points (representing biologically homologous features of the bones) were digitally placed onto each surface scan (Zelditch et al., 2012) using Landmark Editor v.3.0 software (Wiley et al., 2006); landmark points selected follow methods of MacLaren and Nauwelaerts (2016; 2017). Bones analysed with 3D GM included the humerus, radius, cuneiform, lunate, scaphoid, unciform, and the four metacarpals (MCII, MCIII, MCIV MCV), with the remaining forelimb bones being underrepresented in all extinct species in this study. Raw landmark coordinates were aligned using Generalised Procrustes Analysis (GPA) (Rohlf & Slice, 1990) in PAST v.3.19 (Hammer et al., 2001), removing the effects of

Table 5.1. List of taxa included in this study. † = extinct; * = long-bone ratio only. Abbreviations: Eu = Europe, SE As = South-East Asia, CAm = Central America, NAm = North America, SAm = South America; Eo = Eocene, Oli = Oligocene, Mio = Miocene, Ple = Pleistocene, Hol = Holocene.

Higher Taxonomy		Species	Locality	Age
Tapiromorpha				
Tapiridae				
Tapirus		*bairdii*	C/SAm	Ple-Hol
Tapirus		*indicus*	SE As	Ple-Hol
Tapirus		*pinchaque*	SAm	Ple-Hol
Tapirus		*terrestris*	SAm	Ple-Hol
Tapirus		*polkensis* †	NAm	Mio
Helaletidae* †				
*Heptodon** †		*calciculus* †	NAm	Eo
*Heptodon** †		*posticus* †	NAm	Eo
*Colodon** †		*occidentalis* †	NAm	Oli
Lophiodontidae †				
Paralophiodon †		*leptorhynchum* †	Eu	Eo
Lophiodon †		*remense* †	Eu	Eo
Lophiodon †		*tapirotherium* †	Eu	Eo
Rhinocerotoidea*				
*Metamynodon**		*planifrons* †	NAm	Oli
*Teleoceras**		*major* †	NAm	Mio
Teleoceras *		*hicksi* †	NAm	Mio
*Uintaceras**		*radinskyi* †	NAm	Eo
Indeterminate Tapiromorpha †				
Chasmotherium †		*minimus* †	Eu	Eo
Hippomorpha				
Palaeotheriidae †	(*generic prefix*)			
Palaeotherium †	(*Pa.*)	*magnum* †	Eu	Eo
Palaeotherium †	(*Pa.*)	*medium* †	Eu	Eo-Oli
Palaeotherium †	(*Pa.*)	*muelbergi* †	Eu	Eo
Palaeotherium †	(*Pa.*)	*curtum* †	Eu	Eo
Palaeotherium †	(*Pa.*)	*crassum* †	Eu	Eo
Palaeotherium †	(*Pa.*)	*castrense* †	Eu	Eo
Plagiolophus †	(*Pl.*)	*annectens* †	Eu	Eo
Plagiolophus †	(*Pl.*)	*major* †	Eu	Eo
Plagiolophus †	(*Pl.*)	*minor* †	Eu	Eo-Oli
Propalaeotherium †	(*Pr.*)	*hassiacum* †	Eu	Eo
Propalaeotherium †	(*Pr.*)	*isselanum* †	Eu	Eo
Propalaeotherium †	(*Pr.*)	*voigti* †	Eu	Eo
Eurohippus †	(*Eu.*)	*parvulum* †	Eu	Eo
*Eurohippus** †	(*Eu.*)	*messelensis* †	Eu	Eo
Equidae †				
Pliolophus †		*vulpiceps* †	Eu	Eo
*Sifrhippus** †		*granger* †	NAm	Eo
*Mesohippus** †		*bairdii* †	NAm	Eo-Oli
Indeterminate Equoidea †				
Hallensia †		*matthesi* †	Eu	Eo

scale, location and orientation and aligning coordinate configurations based on a geometric center (centroid). Aligned Procrustes coordinates from GPA were input into a Principal Components Analysis (PCA) to extract the main, orthogonal axes of variation, allowing patterns of morphospace occupation by different species to be compared. PCAs were performed in PAST v.3.19 (Hammer et al., 2001), with principal component scores exported and visualised in morphospace plots constructed in RStudio v.1.0.143 (RStudio Team 2016) using the 'ggplot2' library (Wickham, 2009).

Functional Traits

The humerus and ulna were examined for sites of major muscular insertion pertaining to established biomechanical outcomes (e.g., forearm extension; shoulder flexion) (Figure 5.1a); muscles included the *deltoideus*, *teres major*, *supraspinatus* and *infraspinatus* (humeral) and the lateral and long heads of the *triceps brachii* (ulnar) (Figure 5.1a). A series of in-lever measurements were taken between center of tendon attachment and center of joint rotation, with corresponding out-lever measurements taken between the center of joint rotation and the distal joint surface of the bone (recording the functional length from joint to joint along the bone). Measurements were taken on 3D scans using the Geomagic Studio 10 measuring tool, with ratios of out-lever over in-lever (L_o / L_i) calculated following the method of Hildebrand (1985). Linear measurements were taken in three dimensions, assuming perpendicular line of action to the in-lever (L_i) for all muscles. While this does not necessarily represent the true line of action of the muscles in life, the methodology utilised was consistent across all taxa in the analysis, allowing for legitimate functional comparisons based solely on bone material. This method allowed the study of isolated and disarticulated limb elements as well as articulated skeletons. Raw measurements for the in-lever and out-lever were regressed against one another using ordinary least square regression (OLS), and regression plots for each muscle were formatted in RStudio (RStudioTeam, 2016). Regression lines for each extant tapir species were compared to results from Eocene European perissodactyls and regression residuals calculated for lophiodontids and palaeotheres. Regression residuals were species averaged and compared across the four living taxa to test which was most analogous in its lever-arm ratios to Eocene European perissodactyls.

Long-Bone Ratios

To establish whether the forelimb ratios ('speed ratios'; Gregory 1929) of extant tapirs resembled those of Eocene European perissodactyls, the length of the humerus, radius,

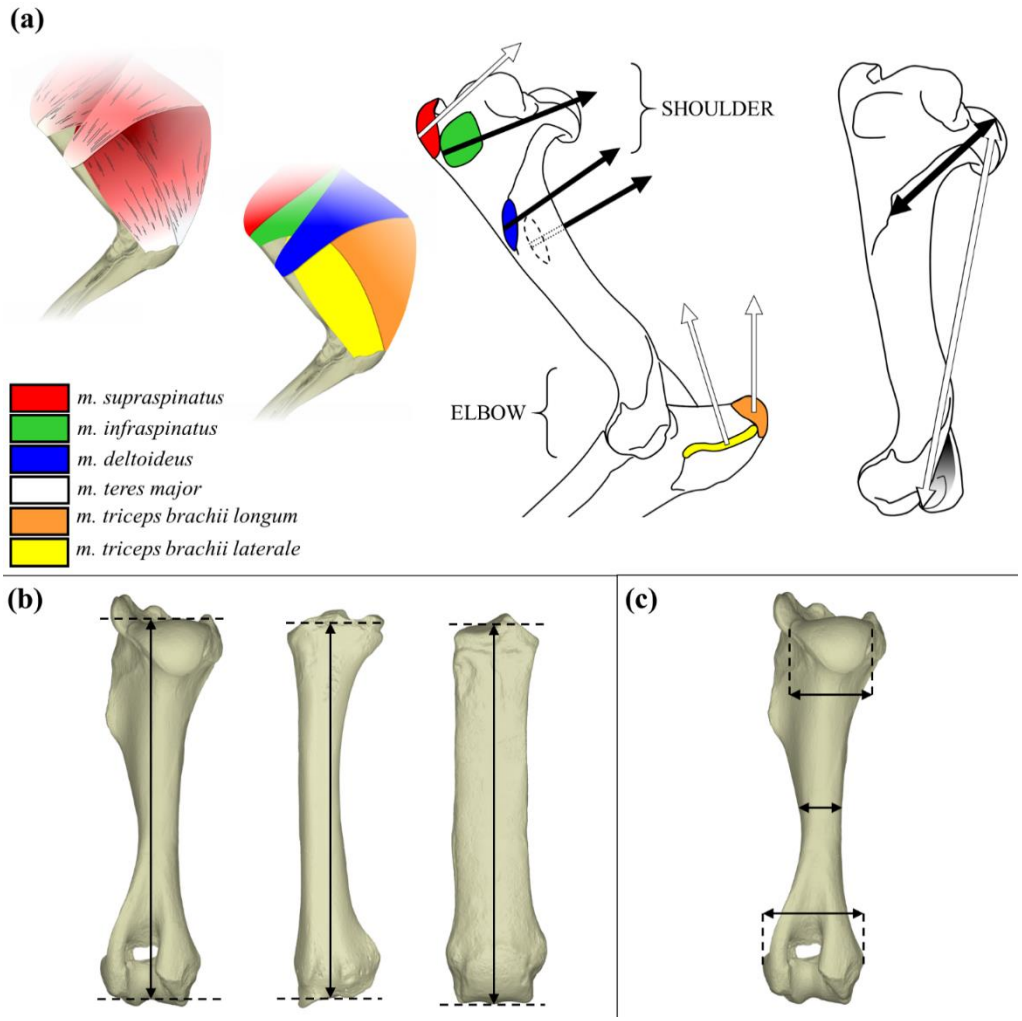

Figure 5.1. Measurement techniques for forelimb functional trait calculation. **(a)** (from left) diagram representing the shoulder and elbow musculature; colour-coded muscles with key; insertions sites in lateral aspect with action of muscles on the shoulder and elbow joints shown in arrows (black = joint flexion; white = joint extension); example of in-lever (black) and out-lever (white) measurements (for *deltoideus*). **(b)** Maximum length from centre of joint articulation (functional length) of humerus (left), radius and third metacarpal (right) for long-bone ratios. Bones not to scale; **(c)** humeral width measurements for body mass estimations.

and third metacarpal from the centre of joint surfaces (representing maximum functional length) were measured (Figure 5.1b). Humeral, radial, and metacarpal length data from

published sources (n = 10 species; see Table 5.1) were also collected and compared to measurements from scanned individuals to expand species coverage for forelimb 'locomotor style' (long bone ratios; Gregory 1929; Scott 1941; Radinsky 1965; Mead 2000; Prothero 2005; Franzen 2010a; Wood et al. 2011). Ratios of these lengths were calculated by dividing the radius length by humerus length x 100 (HR) and third metacarpal length by humerus length x 100 (HMC) (Bai et al., 2017; Gregory, 1929); these ratios were then species averaged. Measurements were also taken on scanned forelimbs of taxa widely believed to demonstrate graviportal (e.g., *Teleoceras* spp.) and cursorial (e.g., *Mesohippus* spp.) locomotion styles (22 specimens across five species), in addition to perissodactyl forelimb measurements from published literature (13 specimens across nine species) (Gregory, 1929; Holbrook & Lucas, 1997; Radinsky, 1965b; W. B. Scott, 1941). It is important to note here that the use of ratios for parametric statistical analyses can pose issues due to certain assumptions of normality and homoscedasticity being violated (Sokal & Rohlf, 2012). Fortunately, several studies have shown that the use of ratio data in multivariate statistics can be robust (e.g., Van Valkenburgh and Koepfli, 1993; Elissamburu and Vizcano, 2004). In addition, due to the small sample sizes attained in this study, non-parametric analyses were favored; we therefore believe that the use of comparative ratio data in this study is valid. Body mass was estimated from the humeri of Eocene European perissodactyls (and additional perissodactyl taxa with cursorial and graviportal characteristics) using humeral width measurements and regression equations from Scott (1990) (Figure 5.1c), successfully applied to tapirs in recent studies (Hulbert et al., 2009; MacLaren et al., 2018).

Statistical Analyses

The first principal axes from shape-based PCA (PC1; accounting for the greatest % variance) were tested for interspecific differences between taxonomic units using an analysis of variance (ANOVA) and Tukey WSD (wholly significant difference) post-hoc test, both in SPSS v.24 (IBM, 2013). In addition, aligned Procrustes coordinates were compared across taxonomic groups using one-way analysis of similarities (ANOSIM) (Clarke, 1993; Warton, Wright, & Wang, 2012). ANOSIM is a non-parametric analysis that compares within-group to between-group variation and generates an R-statistic between 0 (equal dissimilarity between and within groups) and 1 (similarity between all within-group pairs greater than any between-group pairing) (Clarke, 1993). ANOSIM was conducted in RStudio using the 'vegan' library (Oksanen et al., 2018), with pairwise comparisons of R-statistics generated in PAST v.3.19.

Body size has been suggested to affect long-bone ratios, in addition to size affecting the denomination of cursorial locomotor styles (Gregory 1929; Bai et al. 2017). To test this,

long-bone ratios were regressed against estimated body mass using OLS to test for a correlation between body size and 'locomotor style' (Gregory, 1929) for Eocene-Oligocene European perissodactyls and living tapirs; OLS was performed in PAST v.3.19.

Finally, Euclidean distances between species-mean shape configurations were extracted from aligned Procrustes coordinates in Morphologika v.2.5 (O'Higgins & Jones, 1999) and compared using neighbour-joining trees. Neighbour-joining (N-J) trees were used to heuristically visualise morphological proximity of extant tapir forelimb bones to those of extinct European equoids. Euclidean distances between mean long-bone ratios were also calculated to examine which tapir species most closely resembled Eocene European perissodactyls in their long-bone ratio. N-J trees were produced in RStudio using the 'ape' library (Paradis, Claude, & Strimmer, 2004).

Results

Forelimb Shape Variation

Results of principal component analyses (PCA) show that for each bone, certain tapir species exhibit similarities in shape to specific Eocene European perissodactyls. Contrastingly, other tapir species are show to exhibit significant differences in shape to one another, and to both palaeotheres and lophiodontids. The first principal axis (PC1) for the long bones (humerus, radius, and metacarpals) represents an axis of robusticity, with broader bones at one end of the axis and gracile bones at the other end (Figure 5.2) dependent upon the bone. For example, robust humeri are located in negative PC1 morphospace (Figure 5.2a) whereas robust MCIIIs are located in positive PC1 morphospace (Figure 5.2c). Lophiodontidae were excluded from metacarpal analyses due to the scale of morphological difference between this group and the others swamping interspecific differences between palaeotheres and tapirs. Shape analyses for all bones are reported in the Appendix IV, Figure S4.1. Two forelimb bones stand out as showing notable overlap between tapirs and Eocene European perissodactyls: the humerus and third metacarpal (MCIII) (Figure 5.2).

Humeral shape of tapirs overlaps along PC1 with four groups of Eocene European perissodactyls: Lophiodontidae spp., *Pa. magnum*, *Pr. hassiacum*, and *Plagiolophus* spp. (Figure 5.2a). Within the overlapping taxa, *T. pinchaque* demonstrates overlap with *Plagiolophus* and *Pr. hassiacum*, whereas all other extant tapirs and the extinct dwarf *T. polkensis* overlap with *Pa. magnum* and *Paralophiodon*. No tapirs overlap with *Pr. voigti* or the basal equid *Pliolophus* along PC1 (Figure 5.2a). The most robust bones are

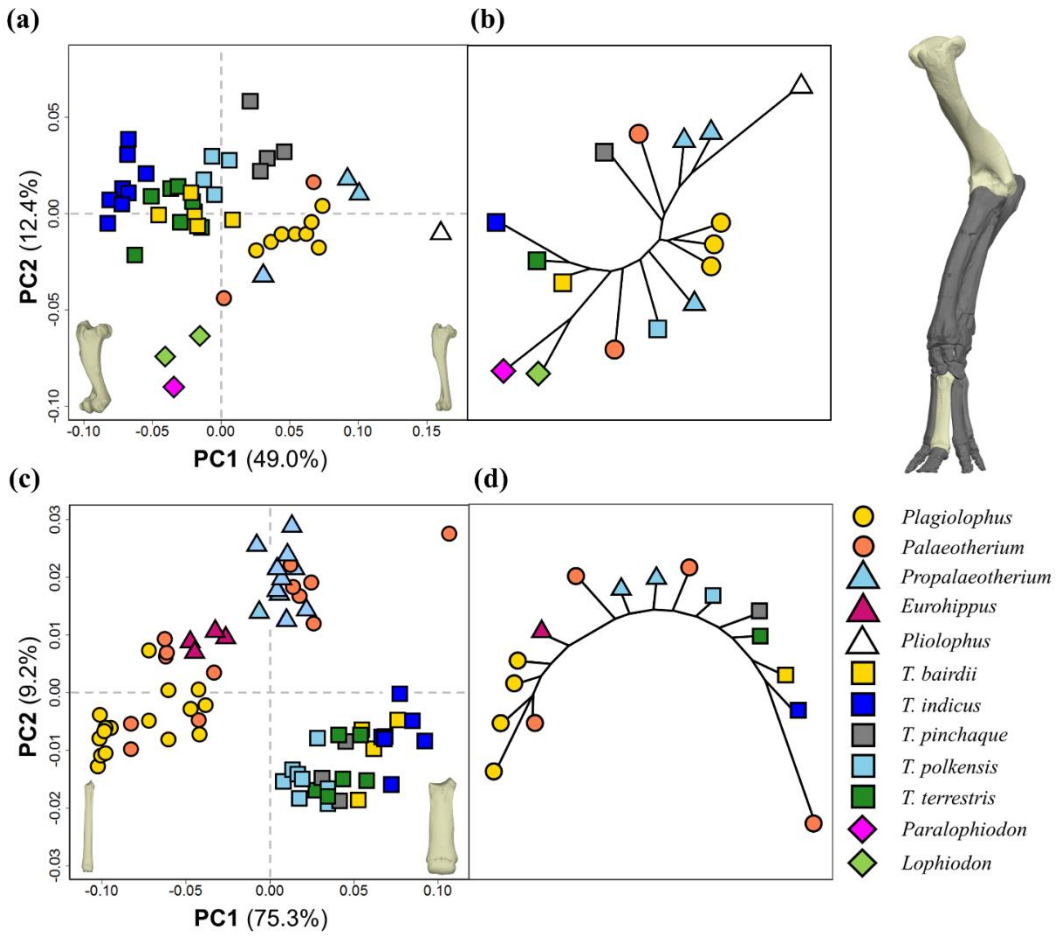

Figure 5.2. Morphological comparison of humerus **(a, b)** and third metacarpal **(c, d)** between *Tapirus* species and extinct European perissodactyls. Principal components 1 and 2 demonstrate variation in shape **(a, c)**, with associated neighbour-joining trees based on Euclidean distances between species mean landmark configurations **(b, d)**. Approximate bone shapes based on PC1 variation shown (bottom). Location of bones shown on scanned forelimb of *Propalaeotherium hassiacum* (top right). Shape key: circles = Palaeotheriinae; triangles = other Palaeotheriidae + *Pliolophus*; square = Tapiridae; diamond = Lophiodontidae.

found in negative PC1 morphospace, and there appear to be diagonal axes of robusticity from bottom left to top right within phylogenetically separated groups: *Tapirus* (squares) and palaeotheres (circles and triangles; excluding *Pliolophus*) (Figure 5.2a). The landmarks most greatly influencing placement along both PC1 and PC2 describe

the proximodistal positioning of the teres tuberosity along the humeral diaphysis, a feature that varies within *Tapirus* as well as between Eocene European perissodactyls. Neighbour joining (N-J) trees confirm that mean humeral landmark configurations of Lophiodontidae are most similar to extant tapirs excluding *T. pinchaque* (Figure 5.2b); N-J tree topology suggests that *T. pinchaque* humeri most closely resemble those of *Plagiolophus* spp. ANOVA and Tukey WSD post-hoc testing suggested that *T. indicus* is separate from all other tapirs and Eocene European perissodactyls; *T. terrestris* and *T. baridii* are grouped with Lophiodontidae, and *T. pinchaque* is grouped with the Palaeotheriinae taxa (Table 5.2). ANOVAs also suggest that both humerus samples exhibit much higher between-group variance than within-group ($F = 37.01$; Table 5.2). This is supported by ANOSIM results, which suggest few similarities in humeral shape (R-statistic = 0.788); pairwise R-statistics suggest *T. pinchaque* and *T. bairdii* show the most similarities to Eocene European perissodactyls (Table 5.3), with the lowest R-statistic recorded between *T. pinchaque* and *Propalaeotherium* ($R = 0.685$).

Shape variation of the third metacarpal demonstrates a clear divide in morphospace between tapirs and Eocene European perissodactyls, although there is a large amount of overlap along PC1 (75.1%) (Figure 5.2c). The slender *Pl. minor* is located in negative PC1 morphospace and the highly robust *Pa. curtum* in positive PC1 morphospace. Landmark loadings suggest that coordinates describing metacarpal narrowing dominate PC1, whereas landmarks describing the relative size and position of the MCII and MCIV joint facets are highly loaded along PC2. Due to the landmarks describing differences in joint facet morphology, two distinct clusters are present in morphospace: one palaeothere group (Figure 5.2c; top) and one tapir group (Figure 5.2c; bottom right). Within these groups, variation in MCIII robusticity is observed, with the most slender bones (*Plagiolophus*; *T. polkensis* respectively) in the bottom left of each group and the most robust MCIIIs (*Pa. curtum*; *T. indicus* respectively) found in the top right of each group (Figure 5.2c). Along PC1, there is overlap between tapirs (*T. polkensis*, *T. terrestris* and *T. pinchaque*) and palaeotheres (*Pr. hassiacum*, *Pa. magnum* and *Pa. crassum*) (see Supplementary Fig S4.2 and Fig S4.3 for species breakdown). No tapirs appear in negative PC1 morphospace, which is predominated by slender tridactyl *Plagiolophus* spp. and *Palaeotherium* spp. (Figure 5.2c). PC2 is most greatly influenced by proximal MCIII shape and joint facet arrangement. Third metacarpal N-J tree suggests that *T. pinchaque* is the most similar extant tapir to Eocene European perissodactyls (*Pa. magnum* and *Pr. hassiacum*) (Figure 5.2d), with the extinct dwarf tapir *T. polkensis* demonstrating the most similar MCIII morphology of all the tapirs in this analysis. ANOVA and Tukey WSD post-hoc tests suggest that both *T. pinchaque* and *T. terrestris* MCIII mean configurations group with *Propalaeotherium* spp. (Table 5.2), whereas *Plagiolophus* spp., *Eurohippus* and *Palaeotherium* spp. grouping

Table 5.2. Tukey WSD post-hoc results following ANOVAs of humerus, third metacarpal and unciform bone shape variation along principal component 1 (PC1). Modern tapirs similar to extinct taxa in bold. Statistical abbreviations: SS (total sum of squares), WG (within-group sum of squares), F (F-statistic), p (p-value of F-statistic; significant at <0.05)

Species	N	Subset 1	2	3	4
Humerus (PC1 scores)					
T. indicus	8	-0.071			
T. terrestris	7		**-0.035**		
Lophiodontidae	3		-0.030		
T. bairdii	5		**-0.019**		
T. polkensis	4		-0.005		
T. pinchaque	4			**0.032**	
Palaeotherium	2			0.034	
Plagiolophus	8			0.054	0.054
Propalaeotherium	3				0.074
ANOVA statistics		SS = 0.111	WG = 0.012	F = 37.01	p < 0.01
Metacarpal III (PC1 scores)					
Plagiolophus	16	-0.077			
Eurohippus	4		-0.038		
Palaeotherium	12		-0.028		
Propalaeotherium	11			0.007	
T. polkensis	8			0.021	
T. pinchaque	3			**0.039**	0.039
T. terrestris	6			**0.043**	0.043
T. bairdii	5				0.062
T. indicus	7				0.076
ANOVA statistics		SS = 0.232	WG = 0.050	F = 29.07	p < 0.01
Unciform (PC1 scores)					
T. polkensis	6	-0.093			
T. indicus	6	-0.082			
T. terrestris	5	-0.071			
T. bairdii	5	-0.048			
T. pinchaque	4	-0.048			
Chasmotherium	2		0.013		
Plagiolophus	2		0.017		
Propalaeotherium	5		0.037		
Palaeotherium	3			0.086	
Paralophiodon	8				0.1671
ANOVA statistics		SS = 0.413	WG = 0.020	F = 77.90	p < 0.01

separately. Despite the large intra-genus variation of *Palaeotherium*, ANOVAs also suggest that MCIIIs in this study exhibit higher between-group variance than within-group (F = 29.07; Table 5.2).When MCIII data were split into individual species of *Palaeotherium* (spp. = 4) and *Plagiolophus* (spp. = 4), *T. pinchaque* and *T. terrestris* grouped with *Pa. magnum*, not *Pr. hassiacum* (see Appendix IV, Table S4.1). By contrast, ANOSIM results again suggest a high level of dissimilarity in MCIII shape (R-statistic = 0.836); pairwise R-statistic results again suggest *T. pinchaque* demonstrates more similarities to Eocene European perissodactyls (Table 5.3) than other living tapirs, with comparatively low R-statistics recorded between *T. pinchaque* and the palaeotheres *Pa. crassum* (R = 0.741) and *Pa. magnum* (R = 0.593). MCIIIs of tetradactyl perissodactyls in this analysis (*Tapirus* spp., *Eurohippus* and *Propalaeotherium*) show much greater within-group similarity than between-group similarities (R = 1) (Table 5.3).

Results for the majority of the carpal complex of the Eocene European perissodactyls were limited by specimen and species availability. Fortunately, sample size and species coverage for the unciform (fourth carpal) were great enough to warrant morphological comparison. The morphological variation in the unciform suggests three morphological groups, separated along PC1 (Figure 5.3a; Table 5.2). All three major groups include functionally tetradactyl taxa (*Tapirus*, *Paralophiodon*, *Propalaeotherium*). Lophiodontids plot separately from all other groups along PC1, overlapping with extant tapirs excluding *T. pinchaque* along PC2; PC2 approximates an axis of body size. Palaeotheres (including *Plagiolophus*, *Palaeotherium*, and *Propalaeotherium* spp.) group together, separate from tapirs and lophiodontids (Figure 5.3a; Table 5.2). The early tetradactyl tapiromorph *Chasmotherium* occupies morphospace between the palaeothere group and the tapir group. The unciform of lophiodontids in this study possesses a flattened distal facet for articulation with the fourth and fifth metacarpals, and (along with the majority of lophiodontid carpal bones) is proximodistally compressed when compared to the unciform of *Tapirus* and palaeotheres (Figure 5.3b). ANOVA and Tukey WSD post-hoc tests demonstrate the deep divisions between the groups, with subsets for tapirs, *Chasmotherium* + palaeotheres (excluding *Palaeotherium*), and individual subsets for *Palaeotherium* and *Paralophiodon* (Table 5.2). In addition, ANOVAs demonstrate much higher between-group variance than within-group (F = 77.90; Table 5.2) for the unciforms in this study.

Lever-arm Calculations

Lever-arms for the muscles of the shoulder demonstrate that tapir lever arms are larger than those of most Eocene European perissodactyls (Figure 5.4). Individual regression

Table 5.3. ANOSIM comparing modern *Tapirus* spp. with Eocene European perissodactyls, based on Procrustes aligned shape coordinates for the humerus, third metacarpal and unciform. R-statistic between 0 and 1; 0 = equal within and between-group dissimilarity, 1 = between-group dissimilarity greater than all within-group similarity interactions. PA= *Palaeotherium* spp.; PL = *Plagiolophus* spp., PR = *Propalaeotherium* spp., EU = *Eurohippus*, LO = Lophiodontidae spp., CH = *Chasmotherium*.

Humerus						
	PA	PL	PR	LO		
T. bairdii	0.836	0.815	0.908	1		
T. indicus	0.978	1	1	1		
T. pinchaque	0.821	0.831	0.685	1		
T. terrestris	0.896	0.950	0.956	0.996		
Metacarpal III						
	Pa. magnum	*Pa. crassum*	*Pa. medium*	PL	PR	EU
T. bairdii	0.939	0.959	1	1	1	1
T. indicus	0.980	1	1	1	1	1
T. pinchaque	0.593	0.741	1	1	1	1
T. terrestris	0.897	0.925	1	1	1	1
Unciform						
	PA	PL	PR	CH	LO	
T. bairdii	0.610	1	0.920	1	1	
T. indicus	0.803	1	0.997	1	1	
T. pinchaque	0.444	0.964	0.888	0.821	1	
T. terrestris	0.651	1	0.956	1	1	

lines for *T. terrestris* and species averaged regression residuals between *T. terrestris* and Eocene European perissodactyls suggest that this species' lever arms exhibit the closest overall affinity to those of the Eocene European perissodactyls in this study (Figure 5.4; Appendix IV, Table S4.2). With the exception of *Pa. magnum*, all Eocene European perissodactyls in this analysis have relatively shorter in-levers for the *supraspinatus* than tapirs (Figure 5.4a). Residuals for the *supraspinatus* suggest that both lophiodontids and palaeotheres resemble *T. terrestris* most closely in their lever arm measurements, although *T. pinchaque* and *Lophiodon* are also very similar. Regression lines and Eocene European perissodactyl residuals for the *infraspinatus* suggest that both *T. bairdii* and *T. terrestris* are similar to lophiodontids and palaeotheres (Figure 5.4b; Appendix IV, Table S4.2). The only tapir that does not show any close similarities

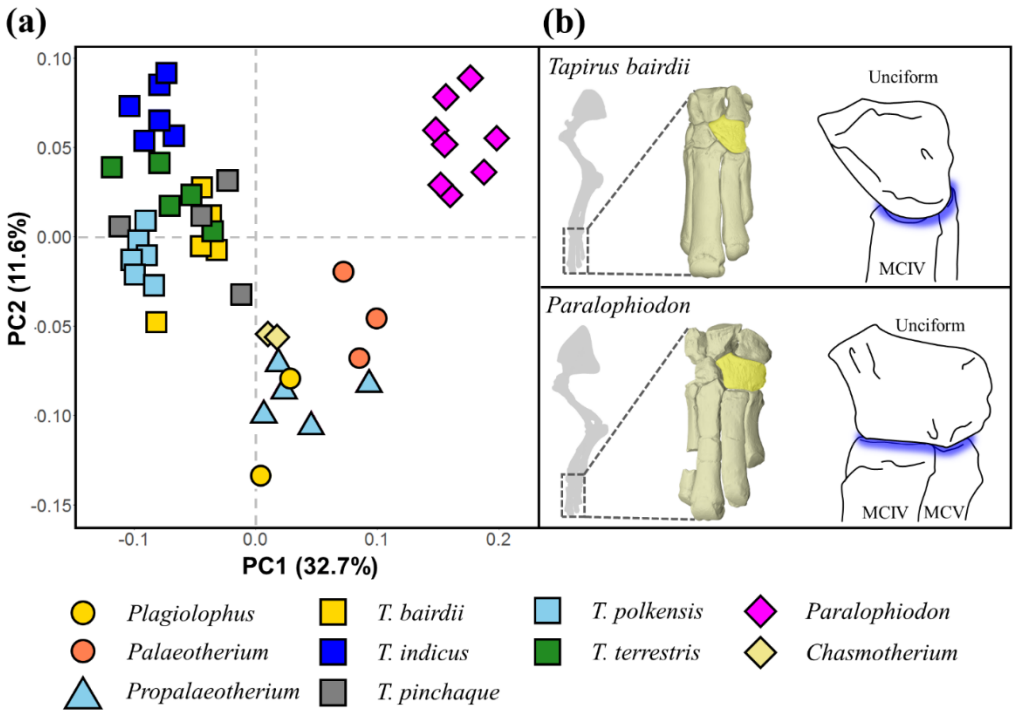

Figure 5.3. Comparison of unciform morphology between *Tapirus* spp. and European Eocene perissodactyls. **(a)** Principal components 1 and 2 demonstrate variation in shape between the groups; **(b)** genus level comparison between *Tapirus* and *Lophiodon* unciform morphology, with unciform-metacarpal joint facet hightlighted. Silhouettes represent skeletal forelimbs of *Tapirus bairdii* (top) and *Lophiodon* (excluding phalanges). Shape key: circles = Palaeotheriinae; triangles = other Palaeotheriidae; square = Tapiridae.

to small-bodied Eocene European perissodactyls in the *deltoideus* is *T. indicus* (similar to *Pa. magnum*;), with *T. bairdii* and *T. terrestris* showing close affinity to all palaeotheres (Figure 5.4c). The *teres major* lever arm of *T. indicus* demonstrates the greatest similarity to all Eocene European perissodactyls in this study excluding *Pa. magnum*, which is closest to *T. terrestris* (Figure 5.4d). In contrast to morphological results from geometric morphometrics, *T. pinchaque* does not demonstrate many close affinities to the lever arms of *Plagiolophus*, *Palaeotherium*, or *Propalaeotherium* (Figure 5.4; Appendix IV, Table S4.2).

No complete ulnae were available from *Plagiolophus* spp., *Chasmotherium*, or *Pliolophus* for comparison with *Tapirus*. For the elbow muscle data available, *T. terrestris* and *T. bairdii* demonstrate the closest residual distances to the lever arm results of *Propalaeotherium* and the lophiodontids (Figure 5.4e-f; Appendix IV, Table S4.2). The putatively cursorial *Pa. medium* represents an outlier for the lever arm of the *triceps brachii* (long head); all Eocene European perissodactyls have relatively shorter in-levers for this muscle than individuals of extant tapir species (Figure 5.4f).

Long-Bone Ratios

The ratios of humerus to radius and third metacarpal lengths for Eocene European perissodactyls display a broad range of measurements, demonstrating exceptionally high levels of variability within the Palaeotheriidae (Figure 5.5; Table 5.4). Long-bone ratio measurements and body mass calculations can be found in Appendix IV, Table S4.3. Ratios calculated for additional taxa from published measurements demonstrate low ratios for the extinct rhinocerotoids *Uintaceras*, *Metamynodon*, and *Teleoceras*, all of which were notably separated from tapirs and Eocene European perissodactyls (Figure 5.5a; triangles). The highest ratios are recorded for the small, tridactyl palaeothere *Plagiolophus* (*Pl. minor*, *Pl. annectens*), which displays long-bone ratios exceeding those of contemporaneous equids (*Mesohippus* spp.) and helaletids (*Heptodon*) (Figure 5.5a; Table 5.4). The ratios displayed by extinct rhinocerotoids, helaletids, *Mesohippus* spp., and *Plagiolophus* spp. were not compared to those of tapirs in subsequent analyses to improve resolution for less specialised taxa (Figure 5.5b).

In both radio-humeral and metacarpo-humeral ratios, the tapiromorphs *Paralophiodon* and *Chasmotherium* are shown to be very similar to *Tapirus* spp. (Figure 5.5a-b; Table 5.5). *Chasmotherium* (HR = 86.9; HMC = 49.9) and *T. terrestris* (86.1; 48.8) share the greatest similarity in forelimb ratios, with *Paralophiodon* (87.45; 45.4) exhibiting a greater similarity to the largest tapirs *T. indicus* (89.4; 47.6) and *T. bairdii* (84.6; 46.9) (Table 5.4). When compared to the Eocene equoids (*Hallensia* + palaeotheres), both *Chasmotherium* and *Paralophiodon* are more reminiscent of tapirs in their long-bone ratios. Within extant tapirs, *T. terrestris* and *T. indicus* are most similar in long-bone ratios to the non-plagiolophine palaeotheres (including *Pr. hassiacum*, *E. messelensis*, and *Pa. magnum*) (Figure 5.5b). Despite demonstrating close similarities to Eocene perissodactyls in humeral shape, the long humerus of *T. pinchaque* causes low HR and HMC ratios when compared to other tapirs. As a result, this taxon does not show close affinities to Eocene European perissodactyls in their long-bone ratios.

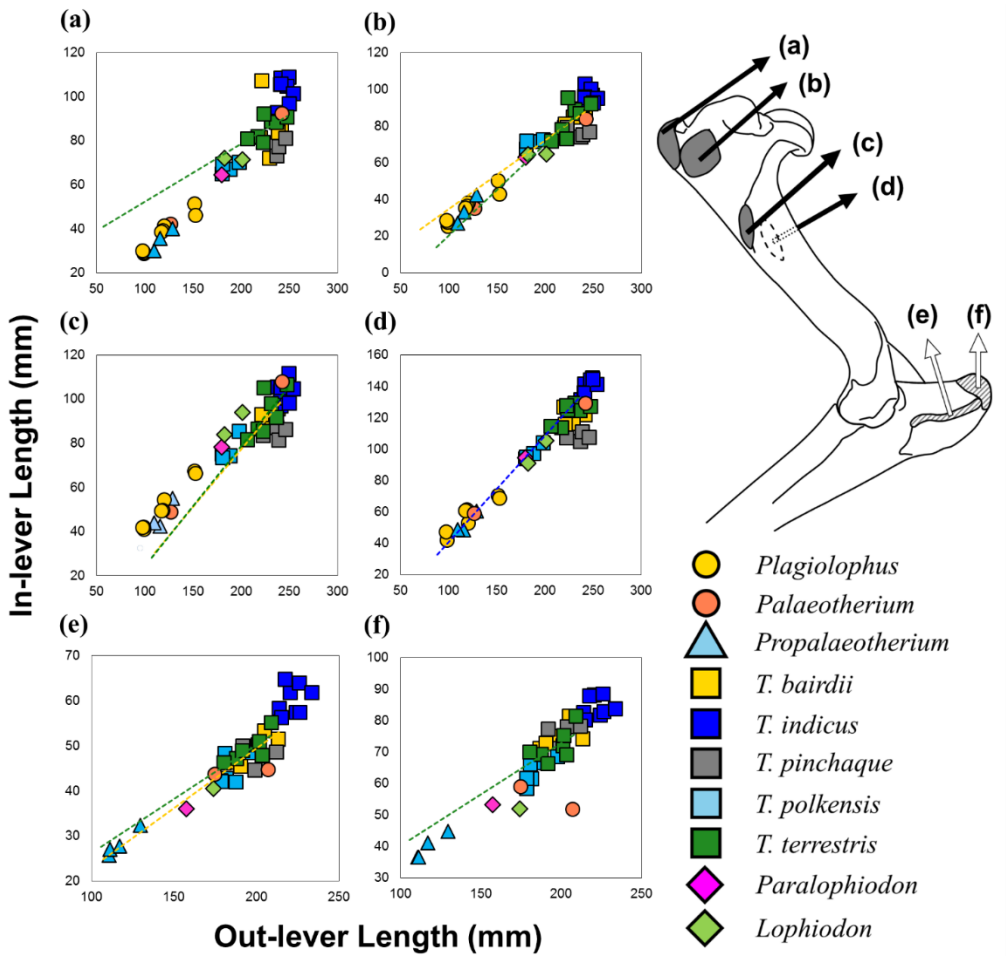

Figure 5.4. Lever-arm comparison of upper forelimb bones of *Tapirus* species with Eocene European perissodactyls. In-lever lengths plotted against out-lever for *supraspinatus* **(a)**, *infraspinatus* **(b)**, *deltoideus* **(c)**, *teres major* **(d)**; lateral **(e)** and long **(f)** head of *triceps brachii*. OLS regression line for individual tapir species best fitting extinct European perissodactyl pattern shown. Insertion sites and action of muscles (arrows) shown on forelimb diagram (right): black arrows = shoulder, white arrows = elbow; bones of left forelimb in lateral view. Shape key: circles = tridactyl Palaeotheriidae; triangles = tetradactyl Palaeotheriidae; square = Tapiridae; diamond = Lophiodontidae.

The extinct dwarf *T. polkensis* displays similar long-bone ratios to those of *Hallensia*, *Pr. voigti*, and the extinct helaletid *Heptodon*; this tapir is not close to any living tapirs

in the proportions of its long forelimb elements. The basal equid *Sifrhippus* exhibits comparable metacarpo-humeral ratios to those of extant tapir species; this taxon also displays a radio-humeral ratio intermediate between the tetradactyl palaeotheres *Eurohippus* and *Propalaeotherium* (Figure 5.5b). OLS regression and permutation of long-bone ratios against log-transformed body mass demonstrates significant negative correlation between mass and radiohumeral ($r = -0.70$; $r^2 = 0.49$; $p < 0.01$) and metacarpohumeral ($r = -0.72$; $r^2 = 0.51$; $p < 0.01$) ratios for available taxa.

Discussion

In this study we used various quantitative approaches to test whether extant species of tapir (*Tapirus*) represent viable morphological and functional forelimb analogues for Eocene European perissodactyls. Previous qualitative comparisons have suggested that the limbs of tapirs morphologically resemble those of species within the tridactyl genus *Palaeotherium* (including *Pa. magnum* and *Pa. crassum*) (W. H. D. Adams & Meunier, 1872; Cuvier, 1812b; Rudwick, 2008), with additional comparisons drawn to the tetradactyl Lophiodontidae and *Propalaeotherium* in overall biology (Agustí & Anton, 2004a; Franzen, 2010a; Prothero, 2016). Here, we demonstrate that no one extant tapir species is a viable analogue for Eocene European perissodactyls; however, several individual tapir species show both morphological and functional attributes of the forelimb that would make them potential analogues for locomotion in certain groups of Eocene European perissodactyls. Using a combination of morphological similarities (quantified using geometric morphometrics), forelimb proportion comparisons (long-bone ratios), and joint functional morphology (lever-arm ratio comparisons), we discuss how variable Eocene European equoid limb morphology is, and how these respective morphologies and associated functions compare to living tapir analogues.

Locomotor diversity within Palaeotheriinae

In recent studies, tapirs have been demonstrated to display significant differences in forelimb morphology pertaining to specific functional outcomes (MacLaren & Nauwelaerts, 2016, 2017). However, this diversity in form and function is meagre when compared to the diversity in forelimb morphology displayed by the Palaeotheriidae. The results of this study categorically support the earliest descriptions of palaeotheres diverging greatly in their forelimb bone morphology from one another (Cuvier, 1812b; Rudwick, 2008), highlighted by the disparity observed in both the radius and third metacarpal (Figure 5.2 and 5.6; Appendix IV, Figure S4.1).

Table 5.4. Long-bone ratios and estimated body masses for tapirs and early European perissodactyls. * = predicted based on sister taxa. **N** = number of articulated specimens; (n) = total specimens for average. **HR** = radius/humerus; **HMC** = third metacarpal/humerus; **BM** = mean estimated body mass.

Genus	**Species**	**N** (n)	**HR**	**HMC**	**BM** (kg)
Tapirus	*bairdii*	**5** (5)	84.6	46.9	228.7
Tapirus	*indicus*	**7** (8)	89.4	47.6	326.4
Tapirus	*pinchaque*	**4** (4)	83.5	47.1	202.4
Tapirus	*terrestris*	**7** (7)	86.1	48.8	216.6
Tapirus	*polkensis*	**2** (15)	96.8	54.5	116.9
Paralophiodon	*leptorhynchum*	**1** (1)	87.45	45.4	232.5
Chasmotherium	*minimus*	**1** (2)	86.9	49.9	-
Palaeotherium	*magnum*	**1** (4)	93.7	49.8	240.3
Plagiolophus	*major**	**0** (5)	107.5*	62.9	78.9
Plagiolophus	*annectens*	**0** (6)	117.0	72.8	34.8
Plagiolophus	*minor*	**0** (11)	126.6	82.1	19.3
Propalaeotherium	*hassiacum*	**0** (24)	93.3	48.6	46.5
Propalaeotherium [a]	*voigti*	**0** (4)	96.4	56.9	23.0
Eurohippus	*parvulum*	**1** (6)	90.5	52.2	-
Eurohippus [b]	*messelensis*	**2** (2)	88.2	49.6	-
Hallensia [c]	*matthesi*	**1** (1)	93.5	55.1	-

References: [a] Franzen (2010); [b] Franzen and Haupzeter (2017); [c] Franzen (1990)

The Palaeotheriidae include both tetradactyl and tridactyl members (Agustí & Anton, 2004a; Danilo et al., 2013; Franzen, 2006, 2010a), and as a result may be expected to demonstrate a high degree of morphological variation in the forelimb. The first descriptions of palaeotheres are those of the currently recognised Palaeotheriinae (Cuvier, 1812b), a monophyletic clade which includes the genera *Palaeotherium* and

Plagiolophus (Bai, 2017; Danilo et al., 2013; Remy, 2015). These two genera are both functionally tridactyl palaeothere clades; however, despite their close phylogenetic affinity, they demonstrate high morphological diversity within the forelimb (Figures 5.2, 5.5 and 5.6). Shape variation in the third metacarpal of the most variable genus, *Palaeotherium*, is shown to be far greater than exhibited by any other in this study, including *Tapirus* (Figure 5.2 and Figure 5.6). Several contemporaneous palaeotheriines exhibited highly divergent manus dimensions (e.g., *Pa. curtum* and *Pl. minor*; Figure 5.6), implying a range of locomotor behaviours (e.g., cursoriality) in similarly sized taxa, and potentially accompanying variation in ecological niche. As observed by Cuvier, *Pa. curtum* possesses highly robust forelimb bones, indicative of a heavily built taxon, whereas *Plagiolophus* spp. and *Pa. medium* demonstrate elongate and gracile metacarpals, akin to their equid cousins (Cuvier, 1812b; Franzen, 2010a; MacFadden, 2005). Despite this divergence in morphology, the metacarpals of *Pa. curtum* and *Pl. minor* are of approximately equal absolute length. A comparable situation is observed in many other perissodactyl communities, including the Miocene of Florida (*Nannipus* (Equidae) and *Aphelops* (Rhinocerotidae); Love Bone Bed) and France (*Anchitherium* (Equidae) and *Hoploaceratherium* (Rhinocerotidae); Sansan) (Alberdi & Rodriguez, 2012; Heissig, 2012; MacFadden & Hulbert, 1990). Palaeotheriines diversified to occupy many available locomotor niches, potentially pertaining to specific partitioning of resources based on taxon mobility. The short and stout manus of *Pa. curtum*, coupled with a comparatively long but robust radius (Figure 5.6), is reminiscent of the basal rhinoceros *Uintaceras* (Holbrook & Lucas, 1997), described as exhibiting multiple features of a graviportal existence (e.g., highly robust limb bones; femur much longer than tibia; Holbrook and Lucas 1997). The plagiolophines and *Pa. medium*, with their elongated distal forelimbs and posteriorly curved radii and ulnae (Figure 5.6), would have represented a cursorial group of palaeotheres. The diminutive plagiolophines (e.g., *Pl. minor*), with small body size and elongate forelimb morphology represent the only members of the clade to survive through the Eocene-Oligocene extinction event (the "Grande Coupure") (Hooker, 2010a; Joomun, Hooker, & Collinson, 2008). The climatic changes throughout Eurasia during this extinction event are hypothesised to have favoured animals adapted to drier, more open habitats (Blondel, 2001). In addition to differential dietary specialisations compared to other late Eocene palaeotheres (Joomun et al., 2008), the elongated limbs and reduced body size may have benefitted plagiolophines in drier, open habitats in Europe immediately following the 'Grande Coupure' (Blondel, 2001; Hooker, 2010a). These cursorial adaptations would allow small browsers to rapidly flee from predators in more open terrain where shelter may have been scarce. In contrast, the more graviportal palaeotheres (e.g., *Pa. curtum*) did not attain the sizes that contemporaneous North American browsing perissodactyls (e.g., brontotheres) achieved, and their truncated manus and robust upper limbs would

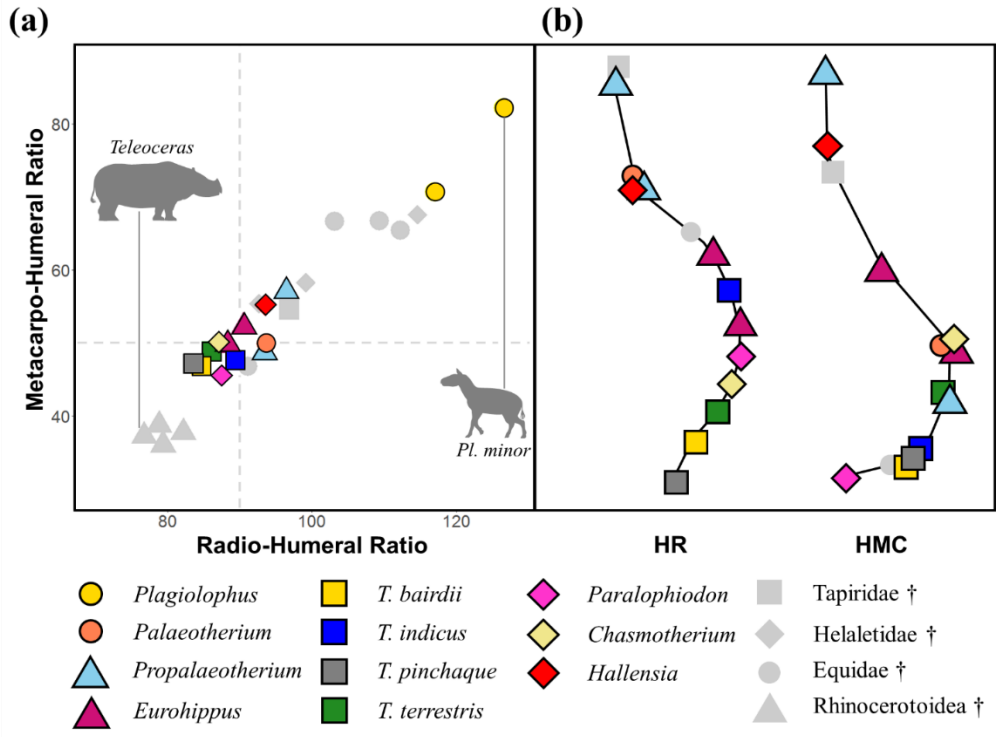

Figure 5.5. Long-bone ratio comparison of *Tapirus* spp. and selected extinct perissodactyls. **(a)** Radio-humeral (HR) and metacarpo-humeral (HMC) ratios plotted against one another. **(b)** Neighbour-joining trees based on distances between mean ratios for extant *Tapirus* and European perissodactyls (excluding *Plagiolophus* spp.). Dotted lines mark approximate boundary between cursorial and mediportal long-bone ratios, according to Gregory (1929). Silhouettes represent taxa demonstrating typically graviportal (Rhinocerotidae: *Teleoceras*) and cursorial (Palaeotheriinae: *Plagiolophus*) limb ratios.

not have been favorable for swift escape or efficient movement over longer distances in the more open environments of Oligocene Europe.

Cursorial palaeothere shoulder analogy

The comparisons drawn between tapir forelimb anatomy and that of palaeotheres in previous studies (e.g., Cuvier, 1812) have been demonstrated to warrant re-evaluation in this study. First, any comparisons of the putatively cursorial palaeotheres

(*Plagiolophus* and *Pa. medium*) to tapirs in terms of their locomotor anatomy and function may be considered erroneous, on the evidence of this study. The long-bone ratios of *Plagiolophus* (Figure 5.5) coupled with the large size difference between this genus and all *Tapirus* in this analysis (Figure 5.4), suggest that locomotor analogy between these taxa and tapirs is unlikely. Conversely, the lever-arm similarities between the palaeotheres *Plagiolophus* and *Propalaeotherium* and the extant *T. terrestris* (Figures 5.4 and 5.7; Appendix IV, Table S4.2) demonstrate that the muscular action on the shoulder and elbow in this tapir may indeed be representative of the functional morphology in smaller palaeotheres. There is also a noteworthy similarity in *teres major* lever-arm ratio between *T. indicus* and all the Eocene European perissodactyls in the analysis (Figure 5.4d). The site of insertion for this muscle (the teres tuberosity of the humerus) is a discriminant feature for living tapirs (MacLaren & Nauwelaerts, 2016), suggestive of interspecific differences within tapirs in mechanical action of the *teres major* and *latissimus dorsi* muscles, both of which insert on the tuberosity. The variation in placement of the teres tuberosity along the shaft of the humerus in *Plagiolophus*, *Palaeotherium* cf. *medium*, and *Propalaeotherium* is akin to the range observed in living *Tapirus* species. The placement of the lateral humeral flexor (the *deltoideus*) in the smaller Eocene European perissodactyls (*Propalaeotherium* and *Plagiolophus*) coupled with comparatively longer in-lever measurements is more reminiscent of the large *T. indicus* than any other living tapir (Figure 5.4c and Figure 5.7).

Based on our understanding of how morphometric features scale with changes in mass (Biewener, 2003, 2005), the similarities in flexor insertions and lever-arm measurements between the cursorial palaeotheres (20-80kg) and the more massive *T. terrestris* (~220kg) and *T. indicus* (~325kg) suggest that muscles acting on the shoulder of cursorial palaeotheres (e.g., *Plagiolophus*) were disproportionately smaller relative to those of extant tapirs. This means that the muscle mass around the shoulder would have been very limited, giving the shoulder region of smaller cursorial palaeotheres a very gracile appearance akin to small antelopes, chevrotains, and goats (Franzen and Haupt 2012; Gewaily et al. 2017). As both adult and juvenile *T. indicus* demonstrate shoulder flexor insertions similar to those observed in cursorial palaeotheres (MacLaren and McHorse, *In review*), it is possible that the functional morphology of juvenile *T. indicus* would be of greater comparative value for small palaeotheres.

Corroborating Cuvier on palaeothere morphology

Whereas many palaeotheres in this analysis are small, presenting a number of scaling issues to consider when drawing conclusions on locomotor analogy, there is one taxon which approximates living tapir species in both size and shape: *Palaeotherium magnum*

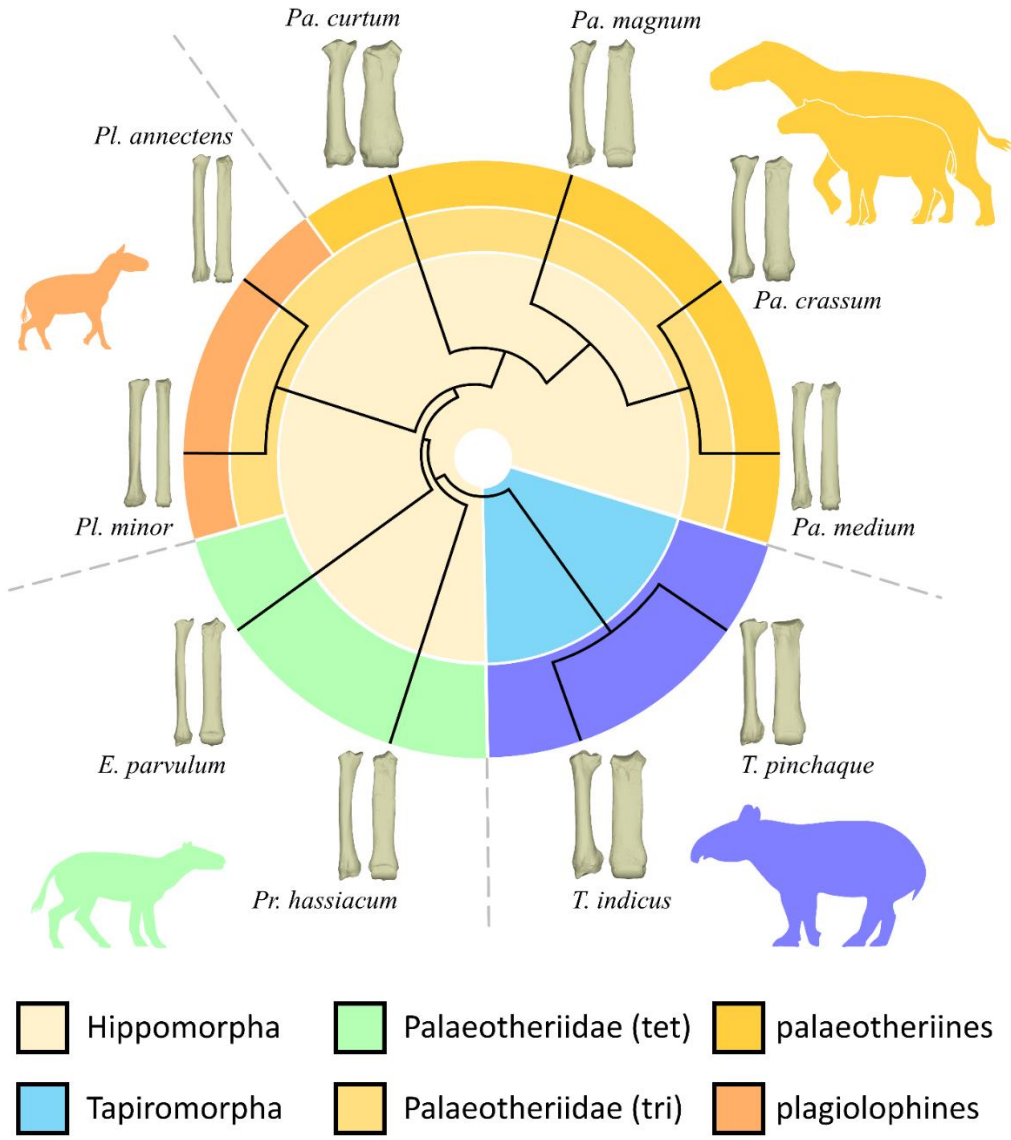

Figure 5.6. Variation of locomotor morphology across Palaeotheriidae. Radius (left) and third metacarpal shown for three clades of Palaeotheriidae alongside modern tapirs for comparison; bones not to scale. Unrooted phylogeny based on Franzen (1992) and Danillo, et al. (2013). Silhouettes represent exemplar *bauplans* for each group. Abbreviations: tet = tetradactyl; tri = functionally tridactyl.

(Table 5.4). This taxon was described by Cuvier as displaying strong similarities to tapirs in the metacarpus, which we corroborate and expand upon with this quantitative analysis. Similarities in MCIII shape between the mountain tapir *T. pinchaque* and *Pa. magnum* were observed (PCA and ANOSIM results; Figure 5.2; Table 5.3), and are likely driven by the comparatively broad metacarpophalangeal joint facet in *Pa. magnum* when compared to other tridactyl palaeotheres (Figure 5.6; Palaeotheriinae), and the more slender profile of the MCIII in *T. pinchaque* (MacLaren & Nauwelaerts, 2017). This is also true for the palaeothere *Pa. crassum*, described in the past as "resembling a tapir even more than [*Pa. magnum*], for it did not differ in its size and proportions" (Cuvier 1812; translation from Rudwick 2008). By contrast, we find that *Pa. magnum* resembles tapirs more closely than *Pa. crassum* (for the bones available for the latter species), principally due to the more gracile shape of the metapodials and radius in *Pa. crassum*. Therefore, from this point on our morphofunctional comparison focuses upon *Pa. magnum*.

From a functional standpoint, results from body mass estimation and lever-arm ratios suggest that *Pa. magnum* may have demonstrated similar muscle mass in the shoulder and upper forelimb region to both *T. indicus* and *T. terrestris* (Table 5.4; Figure 5.4). Other large tapirs with longer limbs not included in this study (e.g., *T. webbi*; Hulbert 2005; MacLaren et al. 2018) may represent a closer proportional analogue for *Pa. magnum* within *Tapirus*. However, as *T. webbi* is itself extinct, it cannot represent a viable living analogue for modelling locomotion in this large palaeothere. It is therefore difficult to isolate one individual tapir species that shows ideal morphofunctional similarities to *Pa. magnum*. First of all, every tapir living today retains all four digits in the manus, whereas *Pa. magnum* (and all other palaeotheriines) have reduced their MCV to a non-functional vestige (Cuvier, 1812b). The more gracile metacarpal morphology of *T. pinchaque* is shown to be similar to that of *Pa. magnum* (Table 5.3). However, this is countered by the proximal shift in muscle insertions on the humerus of this tapir, whereas the upper limb functional morphology of *T. indicus* or *T. terrestris* appears an ideal analogue. The obligate reliance on the lateral fifth digit in *T. indicus* (and the consequent morphological changes in the carpus; Earle 1893; Simpson 1945; MacLaren and Nauwelaerts 2017) rule this tapir out as a model species for a functionally tridactyl *Pa. magnum* (Table 5.4; Figure 5.3). Therefore, we conclude that, due to close similarities in humeral shape and lever-arms, metacarpal shape, predicted body mass, and only facultative use of the lateral MCV, the closest locomotor analogue for *Pa. magnum* within living tapirs is the lowland tapir *T. terrestris*. Any future mechanical modelling undertaken on *Palaeotherium* should naturally account for the differences in the manus morphology and spread of loading forces when compared to the tetradactyl tapir.

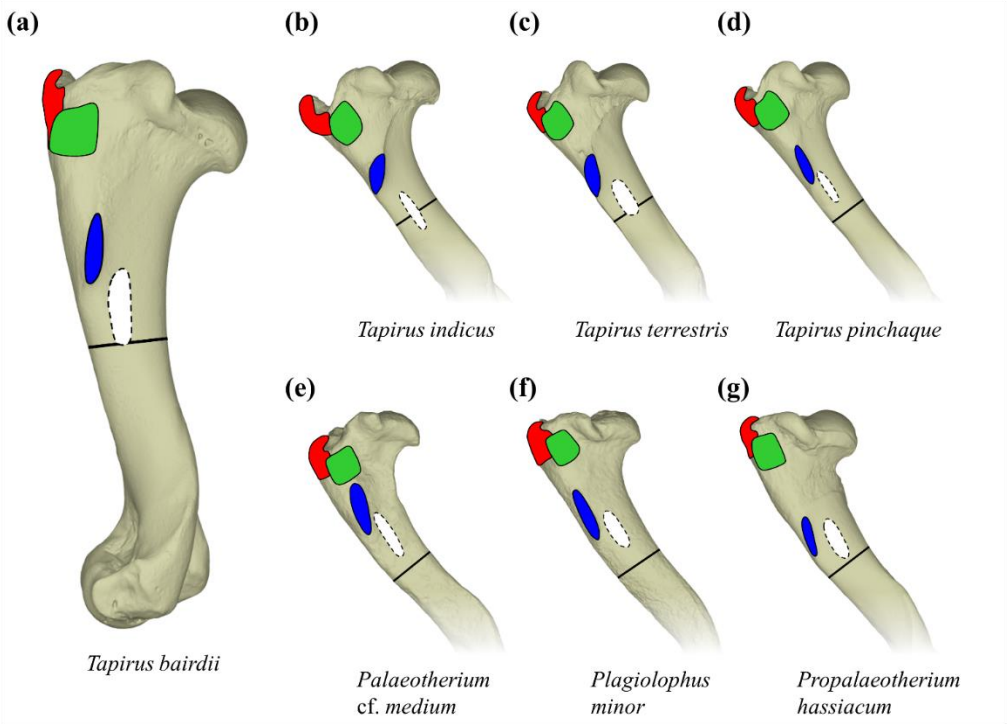

Figure 5.7. Variation of muscular insertion sites on the humerus of tapirs and early European perissodactyls. Humeri of tapirs **(a-d)** shown alongside three palaeothere taxa **(e-g)** in lateral view. Black bar represents midpoint of the humeral shaft. Muscular insertions: *m. supraspinatus* (red); *m. infraspinatus* (green); *m. deltoideus* (blue); *m. teres major* (medial insertion; white). In particular note variation in *teres major* and deltoid insertions across *Tapirus* and between early European perissodactyls.

Lack of tetradactyl palaeothere analogy

The earliest European perissodactyls were (to our knowledge) all functionally tetradactyl; these include taxa such as *Lophiodon* and *Paralophiodon* (Holbrook, 2009), *Eurohippus*, *Propalaeotherium* (Franzen, 2010b), *Hallensia*, and *Chasmotherium* (Franzen, 1990; Radinsky, 1967; Remy, 2015). Functional tetradactyly is present in palaeotheres, albeit in the smaller and more primitive forms (e.g., *Propalaeotherium*). Evidence from this study suggests that the morphology of the metacarpals, lateral carpus, and long-bone ratios in tetradactyl palaeotheres more closely resembles tridactyl palaeotheres (Figure 5.2c-d, Figure 5.3a), in some cases those of much greater size (e.g., *Propalaeotherium* and *Pa. magnum*; Figure 5.2c, Table 5.4). In living tapirs, the

unciform carpal and both third and fourth metacarpals have been shown to demonstrate morphological differences relating to the functional use of the fifth (most lateral) digit. The MCIII is elongate relative to the MCIV in tapirs with reduced lateral metacarpal usage (e.g., *T. bairdii*, *T. terrestris*; Earle, 1893; MacLaren and Nauwelaerts 2017), and the MCIV also exhibits a flattened joint facet with the unciform in species reliant on the MCV for locomotion (e.g., *T. indicus*). The unciform also demonstrates morphological variability across *Tapirus*, both in keeping with greater loading of the fifth metacarpal (Earle, 1893; MacLaren & Nauwelaerts, 2017; Simpson, 1945) and with habitat density (MacLaren et al., 2018). The distribution of loading forces through the carpus therefore appears to be more similar within phylogenetically related groups than between perissodactyls exhibiting functional tetradactyly. In addition, the relatively long and thin fifth metacarpal of tetradactyl palaeotheres has no extant equivalent in ungulates, and is more reminiscent of the manus arrangement in felids or canids (Barone, 2000). This apparent phylogenetic constraint on morphology in the manus, and notable size difference as mentioned earlier, makes the assignment of a living analogue for tetradactyl palaeotheres within the tapirs difficult. Although metacarpal shape and upper forelimb lever-arms are suggestive of similarities between *Propalaeotherium* and *T. terrestris* (Figures 5.2c and 5.4), we feel that assigning this tapir as a viable locomotor analogue for *Propalaeotherium* would require a substantial over-interpretation of the data available.

Locomotion in the Lophiodontidae

Living contemporaneously alongside palaeotheres, the lophiodontids represent an enigmatic extinct group of tetradactyl perissodactyls endemic to Europe that have been compared to tapirs based upon general appearance and feeding ecology (Agustí & Anton, 2004a; Depéret, 1907; Franzen, 2010a; Holbrook, 2001). In this study we find that the morphology of the humerus of lophiodontids (*Paralophiodon leptorhynchum* and *Lophiodon tapirotherium*) cannot be statistically separated from *T. terrestris* or *T. bairdii* (Table 5.2), although between-group variation is greater than that of almost all living tapirs (Table 5.3). The humerus of *Lophiodon* exhibits a prominent deltoid tuberosity and a proximodistally long teres tuberosity (Holbrook, 2009), implying that the *deltoideus* and *teres major* (shoulder flexors) act slightly differently to those of living tapirs. The lateral projection of the deltoid tuberosity increases the mechanical advantage of the *deltoideus*, which acts as the primary lateral shoulder flexor. In addition, the olecranon process of the ulna is rounded in lateral aspect (as observed in *T. indicus*; MacLaren and Nauwelaerts, 2016) and also in caudal aspect; this increases surface area insertion potential for the long head of the *triceps brachii*, one of the major limb extensors involved in gravitational support (Liebich et al., 2007). This large,

rugose insertion site is mirrored by evidence of similarly robust origination sites for the *triceps* on lophiodontid scapulae (Holbrook, 2009). The implication of these muscle attachment morphologies, similar in many ways to those of rhinoceros, hippopotamus, and elephant humeral flexors (Depéret, 1907; Fisher, Scott, & Naples, 2007; Prothero, 2005), is that the lophiodontids possessed a highly muscularised upper arm, ideal for supporting large masses over the forelimb (Prothero, 2005). With regards to the carpus and metacarpals of lophiodontids (principally represented by *Paralophiodon* in this study; see Appendix IV, Figure S4.1), a similar suite of load-bearing adaptations are observed. *Paralophiodon* exhibits several features indicative of comparatively greater loading being applied over the forelimb than in living tapirs. First, the proximal row of carpals (scaphoid, lunate, and cuneiform) demonstrate a large degree of proximodistal compression compared to those of most extant tapirs and palaeotheres. Within recent tapirs, the Central American *T. bairdii* has been shown to demonstrate compressed proximal carpals relative to other tapirs (MacLaren & Nauwelaerts, 2017); due to the decreased reliance on the fifth digit in this taxon, proximal carpal compression was interpreted as an adaptation to higher loading over the manus compared to *T. terrestris* or *T. pinchaque* (MacLaren & Nauwelaerts, 2017; Prothero, 2005). We find a similar condition in *Paralophiodon*, albeit with more extreme proximal carpal compression and more greatly reduced fifth metacarpal in the type manus of *Paralophiodon leptorhynchum* (FSL 2685), as described by Deperet (1907) and Holbrook (2009). Evidence of carpal compression is further observed in the distal carpal row (unciform, magnum, and trapezoid) (Figure 5.3), most markedly in the unciform. The unciform demonstrates a near-flattened distal joint facet for interaction with the fourth and fifth digits (MCIV and MCV) (Figure 5.3b). The flattened distal facet spreads compressive forces across the fourth and fifth metacarpals during the stance phase of locomotion in *Paralophiodon*. This morphology is not observed in tapirs or tetradactyl palaeotheres, which both exhibit a convex distal unciform joint for the MCIV (MacLaren & Nauwelaerts, 2017). Ultimately, this suggests that the MCIV, at least of *Paralophiodon*, was more heavily loaded than that of either tapirs or tetradactyl palaeotheres (Earle, 1893; Gregory, 1929; MacLaren & Nauwelaerts, 2017; Prothero, 2005; Simpson, 1945). Interestingly, a similar condition is observed in the carpus of the pygmy hippopotamus *Hexaprotodon* (*Choeropsis*); although excluded from this study, the potential ecological and locomotor comparisons between lophiodontids and the paraxonic artiodactyl *Hexaprotodon* are an ideal avenue of future investigation.

Paralophiodon is well known from multiple isolated specimens from the middle Eocene deposits at La Livinière (Buffetaut, 1986; Depéret, 1907; J. E. Martin, 2014) (Lutetian, possibly Bartonian in age). Among the specimens incorporated in this study, two distinct fifth metacarpals (MCVs) were found; one belonging to the type manus FSL

2685, the other misidentified as a second metacarpal (MCII) in another associated manus (FSL 2686). The MCV of FSL 2686 is distinctly longer (+33%) than that of the type manus for *Paralophiodon*; this bone does not cluster with the MCV from the type specimen, but is in fact closer to the MCVs of Eocene-Oligocene rhinocerotoids and the relatively cursorial Miocene tapir *T. polkensis* (Appendix IV, Figure S4.1f). On the premise that tapiromorph metacarpals do not differ greatly in length relative to one another through ontogeny (MacLaren, pers. obs.), and that tapiromorphs do not exhibit significant osteological shape differences between sexes (despite demonstrating sexual dimorphism in size; Simpson 1945; Mead 2000), we interpret FSL 2686 as likely representing a different species from the same locality. A thorough phylogenetic examination of all postcranial elements will be necessary to establish this with any certainty. At this point, the presence of this bone in the deposits of La Livinière indicates the likely presence of another species of lophiodontid alongside *Paralophiodon leptorhynchum*, which appears to demonstrate an alternative locomotor niche (functional tetradactyly). Ecologically, the early Eocene locality of La Livinière is well known for terrestrial crocodilians, small artiodactyls, and creodonts, indicative of a drier and more terrestrial habitat than other deposits harboring lophiodontid remains (J. E. Martin, 2014). This represents a similar habitat to that preferred by the living tapirs *T. terrestris* and *T. bairdii* (Bodmer & Brooks, 1997; Matola, Cuarón, & Rubio-Torgler, 1997). The short lateral metacarpal of *Paralophiodon* (based on the type manus) is notably reminiscent of the patterns of metacarpal length observed in *T. bairdii* (MacLaren and Nauwelaerts 2017). Combined, we therefore conclude that the compressed proximal carpal row, reduced fifth metacarpal, lever-arm ratios, and forelimb proportions indicate that the most suitable extant locomotor analogue for *Paralophiodon* within modern tapirs is the Central American tapir *T. bairdii*. It should be noted that lophiodontids demonstrate a large range of mass and shape in the forelimb, although many of these bones were not suitable for analysis in this study. To test whether *Paralophiodon* differs in locomotor ecology to other lophiodontids found in deposits suggesting a moist-habitat (e.g., *Lophiodon remensis* from Monthelon, France (Smith, De Wilde, & Steurbaut, 2004); *L. tapirotherium* from Geiseltal, Germany (Holbrook, 2009)), further three-dimensional quantification of multiple lophiodontid taxa will be necessary, with the aid of retrodeformation of severely crushed remains (e.g., *L. lautricense*).

Conclusions

In this study, we have successfully quantified forelimb variation in Eocene European perissodactyls which, in previous literature, have been compared in their morphology and ecology to extant tapirs. This geometric morphometric study clearly highlights the

extreme variation in Eocene European perissodactyl locomotor morphology. To assign a closest extant analogue within *Tapirus* to (for example) the genus *Palaeotherium* would consequently be impossible, given the variation in form (limb morphology) and function (e.g., rapid vs. slow shoulder flexion) of the forelimb in Eocene European perissodactyls. The plesiomorphic, yet variable, forelimb of *Tapirus* certainly demonstrates similarities in both form and function when compared to some palaeotheres and lophiodontids, as previously noted (albeit qualitatively) by Cuvier and Depéret during the early descriptions of these Eocene taxa (Cuvier, 1812b; Depéret, 1907). Tapir upper forelimb morphology, lever-arms, and limb proportions suggest the closest analogy to members of the Lophiodontidae (e.g., *Paralophiodon leptorhynchum*). The greatest similarities between extant tapirs and lophiodontids are shown between *Paralophiodon* and the Central American tapir *Tapirus bairdii*. The Lophiodontidae may exhibit as much variation in form as is present in palaeotheres, although it was not possible to include all taxa in this study due to extensive taphonomic modification of many limb bones (Depéret, 1907; Holbrook, 2009; Robinet, Remy, Laurent, Danilo, & Lihoreau, 2015). When compared to the highly diverse palaeotheres, tapirs with more gracile metapodials (e.g., *T. pinchaque, T. polkensis*) are shown to be morphologically more similar. In confirmation of Cuvier's work on palaeotheres (Cuvier, 1812b; Rudwick, 2008), both *Pa. magnum* and *Pa. crassum* are demonstrated to resemble tapirs in their overall forelimb morphology (most closely that of *T. pinchaque*). The question of scaling will always be of importance when comparing extant and extinct species in search of potential analogy; in this case, both *Pa. crassum* and *Pa. magnum* approximate living tapirs in their estimated size, further supporting historical claims of morphofunctional similarity. In contrast to the speculations of Cuvier, the 'cursorial palaeotheres' *Pa. medium* and *Plagiolophus* spp. show few similarities to any tapir species in this study. This is indicative of a similar shoulder muscle application and function between palaeotheres and tapirs, but also that the greatest modifications in palaeothere forelimb morphology exist in the distal segments (as is the case in equids; MacFadden 1992) rather than the proximal segments (as evidenced in living tapirs; MacLaren and Nauwelaerts 2016). This study has endeavored to utilise recent techniques and understanding of tapir functional locomotor morphology (MacLaren and Nauwelaerts 2016; 2017; MacLaren et al. 2018) to cast light on the locomotion of poorly understood Eocene European perissodactyls. Future work incorporating other potential analogues (e.g., *Hexaprotodon*, suids, etc.) and combining morphometrics with ecological data (e.g., tooth micro/mesowear, stable isotopes, cranial and lumbar mechanics) will enable these bizarre clades to be better understood as members of Eocene European ecosystems, and facilitate a more fundamental understanding of adaptive radiations within perissodactyl clades.

“all these moments lost in

time, like tears in rain”

- Roy Batty -

– RESEARCH CHAPTER SIX –

Endemism, dietary regime and ecological turnovers influence morphological evolution in equoid limbs through deep time

Jamie A. MacLaren

Thesis Chapter

One of the most well studied examples of a terrestrial macroevolutionary transition in the locomotor apparatus is that of the forelimb Equidae (Perissodactyla: Equoidea). The main joint in the distal limb of equoids – the metacarpophalangeal (fetlock) joint – is a highly specialised joint with multiple functions (shock absorption, stability, and facilitation of efficient elastic recoil to enable sustained, rapid running). Changes in the shape of this joint have not been directly linked to other well-known ecological transitions in equoids (e.g. diet changes), nor has the variation in the shape of this joint been investigated relative to local or global climatic changes through the Cenozoic. Here, we investigate how this joint has changed in shape (and potential function) from extinct tetradactyl equoids (equids + palaeotheres) to modern horses in a quantitative framework, comparing patterns of shape change with internal (mass/diet) and external (geological/climatic) ecological drivers. We used landmark based geometric morphometrics to quantify fetlock shape in Equoidea using landmarks applied to the distal metacarpal. 268 metacarpals were laser scanned and landmarked, including a comparative sample of tapirs (Perissodactyla: Tapiridae) to represent tetradactyl perissodactyls with established forest-dwelling ecology. A hypothetical ancestral fetlock shape was calculated from basal-most taxon metacarpal shapes using a time-calibrated phylogeny. Divergence from the ancestral condition was calculated using ordinary sum of square distances (OSS) from geometric morphometric analysis, averaged per species. First derivatives of time for body mass, hypsodonty and OSS were taken at 1 Ma intervals to compare trait shifts. When examined through time, positive correlations between shape divergence and body mass/hypsodonty occurred at 0–1 Ma intervals, with negative correlations at 5 Ma. The presence of the European equoid *Plagiolophus* drives divergence in fetlock shape in the late Eocene; morphology of the entire manus in this taxon hints at a divergence in phalangeal mobility between tridactyl equids and palaeotheres, facilitated by digital interosseous muscles. Minimal increases in average shape divergence were observed at the "Grande Coupure" extinction event, whereas a large increase occurred following the advent of hypsodonty in the middle

Miocene. Reversion toward a more forest-adapted fetlock shape is hinted at during the Vallesian faunal turnover. Shape divergence in equoids hits its peak during the Quaternary Glaciation with the presence of multiple functionally monodactyl taxa, notably including the South American endemic equinine fauna *Hippidion* spp. and *Equus* (*Amerhippus*). By contrast, tapirid fetlock morphology remains close to the ancestral condition throughout the Cenozoic. Overall, we demonstrate that fetlock morphology in equoids is intricately linked with fluctuations in body mass, diet regime, and major faunal turnover events. Localised morphological evolution plays a key role, with novel exploration of metacarpal morphospace correlating with origination and extinction of specialised endemics (e.g. *Plagiolophus*, *Hippidion*).

Introduction

The interactions between the metapodials and phalanges represent essential morphological and functional aspects of locomotion in numerous terrestrial, volant and aquatic tetrapods (e.g. Thewissen and Fish 1997; Richmond and Strait 2000; Bonnan 2003; Bennett 2008; Clifford 2010; Nyakatura 2012). Within mammalian locomotion alone, the bones, tendons and ligaments involved in metacarpophalangeal joints permit successful negotiation of complex, three-dimensional environments (e.g. climbing in primates; Patel 2010; Druelle et al. 2018), enable efficient high-speed locomotion in open habitat ungulates (e.g. Janis 2007; Clifford 2010), and have even facilitated the conquest of the seas (e.g. cetaceans; Cooper et al. 2007) and skies (chiropterans; Sears et al. 2006). One of the most recognisable and highly specialised metacarpophalangeal joints in mammals is the fetlock joint present in the manus of modern equids (horses and their kin) (N. A. T. Brown et al., 2003; Harrison, Whitton, Kawcak, Stover, & Pandy, 2010; MacFadden, 1992b; Sondaar, 1968). The bones and tendons comprising this joint have evolved to combine as an effective digit rotation and energy release mechanism for the foot during locomotion. The highly derived metacarpal head allows a large range of phalangeal rotation (MacFadden, 1992b; Sondaar, 1968), with an angular range of motion in trotting horses between 80°–103° (Cano, Vivo, Miró, Morales, & Galisteo, 2001; Galisteo et al., 1997). Allied to this large potential rotation for the proximal phalange, several antebrachial muscles developed short muscle fibres and long flexor and extensor tendons well suited for storing elastic strain energy during the stance phase of locomotion (N. A. T. Brown et al., 2003; Harrison et al., 2010). As energy is released during initiation of the swing phase, the phalanges rotate in flexion around the metacarpal joint facet, held in parasagittal alignment by the interaction of the prominent sagittal ridge of the metacarpal with the corresponding groove in the

proximal phalange (Liebich et al., 2007; MacFadden, 1992b). The musculoskeletal adaptation of this joint for efficient, mid-high speed running over long distances represents one of the key innovations in equid locomotor evolution.

The transition from diminutive tetradactyl (four-toed) equids in the early Eocene (c. 56 million years ago; Mya) to the large, extant, monodactyl horses (*Equus* spp.) is a well-known example of terrestrial macroevolution (Cantalapiedra, Prado, Hernández Fernández, & Alberdi, 2017; Janis, 2007; MacFadden, 2005; Maguire & Stigall, 2008; Mihlbachler et al., 2011). Through the Eocene, equids reduced their most lateral manus digit (metacarpal V and associated phalanges), with the remaining metacarpals and phalanges becoming more elongate through the late Eocene–Oligocene (O'Sullivan, 2008; Solounias et al., 2018; Sondaar, 1968). The central third digit became reinforced following the loss of the fifth digit, emphasising the importance of the fetlock joint on the third digit (between metacarpal III and proximal phalange III) for locomotion (MacFadden, 1992b). In later equids, the central third digit became the principal load-bearing digit, with reduction in the side toes in all lineages of late Neogene and Quaternary equids. Modern equids rely solely on their central digit. The sister family to Equidae within the Equoidea (the Palaeotheriidae) also exhibited digit reduction from tetradactyly to tridactyly during their diversification in the Eocene and earliest Oligocene (Bai, 2017; Bronnert et al., 2017; Danilo et al., 2013; Joomun et al., 2008; Sondaar, 1968). Palaeotheres exhibit multiple contemporaneous taxa with limb material demonstrating both tetradactyl (e.g. *Eurohippus*, *Propalaeotherium*) and tridactyl (*Plagiolophus*, *Palaeotherium*) species (Danilo et al., 2013; Franzen, 2010a; Rudwick, 2008); such evidence is not available for equids.

With the loss of the lateral digit and increased reliance on the central third digit for locomotion in both equids and palaeotheres, changes in the shape of the third digit fetlock joint may be expected. Some of these changes have previously been reported in equids, demonstrating the postural and morphological shifts that must have been necessary for modern equids to attain their current locomotor ecology (MacFadden, 1992b; Sondaar, 1968). Identifying the shape changes in the fetlock joint across the equoid phylogenetic tree can enable us to predict the timing of morphological shifts in the antebrachial muscle-tendon arrangements, and develop a greater understanding for why equoids underwent such morphological changes. Using modern tetradactyl perissodactyls (tapirs) as a reference for four-toed morphology and myology, we predict that tetradactyl equoids will exhibit less divergence from an ancestral fetlock shape than tridactyl species. Coupled to that, we anticipate that as the muscles of the antebrachium adjusted to the loss of the lateral digit (i.e. extinction of all tetradactyl equoids; end–

Bartonian 37.2 Mya), the shape of the fetlock will exhibit an increase in divergence away from an ancestral shape.

Traditionally, the evolutionary changes exhibited by equids were assumed to be associated with the exploitation of open grassland habitats, which became more prevalent in the late Oligocene and Miocene (Janis, Damuth, & Theodor, 2002; MacFadden, 1992b; Strömberg, 2006). However, the timing of digit reduction and the acquisition of high-crowned (hypsodont) dentition does not correlate with the spread of grasslands (Cantalapiedra et al., 2017; Damuth & Janis, 2011; Janis et al., 2002; Kaiser et al., 2013; Mihlbachler et al., 2011; Strömberg, 2006), leading researchers to investigate alternative causes of these macroevolutionary changes (Kaiser et al., 2013; McHorse et al., 2017; Nauwelaerts, MacLaren, Kaashoek, & Aerts, 2016). Changes in the morphology of the fetlock across multiple stages of habitat exploitation may offer insights into the shift in function of the joint, and by extension the manner in which the forelimb was being used. For example, the prominence of the sagittal ridge (locking the phalanges in the parasagittal plane) may indicate an increase in straight-line running behaviour (Sondaar, 1968), and the mediolateral expansion of the metacarpal head (increasing resistance to mediolateral bending) may represent exploitation of uneven substrates (e.g. steep mountains). Based on the current understanding that digit reduction in equoids predates the evolution of hypsodont dentition by approximately 23 Ma (MacFadden, 1986, 2005; Mihlbachler et al., 2011), we do not anticipate a strong covariance or temporal correlation between fetlock shape and tooth crown height. However, due to the intimate link between body size and limb bone dimensions (Prothero, 2005; K. M. Scott, 1990), we suggest that fetlock shape will covary with (and correlate with temporal fluctuations in) estimated body mass.

Despite little direct evidence supporting the link between the spread of grasslands and changes in the equoid locomotor anatomy, there is an undoubted effect of climate change and turnover events on equoid diversity and biogeography (Blondel, 2001; Cantalapiedra et al., 2017; Fraser, Gorelick, & Rybczynski, 2015; Hooker, Collinson, & Sille, 2004; Prado & Alberdi, 2014). At the Eocene-Oligocene boundary (33.9 Mya), equoid diversity was curtailed by the near-complete extinction of the Eurasian palaeotheres, termed the "Grand Coupure" (Hooker, 2010a; Hooker et al., 2004; Joomun et al., 2008). This mass turnover of European species is not observed to as great an extent in North American equoid taxa, where true equids continued to thrive (MacFadden, 2005). An explosive diversification of tridactyl equids occurred in North America at the onset of the Mid-Miocene Climatic Optimum (MMCO; Maguire and Stigall 2008; Fraser et al. 2015; Prado and Alberdi 2017), during which the first truly hypsodont equids evolved (e.g. *Protohippus*, *Pliohippus*; Mihlbachler et al. 2011). In

the cooler climate following the MMCO, equids in the Equini lineage began to exhibit increased reliance on their central digit, with some species exhibiting both monodactyl and tridactyl individuals (MacFadden, 1984; Voorhies, 1981). Species vicariance and climate-driven biogeographical shifts have also been shown to greatly affect equid community structure; examples include the Vallesian turnover (Agustí, Cabrera, & Garcés, 2013) and the Great American Biotic Interchange (Cione et al., 2015; Machado et al., 2018). Given the widespread impact of turnover events, biogeographic shifts and climatic optima, we predict that these significant extrinsic events known to affect prehistoric community composition will be reflected in shape variation and disparity of the fetlock in equoids through time.

In this study I use a three-dimensional (3D) based geometric morphometric approach, an increasingly popular method for assessing bone shape in perissodactyls (Bignon et al., 2005; Hanot, Guintard, et al., 2017; Hanot, Herrel, et al., 2017; MacLaren et al., 2018; MacLaren & Nauwelaerts, 2016, 2017; Nauwelaerts, Vangeel, et al., 2016; E. Scott, McHorse, Jass, & Zazula, 2014), based on surface scan data. I investigate the morphological evolution of the equoid fetlock across a broad phylogenetic scope, assessing variation and covariation between intrinsic biological and extrinsic ecological criteria through geological time.

Methodology

Specimens

A total of 268 third metacarpals (MCIIIs) from extant and extinct equoids and tapiroids across a wide geographic and temporal range were laser scanned to compile the three-dimensional shape dataset. MCIIIs were laser scanned with a FARO ScanArm Platinum V2 system combined with an integrated FARO Laser Line Probe (≥50 μm resolution), with additional MCIIIs micro-CT scanned using a Nikon Metrology (X-Tek) HMXST225 Micro-CT setup, processed using Bone Geometry function in BoneJ v.1.0.0 plugin for ImageJ v.1.48v (following methods of McHorse, Biewener and Pierce 2017).

Phylogeny

A composite phylogeny was compiled from a series of published maximum likelihood trees (M. W. Colbert, 2005; Danilo et al., 2013; Hulbert, 2005; Hulbert et al., 2009; Maguire & Stigall, 2008; Prado & Alberdi, 2017b; Remy, 1992, 2004; Ruiz-García et al., 2016; Steiner, Mitelberg, Tursi, & Ryder, 2012; Steiner & Ryder, 2011) to

incorporate all taxa in the current study (including equids, palaeotheres, and tapirs) (see Appendix V, Figure S5.1). The phylogenetic tree was constructed in Mesquite v.3.04, and exported to RStudio v.1.1.456 (RStudioTeam, 2016) for time-calibration using the 'paleotree' package (Bapst, 2012). Branch lengths for time-calibration were based on first-last occurrence dates from published literature and supplemented by records from the Palaeobiology Database (see Appendix V, Table S5.1).

Geometric Morphometrics

Distal metacarpal ('metacarpal head') shape was quantified using three-dimensional landmark-based geometric morphometrics (Rohlf & Slice, 1990; Zelditch et al., 2012). Landmarks representing homologous features of the third metacarpal head for both equoids and tapirids were applied to each surface scan using Landmark Editor v.3.0 software (Wiley et al., 2006); see Appendix V, Figure S5.2 for landmark placements. Landmark configurations for equoids and tapirids were superimposed using Generalised Procrustes Analysis (GPA), removing the effect of scale, location and orientation (Rohlf & Slice, 1990) and aligning configurations around a common centroid. GPA was performed in PAST v.3.19 (Hammer et al., 2001); generalised shape variance was visualised in a Principal Components Analysis (PCA) in RStudio (RStudio Team 2016). Configurations were also iteratively aligned against a hypothetical ancestral fetlock shape (see Appendix V, Section 9 for details) using Ordinary Procrustes Analysis (OPA) to test for divergence in shape from an ancestral condition. Species averaged ordinary sum of square distances (OSS) from OPA were used as a measure of shape divergence from the hypothetical ancestral shape. The OSS values were projected onto the informal time-calibrated phylogeny to examine shape deviation from the ancestral morphology through time using the R packages 'geiger' and 'phytools' (Garland et al., 1993; Revell, 2012, 2013).

The second method of examining shape through time focussed on morphospace occupation across ecological or climatic turnover events: the 'Grand Coupure' turnover event (33.9 Mya)(Hooker, 2010a), the Mid-Miocene Climatic Optimum (c.17–14 Mya) (DeMiguel, Azanza, & Morales, 2010; Holbourn, Kuhnt, Kochhann, Andersen, & Sebastian Meier, 2015; Kürschner, Kvaček, & Dilcher, 2008), the Vallesian Crisis turnover event (c.9.7 Mya) (Agustí et al., 2013; Casanovas-Vilar, Van Den Hoek Ostende, Furió, & Madern, 2014) and the formation of the Panamanian Isthmus (start of Quaternary Glaciation and Great American Biotic Interchange) (c.2.7 Mya) (Cione et al., 2015; O'Dea et al., 2016). Morphospace plots were constructed using PC1 and PC2 scores, including taxa present in the 1 Ma prior to and following the events. 1 Ma time bins on either side of the approximate date of the event was used to maximise the

chance of a morphological signal across the ecological event. The MMCO time bins chosen were at 17 Mya and 14.7 Mya; additional plots for the transition between 17 and 13 Mya during the MMCO are provided in Appendix V, Section 5.

Covariates

Several morphometric and climatic variables were collated from published literature for assessment of covariation with shape of the metacarpophalangeal facet. Here, we utilised estimated body mass and hypsodonty index as covariates, due to their utility as indicators of taxon diet, potential population density and range size (Cantalapiedra et al., 2017). We also calculated gracility index for the complete third metacarpal (proxy for limb gracility) (Guérin, 1980), and the angle of the sagittal ridge of the metacarpophalangeal joint as a proxy for range-of-motion (MacFadden, 1992b).

Hypsodonty indices (HI = third molar crown height ÷ second molar anterior width; Appendix V, Figure S5.3a) were gathered from literature sources (Cantalapiedra et al., 2017; Kaiser et al., 2013; Mihlbachler et al., 2011), and where necessary calculated from images in published articles and first hand photographs (Franzen, 2006; Hellmund, 2016; Hulbert, 2010; Hulbert et al., 2009; Remy, 1992, 2004; W. B. Scott, 1941).

Body mass estimates were taken from recent published literature (Cantalapiedra et al., 2017; MacLaren et al., 2018; MacLaren & Nauwelaerts, 2019; Remy, 2015) or estimated using linear measurements and ungulate regression equations (squared correlation coefficients > 0.90) from Scott (1990) for postcranial elements (humeral or metapodial width measurements) (Appendix V, Figure S5.3b). Postcrania (rather than dental estimates) were favoured for body mass estimates where possible, as they are less influenced by feeding variation than dental measurements (Dagosto & Terranova, 1992; Fortelius, 1990). Resultant estimated body masses (BM) were log-transformed for statistical analyses.

Gracility indices (Gr-I) were calculated by taking the maximum mediolateral width of the proximal metacarpal (mm) x 100 ÷ maximum proximodistal length of the metacarpal (mm) (after Guérin 1980) (Appendix V, Figure S5.3c). This method is the standard procedure for the quantification of metapodial gracility in rhinoceroses (Guérin, 1980) and palaeotheres (Métais & Sen, 2017; Remy, 2004). Here we expand it to include equids and tapirs; equids are included to maintain methodological continuity, with the understanding that equid metapodials also increase in relative dorsopalmar depth through time.

The keeled sagittal ridge of modern equids slides within a corresponding groove in the first phalange, preventing adduction and abduction of the digit, and may be considered a proxy for digit mediolateral movement and indicator of fetlock range of motion (MacFadden, 1992b). Here, we quantify the angle circumscribed by the sagittal ridge of the distal metacarpal across a large sample of equoid species for the first time to explore potential range-of-motion at the fetlock in comparison with fetlock shape. Ridge angles (RA) were measured from two-dimensional images of metacarpals in lateral view, taking the maximum angle the ridge attains with the centre of the metacarpal head acting as the centre of rotation (Appendix V, Figure S5.3d).

Hypsodonty and ridge angle measurements were performed in ImageJ v.1.48 (Schneider, Rasband, & Eliceiri, 2012), and measurements for regression equations and gracility indices were taken using the measurement tool in GeoMagic Studio 10 (Morrisville, NY, USA). Trait values for all covariates were plotted onto the composite phylogenetic tree to inspect maximum likelihood ancestral trait expression across the phylogeny. No quantitative conclusions were drawn from node estimates; only measured trait values were used in statistical analyses. Ancestral states were calculated in RStudio using the 'phytools' library (Revell, 2012) for all nodes and braches, visually illustrating variation in OSS, HI, BM, Gr-I and RA traits across the tree.

Climatic variables through the Cenozoic were taken from Zachos et al. (2008); principally, these included stable oxygen isotope values from benthic foraminifera, used as a proxy for global temperature, and have been used in previous studies to demonstrate correlations and temporal alignments of temperature fluctuations and trait acquisitions (e.g. Mihlbachler et al. 2012).

Statistical Analyses

Variation in distal metacarpal shape was assessed using a principal componenets analysis to extract the major axes of variation. Taxa were pooled into appropriate phylogenetic groups, and Procrustes coordinates were tested for significant differences using a non-parametric multivariate analysis of variance (perMANOVA) in RStudio libraries 'vegan' and 'RVAideMemoire' with 10000 permutations using the FDR (false discovery rate) post-hoc protocol (Hervé, 2014; Oksanen et al., 2018). PerMANOVA was selected due to inequality of sample sizes (M. J. Anderson, 2001). Principal component scores for the first two PCs were also tested to detect significant differences in morphospace overlap along each axis using an ANOVA and Tukey-B Wholly Significant Difference (WSD) post-hoc test, implemented in IBM SPSS Statistics v.25 (IBM, 2013). Covariation between distal metacarpal shape (landmark coordinates) and

ecomorphological variables (HI, BM, Gr-I, RA) was tested for using a two-block phylogenetic partial least squares regression (phyPLS). Aligned Procrustes coordinates (from GPA) were mapped onto the informal phylogeny in MorphoJ, yielding independent contrasts for each node. Two-block PLS was performed on the phylogenetic independent contrasts from landmark coordinate data, testing for covariance with each ecomorphological variable and assessing the significance of any correlation with a permutation test (10000 repetitions) (Rohlf & Corti, 2000). Covariation between shape and ecomorphological variables was assessed using Escoffier coefficients (RV), a multivariate extension of a univariate correlation coefficient (R^2) used for Ordinary Least Squares regression (OLS). Univariate covariate trait values were correlated against one another in a pairwise manner using OLS regression. Covariates which did not exhibit significant covariation with shape were further investigated with a cross-correlation test to investigate whether there was temporal correlation between changes in traits. Average covariate values were calculated for 1 Ma time-bins, and tested for correlations in trait changes from one time-bin to another (the first derivatives for each trait) through 56 Ma using the 'ccf' function in RStudio (Venables & Ripley, 2002).

Results

Shape Variation (PCA)

Principal components analysis (PCA) of GPA aligned coordinates demonstrates clear morphological separations between clades. The first two principal axes account for over 50% of shape variation (Figure 6.1), with a large drop-off to PC3 (7.9%); therefore, PC1 and PC2 will be the focus of the morphological variation comparison. The spread of points along the first and second principal components (PC1 and PC2 respectively) suggest three phylogenetic clusters within distal metacarpal morphospace: basal and browsing taxa (palaeotheres, tapirs and 'hyracotheres'); tridactyl equids; and Equini. Positive PC1 is dominated by taxa which exhibit low sagittal ridges, limited palmar extension of the metacarpophalangeal facet, and little or no flaring of the medial and lateral joint facet (Figure 6.1; wireframe diagrams). Tapirs, palaeotheres, 'hyracotheres' and both New World and European 'anchitheres' are found in this region of morphospace, with the 'hyracothere' (basal equid) taxa *Eohippus* (*Hyracotherium*) and *Sifrhippus* nestled deep within palaeothere morphospace. The 'hyracotheres' exhibit no significant distinction from palaeotheres in their distal metacarpal morphology ($p = 0.110$; Table 6.1). The 'hyracotheres' also exhibit no significant differences to either palaeotheres or tapirs in their occupation of PC1 vs PC2 morphospace (Appendix V, Table S5.3). Within tapirs, the extinct *Tapirus webbi* and the modern *T. indicus* and *T.*

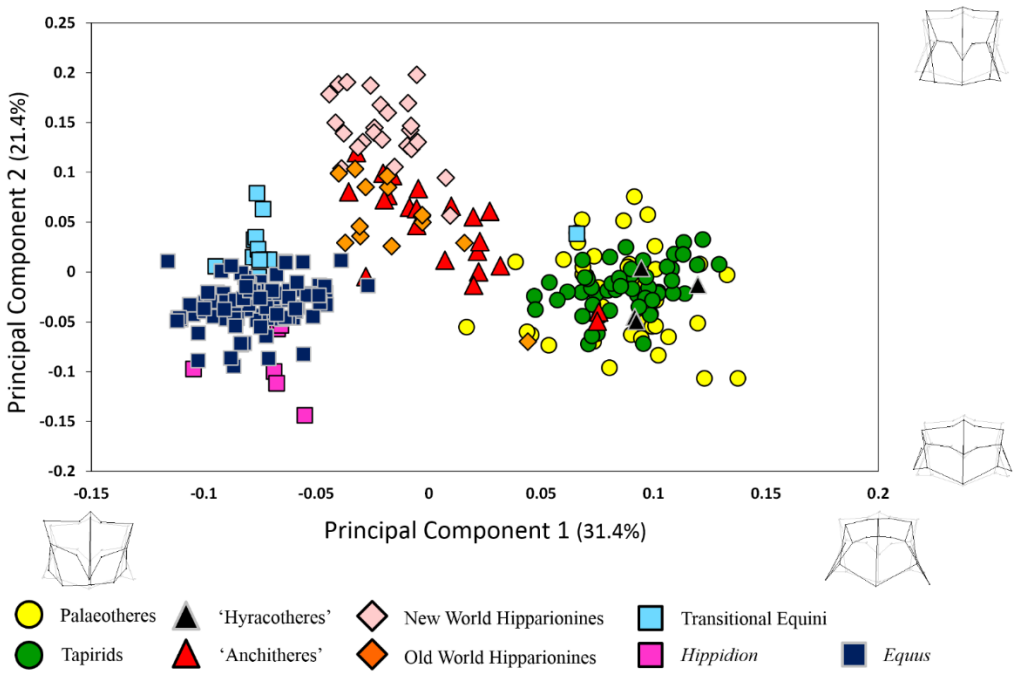

Figure 6.1. Morphospace occupation for distal metacarpal shape in equoids and tapirids based on principal component analysis (PCA). Principal components 1 and 2 account for 52.8% of shape variation. Wireframe diagrams demonstrate representative distal metacarpal shapes along the two PC axes (palmar view). Significant differences between clades listed in Table 6.1; species breakdown in Appendix V (Supplementary Figures S5.6a-h).

pinchaque are found at lower PC1 values (0.047–0.087), whereas the modern *T. bairdii* and European *T. arvernensis* exhibit the highest PC1 values for tapirs (0.098–0.122). Palaeotheres exhibit a large range of PC1 values (0.017–1.317), indicative of the diverse morphologies in this clade. Tapirs and palaeotheres exhibit no significant differences in PC1 vs PC2 morphospace occupation, but Procrustes coordinates do exhibit significant differences between these two browsing clades. Positive PC2 is predominantly occupied by New World 'anchitheres', hipparionines and transitional Equini (e.g. *Astrohippus*, *Pliohippus* etc.). High PC2 values in this region of morphospace are associated with mediolateral constriction of the metacarpophalangeal facet (narrowing of the metacarpal). New World hipparionines exhibit the greatest narrowing of the metacarpophalangeal facet, with specimens of *Nannippus peninsulatus* and *N. westoni*

displaying the highest PC2 values (>0.19). Negative PC1 and PC2 morphospace is dominated by transitional Equini and *Equus* species; metacarpals in this region are characterised by strongly flared joint facets, a prominent sagittal ridge, mediolateral broadening of the metacarpal head, and (in the extreme case of *Hippidion*, *Equus andium* and *E. neogeum*) a reduction in the dorsal and palmar extent of the metacarpophalangeal facet. 'Anchitheres' exhibit a broad spread of morphologies, including taxa within tapir-palaeothere morphospace (e.g. *Mesohippus*) and New World hipparionine morphospace (e.g. *Archaeohippus* spp.). Equid outliers within the tapir-palaeothere cluster include *Eurygnathohippus* ('*Hypsohipparion'*) (derived Old World hipparionine) and *Acritohippus* (basal Equini), both of which exhibit broad distal metacarpals with reduced flaring of the joint facet. Figure 6.1 species breakdown can be found in Appendix V (Supplementary Figures S5.6a-h).

Permutational MANOVA testing suggested an overall significant difference within the data; pairwise comparisons revealed significant differences in distal metacarpal shape between all clades, with the exception of palaeotheres and 'hyracotheres' ($p = 0.110$) (Table 6.1). Tukey-B WSD testing based on morphospace occupation (PC1 v PC2) between clades suggests that for PC1 there are four well separated groupings: 1) tapirs, 'hyracotheres' and palaeotheres; 2) 'anchitheres'; 3) Old and New World hipparionines; and 4) Equini (including *Equus* spp.) (Appendix V, Table S5.3a). For PC2 scores, Tukey-B testing suggests three groupings: 1) New World hipparionines; 2) Old World hipparionine and 'anchitheres'; and 3) tapirs, palaeotheres, 'hyracotheres', and equinines. (Appendix V, Table S5.3b).

Principal component analyses are also plotted for overall equoid morphospace occupation immediately before and after four significant ecological events known to affect perissodactyl communities. Morphospace occupation either side of the "Grand Coupure" extinction event (Figure 6.2a) suggests a marked reduction in palaeothere sample diversity, with only a single species remaining (*Plagiolophus minor*). Equid variation, represented by *Mesohippus* and *Miohippus*, does not decrease across the Eocene–Oligocene boundary. Prior to the Mid-Miocene Climatic Optimum (Figure 6.2b), equid metacarpal head shape is conserved in the negative region of PC1 represented by the derived New World 'anchitheres' *Archaeohippus* and *Parahippus*; following the MMCO, equid morphospace occupation expand with Old World 'anchitheres' and both New World and Old World hipparionines occupy new regions of morphospace compared to the pre-MMCO 'anchitheres'. Following the MMCO, equini metacarpal shape (represented by the single genus *Pliohippus*) is already separate from both New World and Eurasian hipparionines. Additional plots through the MMCO are provided in the Appendix V, Figure S5.4. Equid shape variation does not greatly vary

Table 6.1. Pairwise permutational multivariate analysis of variance (perMANOVA) results between perissodactyl clades based on Procrustes coordinates of distal third metacarpal, based on false discovery rate post-hoc testing. P-values significant ≤ 0.05.

Clade	'Anchi'	n*E* Equini	*Equus*	'Hyrac'	NW Hip	OW Hip	Palaeo
non-*Equus* Equini	<0.01		-	-	-	-	-
Equus species	<0.01	<0.01		-	-	-	-
'Hyracotheres'	<0.01	<0.01	<0.01		-	-	-
NW Hipparionines	<0.01	<0.01	<0.01	<0.01		-	-
OW Hipparionines	0.003	<0.01	<0.01	<0.01	<0.01		-
Palaeotheres	<0.01	<0.01	<0.01	0.110	<0.01	<0.01	
Tapirids	<0.01	<0.01	<0.01	<0.01	<0.01	<0.01	<0.01

Key of terms: 'Anchi.' = 'Anchitheres'; n*E* = non-*Equus*; 'Hyrac.' = 'Hyracotheres'; NW = New World (North + South America); OW = Old World (Eurasia + Africa); Palaeo. = Palaeotheres.

across the Vallesian Crisis (Figure 6.2c), with the exception of a slight decrease in New World hipparionine variation and corresponding increase in Old World hipparionine disparity following the event. Equid shape variation (for the sample in this study) preceding the formation of the Panamanian Isthmus approximates that following the Vallesian crisis, though with notably fewer specimens and lower taxonomic spread (Figure 6.2d). Following the formation of the land-bridge and start of the Quaternary Glaciation, there is a clear diversification of *Equus* and *Hippidion* species with a comprehensive reduction of tridactyl taxa. Morphospace occupation for equids is almost exclusively in negative PC2, with the most extreme examples being the fetlock morphologies of the highly derived and robust equinine *Hippidion* and Old World hipparionine *Eurygnathohippus* ('*Hypsohipparion*') *albertense*.

Shape-Trait Covariation (PLS)

Phylogenetic signal was statistically significant in all covariates, necessitating the use of independent contrasts for PLS analyses. Two-block partial least square regression (PLS) analyses of independent contrasts (of shape variables) and ecomorphological covariates (body mass, hypsodonty index, gracility index and sagittal ridge angle) yielded mixed results (Figure 6.3). Body mass (BM) and hypsodonty index (HI) were poorly correlated with shape (Figure 6.3a and 6.3b). RV coefficients (0 = no covariance; 1 = complete covariance) and permutational p-values indicate limited, non-significant

covariation between both BM (RV = 0.067; p = 0.108) and HI (RV = 0.055; p = 0.202) and distal metacarpal shape; similar results were found for an equoid-only dataset (Appendix V, Table S5.4). Gracility index (Gr-I) covaried most strongly with shape (RV = 0.298; p < 0.01); metacarpal head shapes with negative PLS scores exhibited narrow metacarpophalangeal joint facets and relatively more prominent collateral ligament origination sites, whereas shapes with high scores demonstrated mediolaterally broader joint facets and a generally more proximodistally flattened metacarpal head (Figure 3c; wireframe diagrams). Sagittal ridge angle (RA) also covaried significantly with metacarpal head shape (RV = 0.154; p < 0.01). Nodes with high PLS scores for both shape and RA exhibited more elongate facets for articulation with the proximal sesamoids (Figure 6.3d; wireframe diagrams), whereas the same feature is truncated in shapes with low PLS values. Gracility index and ridge angle were not significantly correlated with one another (all taxa $R^2 = 0.014$; equoid only dataset $R^2 = 0.012$, p-value for both >0.05). Figures 6.4–6.7 demonstrate trait value variation mapped onto the phylogenetic tree, and Appendix V, Table S5.5 offers pairwise regression coefficients between ecomorphological traits.

Trait Covariation through Time

The ordinary sum of square distances (OSS) from ancestral morphology to each individual in the analysis were plotted alongside intrinsic traits which demonstrated no significant covariation with shape in PLS analyses (body mass and hypsodonty) and compared through geological time (Figure 6.8). Average hypsodonty indices for equoid taxa in this study show one very dramatic increase at the start of the Mid-Miocene Climatic Optimum (MMCO; c.18 Mya) (Figure 6.8a). Less dramatic increases are observed in a stepwise fashion through the late Miocene to the Pleistocene, with a generally increasing trend. A similarly sharp increase is observed in average equoid body mass, with an additional early peak in the late Eocene (Bartonian) prior to the "Grande Coupure" (Figure 6.8b). Cross-correlation analyses comparing BM and HI across all equoids in this study suggest a strong positive relationship between these traits at a lag-time of less than 1 Ma (R = 0.459), indicating increases in the value of these two traits are temporally correlated (Supplementary Figure S5.5).

Shape Change through Time

Shape divergence from the hypothesised ancestral morphology for both equoids and tapirs was plotted through time, with standard deviations around the mean values for each 1 Ma time-bin (Figure 6.8c). Average equoid OSS through time suggests a Lutetian-Bartonian increase in shape divergence from the ancestral metacarpal head

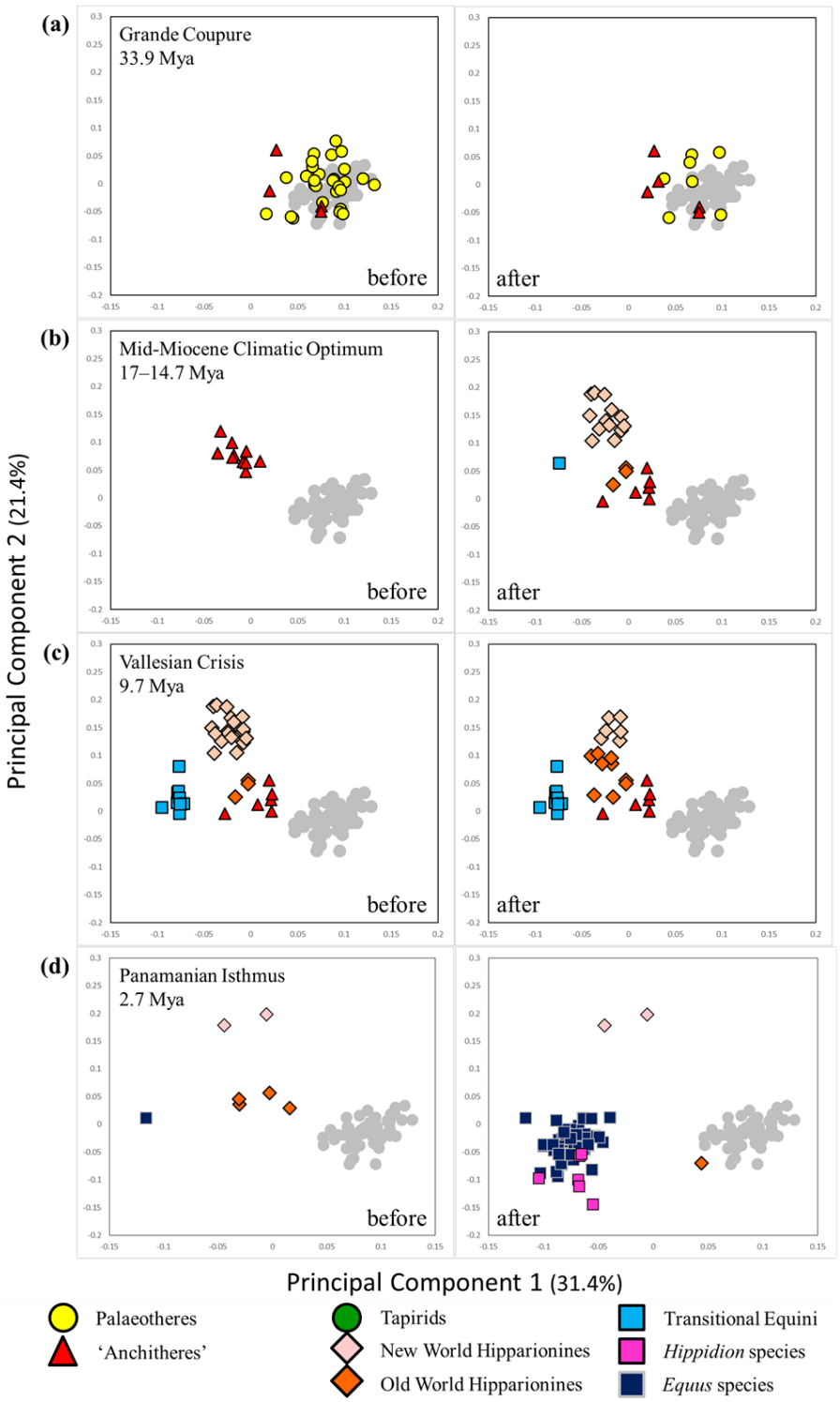
(a)
Grande Coupure
33.9 Mya
before
after
(b)
Mid-Miocene Climatic Optimum
17–14.7 Mya
before
after
(c)
Vallesian Crisis
9.7 Mya
before
after
(d)
Panamanian Isthmus
2.7 Mya
before
after
Principal Component 2 (21.4%)
Principal Component 1 (31.4%)
Palaeotheres
'Anchitheres'
Tapirids
New World Hipparionines
Old World Hipparionines
Transitional Equini
Hippidion species
Equus species

Figure 6.2. Morphospace occupation for distal metacarpal shape in equoids and tapirids across significant ecological events, based on principal component analysis (PCA). Principal components 1 and 2 account for 52.8% of shape variation. Morphospace plots chart changes from before (left) and after (right) each ecological event: **(a)** the "Grande Coupure" extinction event; **(b)** the Mid-Miocene Climatic Optimum; **(c)** the Vallesian Crisis turnover event; and **(d)** the formation of the Isthmus of Panama and initiation of the Quaternary Glaciation.

morphology, with a smaller increase at the "Grande Coupure" (GC) extinction event (33.9 Mya; Figure 6.8c–d). The initial peak in OSS predates the equoid body mass increase at the Bartonian–Priabonian boundary, but does correspond to the first occurrence of tridactyly in this sample (*Plagiolophus annectens*). From the late Eocene to the Mid-Miocene Climatic Optimum, OSS values for equoids fluctuate with a general upwards trend. There is a sharp decrease followed by an immediate increase in OSS at the Rupelian–Chattian boundary (28.4 Mya), repeated through the Langhian–Seravallian transition (c.16–13 Mya) prior to an initial peak in the early Tortonian (c. 11 Mya). This early peak is followed by a series of fluctuations through the late Miocene to the Pleistocene. Equoid OSS maximally peaks in the Quaternary Glaciation (QG), before a decline in the latest Pleistocene. Cross-correlation between OSS and both HI and BM patterns through time suggest strong temporal correlations. Two correlations are present in both HI and BM cross-correlations: a positive correlation with a parallel shift 1 Ma following OSS shift in HI (R = 0.296) and BM (R = 0.364), and a negative correlation at -5 Ma, suggesting OSS shifts correlated with opposite shifts in HI (R = -0.446) and BM (R = -0.419) offset by 5 Ma (see Appendix V, Figure S5.5). A positive correlation is also observed at 0 Ma lag time between OSS and HI (R = 0.367). At no point do HI or BM peaks strongly correlate when prior to a peak in OSS.

The tapir specimen count in this study prior to the MMCO is restricted; however, an overall pattern of divergence from ancestral morphology is evident (Figure 6.8c). In the Eocene, tapiroid OSS is represented by *Chasmotherium* (= *Hyrachyus minimus*), and by *Protapirus obliquidens* in the Oligocene (Figure 6.8c); both *Chasmotherium* and *Protapirus* metacarpal head OSS values fall within the range of *Tapirus* spp. (late Miocene–Holocene). Moreover, *Chasmotherium* and average equoid OSS in the early-middle Eocene are very similar (*Chasmotherium* = 2.396; Equoidea = 2.447); see Appendix V, Section 9 for discussion on methodology. The average OSS for tapirids does not exceed 4.5 (*Tapirus webbi*); by comparison, average equoid OSS exceeds 4.5 prior to the end of the Bartonian (Late Eocene) (Figure 6.8c). From the early Tortonian (11.6 Mya) tapirid OSS is represented exclusively by members of the genus *Tapirus*.

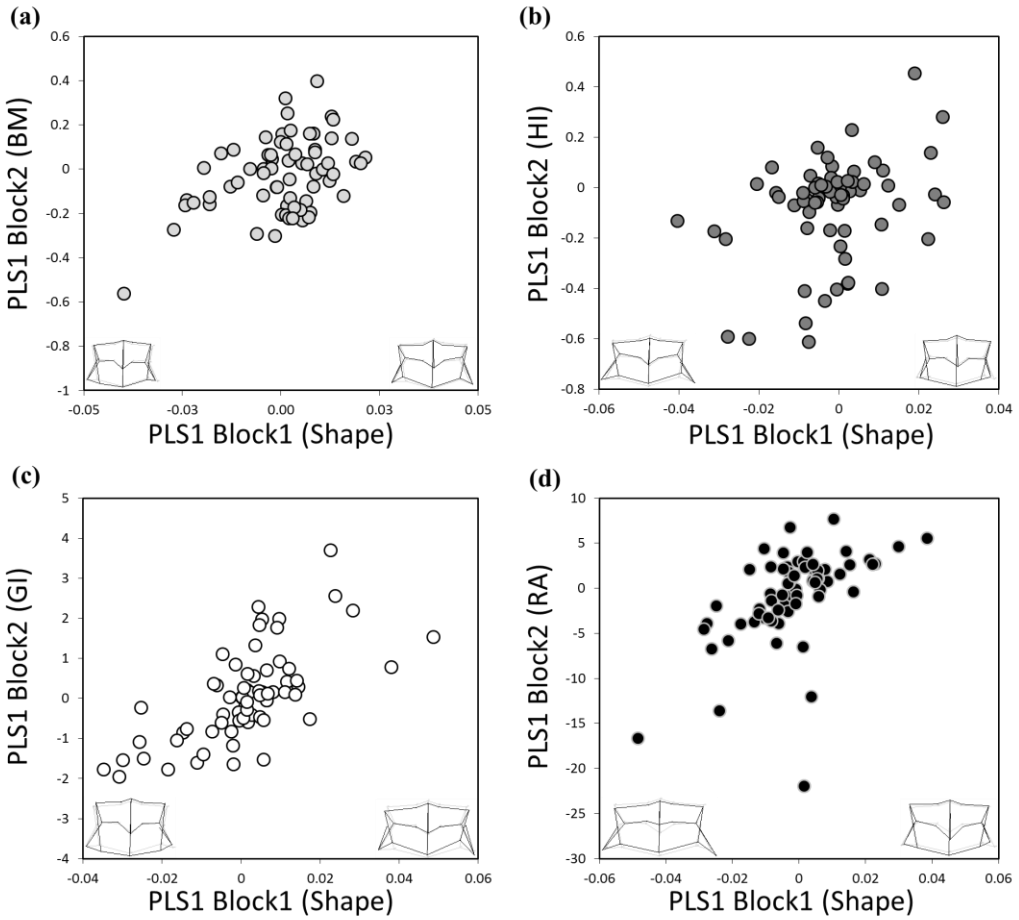

Figure 6.3. Phylogenetic two-block partial least squares analysis of independent contrasts for equoids and tapirid distal metacarpal shape against intrinsic biological covariates. PLS comparisons with Procrustes shape coordinates against **(a)** log-transformed body mass, **(b)** hypsodonty index, **(c)** metacarpal gracility index, and **(d)** sagittal ridge angle. Wireframe diagrams demonstrate representative distal metacarpal shape changes along Block 1 (shape coordinates) of PLS analysis.

Peak average tapir shape divergence occurs in the mid-Pliocene, corresponding with peak absolute OSS values for equoids (3–4 Mya), and preceding peak average equoid values (1–2 Mya). The average negative peak for tapir OSS in this study is observed around the Miocene–Pliocene boundary (5.3 Mya), with tapir metacarpal head

morphologies more similar to the hypothesised ancestral shape at this time slice than are previously observed in Eocene or Oligocene members of the group.

Discussion

Throughout this study, the morphology of the fetlock (distal metacarpal) has been investigated in equoids and tapirids across a broad geographical and temporal scope. As expected from numerous qualitative investigations, shape differences were observed using a quantitative framework based on landmark-based geometric morphometrics and potential covariate morphometric measurements, including tooth crown height (hypsodonty index; HI), overall body size (log body mass; BM), metapodial narrowing (gracility index; Gr-I) and maximum angle circumscribed by the sagittal ridge (ridge angle; RA). We demonstrate that shape and both hypsodonty index and body mass do not covary across the entire sample of species investigated here; however, both these traits do show strong temporal correlations when investigated against divergence in shape from an ancestral condition through deep time.

There are several key components of the fetlock in equoids and tapirs to be discussed here, including comparisons with previous work on the perissodactyl fetlock joint and changes in functionality with different morphologies (MacFadden, 1992b; Sondaar, 1968, 1969); the influence of endemic taxa and importance of provincialism in assessing morphological shifts; and finally, the observed effect of local and global turnover events on fetlock shape change.

Fetlock functional morphology – comparisons to Sondaar (1968)

The changes in the equoid fetlock between species of different ages has been described in previous literature (MacFadden, 1992b; Sondaar, 1968, 1969), with several key innovations highlighted which were interpreted as essential for the development of the elastic recoil mechanism observed in modern equid fetlock joints. Sondaar (1968, 1969) observed several aspects of the fetlock joint which lead him to differentiate equids into four categories of locomotor potential. The first two categories were characterised by four or three digits with short proximal phalanges (‘hyracotheres’, *Mesohippus* and *Plagiolophus*) and some independent adduction or abduction of the digit on the metacarpal head; Sondaar (1968) concluded that all three of these taxonomic groups would have possessed a strongly angular forelimb posture to enable all digits to be in contact with the ground, and that adaptations in the fetlock toward a more specialised, open-habitat running style in equids came into being with the evolution of *Archaeohippus* (category III; Sondaar 1968). For reference, category IV is anatomical

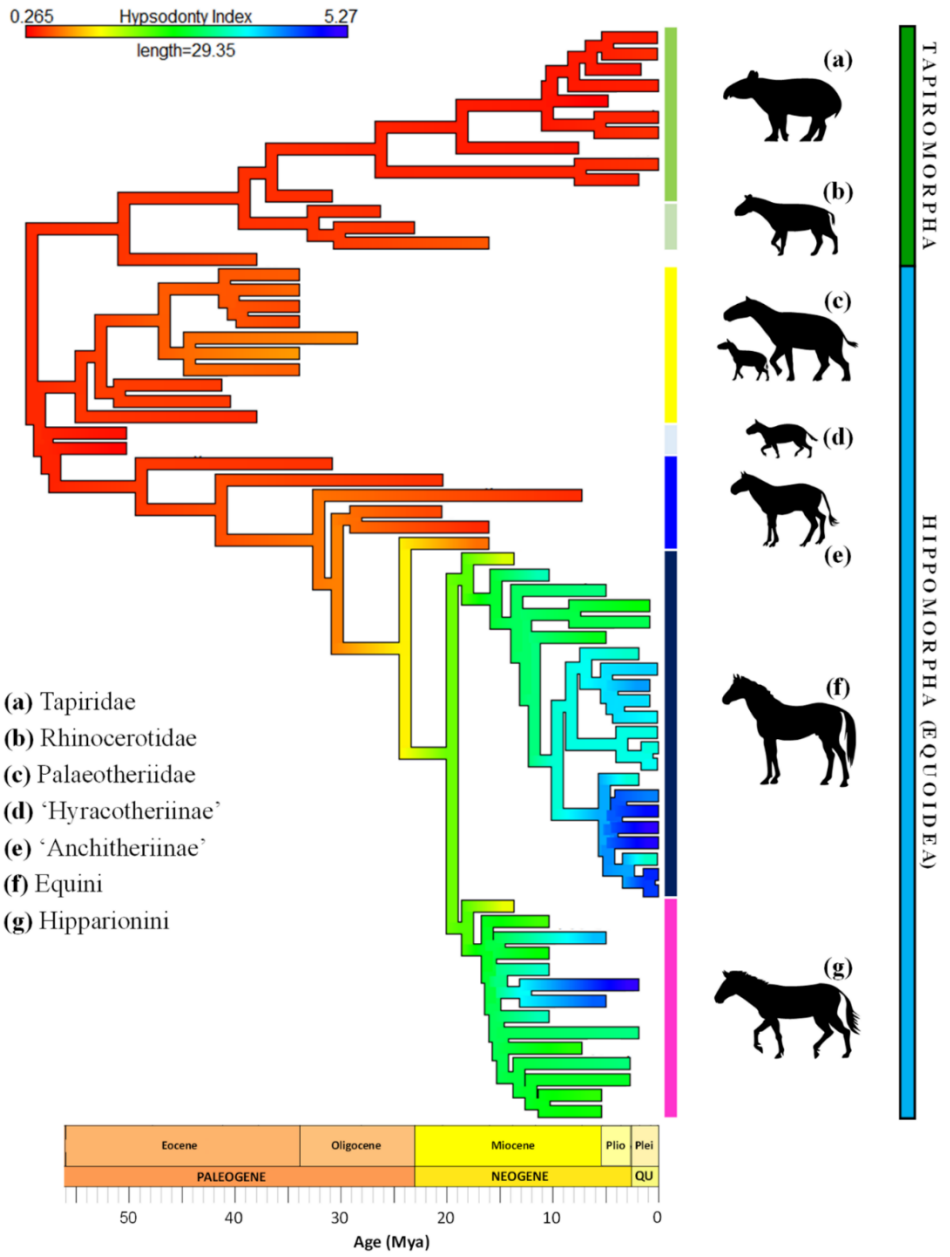

Figure 6.4. Hypsodonty index (HI) plotted onto the composite phylogenetic tree of tapiromorphs and equoids. Warm colours signify low tooth crowns (brachydont); cooler colours signify high tooth crown (hypsodont). Species names provided in Appendix V; Figure S5.1.

and functional monodactyly, with no side toes striking the ground (e.g. side digit condition observed in cervids and some bovids; Marsh 1874); this category includes derived equinines, culminating in the extant *Equus*. While the results of our study do on-the-whole support the morphological divisions in the equoids described by Sondaar (1968, 1969), the morphological evidence across the wide taxonomic scope of this study (especially with the inclusion of tapirs and multiple palaeothere taxa) call into question some of the interpretations and conclusions.

Our morphospace results demonstrate that 'hyracotheres', tetradactyl (and most tridactyl) palaeotheres, and *Mesohippus* fall within the shape-space occupied by tapir distal metacarpals (Figure 6.1). Overall, the manus of tapirs more closely resembles that of palaeotheres than other equoids, with some larger palaeothere taxa showing very close morphological affinity to modern tapir species in their manual elements (MacLaren & Nauwelaerts, 2019). A key difference between the manus of tapirs + palaeotheres and those of equids is the proximal contact between metapodial and carpal complex (Yalden, 1971). In equids as early as *Mesohippus*, the proximal metacarpal is flattened at the joint articulation with the magnum, similar in some respects to modern equids (Wood et al., 2011); tapirs and palaeotheres retain a more basal, saddle-shaped joint facet with the magnum (MacLaren & Nauwelaerts, 2019; Rudwick, 2008; Yalden, 1971). The saddle-shaped articulation with the magnum enables a large surface for bone-bone contact (in this case binding the distal carpal row and the metacarpals together); however, the flatter contact surface between the metacarpal and magnum of *Mesohippus*, and all other subsequent lineages of horses, is well adapted to dissipate compressive forces during locomotion (MacLaren & Nauwelaerts, 2017; Prothero, 2005). This flattened proximal metacarpal morphology is also observed in other clades within the Perissodactyla, associated with large masses over the manus (e.g. *Teleoceras*, Prothero 2005) or the with metapodials incurring increased impact forces during locomotion (e.g. "running rhinoceros" *Hyracodon*, Scott 1941). We interpret the acquisition of this morphology at this early stage in equid evolution as an indicator of increased compressive forces on the central digit; this would warrant a more upright metacarpal (and thus limb) posture for Eocene–Oligocene equids than suggested by Sondaar (1968).

With regards to the locomotion of palaeotheres, Sondaar (1968) argues that the carpal joint of *Plagiolophus* enabled greater flexibility of this joint compared to that of equids, and that this made up for the limited anteroposterior mobility of the fetlock joint in *Plagiolophus* (and by extension other palaeotheres with gracile metapodials, e.g. *Palaeotherium medium*; MacLaren and Nauwelaerts 2019). Our results do not disprove this conclusion; however, we do find that the distal metacarpal shape in both

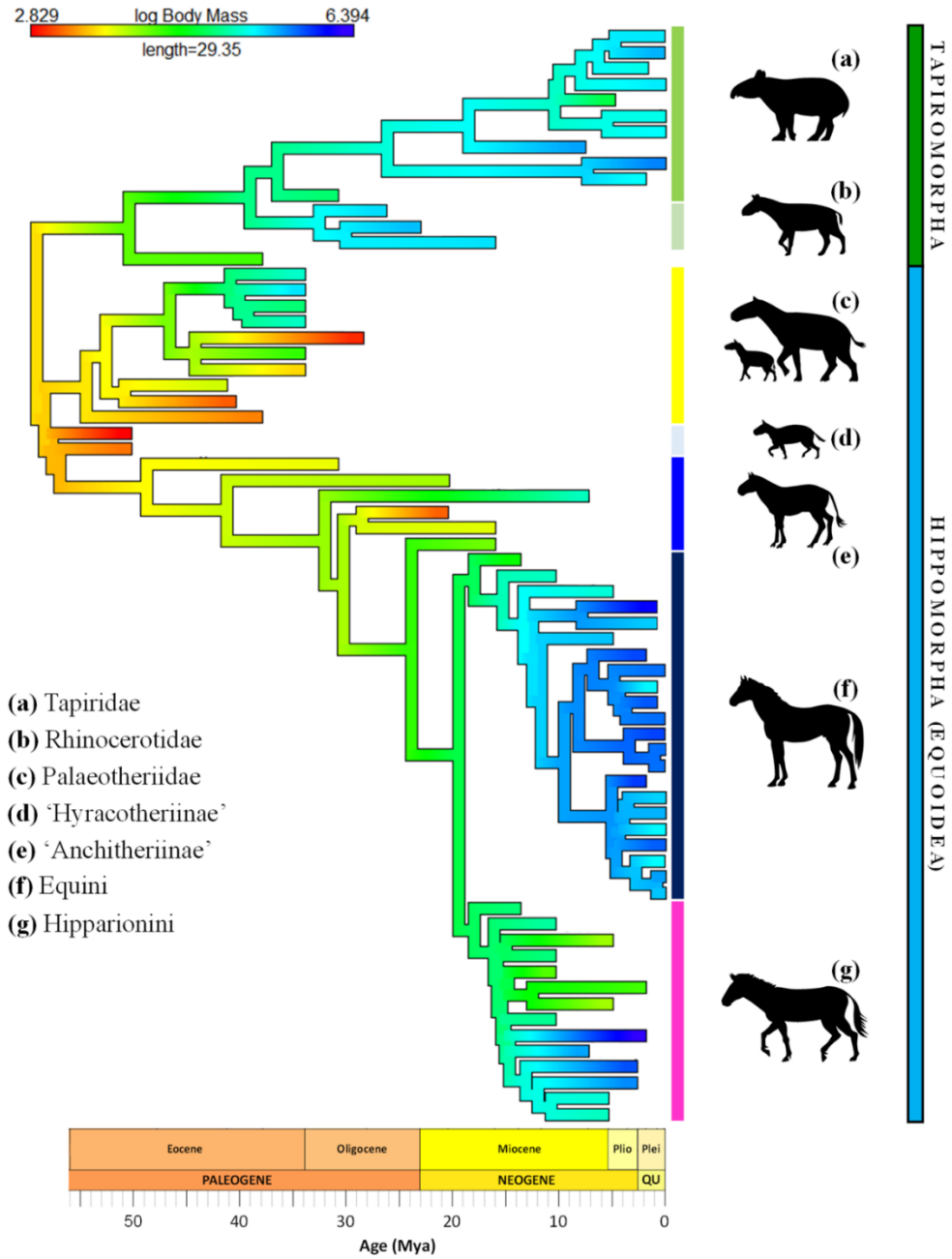

Figure 6.5. Body mass (BM) plotted onto the composite phylogenetic tree of tapiromorphs and equoids. Warm colours signify low estimated body mass; cooler colours signify high body masses. Species names provided in Appendix V; Figure S5.1.

Plagiolophus minor and *Pl. annectens* exhibit sufficient similarities in morphospace occupation and sagittal ridge angle to *Mesohippus* and *Miohippus* to indicate that the fetlock was no less mobile in *Plagiolophus* than in early equids. The additional conclusion of Sondaar (1968) that the carpus joint is more flexible in extension in palaeotheres may indeed be true; however, the range of extension for the similarly mobile carpus of *Tapirus* (Yalden, 1971) does not exceed the range observed in *Equus* species (Kaashoek, pers. comm. February 2019, unpublished data), and as such I believe this remains a contentious comparison between *Plagiolophus* and *Mesohippus* without further study. The presence of stabilizing ligaments attached to the prominent volar processes ('flexor hooks') on the palmar surface of the magnum of *Plagiolophus* and *Palaeotherium* (also in tapirs and rhinoceroses; Osborn 1929; Yalden 1971) has been hypothesised to prevent hyperextension at the carpus. From recent comprehensive investigation, the volar processes of *Tapirus* are shown to be the origination sites for the deep and superficial interosseous muscles, controlling adduction and abduction and preventing hyperextension of the digits (Barone 2000; MacLaren and McHorse, *In review*). Prominent volar processes of the magnum and unciform are known from the palaeotheres *Propalaeotherium* (Hellmund, 2005; MacLaren & Nauwelaerts, 2019), *Plagiolophus* and *Palaeotherium* (MacLaren & Nauwelaerts, 2019), the 'hyracothere' *Sifrhippus* (Wood et al., 2011), and the Eocene tapiroids *Heptodon* (Radinsky 1967a) and *Hyrachyus* (Bai et al. 2017). Large volar processes are not found in *Mesohippus* or any other tridactyl equid; this indicates that, despite the lack of notable differences within the fetlock morphology of tridactyl Eocene equoids, functional aspects of the carpometacarpal joint in the manus appear to have shifted radically in true equids by the early Oligocene.

Our results do not all contrast with those of Sondaar (1968, 1969). Our shape analysis strongly supports previous assertions that the fetlock joint of 'anchitheres' from *Mesohippus* to *Anchtherium* allowed phalangeal adduction and abduction (Sondaar, 1968, 1969) (see Appendix V, Figure S5.1 for species), with these taxa exhibiting sagittal ridge angles within the range observed in tapirs (102°–130°), and overall morphological similarities in the distal joint facet (Figure 6.1). These equids, like their morphological counterparts the palaeotheres, are interpreted as browsing species (Cantalapiedra et al., 2017; Mihlbachler et al., 2011) owing to the presence of brachydont dentition (Figure 6.4a; HI between 0.3 and 0.7, Mihlbachler et al. 2011); the closer affinity with tapir fetlock morphology than is present in other equids also supports this ecological assignment (Figures 6.1 and 6.2a–b). However, supporting the conclusions of Sondaar (1968) with regards to the posture of the browsing equids is more problematic. The presence of flattened carpometacarpal joint facets, elongate medial and lateral phalanges relative to the central third digit (low TRI; see McHorse et

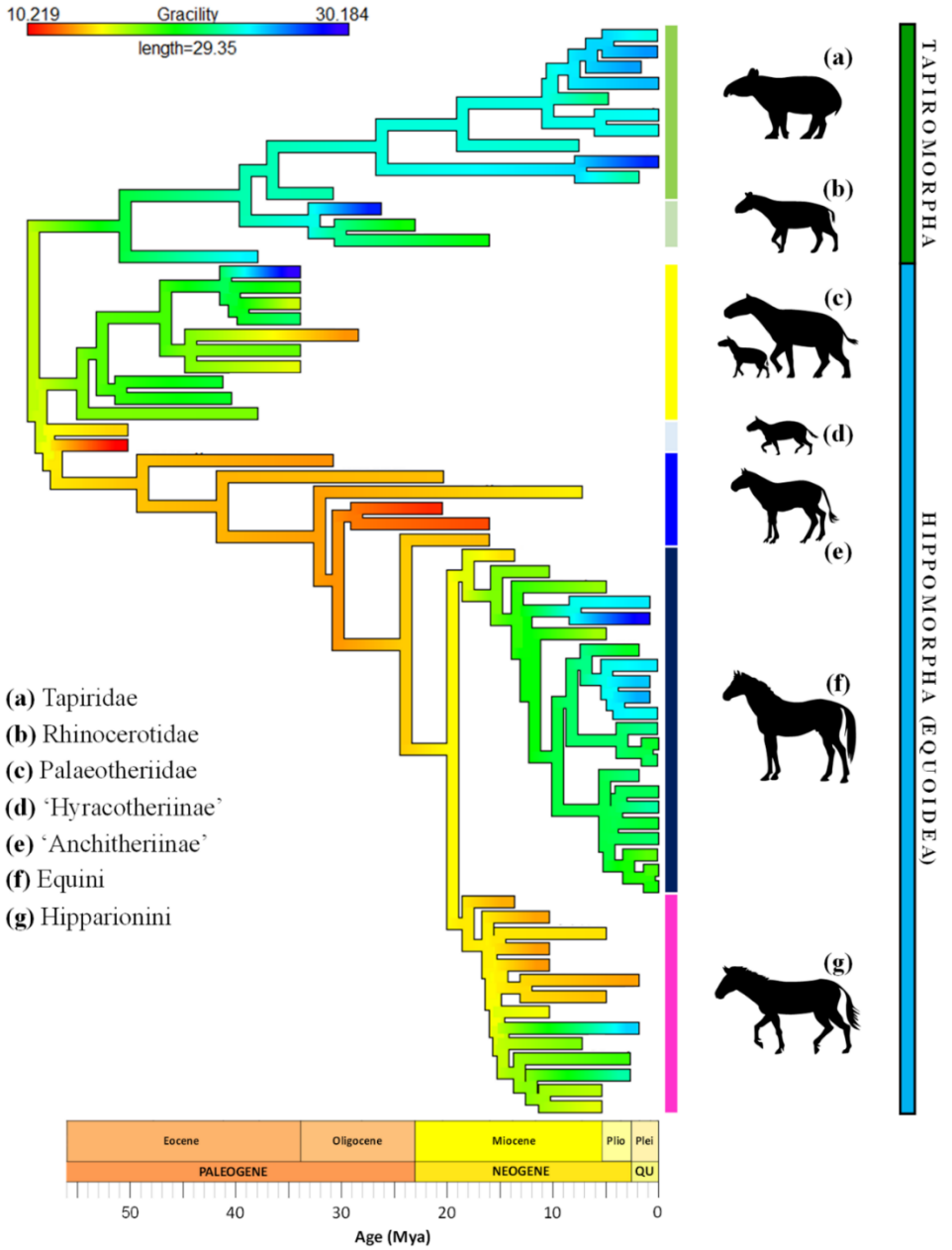

Figure 6.6. Gracility index (Gr-I) plotted onto the composite phylogenetic tree of tapiromorphs and equoids. Warm colours signify mediolaterally narrow, gracile third metacarpals; cooler colours signify mediolaterally broad, robust third metacarpals. Species names provided in Appendix V; Figure S5.1.

al., 2017), and the knowledge that the metacarpals of the tetradactyl tapir manus are capable of near-vertical orientation during locomotion (unlike ± 50° predicted by Sondaar (1968) for *Mesohippus* and *Anchitherium*), all point to basal 'anchitheres' being capable of a more upright stance than implied by phalangeal length alone. Future work with a musculoskeletal modelling-based approach may ultimately answer this particular question.

I believe these comparative morphological results strongly support the notion that the fetlock of basal 'anchitheres' was indeed supported by a fatty foot-pad, as is present in tapirs, and also concur with Sondaar (1968, 1969) that the transition within the Equidae from basal to derived 'anchitheres' lead to the loss, or drastic reduction, of the foot-pad. This transition can be observed with a punctuated shift in fetlock shape (OSS) away from the ancestral condition at the first occurrence in the sample of *Archaeohippus* (represented by the Florida endemic *A. mannulus*) approximately 26 Mya (Figure 6.8c). However, in light of this study and recent evidence from the functional anatomy of the perissodactyl manus (MacLaren and Nauwelaerts 2017, 2019; McHorse et al. 2017; Hanot et al. 2017; Bai et al. 2017; MacLaren and McHorse, *In review*) we have misgivings about the interpretation of locomotor changes by Sondaar (1968) in both equids and palaeotheres across the tetradactyl-tridactyl transition.

Tetradactyl–tridactyl transition of the fetlock

Shape variation in the fetlock of tetradactyl equoids in this study are shown to be similar to that of the hypothetical ancestor, and also statistically inseparable from tapirs (Figure 6.1; Table 6.1; Appendix V, Table S5.3). Initially, this result can be interpreted as supporting our hypothesis, and demonstrating that tetradactyl perissodactyls have a similarly shaped fetlock joint facet on the metacarpal (across all clades present in this analysis; see lophiodontid discussion in MacLaren and Nauwelaerts 2019 for alternative tetradactyl perissodactyl morphotypes). However, it is important to keep in mind the methodology for the ancestral shape reconstruction (see Appendix V). Conclusions based on this will therefore be tempered to account for the absence of other key tetradactyl species within both tapiromorph and equoid groups, and the hypothetical nature of the comparative 'taxon'.

Interestingly, not only do 'hyracotheres' plot deep within the morphospace of both tapirs and palaeotheres (Figure 6.1), but the average ordinary sum of squares (OSS; proxy for shape divergence) for 'hyracotheres' is almost identical to that of the contemporaneous tapiromorph *Chasmotherium* (Figure 6.8c). This may suggest that the level of divergence from the ancestral fetlock morphology remained fairly conserved in both

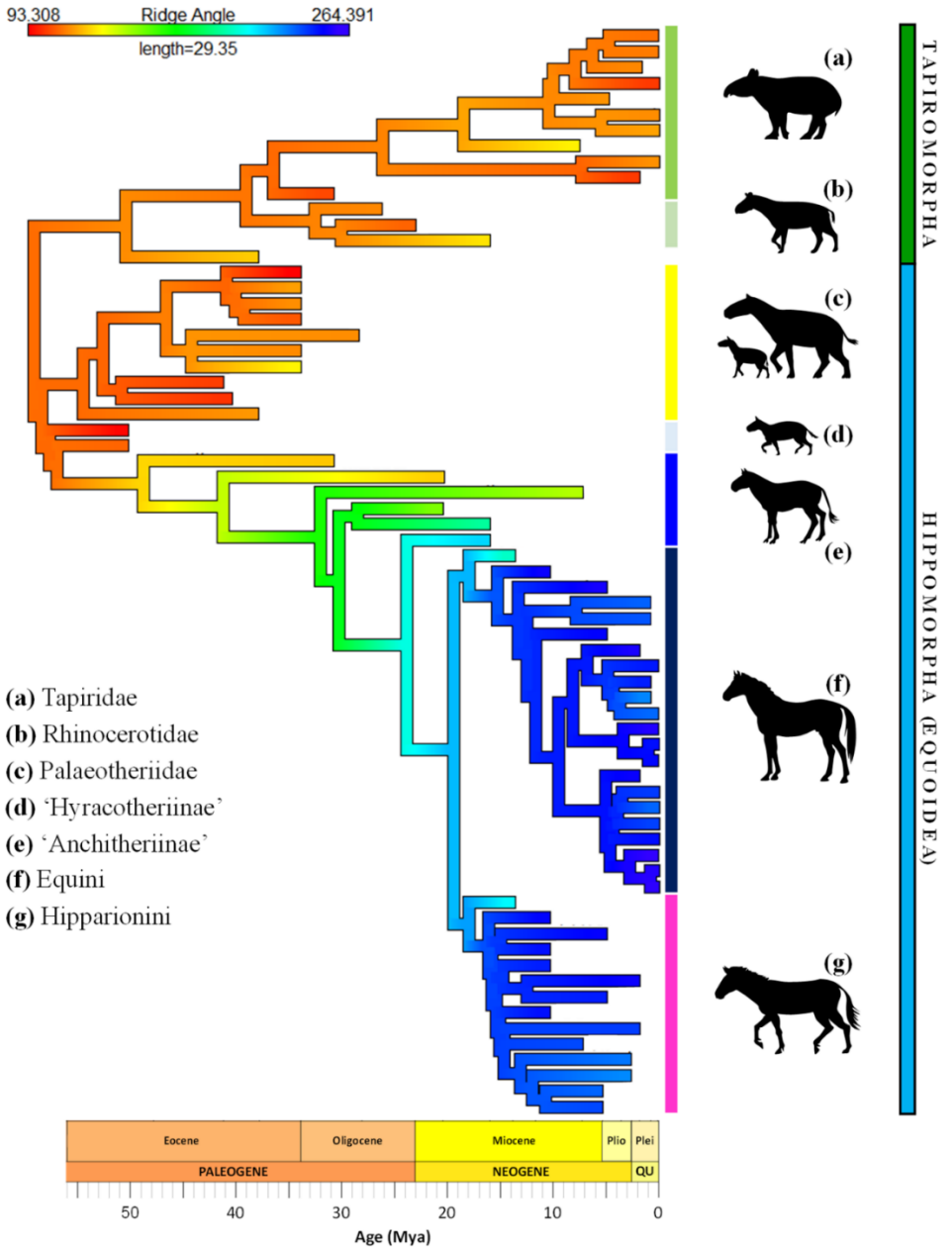

Figure 6.7. Sagittal ridge angle (RA) plotted onto the composite phylogenetic tree of tapiromorphs and equoids. Warm colours signify small angles circumscribed by the sagittal ridge; cooler colours signify large angles. Species names provided in Appendix V; Figure S5.1.

tapiromorphs and equoids until the middle Eocene (Figure 6.8c), although the potential for this pattern being an artefact of ancestral shape generation cannot be discounted (see Appendix V, Section 9 for discussion on this).

From the Paleocene-Eocene Thermal Maximum (PETM, c.55.5 Mya; Secord et al. 2012) until the middle Eocene, global temperatures declined steadily due to increased glaciation in Antarctica (Hren et al., 2013). Whether as a direct result of this temperature shift, or as a consequence of associated aridification of local habitats, the first functionally tridactyl equoids appeared in late Lutetian; in this study, they are represented by the first occurrence of *Plagiolophus* (Badiola & Cuesta, 2008). The origination of definitive tridactyly in the equoid lineage lead to a shift in average OSS away from the ancestral fetlock morphology, associated with a slight mediolateral narrowing of the phalangeal joint facet (making the metacarpal appear thinner), and a small extension of the palmar sagittal ridge for articulation with the proximal sesamoids. The extension of this sagittal ridge has previously been proposed as indicative of increased digit stability and load spreading at the metacarposesamoid and metacarpophalangeal articulations (Hildebrand 1985; Easton and Kawcak 2007; in perissodactyls: MacLaren and Nauwelaerts 2016), and these interpretations would also fit well in this case. It should be noted also here that the volar process of the magnum (site of interosseous muscle attachment) decreases in prominence across the tetradactyl-tridactyl transition in both palaeotheres and equids (Hellmund, 2005; MacLaren & Nauwelaerts, 2019; Wood et al., 2011), likely due to the reduction, or loss, of the deep and superficial interosseous muscles for the (now relict) lateral fifth digit (Barone 2000; MacLaren and McHorse, *In review*). This would have resulted in a reduced ability for digital adduction and abduction in both equoid lineages, though less so in palaeotheres due to the retention of a notable volar process of both the magnum and unciform (MacLaren & Nauwelaerts, 2019).

The loss of the lateral digit in equoids has been shown to be associated with elongation (= increased gracility) of the central digit (Franzen, 2010b; MacFadden, 1992b). The narrowing of the third metacarpal in the transition between tetradactyly and tridactyly in palaeotheres is reflected in the gracility index (Gr-I). Gracility index decreases from tetradactyl palaeotheres (*Propalaeotherium* and *Eurohippus*; Gr-I = 17-21) to the tridactyl *Plagiolophus* (Gr-I = 13–18) and *Pa. medium* (Gr-I = 15.8) (Figure 6.6); this is not mirrored in true equids, with no great decrease observed between tetradactyl 'hyracotheres' *Sifrhippus* and *Eohippus* (15–10) and the first tridactyl equid *Mesohippus* (15.3). With regards to their fetlock morphology, tetradactyl palaeotheres and 'hyracotheres' occupy similar regions of metacarpal morphospace (Figure 6.1), as do *Mesohoippus* and *Plagiolophus* (as discussed previously). This pattern suggests the

morphological transition from a tetradactyl to tridactyl manus incurred similar changes to the fetlock (slight mediolateral constriction of the metacarpophalangeal joint facet; expanded articular surface for the sesamoids) in both palaeotheres and equids. This is in contrast to the accompanying rearrangement of interosseous muscles, which show evidence of remaining well developed in palaeotheres whereas equids greatly reduced the area for attachment of these muscles between the tetradactyl *Sifrhippus* and tridactyl *Mesohippus*. This finding supports suggestions by Sondaar (1968) that *Plagiolophus* did not specialise its manus in the same manner as equids did, possibly preventing it from exploiting more open terrain. Rather, palaeotheres would have possessed greater muscular control over their three short but comparatively mobile digits, ideal for locomotion in uneven or compliant substrates.

With the extinction of *Eurohippus*, the last tetradactyl equoid in the study sample, we observe another increase in OSS (end-Bartonian; Figure 6.8). This result not only supports our second hypothesis (after tetradactyl equoids died out, average fetlock divergence would increase), but also demonstrates the importance of the inclusion of endemic faunas in the study of equoid locomotor evolution. In reality, endemic faunas played a key role in explaining patterns of shape divergence and trait correlation throughout this study.

The role of provincialism in fetlock shape variation

Throughout evolution there are many occurrences of localised diversification resulting in highly disparate morphologies and ecologies (e.g. Sondaar 1977; Burns et al. 2002; Ribera and Balke 2007; Badiola et al. 2009; Grossnickle and Polly 2013; Velasco et al. 2018). The effect of endemism on the morphology of the equoid fetlock represents another example, with taxa currently understood to be provincial in their distribution driving peaks in shape variation and divergence from the ancestral fetlock shape (Figure 6.8c). Three major examples presented in this study are those of *Palaeotherium* spp., *Archaeohippus mannulus*, and the South American equinines.

1) Palaeotherium *and the endemic European equoids*

Fetlock shape divergence exhibits an Eocene peak at the height of palaeothere diversity and disparity in Europe and Asia (Priabonian; Remy 1992, 2004; Hooker 2005; Figure 6.8c). Within the genus *Palaeotherium*, the locomotor apparatus has been shown to be highly variable between species (Cuvier, 1812a; MacLaren & Nauwelaerts, 2019; Rudwick, 2008), and this is reflected in the large morphospace occupation (Figure 6.1; yellow circles) and notable divergence from the hypothetical ancestral shape observed

from the Lutetian to end-Priabonian (Figure 6.8c). Additionally, the diversification of palaeotheres beyond just their limb skeleton is evident in the isolated spike in body mass observed throughout the occurrence of the genus *Palaeotherium* (Figure 6.8b; Remy 2015; MacLaren and Nauwelaerts 2019). The extinction of *Palaeotherium* spp. at the "Grande Coupure" (Eocene–Oligocene boundary; 28.4 Mya) is not marked by a drop in average OSS values in equoids, thus not supporting our hypothesis regarding the effect on fetlock shape by major turnover events. The extinction of *Palaeotherium* does correspond with a dip in average body mass (Figure 6.5, 6.8b–c). As previously noted in *Plagiolophus* (Sondaar 1968; this study), the articulation with the proximal phalange in *Palaeotherium* is indicative of greater mediolateral adduction and abduction in this taxon than is present in the derived 'anchithere' equids (e.g. *Parahippus*), although younger but less derived 'anchitheres' share a lot of features of the fetlock with palaeotheres (see Figure 6.1 and Figure 6.2b). Equids contemporaneous with *Palaeotherium* are noticeably smaller in their body size range. We propose that the ability for *Palaeotherium* to manipulate its digits via comparatively large digital interosseous muscles may have facilitated this genus maintaining secure footing on compliant substrates while attaining much larger sizes than contemporaneous equids (MacLaren and Nauwelaerts 2019; MacLaren and McHorse, *In review*). The presence of multiple body sizes of *Palaeotherium* spp. exhibiting variable, but 'primitive' for Equoidea, fetlock morphologies goes some way to explaining the lack of correlation between body mass and shape in this study (Figure 6.3a). This particular result supports our hypothesis of poor correlation between shape and mass, albeit only part of the explanation for the decoupling observed.

When observed in a temporal context, the endemic late Eocene equoids of Europe (*Plagiolophus* + *Palaeotherium* spp.) exhibit a high degree of variation compared to the ancestral shape, even though some species of *Palaeotherium* (e.g. *Pa. magnum*) are quantitatively very close in OSS to the hypothesised ancestral condition for the fetlock. The first peak and plateau in equoid body mass and OSS values (c. 38 Mya) correlates with the first appearance of *Palaeotherium* spp.; this radiation of a single genus into multiple locomotor morphologies (including several different fetlock shapes) corresponds with a 3–4 Ma plateau in global temperature following a generally decreasing trend from the PETM (55.8 Mya) (Figure 6.8b–d; Zachos et al. 2008). Evidence from late Eocene palaeoclimate estimates suggest that the Bartonian-Priabonian of Western Europe was comparable to modern South-East Asian subtropical and warm-temperate forests (Hren et al., 2013; Moraweck, Uhl, & Kunzmann, 2015). The generally stable global temperature conditions (Moraweck et al., 2015; Zachos et al., 2008) combined with a seasonally sub-tropical local environment high in primary productivity likely promoted the diversification of *Palaeotherium*. The moist forest

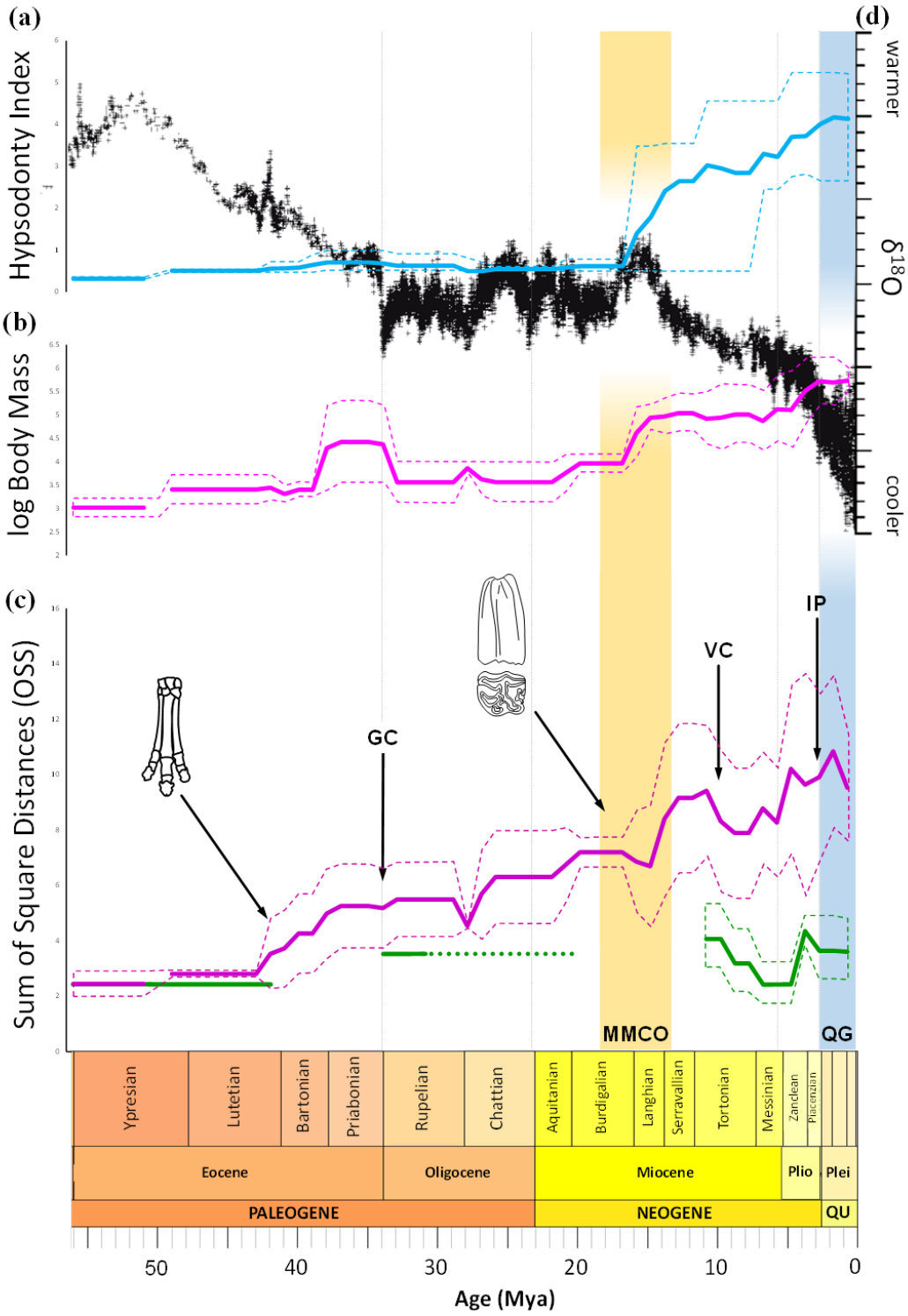
(a)
Hypsodonty Index
(b)
log Body Mass
(c)
Sum of Square Distances (OSS)
(d)
warmer
cooler
δ18O
GC
VC
IP
MMCO
QG
Ypresian
Lutetian
Bartonian
Priabonian
Rupelian
Chattian
Aquitanian
Burdigalian
Langhian
Serravallian
Tortonian
Messinian
Zanclean
Piacenzian
Eocene
Oligocene
Miocene
Plio
Plei
PALEOGENE
NEOGENE
QU
50
40
30
20
10
0
Age (Mya)

Figure 6.8. Equoid and tapirid shape and covariate variation through time. **(a)** Average hypsodonty index (HI) and **(b)** body mass (BM) for equoids alongside **(c)** ordinary sum of square distances representing divergence from a hypothetical ancestor for equoids (purple) and tapirids (green), plotted through geological time. **(d)** Stacked oxygen isotope values ($\delta^{18}O$) from benthic foraminifera plotted as a proxy for global temperature fluctuations (Zachos, Dickens, & Zeebe, 2008). Significant ecological events and evolutionary innovations labelled on OSS plot through time: "Grande Coupure" extinction event (GC); Mid-Miocene Climatic Optimum (MMCO); Vallesian Crisis turnover event (VC); Panamanian Isthmus formation (IP); Quaternary Glaciation (QG); diagrams representing first occurrence of tridactyly in equoids (tridactyl manus) and first occurrence of hypsodont dentition in equoids (HI ≥ 2; after Mihlbachler et al. 2011).

environments predicted for Western Europe during this time also correlates well with the maintenance of a tapir-like fetlock morphology in this group (Hren et al., 2013; Kvaček, 2010; MacLaren & Nauwelaerts, 2017, 2019; Moraweck et al., 2015; Mosbrugger, Utescher, & Dilcher, 2005). The extinction of palaeotheres (predominantly at the "Grande Coupure" and then entirely with the mid-Oligocene extinction of *Plagiolophus*) is clearly marked by a dip in the average OSS values for equoids (Figure 6.8c; 28.4 Mya). Shortly following the last occurrence of *Plagiolophus* in Europe, true equids began to undergo radical changes to the distal metacarpal shape with the evolution of the first advanced anchithere *Archaeohippus mannulus*, a dwarf horse currently recognised as endemic to Florida (O'Sullivan, 2003).

2) Archaeohippus *and the derived 'anchitheres'*

Immediately following the extinction of the endemic European equoids, shape divergence and variation is driven away from the ancestral shape (and indeed from that of the Eocene–Oligocene equid fauna) by the first occurrence of the Florida endemic *Archaeohippus mannulus* (O'Sullivan, 2003) (Figures 6.1 and 6.8). Isolated in the South-East of North America, *A. mannulus* exhibits a very gracile metacarpal, low body mass (approximately 23 kg), a narrow metacarpal head and a sagittal ridge angle intermediate between the earlier Oligocene *Miohippus* and the more derived 'anchitheres' of the early Miocene (e.g. *A. blackbergi* and *Parahippus leonensis* of the Thomas Farm fauna; Hulbert 1984). The presence of this suite of characters, far more derived than *Mesohippus* or *Miohippus*, indicate that this species was already less capable of mediolateral adduction or abduction of the proximal third phalange, in favour of a slight increase in range of motion. However, *A. mannulus* was likely to have relied upon the remaining medial and lateral digits to stabilise itself during locomotion

(McHorse et al., 2017; Thomason, 1986), especially if this taxon was one of the first to exhibit a 'spring-foot' style of locomotion independent of foot-pad (O'Sullivan, 2008; Sondaar, 1969). The later North American 'anchitheres' *A. blackbergi* and *Parahippus* both exhibit similarly narrow metacarpal heads and progressively greater sagittal ridge angles (Figure 6.7), strongly supporting the claims of Sondaar (1968) that the *Archaeohippus* lineage represents a distinct turning point in the equid fetlock evolution. In this study, the presence of *A. mannulus* has a negligible effect on hypsodonty or body mass patterns through time; however, the very narrow and already specialised fetlock shape of this taxon, and its more widespread sister species *A. blackbergi* (Figure 6.1; far left triangles), caused a divergence from the ancestral fetlock condition greater than the combined variation of *Palaeotherium* and *Plagiolophus* (Figure 6.4c). The fetlock of this species is here revealed as more akin to derived Old World hipparionines than to its predecessor *Miohippus* (Figure 6.1). Due to the combination of highly derived tridactyl fetlock morphology, very small size and low-crowned molars, *A. mannulus* can also be considered as contributing to the decoupling of shape and both body mass and hypsodonty (Figure 6.3a–b).

From a palaeoclimatic standpoint, global temperatures changed profoundly across the Eocene–Oligocene boundary (Figure 6.8d; Zachos et al. 2008). Cooler environments than the Eocene "greenhouse" were coupled with a drop in sea level, leading to the emergence and spread of arid ecosystems in the Northern Hemisphere (Hren et al., 2013; Mosbrugger et al., 2005; Retallack, 2001; Zachos et al., 2008). The emergence of the purportedly 'spring-footed' *Archaeohippus*, and the associated increase in mean OSS by equoids, represents a broader change in the equoid manus driven by this small endemic equid. Principally these changes include: 1) reduction of mediolateral movement of the phalanges (Sondaar, 1968); 2) reduction of metacarpal and phalangeal bone mass, and 3) further reduction of the medial and lateral digital interossei in favour of a single, central, and potentially more fibrous digital interosseous muscle attaching to the proximal phalange at the palmar aspect of the fetlock (Barone, 2000; Soffler & Hermanson, 2006). These innovations would be carried forward through all subsequent lineages of equids, including highly gracile tridactyl hipparionines (e.g. *Nannippus* spp.) and the stocky, robust equinine fauna native to South America (*Hippidion* and *Equus* (*Amerhippus*) species).

3) *Stability specialisation in South American endemic equid fetlock*

The formation of the Isthmus of Panama offered a land-bridge for multiple North American taxa to disperse to the South American continent via at least two separate pathways (Cione et al., 2015; O'Dea et al., 2016; Prado & Alberdi, 2014). Two genera

of equids are known from South America, *Equus* (*Amerhippus*) and *Hippidion*, both of which contain several species presenting highly robust metapodia (Alberdi et al. 2003; Machado et al. 2018; among others). In this study, South American *Equus* (*Amerhippus*) and *Hippidion* occupy similar regions of morphospace (Figure 6.1), and are present at similar times (Plio-Pleistocene; Figure 6.8). The *Hippidion* lineage ('hippidiforms') is regarded as endemic to South America (Prado & Alberdi, 2014); however, as the *Equus* (*Amerhippus*) species *E. neogeus* and *E. andium* exhibit comparable morphologies, they will also be discussed in brief here with regards to the specialisation of the metacarpal and fetlock.

The extremely robust metacarpals of *Hippidion* and *E.* (*Amerhippus*) species place them as outliers in fetlock morphospace in this study (Figure 6.1). The metacarpal head is broader than other equinine species (low PC2 values). This robusticity is not confined to the fetlock, with both *Hippidion* and *E.* (*Amerhippus*) species exhibiting gracility indices higher than any other equinine taxa (Figure 6.6). Finally, the average sagittal ridge angle for South American equinines is 12° lower than that for other *Equus* species, which increases to a 20° difference when compared to hemionine asses e.g. kiangs and onagers. The broad fetlock joint is present in both large and small taxa, ranging between 220–520 kg (Prado & Alberdi, 2017a), and can therefore be discounted as an artefact of body size. Although *Hippidion* species are found in the far east of Brazil, there is sufficient evidence supporting the migration of the ancestral *Hippidion* south along the Andes, whereupon at least three species diverged, all of which exhibit extreme robusticity to their metacarpal shaft and fetlock. Previous interpretations of broad metacarposesamoid and metacarpophalangeal joints have concluded that these features indicate increased stability of the joint (Easton & Kawcak, 2007; MacLaren & Nauwelaerts, 2017). In support of this, and continuing a theme throughout this study, the broad and flat palmar surface of the *Hippidion* metacarpal suggests the presence of a very large and likely highly fibrous interosseous muscle of the third digit (suspensory ligament; Barone 2000; Soffler and Hermanson 2006), conferring a high degree of force to stabilise the fetlock (Soffler & Hermanson, 2006). When compared to the narrow metacarpals of open and arid-habitat equids (e.g. hemionine asses, New World hipparionines), the ~20° reduction in sagittal ridge angle and very robust limbs in South American endemic equinines suggests that these horses possessed a stiffened fetlock joint more suited for stability and shock absorption on uneven terrain than high-speed, high efficiency running in open environments. Similar adaptations for stability can be seen in the robust metapodials of draught horses bred for power rather than speed. Additionally, the ~20° difference in sagittal ridge angle is mirrored in the mountain zebra (*Equus zebra*), a species known to inhabit high altitude, uneven terrain (Mills, 1997; L. H. Watson & Chadwick, 2007). I therefore posit that *Hippidion*, and possibly

also *E.* (*Amerhippus*) species, underwent similar environmental and selective pressures to modern mountain zebra early in their evolution, resulting in broader metacarpals to accommodate larger suspensory ligaments, leading to a more rigid fetlock joint. Considering the morphological similarities to modern draught horses and mountain zebra, I believe this selective pressure to be based upon habitat confinement along the Andean foothills early in the equid radiation into South America (Prado & Alberdi, 2014). The extremely robust fetlock morphology of the Pleistocene South American equids drives the maximal peak in mean OSS values for equoids, occurring 1–2 Mya (Figure 6.8c). This result suggests that the formation of the Panamanian Isthmus certainly did affect equoid fetlock variation. I find it unlikely that this particular morphological shift is an example of metacommunity mechanisms (e.g. species sorting), which may account for other migrations of equids. The specific shift in shape exhibited exclusively by the South American equinine fauna appears to be more in keeping with localised adaptation to a localised selection pressure, and the muscles and bones of the distal forelimb adapting to that pressure (in this case, shock absorption and powerful movement across uneven terrain). It should be noted that no difference in tapirid fetlock OSS was observed at this time, despite this group also migrating into South America during the Great American Biotic Interchange (Cione et al., 2015; Holanda & Ferrero, 2013) and currently occupying upland areas in the cloud forests of the Andes (Padilla et al., 2010; Ruiz-García et al., 2012). The role faunal turnover events have on fetlock shape variation is therefore not a straightforward one.

Perissodactyl fetlock shape change at faunal turnover events

The Cenozoic has played host to a number of significant faunal turnover events (e.g. Retallack 2001; Zachos et al. 2008; Blois and Hadly 2009; Domingo et al. 2009; Damuth and Janis 2011; Figueirido et al. 2012; Agustí et al. 2013; Fraser et al. 2015; O'Dea et al. 2016). Driving forces behind these shifts in local and global community structure have been widely hypothesised, and include temperature fluctuations (e.g. Blondel 2001; Ehlers and Gibbard 2004*c*, *b*, *a*; Hooker et al. 2004; Mosbrugger et al. 2005; Zachos et al. 2008; Kürschner et al. 2008; Mihlbachler et al. 2011; Secord et al. 2012; Hren et al. 2013), faunal dispersal/extinction events (e.g. Agustí et al. 2013; Casanovas-Vilar et al. 2014; Prado and Alberdi 2014; O'Dea et al. 2016), and flora-based habitat modification (e.g. Retallack 2001; Kvaček 2010; Nunez et al. 2010). In this study, I selected four events or periods of established perissodactyl community change with which to compare patterns of fetlock shape divergence: the Eocene–Oligocene extinction event ("Grande Coupure"; 33.9 Mya); the Mid-Miocene Climatic Optimum (c.17–13 Mya); the Vallesian 'Crisis' turnover event (c.9.7 Mya); and the formation of the Isthmus of Panama (c.2.7 Mya). Localised turnover events affecting equid

communities are also known (e.g. Messinian Salinity Crisis; South American megafaunal extinctions) (Tonni, Cione, & Soibelzon, 2003; van der Made, Morales, & Montoya, 2006); however, the four events chosen were anticipated to demonstrate notable shifts in trait conditions across a broad geographical range. Biological changes (e.g. morphology) on any temporal or spatial scale as a response to climatic change are difficult to specifically identify (Blois & Hadly, 2009). With this in mind, we present an overview of patterns in shape and ecomorphological covariate variation, and speculate on the cause of those patterns where they correspond with global turnover events.

1) *The Great Separation – La "Grande Coupure"*

The Eocene–Oligocene extinction event is strongly associated with drastic faunal turnover in Europe, where it is known as the "Grande Coupure" (Hooker, 2010a; Stehlin, 1910), but is also known to have impacted community structure in North American ecosystems (Prothero, 1985). In Europe, the rapid temperature drop and decreased sea-level combined to alter the pre-Oligocene European archipelago (Agustí & Anton, 2004a; Hren et al., 2013; Zachos et al., 2008), forcing previously isolated populations into contact with new competitors and predators (Hren et al., 2013). Principal among these were the endemic perissodactyl family Palaeotheriidae, which saw a catastrophic decline across the Eocene–Oligocene boundary; only *Plagiolopus minor* survived in the more arid early Oligocene of Europe (Hooker, 2010a), restricted to southern European sites (Heissig, 1987). By the end of the Rupelian (28.4 Mya), the perissodactyl-dominated fauna of Europe was replaced by browsing artiodactyls (Agustí & Anton, 2004a; Hooker, 2010a), and in Central Asia by lagomorphs and rodents (Meng & McKenna, 1998). In our data, we observe a small shift in average OSS away from the ancestral condition (Figure 6.8c); this can be explained neatly by the extinction of *Palaeotherium* spp., which overall exhibit more basal fetlock morphologies than the surviving *Plagiolophus* (and *Mesohippus* in North America) (Figure 6.2a). The shift in fetlock morphology away from the ancestral shape also represents a shift away from a forest-adapted fetlock morphology (i.e. tapirid fetlock shape; Figure 1, PC1 > 0.05; Figure 6.8c, green curve). Therefore, these results suggest that post-Eocene equoid fetlocks were already adapted for a more open terrain than the subtropical forest inhabitants of the late Eocene. This result supports previous findings suggesting increased levels of cursorial (running) adaptations in early Oligocene perissodactyls, likely as a consequence of being exposed to drier, more open habitats (e.g. Gregory 1929; Scott 1941; Sondaar 1969; Thomason 1986; Blondel 2001; Agusti and Anton 2004; Bai et al. 2017; MacLaren and Nauwelaerts 2019).

2) *The Great Diversification – Mid–Miocene Climatic Optimum*

A rapid increase in atmospheric CO_2 followed the Oligocene–Miocene transition, causing widespread ecosystem warming (Kürschner et al., 2008). Global temperatures stabilised from c.17–13 Mya; this time interval is known as the Mid–Miocene Climatic Optimum, or MMCO (Anagnostou et al., 2016; Kürschner et al., 2008; Zachos et al., 2008). During the MMCO, ungulate taxonomic diversity increased dramatically, and several adaptations for living in open grassland habitats (including truly hypsodont dentition) became widespread in multiple herbivore clades (Damuth & Janis, 2011; Kaiser et al., 2013). Unfortunately, the MMCO corresponds with the 'tapir vacuum' (van der Made, 2010), a presumably sampling-based phenomenon whereby very few tapirs have been found to bridge the evolutionary gap between non-*Tapirus* tapirs and the first occurrence of *Tapirus* (*T. johnsoni*; Hulbert 2010). This precludes us from observing differences in tapir fetlock shape through the MMCO. Aforementioned patterns of adaptation to grasslands can be tracked in the equids in our study (Figure 6.8a), with a substantial increase in mean tooth crown height observed at 16 Mya (first occurrence of *Pliohippus* in the dataset), and an increase in body mass as equids began to feed upon lower-nutrition fodder (Blois & Hadly, 2009; Fortelius et al., 2014), necessitating greater consumption. At the transition from Burdigalian to Langhian (c.16 Mya), despite overall equid diversity increasing (Maguire & Stigall, 2008; Prado & Alberdi, 2017b), this analysis demonstrates a decrease in average OSS (Figure 6.8c), corresponding with the occurrence of the European browsing equid *Anchitherium aureliense*, which exhibits comparatively basal fetlock morphology (Sondaar, 1968). Although *Anchitherium* was present in Eurasian ecosystems until the Messinian, affecting the mean average OSS for equids long after the MMCO (until approximately 7 Mya), the sharp increase in OSS observed at the end of the MMCO highlights how divergent the newly evolved New World hipparionine fetlock morphology was (Figures 6.1, 6.2b and S5.4). Despite a notable shift in both OSS and morphospace occupation (Figure 6.1, 6.2b, 6.8), no corresponding shift in body mass is observed. In fact, no large bodied (BM > 200kg) hipparionine taxa are present in the New World sample (Figure 6.5), all of which demonstrate gracile metapodials compared to contemporaneous equinines (Figure 6.6). Only after the dispersal of hippaironines into Eurasia in the Vallesian (c.9.7 Mya) do we observe hipparionines rivalling equinine body masses (standard deviation increase; Figure 6.8b).

3) *The Great Migrations – the Vallesian 'Crisis' and GABI*

Large-scale shifts in biogeography have been a hallmark of perissodactyl evolution (MacFadden 1992; Deng et al. 2011; Rose et al. 2014; Bai et al. 2018a). Recent evidence

suggest dispersals from the Indian subcontinent and across Eurasia early in the evolution of both equoids and tapiromorphs (Bai et al., 2018b, 2014; Rose et al., 2014; Smith et al., 2015). The colonisation and subsequent evolution of the equids, rhinoceroses and tapirs in North America was punctuated by several reverse migrations back into Eurasia of progressively more derived clades in the Oligocene (Scherler, Becker, & Berger, 2011; Scherler, Mennecart, Hiard, & Becker, 2013) and Miocene (Agustí et al., 2013; Fortelius et al., 2014; van der Made et al., 2006). The late Miocene Vallesian 'Crisis' represents one of the more major mammalian faunal turnovers to occur in Europe in the Neogene. While there is no doubting the existence of comprehensive shifts in herbivorous community composition at this time, the causes for the Vallesian 'Crisis' remain unclear (Casanovas-Vilar, García-Paredes, Alba, Van Den Hoek Ostende, & Moyà-Solà, 2010; Casanovas-Vilar, Moyà-Solà, Agustí, & Köhler, 2005; Casanovas-Vilar et al., 2014; Fortelius et al., 2014; Fortelius & Hokkanen, 2001). It is possible that the expansion of hipparionine equids and recolonisation of Eurasia in the Vallesian represents a case of migration via species sorting and adaptive radiation, with optimal conditions existing (for approximately 2 Mya) whereby equids could expand into and inhabit regions previously unsuitable for them. What is clear from the results of the present study is that the influx of hipparionine equids into Europe approximately 9–10 Mya heralded a notable increase in body size (Figure 6.5), coupled with a drop in average OSS (Figure 6.8c). Reduction in OSS at this time highlights the shift in hippaironine distal metacarpals to broader, more equinine shape (Figure 6.2c; orange diamonds), and with that shape change a potential mechanical shift towards functional monodactyly. Old World hipparionines demonstrate both robust and gracile taxa from the late Miocene onwards (e.g. Eisenmann 1995; Koufos 2015), whereas New World hipparionines remained small (Figure 6.5) and highly gracile until their extinction in the Pleistocene (Figure 6.6). Current evidence suggests a mixed dry forest, scrub and sporadic grassland environment for Southern Europe following the Vallesian 'Crisis' (Casanovas-Vilar et al., 2010, 2014), with more temperate forests predominating central Europe (Fortelius et al., 2014). The mixture of woodland and grassland habitats in late Miocene–early Pliocene Europe may have influenced the variation in fetlock morphology we observe in Old World hipparionines, with different species inhabiting different areas and partitioning resources accordingly (Agustí & Anton, 2004b). The presence of both browsing and grazing taxa is also supported in this study by the distinct lack of extremely high-crowned (HI > 4.0), grass-land specialised dentition, a feature widespread among New World hipparionines, *Equus* and the South American *Hippidion* lineages (Cantalapiedra et al., 2017; Parker, McHorse, & Pierce, 2018). The expansion of arid grasslands in the Plio–Pleistocene icehouse conditions favoured the high-crowned lineages, as we observe with the last occurrence of European hipparionines (c.2.6 Mya), coinciding with the formation of the Panamanian land-bridge and the

rearrangement of global ocean currents at the onset of the Quaternary Glaciation (Cione et al., 2015; Corliss, Martinson, & Keffer, 1986; Hewitt, 2000; O'Dea et al., 2016).

The formation of the Isthmus of Panama not only impacted climate on a global scale by sealing the Central American Seaway (Bacon et al., 2015; Bartoli et al., 2005; O'Dea et al., 2016), but provided a means by which terrestrial species could intersperse between and across the continents, termed the Great American Biotic Interchange (GABI) (Bacon et al., 2015; Cione et al., 2015; Prado & Alberdi, 2014). Equids and tapirs exploited the land-bridge, and both groups were highly successful until the end-Pleistocene extinctions in the Americas reduced megafaunal taxonomic diversity (Defler, 2019; Tonni et al., 2003). The effect of the formation of the isthmus, subsequent speciation of the *Hippidion* lineage, and the final extinction of New World equids can be tracked clearly in our data (Figure 6.8a–c). Extinction of almost all New World hipparionines at the Plio–Pleistocene boundary triggers an initial dip in OSS through the Zanclean, followed by an increase to an overall equoid peak in the mid–Pleistocene (Figure 6.8c). The overall peak in OSS and expansion of morphospace occupation represents the extinction of European hipparionines possessing a more forest-adapted fetlock (Figure 6.1; Agusti and Anton 2004), the continued presence of the youngest New World hipparionine *Nannippus peninsulatus* (Appendix V, Figure S5.1; MacFadden 2005), and the first occurrence of the morphologically disparate South American endemic equid fauna, including *Hippidion* and *Equus* (*Amerhippus*) (Prado & Alberdi, 2014) (Figure 6.2d). Both *N. peninsulatus* and *E.* (*Amerhippus*) spp. exhibited high-crowned molars, and were likely both open-habitat specialists. *Hippidion* spp. was likely a browser, purportedly sporting a prehensile upper lip (Bernardes, Sicuro, Avilla, & Pinheiro, 2012; Defler, 2019), and would have benefitted from stocky limbs and a stiffened fetlock joint to harvest leafy browse in potentially steep and uneven montane scrub-forest. Following the extinction of hippidiforms (*Hippidion* spp.) and hipparionines (North American *Nannippus* and African *Eurygnathohippus*) in the late Pleistocene, OSS values are reduced, signifying the loss of a morphologically diverse, functionally monodactyl and geographically widespread equid fauna (Figure 6.2d).

It may be concluded that, from the broad biogeographical and temporal sample of equoids investigated in this analysis, that the effect of climate-driven turnover events can be tracked through time using the equoid fetlock joint and other metapodial features (e.g. gracility, sagittal ridge angle). The remaining, highly specialised extant species in the genus *Equus* represent the last survivors of a morphologically diverse and biomechanically progressive glade of ungulates. Despite surviving through the megafaunal extinction at the end of the Pleistocene, the locomotor specialisation of the

modern equid fetlock – an adaptation which made the group so successful in the past – may in turn restrict it from rapid adaptation to a changing environment in the near future.

Conclusions

The fetlock joint of equoids is a pivotal anatomical unit for understanding the locomotor evolution of this clade. I this study have elucidated how the changes in the manus of true equids in the late Eocene may have already been well on the way toward the specialised joint we associate with equids today. The joint morphology itself does not significantly vary between early equids and their sister clade, the palaeotheres. However, additional feature of the manus (e.g. volar processes of the magnum) strongly suggest that tridactyl palaeotheres retained greater muscular control over the adduction and abduction of digits in the manus compared to contemporaneous true equids. Contrary to the interpretations of Sondaar (1968, 1969), my results suggest that the equid manus was capable of being held in a more perpendicular manner than the ±50° limit which has been previously suggested for *Mesohippus*. Placing the fetlock morphology of equids into a quantitative, comparative framework with known forest-dwelling perissodactyls (i.e. tapirids) enabled observations of how the locomotor ecology of equoids diverged, regressed, and diverged again throughout their evolution. Body mass and dietary changes can be correlated with shifts in shape divergence; however, our results also highlight the importance of accounting for multiple taxa from multiple regions. Horse evolution in North America is very well studied, with new interactions, species and evolutionary hypotheses being established on a regular basis (Heintzman et al., 2017; McHorse et al., 2017; Mihlbachler et al., 2011; Parker et al., 2018; E. Scott et al., 2014; Secord et al., 2012; Solounias et al., 2018). Our study has aimed to incorporate a geographically broad sample of equoids (and tapirids) in a comparative morphological framework, with the hope that future studies will be able to do likewise to investigate shape change in equids on a global scale. In conclusion, fluctuations in equoid fetlock shape and specialisation are heavily influenced by turnover events and provincialism. Peaks and troughs in shape divergence correlating with localised origination events (e.g. *Plagiolophus* and *Hippidion*) and biogeographical dispersals (e.g. South American equinines) highlight the importance of regional biodiversity and understanding the effect of climate on vicariance. In light of present-day global climatic disturbance, it is vitally important that conservation efforts on endemic faunas and floras are promoted to preserve both morphological and genetic diversity in highly specialised taxa.

“you know what thinking is? It’s just
a fancy word for changing your mind”

- Twelfth Doctor -

– DISCUSSION –

Within the following synthesis, I will highlight and critically discuss the findings of my research chapters, each with respect to themes and lines of questioning I have explored throughout the thesis. This will be broken down into logical sections, covering the aspects of 1) descriptive and comparative anatomy between tapirs, 2) functional interpretations as pertains to locomotion, 3) challenging the tapir *status quo*, and 4) how the story of the tetradactyl tapir forelimb fits (or does not fit) into the ongoing story of equid locomotor macroevolution.

Unforeseen variation in an enigmatic ungulate

From the initiation of the thesis, it became abundantly clear that tapir locomotor morphology has not been a "top priority" for researchers interested in perissodactyl evolution, with no dedicated assessment of locomotor morphology in the clade since Leonard Radinsky (1963, 1965*a*, *b*). Therefore, the first aim was to establish a grounded, quantitative understanding of the osteology and functional anatomy of the forelimb in modern tapirs, an ambition which was achieved through Research Chapters 1, 2 and 3. In these initial descriptive chapters I demonstrated that, not only are tapirs from different geographical regions dissimilar in their forelimb anatomy (as previously established by Earle in the late 1800s), but also that differences are present in sympatric species phylogenetically separated as recently as 1.5 million years ago (Mya) (Ruiz-García et al., 2016; Steiner & Ryder, 2011). To place this into some historical context, tapirs have been labelled as 'living fossils', due to their plesiomorphic tetradactyl manus, brachydont (i.e. low-crowned) dentition, and propensity to inhabit tropical forest ecosystems. Essentially, the general consensus was that tapirs have not changed in shape or ecology since the first occurrence of the family Tapiridae over 40 Mya (DeSantis & MacFadden, 2007; Janis, 1984; Rustioni & Mazza, 2001). Research Chapters 1 and 2 have disproven that this is the case. Extant tapirs are highly recognisable by their cranial morphology (Cozzuol et al., 2013; Dumbá et al., 2018), and I have shown in Research Chapter 1 that they can just as easily be distinguished from one another based on the shape of their scapula. The mountain tapir *Tapirus pinchaque* emerged from the analyses of both upper and lower forelimbs as a surprisingly divergent taxon, contradicting suggestions that this species represents the most unspecialised tapir alive today (Hershkovitz, 1954; Padilla et al., 2010; Radinsky, 1965b). Furthermore, when investigated against extinct tapir species in Research Chapter 4, *T. pinchaque* once again exhibited morphological features which set it apart from the rest of the *Tapirus* species (*teres major* muscle attachments, parasagittal elbow alignment). Indeed, it was *T. pinchaque* and its morphological divergence from a tapir of near equal size (*T.*

lundeliusi) which formed the most convincing argument to reject the long-held notion that tapir postcranial variation is correlated with differences in body size (Research Chapter 4). Not only did Research Chapter 4 provide evidence that the tapir postcranial skeleton has changed in shape independent of changes in size, but also that the Plio–Pleistocene tapirs of the subgenus *Helicotapirus* exhibit habitat-specific variation in the lateral carpus. Unfortunately, there have been few studies attempting to relate variation in the carpal bones of ungulates to habitat preferences (Schellhorn & Pfretzschner, 2014), and the exact scope of how differences I have observed in the tapir carpus might affect locomotion can, at this point, only be speculated at. But let's do it anyway. The lateral carpus of tapirs is intricately linked to the lateral fifth digit, transmitting compressive forces to that digit during locomotion. As the shape of the more open woodland species *Tapirus* (*Helicotapirus*) *haysii*, *T.* (*H.*) *veroensis* and *T.* (*H.*) *lundeliusi* showed in Research Chapter 4, the connection between the lateral carpus and the ulna appears rigid and adapted for greater loading on this joint. In addition, the forelimb bones of *T. lundeliusi* (most notably the humerus, ulna and metacarpals) are very robust for an animal of such small stature (c. 200kg; equivalent to the gracile *T. pinchaque*), with shoulder flexor attachment sites comparable to the large modern *T. indicus*. One might conclude that this small, robust and compact tapir possessed a low centre of gravity. With greater mechanical advantage for the shoulder flexors and a carpus indicative of higher loading than similarly sized tapirs from South America or Europe, one might venture so far as to suggest that *T. lundeliusi* was capable of rapid sprinting over short distances. Such adaptations would be beneficial for a small tapir to rapidly reach shelter if pursued by ambush predators, with the robust limb skeleton potentially indicative of a medium sized mammal existing in a cold or cooling environment (e.g. neanderthals; Trinkaus 1997). Another intriguing comparison to make is that between the largest tapirs incorporated in my study. These include the giant Pleistocene 'Megatapirus' (*T.* (*Megatapirus*) *augustus*), the modern Malayan tapir (*T. indicus*) and the extinct North American *T. webbi* from the subtropics of the Miocene and *T. haysii* from the more temperate climes of the Plio–Pleistocene (E. H. Colbert & Hooijer, 1953; de Thoisy et al., 2014; Hulbert, 1995, 2005). *T. indicus* is a large, dense-forest taxon, and *T.* (*M.*) *augustus* has been assumed to be much the same it its ecology (E. H. Colbert & Hooijer, 1953); by contrast, both *T. webbi* (Hulbert, 2005) and *T. haysii* (Perez-Crespo, Arroyo-Cabrales, Morales-Puente, Cienfuegos-Alvarado, & Otero, 2016); this study) are interpreted as more open-habitat taxa, with *T. webbi* even being colloquially known as the "savannah" tapir due to a) the combinations of fauna and flora which coexisted with it, and b) due to its very long limbs. Most interestingly, when size is taken into account, the shapes of many of the limb bones of these large tapirs plot in independent regions of morphospace. For the few bones that were available for comparison, it was evident that *T. indicus* does not resemble its giant Pleistocene cousin

T. (*M.*) *augustus*, at least not in the limb skeleton after correcting for size. In fact, despite being estimated to weigh over half a ton (~620kg), *T.* (*M.*) *augustus* is comparatively gracile in its limb bones, both prior to and after correcting for allometric shape variation, and is more reminiscent of the medium sized *T. bairdii* or *T. veroensis*. This then adds a new angle to the story of modern tapir limb evolution and specialisation – if the largest tapir ever known possessed a limb skeleton which (following allometric correction) is *not* exceptional in its morphology (i.e. centre of morphospace – quite an "average tapir"), why does the Malayan tapir exhibit adaptations indicative of a graviportal taxon? It seems as though size itself is not sufficiently explanatory for the limb condition in *T. indicus*, and therefore one might conclude – tentatively – that there are two highly specialised tapirs living today, with highly disparate morphologies, and no adequate explanation for their limb shape. As this project dealt exclusively with dead animals, incapable of exhibiting natural locomotor behaviour, it feels tantalizingly incomplete by way of functional explanations for the morphologies observed. Moreover, this project would not have been possible to complete without the inclusion of zoo animals in the dataset. Unfortunatley, the literature on the morphological effects of captivity on ungulates (compared to wild animals) is very restricted, with next to no information on postcrania. Reports do exist on living rhinoceros autopodial pathologies, which are widespread in captive rhinoceroses (Galateanu et al., 2013). Unfortunately, this study did not compare wild and captive populations; when a limited number of museum specimens of wild rhinoceroses (n = 4) were compared to captive specimens (n = 13), no specific differences were observed in autopodial pathology (Regnault, Hermes, Hildebrandt, Hutchinson, & Weller, 2014). The effect of captivity (if there is one) on tapir skeletal anatomy could be tested using a similar technique to that employed in Research Chapters 1 and 2. Focusing on a single species with numerous specimens in museums (i.e. *T. indicus* or *T. terrestris*), and using discriminant analyses in an attempt to discern zoo and wild populations, may provide evidence that captivity does indeed increase shape variability in tapir postcrania. However, to gather reliable data on kinematics of locomotion in tapirs (and other rare species) in a repeatable manner, zoo populations are essential; this may be all the more reason to pursue investigations into morphological differences between captive and wild populations. Several researchers have tried to extract experimental data from extant tapirs in captive conditions, with mixed success (e.g. Nauwelaerts et al. 2016). To achieve a level of closure which this thesis does not necessarily provide, I would be thrilled to learn about (or contribute to the completion of) studies investigating tapir locomotor kinematics, loading patterns or general locomotor behaviour using non-invasive experimental techniques (e.g. force/pressure measurements, live X-ray imaging) or digital simulations (e.g. musculoskeletal modelling).

Back on topic, it became clear that, due to the large degree of variation in the forelimb of modern *Tapirus* quantified in Research Chapters 1–4, comparisons with extinct, non-*Tapirus* species would be challenging (to put it mildly). As anticipated, expanding the comparative dataset to non-*Tapirus* perissodactyls with the specific aim of assessing the validity of *Tapirus* as a locomotor analogue for extinct European equoids (palaeotheres), yielded mixed results (Research Chapter 5). Does the forelimb morphology of either *Palaeotherium magnum* or *Pa. crassum* closely resemble that of modern tapirs, as suggested by George Cuvier? Yes. And no. The difficulty with assigning a single morphological analogue in this particular case is, ironically, the variation which was observed in modern tapir forelimbs in Research Chapters 1 and 2. Overall however, it must be conceded that the morphological variation within the forelimbs of the genus *Palaeotherium* is so vast that the assignment of one single modern genus as a locomotor analogue was always an uphill struggle (Research Chapter 5; see Discussion). The highly gracile metapodials and radioulnae of *Pa. medium*, for example, exhibit no gross similarity to *Tapirus* except in the shape of the joint facets. It was this similarity in articular surface morphology that was taken forward and explored on a much greater taxonomic extent in Research Chapter 6. The similarities in fetlock joint shape between palaeotheres and tapirs hinted at in Research Chapter 5 offered a quantitative blue-print of a forest-dwelling metacarpal head and semi-mobile central digit (in adduction and abduction) (Sondaar, 1968, 1969). By generating an estimated ancestral fetlock morphology representing the last common ancestor of tapirs and equoids, the morphological transition within a single functional unit was assessed through equid evolution. Critically, the tapir fetlock exhibited no significant differences in fetlock morphospace occupation when compared to palaeothere and early equid fetlock shapes – in this particular feature of the forelimb, the tapir could almost be considered a 'living fossil'! Much of the variation in the equid fetlock aligned with previous morphometric assessments (e.g. Eisenmann and Karchoud 1982; Eisenmann and Beckouche 1986; Eisenmann 1995; Scott et al. 2003, 2014). However, as many of these previous studies utilised measurements in biplot comparisons or as phylogenetic characters, the aim of my final chapter was achieved by providing the additional aspect of comparative locomotor functionality to an already well established morphological variation.

Function of four-fingered forelimb

Although this thesis was not testing specific biomechanical questions about tapir forelimb use or the transition from tetradactyly to monodactyly within equids, it was

always the intention to place the comparative morphological results attained from geometric morphometrics into a functional context where possible. The undertaking and results of Research Chapter 3 went a long way towards informing conclusions on potential functional differences in forelimb proportions, muscle attachment sites, and potential differential movement at joints. For example, prior to the results of Research Chapter 3, literature searching for the function of the palmar 'volar processes' of the carpus in tapiromorphs lead to only speculatory conclusions which implied that they functioned as sites for ligamentous attachment to stiffen the manus in extension (Gregory, 1929; Yalden, 1971). After investigation through quantitative dissection (Research Chapter 3), it was revealed that the volar process of the magnum was the site of origination for the superficial digital interossei – muscles intricately involved with the adduction, abduction and flexion of the lateral and medial phalanges (Barone, 2000). With this knowledge, functional inferences could be made regarding digit employment during locomotion, based on the shape of the volar processes (Research Chapters 2, 5 and 6). This finding suggests that tetradactyl perissodactyls (including members of the Tapiridae, Palaeotheriidae and Equidae) all exhibit elongate volar processes of the magnum, offering improved mechanical advantage for the lateral fifth digit. Moreover, a knowledge of the function of the volar process in tetradactyl species allows the inference of digit condition from isolated fossilised carpals (ideal for estimating functionality of the lateral toe in tetradactyl species).

Research Chapters 1, 2 and 3 combined to provide a great deal of comparative osteological information with the additional benefit of a quantitative myological assessment occurring alongside. Knowing where the muscles of the tetradactyl forelimb attach, and how the proportion of muscle mass is differentiated between tetradactyl and monodactyl limbs not only informed functional inferences in this work, but it is hoped that it will provide a great deal of insight for the further investigation of perissodactyl locomotion beyond just the equid limb transition. Examples of functional hypotheses which have emerged from this thesis, and can be tested with a more experimental approach in the future, include:

1) *Variation in lateral digit recruitment (terrestrial)*: the Central American tapir (*Tapirus bairdii*) will not utilise its lateral fifth digit as much during locomotion as other extant tapirs.

2) *Differences in tapir stride frequency:* the mountain tapir (*Tapirus pinchaque*) will trot and gallop with higher stride frequency than exhibited by other modern tapir species.

3) *Digit interaction with compliant substrate through evolution:* as and when a researcher generates a musculoskeletal model to investigate the tetradactyl to tridactly transition in the equoid manus, the morphology and placement of the superficial and deep interossei will dictate how successfully the limb interacts with a compliant substrate.

4) *Variation in lateral digit recruitment (aquatic):* given the limited adduction/abduction of the lateral digit during the power and recovery strokes of swimming *Tapirus terrestris* (Endo et al. 2019), I would predict that the lateral digit of T. indicus is capable of a greater angle of adduction/abduction, and consequently may be able to displace a greater amount of water during forelimb-powered swimming.

Assigning functional analogues to long extinct taxa with no living descendants is no easy task. In this thesis I have demonstrated morphological similarities in the locomotor apparatus of tapirs and some *Palaeotherium* spp., and inferred behavioural equivalents between some tapirs and lophiodontids (Research Chapter 5). However, sometimes it is possible that there are no functional analogues that can be investigated in an experimental context, and no validation for speculation based on osteology. Sometimes extinct animals are just too weird – where would one start to validate locomotion in a chalicothere, for example? All that being said, the burgeoning field of musculoskeletal modelling is being applied to investigate locomotion in all manner of different species, both modern (e.g. ostrich, Hutchinson et al. 2015; echidna, Regnault and Pierce 2018, etc.) and extinct (e.g. non-avian dinosaurs, Hutchinson et al. 2005; stem-tetrapods, Pierce et al. 2012). It is likely only a matter of time (and funding) before the transition from tetradactyl forest-dwelling 'hyracothere' to monodactyl champion racehorse finds itself under investigation in a virtual modelling environment. This way, morphological variation and functional inferences can be tested, and more theories we hold as gospel can be rigorously examined.

Challenging the tapir *status quo*

Prior to the culmination of Research Chapter 1, it became clear that several concepts which have pervaded the literature regarding tapir osteology were likely to be incorrect. To put these concepts into better context, it is important to understand the limitations of the analyses within which these statements were made. I will begin with the scaling concept put forward by Radinsky (1965*a*) in his comparison of *Tapirus* with *Heptodon* (Perissodactyla: Helaletidae). Radinsky was undertaking a very specific comparison in this study – that of one genus with another to establish what features changed through the evolution of the tapiroid bauplan. The fickleness of the fossil record does not always

allow for multiple examples of an extinct taxon to be compared, or to assess intraspecific variation – this is often a privilege only afforded to researchers who investigate modern taxa. Radinsky (1965*a*) was able to acquire a comparative sample of *Tapirus pinchaque* for his comparison with a single, if rather beautifully preserved, specimen of *Heptodon.* Several of the tapir specimens he observed I was able to include within my study as well, with which I demonstrated that – far from being the least specialised tapir – *T. pinchaque* is most unlike any other tapir from the Americas, and even further removed from the modern Malayan tapir (*T. indicus*) or the extinct giant tapir from China (*T.* (*Megatapirus*) *augustus*). It is my belief that Radinsky was correct in his surmise that between the early Eocene *Heptodon* and the extant Holocene *T. pinchaque*, the effect of body size cannot be understated when investigating changes in postcranial morphology. However, it is also my hope that with the results of Research Chapter 4 of my thesis, the genus *Tapirus* will not be considered as possessing a monomorphic postcranial skeleton. Rather, I believe this is a clade which has persisted at low population densities, specialising their postcranial skeleton (sometimes rapidly; e.g. *T. pinchaque*, Ruiz-García et al. 2016) to facilitate effective locomotion in their respective habitats (González-Maya et al., 2012; Hulbert, 2005, 2010; Momin Khan, 1997; Padilla & Dowler, 1994; Padilla et al., 2010).

Secondly, I will briefly touch on the concept of 'living fossils'. Tapirs have famously been considered as 'living fossils' due to their suite of characteristics plesiomorphic for perissodactyls (tetradactyl forelimb, brachydont dentition, rainforest habitat etc.) (Janis 1984; Rustioni and Mazza 2001, among others). When we examine the origins of the term, 'living fossils' was initially introduced in Darwin's "On the Origin of Species", where he states:

"[remarking on the biology of the lungfish *Lepidosiren*] *These anomalous forms may almost be called living fossils; they have endured to the present day, from having inhabited a confined area, and from having thus been exposed to less severe competition*"

Charles Darwin – *On the Origin of Species* (1859)

At the inception of this project, it was my firm belief that tapirs were indeed an anatomical relic of a bygone epoch – a peculiar amalgam of plesiomorphic traits from a time the world forgot. The first presentation I gave as a PhD student utilised 'living fossil' in the title, and at that point I believed it. In recent years, the term 'living fossil' has been put under intense scrutiny for its use in describing species with cult status as plesiomorphic in their anatomy and behaviour, such as the tuatara *Sphenodon* (Herrera-

Flores, Stubbs, & Benton, 2017, 2019; Meloro & Jones, 2012) and the coelacanth *Latimeria* (Casane & Laurenti, 2013; Naville, Chalopin, Casane, Laurenti, & Volff, 2015). If we consider the description of living fossils by Darwin (1859), tapirs do not seem to fit in particularly well. Tapirs as recently as the Last Great Ice Age are known to have ranged from China to North America, across Europe and South America. At present, despite notable habitat loss (de Thoisy et al., 2014), their range remains impressive, with three (or possibly four; Cozzuol et al. 2013) species in the neotropics and the Malayan tapir in fragmented primary rainforest of South East Asia. Modern lowland tapirs have been known to roam in rainforest and open floodplain, and mountain tapirs inhabit both upland wet grassland and tropical cloud-forest (Padilla and Dowler 1994; Padilla et al. 2010). Add to that fossils of *T. veroensis* proximate to the glacial front during the Pleistocene ice age (Czaplewski et al. 2002), it is fair to say that tapirs may not truly be confined to the moist rainforest they are so often associated with. If we consider morphometric criteria put forward by Herrera-Flores et al. (2017), living fossils are expected to exhibit 'conservative occupation of morphospace'. To this point, I can certainly agree that the fetlock joint of *Tapirus* is indicative of a 'living fossil'. However, from a recent assessment of tapirs and tapiroids, it is clear that modern tapirs have not remained morphologically conserved in their crania at all (Dumbá et al., 2018). My study also suggests that modern tapirs (most particularly *T. indicus* and *T. pinchaque*) occupy regions of morphospace far removed from the average tapir form (see results of Research Chapters 4, 5 and 6). In conclusion, it is my revised opinion that rather than being 'living fossils', it seems more likely that *Tapirus* have existed at low numerical and taxonomic densities within tropical, subtropical and temperate biomes since the early Miocene, rather than being the last few of a dynamic and explosive radiation…if that were to be the definition of a 'living fossil', then our gaze should shift toward *Equus* rather than *Tapirus*!

Looking Back, and to the Future

As, I suspect, with all doctoral projects, there have been times and opportunities within this project where the scope of possible research has drifted along side-projects or bolted down academic rabbit-holes, often finding new and exciting avenues of study just over the horizon. As a final word on the research scope of this project, I will touch briefly on a few side-projects which have come from it, and where they may lead me (or others) in the near future.

Mystery tapir identification – using postcrania and discriminant function analysis

During my initial forays into the museums of Western Europe, I found several skeletons of tapirs which were not identified to species level. This was likely because no one had looked at the boxes for many years, or possibly due to there being no cranium associated with the skeleton. Part of onus my first two research chapters was to generate a training set of discriminatory characteristics which defined each modern species of tapir, enabling the measurement of a few bones in an unidentified skeleton to provide an accurate species level determination. The aim was to test the ability of discriminant function results from Research Chapter 1 and 2 to predict the species of the specimen in question, while a genetic assessment on DNA from bone-cores would be conducted to ascertain the true species using a molecular framework.

It was hoped that the discriminant function results would be sufficiently accurate to be disseminated to museums with unidentified tapir skeletons as a tool for the curators to use for updating their collection information. As I write this thesis, the molecular aspect of the project remains incomplete. It is my hope that, after further training of the discriminant functions on new, *a priori* identified specimens of all four species, someone will be able to sequence the DNA from the mystery tapirs and accurately identify the unknown tapir specimens both using morphometric and molecular tools.

Equid metacarpal discrimination and postcranial landmark error

During the initial stages of this project, I partook in a study lead by UAntwerpen masters student Hester Hanegraef which focussed on the sources of error in landmark placement on perissodactyl postcrania (humerus, metacarpal, trapezoid and sesamoid). To my knowledge, this remains the first study of its kind (i.e. landmark error focussing exclusively on postcranial elements). From this study, several very interesting results came out. Firstly, the error analysis revealed both inter- and intra-observer precision in landmark placement were comparable with those from published craniodental landmark error studies. Furthermore the results are very promising for researchers who compile multiple datasets from different observers. Secondly, the use of different scanners to collect scan data for landmarking did not greatly affect the resultant landmark placement per observer – also good for researchers collecting 3D scanned postcranial material from multiple sources. Finally, and perhaps most interestingly from a biological viewpoint, a comparison of inter-specific differences and intra-observer variability suggests a) the variability within landmark placements by an observer is lower than interspecific variability (good!), and b) that landmark based geometric morphometrics can separate taxa within modern equids into broad phylogenetic groups (caballines, zebras, Asiatic

asses, and African asses), but cannot differentiate between species-level shapes within the groups. This is a perfect study to be expanded upon with the inclusion of more specimens and observers, and may have implications for the broad phylogenetic identification of palaeotaxa based on individual postcranial bones.

(based on: "H. Hanegraef (2015) Validating the use of geometric morphometrics: a case study on the forelimb anatomy of Perissodactyla. *Masters Project* [supervisors: J.A. MacLaren, S. Nauwelaerts])

Scapular Fossa Ratios as ecomorphological tools in equid evolution

Initially seen as a means to graphically illustrate how truly odd the mountain tapir (*Tapirus pinchaque*) is in its scapula morphology, the scapular fossa ratio (or SFR) has continued to throw up some very intresting findings, beyond just the differences between tapir species. The SFR describes a ratio between the two deep lateral fossae of the scapula, and is defined as the three-dimensional area of the supraspinous fossa divided by the total fossa area (supraspinous + infraspinous). This essentially quantifies the relative attachment areas of the deep lateral shoulder muscles – *supraspinatus* and *infraspinatus* – both of which are used for shoulder stability, although the *supraspinatus* also has a role in limb extension. From this simple ratio, several very interesting findings have come out which were not able to fit comfortably into the commentary of the project, but remain ripe for future investigation. For example, my student and I have shown that through equid evolution the SFR changes quite dramatically from tetradactyl to tridactyl species, and that tridactyl equids of comparable size to modern monodactyl equids have very different SFRs. This shift may (and I stress, *may*) be correlated with increased distal limb instability with the loss of the lateral fifth toe (tetradactyl tapirs and palaeotheres both have much higher SFRs than tridactyl equids), and as such the infraspinous fossa expanded to provide a larger attachment for the infraspinatus muscle (which acts as a lateral collateral ligament for the shoulder). Of further interest is the fact that monodactyl species have a less expanded infraspinous fossa. At present, it is our hypothesis that the reduced necessity for a large infraspinatus attachment site in monodactyl equids occurred following the evolution of an advanced stay apparatus at the shoulder – a locking mechanism of tendons enabling equids to stand for long periods with relatively low energetic expenditure. We have observed a similar divergence in SFR between dense forest and open-savannah bovids (bongo vs. gnu). I hope that this will be validated (by someone), and the relationship between the SFR and locomotor ecology clarified, and potentially demonstrate the utility of the SFR as a tool for determining habitat preference, digit condition or stay-apparatus advancement through the equid evolutionary transition.

(based on: "K. Van Houtven, J.A. MacLaren. (2018) Evidence of locomotor and ecological analogy between modern cervids and extinct equids demonstrated by scapula fossa ratios. *25th Benelux Congress of Zoology, Antwerp*." and "J.A. MacLaren, S. Nauwelaerts (2016) A novel method to track changes in perissodactyl locomotion: the scapular fossa ratio. *23rd Benelux Congress of Zoology, Antwerp*")

Expansion of these side projects are but two of a multitude of directions that this study could be taken in the future. With the strong, quantitative and functionally-minded base now established for tapir forelimb morphology, options open up for quantification and comparison of other groups of extant and extinct perissodactyl with this established dataset. The geographically and phylogenetically broad dataset of scanned metacarpals which has been developed within this project can only be built upon and improved to enable more investigations into the locomotor apparatus of these bizarre and wonderous ungulates. It is my hope and ambition to remain linked with such studies long into my career as an academic.

A final word – the tapir forelimb in the tale of equid locomotion

Within the final two Research Chapters of my thesis, I was able to investigate how variation in the forelimb elements of *Tapirus* can cast light into the dark shadows remaining to be explored in the morphological transition from forest-dwelling equoids to modern, open-habitat monodactyl equids. After a comprehensive analysis of the upper and lower forelimb elements in Research Chapters 1 and 2, revealing obligate functionality of all digits in *Tapirus indicus* and the potential for rapid shoulder flexion in *T. pinchaque*, a comparison with equids seemed a bridge too far. After all, 'hyracotheres' may exhibit obligate tetradactyly (McHorse et al., 2017; Wood et al., 2011) as *T. indicus* does, but the potential confounding factors of a) scale, b) extinct equid availability, and c) specimen preservation were (and still are) causes for concern when comparing these clades. As established in Research Chapter 1 and 2, tetradactyl perissodactyls are *not* all alike in their locomotor morphology even within the same genus. The decision to isolate comparisons to a single, quantifiable morphological feature with known functionality in modern equids – the fetlock joint – was therefore the only logical approach for comparing these quite disparate groups. The scope of positive and meaningful results that has come from Research Chapter 6 vindicated this decision, highlighting themes which are not always explored in equid evolution, including: 1) the rapid specialisation of the interosseous muscles early in equid evolution forming the blueprint for the spring-foot style of locomotion horses are known for in modern day; 2) far from being crouched at a near 45° angle, late Eocene equids would have stood more upright at the expense of the digital manipulation exhibited by their cousins the palaeotheres; and 3) the effect of disparate endemic faunas on global

variation (e.g. *Palaeotherium* and *Hippidion* spp.), and, more poignantly, the effect that the loss of such endemics may have on the adaptability of a clade.

Being able to examine the equid locomotor transition by barely looking at equids at all has provided me with a unique insight into this radical shift in morphology; I can only hope that the efforts I have made throughout this thesis to utilise modern tetradactyl perissodactyls to offer new explanations for changes in past species can be taken forward in new and exciting ways in the not too distant future.

– ACKNOWLEDGEMENTS –

So, now that you have skipped past my research articles without reading them, pausing to glance at the occasional figure, I would like you to take some time to read about the real heroes of this story. Off the top, I will apologise for the lack of tapir picture for the *Acknowledgements* section. There is only so much glorified colouring-in a student can make time for in the run-up to a doctoral defense.

Anyone who has spent more than five minutes with me has probably worked out I'm never short of a word or two. So strap yourselves in, people – this may take a while…

In no particular order: (*there is totally an order*…)

From the start of my failed Skype interview for the doctoral position at the FunMorph lab, it became abundantly clear that this was not going to be a conventional PhD…at the heart of it was a fundamental clash of styles and experience. There was no conceivable reason why it would work. The fact you are reading this right now is evidence that such clashes need not lead to failure. And for that, **Sandra** needs the highest of acknowledgement. The success we have achieved in spite of our very different styles, thought processes, knowledge bases and ideas for the project is a credit to Sandra as a supervisor; she worked to mould the brash and somewhat irritating past-Me into a researcher who understands *WHY* he is doing something, not just *WHAT* he is doing. This is probably the greatest gift a supervisor can offer to their student, setting them up to work independently and (*with any luck*) to know what they are doing in a terrifying post-doctoral landscape! On top of that, Sandra introduced me to the most enjoyable conference I've every been to (ICVM), and has always been supportive of me taking the project in new and interesting directions – with the caveat that she doesn't have to put up with too many latin names! I feel privileged to have been Sandra's first doctoral student; she has taught me such a lot about being a researcher, and also about being a person. I will carry her teachings with me in all I do – and I thank her so very much for taking me on. Hartelijk bedankt, Sandra!

"Who's the guy with all the dance moves?" "Oh, that's the head of the lab…it's a fun lab". Rolling back the clock to November 2013, **Peter** asks me straight away "do you play a musical instrument?" Immediately, I could tell that this guy had a 'different dynamic' to the professors and academics who I was used to! And I don't think we would have him any other way. Peter has an infectious enthusiasm for everything he does (*with the possible exception of marking exam papers*), and his balance of wonder and wisdom is something that any student under his tutorage should aspire to. While it

is fair to say that Peter took more of a back-seat role in my supervision, he was always there for discussions on ideas and concepts, and his open-door policy and willingness to help is something I will take with me through my career, irrespective of where it takes me. Thank you so much Peter – zie je op de dansvloer!

Alexandra, Chris, Luke, Stefan and **Raoul**: To my IDC and external jury members, I thank you for your time, your insights, your patience, and ultimately your verdict. I believe having such a diverse doctoral jury (in multiple senses of the word) has benefitted the thesis to no end, and for this you have my eternal gratitude. I had fun writing the little monster, and I hope you have enjoyed reading it. Luke & Alexandra – I am especially grateful that you were both willing and able to travel for my defences, and I trust you will enjoy celebrations FunMorph style!

Family: Funmorphidae

Before I say anyone in particular, I want you all to know that each and every one of you has contributed to this thesis, whether you know it or not, and I thank you. I would also like to give special thanks to all those who I have shared offices with – and especially those who have allowed me to play my fairly eclectic music without headphones …(*speaking of which*)…

Gilles and **Diego** – an Englishman, an Argentinian and a Belgian walk into an office (*rarely at the same time*). It's the start to a bad joke. The sort of joke even your dad thinks is a bad joke. Nevertheless, this 'bad joke' has kept me going through the final years of my PhD. The intricate combination of Gilles' tact, my bluntness and Diego's hilarious insights on the Belgian Experience has led to more laughs, lectures and (for want of a better word) "good ideas" than I could ever have dreamt of for my final doctoral years. I feel sorry for most people reading this, because frankly "you had to be there" for most of this stuff – but for what it's worth, these two have contributed to the best years of my life as an academic. So gentlemen, here's to you. Diego, with your continuous whistling of the same nine notes of the Lord of the Rings theme through your teeth, and Gilles, with your sodding grapes, this is not goodbye.

Glenn – Many may be aware of Glenn and I as the Bordeaux Bros (a working title, to be sure, but understandably founded on our mutual ownership of dark red hoodies). If we were indeed bros, I can tell you three things of our siblingship. One, our mother was bipolar and exposed us to very different music during our upbringing. Two, our selection of home videos was catastrophically limited to all titles between the letters "Star" and "Wars". Three. I can't remember three – but it's ok, everyone, because Glenn will look it up on Google. I challenge any lab in the cosmos to fit that much useless yet fascinating information into one (freshly graduated) doctoral student. You're one of a

kind, Glenn – and I look forward to growing old hearing more pointless facts from you, brother.

OK, so I thought I'd go for a slightly different way of mentioning everyone in the FunMorph family. So this is what you get. Deal with it:

Room 1.38 – Residing in what is essentially the FunMorph Living Room/Woonkamer, these three have been such great fun throughout my PhD. **Simon**, your support and assistance with work and leisure have been invaluable. I covet your hair. May you remain a constant source of great amusement, knowledge, common sense, and (of course) smoskes. **Menelia**, your refreshing Mediterranean attitude towards all things has really added an extra dimension to the lab. I will not soon forget your culinary delights, your inspiring artwork, your knowledge of the bars of Antwerp, and your occasional hilarious rants at reviewer comments. **Mariëlle**, so many fun times with the perissodactyl posse, most relating to re-animating dead things and ending the day covered in carcass #phdlife. One of the most social people I have come to know in Antwerp, always up for a laugh and a damn-good baker, my only regret is that we could not have worked closer on perisso-projects. Never say never!

Room 1.39 – I was going to list this as the calm and sensible room, and then I remembered Emina lived here for some time, so I guess that label doesn't quite fit…anywho…**Charlotte**, my good friend, there are few people in my life who can sit patiently watching a guy playing golf without ball or club, talking to himself about some problem with R (*lets face it, it's always a problem with R*), and yet without saying a word you are able to help. It's like magic. Add to that our ever-so-fun squash sessions, Game of Thrones viewings and two-person TGIFs, you have been a great colleague and friend, and I wish you all the very best for the finalisation of your own doctorate. **Jana**, my first room-mate, and an ever-present voice of reason. Your excitement and energy for your work always translates into excellent science and (*dare I say it*) even better Twitter posts! As a permanent member of the lab since my inception (aside from hatching little Linde with her lightsabre), you probably have one of the best perspectives on how I have changed through my doctorate – I would encourage you to keep that opinion to yourself for the good of my academic career! **Chris**, although our time together in the lab has been brief, I immediately sense that we share many interests, and I believe collaborations and Game of Thrones discussions over a bottle or two of excellent South African wine are fixed in our futures! **Emina**, every great lab needs an agent of chaos; a perennial tornado delivering baby pictures and casual violence. Ever since you kicked me in the face at the Christmas party, I knew our friendship was going

to be entertaining – and you can never be accused of not being entertaining! I wish you and Jeroen all the very best in your latest adventure with Achil!

Room 1.40 – On a good day, this room is full of super-knowledgeable post-doc researchers, all of whom will jump to assist with any problems big or small…it is sad to see it empty half the time. **Francois**, my French Connection, you have been such fun to work with in the lab in my final few years. Whether it be your misunderstood musical taste, your delightful edible treats, your unwillingness to give up on a point at squash, or the way you say "baboon" (*don't know why, just love it!*), I will miss you greatly and I wish you all the very best in the future. **Sam**, senior-most of my first generation room-mates! Your guidance with the apparatus I have been using throughout my PhD and your invaluable insights on biomechanics have been so helpful, and your stalwart dedication to one single carbonated beverage throughout my time at the UA should be an inspiration to us all.

Room 2.36 – Despite being a liberal and progressive labgroup, it's fair to say that there are "no girls allowed" in the Boys Room. **Jan** and **Jorrit**, suffice it to say that without you guys I would be one or two chapters short of a thesis – your assistance with logistics is rivalled only by your dedication to the lab as a whole, providing lunchtime food for the needy (= *lazy = me*), endless entertainment, and just great comradery. Every other lab should be envious of the help we have at FunMorph, and I thank you so much for all yours during my time here. **Raf**, pretty much the first non-supervisor I spoke to at any length during my PhD! It has been a pleasure to see you conduct your masters and PhD studies in FunMorph, finalising both before either Glenn or I had defended our PhDs…that should give anyone an impression of the work this guy puts in. Most importantly, Raf taught me that zebras are [*insert expletive here*], reaffirming the old adage of "never work with children or animals". **Alex**, not sure you've been here long enough to earn a spot in the *Acknowledgements*…

…oh ok, go one then. Your brief time here has been ever so exciting – the laser scanner has not seen this much action since Florida 2017! As with all visiting researchers, I am certain your time here will be too brief, and I sincerely hope you enjoy yourself here sufficiently to want to return to continue your career. All the best fella.

Room 1.36 – Whoever you are reading this (*yeah, YOU!*), if a lab group tells you that their secretariat is the best, kindly inform them that they do not have a sufficient sample size, and are likely to be incorrect – if they need proof, then they should ask anyone from FunMorph / BECO to point them toward Room 1.36, the Boss Room (*Legend of Zelda reference*). **Josie**, The Boss (*capital T, capital B*), my source of tuck-shop

chocolates, my first port of call for issues, and the keeper of the keys to unlock everyone's potential. It has been too much fun to be able to wander into your office and be my miserable self, and then leave some minutes later much happier (*probably with a Kit-Kat and some coloured paper*). Your ability to make sure that everyone in the lab(s) have the funds they need to conduct their PhD to the best of their ability is an invaluable skill, and one which I am sure to miss in future endevours. I am glad to have been able to share the lab with you, and I wish you all the very best for the future.

Superfamily: Funmorphoidea (*all members of Funmorph + random adoptees*)

Honestly, this time there is no particular order. **Nolwenn**, too much fun has been had between us to sum it up in a sentence or two – all I will say is that you have been an inspiration for me to keep going, never give up and never give in, and the rewards will sort themselves out. You have yours, and I hope you continue to enjoy great success. Your ability to mimic a lemming falling off a cliff with your laughter is frankly disturbing, and yet brings such joy to hear it. Santé, mon ami. **Lotte** and **Lisa** (and **Krijn** and **Diana**), for dragging me kicking and screaming out of my comfort zone of Wilrijk and into town on more than several occasions, I thank you all. My social diability has been at least partially relieved thanks to you all, and no words can adequately sum up how much that has meant over the years – so I'll keep it simple: cheers! **Maaike**, from our first conversation across the table discussing whether Glenn or Marwa would eat "all of the ribs", I knew ours would be a great friendship. Whether it be chilling with wine and horror-films, or just being there as a colleague and friend during times of great PhD strife, I thank you and wish you all the very best for the completion of yours! **Alexia**, **Arne**, **Bert**, **Gerardo**, **Laura**, **Manrico**, **Marwa**, **Natalie**, **Simone**, **Stijn**, and everyone else I've not named – so many happy memories in and out of the lab have come about and you have been part of them. You all have my thanks for making this strange and peculiar city my home-from-home, a home I will be reluctant to leave and in a hurry to return to!

Some special mentions now. Several are obvious. Some are not. They all matter.

Hester, **Eleni**, **Wouter**, **Paul** and **Karianne**, my students (one way or another), my minions, my helpers in many things. Without your scanning assistance, model reconstructions, and willingness to wander off in museums to find fun things to scan, my project would be so much the poorer. Should you choose to continue, I look forward to following your careers in academia in the future. Thank you all so very much.

Dr. Júlia Arias-Martorell, for the timely donation of a full version of GeoMagic (*with all the bells and whistles*). Without Julia, I would not have been able to record even half

the amount of scans that I have done for my PhD, and that deserves no small acknowledgement – thank you so much Júlia!

Dr. Chris Basu and **Prof. John Hutchinson**, the tag-team who inadvertently lead me to the Universieit Antwerpen in the first place! Chris was the successful applicant who received a doctoral position ahead of me at another university; John was the one who broke this news to me, and then directed me toward another project that was looking for applicants like me, sending me the email address of someone called Dr. Sandra Nauwelaerts…

Dr. Mark Jervis, my Bachelor's thesis supervisor. Mark was a wonderful, sarcastic and smiling fellow, who always gave us handouts the size of a small encyclopedia, and then proceeded to tell us the questions he would set on the exam. He was also the only researcher at Cardiff University in my year who was looking into aspects of vertebrate palaeontology and evolution. Without Mark allowing me to pursue a project on vertebrate evolution (*cetaceans, if anyone was wondering*), I would not have come across geometric morphometrics as a method for quantifying fossil and extant morphology. I may never have then gone on to use GM in my Master's, and ultimately my journey to Antwerp may never have been paved. The late, great Mark Jervis laid the first academic cobble on the street to where I am now. Thanks Mark.

Un-named Tutor, my Bachelor's individual tutor. I don't want to name names in this instance – but the story is important enough to warrant telling, and I am indebted to this person. After my second-year exam results, I suggested to this person that I would like to pursue a career in academia, and maybe do a follow-up degree after my BSc. "*You don't have the grades, and you can't just carry on being a student forever*". You can probably imagine how that went down in my stubborn little head – actually, I'm a bit of a softie, so it hurt like hell. From then I set out to prove to myself that if I want something enough, and I love doing it, I can learn more and more about it every day. And yeah, I ***can*** be a student forever…just like everyone else.

As both Gilles and Diego (*and Mariëlle, and Sandra…*) can testify to, I play my music quite loud. For this, I apologise here and now. Irrespective of volume, there is one piece of music which has influenced me through my PhD more so than any other. It is no exaggeration to say that more than half of my research chapters were written to this albumn. And I suspect two thirds of the people reading this will never have heard of it. But, as it has been such an enormous part of my life for the past five years, it would be remiss of me to not acknowledge the genius of **Hans Zimmer** and his soundtrack to the film *Man of Steel*. Listening to it, you might even believe that a man can fly…

Back to thanks of a more academic nature, there are a great number of people to thank from institutions which I have visited / collaborated with. Therefore, I extend thanks to:

AMNH; Eleanor Hoeger, Jin Meng, Ruth O'Leary (*American Museum of Natural History*).

ETSU / GFS; Chris Widga, Steve "Wally" Wallace (*East Tennessee State University and General Shale Museum at Gray Fossil Site*).

FLMNH / UF; Richard Hulbert Jr., Bruce MacFadden, Jeanette Pirlo, Natasha Vitek, Lauren Gonzalez, Paul Morse, Sean Moran, Sharon Holte, John Bloch (*Florida Museum of Natural History*).

GMH; Michael Stache, Frank Steinheimer, Oliver Wings (*Geiseltalmuseum Halle*).

KMDA, Francis Vercammen and all Antwerp Zoo and Planckendael staff (*Koninklijke Maatschappij voor Dierkunde van Antwerpen*).

MCZ; Brianna McHorse, Stephanie Pierce, Jessica Cundiff (*Harvard Museum of Comparative Zoology*).

MEO; Luc Tyteca and Leentje Vandenhoudt (*MuseOs Natuurhistorisch Museum*).

MfN / ZMB MAM; Christiane Funk, Stefan Bock, Thomas Schossleitner, Frieder Meyer (*Museum für Naturkunde Berlin*).

MNHN; Guillaume Billet, Josephine Lesur, Alexandra Houssaye, Christophe Mallet (*Museum National d'Histoire Naturelle*).

MVZ; Chris Conroy, Marisa Fong (*Museum of Vertebrate Zoology*)

NHMUK; Pip Brewer, Roula Pappa, Jerry Hooker (*British Museum of Natural History*)

NHMW; Frank Zachos (*Naturhistoriches Museum Wien*).

NMS; Andrew Kitchener (*National Museums of Scotland*).

OMNH; Nick Czaplewski (*Sam Noble Museum* / *Oklahoma Museum of Natural History*).

RBINS; Thierry Smith, Annelise Folie, Terry Walschaerts, Sebastian Bruaux, Olivier Pauwels (*Royal Belgian Institute for Natural Sciences*).

RMCA; Wim Wendelen, Emmanuel Gilissen (*Royal Museum of Central Africa*).

RMNH; Pepijn Kamminga, Steven Van der Mije, Marianne Fokkens (*Naturalis Biodiversity Center*).

SMNK; Eberhard "Dino" Frey (*Staatliches Museum für Naturkunde Karlsruhe)*

UCBL / FSL; Emmanuel Robert (*Université Claude Bernard Lyon-1*)

I also extend thanks to researchers who have provided me with raw data or offered helpful discussions regarding their own work: Larisa De Santis, Luke Holbrook, Jerry Hooker, Christophe Mallet, Bruce MacFadden, Brianna McHorse, Aaron Wood

Last, and by no means least, the people closest to me.

Carol, **Dan**, **Pete**, **Judy** and **Ceal** – you have always been so supportive of the work I have been doing, without me necessarily explaining it particularly well! Your help, well-wishes and enthusiasm to learn what I am up to have been inspiring, and I thank you all so much for it. I'm sorry none of you could make the defense, but I know you were here in spirit…non-alcoholic spirit, that is…

Heleen – you came into my life during the calm before the storm, and yet you have risen to the occasion as the metaphorical hurricane made landfall. You have kept a cool head when I've been stressed, offering me opportunities to get away from it all and relax precisely when I needed it most. Your constant support in this has spurred me on to make the very best version of this thesis I can, and in turn become the very best version of myself. You and your family have been amazing, especially these past months, and I hope that I can repay your patience with a lot more quality time now the storm has passed. I cannot thank you enough. Love you.

Mum and **Dad** – when I told you both I had been offered the position here in Antwerp, it seemed as though you couldn't wait to get me out of the house! Ironically, for that I cannot thank you enough. I would have just made a mess if I had stayed at home much longer. I am so glad you ejected me from my comfort zone to live in a foreign country – something which might have been a good idea for 51.8% of the voting public a few years ago… (…*yeah, that's right, I went there*)

Ultimately, I know you just wanted me to come here so you had an excuse to visit and eat chocolate while I was at work! Whatever your reasons, thank you so much for supporting my decision. I love what I do, and I think I'm kinda good at it, and I wouldn't have had the opportunity to find that out without you nudging me out the door.

Love you.

– LAYMANS GLOSSARY –

allometry	the relationship between size and shape, anatomy, physiology or behaviour; an **allometric scaling** relationship is any change that deviates from isometry, wherein proportional changes are preserved
artiodactyl	an even-toed hooved mammal withing the order Artiodactyla (now recombined as Cetartiodactyla to include whales); examples include cows, goats, pigs, hippos, giraffes, camels
browser	a browsing animal (herbivore) is considered to acquire its food predominantly from trees or bushes rather than from grass (**grazer**); food may include leaves, fruits, twigs etc.
carpal	wrist bones; a '**carpal complex**' refers to the intricate combination of ligaments and bones in the wrist.
centroid	mathematical term for the geometric centre of an object
clade	a group of organisms believed to comprise all the evolutionary descendants of a common ancestor
covariation	correlated variation; the degree of relationship between two variables which vary together over a period
craniocaudal	anatomy: description of a direction from (or between) the cranial (head) and caudal (tail) regions
cursorial	having limbs (legs) adapted for running
digitigrade	anatomy: (of a mammal) walking on its toes and not touching the ground with its palm (front leg) or heel (back leg)
dorsoventral	anatomy: description of a direction from (or between) the dorsal (upper) and ventral (lower) regions; dorsal usually the back of a quadruped (e.g. tapir), and ventral is the belly.
geometric morphometrics	a method for analysing shape using the geometric coordinates rather than linear, area or volumetric variables
graviportal	having limbs adapted only for moving slowly, usually associated with animals bearing large mass (e.g. elephants).

isometry	proportional relationship between two attibutes; an **isometric scaling** relationship suggests that the proportions of an object remain constant at different sizes.
linear morphometrics	a method for analysing shape using linear, area or volumetric variables rather than geometric coordinates
log-transformation	a method for transforming skewed data to approximately conform to normality; multiplication of data values by log (base 10) or natural logarithm are most common
macroevolution	major evolutionary change, often referring to the evolution of a whole group of organisms over long periods of time
mediolateral	anatomy: description of a direction from (or between) the inside (medial) and outer (lateral) regions
mediportal	a poorly described definition of animals having limbs that are neither cursorial nor graviportal
megafauna	in basic terms, "large animals"; more specifically, often termed as animals exceeding 1000kg
meridioungulate	extinct group of hooved mammals native to South America, with currently unresolved phylogenetic relationships to other hooved mammals (e.g. **perissodactyls / artiodactyls**)
metacarpals	the 'hand bones'; metacarpals form the palm in the human hand, with phalanges associated with each metacarpal
metapodial	collective term for **metacarpals** (front leg) and **metatarsals** (hind leg)
morphofunctional	relating to the interaction of form and function of a system (e.g. the musculoskeletal system)
osteological	relating to bones
parasagittal	in line with the sagittal plane – the long axis of the body
perissodactyl	odd-toed hooved mammals; members include horses, rhinos and tapirs, which have an odd number of toes on the *hind* leg
phylogenetics	the study of the evolutionary history and relationships among individuals or groups of organisms

postcranial	(of a quadrupedal animal) relating to parts of the body behind the head; (of bipedal animal) relating to parts of the body below the head
proximodistal	anatomy: description of a direction from (or between) the proximal (closer) and distal (further away) regions, relative to the main trunk of the body (torso)
rotational inertia	a quantity which determines the rotational equivalent of force (torque) needed for a desired acceleration around a rotational axis
sister taxa	closest phylogenetic relative within a clade; for example, chimpanzees (genus *Pan*) are the sister taxa to humans (genus *Homo*)
substrate	an underlying substance or layer
superimposition	the act of superimposing two (or more) objects on top of one another
systematics	in biology, systematics is the study of the diversification of living forms, both past and present, and the relationships among living things through time
taphonomy	a branch of palaeontology concerned with the processes of fossilisation; how organisms decay and become fossilised.
telescoping	(of limbs) the elongating of limb bones without a notable corresponding increase in radius or circumference
terminal taxa	the organism at the tip of a branch on a phylogenetic tree
unguligrade	anatomy: (of a mammal) walking on its toe-nails/hooves and not touching the ground with its digits, palm or heel
vicariance	the geographical separation of a population, typically by a physical barrier such as a mountain range or river, resulting in a pair of closely related species

“what we do in life echoes in eternity”

- Maximus -

– BIBLIOGRAPHY –

Acuña, F., Sidorkewicj, N. S., Popp, A. I., & Casanave, E. B. (2017). A geometric morphometric study of sex differences in the scapula, humerus and ulna of *Chaetophractus villosus* (Xenarthra, Dasypodidae). *Iheringia. Série Zoologia*, *107*, 1–12.

Adams, D. C., Rohlf, F. J., & Slice, D. E. (2004). Geometric morphometrics: Ten years of progress following the 'revolution.' *Italian Journal of Zoology*, *71*, 5–16.

Adams, W. H. D., & Meunier, V. (1872). The Pachydermata. In W. H. D. Adams & V. Meunier (Eds.), *Life in the Primeval World* (pp. 107–142). New York: T. Nelson & Sons.

Agustí, J., & Anton, M. (2004a). The Eocene: Reaching the Climax. In *Mammoths, Sabertooths, and Hominids: 65 Million Years of Mammalian Evolution in Europe* (pp. 23–66). New York: Columbia University Press.

Agustí, J., & Anton, M. (2004b). The Late Miocene: The Beginning of the Crisis. In *Mammoths, Sabertooths, and Hominids: 65 Million Years of Mammalian Evolution in Europe* (pp. 151–210). New York: Columbia University Press.

Agustí, J., Cabrera, L., & Garcés, M. (2013). The Vallesian Mammal Turnover: a Late Miocene record of decoupled land-ocean evolution. *Geobios*, *46*, 151–157.

Alberdi, M. T., Cartelle, C., & Prado, J. L. (2003). El registro Pleistoceno de *Equus* (*Amerhippus*) e <i>Hippidion</> (Mammalia , Perissodactyla) de Brasil: consideraciones paleoecológicas y biogeográficas. *Ameghiniana*, *40*, 173–196.

Alberdi, M. T., & Rodriguez, J. (2012). Anchitherium Meyer, 1844 (Perissodactyla, Equidae) de Sansan. In S. Peigné & S. Sen (Eds.), *Mammiferes de Sansan* (pp. 487–533). Paris: Publication Scientifiques du Museum.

Alexander, R. M., & Pond, C. M. (1992). Locomotion and bone strength of the white rhinoceros, *Ceratotherium simum*. *Journal of Zoology*, *227*, 63–69.

Alrtib, A. M., Philip, C. J., Abdunnabi, A. H., & Davies, H. M. S. (2013). Morphometrical study of bony elements of the forelimb fetlock joints in horses. *Anatomia, Histologia, Embryologia*, *42*, 9–20.

Anagnostou, E., John, E. H., Edgar, K. M., Foster, G. L., Ridgwell, A., Inglis, G. N., … Pearson, P. N. (2016). Changing atmospheric CO2 concentration was the primary driver of early Cenozoic climate. *Nature*, *533*, 380–384.

Anderson, M. J. (2001). A new method for non-parametric multivariate analysis of variance. *Austral Ecology*, *26*, 32–46.

Anderson, P. S. L., Friedman, M., Brazeau, M. D., & Rayfield, E. J. (2011). Initial radiation of jaws demonstrated stability despite faunal and environmental change. *Nature*, *476*, 206–209.

Anderson, P. S. L., Friedman, M., & Ruta, M. (2013). Late to the table: diversification

of tetrapod mandibular biomechanics lagged behind the evolution of terrestriality. *Integrative and Comparative Biology*, *53*, 197–208.

Andersson, K. (2004). Elbow-joint morphology as a guide to forearm function and foraging behaviour in mammalian carnivores. *Zoological Journal of the Linnean Society*, *142*, 91–104.

Andersson, K., & Werdelin, L. (2003). The evolution of cursorial carnivores in the Tertiary: implications of elbow-joint morphology. *Proceedings of the Royal Society B: Biological Sciences*, *270 Suppl*, S163-5.

Anton, M., Galobart, A., & Turner, A. (2005). Co-existence of scimitar-toothed cats, lions and hominins in the European Pleistocene. Implications of the post-cranial anatomy of *Homotherium latidens* (Owen) for comparative palaeoecology. *Quaternary Science Reviews*, *24*, 1287–1301.

Argot, C. (2013). Postcranial analysis of a carnivoran-like archaic ungulate: the case of *Arctocyon primaevus* (Arctocyonidae, Mammalia) from the Late Paleocene of France. *Journal of Mammalian Evolution*, *20*, 83–114.

Arias-Martorell, J., Potau, J. M., Bello-Hellegouarch, G., Pastor, J. F., & Pérez-Pérez, A. (2012). 3D geometric morphometric analysis of the proximal epiphysis of the hominoid humerus. *Journal of Anatomy*, *221*, 394–405.

Arruda, A. F. D. P., Muzzi, L. A. L., Lacreta Junior, A. C. C., Muzzi, R. A. L., Sampaio, G. R., Moreira, S. H., & Mesquita, L. R. (2018). Radiographic assessment of the proximal tibial angles in dogs and cats with and without cranial cruciate ligament rupture. *Pesquisa Veterinária Brasileira*, *38*, 1190–1195.

Astúa, D. (2009). Evolution of scapula size and shape in didelphid marsupials (Didelphimorphia: Didelphidae). *Evolution; International Journal of Organic Evolution*, *63*, 2438–2456.

Back, W., Schamhardt, H. C., Savelberg, H. H. C. M., Bogert, A. J., Bruin, G., Hartman, W., & Barneveld, A. (1995). How the horse moves: 1. Significance of graphical representations of equine forelimb kinematics. *Equine Veterinary Journal*, *27*, 31–38.

Bacon, C. D., Silvestro, D., Jaramillo, C., Smith, B. T., Chakrabarty, P., & Antonelli, A. (2015). Biological evidence supports an early and complex emergence of the Isthmus of Panama. *Proceedings of the National Academy of Sciences of the United States of America*, *112*, 6110–6115.

Badiola, A., Checa, L., Cuesta, M.-Á., Quer, R., Hooker, J. J., & Astibia, H. (2009). The role of new Iberian finds in understanding European Eocene mammalian paleobiogeography. *Geologica Acta*, *7*, 243–258.

Badiola, A., & Cuesta, M.-Á. (2008). New endemic Eocene equoids from the Iberian Peninsula (western Europe). *Journal of Vertebrate Paleontology*, *28*, 1149–1161.

Bai, B. (2017). Eocene Pachynolophinae (Perissodactyla, Palaeotheriidae) from China, and their palaeobiogeographical implications. *Palaeontology*, *60*, 837–852.

Bai, B., Meng, J., Wang, Y.-Q., Wang, H.-B., & Holbrook, L. T. (2017). Osteology of the middle Eocene ceratomorph Hyrachyus modestus (Mammalia, Perissodactyla). *Bulletin of the American Museum of Natural History*, *413*, 1–70.

Bai, B., Wang, Y.-Q., & Meng, J. (2018a). Postcranial morphology of the Middle Eocene deperetellid *Teleolophus* (Perissodactyla, Tapiroidea) from Shara Murun region of the Erlian Basin, Nei Mongol, China. *Vertebrata Palasiatica*, *56*, 1–27.

Bai, B., Wang, Y.-Q., & Meng, J. (2018b). The divergence and dispersal of early perissodactyls as evidenced by early Eocene equids from Asia. *Communications Biology*, *1*, 115.

Bai, B., Wang, Y., Meng, J., Li, Q., & Jin, X. (2014). New Early Eocene basal tapiromorph from southern China and its phylogenetic implications. *PloS One*, *9*, e110806.

Bales, G. S. (1996). Skull evolution in the rhinocerotidae (Mammalia, Perissodactyla): Cartesian transformations and functional interpretations. *Journal of Mammalian Evolution*, *3*, 261–279.

Bapst, D. W. (2012). paleotree: an R package for paleontological and phylogenetic analyses of evolution. *Methods in Ecology and Evolution*, *3*, 803–807.

Barone, R. (2000). Muscles de la ceinture et du membre thoraciques. In *Anatomie Comparée des Mammiferes Domestique* (Fourth, pp. 719–842). Paris: Editions Vigot.

Bartoli, G., Sarnthein, M., Weinelt, M., Erlenkeuser, H., Garbe-Schönberg, D., & Lea, D. W. (2005). Final closure of Panama and the onset of northern hemisphere glaciation. *Earth and Planetary Science Letters*, *237*, 33–44.

Bassarova, M., Janis, C. M., & Archer, M. (2008). The calcaneum—on the heels of marsupial locomotion. *Journal of Mammalian Evolution*, *16*, 1–23.

Basu, C., Falkingham, P. L., & Hutchinson, J. R. (2016). The extinct, giant giraffid Sivatherium giganteum: skeletal reconstruction and body mass estimation. *Biology Letters*, *12*, 20150940.

Becker, D., Antoine, P.-O., & Maridet, O. (2013). A new genus of Rhinocerotidae (Mammalia, Perissodactyla) from the Oligocene of Europe. *Journal of Systematic Palaeontology*, *11*, 947–972.

Bello-Hellegouarch, G., Potau, J. M., Arias-Martorell, J., Pastor, J. F., & Pérez-Pérez, A. (2013). A comparison of qualitative and quantitative methodological approaches to characterizing the dorsal side of the scapula in Hominoidea and its relationship to locomotion. *International Journal of Primatology*, *34*, 315–336.

Benjamini, Y., & Hochberg, Y. (1995). Controlling the false discovery rate: a practical and powerful approach to multiple testing. *Journal of the Royal Statistical Society. Series B (Methodological)*, 289–300.

Bennett, S. C. (2008). Morphological evolution of the wing of pterosaurs: myology and function. *Zitteliana Reihe B: Abhandlungen Der Bayerischen*

Staatssammlung Fur Palaontologie Und Geologie, 127–141.

Bernardes, C., Sicuro, F. L., Avilla, L. S., & Pinheiro, A. E. P. (2012). Rostral reconstruction of South American hippidiforms (Mammalia, Perissodactyla, Equidae): New anatomical and ecomorphological inferences. *Acta Palaeontologica Polonica*, *58*, 669–678.

Bernor, R. L., Gilbert, H., Semprebon, G. M., Simpson, S., & Semaw, S. (2013). *Eurygnathohippus woldegabrieli*, sp. nov. (Perissodactyla, Mammalia), from the Middle Pliocene of Aramis, Ethiopia. *Journal of Vertebrate Paleontology*, *33*, 1472–1485.

Bernor, R. L., & Kaiser, T. M. (2006). Systematics and paleoecology of the earliest Pliocene equid, *Eurygnathohippus hooijeri* n. sp. from Langebaanweg, South Africa. *Mitteilungen Aus Dem Hamburgischen Zoologischen Museum Und Institut*, *946*, 149–185.

Bernor, R. L., Kaiser, T. M., Nelson, S. V., & Rook, L. (2011). Systematics and paleobiology of *Hippotherium malpassii* n. sp. (Equidae, Mammalia) from the latest Miocene of Baccinello V3 (Tuscany, Italy). *Bollettino Della Societa Paleontologica Italiana*, *50*, 175–208.

Bernor, R. L., Scott, R. S., & Haile-Selassie, Y. (2005). A contribution to the evolutionary history of Ethiopian hipparionine horses (Mammalia, Equidae): morphometric evidence from the postcranial skeleton. *Geodiversitas*, *27*, 133–158.

Biewener, A. A. (2003). *Animal Locomotion*. Oxford: Oxford University Press.

Biewener, A. A. (2005). Biomechanical consequences of scaling. *Journal of Experimental Biology*, *208*, 1665–1676.

Biewener, A. A., & Patek, S. N. (2018a). Movement on land. In *Animal Locomotion* (2nd ed., pp. 61–89). Oxford: Oxford University Press.

Biewener, A. A., & Patek, S. N. (2018b). Physical and Biological Properties and Principles Related to Animal Locomotion. In *Animal Locomotion* (Second, pp. 1–12). Oxford: Oxford University Press.

Biewener, A. A., & Roberts, T. J. (2000). Muscle and tendon contributions to force, work, and elastic energy savings: a comparative perspective. *Excersice and Sport Sciences Reviews*, *28*, 99–107.

Bignon, O., Baylac, M., Vigne, J.-D., & Eisenmann, V. (2005). Geometric morphometrics and the population diversity of Late Glacial horses in Western Europe (*Equus caballus arcelini*): phylogeographic and anthropological implications. *Journal of Archaeological Science*, *32*, 375–391.

Bininda-Emonds, O. R. P. (2004). The evolution of supertrees. *Trends in Ecology & Evolution*, *19*, 315–322.

Blagojević, M., & Aleksić, J. (2012). Forensic analysis of bone in Regio antebrachii of deer (*Capreolus capreolus*) and sheep (*Ovis aries*) in order to determine origin of

animal species. *Veterinarski Glasnik*, *66*, 325–331.

Blois, J. L., & Hadly, E. A. (2009). Mammalian response to Cenozoic climatic change. *Annual Review of Earth and Planetary Sciences*, *37*, 181–208.

Blondel, C. (2001). The Eocene-Oligocene ungulates from Western Europe and their environment. *Palaeogeography, Palaeoclimatology, Palaeoecology*, *168*, 125–139.

Boardman, G. S., & Secord, R. (2013). Stable isotope paleoecology of White River ungulates during the Eocene–Oligocene climate transition in northwestern Nebraska. *Palaeogeography, Palaeoclimatology, Palaeoecology*, *375*, 38–49.

Bocherens, H., Schrenk, F., Chaimannee, Y., Kullmer, O., Morike, D., Pushinka, D., & Jaeger, J.-J. (2017). Flexibility of diet and habitat in Pleistocene South Asian mammals: Implications for the fate of the giant fossil ape Gigantopithecus. *Quaternary International*, *434*, 148–155.

Bodmer, R. E., & Brooks, D. M. (1997). Status and action plan of the Lowland Tapir (*Tapirus terrestris*). In D. M. Brooks, R. E. Bodmer, & S. Matola (Eds.), *Tapirs: Status Survey and Conservation Action Plan* (pp. 46–56). Cambridge: IUCN/SSC Tapir Specialist Group.

Bonnan, M. F. (2003). The evolution of manus shape in sauropod dinosaurs: implications for functional morphology, forelimb orientation, and phylogeny. *Journal of Vertebrate Paleontology*, *23*, 595–613.

Bookstein, F. L. (1991). Landmarks. In *Morphometric Tools for Landmark Data - Geometry and Biology* (pp. 55–87). Cambridge: Cambridge University Press.

Botton-Divet, L., Cornette, R., Houssaye, A., Fabre, A.-C., & Herrel, A. (2017). Swimming and running: A study of the convergence in long bone morphology among semi-aquatic mustelids (Carnivora: Mustelidae). *Biological Journal of the Linnean Society*, *121*, 38–49.

Brennan, L. A., Buchanan, J. B., Schick, C. T., & Herman, S. G. (1991). Estimating sex ratios with discriminant function analysis: the influence of probability cutpoints and sample size. *Journal of Field Ornithology*, *62*, 357–366.

Bressou, C. (1961). La myologie du tapir (*Tapirus indicus* L.). *Mammalia*, *25*, 358–400.

Bronnert, C., Gheerbrant, E., Godinot, M., & Métais, G. (2017). A primitive perissodactyl (Mammalia) from the early Eocene of Le Quesnoy (MP7, France). *Historical Biology*, *30*, 237–250.

Brown, J. C., & Yalden, D. W. (1973a). The description of mammals - 2 Limbs and locomotion of terrestrial mammals. *Mammal Review*, *3*, 107–134.

Brown, J. C., & Yalden, D. W. (1973b). The description of mammals – 2 Limbs and locomotion of terrestial mammals. *Mammal Review*, *3*, 107–134.

Brown, N. A. T., Kawcak, C. E., McIlwraith, C. W., & Pandy, M. G. (2003). Architectural properties of distal forelimb muscles in horses, Equus caballus.

Journal of Morphology, *258*, 106–114.

Budras, K.-D., Sack, W. O., & Rock, S. (2003). Thoracic Limb. In K.-D. Budras, W. O. Sack, & S. Rock (Eds.), *Anatomy of the Horse* (Fourth, pp. 2–13). Stuttgart: Schlutersche.

Buffetaut, É. (1986). Un Mésosuchien ziphodonte dans l'Éocène supérieurde La Livinière (Hérault, France). *Geobios*, *19*, 101–113.

Burns, K. J., Hackett, S. J., & Klein, N. K. (2002). Phylogenetic relaitonships and morphological diversity in Darwin's finches and their relatives. *Evolution*, *56*, 1240–1252.

Button, D. J., Rayfield, E. J., & Barrett, P. M. (2014). Cranial biomechanics underpins high sauropod diversity in resource-poor environments. *Proceedings of the Royal Society B: Biological Sciences*, *281*, 20142114–20142114.

Campbell, B. (1936). The comparative myology of the forelimb of the hippopotamus, pig and tapir. *Americal Journal of Anatomy*, *59*, 201–247.

Cano, M. R., Vivo, J., Miró, F., Morales, J. L., & Galisteo, A. M. (2001). Kinematic characteristics of Andalusian, Arabian and Anglo-Arabian horses: A comparative study. *Research in Veterinary Science*, *71*, 147–153.

Cantalapiedra, J. L., Prado, J. L., Hernández Fernández, M., & Alberdi, M. T. (2017). Decoupled ecomorphological evolution and diversification in Neogene-Quaternary horses. *Science*, *355*, 627–630.

Carrano, M. T. (1998). Locomotion in non-avian dinosaurs: Integrating data from hindlimb kinematics, in vivo strains, and bone morphology. *Paleobiology*, *24*, 450–469.

Carrano, M. T. (1999). What, if anything, is a cursor? Categories versus continua for detemining locomotor habit in mammals and dinosaurs. *Journal of Zoology*, *247*, 29–42.

Casane, D., & Laurenti, P. (2013). Why coelacanths are not 'living fossils.' *BioEssays*, *35*, 332–338.

Casanovas-Vilar, I., García-Paredes, I., Alba, D. M., Van Den Hoek Ostende, L. W., & Moyà-Solà, S. (2010). The European Far West: Miocene mammal isolation, diversity and turnover in the Iberian Peninsula. *Journal of Biogeography*, *37*, 1079–1093.

Casanovas-Vilar, I., Moyà-Solà, S., Agustí, J., & Köhler, M. (2005). The geography of a faunal turnover: tracking the vallesian crisis. In *Migration of Organisms* (pp. 247–300). Berlin/Heidelberg: Springer-Verlag.

Casanovas-Vilar, I., Van Den Hoek Ostende, L. W., Furió, M., & Madern, P. A. (2014). The range and extent of the Vallesian Crisis (Late Miocene): new prospects based on the micromammal record from the Vallès-Penedès basin (Catalonia, Spain). *Journal of Iberian Geology*, *40*, 29–49.

Cerling, T. E., Harris, J. M., Ambrose, S. H., Leakey, M. G., & Solounias, N. (1997).

Dietary and environmental reconstruction with stable isotope analyses of herbivore tooth enamel from the Miocene locality of Fort Ternan, Kenya. *Journal of Human Evolution*, *33*, 635–650.

Cerling, T. E., Harris, J. M., & Leakey, M. G. (1999). Browsing and grazing in elephants: the isotope record of modern and fossil proboscideans. *Oecologia*, *120*, 364–374.

Cerling, T. E., Hart, J. A., & Hart, T. B. (2004). Stable isotope ecology in the Ituri Forest. *Oecologia*, *138*, 5–12.

Christiansen, P., & Adolfssen, J. S. (2007). Osteology and ecology of *Megantereon cultridens* SE311 (Mammalia; Felidae; Machairodontinae), a sabrecat from the Late Pliocene - Early Pleistocene of Senéze, France. *Zoological Journal of the Linnean Society*, *151*, 833–884.

Cignoni, P., Callieri, M., Corsini, M., Dellapiane, M., Ganovelli, F., & Ranzuglia, G. (2008). MeshLab: an open-source mesh processing tool. In V. Scarano, R. De Chiara, & U. Erra (Eds.), *Eurographics Italian Chapter Conference* (pp. 1–8). Salerno.

Cione, A. L., Gasparini, G. M., Soibelzon, E., Leopoldo, H. S., & Eduardo, P. T. (2015). *The great American biotic interchange: a South American perspective* (A. L. Cione, G. M. Gasparini, E. Soibelzon, H. S. Leopoldo, & P. T. Eduardo, Eds.). New York: Springer.

Clarke, K. R. (1993). Non-parametric multivariate analyses of changes in community structure. *Austral Ecology*, *18*, 117–143.

Clayton, H. M., Chateau, H., & Back, W. (2013). Forelimb function. In W. Back & H. M. Clayton (Eds.), *Equine Locomotion* (Second, pp. 99–125). London: Saunders Elsevier.

Clifford, A. B. (2010). The evolution of the unguligrade manus in artiodactyls. *Journal of Vertebrate Paleontology*, *30*, 1827–1839.

Codron, J., Codron, D., Lee-Thorp, J. A., Sponheimer, M., Bond, W. J., de Ruiter, D., & Grant, R. (2005). Taxonomic, anatomical, and spatio-temporal variations in the stable carbon and nitrogen isotopic compositions of plants from an African savanna. *Journal of Archaeological Science*, *32*, 1757–1772.

Colbert, E. H., & Hooijer, D. A. (1953). Pleistocene mammals from the limestone fissures of Szechwan, China. *Bulletin of the American Museum of Natural History*, *102*, 1–134.

Colbert, M. W. (2005). The facial skeleton of the early Oligocene *Colodon* (Perissodactyla, Tapiroidea). *Palaeontologia Electronica*, *8*, 1–27.

Constantinescu, G. M., Habel, R. E., Hillebrand, A., Sack, W. O., Schaller, O., Simoens, P., & de Vos, N. R. (2012). Osteologia. In G. M. Constantinescu & O. Schaller (Eds.), *Illustrated Veterinary Anatomical Nomenclature* (Third, pp. 10–62). Stuttgart: Enke.

Cooper, L. N., Berta, A., Dawson, S. D., & Reidenberg, J. S. (2007). Evolution of hyperphalangy and digit reduction in the cetacean manus. *The Anatomical Record: Advances in Integrative Anatomy and Evolutionary Biology*, *290*, 654–672.

Corliss, B. H., Martinson, D. G., & Keffer, T. (1986). Late Quaternary deep-ocean circulation. *Geological Society of America Bulletin*, *97*, 1106.

Cozzuol, M. A., Clozato, C. L., Holanda, E. C., Rodrigues, F. H. G., Nienow, S., de Thoisy, B., … Santos, F. R. (2013). A new species of tapir from the Amazon. *Journal of Mammalogy*, *94*, 1331–1345.

Cucchi, T., Mohaseb, A., Peigné, S., Debue, K., Orlando, L., & Mashkour, M. (2017). Detecting taxonomic and phylogenetic signals in equid cheek teeth: towards new palaeontological and archaeological proxies. *Royal Society Open Science*, *4*, 160997.

Cuff, A. R., Sparkes, E. L., Randau, M., Pierce, S. E., Kitchener, A. C., Goswami, A., & Hutchinson, J. R. (2016). The scaling of postcranial muscles in cats (Felidae) I: forelimb, cervical, and thoracic muscles. *Journal of Anatomy*, *229*, 128–141.

Curran, S. C. (2012). Expanding ecomorphological methods: geometric morphometric analysis of Cervidae post-crania. *Journal of Archaeological Science*, *39*, 1172–1182.

Curran, S. C. (2015). Exploring Eucladoceros ecomorphology using geometric morphometrics. *Anatomical Record*, *298*, 291–313.

Cuvier, G. (1812a). *Recherches sur les ossemens fossiles de quadrupèdes: Tome II* (G. Cuvier, Ed.). Paris: Chez Deterville Libraire.

Cuvier, G. (1812b). *Recherches sur les ossemens fossiles de quadrupèdes: Tome III* (G. Cuvier, Ed.). Paris: Chez Deterville Libraire.

Czaplewski, N. J., Puckette, W. L., & Russell, C. (2002). A Pleistocene tapir and associated mammals from the southwestern Ozark Highland. *Journal of Cave and Karst Studies*, *64*, 97–107.

Dagosto, M., & Terranova, C. J. (1992). Estimating the body size of eocene primates: A comparison of results from dental and postcranial variables. *International Journal of Primatology*, *13*, 307–344.

Damuth, J., & Janis, C. M. (2011). On the relationship between hypsodonty and feeding ecology in ungulate mammals, and its utility in palaeoecology. *Biological Reviews*, *86*, 733–758.

Damuth, J., & MacFadden, B. J. (1990). Appendix: Prediction Equations. In J. Damuth & B. J. MacFadden (Eds.), *Body Size in Mammalian Paleobiology: Estimation and Biological Implications* (pp. 365–390). Cambridge: Cambridge University Press.

Danilo, L., Remy, J. A., Vianey-Liaud, M., Marandat, B., Sudre, J., & Lihoreau, F. (2013). A new Eocene locality in southern France sheds light on the basal

radiation of Palaeotheriidae (Mammalia, Perissodactyla, Equoidea). *Journal of Vertebrate Paleontology*, *33*, 195–215.

Darwin, C. (1859). *On the Origin of Species by Means of Natural Selection, or the Preservation of Favoured Races in the Struggle for Life*. London: John Murray.

Davis, E. B., & McHorse, B. K. (2013). A method for improved identification of postcrania from mammalian fossil assemblages: multivariate discriminant function analysis of camelid astragali. *Palaeontologia Electronica*, *16*, 27A.

Day, L. M., & Jayne, B. C. (2007). Interspecific scaling of the morphology and posture of the limbs during the locomotion of cats (Felidae). *Journal of Experimental Biology*, *210*, 642–654.

de Muizon, C., & Argot, C. (2003). Comparative anatomy of the Tiupampa didelphimorphs; an approach to locomotory habits of early marsupials. In M. Jones, C. Dickman, & M. Archer (Eds.), *Predators with Pouches: The Biology of Carnivorous Marsupials* (pp. 43–62). Collingwood: Csiro.

de Oliveira, A. M., & Santos, C. M. D. (2018). Functional morphology and paleoecology of *Pilosa* (Xenarthra, Mammalia) based on a two-dimensional geometric morphometrics study of the humerus. *Journal of Morphology*, *279*, 1455–1467.

de Soler, B. G., Vall-llosera, G. C., van der Made, J., Oms, O., Jordi, A. B., Sala, R., … Rosillo, R. (2012). A new key locality for the Pliocene vertebrate record of Europe: the Camp dels Ninots maar (NE Spain). *Geologica Acta*, *10*, 1–17.

de Thoisy, B., Pukazhenthi, B., Janssen, D. L., Torres, I. L., May Jr., J. A., Medici, P., … Quse, V. (2014). *Tapir Veterinary Manual* (2nd ed.; R. C. Quse, V., Fernandes-Santos, Ed.). IUCN/SSC Tapir Specialist Group.

Defler, T. (2019). *The Great American Biotic (Faunal) Interchange*. Springer, Cham.

Deka, A., Baishya, G., Das, B. J., Talukdar, M., & Kalita, P. C. (2013). Gross anatomy of the scapula of pygmy hog (*Porcula salvania*). *Indian Journal of Veterinary Anatomy*, *25*, 109–110.

DeMiguel, D., Azanza, B., & Morales, J. (2010). Trophic flexibility within the oldest Cervidae lineage to persist through the Miocene Climatic Optimum. *Palaeogeography, Palaeoclimatology, Palaeoecology*, *289*, 81–92.

Depéret, M. C. (1907). Études des Membres du *Lophiodon*. In M. C. Depéret (Ed.), *Études Paléontologiques sur les Lophiodon du Minervois: Structure du Cran, des Membres et Affinités Générales des Lophiodon* (pp. 34–40). Lyon: A. Rey & Company.

DeSantis, L. R. G. (2011). Stable isotope ecology of extant tapirs from the Americas. *Biotropica*, *43*, 746–754.

DeSantis, L. R. G., Feranec, R. S., MacFadden, B. J., Robinson, T., & Roeder, B. (2009). Effects of global warming on ancient mammalian communities and their environments. *PLoS ONE*, *4*, e5750.

DeSantis, L. R. G., & MacFadden, B. J. (2007). Identifying forested environments in deep time using fossil tapirs: evidence from evolutionary morphology and stable isotopes. *Courier-Forschungsinstitut Senckenberg*, *258*, 147–157.

DeSantis, L. R. G., & Wallace, S. C. (2008). Neogene forests from the Appalachians of Tennessee, USA: Geochemical evidence from fossil mammal teeth. *Palaeogeography, Palaeoclimatology, Palaeoecology*, *266*, 59–68.

Dive, J., & Eisenmann, V. (1991). Identification and discrimination of first phalanges from the Pleistocene and modern *Equus*, wild and domestic. In R. H. Meadow & H.-P. Uerpmann (Eds.), *Equids in the Ancient World* (Second, pp. 278–333). Wiesbaden: Ludwig Reichert Verlag.

Domingo, L., Grimes, S. T., Domingo, M. S., & Alberdi, M. T. (2009). Paleoenvironmental conditions in the Spanish Miocene-Pliocene boundary: Isotopic analyses of Hipparion dental enamel. *Naturwissenschaften*, *96*, 503–511.

Downer, C. C. (1995). The gentle botanist. *Wildlife Conservation*, *98*, 30–35.

Downer, C. C. (1996). The mountain tapir, endangered 'flagship' species of the high Andes. *Oryx*, *30*, 45–58.

Downer, C. C. (1997). Status and action plan of the Mountain Tapir (*Tapirus pinchaque*). In D. M. Brooks, R. E. Bodmer, & S. Matola (Eds.), *Tapirs: Status Survey and Conservation Action Plan* (pp. 10–22). Cambridge: IUCN/SSC Tapir Specialist Group.

Downer, C. C. (2001). Observations on the diet and habitat of the mountain tapir (*Tapirus pinchaque*). *Journal of Zoology*, *254*, 279–291.

Druelle, F., Young, J., & Berillon, G. (2018). Behavioral implications of ontogenetic changes in intrinsic hand and foot proportions in olive baboons (*Papio anubis*). *American Journal of Physical Anthropology*, *165*, 65–76.

Dumbá, L. C. C. S., Dutra, R. P., & Cozzuol, M. A. (2018). Cranial geometric morphometric analysis of the genus Tapirus. *Journal of Mammalian Evolution*. https://doi.org/doi.org/10.1007/s10914-018-9432-2

Duncan, M. (2018). Perissodactyls. In K. A. Terio, D. McAloose, & J. St.Ledger (Eds.), *Pathology of Wildlife and Zoo Animals* (pp. 433–454). London: Elsevier Academic Press.

Earle, C. (1893). Some points in the comparative osteology of the tapir. *Science*, *21*, 118.

Earle, C. (1896). Tapirs past and present. *American Journal of Science*, *4*, 934–935.

Easton, K. L., & Kawcak, C. E. (2007). Evaluation of increased subchondral bone density in areas of contact in the metacarpophalangeal joint during joint loading in horses. *American Journal of Veterinary Research*, *68*, 816–821.

Ehleringer, J. R., Lin, Z. F., Field, C. B., Sun, G. C., & Kuo, C. Y. (1987). Leaf carbon isotope ratios of plants from a subtropical monsoon forest. *Oecologia*, *72*, 109–

114.

Ehlers, J., & Gibbard, P. L. (2004a). *Quaternary Glaciations - Extent and Chronology: Part 1 - Europe* (2nd ed.; J. Ehlers & P. L. Gibbard, Eds.). London: Elsevier.

Ehlers, J., & Gibbard, P. L. (2004b). *Quaternary Glaciations - Extent and Chronology: Part II - North America* (2nd ed.; J. Ehlers & P. L. Gibbard, Eds.). London: Elsevier.

Ehlers, J., & Gibbard, P. L. (2004c). *Quaternary Glaciations - Extent and Chronology: Part III - South America, Asia, Africa, Australasia, Antarctica* (2nd ed.; J. Ehlers & P. L. Gibbard, Eds.). London: Elsevier.

Eisenmann, V. (1979). Les métapodes d'*Equus* sensu lato (Mammalia, Périssodactyla). *Geobios*, *12*, 863–886.

Eisenmann, V. (1995). What metapodial morphometry has to say about some Miocene hipparions. In E. S. Vrba, G. H. Denton, T. C. Partridge, & L. H. Burckle (Eds.), *Paleoclimate and Evolution, with emphasis on Human Origins* (pp. 149–164). London: Yale University Press.

Eisenmann, V. (2006). Pliocen and Pleistocene equids: palaeontology versus molecular biology. *Courier-Forschungsinstitut Senckenberg*, *256*, 71–89.

Eisenmann, V., & Beckouche, S. (1986). Identification and discrimination of metapodials from Pleistocene and modern *Equus*, wild and domestic. In R. H. Meadow & H.-P. Uerpmann (Eds.), *Equids in the Ancient World* (pp. 117–163). Wiesbaden: Ludwig Reichert Verlag.

Eisenmann, V., & Guérin, C. (1992). *Tapirus priscus* Kaup from the Upper Miocene of Western Europe: palaeontology, biostratigraphy and palaeoecology. *Paleontologia i Evolucio*, *24–25*, 113–122.

Eisenmann, V., & Karchoud, A. (1982). Analyses multidimensionnelles de métapodes d'Equus sensu lato (Mammalia, Perissodactyla). *Bulletin Du Muséum National d'Histoire Naturelle*, Vol. 4, pp. 75–103.

Elissamburu, A., & DeSantis, L. R. G. (2011). Forelimb proportions and fossorial adaptations in the scratch-digging rodent Ctenomys (Caviomorpha). *Journal of Mammalogy*, *92*, 683–689.

Elissamburu, A., & Vizcaíno, S. F. (2004). Limb proportions and adaptations in caviomorph rodents (Rodentia: Caviomorpha). *Journal of Zoology*, *262*, S0952836903004485.

Endo, H., Yoshida, M., Nguyen, T. S., Akiba, Y., Takeda, M., & Kudo, K. (2019). Three-dimensional CT examination of the forefoot and hindfoot of the hippopotamus and tapir during a semiaquatic walking. *Anatomia, Histologia, Embryologia*, *48*, 3–11.

Evans, H. E., & de Lahunta, A. (2013). Appendicular Skeleton. In H. E. Evans & A. de Lahunta (Eds.), *Miller's Anatomy of the Dog* (Fourth, pp. 127–151). Elsevier.

Fabre, A.-C., Cornette, R., Goswami, A., & Peigné, S. (2015). Do constraints associated with the locomotor habitat drive the evolution of forelimb shape? A case study in musteloid carnivorans. *Journal of Anatomy*, *226*, 596–610.

Fabre, A.-C., Cornette, R., Peigné, S., & Goswami, A. (2013). Influence of body mass on the shape of forelimb in musteloid carnivorans. *Biological Journal of the Linnean Society*, *110*, 91–103.

Fabre, A.-C., Cornette, R., Perrard, A., Boyer, D. M., Prasad, G. V. R., Hooker, J. J., & Goswami, A. (2014). A three-dimensional morphometric analysis of the locomotory ecology of *Deccanolestes*, a eutherian mammal from the Late Cretaceous of India. *Journal of Vertebrate Paleontology*, *34*, 146–156.

Fabre, A.-C., Cornette, R., Slater, G. J., Argot, C., Peigné, S., Goswami, A., & Pouydebat, E. (2013). Getting a grip on the evolution of grasping in musteloid carnivorans: a three-dimensional analysis of forelimb shape. *Journal of Evolutionary Biology*, *26*, 1521–1535.

Fabre, A.-C., Marigó, J., Granatosky, M. C., & Schmitt, D. (2017). Functional associations between support use and forelimb shape in strepsirrhines and their relevance to inferring locomotor behavior in early primates. *Journal of Human Evolution*, *108*, 11–30.

Fabre, A.-C., Salesa, M. J., Cornette, R., Antón, M., Morales, J., & Peigné, S. (2015). Quantitative inferences on the locomotor behaviour of extinct species applied to *Simocyon batalleri* (Ailuridae, Late Miocene, Spain). *Die Naturwissenschaften*, *102*, 1280.

Fadda, C., & Corti, M. (2001). Three-dimensional geometric morphometrics of *Arvicanthis*: implications for systematics and taxonomy. *Journal of Zoological Systematics and Evolutionary Research*, *39*, 235–245.

Famoso, N. A., Davis, E. B., Feranec, R. S., Hopkins, S. S. B., & Price, S. A. (2016). Are hypsodonty and occlusal enamel complexity evolutionarily correlated in ungulates? *Journal of Mammalian Evolution*, *23*, 43–47.

Fedak, M., Heglund, N. C., & Taylor, C. R. R. (1982). Energetics and mechanics of terrestrial locomotion. II. kinetic energy changes of the limbs and body as a function of speed and body size in birds and mammals. *Journal of Experimental Biology*, *97*, 23–40.

Feranec, R. S., & MacFadden, B. J. (2006). Isotopic discrimination of resource partitioning among ungulates in C_3-dominated communities from the Miocene of Florida and California. *Paleobiology*, *32*, 191–205.

Ferrero, B. S., & Noriega, J. I. (2007). A new upper Pleistocene tapir from Argentina: remarks on the phylogenetics and diversification of neotropical Tapiridae. *Journal of Vertebrate Paleontology*, *27*, 504–511.

Ferrero, B. S., Soibelzon, E., Holanda, E. C., Gasparini, G. M., Zurita, A. E., & Mino-Boilini, A. R. (2013). A taxonomic and biogeographic review of the fossil tapirs from Bolivia. *Acta Palaeontologica Polonica*, *59*, 505–516.

Figueirido, B., Janis, C. M., Pérez-Claros, J. A., De Renzi, M., & Palmqvist, P. (2012). Cenozoic climate change influences mammalian evolutionary dynamics. *Proceedings of the National Academy of Sciences of the United States of America*, *109*, 722–727.

Fisher, R. E., Scott, K. M., & Naples, V. L. (2007). Forelimb myology of the pygmy hippopotamus (*Choeropsis liberiensis*). *Anatomical Record*, *290*, 673–693.

Flores, D. A., & Díaz, M. M. (2009). Postcranial skeleton of *Glironia venusta* (Didelphimorphia, Didelphidae, Caluromyinae): description and functional morphology. *Zoosystematics and Evolution*, *85*, 311–339.

Fortelius, M. (1990). Problems with using fossil teeth to estimate body sizes of extinct mammals. In B. J. Damuth, J., MacFadden (Ed.), *Body Size in Mammalian Paleobiology: Estimation and Biological Implications* (pp. 207–228). Cambridge: Cambridge University Press.

Fortelius, M., Eronen, J. T., Kaya, F., Tang, H., Raia, P., & Puolamäki, K. (2014). Evolution of Neogene Mammals in Eurasia: Environmental Forcing and Biotic Interactions. *Annual Review of Earth and Planetary Sciences*, *42*, 579–604.

Fortelius, M., & Hokkanen, A. (2001). The trophic context of hominoid occurrence in the later Miocene of western Eurasia: a primate-free view. In L. de Bonis, G. D. Koufos, & P. Andrews (Eds.), *Hominoid evolution and climatic change in Europe Volume 2: Phylogeny of Neogene Primates of Eurasia* (pp. 19–47). Cambridge: Cambridge University Press.

Fox, A. N., & Bloom, A. L. (1994). Snowline altitude and climate in the Peruvian Andes (5-17°S) at present and during the latest Pleistocene glacial maximum. *Journal of Geography*, *103*, 867–885.

Franzen, J. L. (1990). Hallensia (Mammalia, Perissodactyla) aus Messel und dem Pariser Becken sowie Nachtrage aus dem Geiseltal. *Bulletin de l'Institut Royal Des Sciences Naturelles de Belgique, Sciences de La Terre*, *60*, 175–201.

Franzen, J. L. (2006). *Eurohippus* n.g., a new genus of horses from the Middle to Late Eocene of Europe. *Senckenbergiana Lethaea*, *86*, 97–102.

Franzen, J. L. (2010a). Pseudo Horses and Relatives of Horses. In *The Rise of Horses: 55 Million Years of Evolution* (pp. 145–164). Baltimore: Johns Hopkins University Press.

Franzen, J. L. (2010b). The Dawn Horses of the Morning Cloud. In *The Rise of Horses: 55 Million Years of Evolution* (pp. 45–76). Baltimore: Johns Hopkins University Press.

Fraser, D., Gorelick, R., & Rybczynski, N. (2015). Macroevolution and climate change influence phylogenetic community assembly of North American hoofed mammals. *Biological Journal of the Linnean Society*, *114*, 485–494.

Froehlich, D. J. (1999). Phylogenetic systematics of basal perissodactyls. *Journal of Vertebrate Paleontology*, *19*, 140–159.

Froehlich, D. J. (2002). Quo vadis eohippus? The systematics and taxonomy of the early Eocene equids (Perissodactyla). *Zoological Journal of the Linnean Society*, *134*, 141–256.

Galateanu, G., Hildebrandt, T. B., Maillot, A., Etienne, P., Potier, R., Mulot, B., … Hermes, R. (2013). One small step for rhinos, one giant leap for wildlife management--imaging diagnosis of bone pathology in distal limb. *PloS One*, *8*, e68493.

Galisteo, A. M., Vivo, J., Cano, M. R., Morales, J. L., Miró, F., & Agüera, E. (1997). Differences between breeds (Dutch Warmblood vs Andalusian Purebred) in forelimb kinematics. *Journal of Equine Science*, *8*, 43–47.

Gambaryan, P. P. (1974). *How Mammals Run: Anatomical Adaptations*. New York: John Wiley & Sons.

García, M. J., Medici, P., Naranjo, E. J., Novarino, W., & Leonardo, R. S. (2012). Distribution, habitat and adaptability of the genus Tapirus. *Integrative Zoology*, *7*, 346–355.

Garcia, N. G., Feranec, R. S., Arsuaga, J. L., Bermudez de Castro, J. M., & Carbonell, E. (2009). Isotopic analysis of the ecology of herbivores and carnivores from the Middle Pleistocene deposits of the Sierra De Atapuerca, northern Spain. *Journal of Archaeological Science*, *36*, 1142–1151.

Garland, T., Dickerman, A. W., Janis, C. M., & Jones, J. A. (1993). Phylogenetic analysis of covariance by computer simulation. *Systematic Biology*, *42*, 265–292.

Gasc, J.-P. (2001). Comparative aspects of gait, scaling and mechanics in mammals. *Comparative Biochemistry and Physiology Part A: Molecular & Integrative Physiology*, *131*, 121–133.

Gewaily, M. S., Fayed, M. H., & Farrag, F. A. (2017). Architectural and functional specifications of the intrinsic muscles of the forelimb of the Egyptian Baladi Goats (*Capra hircus*). *Alexandria Journal of Veterinary Sciences*, *55*, 110–124.

Gilmore, M. (2001). *Tapir Behaviour - an examination of activity patterns, mother-young interactions, spatial use, and environmental effects in captivity on two species (*Tapirus indicus & Tapirus *)*. Oregon State University.

González-Maya, J. F., Schipper, J., Polidoro, B., Hoepker, A., Zárrate-Charry, D., & Belant, J. L. (2012). Baird's tapir density in high elevation forests of the Talamanca region of Costa Rica. *Integrative Zoology*, *7*, 381–388.

Goodall, C. (1991). Procrustes methods in the statistical analysis of shape. *Journal of the Royal Statistical Society. Series B (Methodological)*, *53*, 285–339.

Gould, F. D. H. (2014). To 3D or not to 3D, that is the question: do 3D surface analyses improve the ecomorphological power of the distal femur in placental mammals? *PloS One*, *9*, e91719.

Graham, R. W. (2003). Pleistocene tapir from Hill Top Cave, Trigg County, Kentucky, and a review of Plio-Pleistocene tapirs of North America and their

paleoecology. In R. W. Schubert, B. W., Mead, J. I., Graham (Ed.), *Ice Age cave faunas of North America* (pp. 87–118). Indianapolis: Indiana University Press.

Gregory, W. K. (1929). Mechanics of locomotion in the evolution of limb structure as bearing on the form and habits of the titanotheres and the related odd-toed ungulates. In H. F. Osborn (Ed.), *The titanotheres of ancient Wyoming, Dakota and Nebraska* (pp. 727–756). Washington D.C.: United States Government Printing Office.

Grossnickle, D. M., & Polly, P. D. (2013). Mammal disparity decreases during the Cretaceous angiosperm radiation. *Proceedings of the Royal Society B: Biological Sciences*, *280*, 20132110–20132110.

Groves, C. P., Fernando, P., & Robovský, J. (2010). The sixth rhino: a taxonomic re-assessment of the critically endangered northern white rhinoceros. *PLoS ONE*, *5*, 1–15.

Guérin, C. (1980). Les rhinocéros (Mammalia, Perissodactyla) du Miocèneterminal au Pléistocène supérieur en Europe occidentale: comparaison avec les espèces actuelles. *Documents Du Laboratoire de Géologie de l'Université de Lyon, Sciences d*, 1–1184.

Guérin, C., & Eisenmann, V. (1982). Répartition stratigraphique des tapirs (Mammalia, Perissodactyla) dans le Néogène et le Quaternaire d'Europe occidentale. *XIXeme Réunion Annuelle Des Sciences de La Terre, Societe Geologique de France*, 298.

Guérin, C., & Eisenmann, V. (1994). Les Tapirs (Mammalia, Perissodactyla) du Miocène supérieur d'Europe occidentale. *Geobios*, *27*, 113–127.

Guérin, C., & Tsoukala, E. (2013). The Tapiridae, Rhinocerotidae and Suidae (Mammalia) of the Early Villafranchian site of Milia (Grevena, Macedonia, Greece). *Geodiversitas*, *35*, 447–489.

Hady, L. L., Fosgate, G. T., & Weh, J. M. (2015). Comparison of range of motion in Labrador Retrievers and Border Collies. *Journal of Veterinary Medicine and Animal Health*, *7*, 122–127.

Halenar, L. B. (2011). Reconstructing the locomotor repertoire of *Protopithecus brasiliensis*. II. Forelimb morphology. *Anatomical Record*, *294*, 2048–2063.

Hames, R. B. (1979). A comparison of the efficiencies of the shotgun and the bow in neotropical forest hunting. *Human Ecology*, *7*, 219–252.

Hammer, Ø., Harper, D. A. T., & Ryan, P. D. (2001). PAST: Paleontological statistics software package for education and data analysis. *Palaeontologia Electronica*, *4*, 9.

Hanegraef, H. (2015). *Validating the use of geometric morphometrics: a case-study on the forelimb in Perissodactyla*. Universiteit Antwerpen.

Hanot, P., Guintard, C., Lepetz, S., & Cornette, R. (2017). Identifying domestic horses, donkeys and hybrids from archaeological deposits: A 3D morphological

investigation on skeletons. *Journal of Archaeological Science*, *78*, 88–98.

Hanot, P., Herrel, A., Guintard, C., & Cornette, R. (2017). Morphological integration in the appendicular skeleton of two domestic taxa: the horse and donkey. *Proceedings of the Royal Society B: Biological Sciences*, *284*, 20171241.

Harrison, S. M., Whitton, R. C., Kawcak, C. E., Stover, S. M., & Pandy, M. G. (2010). Relationship between muscle forces, joint loading and utilization of elastic strain energy in equine locomotion. *Journal of Experimental Biology*, *213*, 3998–4009.

Hawkins, P. L. (2011). *Variation in the modified first metatarsal of a large sample of* Tapirus polkensis*, and the functional implication for ceratomorphs*. East Tennessee State University.

Heck, L., Wilson, L. A. B., Evin, A., Stange, M., & Sánchez-Villagra, M. R. (2018). Shape variation and modularity of skull and teeth in domesticated horses and wild equids. *Frontiers in Zoology*, *15*, 14.

Heintzman, P. D., Zazula, G. D., MacPhee, R. D. E., Scott, E., Cahill, J. A., McHorse, B. K., … Shapiro, B. (2017). A new genus of horse from Pleistocene North America. *ELife*, *6*. https://doi.org/10.7554/eLife.29944

Heissig, K. (1987). Changes in the rodent and ungulate fauna in the Oligocene fissure fillings of Germany. *Münchner Geowissenschaftliche Abhandlungen, A*, 101–108.

Heissig, K. (2012). Les Rhinocerotidae (Perissodactyla) de Sansan. In S. Peigné & S. Sen (Eds.), *Mammiferes de Sansan* (pp. 317–486). Paris: Publication Scientifiques du Museum.

Hellmund, M. (2005). A three-dimensional skeletal reconstruction of the Middle Eocene *Propalaeotherium hassiacum* Haupt 1925 (Equidae, Perissodactyla, Mammalia) and a modern synoptic painting of some individuals within their habitat. *Current Research in Vertebrate Palaeontolgy 3rd Annual Meeting of the European Association of Vertebrate Palaeontologists (EAVP)*, 15. Hessisches Landesmuseum Darmstadt.

Hellmund, M. (2016). Tooth emergence and replacement in the European *Hyrachyus minimus* (Fischer, 1829) (Mammalia, Perissodactyla) from the Geiseltal Fossillagerstätte - a further example for "Schultz's rule" in ungulates. *Neues Jahrbuch Für Geologie Und Paläontologie - Abhandlungen*, *282*, 157–180.

Hermanson, J. W., & MacFadden, B. J. (1992). Evolutionary and functional morphology of the shoulder region and stay-apparatus in fossil and extant horses (Equidae). *Journal of Vertebrate Paleontology*, *12*, 377–386.

Herrera-Flores, J. A., Stubbs, T. L., & Benton, M. J. (2017). Macroevolutionary patterns in Rhynchocephalia: is the tuatara (*Sphenodon punctatus*) a living fossil? *Palaeontology*, *60*, 319–328.

Herrera-Flores, J. A., Stubbs, T. L., & Benton, M. J. (2019). Reply to comments on: Macroevolutionary patterns in Rhynchocephalia: is the tuatara (*Sphenodon punctatus*) a living fossil? *Palaeontology*, *62*, 335–338.

Hershkovitz, P. (1954). Mammals of Northern Colombia, Preliminary Report No. 7: Tapirs (genus *Tapirus*) with a systematic review of American species. *Proceedings of the United States National Museum*, *103*, 465–496.

Hervé, M. (2014). Aide-mémoire de statistique appliquée à la biologie. *Construire Son Étude et Analyser Les Résultats à l'aide Du Logiciel R*, pp. 1–203.

Hewitt, G. (2000). The genetic legacy of the Quaternary ice ages. *Nature*, *405*, 907–913.

Hildebrand, M. (1985). Walking and Running. In D. B. Hildebrand, M., Bramble, D. M., Liem, K. F., Wake (Ed.), *Functional Vertebrate Morphology* (pp. 38–57). Cambridge: Harvard University Press.

Holanda, E. C., & Ferrero, B. S. (2013). Reappraisal of the genus *Tapirus* (Perissodactyla, Tapiridae): systematics and phylogenetic affinities of the South American tapirs. *Journal of Mammalian Evolution*, *20*, 33–44.

Holanda, E. C., Ribeiro, A. M., & Ferigolo, J. (2012). New material of *Tapirus* (Perissodactyla: Tapiridae) from the Pleistocene of southern Brazil. *Revista Mexicana de Ciencias Geologicas*, *29*, 308–318.

Holbourn, A., Kuhnt, W., Kochhann, K. G. D., Andersen, N., & Sebastian Meier, K. J. (2015). Global perturbation of the carbon cycle at the onset of the Miocene Climatic Optimum. *Geology*, *43*, 123–126.

Holbrook, L. T. (1999). The phylogeny and classification of tapiromorph perissodactyls (Mammalia). *Cladistics*, *15*, 331–350.

Holbrook, L. T. (2001). Comparative osteology of early Tertiary tapiromorphs (Mammalia, Perissodactyla). *Zoological Journal of the Linnean Society*, *132*, 1–54.

Holbrook, L. T. (2009). Osteology of Lophiodon Cuvier, 1822 (Mammalia, Perissodactyla) and its phylogenetic implications. *Journal of Vertebrate Paleontology*, *29*, 212–230.

Holbrook, L. T., & Lucas, S. G. (1997). A new genus of rhinocerotoid from the Eocene of Utah and the status of North American "Forstercooperia." *Journal of Vertebrate Paleontology*, *17*, 384–396.

Holbrook, L. T., Lucas, S. G., & Emry, R. J. (2004). Skulls of the Eocene perissodactyls (Mammalia) Homogalax and Isectolophus. *Journal of Vertebrate Paleontology*, *24*, 951–956.

Hooker, J. J. (2005). Perissodactyla. In K. D. Rose & J. D. Archibald (Eds.), *The Rise of Placental Mammals* (1st ed., pp. 199–215). London: Johns Hopkins University Press.

Hooker, J. J. (2010a). The "Grande Coupure" in the Hampshire Basin, UK: taxonomy and stratigraphy of the mammals on either side of this major Paleogene faunal turnover. In J. E. Whittaker & M. B. Hart (Eds.), *Micropalaeontology, Sedimentary Environments and Stratigraphy: A Tribute to Dennis Curry (1912-*

2001) (pp. 147–215). Bath: The Geological Society Publishing House.

Hooker, J. J. (2010b). The mammal fauna of the Early Eocene Blackheath Formation of Abbey Wood, London. *Monograph of the Palaeontographical Society*, *624*, 1–162.

Hooker, J. J., Collinson, M. E., & Sille, N. P. (2004). Eocene-Oligocene mammalian faunal turnover in the Hampshire Basin, UK: calibration to the global time scale and the major cooling event. *Journal of the Geological Society*, *161*, 161–172.

Hooker, J. J., & Dashzeveg, D. (2004). The origin of chalicotheres (Perisodactyla, Mammalia). *Palaeontology*, *47*, 1363–1386.

Hoppe, K. A., & Koch, P. L. (2006). The Biogeochemistry of the Aucilla River Fauna. In *First Floridians and Last Mastodons: The Page-Ladson Site in the Aucilla River* (pp. 379–401). Springer Netherlands.

Hren, M. T., Sheldon, N. D., Grimes, S. T., Collinson, M. E., Hooker, J. J., Bugler, M., & Lohmann, K. C. (2013). Terrestrial cooling in Northern Europe during the eocene-oligocene transition. *Proceedings of the National Academy of Sciences of the United States of America*, *110*, 7562–7567.

Hulbert, R. C. (1984). Paleoecology and population dynamics of the early Miocene (Hemingfordian) horse *Parahippus leonensis* from the Thomas Farm site, Florida. *Journal of Vertebrate Paleontology*, *4*, 547–558.

Hulbert, R. C. (1995). The giant tapir, *Tapirus haysii* , from Leisey Shell Pit 1A and other Florida Irvingtonian localities. *Bulletin of the Florida Museum of Natural History*, *37*, 515–551.

Hulbert, R. C. (2005). Late Miocene *Tapirus* (Mammalia, Perissodactyla) from Florida, with description of a new species, *Tapirus webbi*. *Bulletin of the Florida Museum of Natural History*, *45*, 465–494.

Hulbert, R. C. (2010). A new early Pleistocene tapir (Mammalia: Perissodactyla) from Florida, with a review of Blancan tapirs from the state. *Bulletin of the Florida Museum of Natural History*, *49*, 67–126.

Hulbert, R. C., Bloch, J. I., & Poyer, A. R. (2006). Exceptional preservation of vertebrates from Haile 7G, a new late Pliocene site from Florida. *Journal of Vertebrate Paleontology*, *26*, 78A–79A.

Hulbert, R. C., Wallace, S. C., Klippel, W. E., & Parmalee, P. W. (2009). Cranial morphology and systematics of an extraordinary sample of the Late Neogene dwarf tapir, *Tapirus polkensis* (Olsen). *Journal of Paleontology*, *83*, 238–262.

Hutchinson, J. R., Anderson, F. C., Blemker, S. S., & Delp, S. L. (2005). Analysis of hindlimb muscle moment arms in Tyrannosaurus rex using a three-dimensional musculoskeletal computer model: implications for stance, gait, and speed. *Paleobiology*, *31*, 676.

Hutchinson, J. R., & Gatesy, S. M. (2006). Beyond the bones. *Nature*, *440*, 292–294.

Hutchinson, J. R., Rankin, J. W., Rubenson, J., Rosenbluth, K. H., Siston, R. A., &

Delp, S. L. (2015). Musculoskeletal modelling of an ostrich (Struthio camelus) pelvic limb: influence of limb orientation on muscular capacity during locomotion. *PeerJ*, *3*, e1001.

IBM. (2013). *IBM SPSS Statistics for Windows*. Armonk, New York.

Janis, C. M. (1984). Tapirs as Living Fossils. In S. M. Eldredge, N., Stanley (Ed.), *Living Fossils* (pp. 80–86). New York, NY: Springer New York.

Janis, C. M. (1989). A climatic explanation for patterns of evolutionary diversity in ungulate mammals. *Palaeontology*, *32*, 463–481.

Janis, C. M. (2007). The horse series. In B. Regal (Ed.), *Icons of Evolution* (pp. 257–280). Westport: Greenwood Press.

Janis, C. M., Buttrill, K., & Figueirido, B. (2014). Locomotion in extinct giant kangaroos: were sthenurines hop-less monsters? *PLoS ONE*, *9*, e109888.

Janis, C. M., Damuth, J., & Theodor, J. M. (2002). The origins and evolution of the North American grassland biome: the story from the hoofed mammals. *Palaeogeography, Palaeoclimatology, Palaeoecology*, *177*, 183–198.

Janis, C. M., & Wilhelm, P. B. (1993). Were there mammalian pursuit predators in the tertiary? Dances with wolf avatars. *Journal of Mammalian Evolution*, *1*, 103–125.

Jenkins Jr., F. A. (1973). The functional anatomy and evolution of the mammalian humero-ulnar articulation. *The American Journal of Anatomy*, *137*, 281–297.

Jones, K. E. (2016). New insights on equid locomotor evolution from the lumbar region of fossil horses. *Proceedings of the Royal Society B: Biological Sciences*, *283*, 20152947.

Joomun, S. C., Hooker, J. J., & Collinson, M. E. (2008). Dental wear variation and implications for diet: an example from Eocene perissodactyls (Mammalia). *Palaeogeography, Palaeoclimatology, Palaeoecology*, *263*, 92–106.

Kaiser, T. M., Müller, D. W. H., Fortelius, M., Schulz, E., Codron, D., & Clauss, M. (2013). Hypsodonty and tooth facet development in relation to diet and habitat in herbivorous ungulates: implications for understanding tooth wear. *Mammal Review*, *43*, 34–46.

Kaplan, H., & Kopischke, K. (1992). Resource use, traditional technology, and change among native peoples of Lowland South America. In K. H. Redford & C. Padoch (Eds.), *Conservation of Neotropical Forests: Working From Traditional Resource Use* (pp. 83–107). New York: Columbia University Press.

Kaushik, N. (2009). *A quantitative analysis of European horses from Pleistocene to Holocene*. Universidade de Trás-os-Montes e Alto Douro, Vila Real.

Kendall, D. G. (1977). The diffusion of shape. *Advances in Applied Probability*, *9*, 428–430.

Kendall, D. G. (1989). A survey of the statistical theory of shape. *Statistical Science*,

4, 87–99.

Kendall, D. G., Barden, D., Carne, T. K., & Le, H. (1999). *Shape & Shape Theory*. Chichester: John Wiley & Sons, Ltd.

Kitts, D. B. (1956). American *Hyracotherium* (Perissodactyla, Equidae). *Bulletin of the American Museum of Natural History*, *110*, 1–60.

Klaits, B. G. (1972). The moving mesaxonic manus - a comparison of tapirs and rhinoceroses. *Mammalia*, *36*, 126–145.

Klingenberg, C. P. (1998). Heterochrony and allometry: the analysis of evolutionary change in ontogeny. *Biological Reviews of the Cambridge Philosophical Society*, *73*, 79–123.

Klingenberg, C. P. (2009). Morphometric integration and modularity in configurations of landmarks: tools for evaluating a priori hypotheses. *Evolution & Development*, *11*, 405–421.

Klingenberg, C. P. (2011). MorphoJ: an integrated software package for geometric morphometrics. *Molecular Ecology Resourses*, *11*, 353–357.

Klingenberg, C. P. (2016). Size, shape, and form: concepts of allometry in geometric morphometrics. *Development Genes and Evolution*, *226*, 113–137.

Koch, P. L., Hoppe, K. A., & Webb, S. D. (1998). The isotopic ecology of late Pleistocene mammals in North America. *Chemical Geology*, *152*, 119–138.

Kohn, M. J., McKay, M. P., & Knight, J. L. (2005). Dining in the Pleistocene - who's on the menu? *Geology*, *22*, 164.

Koster, J. M. (2006). Assessing the sustainability of Baird's tapir hunting in the Bosawas Reserve, Nicaragua. *Tapir Conservation*, *15*, 23–28.

Koufos, G. (2015). Hipparion macedonicum revisited: New data on evolution of hipparionine horses from the Late Miocene of Greece. *Acta Palaeontologica Polonica*, *61*, 519–536.

Kubo, T., Sakamoto, M., Meade, A., & Venditti, C. (2019). Transitions between foot postures are associated with elevated rates of body size evolution in mammals. *Proceedings of the National Academy of Sciences*, 201814329.

Kuncova, P., & Frynta, D. (2009). Interspecific morphometric variation in the postcranial skeleton in the genus *Apodemus*. *Belgian Journal of Zoology*, *139*, 133–146.

Kürschner, W. M., Kvaček, Z., & Dilcher, D. L. (2008). The impact of Miocene atmospheric carbon dioxide fluctuations on climate and the evolution of terrestrial ecosystems. *Proceedings of the National Academy of Sciences of the United States of America*, *105*, 449–453.

Kvaček, Z. (2010). Forest flora and vegetation of the European early Palaeogene – a review. *Bulletin of Geoscience*, *85*, 3–16.

Labonte, D., Clemente, C. J., Dittrich, A., Kuo, C.-Y., Crosby, A. J., Irschick, D. J., &

Federle, W. (2016). Extreme positive allometry of animal adhesive pads and the size limits of adhesion-based climbing. *Proceedings of the National Academy of Sciences of the United States of America*, *113*, 1297–1302.

Lachenbruch, P. A. (1968). On expected probabilities of misclassification in discriminant analysis, necessary sample size, and a relation with the multiple correlation coefficient. *Biometrics*, *24*, 823.

Lang, A., Motta, P., Habegger, M. L., & Hueter, R. (2012). Shark Skin Boundary Layer Control. In S. Childress, A. Hosoi, W. W. Schultz, & Z. J. Wang (Eds.), *Natural Locomotion in Fluids and on Surfaces* (pp. 139–150). New York: Springer New York.

Lanovaz, J. L., Clayton, H. M., & Watson, L. G. (2010). In vitro attenuation of impact shock in equine digits. *Equine Veterinary Journal*, *30*, 96–102.

Larson, S. G., & Stern, J. T. (2013). Rotator cuff muscle function and its relation to scapular morphology in apes. *Journal of Human Evolution*, *65*, 391–403.

Liebich, H.-G., Konig, H. E., & Maierl, J. (2007). Forelimb or thoracic limb (membra thoracica). In H. E. Konig & H.-G. Liebich (Eds.), *Veterinary Anatomy of Domestic Animals: Textbook and Colour Atlas* (Third, pp. 145–214). Stuttgart: Schlutersche.

Lizcano, D. J., Pizarro, V., Cavelier, J., & Carmona, J. (2002). Geographic distribution and population size of the mountain tapir (*Tapirus pinchaque*) in Colombia. *Journal of Biogeography*, *29*, 7–15.

Lockley, M. G. (2009). New perspectives on morphological variation in tridactyl foot prints : clues to widespread convergence in developmental dynamics. *Geological Quarterly*, *53*, 415–432.

MacFadden, B. J. (1984). *Astrohippus* and *Dinohippus* from the Yepómera local fauna (Hemphillian, Mexico) and implications for the phylogeny of one-toed horses. *Journal of Vertebrate Paleontology*, *4*, 273–283.

MacFadden, B. J. (1986). Fossil horses from "*Eohippus*" (*Hyracotherium*) to *Equus*; scaling, Cope's law, and the evolution of body size. *Paleobiology*, *12*.

MacFadden, B. J. (1992a). *Fossil Horses: Systematics, Paleobiology and Evolution of the Family Equidae*. Cambridge: Cambridge University Press.

MacFadden, B. J. (1992b). What's the use? Functional morphology of feeding and locomotion. In *Fossil Horses: Systematics, Paleobiology, and Evolution of the Family Equidae* (pp. 229–262). Cambridge: Cambridge University Press.

MacFadden, B. J. (2005). Evolution. Fossil horses - evidence for evolution. *Science*, *307*, 1728–1730.

MacFadden, B. J., & Cerling, T. E. (1996). Mammalian herbivore communities, ancient feeding ecology, and carbon isotopes: A 10 million-year sequence from the Neogene of Florida. *Journal of Vertebrate Paleontology*, *16*, 103–115.

MacFadden, B. J., & Hulbert, R. C. (1990). Body size estimates and size distribution

of ungulate mammals from the Late Miocene Love Bone Bed of Florida. In B. J. Damuth, J., MacFadden (Ed.), *Body Size in Mammalian Paleobiology: Estimation and Biological Implications* (pp. 337–363). Cambridge: Cambridge University Press.

Machado, H., Grillo, O., Scott, E., & Avilla, L. S. (2018). Following the footsteps of the South American *Equus*: are autopodia taxonomically informative? *Journal of Mammalian Evolution*, *25*, 397–405.

MacLaren, J. A., Anderson, P. S. L., Barrett, P. M., & Rayfield, E. J. (2017). Herbivorous dinosaur jaw disparity and its relationship to extrinsic evolutionary drivers. *Paleobiology*, *43*, 15–33.

MacLaren, J. A., Hulbert, R. C., Wallace, S. C., & Nauwelaerts, S. (2018). A morphometric analysis of the forelimb in the genus Tapirus (Perissodactyla: Tapiridae) reveals influences of habitat, phylogeny and size through time and across geographical space. *Zoological Journal of the Linnean Society*, *184*.

MacLaren, J. A., & Nauwelaerts, S. (2016). A three-dimensional morphometric analysis of upper forelimb morphology in the enigmatic tapir (Perissodactyla: Tapirus) hints at subtle variations in locomotor ecology. *Journal of Morphology*, *277*, 1469–1485.

MacLaren, J. A., & Nauwelaerts, S. (2017). Interspecific variation in the tetradactyl manus of modern tapirs (Perissodactyla: Tapirus) exposed using geometric morphometrics. *Journal of Morphology*, *278*, 1515–1535.

MacLaren, J. A., & Nauwelaerts, S. (2019). Modern tapirs as morphofunctional analogues for extinct Eocene European perissodactyls. *Journal of Mammalian Evolution*.

Maguire, K. C., & Stigall, A. L. (2008). Paleobiogeography of Miocene Equinae of North America: a phylogenetic biogeographic analysis of the relative roles of climate, vicariance, and dispersal. *Palaeogeography, Palaeoclimatology, Palaeoecology*, *267*, 175–184.

Mallet, C., Cornette, R., Billet, G., & Houssaye, A. (2018). Morphofunctional 3D analysis of long bone shape variation among rhinos. *5th International Paleontological Congress*, 401. Paris.

Marsh, O. C. (1874). Fossil horses in America. *The American Naturalist*, *8*, 288–294.

Martín-Serra, A., Figueirido, B., & Palmqvist, P. (2014). A three-dimensional analysis of morphological evolution and locomotor performance of the carnivoran forelimb. *PloS One*, *9*, e85574.

Martin, J. E. (2014). A sebecosuchian in a middle Eocene karst with comments on the dorsal shield in Crocodylomorpha. *Acta Palaeontologica Polonica*, *60*, 673–680.

Martin, M. L., Warburton, N. M., Travouillon, K. J., & Fleming, P. A. (2019). Mechanical similarity across ontogeny of digging muscles in an Australian marsupial (*Isoodon fusciventer*). *Journal of Morphology*, *280*, 423–435.

Martínez-Navarro, B., & Rabinovich, R. (2011). The fossil Bovidae (Artiodactyla, Mammalia) from Gesher Benot Ya'aqov, Israel: Out of Africa during the Early-Middle Pleistocene transition. *Journal of Human Evolution*, *60*, 375–386.

Mathewson, M. A., Kwan, A., Eng, C. M., Lieber, R. L., & Ward, S. R. (2014). Comparison of rotator cuff muscle architecture between humans and other selected vertebrate species. *The Journal of Experimental Biology*, *217*, 261–273.

Matola, S., Cuarón, A. D., & Rubio-Torgler, H. (1997). Status and action plan of the Baird's Tapir (*Tapirus bairdii*). In D. M. Brooks, R. E. Bodmer, & S. Matola (Eds.), *Tapirs: Status Survey and Conservation Action Plan* (pp. 29–45). Cambridge: IUCN/SSC Tapir Specialist Group.

Maynard Smith, J., & Savage, R. J. G. (1956). Some locomotory adaptations in mammals. *Journal of the Linnean Society of London, Zoology*, *42*, 603–622.

McHorse, B. K., Biewener, A. A., & Pierce, S. E. (2017). Mechanics of evolutionary digit reduction in fossil horses (Equidae). *Proceedings of the Royal Society B: Biological Sciences*, *284*, 20171174.

McKenna, M. C., & Bell, S. K. (1997). *Classification of mammals above the species level*. New York: Columbia University Press.

Mead, A. J. (2000). Sexual dimorphism and paleoecology in Teleoceras , a North American Miocene rhinoceros. *Paleobiology*, *26*, 689–706.

Meloro, C. (2011). Locomotor adaptations in Plio-Pleistocene large carnivores from the Italian Peninsula: Palaeoecological implications. *Current Zoology*, *57*, 269–283.

Meloro, C., & Jones, M. E. H. (2012). Tooth and cranial disparity in the fossil relatives of Sphenodon (Rhynchocephalia) dispute the persistent 'living fossil' label. *Journal of Evolutionary Biology*, *25*, 2194–2209.

Mendez, J., & Keys, A. (1960). Density and composition of mammalian muscle. *Metabolism*, *9*, 184–188.

Meng, J., & McKenna, M. C. (1998). Faunal turnovers of Palaeogene mammals from the Mongolian Plateau. *Nature*, *394*, 364–367.

Métais, G., & Sen, S. (2017). First occurrence of Palaeotheriidae (Perissodactyla) from thelate–middle Eocene of eastern Thrace (Greece). *Comptes Rendus - Palevol*, *16*, 382–396.

Mihlbachler, M. C. (2008). Species taxonomy, phylogeny, and biogeography of the Brontotheriidae (Mammalia: Perissodactyla). *Bulletin of the American Museum of Natural History*.

Mihlbachler, M. C., Rivals, F., Solounias, N., & Semprebon, G. M. (2011). Dietary change and evolution of horses in North America. *Science*, *331*, 1178–1181.

Miller, C. E., Basu, C., Fritsch, G., Hildebrandt, T. B., & Hutchinson, J. R. (2008). Ontogenetic scaling of foot musculoskeletal anatomy in elephants. *Journal of The Royal Society Interface*, *5*, 465–475.

Mills, G. (1997). *Complete Book of Southern African Mammals*.

Milne, N. (2016). Curved bones: An adaptation to habitual loading. *Journal of Theoretical Biology*, *407*, 18–24.

Milne, N., Vizcaíno, S. F., & Fernicola, J. C. (2009). A 3D geometric morphometric analysis of digging ability in the extant and fossil cingulate humerus. *Journal of Zoology*, *278*, 48–56.

Mitteroecker, P., Gunz, P., Bernhard, M., Schaefer, K., & Bookstein, F. L. (2004). Comparison of cranial ontogenetic trajectories among great apes and humans. *Journal of Human Evolution*, *46*, 679–698.

Mitteroecker, P., Gunz, P., & Bookstein, F. L. (2005). Heterochrony and geometric morphometrics: a comparison of cranial growth in *Pan paniscus* versus *Pan troglodytes*. *Evolution & Development*, *7*, 244–258.

Mitteroecker, P., Gunz, P., Windhager, S., & Schaefer, K. (2013). A brief review of shape, form, and allometry in geometric morphometrics, with applications to human facial morphology. *Hystrix*, *24*, 59–66.

Momin Khan, M. K. (1997). Status and action plan of the Malayan Tapir (Tapirus indicus). In D. M. Brooks, R. E. Bodmer, & S. Matola (Eds.), *Tapirs: Status Survey and Conservation Action Plan* (pp. 23–29). Cambridge: IUCN/SSC Tapir Specialist Group.

Monteiro, L. R. (1999). Multivariate regression models and geometric morphometrics: the search for causal factors in the analysis of shape. *Systematic Biology*, *48*, 192–199.

Mooney, H. A., Bullock, S. H., & Ehleringer, J. R. (1989). Carbon isotope ratios of plants of a tropical dry forest in Mexico. *Functional Ecology*, *3*, 137.

Moraweck, K., Uhl, D., & Kunzmann, L. (2015). Estimation of late Eocene (Bartonian–Priabonian) terrestrial palaeoclimate: Contributions from megafloral assemblages from central Germany. *Palaeogeography, Palaeoclimatology, Palaeoecology*, *433*, 247–258.

Mosbrugger, V., Utescher, T., & Dilcher, D. L. (2005). Cenozoic continental climatic evolution of Central Europe. *Proceedings of the National Academy of Sciences of the United States of America*, *102*, 14964–14969.

Moyano, S. R., & Giannini, N. P. (2017). Comparative cranial ontogeny of *Tapirus* (Mammalia: Perissodactyla: Tapiridae). *Journal of Anatomy*, *231*, 665–682.

Muñoz, N. A., Cassini, G. H., Candela, A. M., & Vizcaíno, S. F. (2017). Ulnar articular surface 3-D landmarks and ecomorphology of small mammals: A case study of two early Miocene typotheres (Notoungulata) from Patagonia. *Earth and Environmental Science Transactions of the Royal Society of Edinburgh*, *106*, 315–323.

Murie, J. (1871). The Malayan tapir. *Journal of Anatomy and Physiology*, *6*, 131–512.

Nauwelaerts, S., MacLaren, J. A., Kaashoek, M., & Aerts, P. (2016). Ecomorphology

and biomechanics of digit reduction. *11th International Congress of Vertebrate Morphology*, 36. Washington D.C.

Nauwelaerts, S., Vangeel, K., MacLaren, J. A., & Aerts, P. (2016). Loading distribution over the four fingers of the tapir during locomotion. *11th International Congress of Vertebrate Morphology*. Washington D.C.

Naville, M., Chalopin, D., Casane, D., Laurenti, P., & Volff, J.-N. (2015). The coelacanth: can a "living fossil" have active transposable elements in its genome? *Mobile Genetic Elements*, *5*, 55–59.

Nelson, S. V. (2014). The paleoecology of early Pleistocene *Gigantopithecus blacki* inferred from isotopic analyses. *American Journal of Physical Anthropology*, *155*, 571–578.

Norman, J. E., & Ashley, M. V. (2000). Phylogenetics of Perissodactyla and tests of the molecular clock. *Journal of Molecular Evolution*, *50*, 11–21.

Nunez, E. E., Macfadden, B. J., Mead, J. I., & Baez, A. (2010). Ancient forests and grasslands in the desert: Diet and habitat of Late Pleistocene mammals from Northcentral Sonora, Mexico. *Palaeogeography, Palaeoclimatology, Palaeoecology*, *297*, 391–400.

Nyakatura, J. A. (2012). The convergent evolution of suspensory posture and locomotion in tree sloths. *Journal of Mammalian Evolution*, *19*, 225–234.

O'Dea, A., Lessios, H. A., Coates, A. G., Eytan, R. I., Restrepo-Moreno, S. A., Cione, A. L., … Jackson, J. B. C. (2016). Formation of the Isthmus of Panama. *Science Advances*, *2*, 1–12.

O'Higgins, P., & Jones, N. (1999). Morphologika. *Tools for Shape Analysis. University College London, London, United Kingdom*.

O'Sullivan, J. A. (2003). A new species of *Archaeohippus* (Mammalia, Equidae) from the Arikareean of central Florida. *Journal of Vertebrate Paleontology*, *23*, 877–885.

O'Sullivan, J. A. (2008). Evolution of the proximal third phalanx in Oligocene-Miocene equids, and the utility of phalangeal indices in phylogeny reconstruction. In E. J. Sargis & M. Dagosto (Eds.), *Mammalian Evolutionary Morphology: A Tribute to Frederick S. Szalay* (pp. 159–165). Dordrecht, Netherlands: Springer.

Oksanen, J., Blanchet, F. G., Friendly, M., Kindt, R., Legendre, P., McGlinn, D., … Wagner, H. (2018). *vegan: Community Ecology Package*. https://CRAN.R-project.org/package=vegan.

Oliver, W. L. R. (1993). *Status Survey and Conservation Action Plan: Pigs, Peccaries and Hippos* (W. L. R. Oliver, Ed.). Gland, Switzerland: IUCN/SSC Pigs and Peccary Specialist Group.

Olson, R. A., Glenn, Z. D., Cliffe, R. N., & Butcher, M. T. (2018). Architectural properties of sloth forelimb muscles (Pilosa: Bradypodidae). *Journal of*

Mammalian Evolution, *25*, 573–588.

Orlando, L., Mashkour, M., Burke, A., Douady, C. J., Eisenmann, V., & Hanni, C. (2006). Geographic distribution of an extinct equid (Equus hydruntinus: Mammalia, Equidae) revealed by morphological and genetical analyses of fossils. *Molecular Ecology*, *15*, 2083–2093.

Osborn, H. F. (1929). Theories as to the origin, ancestry, and adaptive radiation of the titanotheres and other odd-toed ungulates. In H. F. Osborn (Ed.), *The titanotheres of ancient Wyoming, Dakota and Nebraska* (pp. 757–804). Washington D.C.: United States Government Printing Office.

Owen, R. (1838). Notes on the anatomy of the Nubian giraffe. *Transactions of the Zoological Society of London*, *2*, 217–248.

Padilla, M., & Dowler, R. C. (1994). *Tapirus terrestris*. *Mammalian Species*, *481*, 1–8.

Padilla, M., Dowler, R. C., & Downer, C. C. (2010). *Tapirus pinchaque* (Perissodactyla: Tapiridae). *Mammalian Species*, *42*, 166–182.

Panagiotopoulou, O., Pataky, T. C., & Hutchinson, J. R. (2018). Foot pressure distribution in white rhinoceroses (Ceratotherium simum) during walking. *PeerJ Preprints*, *6*, e27365v1.

Paradis, E., Claude, J., & Strimmer, K. (2004). APE: Analyses of Phylogenetics and Evolution in R language. *Bioinformatics*, *20*, 289–290.

Parés-Casanova, P. M., Salamanca-Carreño, A., Alejandro-Crosby, R., Carolino, N., Carolino, I., Leite, J. V., … Lopes, S. (2017). Estudio comparativo de diferentes poblaciones equinas, basado en la morfometría geométrica craneal. *Actas Iberoamericanas de Conservación Animal*, *10*, 14–18.

Parker, A. K., McHorse, B. K., & Pierce, S. E. (2018). Niche modeling reveals lack of broad-scale habitat partitioning in extinct horses of North America. *Palaeogeography, Palaeoclimatology, Palaeoecology*, *511*, 103–118.

Patel, B. A. (2010). Functional morphology of cercopithecoid primate metacarpals. *Journal of Human Evolution*, *58*, 320–337.

Payne, R. C., Veenman, P., & Wilson, A. M. (2004). The role of the extrinsic thoracic limb muscles in equine locomotion. *Journal of Anatomy*, *205*, 479–490.

Pereira, S. G. (2013). *Anatomia ossea, muscular e consideracoes adaptativas do membro toracico de* Tapirus terrestris *(Perissodactyla, Tapiridae)*. Universidade Federal de Uberlandia.

Perez-Crespo, V. A., Arroyo-Cabrales, J., Alva-Valdivia, L. M., Morales-Puente, P., & Cienfuegos-Alvarado, E. (2012). Diet and habitat definitions for Mexican glyptodonts from Cedral (San Luis Potosí, México) based on stable isotope analysis. *Geological Magazine*, *149*, 153–157.

Perez-Crespo, V. A., Arroyo-Cabrales, J., Morales-Puente, P., Cienfuegos-Alvarado, E., & Otero, F. J. (2016). Diet and habitat of mesomammals and megamammals

from Cedral, San Luis Potosí, México. *Geological Magazine*, *155*, 674–684.

Perez, S. I., Bernal, V., & Gonzalez, P. N. (2006). Differences between sliding semi-landmark methods in geometric morphometrics, with an application to human craniofacial and dental variation. *Journal of Anatomy*, *208*, 769–784.

Pierce, S. E., Clack, J. A., & Hutchinson, J. R. (2012). Three-dimensional limb joint mobility in the early tetrapod Ichthyostega. *Nature*, *486*, 523–526.

Piras, P., Maiorino, L., Raia, P., Marcolini, F., Salvi, D., Vignoli, L., & Kotsakis, T. (2010). Functional and phylogenetic constraints in Rhinocerotinae craniodental morphology. *Evolutionary Ecology Research*, *12*, 897–928.

Platt, S. G., Rainwater, T. R., Snider, S., Garel, A., Anderson, T. A., & McMurry, S. T. (2007). Consumption of large mammals by *Crocodylus moreletii*: field observations of necrophagy and interspecific kleptoparasitism. *Https://Doi.Org/10.1894/0038-4909(2007)52[310:COLMBC]2.0.CO;2*, *52*, 310–317.

Prado, J. L., & Alberdi, M. T. (2014). Global evolution of Equidae and Gomphotheriidae from South America. *Integrative Zoology*, *9*, 434–443.

Prado, J. L., & Alberdi, M. T. (2017a). Nomenclature and Taxonomy. In *Fossil Horses of South America: Phylogeny, Systemics and Ecology* (pp. 7–60). Cham, Switzerland: Springer.

Prado, J. L., & Alberdi, M. T. (2017b). Phylogeny. In *Fossil Horses: Systematics, Paleobiology, and Evolution of the Family Equidae* (pp. 73–84). Cham, Switzerland: Springer.

Prothero, D. R. (1985). North American mammalian diversity and Eocene–Oligocene extinctions. *Paleobiology*, *11*, 389–405.

Prothero, D. R. (2005). Postcranial Osteology. In *The Evolution of North American Rhinoceroses* (pp. 146–181). Cambridge: Cambridge University Press.

Prothero, D. R. (2016). Perissodactyla. In D. R. Prothero (Ed.), *The Princeton Guide to Prehistoric Mammals* (pp. 186–202). Oxford: Princeton University Press.

Prothero, D. R., & Sereno, P. C. (1982). Allometry and paleoecology of medial Miocene dwarf rhinoceroses from the Texas Gulf coastal plain. *Paleobiology*, *8*, 16–30.

Qu, Y., Jin, C., Zhang, Y., Hu, Y., Shang, X., & Wang, C. (2014). Preservation assessments and carbon and oxygen isotopes analysis of tooth enamel of *Gigantopithecus blacki* and contemporary animals from Sanhe Cave, Chongzuo, South China during the Early Pleistocene. *Quaternary International*, *354*, 52–58.

R Core Development Team. (2008). *R: a language and environment for statistical computing*. Vienna, Austria: R Foundation for Statistical Computing.

Radinsky, L. B. (1963). Origin and early evolution of North American Tapiroidea. *Bulletin of the Peabody Museum of Natural History, Yale University*, *17*, 1–106.

Radinsky, L. B. (1965a). Early Tertiary Tapiroidea of Asia. *Bulletin American Museum of National History*, *129*, 181–263.

Radinsky, L. B. (1965b). Evolution of the tapiroid skeleton from *Heptodon* to *Tapirus*. *Bulletin of The Museum of Comparative Zoology*, *134*, 69–106.

Radinsky, L. B. (1966). The adaptive radiation of the phenacodontid condylarths and the origin of the Perissodactyla. *Evolution*, *20*, 408–417.

Radinsky, L. B. (1967). *Hyrachyus*, *Chasmotherium*, and the early evolution of helaletid tapiroids. *American Museum Novitates*, *2313*, 1–23.

Rajkumar, H. S., & Klein, H. (2014). First perissodactyl footprints from Flysch deposits of the Barail Group (Lower Oligocene) of Manipur , India. *Proceedings of the Indian Academy of Sciences. Earth and Planetary Sciences*, *123*, 413–420.

Reghem, E., Byron, C., Bels, V., & Pouydebat, E. (2012). Hand posture in the grey mouse lemur during arboreal locomotion on narrow branches. *Journal of Zoology*, *288*, 76–81.

Regnault, S., Hermes, R., Hildebrandt, T. B., Hutchinson, J. R., & Weller, R. (2014). Osteopathology in the feet of rhinoceroses: lesion type and distribution. *Journal of Zoo and Wildlife Medicine*, *44*, 918–927.

Regnault, S., & Pierce, S. E. (2018). Pectoral girdle and forelimb musculoskeletal function in the echidna (*Tachyglossus aculeatus*): insights into mammalian locomotor evolution. *Royal Society Open Science*, *5*, 181400.

Reilly, S. M., McElroy, E. J., & Biknevicius, A. R. (2007). Posture, gait and the ecological relevance of locomotor costs and energy-saving mechanisms in tetrapods. *Zoology*, *110*, 271–289.

Remy, J. A. (1992). Observations sur l'anatomie cranienne du genre Palaeotheium (Perissodactyla, Mammalia); mise en evidence d'un nouveu sous-genre, Franzenitherium. *Palaeovertebrata*, *21*, 105–221.

Remy, J. A. (2004). Le genre *Plagiolophus* (Palaeotheriidae, Perissodactyla, Mammalia): révision systématique, morphologie et histologie dentaires, anatomie crânienne, essai d'interprétation fonctionnelle. *Palaeovertebrata*, *33*, 17–281.

Remy, J. A. (2015). Les Périssodactyles (Mammalia) du gisement Bartonien supérieur de Robiac (Éocène moyen du Gard, Sud de la France). *Palaeovertebrata*, *39*, 1–99.

Retallack, G. J. (2001). Cenozoic expansion of grasslands and climatic cooling. *The Journal of Geology*, *109*, 407–426.

Revell, L. J. (2012). phytools: an R package for phylogenetic comparative biology (and other things). *Methods in Ecology and Evolution*, *3*, 217–223.

Revell, L. J. (2013). Two new graphical methods for mapping trait evolution on phylogenies. *Methods in Ecology and Evolution*, *4*, 754–759.

Ribera, I., & Balke, M. (2007). Recognition of a species-poor, geographically restricted but morphologically diverse Cape lineage of diving beetles (Coleoptera: Dytiscidae: Hyphydrini). *Journal of Biogeography*, *34*, 1220–1232.

Richmond, B. G., & Strait, D. S. (2000). Evidence that humans evolved from a knuckle-walking ancestor. *Nature*, *404*, 382–385.

Robinet, C., Remy, J. A., Laurent, Y., Danilo, L., & Lihoreau, F. (2015). A new genus of Lophiodontidae (Perissodactyla, Mammalia) from the early Eocene of La Borie (Southern France) and the origin of the genus *Lophiodon* Cuvier, 1822. *Geobios*, *48*, 25–38.

Rohlf, F. J., & Corti, M. (2000). Use of two-block partial least-squares to study covariation in shape. *Systematic Biology*, *49*, 740–753.

Rohlf, F. J., & Slice, D. E. (1990). Extensions of the Procrustes method for the optimal superimposition of landmarks. *Systematic Zoology*, *39*, 40–59.

Roman, F. (1914). Le Rhinoceros (Ceratorhinus) tagicus du Musee de Francfort-sur-Main (Oligocene superieur de Budenheim, pres Mayence). *Bulletin de La Société Géologique de France*, *14*, 349–365.

Rosas, A., Pérez-Criado, L., Bastir, M., Estalrrich, A., Huguet, R., García-Tabernero, A., … Rasilla, M. de la. (2015). A geometric morphometrics comparative analysis of Neandertal humeri (epiphyses-fused) from the El Sidrón cave site (Asturias, Spain). *Journal of Human Evolution*, *82*, 51–66.

Rose, K. D. (1996). Skeleton of early Eocene Homogalax and the origin of Perissodactyla. *Palaeovertebrata*, *25*, 243–260.

Rose, K. D., Holbrook, L. T., Rana, R. S., Kumar, K., Jones, K. E., Ahrens, H. E., … Smith, T. (2014). Early Eocene fossils suggest that the mammalian order Perissodactyla originated in India. *Nature Communications*, *5*, 5570.

RStudioTeam. (2016). *RStudio: Integrated Development for R*. Boston: RStudio, Inc.

Rubenstein, D. (2011). Family Equidae (Horses and relatives). In D. E. Wilson & R. A. Mittermeier (Eds.), *Handbook of the Mammals of the World - Volume 2: Hoofed Mammals*. Lynx Edicions.

Rudwick, M. J. S. (2008). The animals from the Gypsum Beds around Paris. In M. J. S. Rudwick (Ed.), *George Cuvier, Fossil Bones and Geological Catastrophes: New Translations and Interpretations of the Primary Texts* (pp. 59–67). Chicago: University of Chicago Press.

Ruiz-García, M., Castellanos, A., Bernal, L. A., Pinedo-Castro, M., Kaston, F., & Shostell, J. M. (2016). Mitogenomics of the mountain tapir (*Tapirus pinchaque*, Tapiridae, Perissodactyla, Mammalia) in Colombia and Ecuador: phylogeography and insights into the origin and systematics of the South American tapirs. *Mammalian Biology - Zeitschrift Für Säugetierkunde*, *81*, 163–175.

Ruiz-García, M., Vásquez, C., Pinedo-Castro, M., Sandoval, S., Castellanos, A.,

Kaston, F., … Shostell, J. M. (2012). Phylogeography of the mountain tapir (Tapirus pinchaque) and the Central American tapir (Tapirus bairdii) and the origins of the three Latin-American tapirs by means of mtCyt-B sequences. In K. Anamthawat-Jnsson (Ed.), *Current Topics in Phylogenetics and Phylogeography of Terrestrial and Aquatic Systems* (pp. 83–116). Available from: https://www.intechopen.com/books/: InTech.

Rustioni, M., & Mazza, P. (2001). Taphonomic analysis of *Tapirus arvernensis* remains from the lower valdarno (Tuscany, central Italy). *Geobios*, *34*, 469–474.

Ryder, O. A. (2009). Rhinoceroses, tapirs, and horses (Perissodactyla). In S. B. Hedges & S. Kumar (Eds.), *The Timetree of Life* (pp. 508–510). Oxford: Oxford University Press.

Samuels, J. X., Meachen, J. A., & Sakai, S. A. (2013). Postcranial morphology and the locomotor habits of living and extinct carnivorans. *Journal of Morphology*, *274*, 121–146.

Samuels, J. X., & Van Valkenburgh, B. (2008). Skeletal indicators of locomotor adaptations in living and extinct rodents. *Journal of Morphology*, *269*, 1387–1411.

Schellhorn, R. (2018). Mediportal rhinoceroses from the Miocene Sandelzhausen locality (Germany). *78th Annual Meeting of the Society of Vertebrate Paleontology*, 211. Albuquerque.

Schellhorn, R., & Pfretzschner, H.-U. (2014). Biometric study of ruminant carpal bones and implications for phylogenetic relationships. *Zoomorphology*, *133*, 139–149.

Scherler, L., Becker, D., & Berger, J.-P. (2011). Tapiridae (Perissodactyla, Mammalia) of the Swiss Molasse Basin during the Oligocene–Miocene transition. *Journal of Vertebrate Paleontology*, *31*, 479–496.

Scherler, L., Mennecart, B., Hiard, F., & Becker, D. (2013). Evolutionary history of hoofed mammals during the Oligocene–Miocene transition in Western Europe. *Swiss Journal of Geosciences*, *106*, 349–369.

Scherler, L., Tütken, T., & Becker, D. (2014). Carbon and oxygen stable isotope compositions of late Pleistocene mammal teeth from dolines of Ajoie (Northwestern Switzerland). *Quaternary Research*, *82*, 378–387.

Schmidt, M., & Fischer, M. S. (2009). Morphological integration in mammalian limb proportions: dissociation between function and development. *Evolution; International Journal of Organic Evolution*, *63*, 749–766.

Schneider, C. A., Rasband, W. S., & Eliceiri, K. W. (2012). NIH Image to ImageJ: 25 years of image analysis. *Nature Methods*, *9*, 671–675.

Schoch, R. M. (1989). A review of the tapiroids. In D. R. Prothero & R. M. Schoch (Eds.), *The evolution of perissodactyls* (pp. 299–320). New York: Oxford University Press.

Scott, E., McHorse, B. K., Jass, C., & Zazula, G. D. (2014). A morphometric assessment of Pleistocene horse metapodials across western North America. *74th Meeting of the Society of Vertebrate Paleontology*, 226. Berlin.

Scott, K. M. (1990). Postcranial dimensions of ungulates as predictors of body size. In B. J. Damuth, J., MacFadden (Ed.), *Body Size in Mammalian Paleobiology: Estimation and Biological Implications* (pp. 301–335). Cambridge: Cambridge University Press.

Scott, R. S., Bernor, R. L., & Raba, W. (2003). Hipparionine horses of the Greater Pannonian Basin: morphometric evidence from the postcranial skeleton. *Palaeontographia Italica*, *90*, 189–209.

Scott, W. B. (1941). The mammalian fauna of the White River Oligocene: Part V. Perissodactyla. *Transactions of the American Philosophical Society, New Series*, *28*, 747–964.

Sears, K. E., Behringer, R. R., Rasweiler, J. J., & Niswander, L. A. (2006). Development of bat flight: morphologic and molecular evolution of bat wing digits. *Proceedings of the National Academy of Sciences of the United States of America*, *103*, 6581–6586.

Seckel, L., & Janis, C. M. (2008). Convergences in scapula morphology among small cursorial mammals: an osteological correlate for locomotory specialization. *Journal of Mammalian Evolution*, *15*, 261–279.

Secord, R., Bloch, J. I., Chester, S. G. B., Boyer, D. M., Wood, A. R., Wing, S. L., … Krigbaum, J. (2012). Evolution of the earliest horses driven by climate change in the Paleocene-Eocene thermal maximum. *Science*, *335*, 959–962.

Secord, R., Wing, S. L., & Chew, A. (2008). Stable isotopes in early Eocene mammals as indicators of forest canopy structure and resource partitioning. *Paleobiology*, *27*, 539–563.

Seetah, K., Cucchi, T., Dobney, K., & Barker, G. (2014). A geometric morphometric re-evaluation of the use of dental form to explore differences in horse (*Equus caballus*) populations and its potential zooarchaeological application. *Journal of Archaeological Science*, *41*, 904–910.

Simpson, G. G. (1945). Notes on Pleistocene and recent tapirs. *Bulletin of the American Museum of Natural History*, *86*, 33–82.

Slice, D. E. (2007). Geometric Morphometrics. *Annual Review of Anthropology*, *36*, 261–281.

Smith, T., De Wilde, B., & Steurbaut, E. (2004). Primitive equoid and tapiroid mammals: keys for interpreting the Ypresian-Lutetian transition in Belgium. *Bulletin de l'Institut Royal Des Sciences Naturelles de Belgique, Sciences de La Terre*, *74*, 165–175.

Smith, T., Sole, F., Missiaen, P., Rana, R. S., Kumar, K., Sahni, A., & Rose, K. D. (2015). First early Eocene tapiroid from India and its implication for the paleobiogeographic origin of perissodactyls. *Palaeovertebrata*, *39*, e5.

Soffler, C., & Hermanson, J. W. (2006). Muscular design in the equine interosseus muscle. *Journal of Morphology*, *267*, 696–704.

Sokal, R. R., & Rohlf, F. J. (2012). *Biometry: The Principles and Practice of Statistics in Biological Research* (Fourth). New York: W. H. Freeman & Co.

Solounias, N., Danowitz, M., Stachtiaris, E., Khurana, A., Araim, M., Sayegh, M., & Natale, J. (2018). The evolution and anatomy of the horse manus with an emphasis on digit reduction. *Royal Society Open Science*, *5*, 171782.

Sondaar, P. Y. (1968). The osteology of the manus of fossil and recent Equidae. *Verhandelingen Der Koninklijke Nederlandse Akademie van Wetenschappen, Natuurkunde*, *25*, 1–76.

Sondaar, P. Y. (1969). Some remarks on horse evolution and classification. In P. J. H. van Bree, H. Dathe, E. Herre, K. Herter, H.-G. Klos, B. Lanza, … W. Verheyen (Eds.), *Zeitschrift fur Saugetierkunde* (pp. 307–310). Hannover: M. Rohrs.

Sondaar, P. Y. (1977). Insularity and its effect on mammal evolution. In *Major Patterns in Vertebrate Evolution* (pp. 671–707). Boston, MA: Springer US.

Spoor, C. F., & Badoux, D. M. (1986). Descriptive and functional myology of the neck and forelimb of the striped hyena (*Hyaena hyaena*, L. 1758). *Anatomischer Anzeiger*, *161*, 375–387.

Stacklyn, S., Wang, Y., Jin, C., Wang, Y., Sun, F., Zhang, C., … Deng, T. (2017). Carbon and oxygen isotopic evidence for diets, environments and niche differentiation of early Pleistocene pandas and associated mammals in South China. *Palaeogeography, Palaeoclimatology, Palaeoecology*, *468*, 351–361.

Stehlin, H. G. (1910). Remarques sur les faunules de Mammifères des couches éocènes et oligocènes du Bassin de Paris. *Bulletin de La Société Géologique de France*, *4*, 488–520.

Steiner, C. C., Mitelberg, A., Tursi, R., & Ryder, O. A. (2012). Molecular phylogeny of extant equids and effects of ancestral polymorphism in resolving species-level phylogenies. *Molecular Phylogenetics and Evolution*, *65*, 573–581.

Steiner, C. C., & Ryder, O. A. (2011). Molecular phylogeny and evolution of the Perissodactyla. *Zoological Journal of the Linnean Society*, *163*, 1289–1303.

Stirling, I., & Derocher, A. E. (1990). Factors affecting the evolution and behavioral ecology of the modern bears. *Bears: Their Biology and Management*, *8*, 189.

Strömberg, C. A. E. (2006). Evolution of hypsodonty in equids: testing a hypothesis of adaptation. *Paleobiology*, *32*, 236–258.

Stubbs, T. L., Pierce, S. E., Rayfield, E. J., & Anderson, P. S. L. (2013). Morphological and biomechanical disparity of crocodile-line archosaurs following the end-Triassic extinction. *Proceedings of the Royal Society B: Biological Sciences*, *280*, 20131940.

Thewissen, J. G. M., & Fish, F. E. (1997). Locomotor evolution in the earliest cetaceans: Functional model, modern analogues, and paleontological evidence.

Paleobiology, *23*, 482–490.

Thomason, J. J. (1985). Estimation of locomotory forces and stresses in the limb bones of recent and extinct equids. *Paleobiology*, *11*, 209–220.

Thomason, J. J. (1986). The functional morphology of the manus in the tridactyl equids *Merychippus* and *Mesohippus* : paleontological inferences from neontological models. *Journal of Vertebrate Paleontology*, *6*, 143–161.

Tong, H. (2005). Dental characters of the Quaternary tapirs in China, their significance in classification and phylogenetic assessment. *Geobios*, *38*, 139–150.

Tong, H., Liu, J., & Han, L. (2002). On fossil remains of Early Pleistocene tapir (Perissodactyla, Mammalia) from Fanchang, Anhui. *Chinese Science Bulletin*, *47*, 586.

Tong, H., & Qiu, Z.-X. (2008). The Perissodactyla. In J. Changzhu & L. Jinyi (Eds.), *Paleolithic Site - The Renzidong Cave, Fangchang, Anhui Province* (pp. 286–320). Beijing: Science Press.

Tonni, E. P., Cione, A. L., & Soibelzon, L. H. (2003). The broken zig-zag: Late Cenozoic large mammal and tortoise extinction in South America. *Revista Del Museo Argentino de Ciencias Naturales*, *5*, no. *1*. Retrieved from http://sedici.unlp.edu.ar/handle/10915/5371

Tougard, C., Delefosse, T., Hänni, C., & Montgelard, C. (2001). Phylogenetic relationships of the five extant Rhinoceros species (Rhinocerotidae, Perissodactyla) based on mitochondrial cytochrome b and 12S rRNA genes. *Molecular Phylogenetics and Evolution*, *19*, 34–44.

Trinkaus, E. (1997). Appendicular robusticity and the paleobiology of modern human emergence. *Proceedings of the National Academy of Sciences of the United States of America*, *94*, 13367–13373.

van der Made, J. (2010). Els macrovertebrats del Camp dels Ninots i el seu context: canvis ambientals, evolució i estructura social. In B. Campeny Vall-llosera, G., Gómez de Soler (Ed.), *El Camp dels Ninots - Restres de l'Evolució* (pp. 105–128). Tarragona: Ayuntament de Caldes de Malavella, Caldes de Malavella, & Institut Català de Paleoecologia Humana i Evolució Social.

van der Made, J., Morales, J., & Montoya, P. (2006). Late Miocene turnover in the Spanish mammal record in relation to palaeoclimate and the Messinian Salinity Crisis. *Palaeogeography, Palaeoclimatology, Palaeoecology*, *238*, 228–246.

van der Made, J., & Stefanovic, I. (2006). A small tapir from the Turolianof Kreka (Bosnia) and a discussion on the biogeography andstratigraphy of the Neogene tapirs. *Neues Jahrbuch Für Geologie Und Paläontologie - Abhandlungen*, 207–240.

Van Valkenburgh, B. (1987). Skeletal indicators of locomotor behavior in living and extinct carnivores. *Journal of Vertebrate Paleontology*, *7*, 162–182.

Van Valkenburgh, B., & Koepfli, K. (1993). Cranial and dental adaptations to predation in canids. *Symposia of the Zoological Society of London*, *65*, 15–37.

Velasco, J. A., Martínez-Meyer, E., & Flores-Villela, O. (2018). Climatic niche dynamics and its role in the insular endemism of *Anolis* lizards. *Evolutionary Biology*, *45*, 345–357.

Venables, W. N., & Ripley, B. D. (2002). Time Series Analysis. In W. N. Venables & B. D. Ripley (Eds.), *Modern Applied Statistics with S* (Fourth, pp. 387–418). Springer-Verlag.

Vercammen, F., Bosseler, L., Tignon, M., & Cay, A. B. (2017). Encephalomyocarditis virus in a captive Malayan tapir (*Tapirus indicus*). *Open Veterinary Journal*, *7*, 100–103.

Voorhies, M. R. (1981). Dwarfing the St. Helens eruption: an ancient ashfall creates a Pompeii of prehistoric animals. *National Geographic*, *159*, 66–75.

Wallace, R., Ayala, G., & Viscarra, M. (2012). Lowland tapir (*Tapirus terrestris*) distribution, activity patterns and relative abundance in the Greater Madidi-Tambopata Landscape. *Integrative Zoology*, *7*, 407–419.

Walmsley, A., Elton, S., Louys, J., Bishop, L. C., & Meloro, C. (2012). Humeral epiphyseal shape in the felidae: the influence of phylogeny, allometry, and locomotion. *Journal of Morphology*, *273*, 1424–1438.

Walter, R. M., & Carrier, D. R. (2007). Ground forces applied by galloping dogs. *Journal of Experimental Biology*, *210*, 208–216.

Wareing, K., Tickle, P. G., Stokkan, K. A., Codd, J. R., & Sellers, W. I. (2011). The musculoskeletal anatomy of the reindeer (*Rangifer tarandus*): fore- and hindlimb. *Polar Biology*, *34*, 1571–1578.

Warner, S. E., Pickering, P., Panagiotopoulou, O., Pfau, T., Ren, L., & Hutchinson, J. R. (2013). Size-related changes in foot impact mechanics in hoofed mammals. *PLoS ONE*, *8*, e54784.

Warton, D. I., Wright, S. T., & Wang, Y. (2012). Distance-based multivariate analyses confound location and dispersion effects. *Methods in Ecology and Evolution*, *3*, 89–101.

Watson, J. C., & Wilson, A. M. (2007a). Muscle architecture of biceps brachii, triceps brachii and supraspinatus in the horse. *Journal of Anatomy*, *210*, 32–40.

Watson, J. C., & Wilson, A. M. (2007b). Muscle architecture of biceps brachii, *triceps brachii* and *supraspinatus* in the horse. *Journal of Anatomy*, *210*, 32–40.

Watson, L. H., & Chadwick, P. (2007). Management of Cape mountain zebra in the Kammanassie Nature Reserve, South Africa. *South African Journal of Wildlife Research*, *37*, 31–39.

Weisbecker, V., & Warton, D. I. (2006). Evidence at hand: diversity, functional implications, and locomotor prediction in intrinsic hand proportions of diprotodontian marsupials. *Journal of Morphology*, *267*, 1469–1485.

Wickham, H. (2009). *ggplot2: Elegent Graphics for Data Analysis* (1st ed.; R. Gentleman, K. Hornik, & G. Parmigiani, Eds.). New York: Springer-Verlag.

Wiley, D. F., Amenta, N., Alcantara, D. A., Ghosh, D., Kil, Y. J., Delson, E., … O'Neill, R. (2006). Landmark Editor 3.0. *Institute for Data Analysis and Visualization (IDAV) and the University of California, Davis*.

Wilson, A. M., McGuigan, M. P., Su, A., & van Den Bogert, A. J. (2001). Horses damp the spring in their step. *Nature*, *414*, 895–899.

Wilson, A. M., Watson, J. C., & Lichtwark, G. A. (2003). A catapult action for rapid limb protraction. *Nature*, *421*, 35–36.

Wilson, D. E., & Reeder, D. M. (2005). *Mammal Species of the World: A Taxonomic and Geographical Reference* (3rd ed.; D. E. Wilson & D. M. Reeder, Eds.). Johns Hopkins University Press.

Windle, H. C. A., & Parsons, F. G. (1902). On the muscles of the Ungulata. *Proceedings of the Zoological Society of London*, *71*, 656–704.

Witmer, L. M. (1995). The Extant Phylogenetic Bracket and the importance of reconstructing soft tissues in fossils. In J. J. Thomason (Ed.), *Functional Morphology in Vertebrate Paleontology* (pp. 19–33). Cambridge: Cambridge University Press.

Wood, A. R., Bebej, R. M., Manz, C. L., Begun, D. L., & Gingerich, P. D. (2011). Postcranial functional morphology of *Hyracotherium* (Equidae, Perissodactyla) and locomotion in the earliest horses. *Journal of Mammalian Evolution*, *18*, 1–32.

Wortman, J. L., & Earle, C. (1892). Ancestors of the tapir from the lower Miocene of Dakota. *Bulletin American Museum of National History*, *5*, 159–180.

Yalden, D. W. (1971). The functional morphology of the carpus in ungulate mammals. *Cells Tissues Organs*, *78*, 461–487.

Zachos, J. C., Dickens, G. R., & Zeebe, R. E. (2008). An early Cenozoic perspective on greenhouse warming and carbon-cycle dynamics. *Nature*, *451*, 279–283.

Zanazzi, A., & Kohn, M. J. (2008). Ecology and physiology of White River mammals based on stable isotope ratios of teeth. *Palaeogeography, Palaeoclimatology, Palaeoecology*, *257*, 22–37.

Zelditch, M. L., Swiderski, D. L., & Sheets, H. D. (2012). *Geometric Morphometrics for Biologists: A Primer* (Second). New York: Elsevier Academic Press.

Zhang, K. Y., Wiktorowicz-Conroy, A., Hutchinson, J. R., Doube, M., Klosowski, M., Shefelbine, S. J., & Bull, A. M. J. (2012). 3D Morphometric and posture study of felid scapulae using statistical shape modelling. *PloS One*, *7*, e34619.

– SUPPLEMENTARY CONTENTS –

page

– RESEARCH CHAPTER ONE: APPENDIX I –

A three-dimensional morphometric analysis of upper forelimb morphology in the enigmatic tapir (Perissodactyla: *Tapirus*) hints at subtle variations in locomotor ecology

Jamie A. MacLaren and Sandra Nauwelaerts

Table of Contents

1. List of landmark positions with diagrammatic representations

Bone	Lm	Description
Scapula	$_{S}$Lm1	Cranial angle of the scapula
	$_{S}$Lm2	Caudal angle of the scapula
	$_{S}$Lm3	Proximal margin of tuber of scapula spine
	$_{S}$Lm4	Ventral margin of tuber of scapula spine
	$_{S}$Lm5	Distal margin of tuber of scapula spine
	$_{S}$Lm6	Cranial margin of tuber of scapula spine
	$_{S}$Lm7	Distal-most point of the scapular spine
	$_{S}$Lm8	Cranial margin of glenoid cavity
	$_{S}$Lm9	Lateral margin of glenoid cavity
	$_{S}$Lm10	Ventral margin of glenoid cavity
	$_{S}$Lm11	Medial margin of glenoid cavity
	$_{S}$Lm12	Deepest point of glenoid cavity
	$_{S}$Lm13	Distal angle of cranial margin process (of coracoscapular notch)
	$_{S}$Lm14	Proximal angle of coracoscapular notch
	$_{S}$Lm15	Deepest point of coracoscapular notch
	$_{S}$Lm16	Distal angle of coracoscapular notch
	$_{S}$Lm17	Greatest angle of supraglenoid process
	$_{S}$Lm18	Glenoid margin of *m. biceps brachii* origination

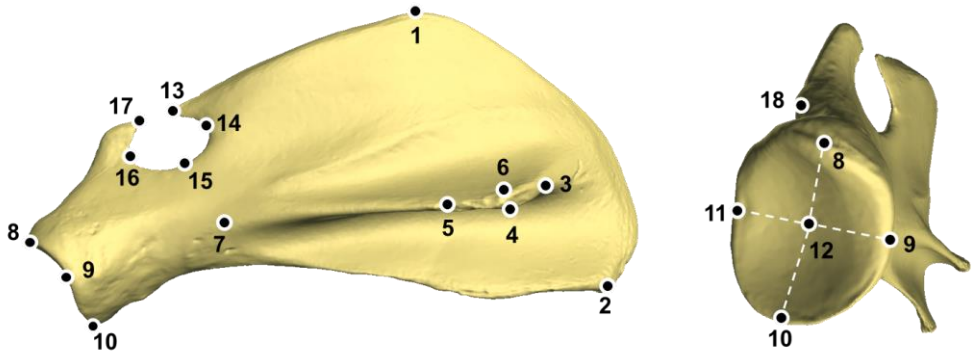

Humerus	$_{H}$Lm1	Inner angle of greater tubercle
	$_{H}$Lm2	Proximal-most point of anterior greater tubercle
	$_{H}$Lm3	Inner angle of lesser tubercle
	$_{H}$Lm4	Proximal-most point of lesser tubercle
	$_{H}$Lm5	Deepest point of intertubercular sulcus
	$_{H}$Lm6	Deepest point of division within two heads of greater tubercle
	$_{H}$Lm7	Proximal-most point of posterior greater tubercle
	$_{H}$Lm8	Antero-proximal angle of *m. infraspinatus* insertion
	$_{H}$Lm9	Anterior-most point of the humeral head (articular surface)
	$_{H}$Lm10	Lateral-most point of the humeral head (articular surface)

$_{H}$Lm11 Distal-most point of humeral head (articular surface)
$_{H}$Lm12 Medial-most point of humeral head (articular surface)
$_{H}$Lm13 Centre of humeral head (articular surface)
$_{H}$Lm14 Proximal origin of deltoid tuberosity
$_{H}$Lm15 Apex of deltoid tuberosity
$_{H}$Lm16 Distal terminus of deltoid tuberosity
$_{H}$Lm17 Proximal margin of teres tuberosity
$_{H}$Lm18 Medial margin of teres tuberosity
$_{H}$Lm19 Distal margin of teres tuberosity
$_{H}$Lm20 Lateral margin of teres tuberosity
$_{H}$Lm21 Apex of lateral epicondyle
$_{H}$Lm22 Apex of medial epicondyle
$_{H}$Lm23 Caudodistal angle of medial epicondyle
$_{H}$Lm24 Caudodistal angle of lateral epicondyle
$_{H}$Lm25 Lateral angle of trochlear notch (olecranon fossa aspect)
$_{H}$Lm26 Medial angle of trochlear notch (olecranon fossa aspect)
$_{H}$Lm27 Distal-most point of sagittal ridge between capitulum and trochlea
$_{H}$Lm28 Distal-most point of medial trochlea
$_{H}$Lm29 Anterior-most point of lateral capitulum
$_{H}$Lm30 Anterior-most point of medial trochlea
$_{H}$Lm31 Proximolateral angle of capitulum (anterior aspect)
$_{H}$Lm32 Proximomedial angle of trochlea (anterior aspect)
$_{H}$Lm33 Deepest point of proximal trochlear margin (anterior aspect)
$_{H}$Lm34 Centre of trochlear groove (anterior aspect; between $_{H}$Lm 29 and 30)
$_{H}$Lm35 Distal-most point of trochlear groove (between $_{H}$Lm 27 and 28)
$_{H}$Lm36 Deepest point of proximal trochlear margin (olecranon fossa aspect)
$_{H}$Lm37 Proximomedial angle of capitulum (anterior aspect; origin of sagittal ridge)
$_{H}$Lm38 Anterior-most point of sagittal ridge between capitulum and trochlea
$_{H}$Lm39 Antero-distal angle of *m. infraspinatus* insertion
$_{H}$Lm40 Caudodistal extremity of *m. infraspinatus* insertion
$_{H}$Lm41 Distolateral angle of capitulum (anterior aspect)
$_{H}$Lm42 Distal angle between capitulum and ridge; terminus of capitulum

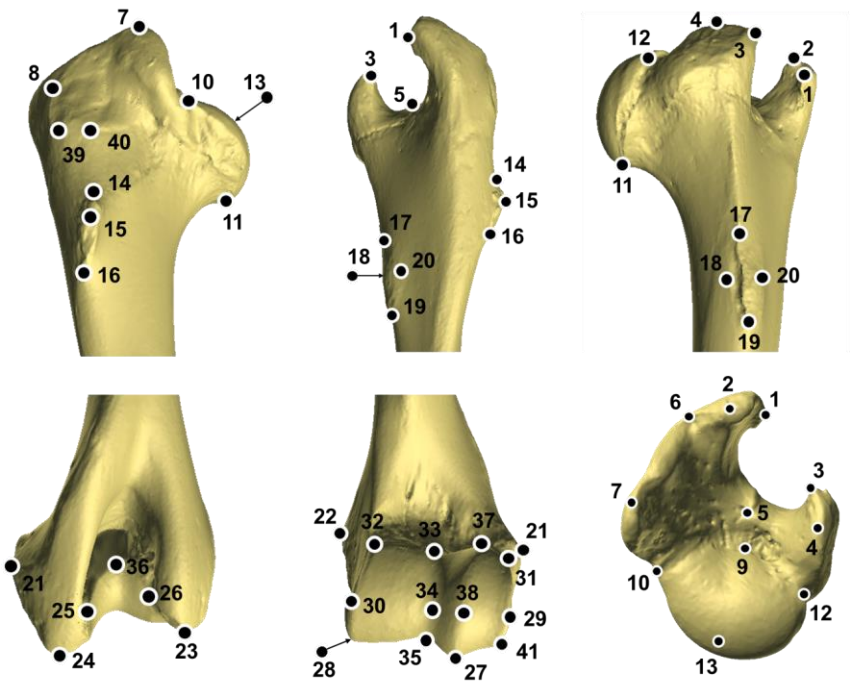

Radius	$_{R}$Lm1	Posterior margin of medial sagittal crest of radial head
	$_{R}$Lm2	Posterior margin of sagittal groove of radial head
	$_{R}$Lm3	Posterior margin of lateral sagittal crest of radial head
	$_{R}$Lm4	Lateral margin of radial head
	$_{R}$Lm5	Anterior margin of medial sagittal crest of radial head
	$_{R}$Lm6	Anterior margin of sagittal groove of radial head
	$_{R}$Lm7	Anterior margin of lateral sagittal crest of radial head
	$_{R}$Lm8	Anteromedial angle of radial head
	$_{R}$Lm9	Posteromedial angle of radial head
	$_{R}$Lm10	Deepest point of lateral sagittal crest of radial head
	$_{R}$Lm11	Lateral tuberosity of the radius (insertion of the lateral collateral ligament)
	$_{R}$Lm12	Highest point of medial distal ridge of the radius
	$_{R}$Lm13	Distal margin of medial distal ridge of the radius
	$_{R}$Lm14	Highest point of lateral distal ridge of the radius
	$_{R}$Lm15	Distal margin of lateral distal ridge of the radius
	$_{R}$Lm16	Distal-most point of anterodistal radiocarpal articulation (lateral side)
	$_{R}$Lm17	Antero-lateral point of distal ulnar facet
	$_{R}$Lm18	Postero-lateral point of distal ulnar facet
	$_{R}$Lm19	Greatest angle of the radio-carpal articulation (posterior aspect)
	$_{R}$Lm20	Posterior extremity of radio-carpal articulation (laterodistal)
	$_{R}$Lm21	Lateral angle of scaphoid facet (radiocarpal articulation)
	$_{R}$Lm22	Medial angle of scaphoid facet (radiocarpal articulation)

	$_{R}$Lm23	Posterior extremity of radio-carpal articulation (mediodistal)
	$_{R}$Lm24	Distal-most point of anterodistal radiocarpal articulation (medial side)
	$_{R}$Lm25	Deepest point of distal radial sulcus (passage of radial carpal extensor muscle)

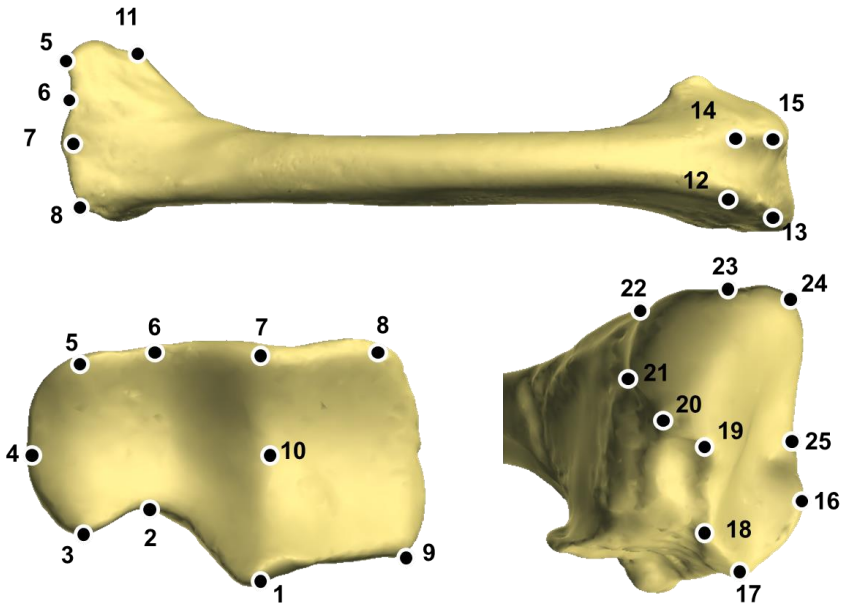

Ulna	$_{U}$Lm1	Apex of anconeal process
	$_{U}$Lm2	Medial prominence angle of anconeal process
	$_{U}$Lm3	Lateral facet angle of anconeal process
	$_{U}$Lm4	Deepest point of medial margin of trochlear notch
	$_{U}$Lm5	Deepest point of lateral margin of trochlear notch
	$_{U}$Lm6	Apex of medial coronoid process
	$_{U}$Lm7	Medial angle of the radial notch of the trochlear notch
	$_{U}$Lm8	Distal angle of lateral radial notch
	$_{U}$Lm9	Proximal angle of trochlear notch (angle alongside radial notch $_{U}$Lm8)
	$_{U}$Lm10	Apex of lateral coronoid process
	$_{U}$Lm11	Medial angle of medial margin (proximal to the interosseous space)
	$_{U}$Lm12	Deepest point of margin between lateral coronoid process and lateral ulnar margin
	$_{U}$Lm13	Deepest point of anterior anconeal/olecranon process
	$_{U}$Lm14	Antero-medial apex of *m. triceps brachii* insertion
	$_{U}$Lm15	Postero-medial apex of *m. triceps brachii* insertion
	$_{U}$Lm16	Lateral apex of *m. triceps brachii* insertion
	$_{U}$Lm17	Proximal-most point of olecranon process

ULm18	Apex of lateral protuberance on olecranon tuber (insertion of medial arm of *m. triceps brachii*)
ULm19	Distal-most point of *m. palmaris longus* origination (posterlateral aspect)
ULm20	Proximal-most point of distal radio-ulnar joint (lateral aspect)
ULm21	Apex of the styloid process of the ulna
ULm22	Proximal extent of the pisiform facet
ULm23	Lateral extent of the pisiform/pyramidal facet
ULm24	Distal extent of the pyramidal facet
ULm25	Medial angle of the pisiform/pyramidal facet
ULm26	Medio-proximal extent of pyradimal facet
ULm27	Latero-proximal extent of pyramidal facet

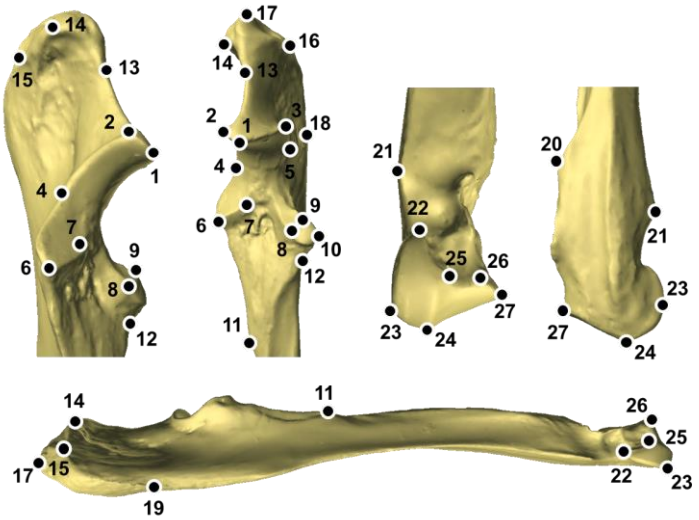

2. Centroid Sizes

Table S1.1. Centroid sizes from landmark analysis for tapir upper forelimb bones.

Specimen	**Species**	**Centroid Sizes**			
		Scap.	Hum.	Radius	Ulna
RMNH 43495	*T. bairdii*	5.955	6.544	6.321	6.306
AMNH 90128	*T. bairdii*	5.837	6.424	6.159	6.170
AMNH 130104	*T. bairdii*	6.006	6.526	6.258	6.283
MVZ 141173	*T. bairdii*	5.850	6.477	6.221	6.213
MVZ 141296	*T. bairdii*	5.801	6.444	6.188	6.191
Average	*T. bairdii*	5.890	6.483	6.230	6.233
NHMW 1938	*T. indicus*	6.009	6.525	6.343	6.342
NHMW 42298	*T. indicus*	6.056	6.545	6.329	6.353
RMNH 17923	*T. indicus*	5.999	6.556	6.368	6.368
RMNH 43543	*T. indicus*	5.961	6.510	6.318	6.310
RMNH 21056	*T. indicus*	5.960	6.502	*n/a*	6.319

RMNH 1014	*T. indicus*	6.045	6.505	6.367	6.352
ZMB MAM 47503	*T. indicus*	6.054	6.585	6.369	6.379
ZMB MAM 4950	*T. indicus*	6.032	6.558	6.392	6.375
Average	*T. indicus*	6.014	6.536	6.355	6.350
MNHN 1982-34	*T. pinchaque*	5.884	6.517	6.252	6.263
MEO 2203a	*T. pinchaque*	5.833	6.534	6.220	6.223
ZMB MAM 62085	*T. pinchaque*	5.904	6.553	6.292	6.303
AMNH 149424	*T. pinchaque*	5.837	6.491	6.198	6.212
Average	*T. pinchaque*	5.865	6.524	6.241	6.250
NHMW 58178	*T. terrestris*	5.965	6.505	6.243	6.233
MEO 2204e	*T. terrestris*	5.978	6.490	6.235	6.235
MEO 2204b	*T. terrestris*	5.850	6.444	6.264	6.239
RMNH 12827	*T. terrestris*	5.884	6.417	6.185	6.175
RMNH 12913	*T. terrestris*	5.978	6.544	6.302	6.294
RMNH 1163.2b	*T. terrestris*	5.827	6.388	6.147	6.148
ZMB MAM 12999	*T. terrestris*	5.909	6.454	6.208	6.194
Average	*T. terrestris*	5.913	6.463	6.226	6.217

3. Maximum length measurements

Maximum bone lengths were approximated from the most proximal and most distal landmark points. The distances were calculated using Euclidean Distance Matrix Analysis:

$$\sqrt{(x_i - x_j)^2 + (y_i - y_j)^2 + (z_i - z_j)^2}$$

where x_i is the x-coordinate for landmark *i*, y_i is the y-coordinate for landmark *i*, and z_i is the z-coordinate for landmark *i*. Landmark *i* represents one end of the linear measurement; landmark *j* represents the other end. Dorsal angle of the scapula is not possible to calculate, and so scapular length is calculated from the caudal angle (acting as a proxy for the maximum length).

Table S1.2. Maximum bone lengths from landmark analysis for tapir upper forelimb bones.

Specimen	**Species**	**Proxy for Maximum Bone Length (mm)**			
		Scap.	Hum.	Radius	Ulna
RMNH 43495	*T. bairdii*	249.61	253.63	228.51	293.84
AMNH 90128	*T. bairdii*	231.36	231.29	192.12	259.76
AMNH 130104	*T. bairdii*	269.53	248.58	213.92	292.95
MVZ 141173	*T. bairdii*	231.69	240.37	206.83	271.65
MVZ 141296	*T. bairdii*	226.49	232.18	198.76	267.55
Average	*T. bairdii*	241.74	241.2	208.03	277.15
NHMW 1938	*T. indicus*	246.05	250.19	235.37	306.88
NHMW 42298	*T. indicus*	273.18	260.30	233.58	308.87

RMNH 17923	*T. indicus*	269.36	256.34	241.69	310.63
RMNH 43543	*T. indicus*	254.99	242.66	230.29	292.64
RMNH 21056	*T. indicus*	230.10	244.21	n/a	297.97
RMNH 1014	*T. indicus*	257.30	244.56	245.25	310.65
ZMB MAM 47503	*T. indicus*	261.96	263.40	242.85	314.74
ZMB MAM	*T. indicus*	264.24	256.00	247.80	313.93
Average	*T. indicus*	257.15	252.21	239.55	307.04
MNHN 1982-34	*T. pinchaque*	243.44	249.75	214.01	284.76
MEO 2203a	*T. pinchaque*	222.22	248.58	206.50	270.67
ZMB MAM 62085	*T. pinchaque*	250.89	255.05	219.61	294.71
AMNH 149424	*T. pinchaque*	224.88	239.01	199.67	270.35
Average	*T. pinchaque*	235.35	248.10	209.95	280.17
NHMW 58178	*T. terrestris*	257.20	246.03	210.04	277.77
MEO 2204e	*T. terrestris*	254.83	245.50	208.34	272.75
MEO 2204b	*T. terrestris*	235.25	239.10	214.02	276.28
RMNH 12827	*T. terrestris*	233.64	226.45	197.96	256.26
RMNH 12913	*T. terrestris*	266.44	260.18	223.12	288.62
RMNH 1163.2b	*T. terrestris*	225.04	220.90	193.73	255.36
ZMB MAM 12999	*T. terrestris*	239.29	232.85	200.03	256.04
Average	*T. terrestris*	244.53	238.71	206.75	269.01

4. Mahalanobis distances

Table S1.3. Squared Mahalanobis distances (MD^2) from linear discriminant function analyses of tapir upper forelimb bones

Specimen	Species	Scap. MD^2	Hum. MD^2	Radius MD^2	Ulna MD^2
RMNH 43495	*T. bairdii*	3.737	1.224	0.802	1.212
AMNH 90128	*T. bairdii*	4.335	2.012	1.484	0.053
AMNH 130104	*T. bairdii*	2.195	2.443	1.085	2.997
MVZ 141173	*T. bairdii*	1.247	0.819	3.468	2.725
MVZ 141296	*T. bairdii*	4.298	1.229	2.373	0.394
NHMW 1938	*T. indicus*	1.295	10.588	5.402	1.501
NHMW 42298	*T. indicus*	3.427	2.056	3.882	2.741
RMNH 17923	*T. indicus*	3.234	7.068	0.356	1.4
RMNH 43543	*T. indicus*	1.852	1.749	0.67	1.288
RMNH 21056	*T. indicus*	3.284	3.802	n/a	1.391
RMNH 1014	*T. indicus*	0.258	0.933	3.803	2.314
ZMB MAM 47503	*T. indicus*	0.997	1.83	0.566	1.783
ZMB MAM	*T. indicus*	0.924	9.093	5.348	4.925
MNHN 1982-34	*T. pinchaque*	3.173	0.499	2.618	3.984

MEO 2203a	*T. pinchaque*	0.356	1.564	4.373	0.273
ZMB MAM 62085	*T. pinchaque*	1.303	1.059	5.71	1.681
AMNH 149424	*T. pinchaque*	4.735	0.929	0.554	2.022
NHMW 58178	*T. terrestris*	0.929	0.267	0.779	2.943
MEO 2204e	*T. terrestris*	3.841	4.757	1.382	2.613
MEO 2204b	*T. terrestris*	1.135	1.024	1.609	3.534
RMNH 12827	*T. terrestris*	3.341	2.444	2.249	3.599
RMNH 12913	*T. terrestris*	5.542	0.979	4.289	6.278
RMNH 1163.2b	*T. terrestris*	3.178	1.437	0.056	3.424
ZMB MAM 12999	*T. terrestris*	1.383	0.193	4.142	4.927

5. Scapular Fossa Ratio (SFR) calculations

Table S1.4. Calculations for scapular fossa ratios (SFRs) in selected perissodactyls. Areas in cm^2. A*s* = area of supraspinous fossa; A*i* = area of infraspinous fossa.

Specimen	**Genus**	**Species**	**A*s***	**A*i***	**Ratio**
ZMB MAM 46075	*Equus*	*africanus*	42.85	103.29	0.293
NMW 7795	*Equus*	*hemionus*	46.17	108.13	0.299
MEO 2194f	*Equus*	*hemionus*	61.64	127.23	0.326
NMW 7222	*Equus*	*kiang*	73.06	131.12	0.358
ZMB MAM 7942	*Equus*	*kiang*	62.09	127.60	0.327
ZMB MAM 33809	*Equus*	*kiang*	71.84	125.74	0.364
ZMB MAM 60363	*Equus*	*przewalski*	81.15	150.37	0.351
ZMBMAM 60606	*Equus*	*przewalski*	96.00	150.68	0.389
RMCA 38121	*Equus*	*zebra*	68.59	135.46	0.336
RMCA 38121	*Equus*	*quagga*	69.54	129.86	0.349
RMCA 30664	*Equus*	*quagga*	59.35	140.58	0.297
MNHN 1982-34	*Tapirus*	*pinchaque*	153.83	90.76	0.628
MEO 2203a	*Tapirus*	*pinchaque*	115.17	68.20	0.628
AMNH 149424	*Tapirus*	*pinchaque*	134.98	100.65	0.572
ZMB MAM 62085	*Tapirus*	*pinchaque*	132.25	89.64	0.596
MNHN 1974-101	*Tapirus*	*pinchaque*	151.18	105.53	0.589
RMNH 43495	*Tapirus*	*bairdii*	154.49	111.08	0.581
AMNH 130104	*Tapirus*	*bairdii*	176.48	130.20	0.575
MVZ 141296	*Tapirus*	*bairdii*	125.35	99.14	0.558
AMNH 90128	*Tapirus*	*bairdii*	125.89	88.05	0.588
MVZ 141173	*Tapirus*	*bairdii*	105.56	83.81	0.557
NMHW 58178	*Tapirus*	*terrestris*	146.22	138.56	0.513

MEO 2204e	*Tapirus*	*terrestris*	160.29	100.26	0.615
MEO 2204b	*Tapirus*	*terrestris*	146.64	114.05	0.562
RMNH 12827	*Tapirus*	*terrestris*	145.83	113.77	0.561
RMNH 12913	*Tapirus*	*terrestris*	170.84	144.88	0.541
RMNH 1163.2b	*Tapirus*	*terrestris*	133.11	109.32	0.549
NMHW 1938	*Tapirus*	*indicus*	164.36	187.54	0.467
NMHW 42298	*Tapirus*	*indicus*	179.77	211.56	0.459
RMNH 17923	*Tapirus*	*indicus*	168.32	194.79	0.463
RMNH 43543	*Tapirus*	*indicus*	162.34	152.65	0.515
RMNH 21056	*Tapirus*	*indicus*	150.66	168.05	0.472
RMNH 1014	*Tapirus*	*indicus*	166.50	156.70	0.515
ZMB MAM 47503	*Tapirus*	*indicus*	143.27	156.63	0.477
ZMB MAM 4950	*Tapirus*	*indicus*	174.24	190.00	0.478
RMCA 35146	*Ceratotherium*	*simim*	242.45	315.38	0.434
RMCA 31727	*Diceros*	*bicornis*	184.93	181.50	0.504
NHMUK com. coll.	*Rhinoceros*	*uniconis*	187.97	141.59	0.570
MNHN com. coll.	*Dicerorhinus*	*sumatrensis*	278.71	253.61	0.524

6. MANOVA and power analyses

Supplementary Table S1.6. Results of MANOVA and power analysis on upper forelimb bones. DF = degrees of freedom; Err. DF = degrees of freedom associated with model errors; p = significance value associated with multivariate F statistic (0.05 ≥ reject null hypothesis that species has no effect on shape); η_p^2 = partial eta squared, the proportion of variance in the variable (shape) which is attributable to group (species). Pillai's = Pillai's Trace statistic (preferred); Wilk's = Wilk's Lambda statistic.

Bone	Statistic	Value	F	DF	Err. DF	p	η_p^2	Power
Scapula	Pillai's	2.85	2.93	60	9	0.04	0.951	0.81
	Wilks'	0	2.52	60	3.818	0.20	0.975	0.33
Humerus	Pillai's	2.87	3.38	60	9	0.03	0.958	0.87
	Wilks'	0	6.95	60	3.818	0.04	0.991	0.72
Radius	Pillai's	2.74	1.66	57	9	0.21	0.913	0.52
	Wilks'	0	2.33	57	3.808	0.22	0.971	0.30
Ulna	Pillai's	2.86	2.99	60	9	0.04	0.952	0.82
	Wilks'	0	12.52	60	3.818	0.01	0.995	0.92

– RESEARCH CHAPTER TWO: APPENDIX II –

Interspecific variation in the tetradactyl manus of modern tapirs (Perissodactyla: *Tapirus*) exposed using geometric morphometrics

Jamie A. MacLaren and Sandra Nauwelaerts

Table of Contents

1. List of specimens

List of specimens scanned for geometric morphometric analysis. Limb elements used: **pi** = pisiform, **cu** = cuneiform, **lu** = lunate, **sc** = scaphoid, **tr** = trapezoid, **ma** = magnum, **un** = unciform, **2** = second metacarpal, **3** = third metacarpal, **4** = fourth metacarpal, **5** = fifth metacarpal. Dashes represent unknown gender for specimen. Prox. = proximal carpal row; Dist. = distal carpal row; s/adult = subadult (scapula not fully ossified).

Taxon	Specimen No.	Prox.	Dist.	MCs	Sex	Age
Tapirus indicus	NHMW 1938	cu, lu, sc	tr, ma, un	2, 3, 4, 5	-	adult
	NHMW 42298	pi, cu, lu, sc	tr, ma, un	2, 3, 4, 5	F	adult
	RMNH 17923	lu, sc	ma	2, 3, 4, 5	-	adult
	RMNH 43543	pi, cu, sc	ma, un	2, 3, 4, 5	-	adult
	RMNH 21056	pi, cu, lu, sc	tr, ma, un	2, 3, 4, 5	-	adult
	RMNH 1014	pi, cu, lu, sc	ma, un	2, 3, 4, 5	-	adult
	ZMB MAM 47503	pi, cu, lu, sc	tr, ma, un	2, 3, 4, 5	F	adult
Tapirus bairdii	RMNH 43495	pi, cu, lu, sc	tr, ma, un	2, 3, 4, 5	-	adult
	AMNH 90128	pi, cu, lu, sc	tr, ma, un	2, 3, 4, 5	-	s/adult
	AMNH 130104	pi, cu, lu, sc	tr, ma, un	2, 3, 4, 5	-	adult
	MVZ 141173	pi, cu, lu, sc	tr, ma, un	2, 3, 4, 5	F	adult
	MVZ 141296	pi, cu, lu	tr, ma, un	2, 3, 4, 5	M	s/adult
Tapirus pinchaque	MNHN 1982-34	pi, cu, lu, sc	tr, un	2, 3, 4, 5	-	adult
	MEO 2203a	pi, cu, lu, sc	tr, ma, un	2, 3, 4, 5	M	adult
	ZMB MAM 62085	pi, cu, lu, sc	tr, ma, un	2, 3, 4, 5	M	adult
	AMNH 149424	pi, cu, lu, sc	tr, ma, un	2, 3, 4, 5	F	s/adult
Tapirus terrestris	NHMW 58178	pi, cu, lu, sc	tr, ma, un	2, 3, 4, 5	F	adult
	MEO 2204b	-	tr, ma, un	2, 3, 4, 5	M	adult
	RMNH 12827	pi, cu, lu, sc	tr, ma, un	2, 3, 4, 5	M	adult
	RMNH 12913	pi, cu, lu, sc	ma, un	2, 3, 4, 5	-	adult
	RMNH 1163.2b	pi, cu, lu, sc	tr, ma	2, 3, 4, 5	M	adult
	ZMB MAM 12999	pi, cu, lu, sc	tr, ma, un	2, 3, 4, 5	F	adult

2. Landmark placements on autopodial bones

Landmark placements on each bone from the autopodium, from proximal carpal row to metacarpals. Description of landmarks (left) alongside numbered landmarks placed onto images of scans (right)

Pisiform	
1. Proximolateral angle between ulna facet and ‘styloid’ facet	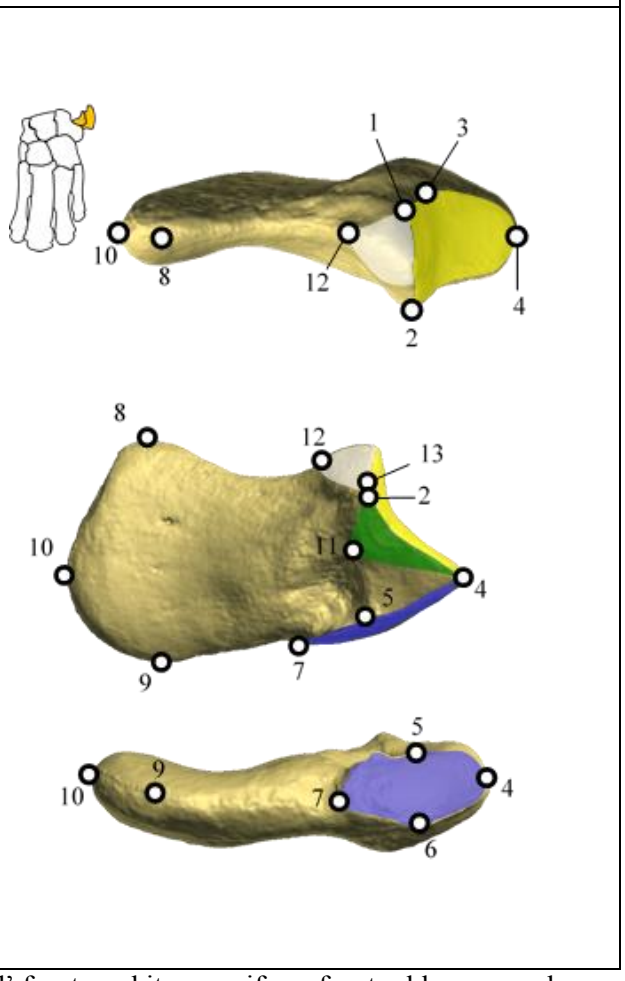
2. Most medial angle of ulna facet	
3. Most lateral angle of ulna facet	
4. Apex of ulna facet meeting cuneiform facet	
5. Most medial angle of cuneiform facet	
6. Most lateral angle of cuneiform facet	
7. Most posterior angle of cuneiform facet	
8. Most proximal angle of pisiform blad	
9. Most distal angle of pisiform blade	
10. Most posterior point on pisiform blade	
11. Most posterior angle of secondary cuneiform facet	
12. Most posterior angle of ‘styloid facet’	
13. Proximomedial angle between ulna facet and ‘styloid’ facet	

Key:- ulna facet = yellow; ‘styloid’ facet = white; cuneiform facet = blue; secondary cuneiform facet = green.

Cuneiform (pyramidal)	
1. Most posterior angle of unciform facet	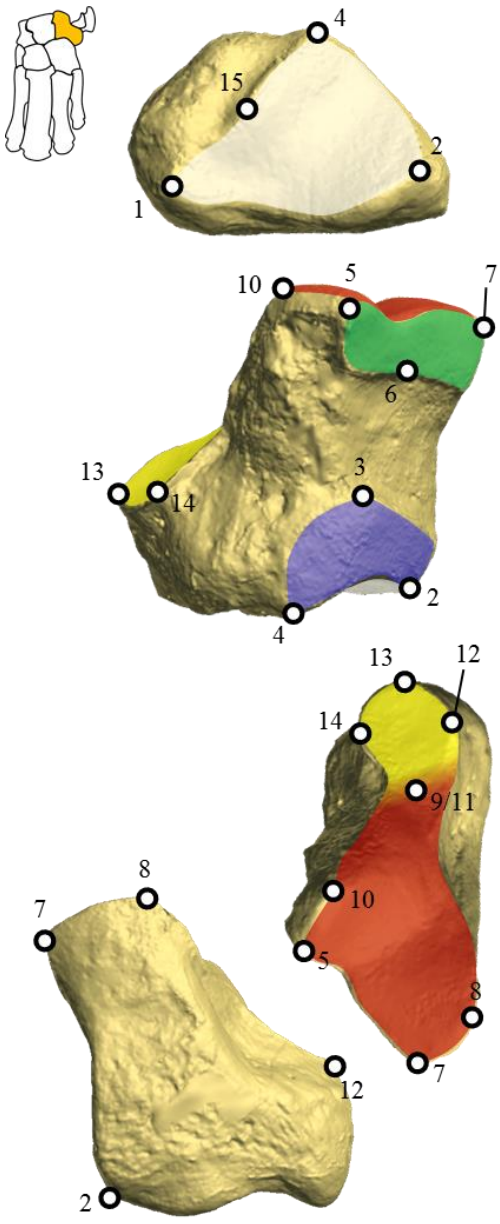
2. Most anterior angle of unciform facet / anterior apex of distal lunate facet meeting unciform facet	
3. Most proximal angle of distal lunate facet	
4. Posterior apex of distal lunate facet meeting unciform facet	
5. Posterior apex of proximal lunate facet meeting ulnar facet	
6. Most distal angle of proximal lunate facet	
7. Most anterior angle of ulnar facet / anterior apex of proximal lunate facet meeting ulnar facet	
8. Most proximal angle of lateral face of cuneiform	
9. Most posterior point of ulnar facet (*ulnar facet often merged with pisiform facet; point taken as narrowest point of merger*)	
10. Most proximal angle of medial face of cuneiform	
11. Most anterior point of pisiform facet (*ulnar facet often merged with pisiform facet; point taken as narrowest point of merger*)	
12. Most lateral angle of pisiform facet	
13. Most posterior angle of pisiform facet	
14. Most medial angle of pisiform facet	
15. Proximomedial angle of unciform facet	

Key:- pisiform facet = yellow; unciform facet = white; distal lunate facet = blue; proximal lunate facet = green; ulnar facet = red.

Lunate (semi-lunar; lunar)	
1. Most proximal angle of distal cuneiform facet	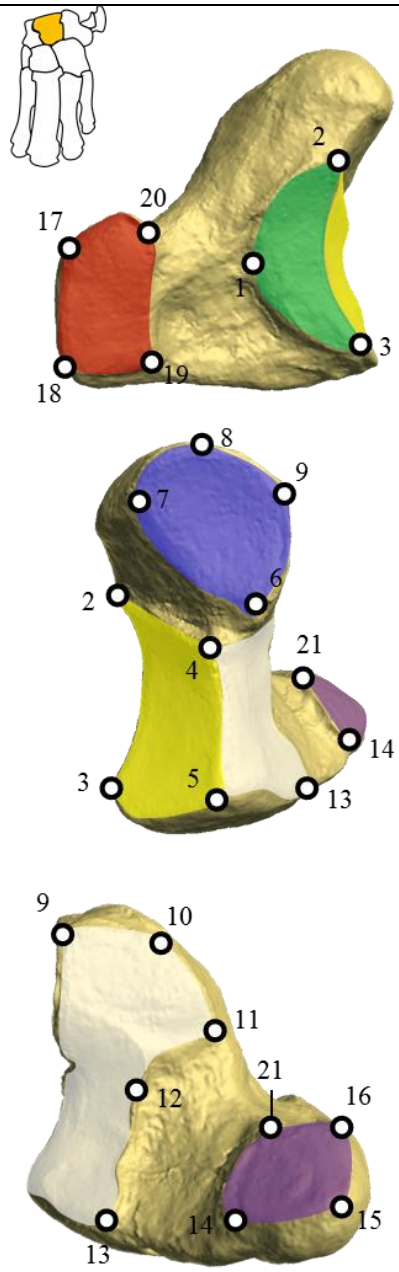
2. Most posterior angle of distal cuneiform facet / posterolateral angle of unciform facet (*meeting cuneiform facet*)	
3. Most anterior angle of distal cuneiform facet / anterolateral angle of unciform facet (meeting cuneiform facet)	
4. Posterior apex of unciform/anterior magnum facet	
5. Anterior apex of anterior magnum facet	
6. Most anterior angle of posterior magnum facet (*volar magnum facet*)	
7. Most medial angle of posterior magnum facet	
8. Most posterior angle of posterior magnum facet	
9. Most lateral angle of posterior magnum facet; meeting with posteromedial angle of distal scaphoid facet	
10. Most posterior angle of distal scaphoid facet	
11. Most proximal angle of distal scaphoid facet	
12. Deepest angle of concave edge of distal scaphoid facet	
13. Most proximal angle of anterodistal scaphoid facet	
14. Most distal angle of anteroproximal scaphoid facet	
15. Most anteroproximal angle of proximal scaphoid facet	
16. Most posteroproximal angle of proximal scaphoid facet	
17. Most posterior angle of proximal cuneiform facet	
18. Most anterior angle of proximal cuneiform facet	
19. Most anterodistal angle of proximal cuneiform facet	Key:- unciform (+ magnum) facet = yellow; distal scaphoid facet = white; proximal scaphoid facet = purple; distal cuneiform facet = green; proximal cuneiform facet = red.
20. Most posterodistal angle of proximal cuneiform facet	
21. Most posterodistal angle of proximal scaphoid facet	

Scaphoid	
1. Most posterior angle of radius facet	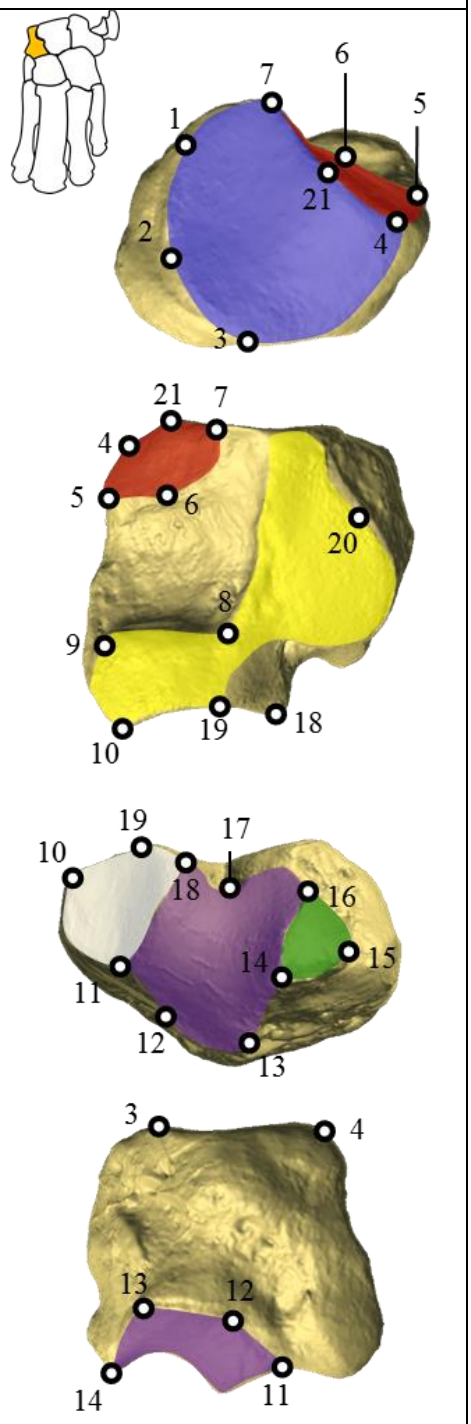
2. Most posterolateral angle of radius facet	
3. Most lateral angle of radius facet	
4. Anteroproximal angle between radial facet and lateral lunate facet	
5. Anterodistal angle of proximal lunate facet	
6. Deepest point of distal edge of proximal lunate facet	
7. Most posteromedial angle of radial facet	
8. Deepest angle of proximal edge of distal lunate facet	
9. Anteroproximal angle of distal lunate facet	
10. Anterodistal angle of distal lunate facet	
11. Lateral angle between trapezoid facet and magnum facet	
12. Deepest point of concave edge of trapezoid facet	
13. Most proximal point of concave edge of trapezoid facet; most lateral point of concave edge of trapezoid facet	
14. Most anterolateral angle of trapezium facet (meeting trapezoid facet)	
15. Most posterior angle of trapezium facet	
16. Most medial angle of trapezium facet	
17. Most concave point of trapezium facet (medial aspect)	
18. Most posteroproximal angle of trapezoid faced (meeting magnum facet)	
19. Most medial angle of magnum facet (meeting posterodistal angle of distal lunate facet)	
20. Most proximal angle of distal lunate facet	
21. Deepest point of proximal edge of proximal lunate facet	

Key:- distal lunate facet = yellow; magnum facet = white; trapezoid facet = purple; trapezium facet = green; proximal lunate facet = red; radial facet = blue.

Trapezoid	
1. Most posterodistal angle of trapezium facet	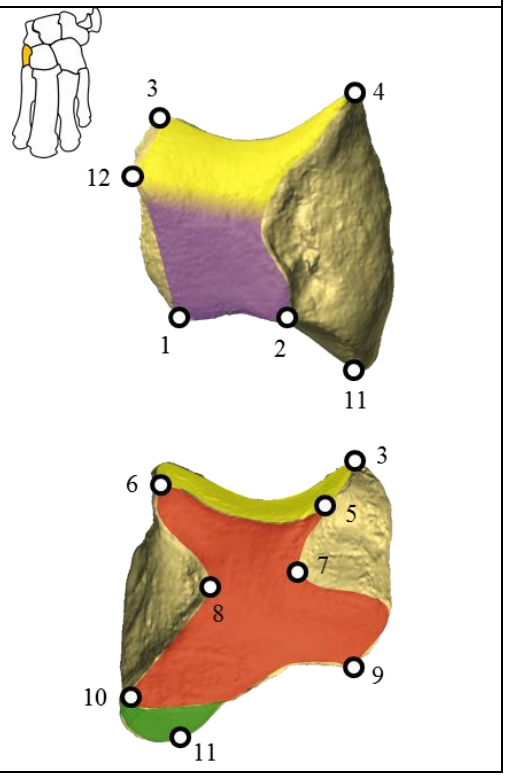
2. Most anterodistal angle of trapezium facet	
3. Most proximal angle of scaphoid facet (posterior)	
4. Most proximal angle of scaphoid facet (anterior)	
5. Posteroproximal angle of magnum facet	
6. Anteroproximal angle of magnum facet	
7. Deepest point of posterior concave surface	
8. Deepest point of anterior concave surface	
9. Posterodistal angle of magnum facet	
10. Anterodistal angle of magnum facet	
11. Most distal angle of MCII facet (anterior)	
12. Posteroproximal angle of trapezium facet meeting the scaphoid facet	

Key:- scaphoid facet = yellow; magnum facet = red; trapezium facet = purple; MCII facet = green.

Magnum (Capitate)	
1. Posteroproximal angle of MCII facet meeting trapezoid facet	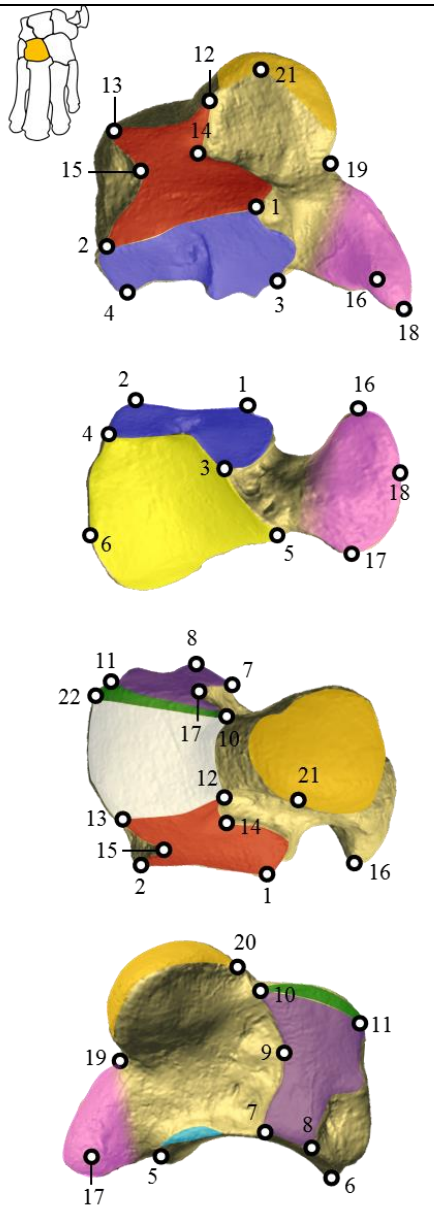
2. Anteroproximal angle of MCII facet meeting trapezoid facet	
3. Posterodistal angle of MCII facet meeting MCIII facet	
4. Anterodistal angle of MCII facet meeting MCIII facet	
5. Most posterior angle of MCIII facet (beneath volar process)	
6. Most distal angle of MCIII facet (anterior)	
7. Posterodistal angle of primary unciform facet	
8. Anterodistal angle of primary unciform facet	
9. Deepest point of posterior edge of primary unciform facet	
10. Posteroproximal angle of primary unciform facet meeting the scaphoid facet and lunate primary facet	
11. Anteroproximal angle of primary unciform facet meeting the primary lunate facet	
12. Posteroproximal angle of trapezoid facet meeting scaphoid facet	
13. Anteroproximal angle of trapezoid facet meeting scaphoid facet	
14. Deepest angle of posterior concave edge of trapezoid facet	
15. Deepest angle of anterior concave edge of trapezoid facet	
16. Most medial angle of volar process of the magnum	
17. Most distal angle of volar process of the magnum	
18. Most lateral angle of volar process of the magnum	
19. Deepest point of the magnum surface between secondary lunate facet and volar process	
20. Anterolateral angle of secondary lunate facet	
21. Deepest point of medial edge of secondary lunate facet	
22. Anteroproximal angle of scaphoid facet meeting the primary lunate facet	

Key:- MCII facet = blue; MCIII facet = yellow; scaphoid facet = white; primary unciform facet = purple; secondary unciform facet (not always present) = light blue; trapezoid facet = red; posterior (volar) lunate facet = orange; anterior lunate facet = green. Volar process of magnum shaded pink.

Unciform (Hamate)	
1. Most distal angle of volar process of the unciform	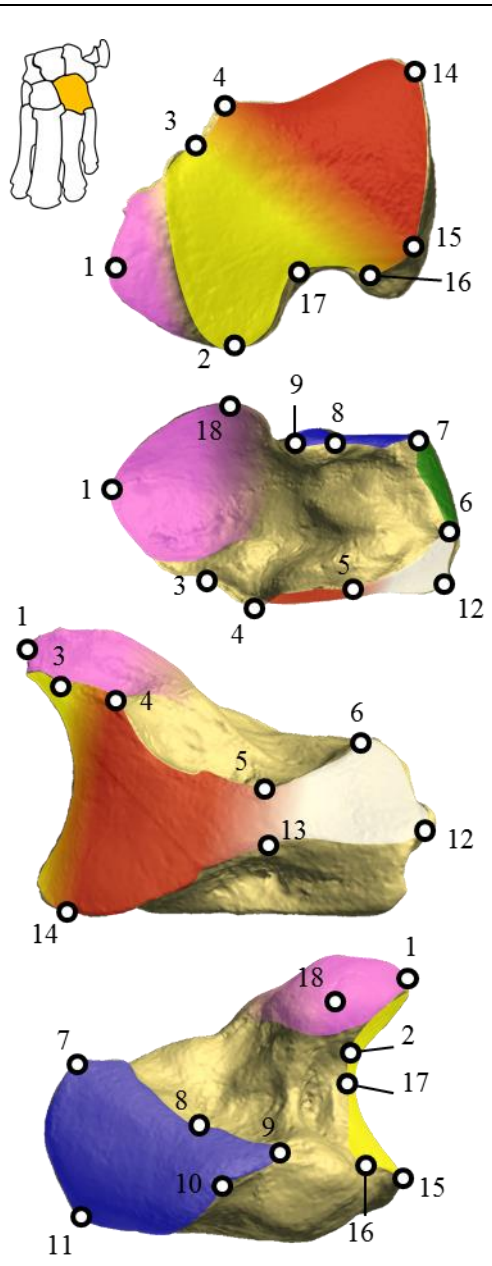
2. Posteroproximal angle of MCV facet (volar)	
3. Angle between volar process of unciform and MCIV/MCV facet (and secondary magnum facet where present)	
4. Posterior angle between MCV and MCIV facets; posterior apex of secondary magnum facet (where present)	
5. Deepest point of posterior concave edge of MCIV/primary magnum facet	
6. Posteroproximal angle between primary magnum facet and lunate facet	
7. Posteroproximal angle between lunate facet and cuneiform facet	
8. Medial angle of cuneiform facet (volar aspect)	
9. Lateral angle of cuneiform facet (volar aspect)	
10. Lateral apex between volar aspect and proximal aspect of cuneiform facet	
11. Anteroproximal angle between lunate facet and cuneiform facet	
12. Anteroproximal angle between lunate facet and primary magnum facet	
13. Deepest point of anterior concave edge of MCIV/primary magnum facet	
14. Most distal angle of MCIV/MCV facet (anterior aspect)	
15. Most lateral angle of MCIV/MCV facet (anterior aspect)	
16. Anteroproximal angle of MCV facet (volar)	
17. Deepest point of proximal concave edge of MCV facet	
18. Most lateral angle of volar process of the unciform	

Key:- cuneiform facet = blue; MCV facet = yellow; magnum facet = white; MCIV facet = red; lunate facet = green. Volar process of unciform shaded pink.

Metacarpal 2 / MCII
(*medial and lateral sides defined relative to entire limb*)

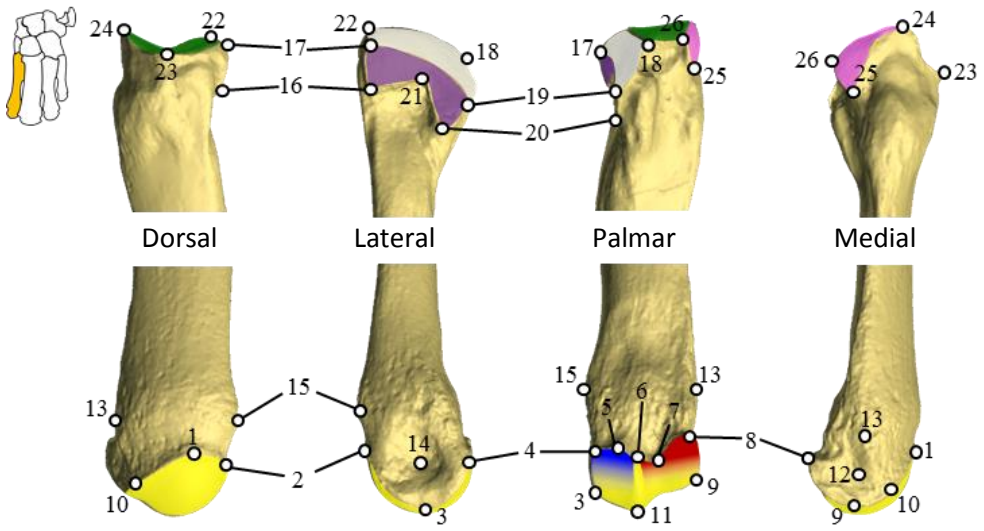

1. Most proximal angle of dorsal surface of MCII metacarpophalangeal facet	2. Most lateral angle of dorsal surface of MCII metacarpophalangeal facet
3. Deepest point of lateral concave edge of MCII metacarpophalangeal facet	4. Most lateroproximal angle of MCII metacarpophalangeal facet (palmar aspect)
5. Deepest point of lateral sesamoid / metacarpophalangeal facet (palmar aspect)	6. Most proximal angle of MCII sagittal ridge (palmar aspect of metacarpophalangeal joint)
7. Deepest point of medial sesamoid / metacarpophalangeal facet (palmar aspect)	8. Most medioproximal angle of MCII metacarpophalangeal facet (palmar aspect)
9. Deepest point of medial concave edge of MCII metacarpophalangeal facet	10. Most medial angle of dorsal surface of metacarpophalangeal facet
11. Most distal point of MCII (along sagittal ridge)	12. Centre of medial depression, distal to medial-collateral ligament origination
13. Apex of metacarpophalangeal medial-collateral ligament origination site	14. Centre of lateral depression, distal to lateral-collateral ligament origination
15. Apex of metacarpophalangeal lateral-collateral ligament origination site	16. Dorsodistal angle of MCIII facet
17. Dorsoproximal angle of MCIII facet	18. Palmoproximal angle of magnum facet
19. Palmoproximal angle of MCIII facet	20. Palmodistal angle of MCIII facet
21. Deepest point of distal concave edge of MCIII facet	22. Dorsoproximal angle of magnum facet
23. Deepest point along concave edge of trapezoid facet (dorsal aspect)	24. Most anterior angle of trapezium facet
25. Most distal angle of trapezium facet	26. Most posterior angle of trapezium facet

Key:- Metacarpophalangeal facet = yellow; medial sesamoid facet = red; lateral sesamoid facet = blue; magnum facet = white; MCIII facet = purple; trapezoid facet = green; trapezium facet = pink.

Metacarpal 3 / MCIII
(*medial and lateral sides defined relative to entire limb*)

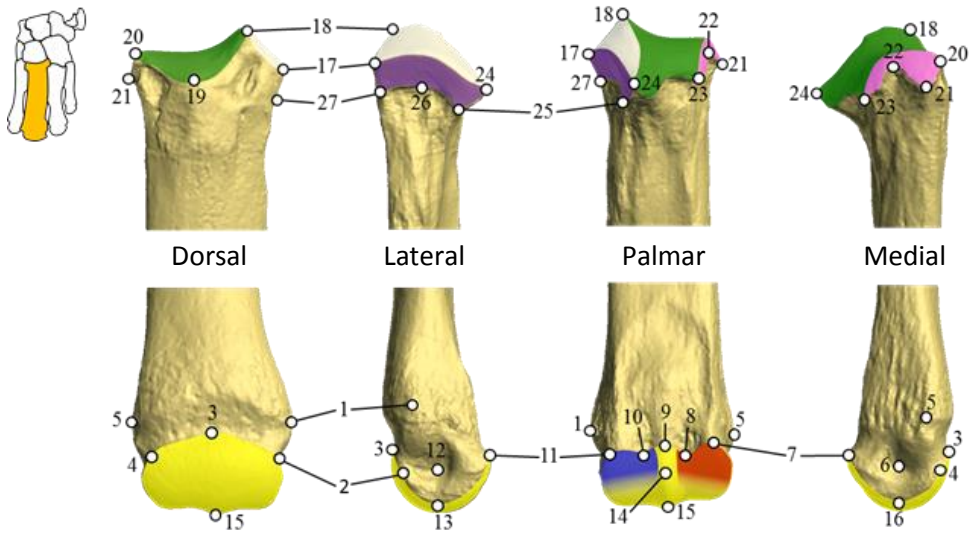

1. Apex of lateral-collateral ligament origination site	2. Lateroproximal angle of MCIII metacarpophalangeal joint facet
3. Most proximal angle of MCIII metacarpophalangeal joint facet	4. Medioproximal angle of MCIII metacarpophalangeal joint facet
5. Apex of medial-collateral ligament origination site	6. Centre of medial depression, distal to medial-collateral ligament origin
7. Most medioproximal angle of MCIII metacarpophalangeal facet	8. Deepest point of medial sesamoid / metacarpophalangeal facet
9. Most proximal angle of MCIII sagittal ridge	10. Deepest point of lateral sesamoid / metacarpophalangeal facet
11. Most lateroproximal angle of MCIII metacarpophalangeal joint facet	12. Centre of lateral depression, distal to lateral-collateral ligament origin
13. Deepest point of lateral concave edge of MCIII metacarpophalangeal facet	14. Most palmar point of MCIII sagittal ridge
15. Most distal point of MCIII (along sagittal ridge)	16. Deepest point of medial concave edge of MCIII metacarpophalangeal joint facet
17. Anteroproximal angle of MCIV facet meeting unciform facet	18. Anteroproximal angle of unciform facet meeting magnum facet
19. Deepest point along concave dorsal edge of magnum facet	20. Anteroproximal angle of MCII facet meeting magnum facet
21. Most distal angle of MCII facet	22. Deepest point along distal edge of MCII facet
23. Palmar angle of (or extent of) MCII facet meeting palmar margin of magnum facet	24. Palmar angle of MCIV facet (in some species doubles as most palmar extent of magnum facet)
25. Palmodistal angle of MCIV facet	26. Deepest point along distal concave edge of MCIV facet
27. Anterodistal angle of MCIV facet	

Key:- Metacarpophalangeal facet = yellow; medial sesamoid facet = red; lateral sesamoid facet = blue; unciform facet = white; MCIV facet = purple; magnum facet = green; MCII facet = pink.

Metacarpal 4 / MCIV
(*medial and lateral sides defined relative to entire limb*)

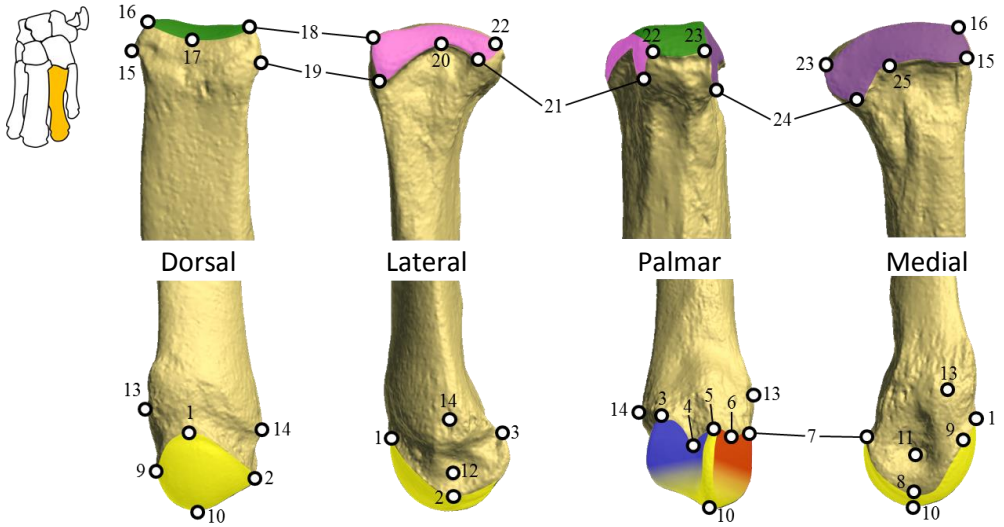

1. Most proximal point along edge of metacarpophalangeal joint facet	2. Deepest point of lateral concave edge of MCIV metacarpophalangeal facet
3. Most lateroproximal angle of MCIV metacarpophalangeal joint facet	4. Deepest point of lateral sesamoid / metacarpophalangeal facet
5. Most proximal angle of MCIV sagittal ridge (palmar aspect of metacarpophalangeal joint)	6. Deepest point of medial sesamoid / metacarpophalangeal facet (palmar aspect)
7. Most medioproximal angle of MCIV metacarpophalangeal joint facet	8. Deepest point of medial concave edge of MCIV metacarpophalangeal facet
9. Most medial angle along dorsal edge of metacarpophalangeal joint facet	10. Most distal point of MCIV (along sagittal ridge)
11. Centre of medial depression, distal to medial-collateral ligament origin	12. Centre of lateral depression, distal to lateral-collateral ligament origin
13. Apex of medial-collateral ligament origination site	14. Apex of lateral-collateral ligament origination site
15. Dorsodistal angle of MCIII facet	16. Dorsoproximal angle of MCIII facet meeting unciform facet
17. Deepest point of the anterior concave margin of unciform facet	18. Dorsoproximal angle of MCV facet meeting unciform facet
19. Dorsoproximal angle of MCV facet	20. Deepest point of concave distal margin of MCV facet
21. Palmodistal angle of MCV facet	22. Palmoproximal angle of MCV facet meeting palmar margin of unci. facet
23. Palmoproximal angle of MCIII facet meeting palmar margin of unciform facet	24. Palmodistal angle of MCIII facet
	25. Deepest point of concave distal margin of MCIII facet
Key:- Metacarpophalangeal facet = yellow; medial sesamoid facet = red; lateral sesamoid facet = blue; MCIII facet = purple; unciform facet = green; MCV facet = pink.	

Metacarpal 5 / MCV
(*medial and lateral sides defined relative to entire limb*)

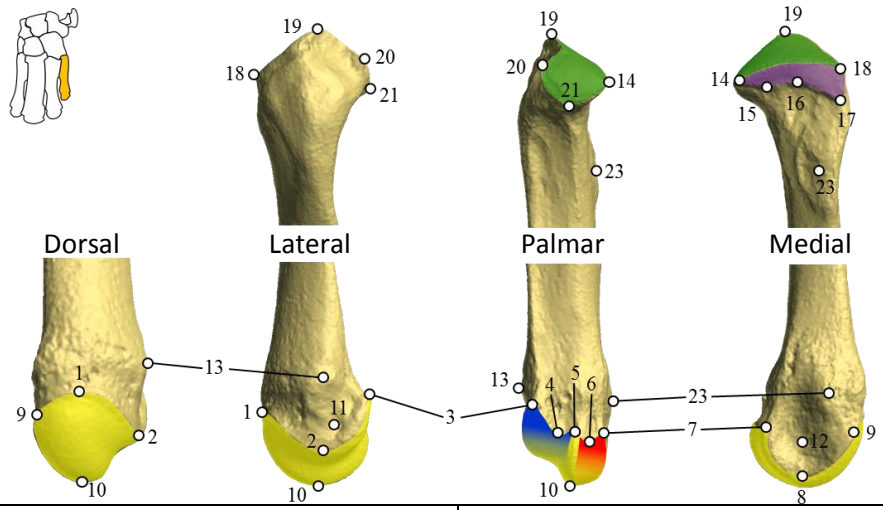

1. Most proximal point along edge of MCV metacarpophalangeal joint facet (dorsal aspect)	2. Deepest point of lateral concave edge of MCV metacarpophalangeal joint facet
3. Most lateroproximal angle of MCV metacarpophalangeal joint facet	4. Deepest point of lateral sesamoid / metacarpophalangeal facet
5. Most proximal angle of MCV sagittal ridge (palmar aspect of metacarpophalangeal joint)	6. Deepest point of medial sesamoid / metacarpophalangeal facet (palmar aspect)
7. Most medioproximal angle of MCV metacarpophalangeal facet	8. Deepest point of medial concave edge of MCV metacarpophalangeal facet
9. Most medial angle along dorsal edge of metacarpophalangeal joint facet	10. Most distal point of MCV (along sagittal ridge)
11. Centre of lateral depression, distal to lateral-collateral ligament origination site	12. Centre of medial depression, distal to medial-collateral ligament origin
13. Apex of lateral-collateral ligament origination site	14. Palmoproximal angle of MCIV facet meeting unciform facet
15. Palmodistal angle of MCIV facet	16. Deepest point of the distal concave margin of MCIV facet
17. Dorsodistal angle of MCIV facet	18. Dorsoproximal angle of MCIV facet meeting unciform facet
19. Dorsal angle along lateral margin of unciform facet; often most proximal point of MCV	20. Palmar angle along lateral margin of unciform facet
21. Posterolateral angle of unciform facet	22. Apex of attachment site for transverse ligaments to MCIII and MCIV
23. Apex of medial-collateral ligament origination site	

Key:- Metacarpophalangeal facet = yellow; medial sesamoid facet = red; lateral sesamoid facet = blue; MCIV facet = purple; unciform facet = green.

Table S2.1. List of bones used in the analysis, corresponding landmark abbreviations and number of landmarks used to describe shape variation.

Bone	Abbreviation	No. Landmarks
pisiform	$_{pi}$Lm	13
cuneiform (pyramidal)	$_{cu}$Lm	15
lunate	$_{lu}$Lm	21
scaphoid	$_{sc}$Lm	21
trapezoid	$_{tr}$Lm	12
magnum (capitate)	$_{ma}$Lm	22
unciform (hamate)	$_{un}$Lm	19
Metacarpal II	$_{2}$Lm	27
Metacarpal III	$_{3}$Lm	28
Metacarpal IV	$_{4}$Lm	26
Metacarpal V	$_{5}$Lm	24

3. Results of MANOVAs and power analyses

Table S2.2. Results of MANOVA and power analysis on upper forelimb bones.

Bone	Test	Value	F	p	η_p^2	Power
Pisiform	Pillai's	2.824	3.213	0.033	0.941	0.842
	Wilks'	0	12.235	0.015	0.993	0.907
Cuneiform	Pillai's	2.864	3.957	0.016	0.955	0.919
	Wilks'	0	4.279	0.091	0.981	0.5
Lunate	Pillai's	2.864	3.957	0.016	0.955	0.919
	Wilks'	0	4.279	0.091	0.981	0.5
Scaphoid	Pillai's	2.852	3.611	0.022	0.951	0.89
	Wilks'	0	5.974	0.053	0.987	0.642
Trapezoid	Pillai's	2.813	3.47	0.026	0.938	0.868
	Wilks'	0	2.844	0.172	0.966	0.342
Magnum	Pillai's	2.696	1.567	0.241	0.899	0.485
	Wilks'	0	9.627	0.023	0.992	0.842
Unciform	Pillai's	2.932	8.049	0.001	0.977	0.999
	Wilks'	0	8.669	0.028	0.991	0.799
MCII	Pillai's	2.799	2.322	0.087	0.933	0.69
	Wilks'	0	2.528	0.199	0.972	0.324
MCIII	Pillai's	2.876	3.858	0.017	0.959	0.915
	Wilks'	0	5.876	0.053	0.988	0.644
MCIV	Pillai's	2.914	5.629	0.004	0.971	0.985
	Wilks'	0	4.727	0.076	0.985	0.549
MCV	Pillai's	2.830	2.774	0.051	0.943	0.781
	Wilks'	0	1.708	0.334	0.96	0.229

4. Discriminant Function plots

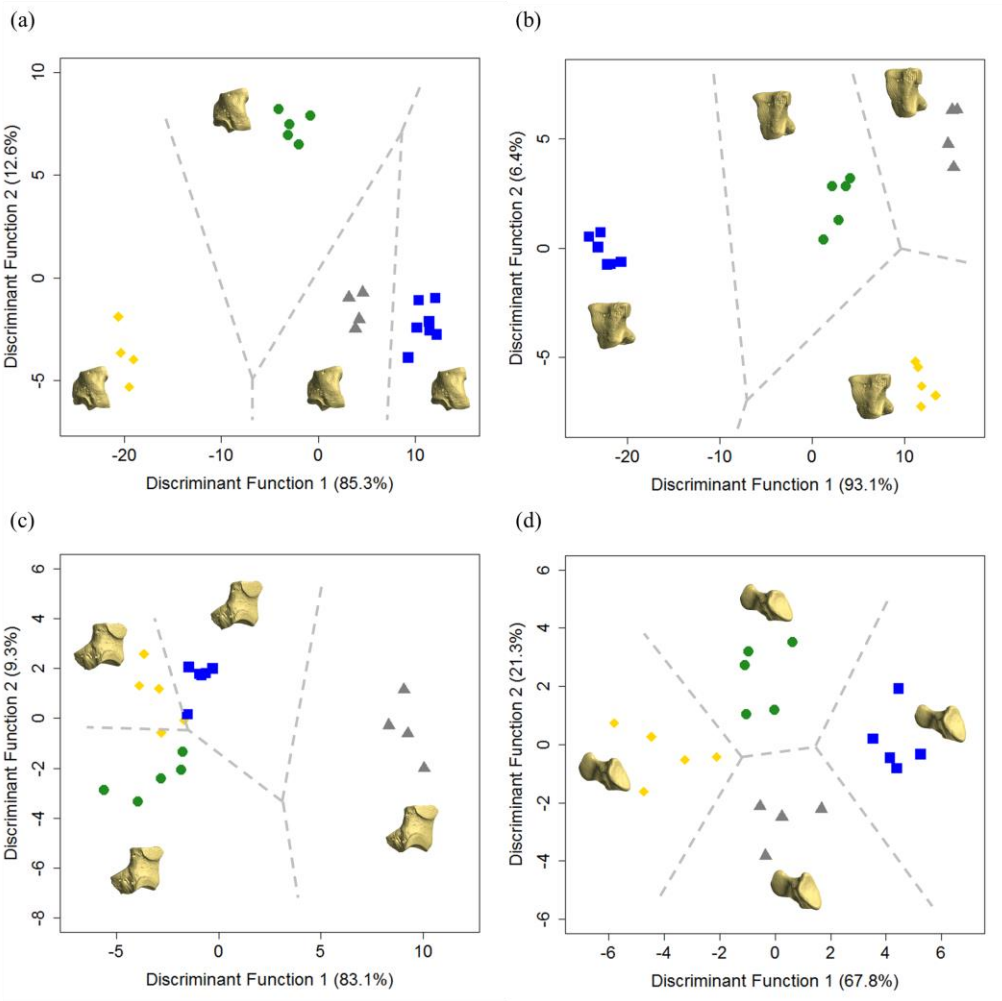

Figure S2.1. Discriminant function plots comparing bones of the tapir proximal carpal row. Proximal carpal row: **(a)** scaphoid (100% accurate); **(b)** lunate (95.0%), **(c)** cuneiform (75.0%), **(d)** pisiform (94.7%). Species: *Tapirus indicus* (squares); *T. bairdii* (diamonds); *T. pinchaque* (triangles); *T. terrestris* (circles). Example bones presented correspond to mean species morphology, oriented to best depict interspecific differences. Variance accounted for by each discriminant function axis is presented in parentheses. Territorial map divisions (grey dotted lines) represent cut-off points between species.

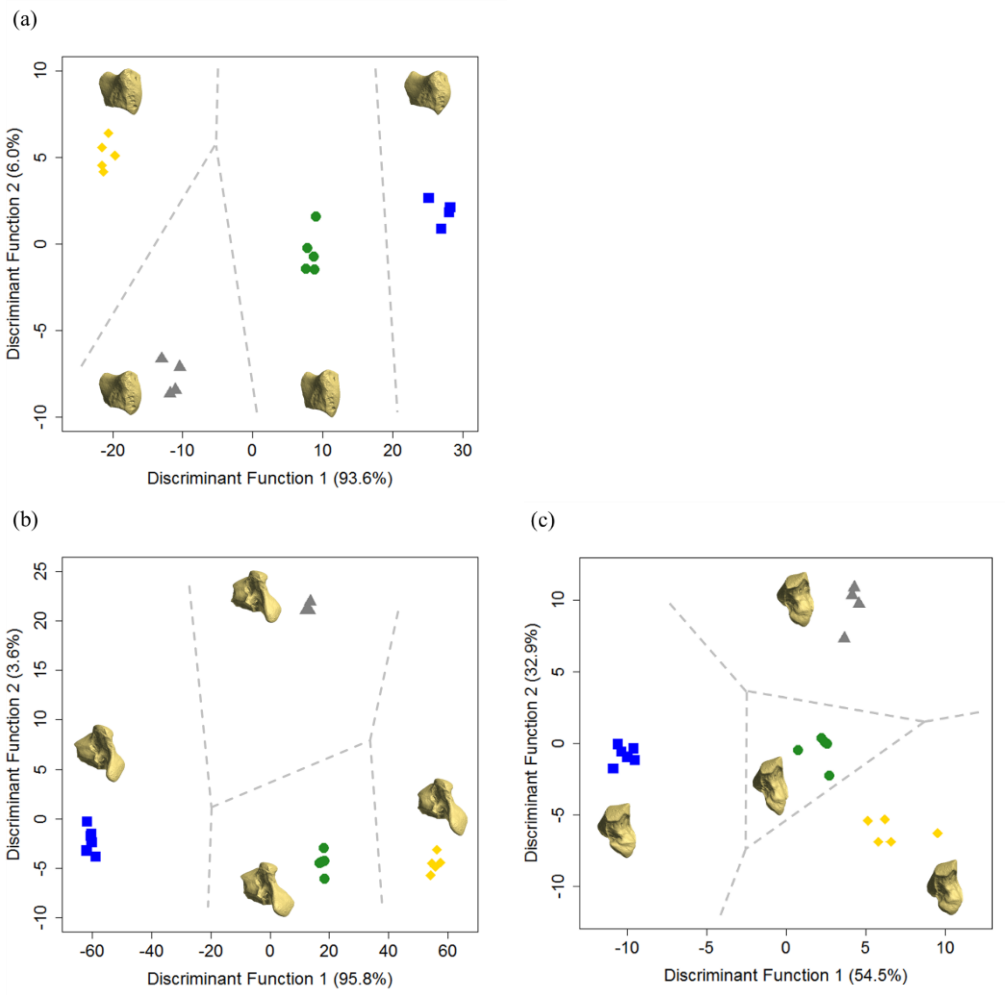

Figure S2.2. Discriminant function plots comparing bones of the tapir distal carpal row. Distal carpal row: **(a)** trapezoid (100% accurate); **(b)** magnum (95.2%), **(c)** unciform (100%). Species: *Tapirus indicus* (squares); *T. bairdii* (diamonds); *T. pinchaque* (triangles); *T. terrestris* (circles). Variance accounted for by each discriminant function axis is presented in parentheses. Territorial map divisions (grey dotted lines) represent cut-off points between species.

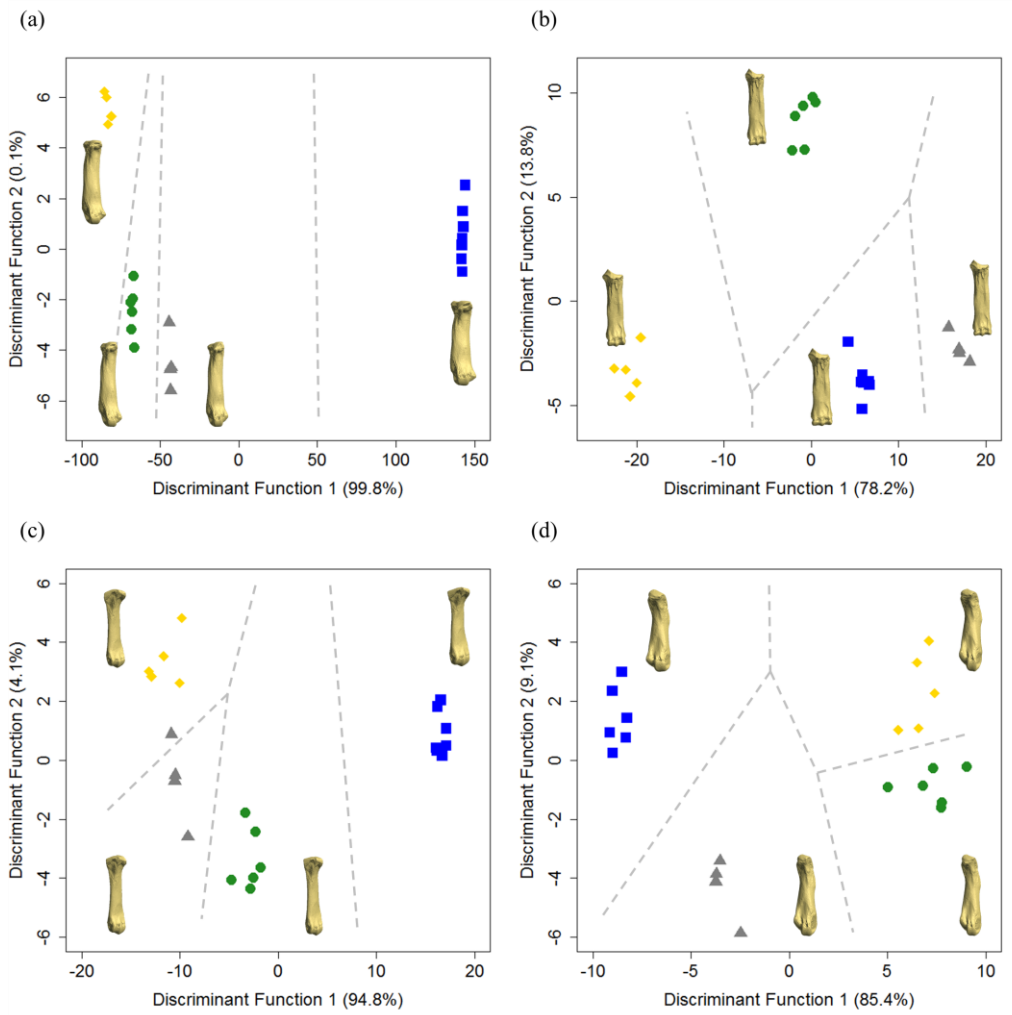

Figure S2.3. Discriminant function plots comparing tapir metacarpals. **(a)** MCII (100% accurate); **(b)** MCIII (100%), **(c)** MCIV (90.9%), **(d)** MCV (95.5%). Species: *Tapirus indicus* (squares); *T. bairdii* (diamonds); *T. pinchaque* (triangles); *T. terrestris* (circles). Example bones presented correspond to mean species morphology, oriented to best depict interspecific differences. Variance accounted for by each discriminant function axis is presented in parentheses. Territorial map divisions (grey dotted lines) represent cut-off points between species.

5. Discriminant functions at group centroids for autopodial bones

Table S2.3. Functions at group centroids from Discriminant Function Analysis

Pisiform	**Discriminant Function**	
Species	1	2
T. bairdii	-4.06	-0.30
T. indicus	4.35	0.10
T. pinchaque	0.25	-2.6
T. terrestris	-0.49	2.33

Cuneiform	**Discriminant Function**	
Species	1	2
T. bairdii	-2.99	0.87
T. indicus	-0.95	1.57
T. pinchaque	9.16	-0.44
T. terrestris	-3.19	-2.41

Lunate	**Discriminant Function**	
Species	1	2
T. bairdii	11.94	-6.17
T. indicus	-22.44	-0.13
T. pinchaque	15.20	5.28
T. terrestris	2.82	2.10

Scaphoid	**Discriminant Function**	
Species	1	2
T. bairdii	-19.87	-3.70
T. indicus	10.97	-2.26
T. pinchaque	3.92	-1.55
T. terrestris	-2.60	7.38

Trapezoid	**Discriminant Function**	
Species	1	2
T. bairdii	-20.90	5.15
T. indicus	27.13	1.85
T. pinchaque	-11.57	-7.71
T. terrestris	8.45	-0.47

Magnum	**Discriminant Function**	
Species	1	2
T. bairdii	55.71	-4.51
T. indicus	-60.56	-2.12
T. pinchaque	12.95	21.3
T. terrestris	17.75	-4.42

Unciform	**Discriminant Function**	
Species	1	2
T. bairdii	6.65	-6.16
T. indicus	-10.12	-0.83
T. pinchaque	4.16	9.56
T. terrestris	2.15	-0.48

MCII	**Discriminant Function**	
Species	1	2
T. bairdii	-83.57	5.69
T. indicus	142.54	0.60
T. pinchaque	-43.63	-4.48
T. terrestris	-67.56	-2.45

MCIII	**Discriminant Function**	
Species	1	2
T. bairdii	-20.80	-3.35
T. indicus	5.85	-3.77
T. pinchaque	16.94	-2.24
T. terrestris	-0.79	8.69

MCIV	**Discriminant Function**	
Species	1	2
T. bairdii	-11.49	3.36
T. indicus	16.56	0.90
T. pinchaque	-10.27	-0.72
T. terrestris	-2.90	-3.37

MCV	**Discriminant Function**	
Species	1	2
T. bairdii	6.63	2.35
T. indicus	-9.06	1.54
T. pinchaque	-3.36	-4.31
T. terrestris	7.28	-0.88

– RESEARCH CHAPTER FOUR: APPENDIX III –

A morphometric analysis of the forelimb in the genus *Tapirus* (Perissodactyla: Tapiridae) reveals influences of habitat, phylogeny and size through time and across geographical space

Jamie A. MacLaren, Richard C. Hulbert, Steven C. Wallace, Sandra Nauwelaerts

Table of Contents

1. Body Mass Calculation

In this study, we estimated body mass in *Tapirus* from measurements of the postcranial skeleton, following the measurements of Scott (1990). There are no established body mass regression equations specifically for tapirs as there are for equids (K. M. Scott, 1990). As such, the equation calculated from a range of ungulate taxa was used to establish body mass estimates for tapirs in this analysis. The measurements utilised included maximal mediolateral width of the humeral head (articular surface); maximal mediolateral width of humeral condyle (epicondyle to epicondyle); maximal mediolateral width of humeral articular surface (trochlea + capitulum) in anterior aspect (Figure S1a). These distances were measured using the measurement tool in Geomagic Studio 10 (GeoMagic Qualify v.10, Morrisville, NY, USA). The same three measurements were recorded for multiple bones per species. Measurements were input into regression equations from Scott (1990) to produce estimates for the body mass based on each measurement. These estimated masses were then averaged across each individual to produce a range of estimated body masses, from which a mean value was then calculated. Where this was not possible (e.g. not all measurements were available), the average of the available measurements was taken as the estimated body mass. Incomplete humeri were excluded where possible. In some species, the distal humerus alone (e.g. *Tapirus haysii*) or only the radius were available (e.g. *T. priscus*, *T. arvernensis*). In these cases, the available measurements were averaged to generate the body mass prediction, although great care was taken when drawing conclusions based on these species.

The European taxa incorporated in this analysis did not have humeral material available, due to lack of specimen availability (*T. arvernensis*) or current lack of identification or existence (*T. priscus*). The radius, a bone which shows strong correlation between size and mass in extant tapirs, was available for scanning in these two European taxa, although only one specimen per taxon was available to the authors. From specimens of extant tapirs with associated humeri and radii (n = 24; 4 spp.) and average scores for humeri and radii of extinct species (humerus n = 26; radial n = 33; 6 spp.), body mass estimates were generated from linear measurements of the humerus and radius (Figure S1) based on all ungulate regression equations with correlation coefficients exceeding 0.95 in both cases (see Scott 1990; Damuth and MacFadden 1990; Appendix). Resultant tapir mass estimates for both humerus and radius were then regressed against one another using OLS regression. This generated a high correlation coefficient for both raw (r^2 = 0.932) and log-transformed predictions (r^2 = 0.886). Body mass estimates from the radii of *T. priscus* and *T. arvernensis* were input into the OLS regression equation for the tapir limbs to generate a body mass prediction for the humerus of these species, which was then compared to those calculated from the other species.

Mass estimates from raw predictions (BMs) predicted a body mass of 349.8kg for *T. priscus* and 214.9kg for *T. arvernensis*; log transformed body masses ($_{log}$BM) from tapir radiohumeral regression predicted comparable body masses for the European specimens under study (*T. priscus* = 347.9kg; *T. arvernensis* = 214.5kg). These artificially generated body mass estimates for *T. arvernensis* and *T. priscus* were used for further

experiments only after close consultation with the published literature. The predicted masses of both *T. priscus* and *T. arvernensis* align with those predicted by Eisenmann and Guerin (1992), who qualitatively estimated *T. priscus* was the same size or slightly larger than *T. indicus* (mean BM = 326.4kg; this study), and hypothesised *T. arvernensis* would be of similar size to *T. terrestris* (mean BM = 216.6kg) (Eisenmann & Guérin, 1992; Guérin & Eisenmann, 1994).

Mass ranges attained for extant taxa (*T. indicus, T. bairdii, T. terrestris* and *T. pinchaque*) fell within published body mass brackets measured from live individuals (de Thoisy et al. 2014). This result provided confidence in the methodology used. To our knowledge, mass estimates in this paper for the *Helicotapirus* tapirs (*T. lundeliusi, T. haysii* and *T. veroensis*) and the Eurasian *T. priscus, T. arvernensis* and *T.* (*Megatapirus*) *augustus* represent the first quantitative mass estimations in these taxa. Extinct taxa which have previously undergone body mass estimations are found to be mostly comparable with results in this study: 117kg for *T. polkensis* (125kg; Hulbert et al., 2009), ~620kg for *T.* (*M.*) *augustus* ("double that of *T. indicus*"; Hooijer and Colbert, 1954), and the European taxa *T. priscus* (~350kg) and *T. arvernensis* (~215kg) ("comparable with *T. indicus* and *T. terrestris* respectively"; Eisenmann and Guérin 1992; Guérin and Eisenmann 1994) (Table 4.1).

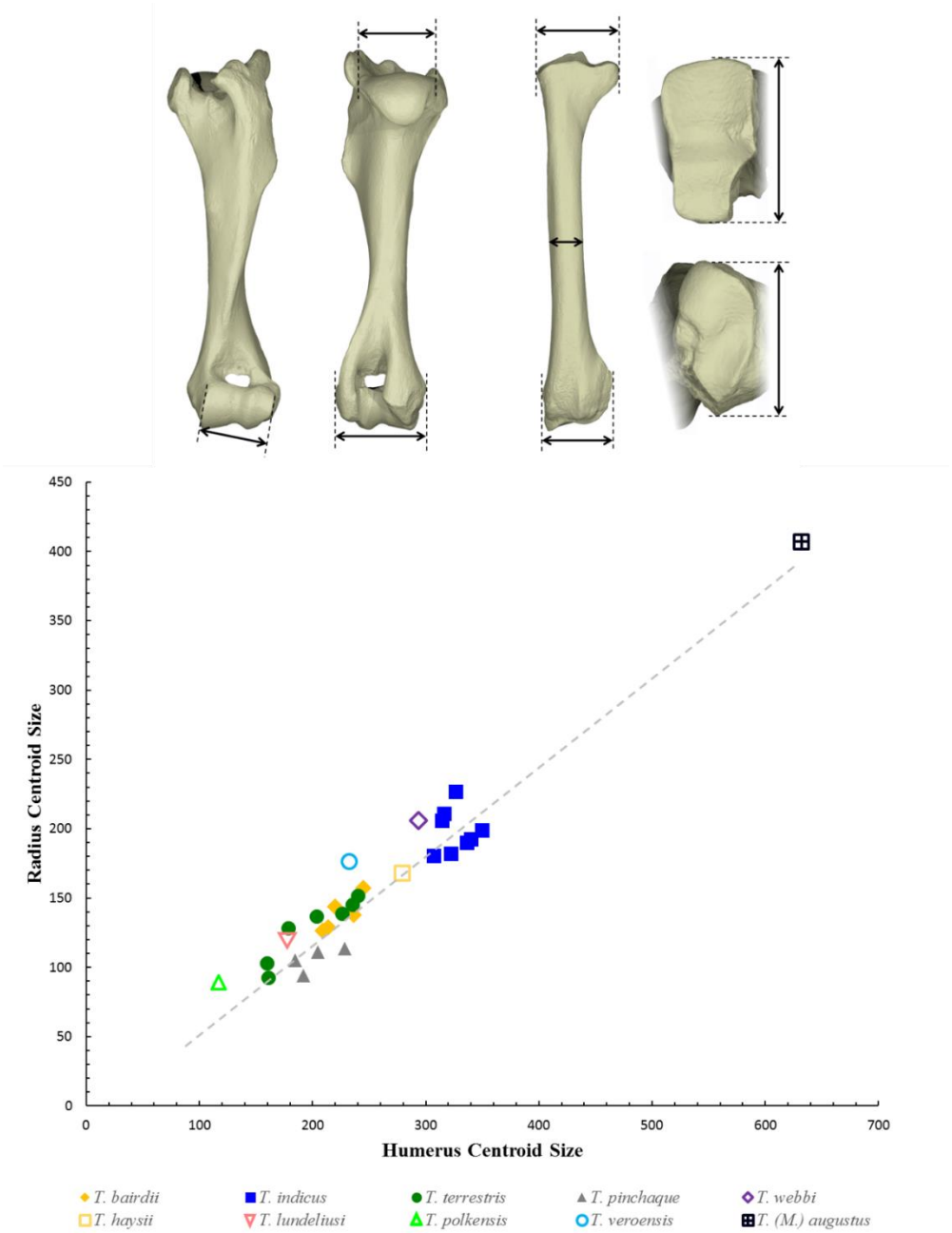

Figure S3.1. Humeral and radial measurements used to estimate body mass, with graphical representation of body mass calculation for *T. priscus* and *T. arvernensis* (only radius preserved). Measurements correspond to humeral and radial measurements in Scott (1990), equations in MacFadden and Damuth (1990). Bones of *T. pinchaque* (ZMB MAM 62085).

2. Allometric Corrections

Assessing the effect of allometric variation (size-dependent shape variation) has been investigated in several different ways (Klingenberg, 2016). These include two fixed frameworks: Gould-Mosimann (shape; Klingenberg, 1998) and Huxley-Jolicoeur (conformation; Kendall, 1989; Goodall, 1991; Kendall *et al.*, 1999), in addition to a synthesis framework drawing on aspects of both (Procrustes form space; Mitteroecker *et al.*, 2004, 2013; Mitteroecker, Gunz and Bookstein, 2005; reiewed in Klingenberg, 2016).

For this study we chose to test whether Procrustes form space could be used to account for allometry in our dataset as an alternative to the widely used multivariate regression of size variable (log-transformed centroid size; $_{log}$CS) (Klingenberg, 1998, 2016). Principal components analyses (PCAs) were performed on the Procrustes coordinates for each bone with no initial allometric or phylogenetic corrections. In Procrustes form space, the first principal component (PC1) is strongly correlated with size (Mitteroecker et al., 2013); in this study, we tested this using an ordinary least squares (OLS) regression of PC1 scores vs. log-transformed body mass ($_{log}$BM) for specimens with articulated skeletons (predominantly extant specimens with intact humeri used for body mass estimation). If body mass were highly correlated with the shape variation along PC1, then PC1 would represent an axis of size and size-associated shape variation, with subsequent PCs describing size independent shape variation; this is often the case in linear morphometrics. The PCAs for all tapir forelimb bones were performed, including specimens without body mass estimates for the specimens. The PC scores for specimens with mass data were then extracted and regressed against $_{log}$BM to test how strongly correlated PC1 and body mass were. In addition, both $_{log}$BM and PC1 scores were regressed against $_{log}$CS to test how well correlated these three morphological metrics are. Finally, species averaged $_{log}$CS and $_{log}$BM were regressed against one another to ascertain whether centroid size could be used as a viable proxy for body mass in tapirs. Results for all these regression calculations can be found in Table S3.1.

Table S3.1. Correlation coefficients from OLS regressions between log-transformed centroid size ($_{log}$CS) and log-transformed body mass ($_{log}$BM), and between the first principal component of shape variables (PC1) of the tapir forelimb and $_{log}$BM (both with ($_{a}r^2$) and without ($_{b}r^2$) extinct taxa). Highest correlation are reported in bold.

Bone	$_{log}$BM / $_{log}$CS (r^2)	$_{log}$BM / PC1 ($_{a}r^2$)	*n*	$_{log}$BM / PC1 ($_{b}r^2$)	*n*
Humerus	0.35	0.45	37	0.46	24
Radius	0.73	0.67	44	0.68	24
Pisiform	0.57	0.02	46	0.05	19
Cuneiform	0.86	0.02	39	0.12	17
Lunate	0.91	0.19	47	0.62	17
Scaphoid	0.90	0.51	42	0.46	18
Magnum	0.90	0.45	48	0.83	18
Unciform	0.89	0.42	48	0.47	17
Metacarpal II	0.53	0.81	51	0.83	22
Metacarpal III	0.44	0.57	50	0.64	22
Metacarpal IV	0.59	0.66	45	0.72	22
Metacarpal V	0.69	0.40	51	0.63	22

In eight of 12 cases, log-transformed centroid size correlated well with estimated body mass; $_{log}$CS was therefore used as a proxy for size in the remainder of the study. On the whole, $_{log}$CS was more highly correlated with body mass than PC1 scores; this was not the case for the three largest metacarpals (MCII, MCIII and MCIV), which displayed higher correlation coefficients for $_{log}$BM vs. PC1 both with and without shape variables from extinct species. However, the argument to use $_{log}$CS rather than PC1 scores as a proxy for body mass (i.e. size) was made based on the majority of bones exhibiting greater r^2 values for $_{log}$CS regressions. With this result in mind, we moved forward with multivariate regressions of shape variables vs. $_{log}$CS. The greatest benefit of this analysis is that it can be performed across all bones in the analysis, whereas regression against estimated body mass can only be performed for limb bones associated with a complete humerus or radius (used for body mass estimation).

3. Phylogenetic Reconstruction

Branch Lengths from the literature. FA = first occurrence; LA = last occurrence.

Species	FA (Mya)	LA (Mya)	Source(s)
T. (*M.*) *augustus*	0.126	0.012	Colbert and Hooijer (1953)
T. arvernensis	3.200	1.806	Rustioni and Mazza (2001); van der Made (2010)
T. bairdii	0.126	0.000	Steiner and Ryder (2011), Ruiz-Garcia et al. (2016)
T. haysii	2.600	0.012	Hulbert, (1995); Hulbert *et al.*, (2009)
T. indicus	2.588	0.000	Steiner and Ryder (2011)
T. lundeliusi	2.600	1.600	Hulbert (2010)
T. pinchaque	0.126	0.000	Steiner and Ryder (2011), Ruiz-Garcia et al. (2016)
T. polkensis	9.000	4.750	Hulbert, Bloch, and Poyer (2006); Hulbert *et al.* (2009)
T. priscus	11.100	7.200	Guérin and Eisenmann (1982); Eisenmann and Guérin (1992)
T. sanyuanensis	2.588	0.781	Tong, Liu, and Han (2002); Tong and Qiu (2008); van der Made (2010)
T. terrestris	0.781	0.000	Steiner and Ryder (2011), Ruiz-Garcia et al. (2016)
T. veroensis	0.300	0.012	Hulbert (1995), Czaplewski, Puckette, and Russell (2002); Hulbert (2010)
T. webbi	10.300	7.500	Hulbert (2005)

Our topology features *T. indicus* nested in a Eurasian clade and *T. bairdii* nested in a North American clade (Ferrero & Noriega, 2007; Hulbert, 2010; Hulbert et al., 2009; Steiner & Ryder, 2011). Based on a combined topology from three maximum parsimony trees (Ferrero & Noriega, 2007; Holanda & Ferrero, 2013; Hulbert, 2010) and several anecdotal descriptions (Eisenmann & Guérin, 1992; Guérin & Eisenmann, 1994; Tong, 2005; Tong et al., 2002), the tree predicts a division between Eurasian and New World tapirs approximately 22.1 Mya (early Aquitanian; supported by Steiner and Ryder 2011; Ruiz-García et al. 2012; Cozzuol et al. 2013; Figure 1). The division between the North and South American taxa is also well correlated between our study and current molecular phylogenies (9.9 Mya in this study; Steiner and Ryder 2011; Ruiz-García et al. 2012; Cozzuol et al. 2013; Ruiz-García et al. 2016). Though informal, our tree represents as accurate a topology as can be provided for all the taxa under investigation without a cladistic matrix or *Tapirus* supertree. Future phylogenetic studies on the genus *Tapirus* will benefit from incorporating Eurasian and New World taxa into an all-inclusive cladistic framework.

4. Multivariate regression of shape against log-transformed centroid size

Figure S3.2. Multivariate regressions of shape variables (Procrustes coordinates) vs. $_{log}$CS from geometric morphometric analysis of 12 forelimb bones of *Tapirus*. (a) humerus, (b) radius, (c) pisiform, (d) cuneiform, (e) lunate, (f) scaphoid, (g) magnum, (h) unciform, (i) MCII, (j) MCIII, (k) MCIV, (l) MCV. Regression score (y-axis) represents combination of shape variables most closely correlated with size variable. Correlation coefficients reported in bottom right of graph.

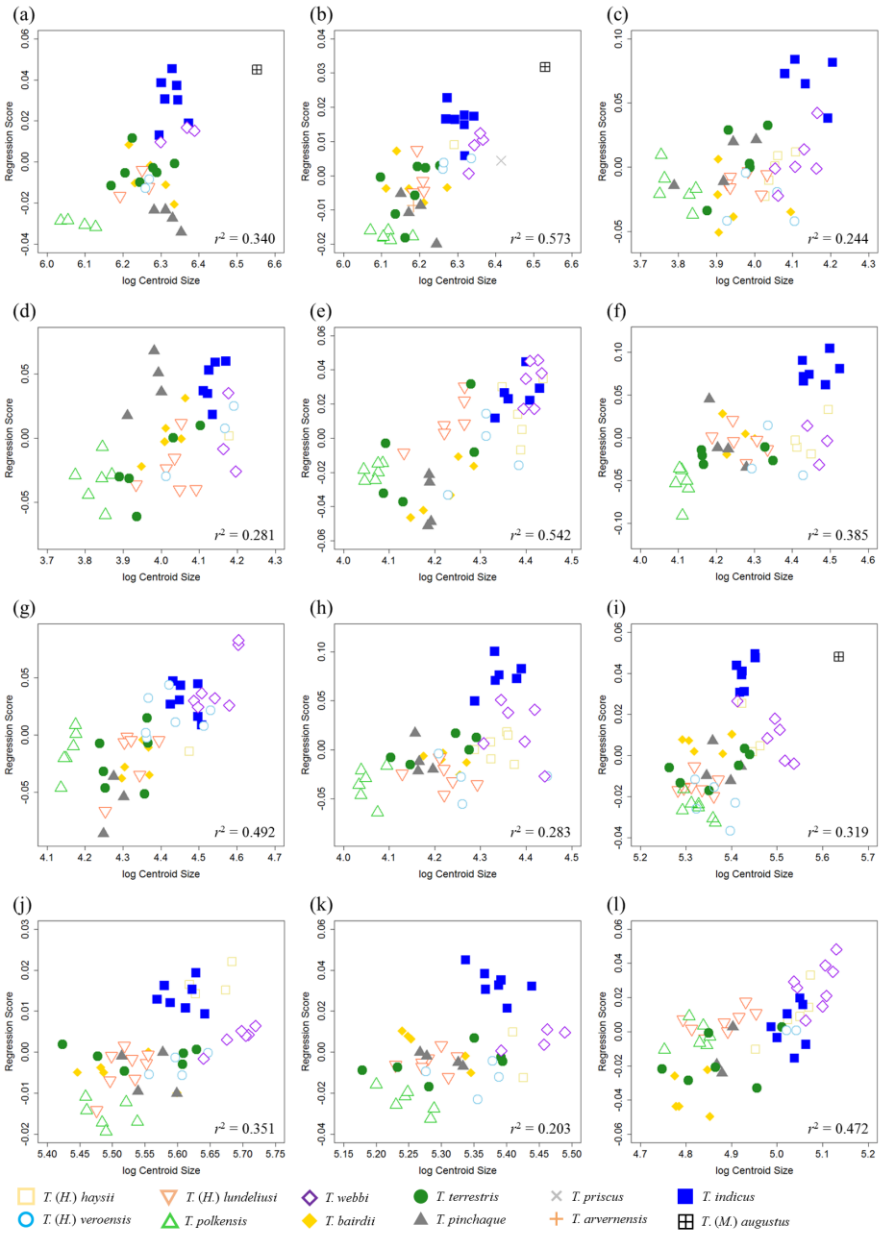

5. Pairwise comparisons from permutational MANOVA

Table S3.2. Results of perMANOVAs of *Tapirus* species, based on regression residuals all forelimb bones corrected for false discovery rate (10000 permutations). Sum of squares and within-group sum of squares reported alongside F-statistic (*F*) and associated *p*-values (*p*). Significant differences in italics.

Bone	Sum of squares	WG SS	*F*	*p*
Humerus	0.116	0.051	4.400	*<0.001*
Radius	0.032	0.015	3.282	*<0.001*
Pisiform	0.578	0.364	2.714	*<0.001*
Cuneiform	0.513	0.295	2.772	*<0.001*
Lunate	0.491	0.287	3.380	*<0.001*
Scaphoid	0.524	0.315	2.730	*<0.001*
Magnum	0.551	0.314	3.672	*<0.001*
Unciform	0.581	0.349	3.249	*<0.001*
Metacarpal II	0.096	0.051	4.520	*<0.001*
Metacarpal III	0.059	0.031	4.661	*<0.001*
Metacarpal IV	0.077	0.042	3.722	*<0.001*
Metacarpal V	0.187	0.099	4.498	*<0.001*

Table S3.3. Pairwise comparisons from perMANOVA testing of regression residuals from landmark analysis of *Tapirus* humeri (10000 permutations). Significant *p*-values (≤0.05) in italics.

Species	*augus.**	*bair*	*indi*	*lund*	*pinc*	*polk*	*terr*	*vero*
*T. augustus**	-							
T. bairdii	0.545	-						
T. indicus	0.295	*0.018*	-					
T. lundeliusi	0.545	*0.049*	*0.030*	-				
T. pinchaque	0.297	*0.030*	*0.022*	*0.049*	-			
T. polkensis	0.823	*0.030*	*0.022*	*0.049*	*0.049*	-		
T. terrestris	0.313	*0.049*	*0.018*	*0.049*	*0.024*	*0.030*	-	
T. veroensis	1.000	0.078	*0.049*	0.741	0.100	0.185	0.085	-
T. webbi	0.545	*0.049*	*0.030*	0.144	*0.049*	*0.049*	*0.030*	0.545

*one specimen only

Table S3.4. Pairwise comparisons from perMANOVA testing of regression residuals from landmark analysis of *Tapirus* radii (10000 permutations). Significant *p*-values (≤0.05) in italics.

Species	*arv* *	*aug* *	*bai*	*hay* *	*ind*	*lun*	*pin*	*pris* *	*pol*	*ter*	*ver*
T. arv.	-										
T. aug.	1.0	-									
T. bai.	0.16	0.16	-								
T. hay.	1.00	1.00	0.16	-							
T. ind.	0.12	0.12	*0.01*	0.12	-						
T. lun.	0.18	0.19	*0.02*	0.40	*0.03*	-					
T. pin.	0.80	0.20	*0.02*	0.20	*0.03*	*0.03*	-				
T. pri.	0.14	0.13	*0.03*	0.14	*0.01*	*0.05*	*0.05*	-			
T. polk.	1.00	1.00	0.16	1.00	0.11	0.19	0.39	0.14	-		
T. terr.	0.25	0.12	*0.02*	0.12	*0.01*	*0.05*	*0.01*	*0.01*	0.38	-	
T. ver.	0.25	0.25	*0.01*	0.49	*0.01*	0.08	*0.02*	*0.01*	0.24	*0.01*	-
T. web.	0.19	0.20	*0.01*	1.00	*0.01*	0.11	*0.02*	*0.01*	0.19	*0.03*	0.06

*one specimen only

Table S3.5. Pairwise comparisons from perMANOVA testing of regression residuals from landmark analysis of *Tapirus* pisiforms (10000 permutations). Significant *p*-values (≤0.05) in italics.

Species	*bai*	*hay*	*ind*	*lund*	*pin*	*polk*	*terr*	*vero*
T. haysii	0.14	-						
T. indicus	*0.03*	*0.02*	-					
T. lundeliusi	0.06	0.78	*0.01*	-				
T. pinchaque	0.16	0.16	0.29	0.16	-			
T. polkensis	0.16	0.42	*0.02*	0.52	0.21	-		
T. terrestris	0.21	*0.02*	0.17	*0.01*	0.20	*0.01*	-	
T. veroensis	0.06	0.72	*0.02*	0.16	0.16	0.08	*0.02*	-
T. webbi	*0.01*	0.09	*0.01*	*0.01*	*0.01*	*0.01*	*0.01*	*0.018*

Table S3.6. Pairwise comparisons from perMANOVA testing of regression residuals from landmark analysis of *Tapirus* cuneiform (10000 permutations). Significant *p*-values (≤0.05) in italics.

Species	*bai*	*hay*	*ind*	*lund*	*pin*	*polk*	*terr*	*vero*
*T. haysii**	0.214	-						
T. indicus	*0.031*	0.190	-					
T. lundeliusi	*0.031*	0.190	*0.032*	-				
T. pinchaque	*0.033*	0.248	*0.039*	*0.032*	-			
T. polkensis	*0.032*	0.623	*0.036*	*0.031*	*0.032*	-		
T. terrestris	*0.039*	0.562	0.163	0.051	*0.031*	0.130	-	
T. veroensis	*0.039*	0.562	*0.038*	0.064	0.051	0.694	0.316	-
T. webbi	*0.039*	0.771	*0.038*	*0.038*	0.051	0.834	0.086	0.150

*one specimen only

Table S3.7. Pairwise comparisons from perMANOVA testing of regression residuals from landmark analysis of *Tapirus* unciforms (10000 permutations). Significant *p*-values (≤0.05) in bold.

Species	*bai*	*hay*	*ind*	*lund*	*pin*	*polk*	*terr*	*vero*
T. haysii	*0.009*	-						
T. indicus	*0.009*	*0.009*	-					
T. lundeliusi	*0.009*	0.111	*0.009*	-				
T. pinchaque	*0.012*	*0.011*	*0.011*	*0.009*	-			
T. polkensis	*0.009*	0.065	*0.009*	*0.009*	*0.011*	-		
T. terrestris	*0.013*	*0.009*	*0.009*	*0.009*	*0.012*	*0.009*	-	
T. veroensis	*0.011*	0.129	*0.011*	*0.011*	0.066	*0.010*	*0.012*	-
T. webbi	0.065	*0.037*	*0.009*	*0.011*	0.229	0.229	0.055	0.082

Table S3.8. Pairwise comparisons from perMANOVA testing of regression residuals from landmark analysis of *Tapirus* third metacarpals (MCIIIs) (10000 permutations). Significant *p*-values (≤0.05) in bold.

Species	*bai*	*hay*	*ind*	*lund*	*pin*	*polk*	*terr*	*vero*
T. haysii	***0.014***	-						
T. indicus	***0.005***	***0.008***	-					
T. lundeliusi	***0.005***	***0.015***	***0.004***	-				
T. pinchaque	***0.012***	***0.032***	***0.008***	***0.006***	-			
T. polkensis	***0.006***	***0.009***	***0.004***	***0.004***	***0.009***	-		
T. terrestris	***0.006***	***0.018***	***0.004***	***0.004***	***0.018***	***0.012***	-	
T. veroensis	***0.018***	***0.032***	***0.007***	***0.006***	***0.032***	***0.015***	***0.015***	-
T. webbi	***0.005***	***0.008***	***0.004***	***0.004***	0.069	***0.039***	0.142	0.129

Table S3.9. Pairwise comparisons from perMANOVA testing of regression residuals from landmark analysis of *Tapirus* fourth metacarpals (MCIVs) (10000 permutations). Significant *p*-values (≤0.05) in bold.

Species	*bai*	*hay*	*ind*	*lund*	*pin*	*polk*	*terr*	*vero*
T. haysii	***0.059***	-						
T. indicus	***0.009***	***0.042***	-					
T. lundeliusi	***0.013***	0.369	***0.006***	-				
T. pinchaque	***0.028***	0.078	***0.013***	***0.014***	-			
T. polkensis	***0.013***	***0.046***	***0.006***	***0.006***	***0.014***	-		
T. terrestris	***0.014***	0.123	***0.006***	***0.013***	0.102	0.013	-	
T. veroensis	***0.016***	0.206	***0.013***	***0.014***	***0.038***	0.201	***0.024***	-
T. webbi	***0.014***	0.077	***0.013***	***0.014***	***0.042***	***0.034***	***0.013***	***0.042***

Table S3.10. Pairwise comparisons from perMANOVA testing of regression residuals from landmark analysis of *Tapirus* lunate (10000 permutations). Significant *p*-values (≤0.05) in bold.

Species	*bai*	*hay*	*ind*	*lund*	*pin*	*polk*	*terr*	*vero*
T. haysii	*0.010*	-						
T. indicus	*0.008*	*0.008*	-					
T. lundeliusi	*0.008*	*0.008*	*0.008*	-				
T. pinchaque	*0.010*	*0.010*	*0.009*	*0.009*	-			
T. polkensis	*0.008*	*0.025*	*0.008*	*0.008*	*0.009*	-		
T. terrestris	*0.010*	*0.010*	*0.008*	*0.010*	*0.010*	*0.010*	-	
T. veroensis	*0.010*	*0.348*	*0.009*	*0.009*	*0.031*	*0.009*	*0.034*	-
T. webbi	*0.008*	*0.010*	*0.008*	*0.008*	*0.009*	*0.167*	*0.031*	*0.010*

Table S3.11. Pairwise comparisons from perMANOVA testing of regression residuals from landmark analysis of *Tapirus* scaphoid (10000 permutations). Significant *p*-values (≤0.05) in bold.

Species	*bai*	*hay*	*ind*	*lund*	*pin*	*polk*	*terr*	*vero*
T. haysii	*0.039*	-						
T. indicus	*0.014*	*0.014*	-					
T. lundeliusi	*0.016*	*0.016*	*0.012*	-				
T. pinchaque	*0.039*	*0.039*	*0.056*	*0.016*	-			
T. polkensis	*0.016*	*0.239*	*0.012*	*0.014*	*0.016*	-		
T. terrestris	*0.019*	*0.019*	*0.012*	*0.014*	*0.060*	*0.019*	-	
T. veroensis	*0.039*	*0.193*	*0.019*	*0.141*	*0.039*	*0.239*	*0.107*	-
T. webbi	*0.039*	*0.039*	*0.019*	*0.027*	*0.039*	*0.200*	*0.031*	*0.212*

Table S3.12. Pairwise comparisons from perMANOVA testing of regression residuals from landmark analysis of *Tapirus* magnum (10000 permutations). Significant *p*-values (≤0.05) in bold.

Species	*bai*	*hay**	*ind*	*lund*	*pin*	*polk*	*terr*	*vero*
*T. haysii**	*0.188*	-						
T. indicus	*0.005*	*0.148*	-					
T. lundeliusi	*0.008*	*0.294*	*0.004*	-				
T. pinchaque	*0.026*	*0.273*	*0.014*	*0.017*	-			
T. polkensis	*0.006*	*0.166*	*0.004*	*0.007*	*0.017*	-		
T. terrestris	*0.008*	*0.294*	*0.004*	*0.010*	*0.017*	*0.007*	-	
T. veroensis	*0.005*	*0.499*	*0.004*	*0.008*	*0.014*	*0.005*	*0.012*	-
T. webbi	*0.004*	*0.149*	*0.004*	*0.004*	*0.014*	*0.043*	*0.004*	*0.004*

*one specimen only

Table S3.13. Pairwise comparisons from perMANOVA testing of regression residuals from landmark analysis of *Tapirus* metacarpal 2 (MCII) (10000 permutations). Significant *p*-values (≤0.05) in bold.

Species	*bai*	*hay*	*ind*	*lund*	*pin*	*polk*	*terr*	*vero*
T. haysii	*0.023*	-						
T. indicus	*0.005*	*0.012*	-					
T. lundeliusi	*0.005*	*0.043*	*0.004*	-				
T. pinchaque	*0.027*	*0.030*	*0.005*	*0.005*	-			
T. polkensis	*0.004*	*0.012*	*0.004*	*0.004*	*0.005*	-		
T. terrestris	*0.005*	*0.014*	*0.004*	*0.004*	*0.007*	*0.004*	-	
T. veroensis	*0.012*	*0.072*	*0.004*	*0.004*	*0.012*	*0.005*	*0.005*	-
T. webbi	*0.011*	*0.015*	*0.004*	*0.004*	*0.008*	*0.005*	*0.005*	*0.025*

Table S3.14. Pairwise comparisons from perMANOVA testing of regression residuals from landmark analysis of *Tapirus* metacarpal 5 (MCV) (10000 permutations). Significant *p*-values (≤0.05) in bold.

Species	*bai*	*hay*	*ind*	*lund*	*pin*	*polk*	*terr*	*vero*
T. haysii	*0.012*	-						
T. indicus	*0.004*	*0.003*	-					
T. lundeliusi	*0.003*	*0.004*	*0.002*	-				
T. pinchaque	*0.024*	*0.058*	*0.012*	*0.009*	-			
T. polkensis	*0.006*	*0.007*	*0.003*	*0.003*	*0.017*	-		
T. terrestris	*0.004*	*0.004*	*0.003*	*0.003*	*0.017*	*0.004*	-	
T. veroensis	*0.196*	*0.054*	*0.032*	*0.028*	*0.106*	*0.041*	*0.328*	-
T. webbi	*0.003*	*0.003*	*0.002*	*0.003*	*0.010*	*0.004*	*0.002*	*0.027*

6. Phylogenetic signal of centroid size

Table S3.15. Results from phylogenetic signal testing on centroid size (CS) and log centroid size ($_{log}$CS). Performed on species averaged bone data; Pagel's Lambda (λ) and significance of λ statistic (*p*; significant <0.05). Significant *p*-value for λ statistic in bold.

Bone	**CS Pagel's λ**	***p***	**$_{log}$CS Pagel's λ**	***p***
Humerus	<0.001	1.000	<0.001	1.000
Radius	0.999	0.253	0.999	0.281
Pisiform	0.999	0.204	0.999	0.289
Cuneiform	<0.001	1.000	<0.001	1.000
Lunate	0.950	0.705	0.981	0.771
Scaphoid	0.932	0.502	0.959	0.560
Magnum	0.999	0.409	0.999	0.521
Unciform	0.999	0.669	<0.001	1.000
Metacarpal II	0.466	1.000	<0.001	1.000
Metacarpal III	<0.001	1.000	<0.001	1.000
Metacarpal IV	<0.001	1.000	<0.001	1.000
Metacarpal V	0.999	0.462	0.999	0.505

7. Stable Carbon Isotopes

Species	Fossil Locality	Region	$\delta^{13}C$	Source
T. bairdii		Nicaragua	16.4	DeSantis 2011
T. bairdii		Nicaragua	14.5	DeSantis 2011
T. bairdii		Nicaragua	15.4	DeSantis 2011
T. bairdii		Honduras	15.0	DeSantis 2011
T. bairdii		Honduras	14.2	DeSantis 2011
T. bairdii		Mexico	14.3	DeSantis 2011
T. bairdii		Mexico	14.7	DeSantis 2011
T. bairdii		Mexico	15.9	DeSantis 2011
T. bairdii		Mexico	13.3	DeSantis 2011
T. bairdii		Mexico	15.6	DeSantis 2011
T. bairdii		Mexico	14.3	DeSantis 2011
T. bairdii		Mexico	15.9	DeSantis 2011
T. bairdii		Mexico	14.3	DeSantis 2011
T. bairdii		Mexico	14.3	DeSantis 2011
T. bairdii		Mexico	15.3	DeSantis 2011
T. bairdii		Mexico	14.0	DeSantis 2011
T. bairdii		Mexico	14.9	DeSantis 2011
T. bairdii		Mexico	15.7	DeSantis 2011
T. bairdii		Mexico	13.0	DeSantis 2011
T. haysii	San Louis Potosi	Mexico	10.6	Perez-Crespo et al. 2012
T. haysii	San Louis Potosi	Mexico	10.7	Perez-Crespo et al. 2012
T. haysii	San Louis Potosi	Mexico	10.7	Perez-Crespo et al. 2012
T. haysii	Leisey 1A	Florida	12.0	DeSantis et al 2009
T. haysii	Leisey 1A	Florida	12.5	DeSantis et al 2009
T. haysii	Leisey 1A	Florida	12.3	DeSantis et al 2009
T. haysii	Leisey 1A	Florida	13.2	DeSantis et al 2009
T. haysii	Leisey 1A	Florida	12.8	DeSantis et al 2009
T. haysii	Leisey 1A	Florida	12.5	DeSantis et al 2009

T. haysii	Leisey 1A	Florida	12.3	DeSantis et al 2009
T. haysii	Leisey 1A	Florida	13.3	DeSantis et al 2009
T. haysii	Leisey 1A	Florida	13.4	DeSantis et al 2009
T. indicus		Sumatra	15.0	Bocherens et al 2017
T. indicus		Sumatra	15.8	Bocherens et al 2017
T. lundeliusi	Inglis 1A	Florida	12.9	DeSantis et al 2009
T. lundeliusi	Inglis 1A	Florida	13.2	DeSantis et al 2009
T. lundeliusi	Inglis 1A	Florida	12.2	DeSantis et al 2009
T. lundeliusi	Inglis 1A	Florida	12.1	DeSantis et al 2009
T. lundeliusi	Inglis 1A	Florida	13.6	DeSantis et al 2009
T. pinchaque		Ecuador	15.9	DeSantis 2011
T. pinchaque		Colombia	13.1	DeSantis 2011
T. pinchaque		Colombia	13.9	DeSantis 2011
T. polkensis	Gray Fossil Site	Tennessee	13.0	DeSantis and Wallace 2008
T. polkensis	Gray Fossil Site	Tennessee	13.9	DeSantis and Wallace 2008
T. polkensis	Gray Fossil Site	Tennessee	12.7	DeSantis and Wallace 2008
T. polkensis	Gray Fossil Site	Tennessee	13.7	DeSantis and Wallace 2008
T. polkensis	Gray Fossil Site	Tennessee	13.1	DeSantis and Wallace 2008
T. polkensis	Gray Fossil Site	Tennessee	12.1	DeSantis and Wallace 2008
T. polkensis	Gray Fossil Site	Tennessee	13.4	DeSantis and Wallace 2008
T. polkensis	Gray Fossil Site	Tennessee	13.3	DeSantis and Wallace 2008
T. polkensis	Gray Fossil Site	Tennessee	11.2	DeSantis and Wallace 2008
T. polkensis	Gray Fossil Site	Tennessee	14.1	DeSantis and Wallace 2008
T. polkensis	Gray Fossil Site	Tennessee	12.7	DeSantis and Wallace 2008
T. polkensis	Gray Fossil Site	Tennessee	13.1	DeSantis and Wallace 2008
T. polkensis	Gray Fossil Site	Tennessee	14.0	DeSantis and Wallace 2008
T. polkensis	Gray Fossil Site	Tennessee	13.9	DeSantis and Wallace 2008
T. polkensis	Gray Fossil Site	Tennessee	11.5	DeSantis and Wallace 2008
T. polkensis	Gray Fossil Site	Tennessee	14.0	DeSantis and Wallace 2008
T. polkensis	Gray Fossil Site	Tennessee	13.7	DeSantis and Wallace 2008
T. polkensis	Gray Fossil Site	Tennessee	12.9	DeSantis and Wallace 2008

T. polkensis	Gray Fossil Site	Tennessee	13.4	DeSantis and Wallace 2008
T. polkensis	Gray Fossil Site	Tennessee	13.7	DeSantis and Wallace 2008
T. polkensis	Gray Fossil Site	Tennessee	13.6	DeSantis and Wallace 2008
T. polkensis	Gray Fossil Site	Tennessee	10.9	DeSantis and Wallace 2008
T. polkensis	Gray Fossil Site	Tennessee	12.4	DeSantis and Wallace 2008
T. terrestris		Colombia	15.7	DeSantis 2011
T. terrestris		Brazil	14.0	DeSantis 2011
T. terrestris		Brazil	12.8	DeSantis 2011
T. terrestris		Brazil	13.0	DeSantis 2011
T. terrestris		Peru	16.4	DeSantis 2011
T. terrestris		Peru	17.0	DeSantis 2011
T. terrestris		Venezuela	16.8	DeSantis 2011
T. terrestris		Venezuela	16.3	DeSantis 2011
T. terrestris		Venezuela	16.6	DeSantis 2011
T. terrestris		Brazil	15.3	DeSantis 2011
T. terrestris		Brazil	15.4	DeSantis 2011
T. terrestris		Brazil	13.5	DeSantis 2011
T. terrestris		Colombia	18.1	DeSantis 2011
T. terrestris		Bolivia	16.3	DeSantis 2011
T. terrestris		Bolivia	16.6	DeSantis 2011
T. veroensis	Page-Ladson	Florida	11.3	Koch et al. 1998
T. veroensis	Page-Ladson	Florida	12.1	Koch et al. 1998
T. veroensis	Hornsby Springs	Florida	12.3	Koch et al. 1998
T. veroensis	Camelot	South Carolina	13.9	Kohn et al. 2005
T. veroensis	Camelot	South Carolina	13.2	Kohn et al. 2005
T. veroensis	Camelot	South Carolina	13.4	Kohn et al. 2005
T. veroensis	Camelot	South Carolina	13.6	Kohn et al. 2005
T. veroensis	Camelot	South Carolina	13.8	Kohn et al. 2005
T. veroensis	Aucilla	Florida	12.0	Hoppe and Koch 2006
T. veroensis	Aucilla	Florida	11.3	Hoppe and Koch 2006
T. veroensis	Aucilla	Florida	13.5	Hoppe and Koch 2006

T. veroensis	Aucilla	Florida	11.4	DeSantis 2009
T. webbi	Love Bone Bed	Florida	11.7	Feranec and MacFadden 2006
T. webbi	Love Bone Bed	Florida	14.3	Feranec and MacFadden 2006
T. webbi	Love Bone Bed	Florida	13.1	MacFadden and Cerling 1996
T. webbi	McGeehee Farm	Florida	13.3	MacFadden and Cerling 1996

Table S3.16. One-way analysis of variance (ANOVA) comparing raw stable isotopic values per species, with Tukey's pairwise comparisons. Tukey's Q below pairwise diagonal and *p*-values above the diagonal; significant *p*-values in bold. Abbreviated column titles correspond to species in rows.

Test	**Sum of squares**	**DF**	***F***	***p***
Equal Means	137.933	8.00	14.74	*<0.01*
Welch *F* test	-	12.46	11.58	*<0.01*

Tukey's p/wise	*bair*	*hays*	*indi*	*lund*	*pinc*	*polk*	*terr*	*vero*	*web*
T. bairdii		*0.04*	*0.99*	*0.07*	*0.99*	*0.17*	*0.97*	*0.03*	*0.19*
T. haysii	5.674		*<0.01*	*0.99*	*0.04*	*0.91*	*<0.01*	*0.998*	*0.894*
T. indicus	1.334	7.008		*0.004*	*0.746*	*0.014*	*1.000*	*0.002*	*0.017*
T. lundeliusi	4.346	1.329	5.679		*0.344*	*1.000*	*0.002*	*1.000*	*1.000*
T. pinchaque	1.069	4.605	2.403	3.276		*0.602*	*0.556*	*0.235*	*0.647*
T. polkensis	3.785	1.889	5.119	0.560	2.716		*0.006*	*1.000*	*1.000*
T. terrestris	1.741	7.416	0.408	6.087	2.810	5.527		*0.001*	*0.007*
T. veroensis	4.640	1.034	5.974	0.295	3.571	0.855	6.382		*0.999*
T. webbi	3.690	1.984	5.024	0.655	2.621	0.095	5.432	0.950	

8. Additional PhyMANOVAs

Table S3.17. phyMANOVAs of size-independent shape variables against average stable carbon isotope ($\delta^{13}C$) ranges, based on rPC scores accounting for >70% variance of species averaged shape data (10000 simulations). Significant values for Wilks' Lambda statistic (Λ) and associated p-value (*p*) and phylogenetically corrected *p*-values (corr. *p*) are in bold.

Bone*	DF	Λ	*F*	*p*	corr. *p*
Humerus	3	0.060	3.078	*0.099*	*0.054*
Radius	3	0.012	2.028	*0.208*	*0.391*
Pisiform	3	0.050	4.605	*0.026*	*0.066*
Cuneiform	3	0.009	4.842	*0.022*	*0.051*
Lunate	3	0.075	1.578	*0.273*	*0.477*
Scaphoid	3	0.018	3.499	*0.051*	*0.120*
Magnum	3	0.013	4.147	*0.033*	*0.082*
Unciform	3	0.012	4.225	*0.031*	*0.072*
Metacarpal 2	3	0.008	5.175	*0.018*	*0.046*
Metacarpal 3	3	0.099	1.315	*0.362*	*0.587*
Metacarpal 4	3	0.079	1.519	*0.291*	*0.494*
Metacarpal 5	3	0.079	1.520	*0.291*	*0.498*

* bones in italics demonstrated significant influence of centroid size on shape data

Table S3.18. phyMANOVAs of size-independent shape variables against average stable carbon isotope ($\delta^{13}C$) ranges, based on the first two rPCs of New World tapir species averaged shape data (10000 simulations). Cumulative % variance accounted for are presented. Significant values for Wilks' Lambda statistic (Λ) and associated p-value (*p*) and phylogenetically corrected *p*-values (corr. *p*) are in bold.

Bone*	Cum. % var.	DF	Λ	*F*	*p*	corr. *p*
Humerus	73.4	3	0.035	2.891	*0.162*	*0.196*
Radius	66.8	3	0.012	2.923	*0.125*	*0.266*
Pisiform	75.7	3	0.066	2.879	*0.112*	*0.239*
Cuneiform	60.9	3	0.008	3.384	*0.096*	*0.201*
Lunate	57.2	3	0.001	10.527	*0.009*	*0.029*
Scaphoid	56.7	3	0.001	8.639	*0.014*	*0.043*
Magnum	60.4	3	0.007	3.752	*0.079*	*0.175*
Unciform	58.8	3	0.004	4.980	*0.046*	*0.107*
Metacarpal 2	53.0	3	0.005	4.014	*0.069*	*0.161*
Metacarpal 3	66.4	3	0.019	2.288	*0.187*	*0.356*
Metacarpal 4	66.9	3	0.027	1.906	*0.247*	*0.456*
Metacarpal 5	64.6	3	0.001	8.639	*0.014*	*0.035*

* bones in italics demonstrated significant influence of centroid size on shape data

9. Specimens of *Tapirus*

A total of 540 bones were laser scanned for this analysis, representing 186 different specimens across 12 species of tapir. These scans were used for both body mass estimations and morphological comparisons. The scapula, ulna, trapezoid and trapezium were excluded due to minimal preservation of fossils; phalanges were not incorporated due to lack of comparative data from extant specimens in previous studies.

The specimens used in this analysis were scanned at four locations: the Universiteit Antwerpen Functional Morphology lab (Antwerpen, Belgium), the Naturalis Biodiversity Centre (Leiden, The Netherlands), the Florida Museum of Natural History (Gainesville (FL), USA) and the East Tennessee State University and General Shale Brick Natural History Museum (Gray (TN), USA). Fossil material that was scanned was chosen based on the completeness of the specimen and lack of taphonomic or post-burial shape change

– RESEARCH CHAPTER FIVE: APPENDIX IV –

Modern tapirs as morphofunctional analogues for locomotion in endemic European perissodactyls

Jamie A. MacLaren and Sandra Nauwelaerts

Table of Contents

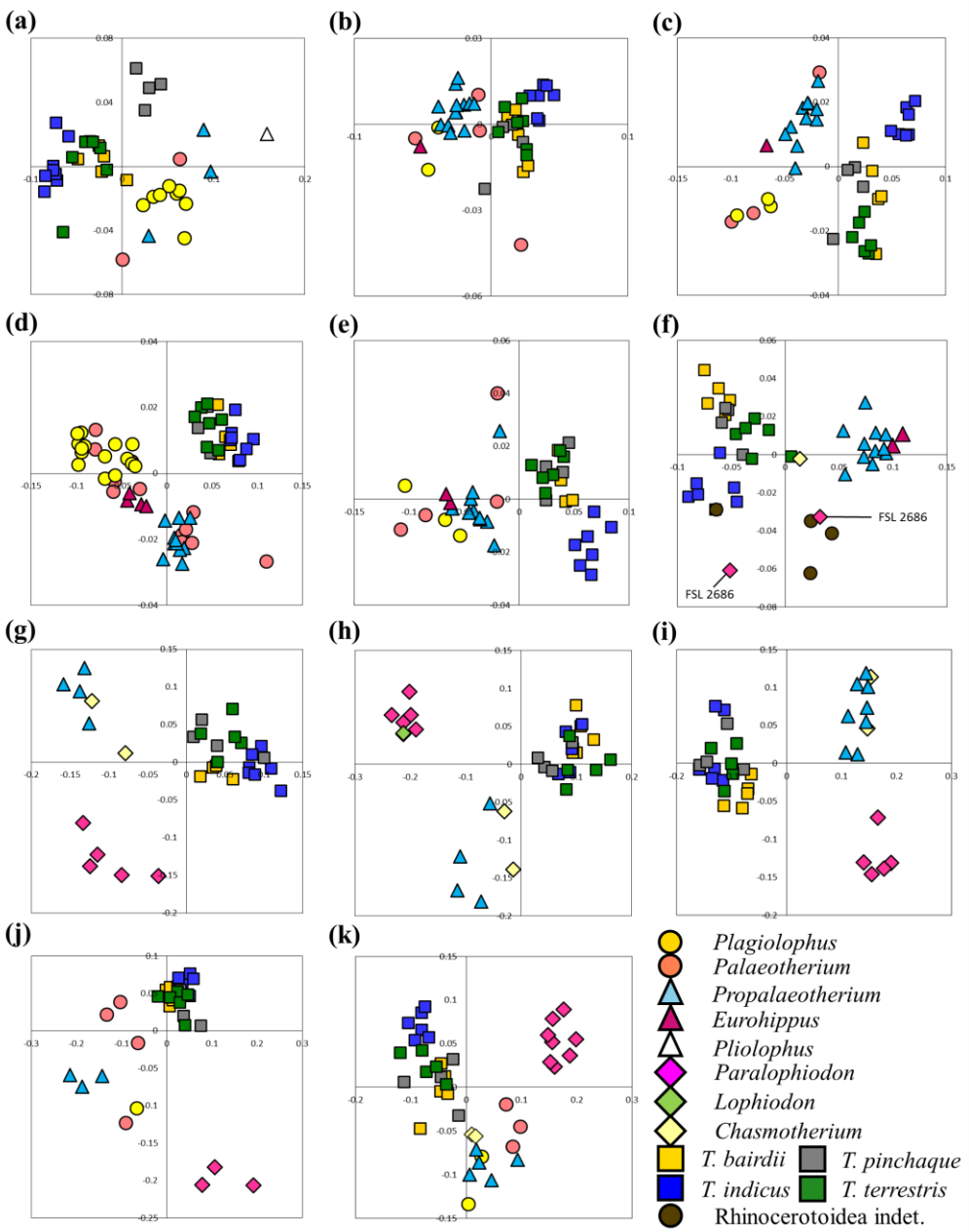

Figure S4.1 Morphospace plots for all forelimb bones investigated. From top left: **(a)** humerus, **(b)** radius, **(c)** metacarpal II, **(d)** metacarpal III, **(e)** metacarpal IV, **(f)** metacarpal V, **(g)** scaphoid, **(h)** lunate, **(i)** cuneiform, **(j)** magnum, **(k)** unciform. Principal components 1 (horizontal) and 2 (vertical) plotted against one another. Species key provided in bottom right.

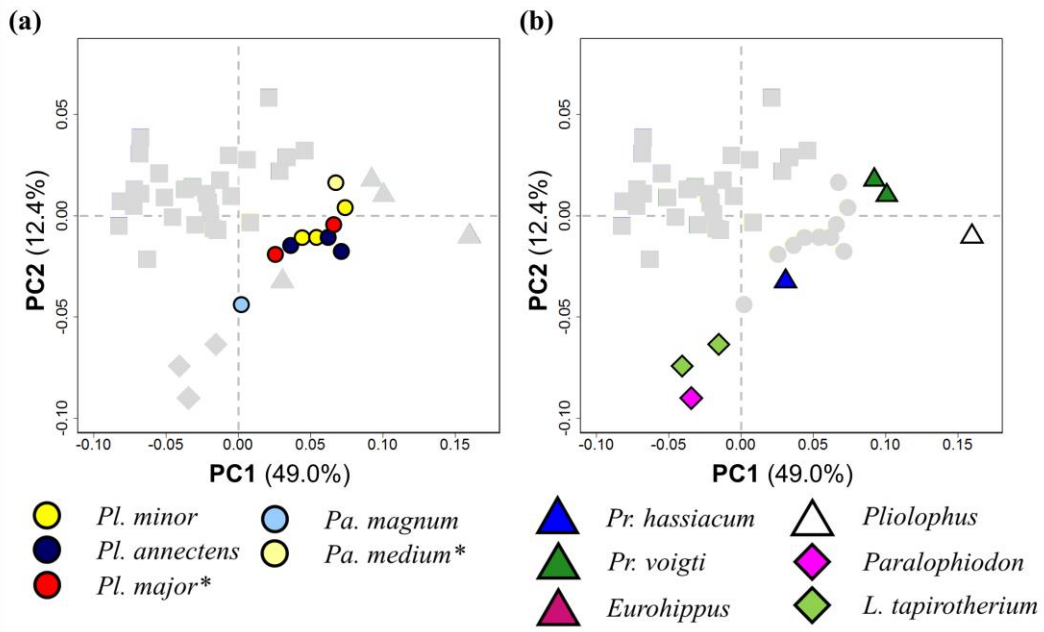

Figure S4.2. Early European perissodactyl species breakdown in humerus morphospace (PC1 vs PC2). **(a)** Palaeotheriinae species and **(b)** early European equoids and lophiodontids. * assigned to species level based on comparisons with other preserved material. Greyed out taxa identified in main document.

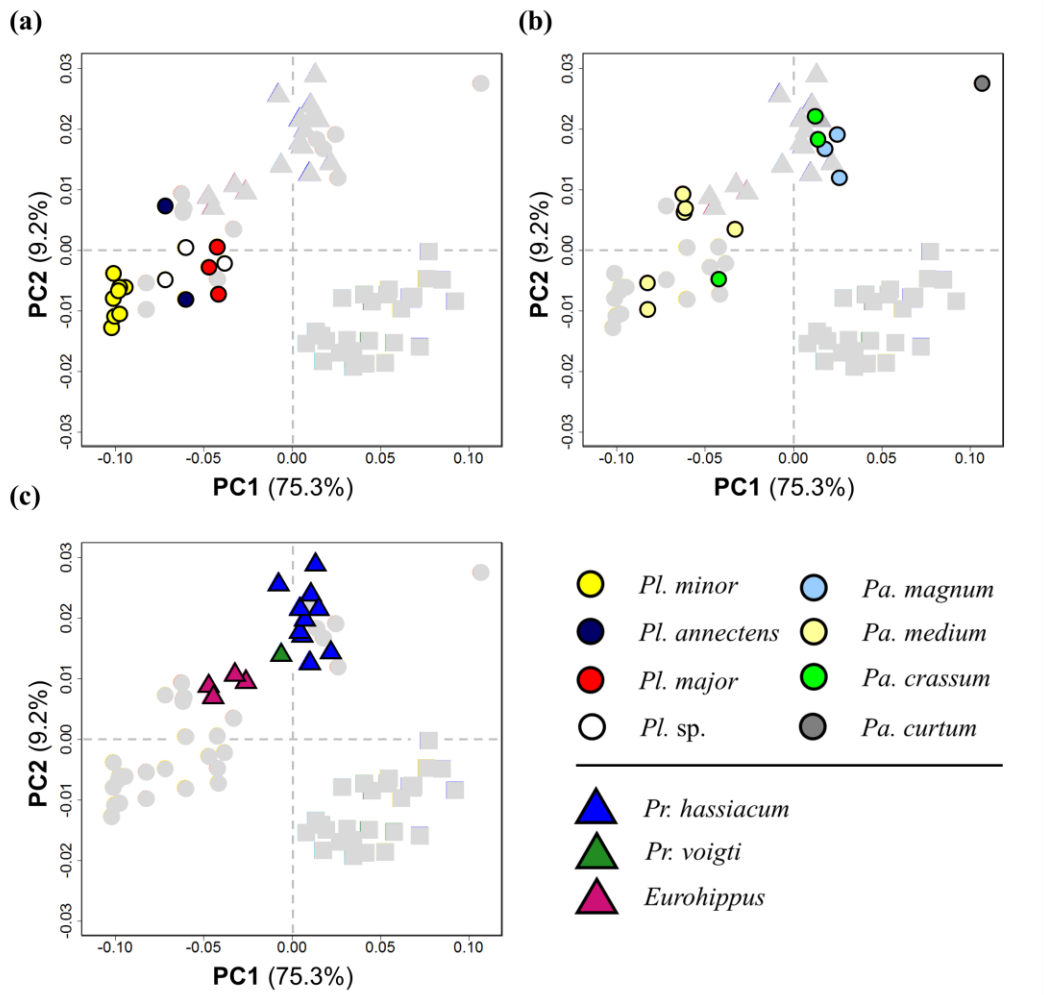

Figure S4.3. Early European perissodactyl species breakdown in third metacarpal morphospace (PC1 vs PC2). **(a)** *Plagiolophus* species, **(b)** *Palaeotherium* species and **(c)** tetradactyl Palaeotheriidae. Greyed out taxa identified in main document. Note the vast span of morphospace occupied by *Palaeotherium* compared with *Plagiolophus* **(a)** and *Propalaeotherium* **(c**; blue and green triangles**)**

2. ANOVA and Tukey WSD Results

Table S4.1. Tukey WSD post-hoc test results for ANOVA based on PC1 scores for third metacarpal.

Species	N	Metacarpal III (PC scores)							
		1	**2**	**3**	**4**	**5**	**6**	**7**	**8**
Pl. minor	8	-0.09							
Pl. annectens	2		-0.06						
Pa. medium	6		-0.06						
Plagiolophus	3		-0.05	-0.05					
Pl. major	3		-0.04	-0.04					
Eurohippus	4			-0.03					
Pa. crassum	3				-0.01				
Propalaeotherium	11				0.01	0.01			
T. polkensis	8					0.02	**0.02**		
Pa. magnum	3					0.02	**0.02**		
T. pinchaque	3						**0.03**	0.03	
T. terrestris	6						**0.04**	0.04	
T. bairdii	5							0.06	0.06
T. indicus	7								0.07

3. Lever arm measurements

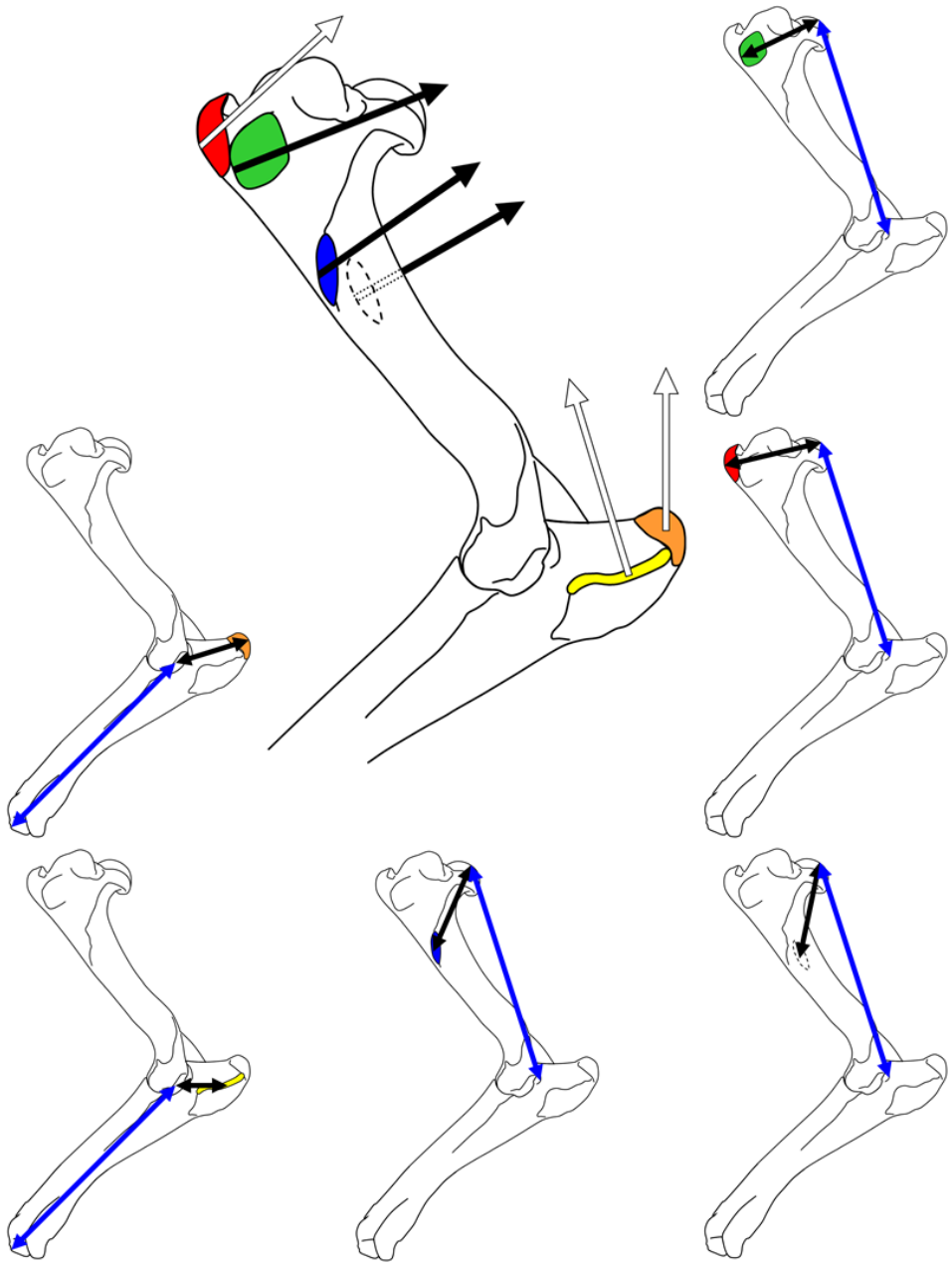

Figure S4.4 Lever arm measurement protocol. In-lever (black) and out-lever (blue) represented for each muscle. Clockwise from top right: (shoulder) *m. infraspinatus*, *m. supraspinatus*, *m. teres major*, *m. deltoideus;* (elbow) *m. triceps brachii laterale*, *m. triceps brachii longum*. Central diagram shows all attachment sites and directions of muscular action: filled arrows = joint flexor; empty arrows = joint extensors.

Table S4.2. Residuals from OLS regression of in-lever and out-lever measurements. Early European perissodactyls listed, with residual distance to regression line of each modern tapir species listed beneath tapir species name (*T. bairdii, T. indicus, T. pinchaque, T. terrestris)*. Residuals calculated as difference between actual inlever (listed) and in-lever predicted by tapir OLS regression lines. The smallest residuals represent the tapir regression line closest to the respective early European perissodactyl values, highlighted in bold. *pinch.* = *T. pinchaque*; *terres.* = *T. terrestris*

Supraspinatus							***Infraspinatus***					
Species	**Inlever**	***bairdii***	***indicus***	***pinch.***	***terres.***		**Species**	**Inlever**	***bairdii***	***indicus***	***pinch.***	***terres.***
Paralophiodon	64.6	40.8	33.4	11.0	**8.7**		*Paralophiodon*	62.9	**1.8**	28.0	20.7	2.9
Lophiodon	71.7	29.1	27.2	**4.3**	**4.8**		*Lophiodon*	64.6	**4.6**	27.2	17.4	**4.5**
Pl. annectens	39.5	89.1	54.1	34.1	**17.9**		*Pl. annectens*	36.4	**5.6**	50.0	55.2	6.5
Pl. major	48.6	67.2	47.5	26.2	**17.6**		*Pl. major*	46.2	8.3	42.6	40.9	**4.0**
Pl. minor	29.1	107.2	63.0	43.8	**22.9**		*Pl. minor*	26.9	**7.5**	58.0	67.4	**7.1**
Propalaeotherium	35.2	93.8	58.3	38.4	**21.8**		*Propalaeotherium*	34.2	7.3	52.1	57.5	**4.9**
Pa. magnum	92.2	10.9	10.4	14.5	**2.3**		*Pa. magnum*	83.5	**4.8**	12.0	8.2	7.8
Deltoideus							***Teres major***					
Species	**Inlever**	***bairdii***	***indicus***	***pinch.***	***terres.***		**Species**	**Inlever**	***bairdii***	***indicus***	***pinch.***	***terres.***
Paralophiodon	78.3	11.6	21.1	**1.4**	10.6		*Paralophiodon*	94.4	16.6	**0.5**	10.4	12.4
Lophiodon	88.9	15.8	11.1	**8.2**	14.6		*Lophiodon*	98.3	15.3	**4.8**	7.0	12.7
Pl. annectens	50.9	**15.8**	45.2	23.8	**16.0**		*Pl. annectens*	58.0	40.1	**5.8**	44.0	28.4
Pl. major	66.6	14.1	31.3	**10.8**	13.7		*Pl. major*	69.3	35.9	**7.2**	34.3	28.4
Pl. minor	41.4	**17.0**	53.6	31.6	**17.5**		*Pl. minor*	44.7	49.1	**4.6**	56.5	34.8
Propalaeotherium	47.1	**12.7**	48.8	27.4	**13.0**		*Propalaeotherium*	52.6	45.3	**1.6**	49.4	33.4
Pa. magnum	107.8	8.1	**5.0**	23.0	6.0		*Pa. magnum*	128.9	4.4	8.7	21.3	**0.7**
***Triceps brachii* (lateral)**							***Triceps brachii* (long)**					
Species	**Inlever**	***bairdii***	***indicus***	***pinch.***	***terres.***		**Species**	**Inlever**	***bairdii***	***indicus***	***pinch.***	***terres.***
Paralophiodon	36.0	**2.1**	16.9	12.4	4.0		*Paralophiodon*	53.2	13.4	27.2	17.2	**5.7**
Lophiodon	40.5	**2.0**	14.3	7.6	3.5		*Lophiodon*	51.9	17.9	29.5	20.6	**12.4**
Propalaeotherium	28.2	**0.8**	20.3	20.9	2.1		*Propalaeotherium*	39.7	19.0	38.3	25.6	**6.0**

4. Supplementary Long-Bone Ratio measurements

Table S4.3. Long-bone ratios and estimated body masses for all available taxa in this study. * = predicted based on sister taxa. **N** = number of articulated specimens; (n) = total specimens for average. **HR** = radius/humerus; **HMC** = third metacarpal/humerus; **BM** = mean estimated body mass.

Genus	**Species**	**N** (n)	**HR**	**HMC**	**BM** (kg)
Tapirus	*bairdii*	**5** (5)	84.6	46.9	228.7
Tapirus	*indicus*	**7** (8)	89.4	47.6	326.4
Tapirus	*pinchaque*	**4** (4)	83.5	47.1	202.4
Tapirus	*terrestris*	**7** (7)	86.1	48.8	216.6
Tapirus	*polkensis*	**2** (15)	96.8	54.5	116.9
Colodon [a]	*occidentalis*	**1** (1)	114.6	67.6	-
Heptodon [b]	*calciculus*	**1** (1)	99.1	58.3	-
Heptodon [c]	*posticus*	1 (1)	92.7	55.3	-
Paralophiodon	*leptorhynchum*	**1** (1)	87.45	45.4	232.5
Metamynodon [a]	*planifrons*	**1** (1)	76.7	37.2	1047.4
Teleoceras [d]	*major*	**0** (20)	82.2	37.7	780.7
Teleoceras [d]	*hicksi*	**0** (14)	79.4	36.0	1296.5
Uintaceras [e]	*radinskyi*	**1** (1)	78.8	38.7	-
Chasmotherium	*minimus*	**1** (2)	86.9	49.9	-
Palaeotherium	*curtum*	**0** (3)	75.0*	38.2*	
Palaeotherium	*magnum*	**1** (4)	93.7	49.8	240.3
Palaeotherium	*crassum*	**0** (6)	105.1*	58.7*	
Palaeotherium	*medium*	**0** (6)	112.6*	100.4*	
Plagiolophus	*major**	**0** (5)	107.5*	62.9	78.9
Plagiolophus	*annectens*	**0** (6)	117.0	72.8	34.8
Plagiolophus	*minor*	**0** (11)	126.6	82.1	19.3
Propalaeotherium	*hassiacum*	**0** (24)	93.3	48.6	46.5
Propalaeotherium [f]	*voigti*	**0** (4)	96.4	56.9	23.0
Eurohippus	*parvulum*	**1** (6)	90.5	52.2	-
Eurohippus [g]	*messelensis*	**2** (2)	88.2	49.6	-
Arenahippus [h]	*grangeri*	**1** (1)	91.2	46.7	7.9
Mesohippus [a]	*bairdii*	**2** (4)	109.4	66.7	24.2
Hallensia [i]	*matthesi*	**1** (1)	93.5	55.1	-

References: [a] Scott (1941); [b] Gregory (1929); [c] Radinsky (1965); [d] Prothero (2005); [e] Holbrook and Lucas (1997); [f] Franzen (2010); [g] Franzen and Haupzeter (2017); [h] Wood *et al.* (2011); [i] Franzen

5. Fossil Locations

Figure S4.5. Map of fossil localities for specimens used in this study. Present-day western European geography overlaid with predicted landmass from c.50Mya (Ypresian), based on Franzen (2010; Ch. 4: Europe in the Eocene; p.41) (brown). Taxon key and localities listed surrounding map. Genus abbreviations: *Pa.* = *Palaeotherium*, *Pl.* = *Plagiolophus*, *Pr.* = *Propalaeotherium*, *Eu.* = *Eurohippus*, *L.* = *Lophiodon*, *Pliolophus* = *P. vulpiceps*, *Hallensia* = *H. matthesi*, *Chasmotherium (=Hyrachyus) minimus*

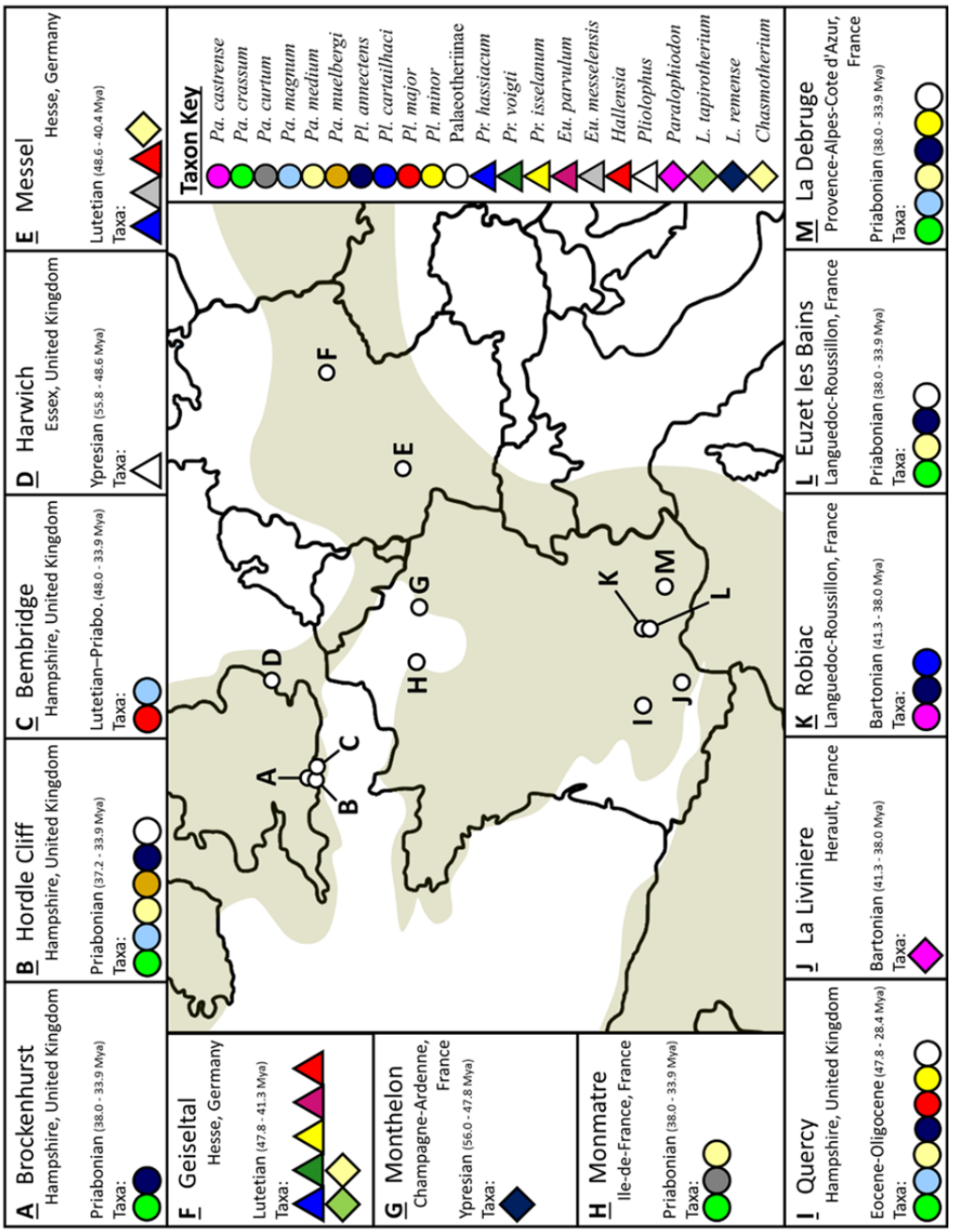

– RESEARCH CHAPTER SIX: APPENDIX V –

Endemism, dietary regime and ecological turnovers influence morphological divergence in equoid limbs through deep time

Jamie A. MacLaren

Table of Contents

1. Composite Phylogeny

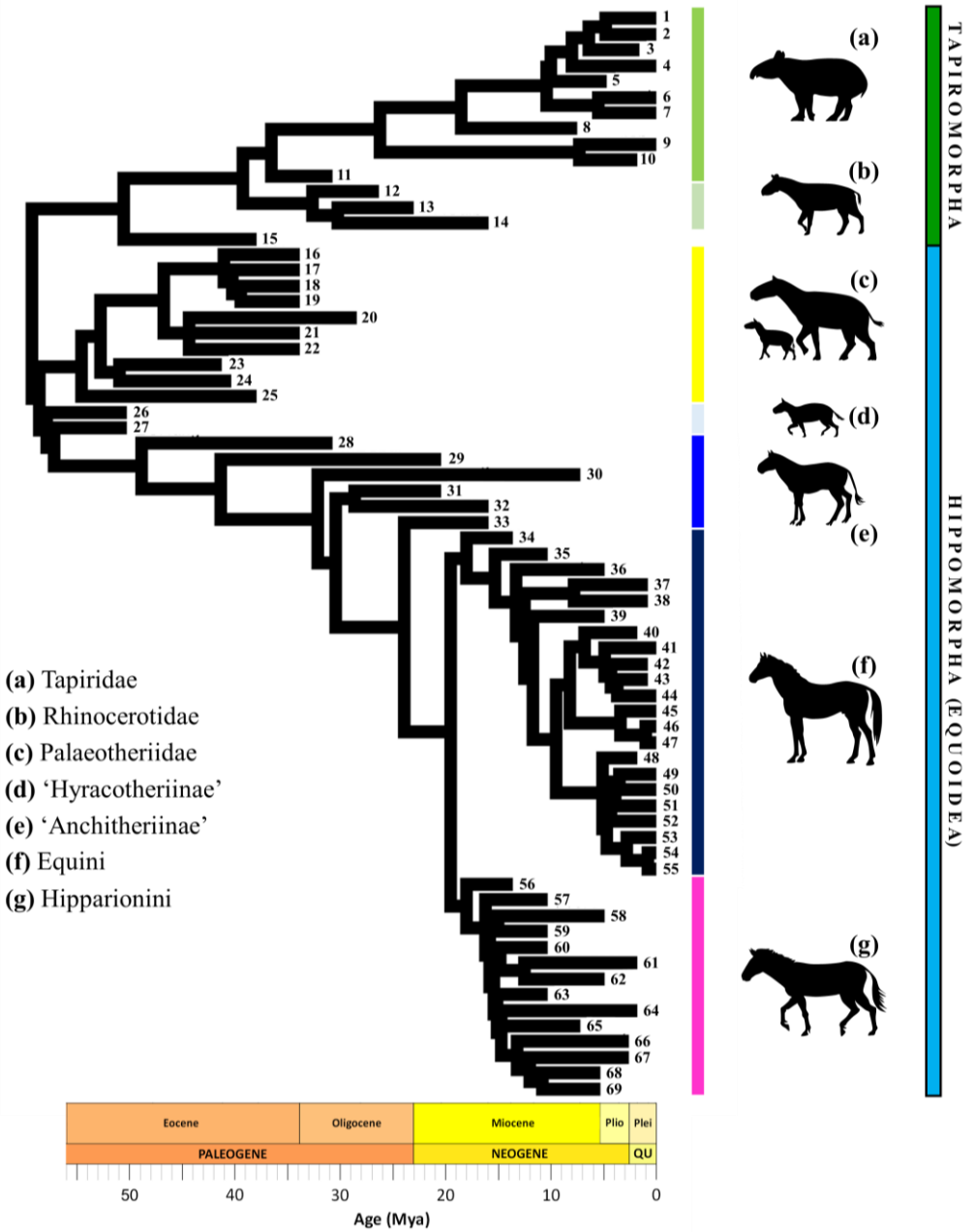

Figure S5.1. Composite phylogenetic tree used for phylogenetic comparative methods. Tree compiled from multiple published trees: Remy 1992, 2004; Colbert 2005; Hulbert 2005; Maguire and Stigall 2008; Hulbert et al. 2009; Steiner and Ryder 2011; Steiner et al. 2012; Danilo et al. 2013; Ruiz-García et al. 2016; Prado and Alberdi 2017. Silhouettes of representative taxa: **(a)** *Tapirus*; **(b)** *Subhyracodon*; **(c)** *Plagiolophus* (left) and *Palaeotherium magnum*; **(d)** *Sifrhippus*; **(e)** *Miohippus*; **(f)** *Equus f. caballus*; **(g)** *Nannippus*.

Figure S5.1 Species list. **Tapiridae**: **1.** *Tapirus veroensis,* **2.** *T. haysii*, **3.** *T. lundeliusi,* **4.** *T. bairdii,* **5.** *T. polkensis,* **6.** *T. pinchaque,* **7.** *T. terrestris,* **8.** *T. webbi*, **9.** *T. indicus,* **10.** *T. arvernensis,* **11.** *Protapirus obliquidens*; **Rhinocerotidae**: **12.** *Subhyracodon occidentalis,* **13.** *Protaceratherium albigense,* **14.** *P. minutum*; **Tapiromorpha indeterminate**: **15.** *Chasmotherium*; **Palaeotheriidae**: **16.** *Palaeotherium curtum,* **17.** *Pa. magnum,* **18.** *Pa. medium,* **19.** *Pa. crassum,* **20.** *Plagiolophus minor,* **21**. *Pl. major,* **22.** *Pl. annectens,* **23.** *Propalaeotherium hassiacum,* **24.** *Pr. voigti,* **25.** *Eurohippus parvulum*; **Equidae**: **26.** *Sifrhippus sandrae,* **27.** *Eohippus angustidens,* **28.** *Mesohippus barbouri*, **29.** *Miohippus gidleyi*, **30.** *Anchitherium aureliense,* **31.** *Archaeohippus manulus,* **32.** *Ar. blackbergi,* **33.** *Parahippus leonensis*; **Equini**: **34.** *Acritohippus isoneus,* **35.** *Pliohippus pernix,* **36.** *Astrohippus ansae,* **37.** *Hippidion principale,* **38.** *H. devellei,* **39.** *Dinohippus interpolates,* **40.** *Equus (Plesippus) simplicidens,* **41.** *Equus* (*Amerhippus*) *insulatus,* **42.** *E.* (*A.*) *andium,* **43.** *E.* (*A.*) *neogeum,* **44.** *E.* (*A.*) *santaelenae,* **45.** *E. ferus gallicus,* **46.** *E. f. przewalski,* **47.** *E. f. germanicus,* **48.** *E. stenonis,* **49.** *E. quagga,* **50.** *E. zebra,* **51.** *E. africanus,* **52.** *E. grevyi,* **53.** *E. hyrudinatus,* **54.** *E. kiang,* **55.** *E. hemionus*; **Hipparionini**: **56.** *Merychippus,* **57.** *Protohippus simum,* **58.** *Pseudohipparion skinneri,* **59.** *Neohipparion affine,* **60.** *Nannippus westoni*, **61.** *N. penninsulatus,* **62.** *N. aztecus,* **63.** *Cormohipparion occidentale,* **64.** *Eurygnathohippus* ("*Hypsohipparion*") *albertense,* **65.** *Hippotherium primigenium,* **66.** *Hipparion* (*Plesiohipparion*) *rocinantis,* **67.** *Hipparion crassum,* **68.** *Hipparion* (*Cremohipparion*) *mediterraneum,* **69.** *Hipparion prostylum.*

2. Branch Lengths

Table S5.2. First-Last occurrence ages for species in this study. FA = first occurrence; LA = last occurrence (occurrence data taken from reference in table and PaleoDB

Genus	Species	FA (Mya)	LA (Mya)	Reference
Tapirus	*veroensis*	0.3	0.012	Hulbert et al. 2010
Tapirus	*haysii*	2.6	0.012	Hulbert et al. 2010
Tapirus	*lundeliusi*	2.6	1.6	Hulbert et al. 2010
Tapirus	*bairdii*	0.126	0	Ruiz-Garcia et al. 2016
Tapirus	*polkensis*	9	4.75	Hulbert et al. 2009
Tapirus	*pinchaque*	0.126	0	Ruiz-Garcia et al. 2016
Tapirus	*terrestris*	0.781	0	Ruiz-Garcia et al. 2016
Tapirus	*webbi*	10.3	7.5	Hulbert 2005
Tapirus	*indicus*	2.588	0	Steiner and Ryder 2011
Tapirus	*arvernensis*	3.2	1.806	Van der Made 2010
Protapirus	*obliquidens*	33.3	30.8	Scott 1941
Subhyracodon	*occidentalis*	30.8	26.3	Scott 1941
Protaceratherium	*albigense*	28.4	23.03	Becker et al. 2013
Protaceratherium	*minutum*	20.43	15.97	Roman 1914
Chasmotherium	sp.	41.3	38	Radinsky 1967
Palaeotherium	*curtum*	38	33.9	Remy 1992
Palaeotherium	*magnum*	37.2	33.9	Remy 1992
Palaeotherium	*medium*	38	33.9	Remy 1992
Palaeotherium	*crassum*	38	33.9	Remy 1992
Plagiolophus	*minor*	38	28.4	Remy 2004
Plagiolophus	*major*	37.8	33.9	Remy 2004
Plagiolophus	*annectens*	41.3	33.9	Remy 2004
Propalaeotherium	*hassiacum*	48.6	41.3	Hellmund 2005
Propalaeotherium	*voigti*	48.6	40.4	Franzen 2010*a*
Eurohippus	*parvulum*	48.6	38	Franzen 2010*a*
Sifrhippus	*sandrae*	55.8	50.3	Secord et al. 2012
Eohippus	*angustidens*	55.8	50.3	Froelich 2002
Mesohippus	*barbouri*	33.3	30.8	Scott 1941
Miohippus	*gidleyi*	33.3	20.4	Scott 1941
Anchitherium	*aureliense*	15.97	7.246	Alberdi and Rodriguez 2012
Archaeohippus	*manulus*	26.3	20.43	O'Sullivan 2003
Archaeohippus	*blackbergi*	20.43	15.97	O'Sullivan 2003
Parahippus	*leonensis*	20.43	15.97	O'Sullivan 2003
Acritohippus	*isoneus*	15.97	13.6	Mihlbachler et al. 2011
Pliohippus	*pernix*	13.6	10.3	Mihlbachler et al. 2011
Astrohippus	*ansae*	10.3	4.9	Mihlbachler et al. 2011
Hippidion	*principale*	2.6	0.8	Mihlbachler et al. 2011
Hippidion	*devellei*	2.588	0.781	Mihlbachler et al. 2011
Dinohippus	*interpolatus*	10.3	4.9	Mihlbachler et al. 2011
Equus (*Plesippus*)	*simplicidens*	4.9	1.8	Prado and Alberdi 2017
Equus (*Amerhippus*)	*insulates*	0.126	0.0117	Prado and Alberdi 2017
Equus (*Amerhippus*)	*andium*	2.6	0.8	Prado and Alberdi 2017
Equus (*Amerhippus*)	*neogeum*	2.6	0.8	Prado and Alberdi 2017
Equus (*Amerhippus*)	*santaelenae*	0.126	0.012	Prado and Alberdi 2017
Equus	*ferus gallicus*	0.781	0.0117	Prado and Alberdi 2017
Equus	*f. przewalski*	0.126	0	Prado and Alberdi 2017

Equus	*f. germanicus*	0.126	0.0117	Prado and Alberdi 2017
Equus	*stenonis*	2.588	1.806	Prado and Alberdi 2017
Equus	*quagga*	2.588	0	Prado and Alberdi 2017
Equus	*zebra*	2.588	0	Prado and Alberdi 2017
Equus	*africanus*	2.31	0	Prado and Alberdi 2017
Equus	*grevyi*	2.588	0	Prado and Alberdi 2017
Equus	*hyrudinatus*	0.35	0.0117	Prado and Alberdi 2017
Equus	*kiang*	0.126	0	Prado and Alberdi 2017
Equus	*hemionus*	0.126	0	Prado and Alberdi 2017
Merychippus	sp.	15.97	13.6	Mihlbachler et al. 2011
Protohippus	*simum*	13.6	10.3	Prado and Alberdi 2017
Pseudhipparion	*skinneri*	10.3	4.9	Prado and Alberdi 2017
Neohipparion	*affine*	13.6	10.3	Prado and Alberdi 2017
Nannippus	*westoni*	13.6	10.3	Prado and Alberdi 2017
Nannippus	*penninsulatus*	4.9	1.8	Prado and Alberdi 2017
Nannippus	*aztecus*	10.3	4.9	Prado and Alberdi 2017
Cormohipparion	*occidentale*	13.6	10.3	Prado and Alberdi 2017
Eurygnathohippus ("*Hypsohipparion*")	*albertense*	2.588	1.8	Bone and Singer 1965
Hippotherium	*primigenium*	13.8	7.2	Prado and Alberdi 2017
Hipparion (*Plesiohipparion*)	*rocinantis*	5.3	2.6	Prado and Alberdi 2017
Hipparion (*Cremohipparion*)	*mediterraneum*	8.7	5.333	Prado and Alberdi 2017
Hipparion	*crassum*	5.3	2.6	Prado and Alberdi 2017
Hipparion	*prostylum*	9	5.3	Prado and Alberdi 2017

3. Landmark Configurations

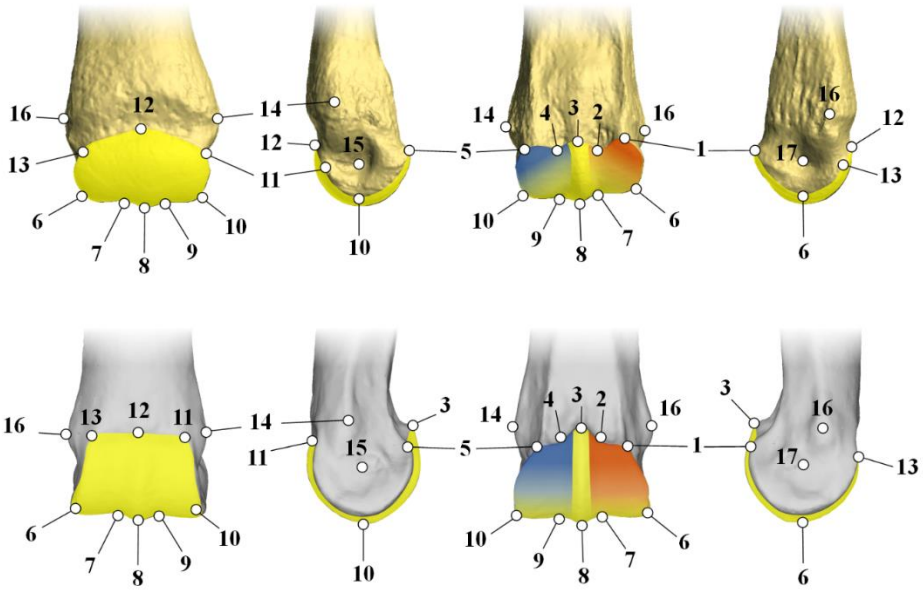

Figure S5.2. Landmark configurations for shape analysis. Landmark points displayed on *Tapirus* (Tapiridae; top) and *Nannippus* (Equidae; bottom) distal metacarpals. From left: dorsal view; lateral view; palmar view; medial view. Yellow region marks metacarpophalangeal joint facet and sagittal ridge; blue region represents the joint facet interaction between the lateral proximal sesamoid and the metacarpal; the red region marks the interaction between the medial proximal sesamoid and the metacarpal head.

1. Medioproximal angle of palmar metacarpophalangeal joint facet	**2.** Medioproximal point of contact between sagittal ridge and palmar metacarpophalangeal joint facet
3. Most proximal angle of palmar metacarpophalangeal joint facet	**4.** Lateroproximal point of contact between sagittal ridge and palmar metacarpophalangeal joint facet
5. Lateroproximal angle of palmar metacarpophalangeal joint facet	**6.** Distal point of medial edge of metacarpophalangeal joint facet
7. Most distal point of contact between sagittal ridge and articular surface of medial metacarpophalangeal facet	**8.** Most distal point of sagittal ridge
9. Most distal point of contact between sagittal ridge and articular surface of lateral metacarpophalangeal facet	**10.** Distal point of lateral edge of metacarpophalangeal joint facet
11. Lateroproximal angle of dorsal metacarpophalangeal joint facet	**12.** Proximal point of dorsal metacarpophalangeal joint facet
13. Medioproximal angle of dorsal metacarpophalangeal joint facet	**14.** Apex of lateral-collateral ligament origination site
15. Deepest point of lateral sulcus of metacarpal head	**16.** Apex of medial-collateral ligament origination site
17. Deepest point of medial sulcus of metacarpal head	

4. Tukey-B Testing of PC scores

Table S5.3. Tukey-B clustering of clades for all taxa along **(a)** PC1 and **(b)** PC2.

(a) Clade	Sample N	Cluster 1	Cluster 2	Cluster 3	Cluster 4
'Hyracotheres'	4	-1.349			
Tapirids	51	-1.191			
Palaeotheres	43	-1.179			
'Anchitheres'	22		-0.081		
OW Hipparionines	14			0.203	
NW Hipparionines	25			0.290	
Non-*Equus* Equini	18				0.875
Equus species	94				0.987

(b) Clade	Sample N	Cluster 1	Cluster 2	Cluster 3
NW Hipparionines	25	-2.247		
OW Hipparionines	14		-0.816	
'Anchitheres'	22		-0.687	
Tapirids	51			0.224
Non-*Equus* Equini	18			0.241
Palaeotheres	43			0.314
'Hyracotheres'	4			0.379
Equus species	94			0.553

5. Trait Quantification Methodologies

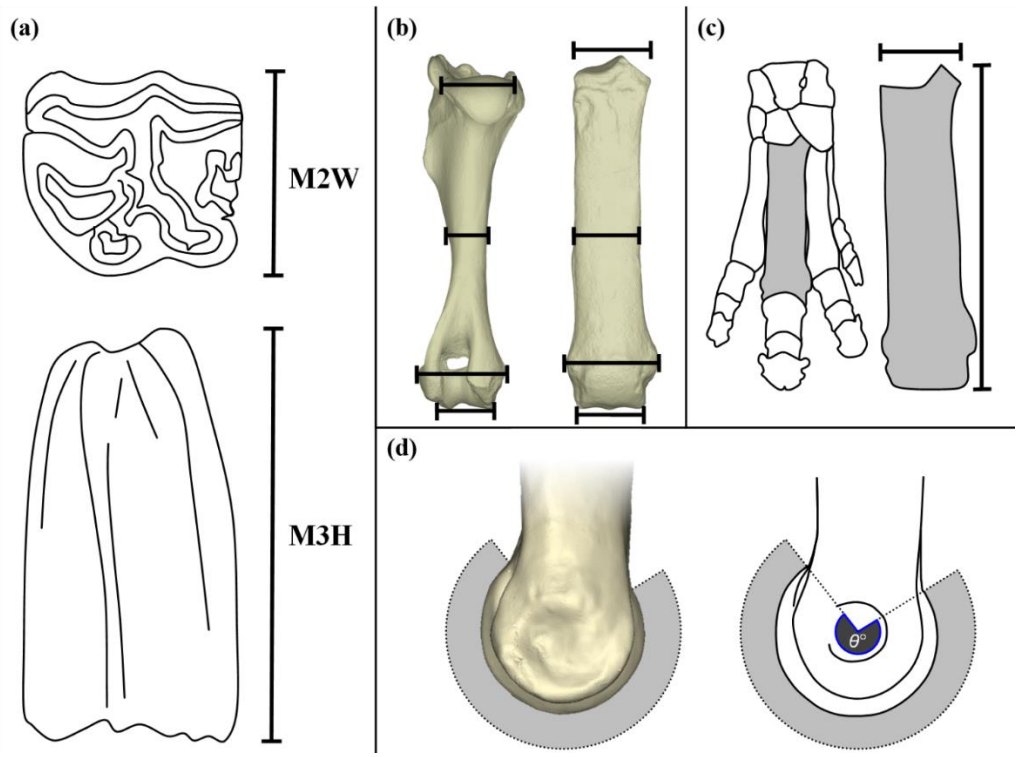

Figure S5.3. Methodology for quantifying tapirid and equoid covariate traits. **(a)** Hypsodonty index, after Mihlbachler et al. (2011): (upper third molar crown height ÷ upper second molar labiolingual width; i.e. max. molar height ÷ max. molar width); **(b)** body mass, using linear measurements and regression equations for 'all ungulate' datasets in Scott (1990), in addition to published values; **(c)** gracility index, after Guerin (1980); **(d)** sagittal ridge angle, after MacFadden (1992).

6. Shape Change through the Mid-Miocene Climatic Optimum

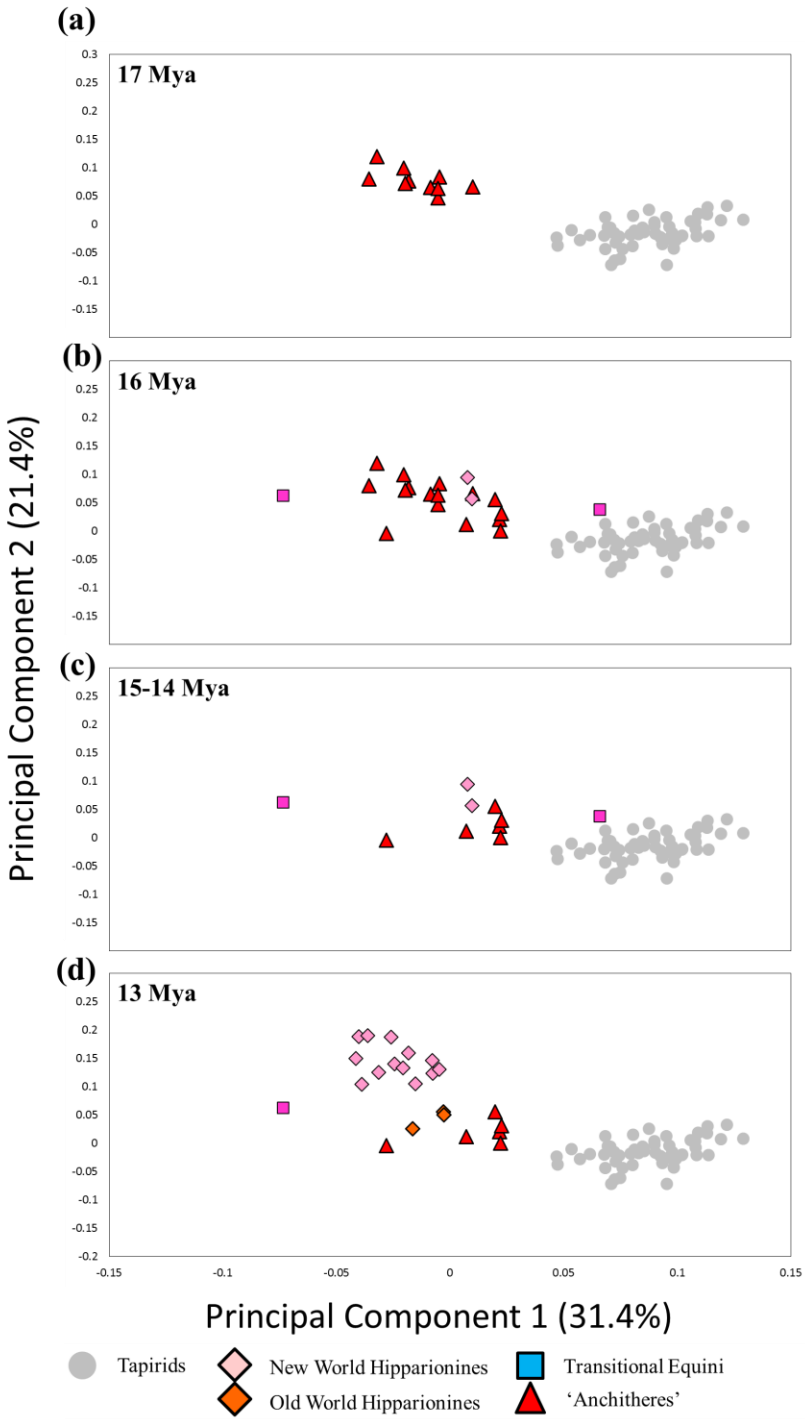

Figure S5.4. Breakdown of metacarpal morphospace occupation through the latter section of the Mid-Miocene Climatic Optimum (MMCO), with time bins between 17 and 13 Mya.

7. Phylogenetic Partial Least Square analyses (Equoid only)

Table S5.4. phyPLS coefficients, multivariate regressions and associated permutational *p*-values for the full data set and equoid only dataset. Permutations with 10000 replicates. Significant p-values at $p \leq 0.05$. HI = hypsodonty index; log BM = log-transformed body mass; Gr-I = gracility index; RA = maximum angle of sagittal ridge.

Statistic	**Dataset**	**HI**	**log BM**	**Gr-I**	**RA**
RV coefficient	all taxa	0.055	0.067	0.242	0.154
	equoid only	0.060	0.093	0.298	0.149
Permutational *p*-value	all taxa	0.202	0.108	<0.01	<0.01
	equoid only	0.268	0.071	<0.01	<0.01
Pairwise correlation	all taxa	0.363	0.429	0.672	0.556
	equoid only	0.368	0.499	0.711	0.537
Correlation *p*-value	all taxa	0.468	0.318	<0.01	<0.01
	equoid only	0.642	0.685	<0.01	0.051
Multivariate Regression (shape variables vs. individual covariates)					
% prediction	all taxa	1.886	2.314	8.326	5.323
	equoid only	2.182	3.392	10.815	5.412
Permutational *p*-value	all taxa	0.204	0.109	<0.01	<0.01
	equoid only	0.260	0.066	<0.01	0.011

Table S5.5. Ordinary Least Squares regression of ecomorphological traits against one another. Permutations with 10000 replicates. Correlation coefficient (R^2) above diagonal, permutational *p*-value below (significant $p \leq 0.05$). All taxa (top) and only equoids only (below).

All Taxa	Hypsodonty	Body Mass	Gracility	Ridge Angle
Hypsodonty		0.117	<0.001	0.844
Body Mass	<0.001		0.392	0.196
Gracility	0.989	<0.001		0.014
Ridge Angle	<0.001	<0.001	0.320	
Equoids only	Hypsodonty	Body Mass	Gracility	Ridge Angle
Hypsodonty		0.394	0.107	0.795
Body Mass	<0.001		0.394	0.471
Gracility	0.016	<0.001		0.037
Ridge Angle	<0.001	<0.001	0.154	

8. Cross Correlation Analyses

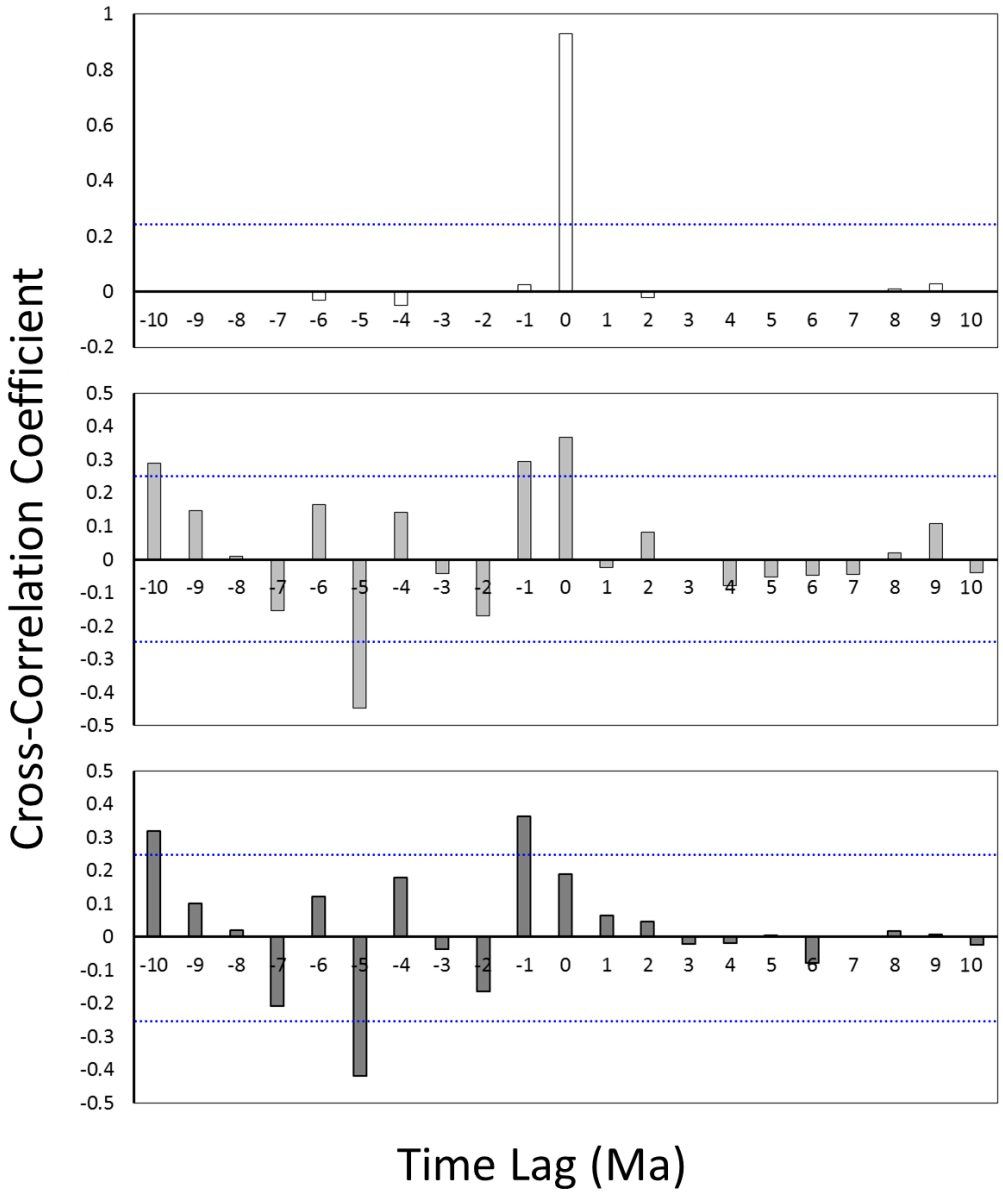

Figure S5.9. Cross correlation coefficients for traits through time: (from top) hypsodonty index vs. log body mass; ordinary sum of squares vs. hypsodonty index; ordinary sum of squares vs. log body mass. Blue dotted lines indicate 95% confidence intervals. Correlations above 95% confidence intervals were chosen for discussion; correlations with lag times less than 5 Ma (positive or negative) are discussed in the main document. Here, we comment on the strong positive correlation between shape and both hypsodonty and body mass at -10 Ma lag time.

10 Ma Cross Correlation

Cross-correlation analysis suggests a strong positive correlation between ordinary sum of squares (i.e. divergence in shape from ancestral morphology; OSS) and both hypsodonty index (HI) and log body mass (BM). When we observe the changes which drive this correlation, it is difficult to conclude whether there is a biological signal associated with the correlation. Examples of events that correlate across 10 Ma include:

1. The shift from 'hyracotheres' to palaeotheres as the main equoid representatives resulted in an ingreat in body mass and tooth crown height (HI and BM); (**10 Ma later**) the early Bartonian expansion of palaeothere taxon count increasing the diversity of shapes(OSS);
2. The early Bartonian palaeothere taxonomic increase (BM); (**10 Ma later**) the origination of the anchithere *Archaeohippus* following the extinction of the last palaeothere *Plagiolophus minor* (c.28 Mya) drove a shift away from the ancestral shape (OSS);
3. Origination of the comparatively large anchithere (*Parahippus leonensis*) increased mean size for equids (BM); (**10 Ma later**) the North American equid turnover in the early Tortonian, including first occurrence of two monodactyl equids (*Astrohippus ansae* and *Dinohippus interpolatus*) and the extinction of the more basal hipparionines (e.g. *Protohippus*), driving average fetlock shape away from ancestral morphology (OSS);
4. Increases in tooth crown height and body mass with the first occurrence of *Merychippus* (and Acritohippus, formerly *Merychippus*) and *Pliohippus* (BM and HI); (**10 Ma later**) origination of several advanced tridactyl taxa (*Nannippus peninsulatus*; *Hipparion crassum*) and the first occurrence of *Equus*, shifting fetlock morphology further from the ancestral shape (OSS).
5. An increase in abundance of tridactyl taxa in both hipparionine and equinine lineages promoting an increase in tooth crown height and (more discretely) body mass at the end of the Mid-Miocene Climatic Optimum (c.13 Mya); (**10 Ma later**) shape divergence increases with the first occurrences of South American equids between 2 and 3 Mya (including *Equus* (*Amerhippus*) spp. and *Hippidion* spp.) following the formation of the Panamanian Isthmus.

There are also multiple small fluctuations in HI and BM which correlate positively with small fluctuations in OSS, especially following the MMCO. None of the five correlated increases in trait values appear to be biologically linked to one another, but rather come about due to climatic changes, shifts in biogeographical range, or are due to first and last occurrences of key taxa. For these reasons, we focussed upon occurrences of trait correlations which were up to 5 Ma appart (positively or negatively); this span of time has more potential to harbour biologically or anatomically relevant correlations, rather than those which may be caused by unrelated events (e.g. proliferation of tridactyl, mid-high crowned equids and the formation of the Panamanian Isthmus).

9. Hypothetical ancestral fetlock generation

To examine the divergence in shape of the fetlock from an ancestral form through time, a hypothetical morphology was necessary to test against modern and fossil perissodactyl metacarpals. Firstly, raw landmark data points from geometric morphometric analysis were mapped onto the time-calibrated phylogeny in MorphoJ (Klingenberg, 2011); the root node morphology was then extracted and used as a hypothetical 'ancestral metacarpal morphology' for comparisons with derived taxa. Inclusion and exclusion of basal taxa in the composite tree were performed to validate the construction of the hypothetical ancestral shape; basal-most taxa included the tetradactyl palaeotheres (*Propalaeotherium, Eurohippus*), 'hyracotheres' (*Sifrhippus, Eohippus*) and the tapiromorph *Chasmotherium*. Sensitivity analyses were performed on the hypothetical shapes which were generated using the most basal taxa using a simple jack-knifing approach (leave-one-out cross validation). All hypothetical metacarpal morphologies fell within the variance of the basal taxa used to generate the ancestor, and as such were deemed suitable for comparative analyses given the caveat that the ancestor was generated predominantly based on shapes of the most basal taxa. The availability of these early taxa, representing each major lineage in this study, was vitally important for the ancestral taxon generation as well as maintaining as many opportunities for comparison through time as possible. The exclusion of other tapirids, helaletids and equoids was purely a matter of specimen availability. Each landmark configuration was finally aligned iteratively to the validated hypothetical ancestral configuration using Ordinary Procrustes Analysis (OPA) in the R-library 'shapes' (citation). OPA translated, scaled and oriented each individual landmark configuration to the geometric centre (centroid) of the ancestral taxon, rather than aligning all taxa at the same time as in Generalised Procrustes Analysis (Zelditch et al., 2012). The OPA produced individual ordinary sum of squares (OSS) values for each metacarpal, representing a value of shape deviation from the ancestral shape.

Ultimately, the accuracy of the hypothetical ancestral condition relies upon several key criteria: 1) the selection of the most basal taxa in each clade, 2) accurate phylogenetic affinity and nomenclature, and 3) accurate dating of branch lengths within the phylogenetic tree used for the ancestor reconstruction. Within this analysis, we believe that the branch lengths are robust, although finer-scale determination for all taxa would have been more ideal. As this was not within the scope of this study, we employed the most viable alternative by generating a tree based on maximum likelihood trees from published articles and taking branch lengths as first and last occurrence dates. This method has been implemented in a variety of studies on different extinct vertebrate clades, principally for taxonomic groups which have no supermatrix or published supertree available (Bininda-Emonds 2004; examples include Button et al. 2014; Famoso et al. 2016, etc.). These dates are unlikely to represent the accurate first and last appearance of the taxon; however, using a uniform methodology within a phylogenetic reconstruction with no available supermatrix may be considered the best option for this study (Bininda-Emonds, 2004). Unsurprisingly, the tetradactyl palaeotheres (*Propalaeotherium, Eurohippus*), 'hyracotheres' (*Sifrhippus, Eohippus*) and the tapiromorph *Chasmotherium* do not diverge greatly

from the hypothetical ancestral taxon. This may be interpreted as an artefact of the methodology used to generate the hypothetical ancestor.

10. Species breakdown of metacarpal morphospace

Supplementary Figures 5.6. Species breakdowns for PC1 and PC2 morphospace occupation based on Procrustes coordinates from distal metacarpal landmarks. Over following pages: **(a)** Tapiroids; **(b)** Palaeotheres; **(c)** Hyracotheres + Anchitheres; **(d)** New World Hipparionines; **(e)** Old World Hipparionines; **(f)** non-Equus equinines; **(g)** extinct Equus species; **(h)** extant Equus species

(a) Species breakdowns for tapiroid morphospace occupation

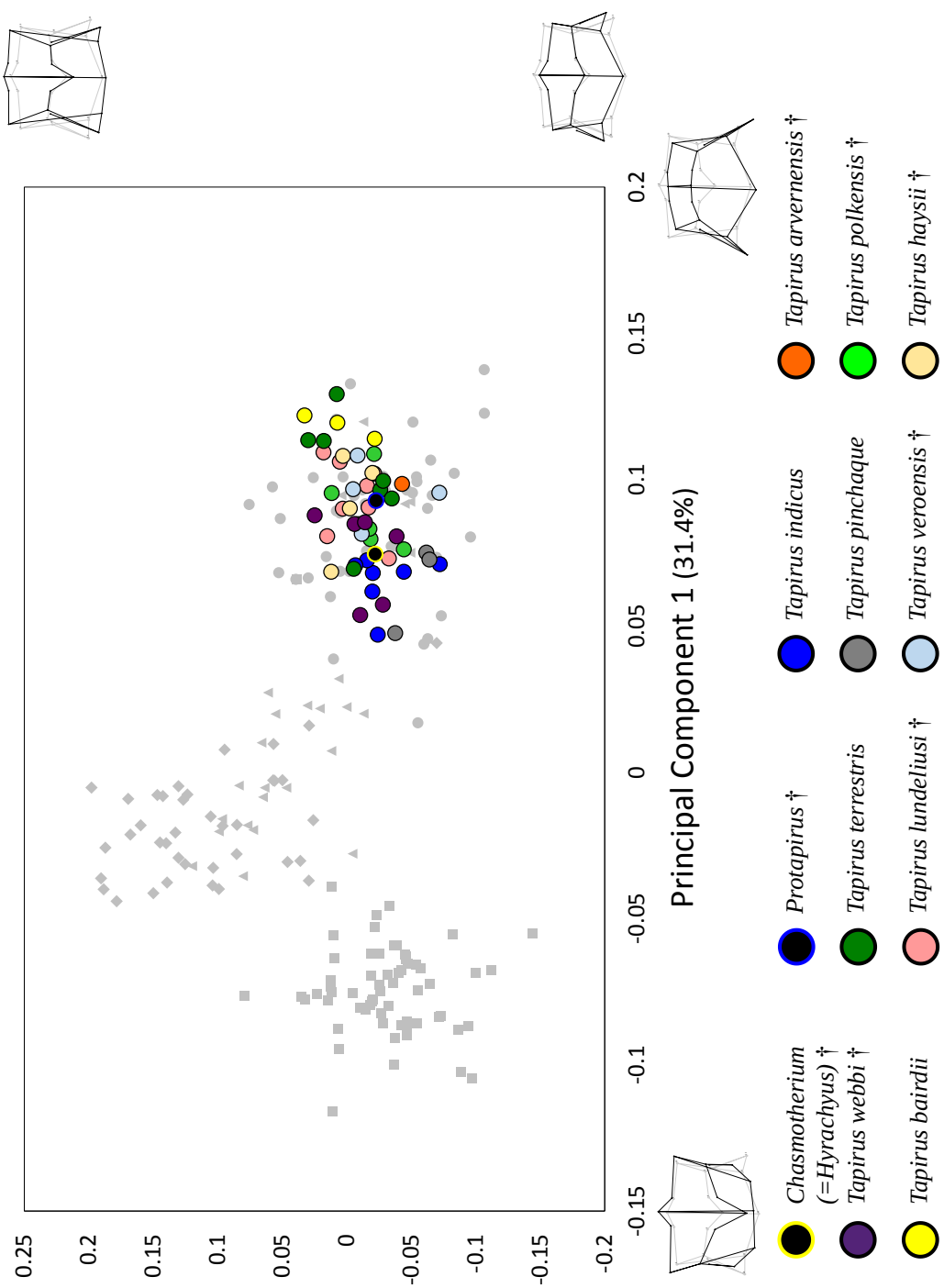

(b) Species breakdowns for palaeothere morphospace occupation

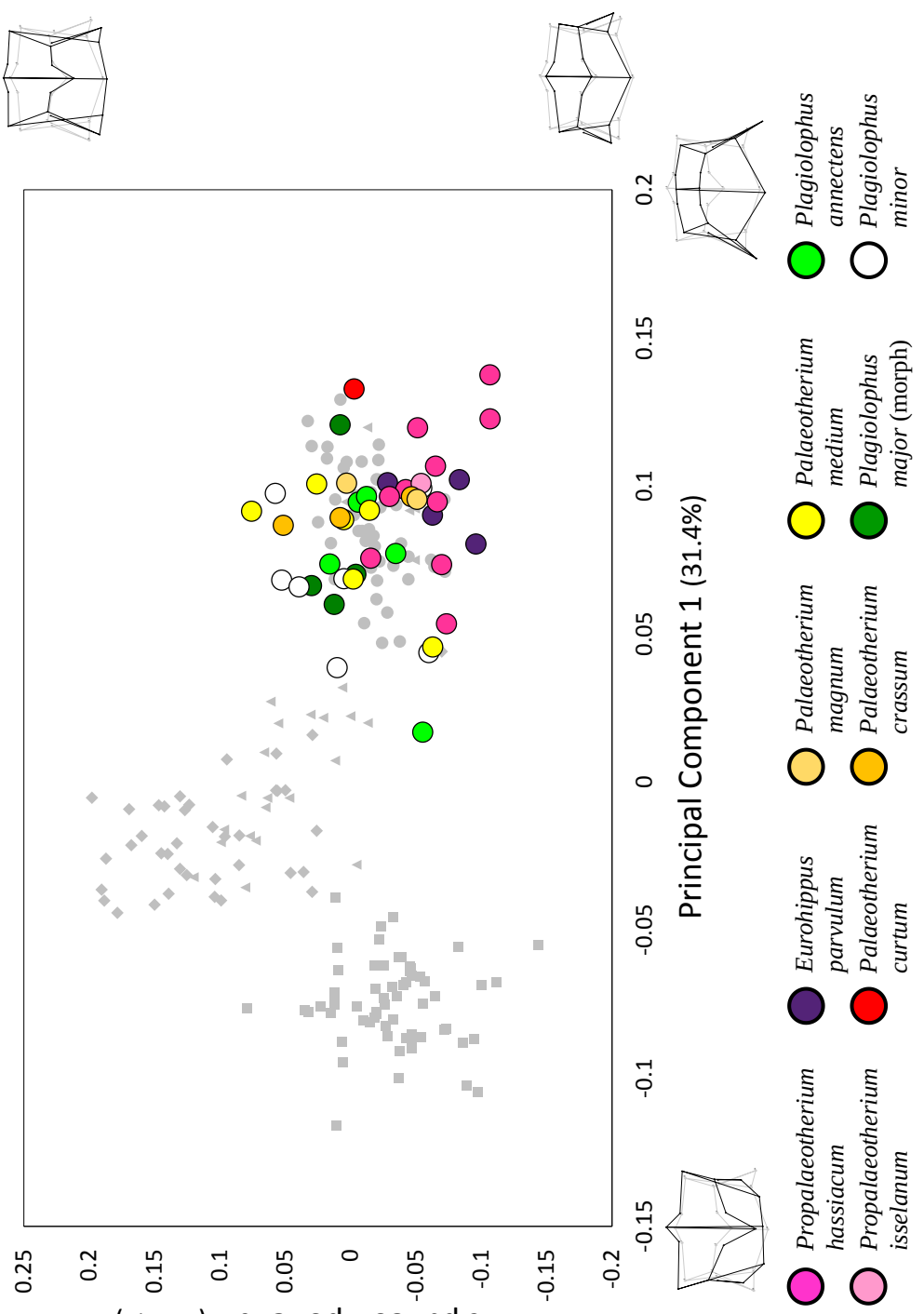

(c) Species breakdowns for ‘hyracothere’ + ‘anchithere’ morphospace occupation

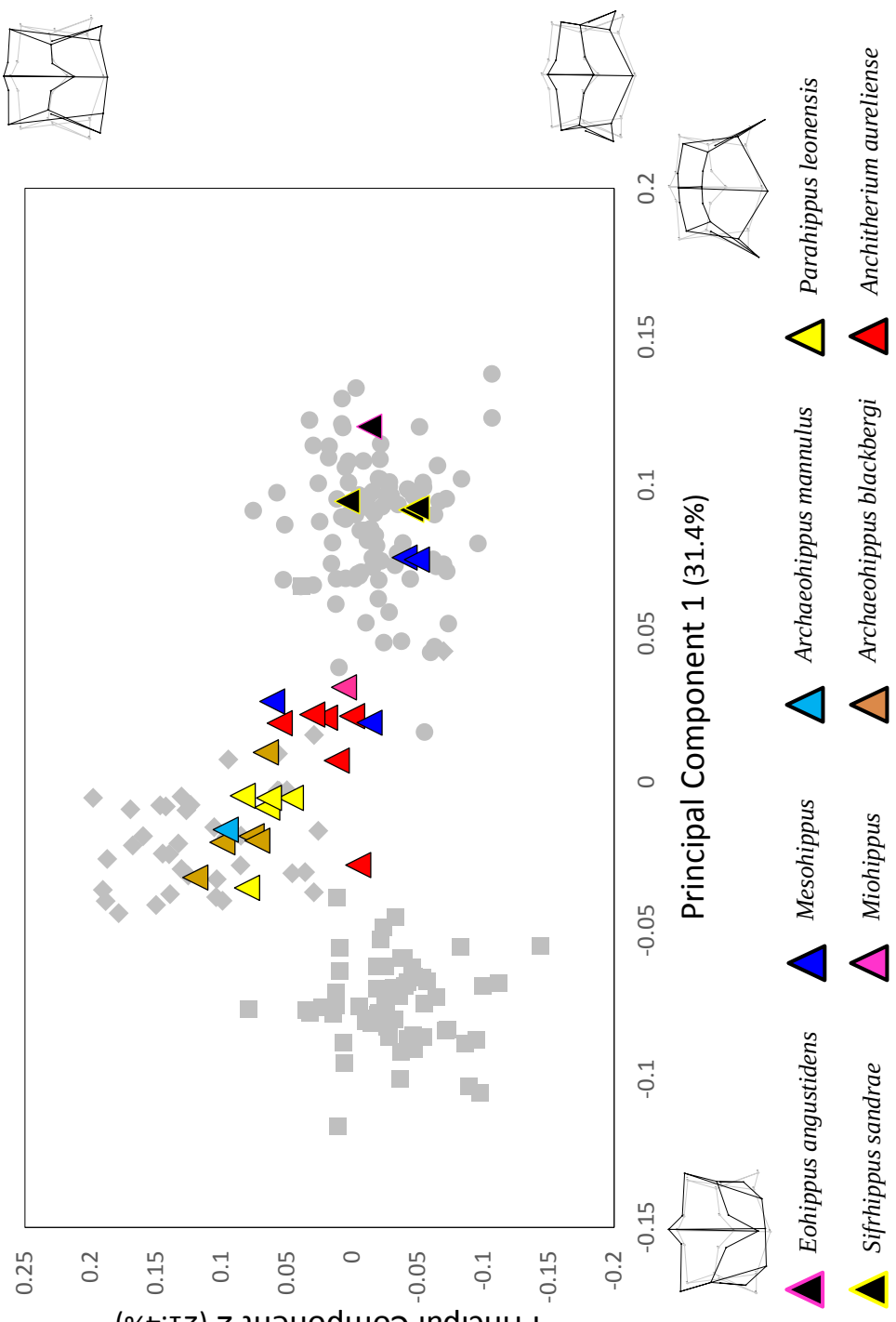

(d) Species breakdowns for New World hipparionine morphospace occupation

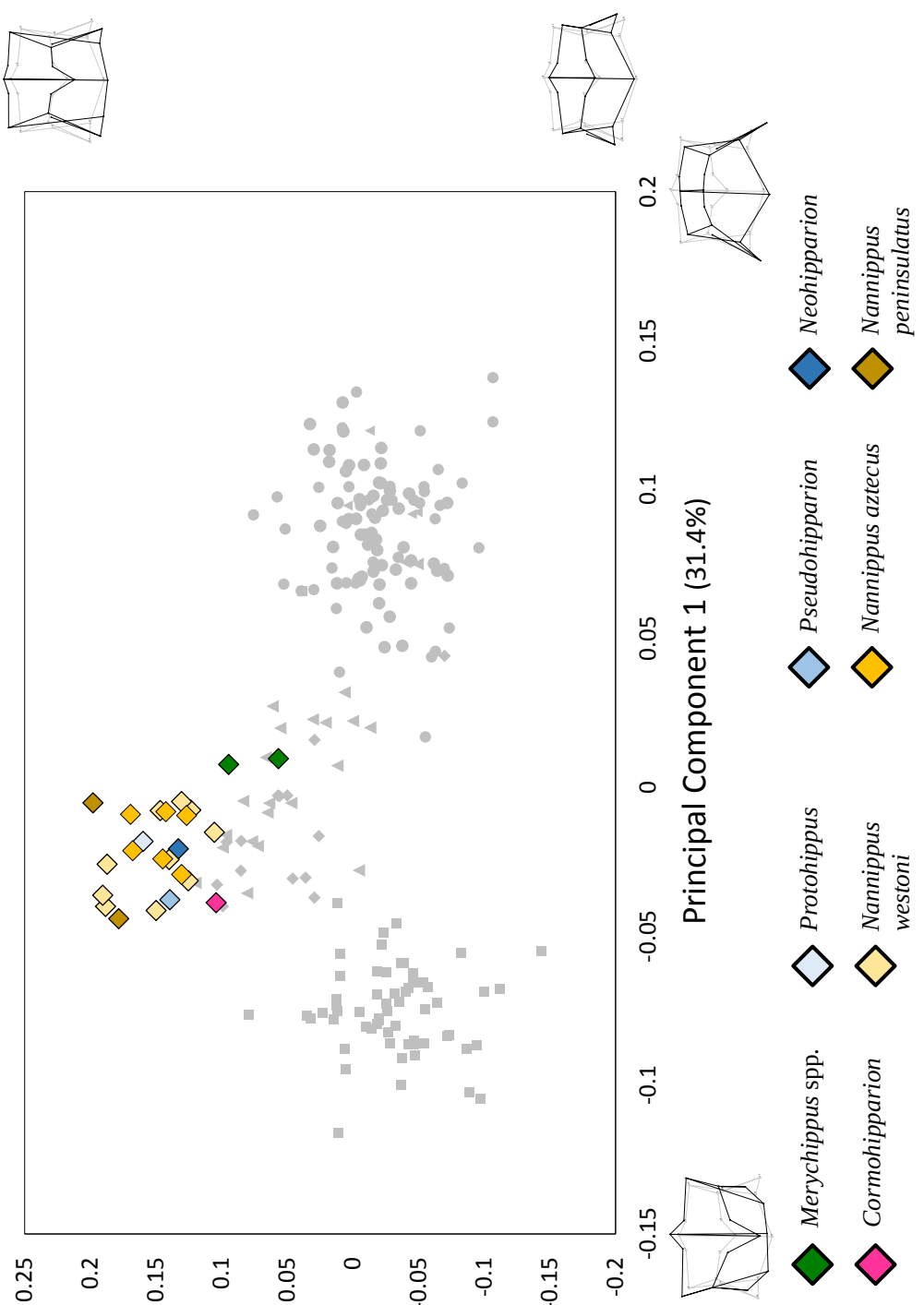

(e) Species breakdowns for Old World hipparionine morphospace occupation

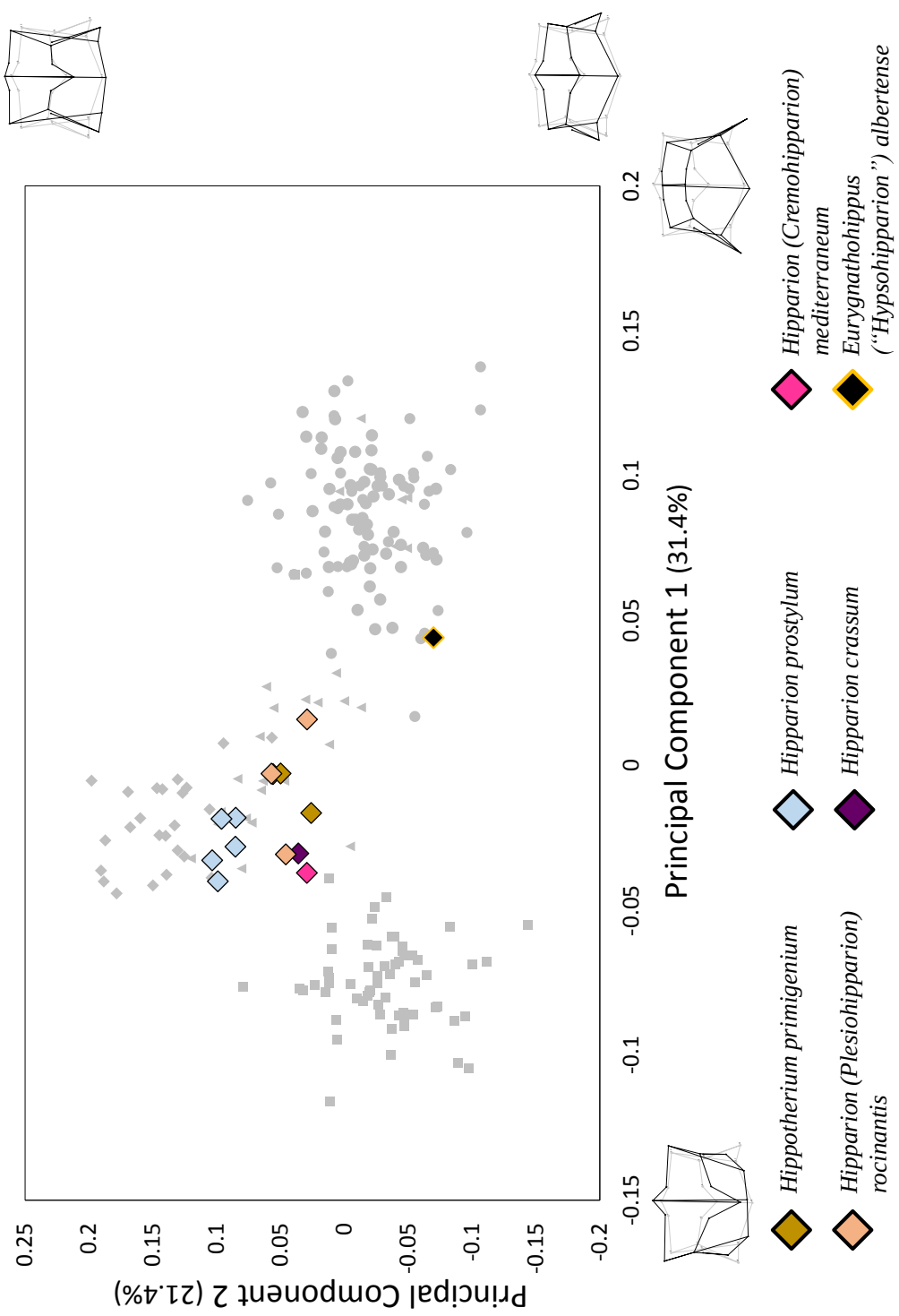

(f) Species breakdowns for non-*Equus* equinine morphospace occupation

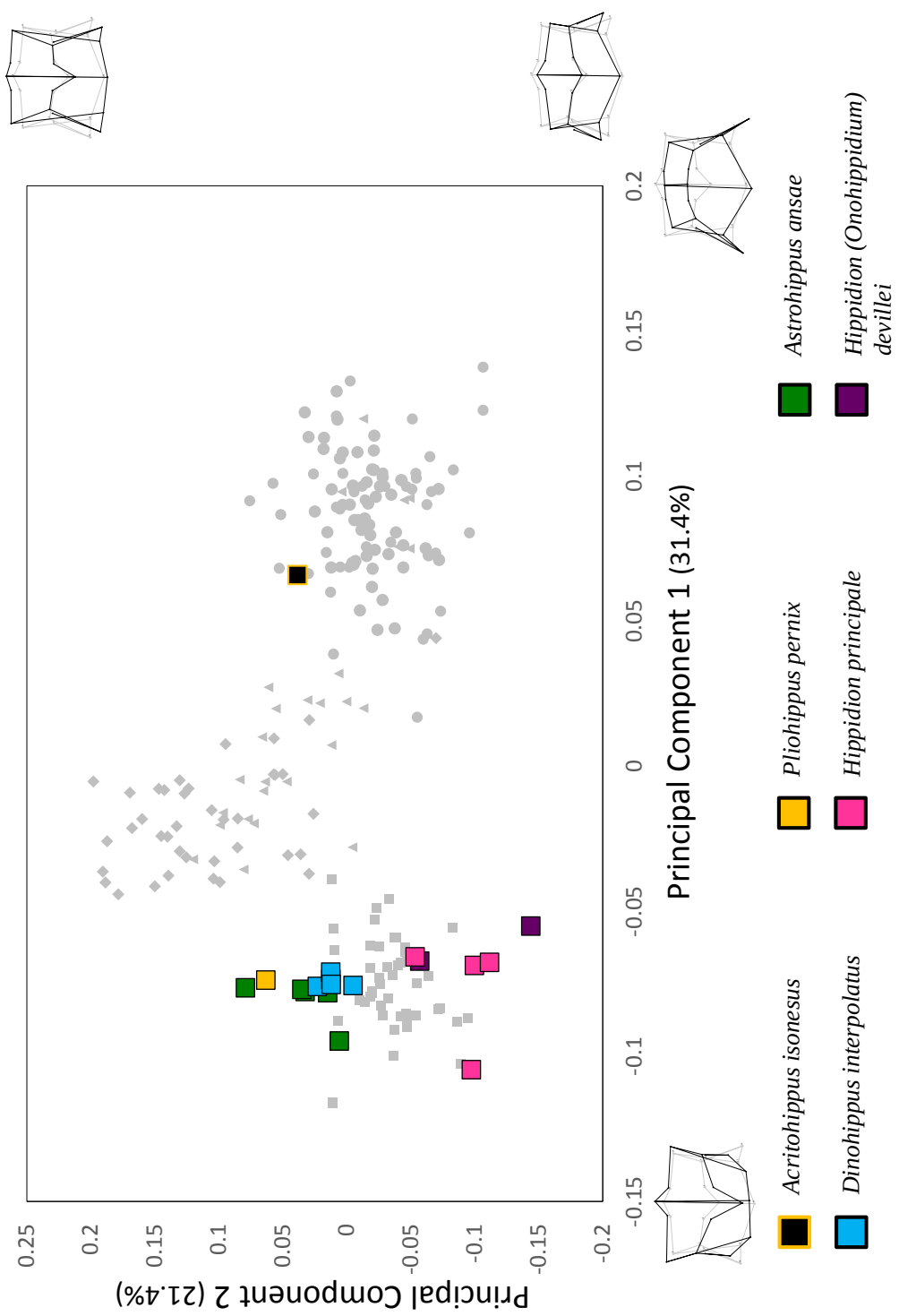

(g) Species breakdowns for extinct *Equus* species morphospace occupation

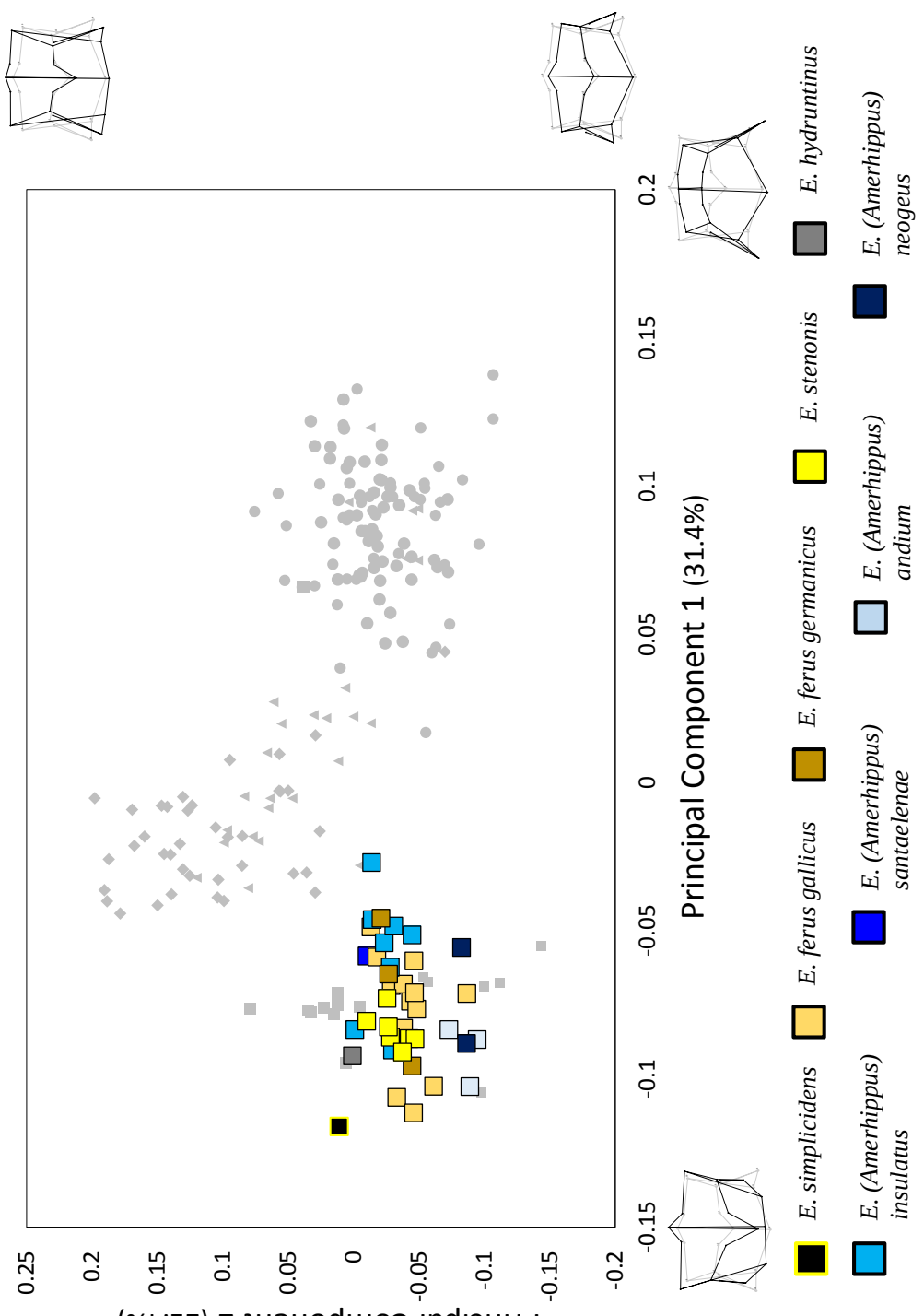

(h) Species breakdowns for extant *Equus* species morphospace occupation